

**A NEW DETERMINATION OF MOLECULAR MOBILITY IN AMORPHOUS
MATERIALS.**

by

RASHMI SATYANARAYAN TIWARI

A Dissertation submitted to the
Graduate School-New Brunswick
Rutgers, The State University of New Jersey
in partial fulfillment of the requirements

for the degree of

Doctor of Philosophy

Graduate Program in Food Science

Written under the direction of

Dr Richard D. Ludescher

And approved by

New Brunswick, New Jersey

[Oct, 2008]

ABSTRACT OF THE DISSERTATION

A New Determination of Molecular Mobility in Amorphous Materials.

By

RASHMI SATYANARAYAN TIWARI

Dissertation Director: Dr. Richard D. Ludescher

This research investigated how the steady-state and time-resolved emission and intensity of phosphorescence from vanillin (4-hydroxy-3-methoxy benzaldehyde), a commonly used flavor compound, can be used to probe molecular mobility when dispersed within amorphous pure sucrose films. The luminescence properties and photophysical events of vanillin as a triplet state probe in amorphous sucrose films as a function of temperature was successfully characterized. The peak energy, bandwidth and lifetime data suggest that it is sensitive to molecular mobility and can be used monitor molecular mobility in amorphous sucrose films. Time-resolved phosphorescence intensity decays from vanillin were multiexponential both below and above the glass transition temperature, indicating that the pure (single component) amorphous matrix was dynamically heterogeneous on the molecular level.

Vanillin analogs (hydroxy, dihydroxy and ethyl vanillin)) phosphorescence lifetime were found to be extremely sensitive to the local environment in the amorphous sucrose in the glassy state and at the glass-to-rubber transition into the melt, and provided useful insight about the mechanism of vanillin sensitivity to molecular mobility. Based on this the capability of movement of methoxyl group about the C-O bond is thought to be the contributor to sensitivity of vanillin to matrix molecular mobility. The other possibility is

that the effect is not that of larger group but rather that of group (like methoxy and ethoxy) not able to hydrogen bond to matrix, which can have an coupling the probe vibrations to the matrix.

Vanillin phosphorescence demonstrated that the average rate of matrix molecular mobility rates increases with an increase in the molecular size and T_g of the sugar in the glucose homologous series. A comparative study of mobility in three excipients sucrose, trehalose and PVP, using vanillin phosphorescence provided useful insight about their stabilizing effect.

The phosphorescence from probes erythrosin B, vanillin and tryptophan was successfully utilized to measure molecular mobility on three different time scales corresponding to each probe in amorphous sucrose and protein film. Molecular mobility was successfully studied in amorphous sucrose films by monitoring phosphorescence from the dual probe combination of erythrosin B: vanillin, erythrosin B: tryptophan and vanillin:tryptophan.

ACKNOWLEDGEMENT

I would sincerely like to thank my mentor Dr. Richard Ludescher for all his support and encouragement and for being a great advisor. I am very grateful to him for giving me the freedom and leaving endless sky as the limit to choose my research topic. This research has shaped into a great piece of work under his guidance.

I would like to specially thank Dr. Jane Vanderkooi for serving on my committee and providing her lab space for some of the important experiments. I would also like to thank my committee member Dr. Paul Takhistov for his valuable guidance. I would also like to extend my sincere thanks to Dr. Qingrong Huang for his helpful inputs and guidance. I want to thank

Dr. Bogumil Zelent and Dr. Peter Kahn for helping with some of my research problems. A special thanks to my lab mates Kasi, Tom, Yumin, Sonali, Melinda, Sanaz, Xiang and Andrew for great environment in the lab. This process was much easier with all the help and support from you all. I would like to extend a special thanks to all my friends and well wishers in and outside the department.

And last but not the least my loving family. My deepest gratitude to my mom (Naina Tiwari) and dad (Satyanarayan Tiwari) for all their love and support. I would like to thank my brother Ashish and sisters Sushma, Priti, Sarita and Varsha for encouraging me in many different ways and providing all the confidence and belief that I needed. My

special and sincere thanks to my husband Rajiv Savai without his support and encouragement I could not have ever achieved this.

DEDICATION

This dissertation is dedicated to my mom for all her support, encouragement. Her love and belief in me has made everything possible for me.

TABLE OF CONTENTS

	<u>Page</u>
ABSTRACT.....	ii
ACKNOWLEDGEMENT.....	iv
DEDICATION.....	vi
TABLE OF CONTENTS.....	vii
LIST OF TABLES.....	xi
LIST OF FIGURES.....	xiv
CHAPTER I: a. Introduction.....	1
b. References.....	25
CHAPTER II: Characterizing the luminescence properties and photo-physical events of vanillin as a triplet state probe in amorphous sucrose films.	
a. Introduction.....	32
b. Materials and Methods.....	35
c. Results.....	42
d. Discussions.....	48
e. Conclusion.....	58
f. Tables and Figures.....	59
g. References.....	85
CHAPTER III: Investigating the mechanism of environmental sensitivity of vanillin to molecular motions: using vanillin analogs in amorphous sucrose films.	
a. Introduction.....	91
b. Materials and Methods.....	94
c. Results.....	101
d. Discussion.....	111
e. Conclusion.....	117
f. Tables and Figures.....	118
g. References.....	169
CHAPTER IV: Vanillin sensitivity to molecular mobility as a function of molecular weight and glass transition temperature in glucose homologous series.	
a. Introduction.....	172
b. Materials and Methods.....	175
c. Results.....	180
d. Discussion.....	187
e. Conclusion.....	190
f. Tables and Figures.....	191
g. References.....	245
CHAPTER V: Characterizing molecular mobility of different amorphous matrices (excipients) used for various controlled release application.	
a. Introduction.....	249
b. Material and Methods.....	253
c. Results.....	258

d. Discussion.....	265
e. Conclusion.....	270
f. Tables and Figures.....	271
g. References.....	307
CHAPTER VI: Investigating molecular mobility in amorphous sucrose films using erythrosin B, tryptophan and vanillin as a triplet state probe.	
a. Introduction.....	312
b. References.....	315
CHAPTER VIa: Investigating molecular mobility in amorphous sucrose films using erythrosin B as a triplet state probe.	
a. Introduction.....	317
b. Material and Methods.....	319
c. Results.....	325
d. Discussion.....	329
e. Conclusion.....	331
f. Figures.....	332
g. References.....	340
CHAPTER VIb: Investigating molecular mobility in amorphous sucrose films using tryptophan as a triplet state probe.	
a. Introduction.....	342
b. Material and Methods.....	344
c. Results.....	351
d. Discussion.....	356
e. Conclusion.....	359
f. Tables and Figures.....	360
g. References.....	382
CHAPTER VIc: Comparing the molecular mobility in amorphous sucrose films for erythrosin B, tryptophan and vanillin as a triplet state probe.	
a. Discussion.....	384
b. Conclusion.....	390
c. Tables and Figures.....	391
d. References.....	404
CHAPTER VII: Investigating molecular mobility using intrinsic (tryptophan) and extrinsic probes (erythrosin B and vanillin) in amorphous protein films.	
a. Introduction.....	406
b. References.....	415
CHAPTER VIIa: Molecular mobility, oxygen permeability and site heterogeneity in amorphous protein films using erythrosin B.	
a. Introduction.....	419
b. Material and Methods.....	422
c. Results.....	428
d. Discussion.....	438
e. Conclusion.....	448
f. Figures.....	449
g. References.....	467

CHAPTER VIIb: Investigating molecular mobility using intrinsic probes tryptophan in amorphous protein films.	
a. Introduction.....	470
b. Material and Methods.....	473
c. Results.....	479
d. Discussion.....	483
e. Conclusion.....	492
f. Tables and Figures.....	493
g. References.....	511
CHAPTER VIIc: Investigating molecular mobility using extrinsic probes vanillin in amorphous protein films.	
a. Introduction.....	515
b. Material and Methods.....	516
c. Results.....	522
d. Discussion.....	525
e. Conclusion.....	528
f. Tables and Figures.....	529
g. References.....	542
CHAPTER VIId: Comparing the molecular mobility maps in amorphous protein films for erythrosin B, tryptophan and vanillin as a triplet state probe.	
a. Results and Discussion.....	543
b. Conclusion.....	546
c. Tables and Figures.....	547
CHAPTER VIII: Investigating the potential of using multiple probes erythrosin B and vanillin in amorphous sucrose films to report molecular mobility.	
a. Introduction.....	554
b. Material and Methods.....	559
c. Results.....	569
d. Discussion.....	578
e. Conclusion.....	582
f. Figures.....	583
g. References.....	602
CHAPTER IX: Investigating the potential of using multiple probes erythrosin B and tryptophan in amorphous sucrose films to report molecular mobility.	
a. Introduction.....	606
b. Material and Methods.....	609
c. Results and Discussion.....	618
d. Conclusion.....	626
e. Figures.....	627
f. References.....	644
CHAPTER X: Investigating the potential of using multiple probes tryptophan and vanillin in amorphous sucrose films to report molecular mobility.	
a. Introduction.....	647

b. Material and Methods.....	649
c. Results and Discussion.....	656
d. Conclusion.....	662
e. Figures.....	663
f. References.....	688
CURRICULUM VITAE.....	690

LIST OF TABLES

	<u>Page</u>
Table I-1: Various transitions in carbohydrates (T_g , T_α , T_β) & proteins (T_d).....	10
Table I-2: Spectroscopic properties of some triplet state probes.....	15
Table II-1: Excitation and emission wavelength and phosphorescence lifetime of vanillin in glycerol water, EPA and amorphous sucrose film at 77K after degassing.....	83
Table II-2: Calculated activation energy E_a for each individual lifetime components τ_1 , τ_2 , τ_3 and τ_4 and average lifetime at low (LT) and high temperature (HT).....	84
Table III-1: Calculated activation energy E_a and transition temperatures for hydroxy, dihydroxy, methyl and ethyl vanillin in amorphous sucrose films at low (LT), intermediate (IT) and high temperature (HT). These values were obtained from $\ln(1/I_p)$ vs. K/T	163
Table III-2: Calculated activation energy E_a for each individual lifetime components τ_1 , τ_2 , τ_3 , τ_4 and τ_5 and average lifetime at low (LT) and high temperature (HT) for hydroxy vanillin in amorphous sucrose films.....	164
Table III-3: Calculated activation energy E_a for each individual lifetime components τ_1 , τ_2 , τ_3 and τ_4 and average lifetime at low and high temperature for dihydroxy vanillin in amorphous sucrose films.....	165
Table III-4: Calculated activation energy E_a for each individual lifetime components τ_1 , τ_2 , τ_3 and τ_4 and average lifetime at low and high temperature for methyl vanillin in amorphous sucrose films.....	166
Table III-5: Calculated activation energy E_a for each individual lifetime components τ_1 , τ_2 , τ_3 and τ_4 and average lifetime at low and high temperature for ethyl vanillin in amorphous sucrose films.....	167
Table III-6: Calculated activation energy E_a for non-radiative decay rate at low and high temperature for hydroxy, dihydroxy, methyl and ethyl vanillin in amorphous sucrose films.....	168
Table IV-1: Calculated activation energy E_a for individual k_p at low and high temperature for vanillin in amorphous films of glucose.....	236
Table IV-2: Calculated activation energy E_a for individual k_p at low, intermediate and high temperature for vanillin in amorphous films of maltose.....	237
Table IV-3: Calculated activation energy E_a for individual k_p at low and high	

	temperature for vanillin in amorphous films of maltotriose.....	238
Table IV-4:	Calculated activation energy E_a for individual k_p at low and high temperature for vanillin in amorphous films of maltotetraose.....	239
Table IV-5:	Calculated activation energy E_a for individual k_p at low and high temperature for vanillin in amorphous films of maltopentaose.	240
Table IV-6:	Calculated activation energy E_a for individual k_p at low and high temperature for vanillin in amorphous films of maltohexaose.....	241
Table IV-7:	Calculated activation energy E_a for individual k_p at low and high temperature for vanillin in amorphous films of and maltoheptaose.....	242
Table IV-8:	Calculated activation energy E_a for average k_p at low, intermediate and high temperature for methyl vanillin in amorphous films of glucose, maltose, maltotriose, maltotetraose, maltopentaose, maltohexaose and maltoheptaose.....	243
Table IV-9:	Calculated activation energy E_a for k_{NR} at low, intermediate and high temperature for methyl vanillin in amorphous films of glucose, maltose, maltotriose, maltotetraose, maltopentaose, maltohexaose and maltoheptaose.....	244
Table V-1a:	Calculated activation energy E_a for $\ln(k_p)$ for individual lifetime at low, intermediate and high temperature for vanillin in amorphous sucrose films.....	302
Table V-1b:	Calculated activation energy E_a for $\ln(k_p)$ for individual lifetime at low, intermediate and high temperature for vanillin in amorphous trehalose films.....	303
Table V-1c:	Calculated activation energy E_a for $\ln(k_p)$ for individual lifetime at low, intermediate and high temperature for vanillin in amorphous PVP films.....	304
Table V-2:	Calculated activation energy E_a for $\ln(k_p)$ for average lifetime at low, intermediate and high temperature for vanillin in amorphous films of sucrose, trehalose and PVP.....	305
Table V-3:	Calculated activation energy E_a for $\ln(k_{NR})$ for average lifetime at low, intermediate and high temperature for vanillin in amorphous films of sucrose, trehalose and PVP.....	306
Table VIb-1a:	Calculated activation energy E_a for k_p and k_{NR} at low, intermediate and high temperature for tryptophan in amorphous films of sucrose using multi-exponential function.....	380
Table VIb-1b:	Calculated activation energy E_a for k_p and k_{NR} at low, intermediate and high temperature for tryptophan in amorphous films of sucrose using two stretched-exponential function.....	381
Table VIc-1:	The activation energies and transition temperatures of erythrosin B, vanillin and tryptophan in amorphous sucrose film.....	403
Table VII-1:	Characteristic motions of globular proteins.....	411

Table VIIb-1:	Calculated activation energy E_a for each individual lifetime components τ_1 , τ_2 , τ_3 and τ_4 and average lifetime at low, intermediate and high temperature.....	510
Table VIIc-1:	Calculated activation energy E_a for each individual lifetime components τ_1 , τ_2 , τ_3 and τ_4 and average lifetime at low, intermediate and high temperature.....	541
Table VIId-1:	Comparison of activation energy and transition temperature for erythrosin B, vanillin and tryptophan in amorphous α -lactalbumin.....	553
Table VIII-1:	Emission Ratios.....	568

LIST OF FIGURES

	<u>Page</u>
Figure I-1:	Molecular mobility..... 5
Figure I-2:	A schematic model of variables playing role in modulating food quality..... 6
Figure I-3:	Molecular mobility and Heterogeneity..... 12
Figure I-4:	Spatially Heterogeneity Dynamics..... 12
Figure I-5:	Jablonski Energy Level Diagram..... 18
Figure II-1a:	Structure of 4-hydroxy-3-methoxy-benzaldehyde (vanillin or methyl vanillin)..... 59
Figure II-1b:	Absorption spectra of vanillin in aqueous solution (50 μ M) and amorphous sucrose (1:10 ³ : dye: sucrose) at 20°C..... 60
Figure II-1c:	Excitation spectra for vanillin phosphorescence at 490 nm in amorphous sucrose (1:10 ³ : dye: sucrose) films (-O ₂) at 20°C..... 61
Figure II-2:	Delayed emission spectra of vanillin in amorphous sucrose films as a function of temperature (excitation at 320 nm). The spectra were collected at 10°C intervals from -20°C to 100°C (the curves follow this order from high to low intensity at ~490 nm)..... 62
Figure II-3:	The effect of temperature on the phosphorescence emission intensity of vanillin in amorphous sucrose films as a function of temperature equilibrated against nitrogen. Intensity (I_P) was determined from analysis of the phosphorescence emission band (Figure II-2) using a log-normal function (eq. (1), Materials and Methods)..... 63
Figure II-4:	Arrhenius plot of the effect of temperature on the phosphorescence emission intensity I_P of vanillin in amorphous sucrose films. Lines drawn over the data points indicate slopes at low and high temperatures..... 64
Figure II-5a:	Peak energy ν_p (♦, left hand scale) and bandwidth (■, right hand scale) for phosphorescence emission from vanillin in amorphous sucrose films as a function of temperature. The delayed emission spectra collected as a function of temperature (Figure II-2) were analyzed using log-normal function..... 65
Figure II-5b:	Peak frequency of phosphorescence emission spectra of vanillin in amorphous sucrose films plotted against temperature. Lines drawn over the data points indicate slopes at low and high temperatures..... 66
Figure II-5c:	FWHM of phosphorescence emission spectra of vanillin in amorphous sucrose films plotted against temperature. Lines drawn over the data points indicate slopes at low and high temperatures..... 67
Figure II-6a:	Decay of the phosphorescence intensity of vanillin in

	degassed glycerol water (6/4 v/v) and EPA at 77K, $\lambda_{\text{excitation}} = 350\text{nm}$, $\lambda_{\text{emission}} = 490\text{nm}$	68
Figure II-6b:	Decay of the phosphorescence intensity of vanillin in degassed amorphous sucrose (1:1000 vanillin: sucrose) film at 77K, $\lambda_{\text{excitation}} = 350\text{nm}$, $\lambda_{\text{emission}} = 490\text{nm}$	69
Figure II-7:	Normalized phosphorescence intensity decay $[I(t)/I(0)]$ of vanillin dispersed in amorphous sucrose film at 20°C in the presence of nitrogen (♦). The solid line through the data is a fit using a multi-exponential function. (b) A plot of modified residuals $[(\text{Data-Fit})/\text{Data}^{1/2}]$ for this fit.....	70
Figure II-7a:	Lifetime components τ_1 (♦), τ_2 (■), τ_3 (▲), τ_4 (●) obtained from a multi-exponential model fit (Eq. (3), Materials and Methods) to phosphorescence intensity decay data from vanillin dispersed in amorphous sucrose films equilibrated against nitrogen as a function of temperature. The data was measured every 10°C from -20°C to 100°C.....	71
Figure II-8:	Intensity decay fit amplitudes for vanillin in amorphous sucrose films in nitrogen as a function of temperature. The data were calculated every 10°C from -20°C to 100°C. The amplitudes a_1 (♦) and a_2 (■) correspond to the longer life time components (τ_1 , τ_2) and a_3 (▲) and a_4 (●) correspond to the shorter lifetime components (τ_3 , τ_4). The amplitudes were obtained from a multi exponential model fit (Eq. (3), Materials and Methods) to phosphorescence intensity decay data from vanillin dispersed in amorphous sucrose films equilibrated against nitrogen as a function of temperature.....	72
Figure II-9a:	Average lifetime from a multi-exponential model fit (Eq. (4), Materials and Methods) to phosphorescence intensity decay data from vanillin dispersed in amorphous sucrose films equilibrated against nitrogen as a function of temperature. The data were calculated every 5°C from -20°C to 100°C.....	73
Figure II-9b:	Average lifetime of vanillin dispersed in amorphous sucrose films equilibrated against nitrogen as a function of T-Tg. The data were calculated every 5°C from -20°C to 100°C. The Tg value used was 65°C.....	74
Figure II-10:	An Arrhenius plot of k_p calculated from the average lifetime of vanillin in amorphous sucrose.....	76
Figure II-11:	An Arrhenius plot of k_p calculated from the individual lifetime components τ_1 (♦), τ_2 (■), τ_3 (▲) and τ_4 (●).....	76
Figure II-12a-d:	Arrhenius plots of k_p for individual lifetime components τ_1 (12a), τ_2 (12b), τ_3 (12c) and τ_4 (12d) of vanillin in amorphous sucrose as a function of inverse of temperature. Lines drawn through the data points indicate slopes at low	

	and high temperatures for each lifetime component.....	77
Figure II-13a:	Temperature dependence of the total non-radiative decay rate of the triplet state k_{NR} ($k_p = k_{RP} + k_{NR}$) to S_0 of vanillin in amorphous sucrose film over the temperature range from -20°C to 100°C; values were calculated from the average lifetime data.....	79
Figure II-13b:	An Arrhenius plot of the total non-radiative decay rate of the triplet state k_{NR} ($k_p = k_{RP} + k_{NR}$) to S_0 of vanillin in amorphous sucrose film.....	80
Figure II-14a:	Temperature dependence of the total non-radiative decay rate of the triplet state k_{NR} ($k_p = k_{RP} + k_{NR}$) to S_0 for individual lifetime components of vanillin in amorphous sucrose film over the temperature range from -20°C to 100°C; values were calculated from the individual lifetime data.....	81
Figure II-14b:	An Arrhenius plot of the total non-radiative decay rate of the triplet state k_{NR} ($k_p = k_{RP} + k_{NR}$) to S_0 for individual lifetime components of vanillin in amorphous sucrose film.....	82
Figure III-1:	Structure of hydroxy vanillin (4-hydroxy-benzaldehyde), dihydroxy vanillin (3, 4-dihydroxy-benzaldehyde), methyl vanillin (4-hydroxy-3-methoxy-benzaldehyde) and ethyl vanillin (4-hydroxy-3-ethoxy-benzaldehyde).....	118
Figure III-2:	Phosphorescence excitation spectra for hydroxyl, dihydroxy, methyl and ethyl vanillin phosphorescence in amorphous sucrose films (1:10 ³ : dye: sucrose) (-O ₂) at 20°C. Emissions were collected for hydroxy (450 nm), dihydroxy (490 nm), methyl (490 nm) and ethyl vanillin (490 nm).....	119
Figure III-3a:	The phosphorescence emission spectra of methyl vanillin (1) and the three analogs hydroxy (3), dihydroxy (4) and ethyl (2) vanillin at 77K in glycerol: water. Excitations were hydroxy (320 nm), dihydroxy (320 nm), methyl (350 nm) and ethyl vanillin (350 nm).....	120
Figure III-3b:	The phosphorescence emission spectra of methyl vanillin (1) and the three analogs hydroxy (3), dihydroxy (4) and ethyl (2) vanillin at 77K in EPA solvent. Excitations were hydroxy (320 nm), dihydroxy (320 nm), methyl (350 nm) and ethyl vanillin (350 nm).....	121
Figure III-3c:	The phosphorescence emission spectra of methyl vanillin (1) and the three analogs hydroxy (3), dihydroxy (4) and ethyl (2) vanillin at 77K in amorphous sucrose films. Excitations were hydroxy (320 nm), dihydroxy (320 nm), methyl (350 nm) and ethyl vanillin (350 nm).....	122
Figure III-4a:	Delayed emission spectra of hydroxy vanillin in amorphous sucrose films as a function of temperature	

	(excitation at 300 nm). The spectra were collected at 10°C intervals from -20°C to 80°C (the curves follow this order from high to low intensity at ~450 nm).....	123
Figure III-4b:	Delayed emission spectra of dihydroxy vanillin in amorphous sucrose films as a function of temperature (excitation at 320 nm). The spectra were collected at 10°C intervals from -20°C to 80°C (the curves follow this order from high to low intensity at ~490 nm).....	124
Figure III-4c:	Delayed emission spectra of methyl vanillin in amorphous sucrose films as a function of temperature (excitation at 320 nm). The spectra were collected at 10°C intervals from -20°C to 100°C (the curves follow this order from high to low intensity at ~490 nm).....	125
Figure III-4d:	Delayed emission spectra of ethyl vanillin in amorphous sucrose films as a function of temperature (excitation at 320 nm). The spectra were collected at 10°C intervals from -20°C to 100°C (the curves follow this order from high to low intensity at ~490 nm).....	126
Figure III-5:	The effect of temperature on the phosphorescence emission intensity of hydroxy, dihydroxy, methyl and ethyl vanillin in amorphous sucrose films as a function of temperature equilibrated against nitrogen. The curves were normalized to -20°C. Intensity (I_p) was determined from analysis of the phosphorescence emission band (Figure III-4a, 4b, 4c, 4d) using a log-normal function (Eq. (1), Materials and Methods).....	127
Figure III-6:	Arrhenius plot ($1/I_p$) of the effect of temperature on the phosphorescence emission intensity I_p of hydroxy, dihydroxy, methyl and ethyl vanillin in amorphous sucrose films.....	128
Figure III-6a-d:	Arrhenius plot of the effect of temperature on the phosphorescence emission intensity $1/I_p$ of hydroxy, dihydroxy, methyl and ethyl vanillin in amorphous sucrose films. Lines drawn over the data points indicate slopes at low, intermediate and high temperatures hydroxy (6a), dihydroxy (6b), methyl (6c) and ethyl (6d) vanillin.....	129
Figure III-7:	Peak energy ν_p (■, left hand scale) and bandwidth (♦, FWHM right hand scale) for phosphorescence emission from hydroxy vanillin in amorphous sucrose films as a function of temperature. The delayed emission spectra collected as a function of temperature (Figure III-4a) were analyzed using log-normal function as described in Materials and Methods using eq. (1) and (2).....	131
Figure III-8a-b:	Peak energy ν_p for phosphorescence emission from dihydroxy (■), methyl (●) and ethyl (▲) vanillin in amorphous sucrose films as a function of temperature (a).	

	Bandwidth for phosphorescence emission from dihydroxy (■), methyl (●) and ethyl (▲) vanillin in amorphous sucrose films as a function of temperature (b). The delayed emission spectra collected as a function of temperature (Figure III-4a, 4b, 4c and 4d) were analyzed using lognormal function as described in Materials and Methods using eq. (1) and (2)...	132
Figure III-9a:	Lifetime obtained from a single-exponential model fit to phosphorescence intensity decay data from hydroxy vanillin dissolved in glycerol: water or EPA at 77K.....	133
Figure III-9b:	Lifetime obtained from a single-exponential model fit to phosphorescence intensity decay data from dihydroxy vanillin dissolved in glycerol: water or EPA at 77K.....	134
Figure III-9c:	Lifetime obtained from a single-exponential model fit to phosphorescence intensity decay data from methyl vanillin dissolved in glycerol: water or EPA at 77K.....	135
Figure III-9d:	Lifetime obtained from a single-exponential model fit to phosphorescence intensity decay data from ethyl vanillin dissolved in glycerol: water or EPA at 77K.....	136
Figure III-10a:	Lifetime obtained from a single-exponential model fit to phosphorescence intensity decay data from hydroxy vanillin dispersed in amorphous sucrose film at 77K.....	137
Figure III-10b:	Lifetime obtained from a single-exponential model fit to phosphorescence intensity decay data from dihydroxy vanillin dispersed in amorphous sucrose film at 77K.....	138
Figure III-10c:	Lifetime obtained from a single-exponential model fit to phosphorescence intensity decay data from methyl vanillin dispersed in amorphous sucrose film at 77K.....	139
Figure III-10d:	Lifetime obtained from a single-exponential model fit to phosphorescence intensity decay data from ethyl vanillin dispersed in amorphous sucrose film at 77K.....	140
Figure III-11a-d:	Normalized phosphorescence intensity decays $[I(t)/I(0)]$ of hydroxy (4a), dihydroxy (4b), methyl (4c) and ethyl (4d) vanillin dispersed in amorphous sucrose films at 20°C in the presence of nitrogen. The solid lines through the data are fits using a multi-exponential function (Eq. (3), Materials and Methods). A plot of modified residuals $[(Data-Fit)/Data^{1/2}]$ for these are shown in the bottom graph.....	141
Figure III-12a1-a2:	Lifetime components τ_1 (◆), τ_2 (■), τ_3 (▲), τ_4 (●) and τ_5 (x) obtained from a multi-exponential model fit (Eq. (3), Materials and Methods) to phosphorescence intensity decay data from hydroxy vanillin dispersed in amorphous sucrose films equilibrated against nitrogen as a function of temperature. The data were measured every 10°C from -20°C to 80°C. The lifetime vs. temperature (12a1) and log	143

	(lifetime) vs. temperature (12a2).....	
Figure III-12b1-b2:	Lifetime components τ_1 (◆), τ_2 (■), τ_3 (▲) and τ_4 (●) obtained from a multi-exponential model fit (Eq. (3), Materials and Methods) to phosphorescence intensity decay data from dihydroxy vanillin dispersed in amorphous sucrose films equilibrated against nitrogen as a function of temperature. The data were measured every 10°C from -20°C to 90°C. The lifetime vs. temperature (12b1) and log (lifetime) vs. temperature (12b2).....	144
Figure III-12c1-c2:	Lifetime components τ_1 (◆), τ_2 (■), τ_3 (▲) and τ_4 (●) obtained from a multi-exponential model fit (Eq. (3), Materials and Methods) to phosphorescence intensity decay data from methyl vanillin dispersed in amorphous sucrose films equilibrated against nitrogen as a function of temperature. The data were measured every 10°C from -20°C to 100°C. The lifetime vs. temperature (12c1) and log (lifetime) vs. temperature (12c2).....	145
Figure III-12d1-d2:	Lifetime components τ_1 (◆), τ_2 (■), τ_3 (▲) and τ_4 (●) obtained from a multi-exponential model fit (Eq. (3), Materials and Methods) to phosphorescence intensity decay data from ethyl vanillin dispersed in amorphous sucrose films equilibrated against nitrogen as a function of temperature. The data were measured every 10°C from -20°C to 100°C. The lifetime vs. temperature (12d1) and log (lifetime) vs. temperature (12d2).....	146
Figure III-13a:	Intensity decay fit amplitudes for hydroxy vanillin in amorphous sucrose films in nitrogen as a function of temperature. The data were measured every 10°C from -20°C to 80°C. The amplitudes a_1 (◆) and a_2 (■) correspond to the longer life time components (τ_1 , τ_2) and a_3 (▲), a_4 (●) and a_5 (x) correspond to the shorter lifetime components (τ_3 , τ_4 , τ_5). The amplitudes were obtained from a multi exponential model fit (Eq. (3), Materials and Methods) to phosphorescence intensity decay data from hydroxy vanillin dispersed in amorphous sucrose films equilibrated against nitrogen as a function of temperature...	147
Figure III-13b:	Intensity decay fit amplitudes for dihydroxy vanillin in amorphous sucrose films in nitrogen as a function of temperature. The data were measured every 10°C from -20°C to 90°C. The amplitudes a_1 (◆) and a_2 (■) correspond to the longer life time components (τ_1 , τ_2) and a_3 (▲) and a_4 (●) correspond to the shorter lifetime components (τ_3 , τ_4). The amplitudes were obtained from a multi exponential model fit (Eq. (3), Materials and Methods) to	

	phosphorescence intensity decay data from dihydroxy vanillin dispersed in amorphous sucrose films equilibrated against nitrogen as a function of temperature.....	148
Figure III-13c:	Intensity decay fit amplitudes for methyl vanillin in amorphous sucrose films in nitrogen as a function of temperature. The data were measured every 10°C from -20°C to 100°C. The amplitudes a_1 (♦) and a_2 (■) correspond to the longer life time components (τ_1 , τ_2), and a_3 (▲) and a_4 (●) correspond to the shorter lifetime components (τ_3 , τ_4). The amplitudes were obtained from a multi exponential model fit (Eq. (3), Materials and Methods) to phosphorescence intensity decay data from methyl vanillin dispersed in amorphous sucrose films equilibrated against nitrogen as a function of temperature.....	149
Figure III-13d:	Intensity decay fit amplitudes for ethyl vanillin in amorphous sucrose films in nitrogen as a function of temperature. The data were measured every 10°C from -20°C to 100°C. The amplitudes a_1 (♦) and a_2 (■) correspond to the longer life time components (τ_1 , τ_2), and a_3 (▲) and a_4 (●) correspond to the shorter lifetime components (τ_3 , τ_4). The amplitudes were obtained from a multi exponential model fit (Eq. (3), Materials and Methods) to phosphorescence intensity decay data from ethyl vanillin dispersed in amorphous sucrose films equilibrated against nitrogen as a function of temperature.....	150
Figure III-14a:	Average lifetime from a multi-exponential model fit (Eq. (4), Materials and Methods) to phosphorescence intensity decay data from hydroxy (♦), dihydroxy (■), methyl (●) and ethyl (▲) vanillin dispersed in amorphous sucrose films equilibrated against nitrogen as a function of temperature. The data were measured every 10°C from -20°C to 100°C.....	151
Figure III-14b:	Arrhenius plots of the average lifetime of hydroxy, dihydroxy, methyl and ethyl vanillin in amorphous sucrose as a function of inverse of temperature.....	152
Figure III-15a:	The Arrhenius plot of the individual lifetime component τ_1 (♦), τ_2 (■), τ_3 (▲), τ_4 (●) and τ_5 (x) of hydroxy vanillin in amorphous sucrose as a function of inverse of temperature.	153
Figure III-15b:	The Arrhenius plot of the individual lifetime component τ_1 (♦), τ_2 (■), τ_3 (▲) and τ_4 (●) dihydroxy vanillin in amorphous sucrose as a function of inverse of temperature.	154
Figure III-15c:	The Arrhenius plot of the individual lifetime component τ_1 (♦), τ_2 (■), τ_3 (▲) and τ_4 (●) methyl vanillin in amorphous	

	sucrose as a function of inverse of temperature.....	155
Figure III-15d:	The Arrhenius plot of the individual lifetime component τ_1 (\blacklozenge), τ_2 (\blacksquare), τ_3 (\blacktriangle) and τ_4 (\bullet) ethyl vanillin in amorphous sucrose as a function of inverse of temperature.....	156
Figure III-16a:	Temperature dependence of the total non-radiative decay rate of the triplet state k_{NR} ($k_p = k_{RP} + k_{NR}$) to S_0 of hydroxy, dihydroxy, methyl and ethyl vanillin in amorphous sucrose film over the temperature range from -20°C to 100°C.....	157
Figure III-16b:	Temperature dependence of the total non-radiative decay rate of the triplet state k_{NR} ($k_p = k_{RP} + k_{NR}$) to S_0 of hydroxy, dihydroxy, methyl and ethyl vanillin in amorphous sucrose film over the temperature range from -20°C to 100°C.....	158
Figure III-17a:	Arrhenius plot of the total non-radiative decay rate of the triplet state k_{NR} ($k_p = k_{RP} + k_{NR}$) to S_0 of hydroxy vanillin in amorphous sucrose film as function of inverse of temperature.....	159
Figure III-17b:	Arrhenius plot of the total non-radiative decay rate of the triplet state k_{NR} ($k_p = k_{RP} + k_{NR}$) to S_0 of dihydroxy vanillin in amorphous sucrose film as function of inverse of temperature.....	160
Figure III-17c:	Arrhenius plot of the total non-radiative decay rate of the triplet state k_{NR} ($k_p = k_{RP} + k_{NR}$) to S_0 of methyl vanillin in amorphous sucrose film as function of inverse of temperature.....	161
Figure III-17d:	Arrhenius plot of the total non-radiative decay rate of the triplet state k_{NR} ($k_p = k_{RP} + k_{NR}$) to S_0 of ethyl vanillin in amorphous sucrose film as function of inverse of temperature.....	162
Figure IV-1a:	Delayed emission spectra of vanillin dispersed in amorphous films of glucose as a function of temperature (excitation at 320 nm). The spectra were collected at 10°C intervals from -10°C to 80°C (the curves follow this order from high to low intensity at ~490 nm).....	191
Figure IV-1b:	Delayed emission spectra of vanillin dispersed in amorphous films of maltose as a function of temperature (excitation at 320 nm). The spectra were collected at 10°C intervals from -10°C to 120°C (the curves follow this order from high to low intensity at ~490 nm).....	192
Figure IV-1c:	Delayed emission spectra of vanillin dispersed in amorphous films of maltotriose as a function of temperature (excitation at 320 nm). The spectra were collected at 10°C intervals from -10°C to 110°C (the curves follow this order from high to low intensity at ~490 nm).....	193

Figure IV-1d:	Delayed emission spectra of vanillin dispersed in amorphous films of maltotetraose as a function of temperature (excitation at 320 nm). The spectra were collected at 10°C intervals from -10°C to 130°C (the curves follow this order from high to low intensity at ~490 nm).....	194
Figure IV-1e:	Delayed emission spectra of vanillin dispersed in amorphous films of maltopentaose as a function of temperature (excitation at 320 nm). The spectra were collected at 10°C intervals from -10°C to 100°C (the curves follow this order from high to low intensity at ~490 nm).....	195
Figure IV-1f:	Delayed emission spectra of vanillin dispersed in amorphous films of maltohexaose as a function of temperature (excitation at 320 nm). The spectra were collected at 10°C intervals from -10°C to 120°C (the curves follow this order from high to low intensity at ~490 nm).....	196
Figure IV-1g:	Delayed emission spectra of vanillin dispersed in amorphous films of maltoheptaose as a function of temperature (excitation at 320 nm). The spectra were collected at 10°C intervals from -10°C to 130°C (the curves follow this order from high to low intensity at ~490 nm).....	197
Figure IV-2:	Intensity (I_p) was determined from analysis of the phosphorescence emission band (Figures IV-1 a, b, c, d, e, f, g) using a log-normal function (eq. (1), Materials and Methods). The effect of temperature on the phosphorescence emission intensity of vanillin in amorphous films of glucose (◆), maltose (■), maltotriose (▲), maltotetraose (×), maltopentaose (*), maltohexaose (●) and maltoheptaose (+) as a function of temperature equilibrated against nitrogen. Intensity normalized to value at -10°C for each sample.....	198
Figure IV-3a-3g:	Peak energy ν_p and bandwidth for phosphorescence emission from methyl vanillin in amorphous films of glucose (3a), maltose (3b), maltotriose (3c), maltotetraose (3d), maltopentaose (3e), maltohexaose (3f) and maltoheptaose (3g) as a function of temperature. The delayed emission spectra collected as a function of temperature (Figure IV-1a to 1g) were analyzed using lognormal function as described in Materials and Methods using eq. (1) and (2).....	199
Figure IV-4a:	Comparison of peak energy ν_p for phosphorescence emission from vanillin in amorphous films of glucose (◆), maltose (■), maltotriose (▲), maltotetraose (×),	

	maltopentaose (*), maltohexaose (●) and maltoheptaose (+) as a function of temperature.....	203
Figure IV-4b:	Comparison of bandwidth for phosphorescence emission from vanillin in amorphous films of glucose (◆), maltose (■), maltotriose (▲), maltotetraose (×), maltopentaose (*), maltohexaose (●) and maltoheptaose (+) as a function of temperature.....	204
Figure IV-5a:	Comparison of peak energy ν_p for phosphorescence emission from vanillin in amorphous films of glucose (◆), maltose (■), maltotriose (▲), maltotetraose (×), maltopentaose (*), maltohexaose (●) and maltoheptaose (+) as a function of T-Tg.....	205
Figure IV-5b:	Comparison of FWHM for phosphorescence emission from vanillin in amorphous films of glucose (◆), maltose (■), maltotriose (▲), maltotetraose (×), maltopentaose (*), maltohexaose (●) and maltoheptaose (+) as a function of T-Tg.....	206
Figure IV-6a-6g:	Normalized phosphorescence intensity decays $[I(t)/I(0)]$ of vanillin dispersed in amorphous films of glucose (6a), maltose (6b), maltotriose (6c), maltotetraose (6d), maltopentaose (6e), maltohexaose (6f) and maltoheptaose (6g) at 20°C in the presence of nitrogen. The solid lines through the data are fits using a multi-exponential function (Eq. (3), Materials and Methods). A plot of modified residuals $[(Data-Fit)/Data^{1/2}]$ for these fits are shown in the bottom graphs.....	207
Figure IV-7a:	Lifetime components τ_1 (◆), τ_2 (■), τ_3 (▲) and τ_4 (●) obtained from a multi-exponential model fit (Eq. (3), Materials and Methods) to phosphorescence intensity decay data from vanillin dispersed in amorphous films of glucose equilibrated against nitrogen as a function of temperature. The data were calculated every 10°C from -10°C to 70°C.....	211
Figure IV-7b:	Lifetime components τ_1 (◆), τ_2 (■), τ_3 (▲) and τ_4 (●) obtained from a multi-exponential model fit (Eq. (3), Materials and Methods) to phosphorescence intensity decay data from vanillin dispersed in amorphous films of maltose equilibrated against nitrogen as a function of temperature. The data were calculated every 10°C from -10°C to 120°C.....	212
Figure IV-7c:	Lifetime components τ_1 (◆), τ_2 (■), τ_3 (▲) and τ_4 (●) obtained from a multi-exponential model fit (Eq. (3), Materials and Methods) to phosphorescence intensity decay data from methyl vanillin dispersed in amorphous films of maltotriose equilibrated against nitrogen as a	

	function of temperature. The data were calculated every 10°C from -10°C to 150°C.....	213
Figure IV-7d:	Lifetime components τ_1 (◆), τ_2 (■) and τ_3 (▲) obtained from a multi-exponential model fit (Eq. (3), Materials and Methods) to phosphorescence intensity decay data from vanillin dispersed in amorphous films of maltotetraose equilibrated against nitrogen as a function of temperature. The data were calculated every 10°C from -10°C to 150°C.	214
Figure IV-7e:	Lifetime components τ_1 (◆), τ_2 (■) and τ_3 (▲) obtained from a multi-exponential model fit (Eq. (3), Materials and Methods) to phosphorescence intensity decay data from vanillin dispersed in amorphous films of maltopentaose equilibrated against nitrogen as a function of temperature. The data were calculated every 10°C from -10°C to 150°C.	215
Figure IV-7f:	Lifetime components τ_1 (◆), τ_2 (■) and τ_3 (▲) obtained from a multi-exponential model fit (Eq. (3), Materials and Methods) to phosphorescence intensity decay data from vanillin dispersed in amorphous films of maltohexaose equilibrated against nitrogen as a function of temperature. The data were calculated every 10°C from -10°C to 150°C.	216
Figure IV-7g:	Lifetime components τ_1 (◆), τ_2 (■) and τ_3 (▲) obtained from a multi-exponential model fit (Eq. (3), Materials and Methods) to phosphorescence intensity decay data from vanillin dispersed in amorphous films of maltoheptaose equilibrated against nitrogen as a function of temperature. The data was calculated every 10°C from -10°C to 150°C...	217
Figure IV-8a-8g:	Intensity decay fit amplitudes for vanillin in amorphous films of glucose (8a), maltose (8b), maltotriose (8c), maltotetraose (8d), maltopentaose (8e), maltohexaose (8f) and maltoheptaose (8g) in nitrogen as a function of temperature. The data were calculated every 10°C from -10°C to 150°C. The amplitudes a_1 (◆) and a_2 (■) correspond to the longer life time components (τ_1 , τ_2), and a_3 (▲) and a_4 (●) correspond to the shorter lifetime components (τ_3 , τ_4). The amplitudes were obtained from a multi exponential model fit (Eq. (3), Materials and Methods) to phosphorescence intensity decay data from vanillin dispersed in amorphous films equilibrated against nitrogen as a function of temperature.....	218
Figure IV-9a:	Average lifetime from a multi-exponential model fit (Eq. (4), Materials and Methods) to phosphorescence intensity decay data from vanillin dispersed in amorphous films of glucose (◆), maltose (■), maltotriose (▲), maltotetraose (×), maltopentaose (*), maltohexaose (●) and maltoheptaose (+) equilibrated against nitrogen as a	222

	function of temperature. The data were calculated every 10°C from -10°C to 150°C.....	
Figure IV-9b:	Average lifetime from a multi-exponential model fit (Eq. (4), Materials and Methods) to phosphorescence intensity decay data from vanillin dispersed in amorphous films of glucose (♦), maltose (■), maltotriose (▲), maltotetraose (×), maltopentaose (*), maltohexaose (●) and maltoheptaose (+) equilibrated against nitrogen as a function of T-Tg. The data were calculated every 10°C from -10°C to 150°C.....	223
Figure IV-10a-10g:	Arrhenius plots of the inverse of individual lifetime component τ_1 , τ_2 , τ_3 and τ_4 of vanillin in amorphous films of glucose (10a), maltose (10b), maltotriose (10c), maltotetraose (10d), maltopentaose (10e), maltohexaose (10f) and maltoheptaose (10g) as a function of inverse of temperature.....	224
Figure IV-11a:	Arrhenius plot of the average lifetime of vanillin in amorphous films of glucose (♦), maltose (■), maltotriose (▲), maltotetraose (×), maltopentaose (*), maltohexaose (●) and maltoheptaose (+) as a function of inverse of temperature.....	228
Figure IV-11b:	Arrhenius plot of the average lifetime of vanillin in amorphous films of glucose (♦), maltose (■), maltotriose (▲), maltotetraose (×), maltopentaose (*), maltohexaose (●) and maltoheptaose (+) as a function of Tg/T.....	229
Figure IV-12:	Temperature dependence of the total non-radiative decay rate of the triplet state k_{NR} ($k_p = k_{RP} + k_{NR}$) to S_0 of vanillin in amorphous glucose, maltose, maltotriose, maltotetraose, maltopentaose, maltohexaose and maltoheptaose film over the temperature range from -10°C to 150°C, values were calculated from the lifetime data in Figures IV-7a to 7g and amplitude data in Figures IV-8a to 8g.....	230
Figure IV-13a:	Temperature dependence of the total non-radiative decay rate of the triplet state k_{NR} ($k_p = k_{RP} + k_{NR}$) to S_0 of vanillin in amorphous glucose, maltose, maltotriose, maltotetraose, maltopentaose, maltohexaose and maltoheptaose film plotted as a function of T-Tg; values were calculated from the lifetime data in Figure IV-7a to 7g.....	231
Figure IV-13b:	Temperature dependence of the total non-radiative decay rate of the triplet state k_{NR} ($k_p = k_{RP} + k_{NR}$) to S_0 of vanillin in amorphous glucose, maltose, maltotriose, maltotetraose, maltopentaose, maltohexaose and maltoheptaose film plotted as a function of T-Tg (expanded for below Tg).....	232
Figure IV-13c:	Temperature dependence of the total non-radiative decay	

	rate of the triplet state k_{NR} ($k_p = k_{RP} + k_{NR}$) to S_0 of vanillin in amorphous glucose, maltose, maltotriose, maltotetraose, maltopentaose, maltohexaose and maltoheptaose film plotted as a function of $T-T_g$ (expanded for above T_g).....	233
Figure IV-14a:	The Arrhenius plot of the total non-radiative decay rate of the triplet state k_{NR} ($k_p = k_{RP} + k_{NR}$) to S_0 of vanillin in amorphous glucose, maltose, maltotriose, maltotetraose, maltopentaose, maltohexaose and maltoheptaose film as function of inverse of temperature.....	234
Figure IV-14b:	The Arrhenius plot of the total non-radiative decay rate of the triplet state k_{NR} ($k_p = k_{RP} + k_{NR}$) to S_0 of vanillin in amorphous glucose, maltose, maltotriose, maltotetraose, maltopentaose, maltohexaose and maltoheptaose film as function of T_g/T	235
Figure V-1a:	Delayed emission spectra of vanillin dispersed in amorphous films of sucrose as a function of temperature (excitation at 320 nm). The spectra were collected at 10°C intervals from -10°C to 100°C (the curves follow this order from high to low intensity at ~490 nm).....	271
Figure V-1b:	Delayed emission spectra of vanillin dispersed in amorphous films of trehalose as a function of temperature (excitation at 320 nm). The spectra were collected at 10°C intervals from -10°C to 120°C (the curves follow this order from high to low intensity at ~490 nm).....	272
Figure V-1c:	Delayed emission spectra of vanillin dispersed in amorphous films of PVP as a function of temperature (excitation at 320 nm). The spectra were collected at 10°C intervals from -10°C to 100°C (the curves follow this order from high to low intensity at ~480 nm).....	273
Figure V-2:	Intensity (I_p) was determined from analysis of the phosphorescence emission band (Figure V-1a, 1b, 1c) using a log-normal function (eq. (1), Materials and Methods). The effect of temperature on the phosphorescence emission intensity of vanillin in amorphous films of sucrose, trehalose and PVP as a function of temperature equilibrated against nitrogen.....	274
Figure V-3:	Arrhenius plot of the effect of temperature on the phosphorescence emission intensity ($1/I_p$) of vanillin in amorphous films of sucrose, trehalose and PVP.....	275
Figure V-4a-4c:	Arrhenius plot of the effect of temperature on the phosphorescence emission intensity I_p of vanillin in amorphous films of sucrose, trehalose and PVP. Lines drawn over the data points indicate slopes at low and high temperatures sucrose, trehalose and PVP.....	276
Figure V-5a:	Peak energy ν_p and bandwidth for phosphorescence emission from vanillin in amorphous films of sucrose as a	278

	function of temperature. The delayed emission spectra collected as a function of temperature (Figure V-1a) were analyzed using log-normal function as described in Materials and Methods using eq. (1) and (2).....	
Figure V-5b:	Peak energy ν_p and bandwidth for phosphorescence emission from vanillin in amorphous films of trehalose as a function of temperature. The delayed emission spectra collected as a function of temperature (Figure V-1b) were analyzed using lognormal function as described in Materials and Methods using eq. (1) and (2).....	279
Figure V-5c:	Peak energy ν_p and bandwidth for phosphorescence emission from vanillin in amorphous films of PVP as a function of temperature. The delayed emission spectra collected as a function of temperature (Figure V-1c) were analyzed using lognormal function as described in Materials and Methods using eq. (1) and (2).....	280
Figure V-6a-6b:	Peak energy ν_p (6a) and bandwidth (6b) for phosphorescence emission from vanillin in amorphous films of sucrose (◆), trehalose (■) and PVP (▲) as a function of temperature.....	281
Figure V-7a-7c:	Normalized phosphorescence intensity decay $[I(t)/I(0)]$ of vanillin dispersed in amorphous films of sucrose (7a), trehalose (7b) and PVP (7c) at 20°C in the presence of nitrogen. The solid lines through the data are fits using a multi-exponential function (Eq. (3), Materials and Methods). A plot of modified residuals $[(Data-Fit)/Data^{1/2}]$ for these fits is shown in the bottom graph.....	282
Figure V-8a:	Lifetime components τ_1 (◆), τ_2 (■), τ_3 (▲) and τ_4 (●) obtained from a multi-exponential model fit (Eq. (3), Materials and Methods) to phosphorescence intensity decay data from vanillin dispersed in amorphous films of sucrose equilibrated against nitrogen as a function of temperature. The data were calculated every 10°C from -20°C to 100°C.....	284
Figure V-8b:	Lifetime components τ_1 (◆), τ_2 (■), τ_3 (▲) and τ_4 (●) obtained from a multi-exponential model fit (Eq. (3), Materials and Methods) to phosphorescence intensity decay data from vanillin dispersed in amorphous films of trehalose equilibrated against nitrogen as a function of temperature. The data were calculated every 10°C from -10°C to 120°C.....	285
Figure V-8c:	Lifetime components τ_1 (◆), τ_2 (■), τ_3 (▲) and τ_4 (●) obtained from a multi-exponential model fit (Eq. (3), Materials and Methods) to phosphorescence intensity decay data from vanillin dispersed in amorphous films of PVP equilibrated against nitrogen as a function of	

	temperature. The data were calculated every 10°C from -10°C to 120°C.....	286
Figure V-9a:	Intensity decay fit amplitudes for vanillin in amorphous films of sucrose in nitrogen as a function of temperature. The data were calculated every 10°C from -20°C to 100°C. The amplitudes a_1 (♦) and a_2 (■) correspond to the longer life time components (τ_1 , τ_2) and a_3 (▲) and a_4 (●) correspond to the shorter lifetime components (τ_3 , τ_4). The amplitudes were obtained from a multi exponential model fit (Eq. (3), Materials and Methods) to phosphorescence intensity decay data from vanillin dispersed in amorphous sucrose films equilibrated against nitrogen as a function of temperature.....	287
Figure V-9b:	Intensity decay fit amplitudes for vanillin in amorphous films of trehalose in nitrogen as a function of temperature. The data were calculated every 10°C from -10°C to 120°C. The amplitudes a_1 (♦) and a_2 (■) correspond to the longer life time components (τ_1 , τ_2) and a_3 (▲) and a_4 (●) correspond to the shorter lifetime components (τ_3 , τ_4). The amplitudes were obtained from a multi exponential model fit (Eq. (3), Materials and Methods) to phosphorescence intensity decay data from vanillin dispersed in amorphous trehalose films equilibrated against nitrogen as a function of temperature.....	288
Figure V-9c:	Intensity decay fit amplitudes for vanillin in amorphous films of PVP in nitrogen as a function of temperature. The data were calculated every 10°C from -10°C to 120°C. The amplitudes a_1 (♦) and a_2 (■) correspond to the longer life time components (τ_1 , τ_2) and a_3 (▲) and a_4 (●) correspond to the shorter lifetime components (τ_3 , τ_4). The amplitudes were obtained from a multi exponential model fit (Eq. (3), Materials and Methods) to phosphorescence intensity decay data from vanillin dispersed in amorphous PVP films equilibrated against nitrogen as a function of temperature.....	289
Figure V-10a-10b:	Comparison of intensity decay fit amplitudes (for longer ($a_1 + a_2$) and shorter ($a_3 + a_4$) lifetime components) for vanillin in amorphous films of sucrose, trehalose and PVP in nitrogen as a function of temperature.....	290
Figure V-11a:	The Arrhenius plot of the individual lifetime component τ_1 (♦), τ_2 (■), τ_3 (▲) and τ_4 (●) of vanillin in amorphous films of sucrose as a function of inverse of temperature.....	291
Figure V-11b:	The Arrhenius plot of the individual lifetime component τ_1 (♦), τ_2 (■), τ_3 (▲) and τ_4 (●) of vanillin in amorphous films of trehalose as a function of inverse of temperature.....	292

Figure V-11c:	The Arrhenius plot of the individual lifetime component τ_1 (♦), τ_2 (■), τ_3 (▲) and τ_4 (●) of vanillin in amorphous films of PVP as a function of inverse of temperature.....	293
Figure V-12a:	Average lifetime from a multi-exponential model fit (Eq. (4), Materials and Methods) to phosphorescence intensity decay data from vanillin dispersed in amorphous films of sucrose (♦), trehalose (■) and PVP (▲) equilibrated against nitrogen as a function of temperature.....	294
Figure V-12b:	Average lifetime from a multi-exponential model fit (Eq. (4), Materials and Methods) to phosphorescence intensity decay data from vanillin dispersed in amorphous films of sucrose (♦), trehalose (■) and PVP (▲) equilibrated against nitrogen as a function of T-Tg.....	295
Figure V-12c:	Arrhenius plot of the average lifetime of vanillin in amorphous films of sucrose (♦), trehalose (■) and PVP (▲) as a function of inverse temperature.....	296
Figure V-12d:	Arrhenius plot of the average lifetime of vanillin in amorphous films of sucrose (♦), trehalose (■) and PVP (▲) as a function of Tg/T.....	297
Figure V-13a:	Temperature dependence of the total non-radiative decay rate of the triplet state k_{NR} ($k_p = k_{RP} + k_{NR}$) to So of vanillin in amorphous sucrose, trehalose and PVP films.....	298
Figure V-13b-13c:	Temperature dependence of the total non-radiative decay rate of the triplet state k_{NR} ($k_p = k_{RP} + k_{NR}$) to So of vanillin in amorphous sucrose, trehalose and PVP films. The graph is showing details below 60°C (13b) and above 60°C (13c).....	299
Figure V-13d:	Temperature dependence of the total non-radiative decay rate of the triplet state k_{NR} ($k_p = k_{RP} + k_{NR}$) to So of vanillin in amorphous sucrose, trehalose and PVP film are plotted as a function of T-Tg.....	300
Figure V-14:	The Arrhenius plot of the total non-radiative decay rate of the triplet state k_{NR} ($k_p = k_{RP} + k_{NR}$) to So of vanillin in amorphous sucrose, trehalose and PVP films.....	301
Figure VIa-1:	Delayed emission spectra of erythrosin B dispersed in amorphous films of sucrose as a function of temperature (excitation at 500 nm). The spectra were collected at 10°C intervals from -20°C to 100°C (the curves follow this order from high to low intensity at ~690 nm).....	332
Figure VIa-2:	Intensity (I_p) was determined from analysis of the phosphorescence emission band (Figure VIa-1) using a log-normal function (eq. (1), Materials and Methods). The effect of temperature on the phosphorescence emission intensity of erythrosin B in amorphous films of sucrose as a function of temperature equilibrated against nitrogen.....	333
Figure VIa-3:	Plot of natural log of the intensity ratio between delayed	

fluorescence and phosphorescence in sucrose glass as a function of inverse temperature. $\Delta E_a = 33.29 \text{ KJ mol}^{-1}$ 334
 1

Figure VIa-4: Peak energy ν_p (◆) and bandwidth (■) for phosphorescence emission from erythrosin B in amorphous films of sucrose as a function of temperature. The delayed emission spectra collected as a function of temperature (Figure VIa-1) were analyzed using lognormal function as described in Materials and Methods using eq. (1) and (2)..... 335

Figure VIa-5: Normalized phosphorescence intensity decay $[I(t)/I(0)]$ of erythrosin B in dispersed in amorphous films of sucrose at 20°C in the presence of nitrogen. The solid line through the data is a fit using a stretch-exponential function (Eq. (3), Materials and Methods). A plot of modified residuals $[(\text{Data-Fit})/\text{Data}^{1/2}]$ for this fit is shown in the bottom graph..... 336

Figure VIa-6: Temperature dependent of lifetime τ (◆, left scale) and stretching exponent β (■, right scale) from fits to a stretched exponential model of the intensity decay of erythrosin B in amorphous sucrose films..... 337

Figure VIa-7: An Arrhenius plot of the lifetime τ of erythrosin B in amorphous films of sucrose as a function of inverse temperature. Lines drawn over the data points indicate slopes at low and high temperatures..... 338

Figure VIa-8: Temperature dependence of the total rate constant for non-radiative decay of the triplet state ($k = k_{RP} + k_{TS0} + k_{TS1}$, ◆), the rate of reverse intersystem crossing to S_1 (k_{TS1} , ■) and the rate of non-radiative decay to S_0 (k_{TS0} , ▲) of erythrosin B in amorphous sucrose over the temperature range from -20°C to 100°C: values were calculated from the lifetime data in Figure VIa-6..... 339

Figure VIb-1: Delayed emission spectra of tryptophan dispersed in amorphous films of sucrose as a function of temperature (excitation at 280 nm). The spectra were collected at 10°C intervals from -10°C to 80°C (the curves follow this order from high to low intensity at ~455 nm)..... 360

Figure VIb-2: Intensity (I_p) was determined from analysis of the phosphorescence emission band (Figure VIb- 1) using a log-normal three function (eq. (1), Materials and Methods). The effect of temperature on the phosphorescence emission intensity of tryptophan in amorphous films of sucrose as a function of temperature equilibrated against nitrogen. The spectra was fitted to a log-normal three function..... 361

Figure VIb-3: Peak energy ν_p (■) and bandwidth (▲) for phosphorescence emission from tryptophan in amorphous films of sucrose as a function of temperature. The delayed emission spectra

	collected as a function of temperature (Figure VIa-1) were analyzed using lognormal three function as described in Materials and Methods using eq. (1) and (2).....	362
Figure VIb-4a-4b:	Normalized phosphorescence intensity decay $[I(t)/I(0)]$ of tryptophan dispersed in amorphous films of sucrose at 20°C in the presence of nitrogen. The solid lines through the data are fits. A plot of modified residuals $[(\text{Data-Fit})/\text{Data}]^{1/2}$ for these fits is shown in the bottom graph. The decay was fitted using a multi-exponential function (3) and two stretch-exponential functions (5). The emissions were collected at 455 nm.....	363
Figure VIb-5a:	Lifetime components τ_1 (◆), τ_2 (■), τ_3 (▲) and τ_4 (●) obtained from a multi-exponential model fit to phosphorescence intensity decay data from tryptophan dispersed in amorphous films of sucrose equilibrated against nitrogen as a function of temperature. The data was calculated every 10°C from -10°C to 100°C.....	364
Figure VIb-5b:	The log plots of lifetime components τ_1 (◆), τ_2 (■), τ_3 (▲) and τ_4 (●) obtained from a multi-exponential model fit to phosphorescence intensity decay data from tryptophan dispersed in amorphous films of sucrose equilibrated against nitrogen as a function of temperature. The data was calculated every 10°C from -10°C to 100°C.....	365
Figure VIb-5c:	Lifetime components τ_1 (◆) and τ_2 (■) obtained from a two stretch exponential function to phosphorescence intensity decay data from tryptophan dispersed in amorphous films of sucrose equilibrated against nitrogen as a function of temperature. The data was calculated every 10°C from -10°C to 100°C.....	366
Figure VIb-5d:	The log plot of lifetime components τ_1 (◆) and τ_2 (■) obtained from a two stretch exponential function to phosphorescence intensity decay data from tryptophan dispersed in amorphous films of sucrose equilibrated against nitrogen as a function of temperature. The data was calculated every 10°C from -10°C to 100°C.....	367
Figure VIb-6a:	Intensity decay fit parameters amplitude for tryptophan in amorphous films of sucrose in nitrogen as a function of temperature. The data was calculated every 10°C from -10°C to 100°C. The amplitudes a_1 (◆) and a_2 (■) correspond to the longer life time components (τ_1 , τ_2) and a_3 (▲) and a_4 (●) correspond to the shorter lifetime components (τ_3 , τ_4).....	368
Figure VIb-6b:	Intensity decay fit amplitudes for stretched exponential fit to tryptophan in amorphous films of sucrose in nitrogen as a function of temperature. The data was calculated every	

	10°C from -10°C to 80°C. The amplitudes a_1 (♦) correspond to the longer life time components (τ_1) and a_2 (■) correspond to the shorter lifetime components (τ_2).....	369
Figure VIb-6c:	Temperature dependent of stretching exponent β_1 (♦) and β_2 (■) from fits to a stretched exponential model of the intensity decay of tryptophan in amorphous sucrose films corresponding to τ_1 (long lifetime) and τ_2 (short lifetime)...	370
Figure VIb-7a:	The Arrhenius plot of the inverse of individual lifetime component τ_1 and τ_2 of tryptophan in amorphous films of sucrose as a function of inverse temperature. The Arrhenius plot is for multi-exponential function.....	371
Figure VIb-7b:	The Arrhenius plot of the inverse of individual lifetime component τ_1 , τ_2 , τ_3 and τ_4 of tryptophan in amorphous films of sucrose as a function of inverse of temperature. The Arrhenius plot is for two stretched-exponential function.....	372
Figure VIb-8a:	Average Lifetime from a multi-exponential model fit to phosphorescence intensity decay data from tryptophan dispersed in amorphous films of sucrose equilibrated against nitrogen as a function of temperature. The data were calculated every 10°C from -10°C to 100°C.....	373
Figure VIb-8b:	Average Lifetime from a two stretched-exponential model fit to phosphorescence intensity decay data from tryptophan dispersed in amorphous films of sucrose equilibrated against nitrogen as a function of temperature. The data was calculated every 10°C from -10°C to 100°C.	374
Figure VIb-8c:	Comparison of average lifetime between multi and a two stretched-exponential model fit to phosphorescence intensity decay data from tryptophan dispersed in amorphous films of sucrose equilibrated against nitrogen as a function of temperature. The data was calculated every 10°C from -10°C to 100°C.....	375
Figure VIb-9a:	Temperature dependence of the total rate constant for decay of the triplet state ($k_P = k_{RP} + k_{TS0} + k_{TS1}$) calculated from multi (♦) and two stretched exponential function (■) of tryptophan in amorphous sucrose over the temperature range from -10°C to 100°C; values were calculated from the lifetime data in Figure 8a and 8b.....	376
Figure VIb-9b:	Temperature dependence of the rate of non-radiative decay to S_0 (k_{NR}) calculated from multi (♦) and two stretched exponential function (■) of tryptophan in amorphous sucrose over the temperature range from -10°C to 100°C...	377
Figure VIb-10a:	The Arrhenius plot of the rate of (k_P) calculated from multi (♦) and two stretched exponential function (■) of tryptophan in amorphous sucrose over the temperature	

	range from -10°C to 100°C.....	378
Figure VIb-10b:	The Arrhenius plot of the rate of non-radiative decay to S_0 (k_{NR}) calculated from multi (◆) and two stretched exponential function (■) of tryptophan in amorphous sucrose over the temperature range from -10°C to 100°C...	379
Figure VIc-1a:	Comparison of average lifetime of erythrosin B (single stretch exponential fit), vanillin (multi exponential fit) and tryptophan (multi exponential fit) dispersed in amorphous films of sucrose equilibrated against nitrogen as a function of temperature. The data was calculated every 10°C from -20°C to 100°C.....	391
Figure VIc-1b:	Comparison of average lifetime of erythrosin B (single stretch exponential fit) and tryptophan (multi exponential fit) dispersed in amorphous films of sucrose equilibrated against nitrogen as a function of temperature. The data was calculated every 10°C from -20°C to 100°C.....	392
Figure VIc-1c:	Comparison of average lifetime of erythrosin B (single stretch exponential fit) and vanillin (multi exponential fit) dispersed in amorphous films of sucrose equilibrated against nitrogen as a function of temperature. The data was calculated every 10°C from -20°C to 100°C.....	393
Figure VIc-1d:	Comparison of average lifetime of vanillin (multi exponential fit) and tryptophan (multi exponential fit) dispersed in amorphous films of sucrose equilibrated against nitrogen as a function of temperature. The data was calculated every 10°C from -20°C to 100°C.....	394
Figure VIc-1e:	Comparison of log of average lifetime of vanillin (multi exponential fit), erythrosin B (stretch exponential fit) and tryptophan (multi exponential fit) dispersed in amorphous films of sucrose equilibrated against nitrogen as a function of temperature. The data was calculated every 10°C from -20°C to 100°C.....	395
Figure VIc-2:	Comparison of temperature dependent of stretching exponent for tryptophan decay (β_1 (◆) and β_2 (■)) and erythrosin B decay (β (▲)) from fits to a stretched exponential model of the intensity decay in amorphous sucrose films.....	396
Figure VIc-3:	Comparison of intensity decay fit parameters amplitude for tryptophan and vanillin in amorphous films of sucrose in nitrogen as a function of temperature. The data was calculated every 10°C from -20°C to 100°C. In case of tryptophan the amplitudes T1 (◆), T2 (■) and T3 (▲) correspond to the longer life time components (τ_1 , τ_2 , τ_3) and T4 (*) correspond to the shorter lifetime components (τ_4). In case of vanillin the amplitudes V1 (*), V2 (●)	

	correspond to the longer life time components (τ_1 , τ_2), V3 (+) and V4 (-) correspond to the shorter lifetime components (τ_3 , τ_4).....	397
Figure VIc-4a-4b:	Comparison of sum of amplitude for longer lifetime components (4a) and shorter lifetime components (4b) for tryptophan and vanillin in amorphous films of sucrose in nitrogen as a function of temperature. The data was calculated every 10°C from -20°C to 100°C.....	398
Figure VIc-5a:	Temperature dependence of the total rate constant for decay of the triplet state ($k_P = k_{RP} + k_{TS0} + k_{TS1}$) for erythrosin B, vanillin and tryptophan in amorphous sucrose over the temperature range from -20°C to 100°C; values were calculated from the lifetime data.....	399
Figure VIc-5b:	Temperature dependence of the rate of non-radiative decay to S_0 (k_{NR}) calculated for erythrosin B, vanillin and tryptophan in amorphous sucrose over the temperature range from -20°C to 100°C.....	400
Figure VIc-6a:	The Arrhenius plot of the rate of (k_P) calculated for erythrosin B, vanillin and tryptophan in amorphous sucrose over the temperature range from -20°C to 100°C.....	401
Figure VIc-6b:	The Arrhenius plot of the rate of non-radiative decay to S_0 (k_{NR}) for erythrosin B, vanillin and tryptophan in amorphous sucrose over the temperature range from -20°C to 100°C.....	402
Figure VII-1	Structure of Bovine α -lactalbumin.....	407
Figure VII-2:	Dynamic transitions in Proteins.....	410
Figure VIIa-1:	Delayed emission spectra of erythrosin B in amorphous α -lactalbumin films as a function of temperature (excitation at 500 nm). The spectra were collected at 10°C intervals from -20 to 120°C (the curves follow this order from high to low intensity at ~690nm).....	449
Figure VIIa-2:	Peak energy ν_p (♦, left hand scale) and bandwidth (■, right hand scale) for phosphorescence emission from erythrosin B in α -lactalbumin films as a function of temperature. The delayed emission spectra collected as a function of temperature (Figure VIIa-1) were analyzed using a log-normal function as described in Materials and Methods.....	450
Figure VIIa-3:	(a) Normalized phosphorescence intensity decay [$I(t)/I(0)$] of erythrosin B dispersed in amorphous α -lactalbumin film at 20°C in the presence of nitrogen (♦) and air (■). The solid lines through the data are fits using a stretched exponential function with following parameters $\tau = 0.475$ ms and $\beta = 0.806$ for data in nitrogen and $\tau = 0.356$ ms and $\beta = 0.806$ for data in air. (b) The modified residuals	

	$[(\text{Data-Fit})/\text{Data}]^{1/2}$ for these fits to data in the presence of nitrogen (dotted line) and air (solid line).....	451
Figure VII-4a:	Lifetime τ (a) from a stretched exponential model fit to phosphorescence intensity decay data from erythrosin B in α -lactalbumin films equilibrated against nitrogen (\blacklozenge) and air (\blacksquare).....	452
Figure VIIa-4b:	Stretched exponential model fit to phosphorescence intensity decay data from erythrosin B in α -lactalbumin films equilibrated against nitrogen (\blacklozenge) and air (\blacksquare).....	453
Figure VIIa-5a:	The effect of temperature on the triplet state de-excitation rates for collisional quenching k_{TS0} (\blacksquare) and oxygen quenching $k_{\text{Q}} [\text{O}_2]$ (\blacklozenge).....	454
Figure VIIa-5b:	Arrhenius plot for the rates of collisional quenching k_{TS0} (\blacksquare) and oxygen quenching $k_{\text{Q}} [\text{O}_2]$ (\blacklozenge). Rates calculated from the lifetime data in Figure VIIa-4a.....	455
Figure VIIa-6:	Dependence of $k_{\text{Q}} [\text{O}_2]$ on k_{TS0}	456
Figure VIIa-7a:	Lifetime from a stretched exponential model fit to phosphorescence intensity decay data from erythrosin B in amorphous α -lactalbumin films collected as a function of emission wavelength (with excitation at 540 nm) and excitation wavelength (with emission at 690 nm). Data collected at 20°C intervals from -20°C to 120°C in presence of nitrogen.....	457
Figure VIIa-7b:	Stretching exponents from a stretched exponential model fit to phosphorescence intensity decay data from erythrosin B in amorphous α -lactalbumin films collected as a function of emission wavelength (with excitation at 540 nm) and excitation wavelength (with emission at 690 nm). Data collected at 20°C intervals from -20°C to 120°C in presence of nitrogen.....	458
Figure VIIa-8a:	Lifetime from a stretched exponential model fit to phosphorescence intensity decay data from erythrosin B in amorphous α -lactalbumin films collected as a function of emission wavelength (with excitation at 540 nm) and excitation wavelength (with emission at 690 nm). Data collected at 20°C intervals from -20°C to 120°C in presence of oxygen.....	459
Figure VIIa-8b:	Stretching exponents from a stretched exponential model fit to phosphorescence intensity decay data from erythrosin B in amorphous α -lactalbumin films collected as a function of emission wavelength (with excitation at 540 nm) and excitation wavelength (with emission at 690 nm). Data collected at 20°C intervals from -20°C to 120°C in	

	presence of oxygen.....	460
Figure VIIa-9a:	Comparison of lifetime in presence and absence of oxygen from a stretched exponential model fit to phosphorescence intensity decay data from erythrosin B in amorphous α -lactalbumin films collected as a function of emission wavelength (with excitation at 540 nm) and excitation wavelength (with emission at 690 nm). Data collected at 20°C intervals from -20°C to 120°C.....	461
Figure VIIa-9b:	Comparison of stretching exponents in presence and absence of oxygen from a stretched exponential model fit to phosphorescence intensity decay data from erythrosin B in amorphous α -lactalbumin films collected as a function of emission wavelength (with excitation at 540 nm) and excitation wavelength (with emission at 690 nm). Data collected at 20°C intervals from -20°C to 100°C.....	462
Figure VIIa-10a:	The temperature dependence for the rate for oxygen quenching $k_Q[O_2]$ in amorphous α -lactalbumin films collected as a function of emission wavelength (with excitation at 540 nm) and excitation wavelength (with emission at 690 nm). Data was calculated from the lifetime data in Figures 7a and 8a, data at -20°C (◆), 0°C (▲), 20°C (*), 40°C (■), 60°C (◐) and 80°C (-).....	463
Figure VIIa-10b:	Activation energies for collisional quenching k_{TS0} at low temperature (◆ from -20°C to 20°C) and high temperature (■ from 40°C to 120°C) and the oxygen quenching $k_Q[O_2]$ (▲) calculated from the lifetime data in Figure 7a and 8a, as a function of emission wavelength (with excitation at 540 nm) and excitation wavelength (with emission at 690 nm). The activation energies were obtained from slopes Arrhenius plots of k_{TS0} and $k_Q[O_2]$	464
Figure VIIa-11:	Effect of delay time on the peak frequency of the phosphorescence emission spectra of erythrosin B dispersed in amorphous α -lactalbumin film at -20°C (◆), 0°C (■), 20°C (▲), 40°C (●), 60°C (▲) and 80°C (●) determined from time resolved emission spectra; peak frequency was calculated from analysis of emission spectra using a log-normal function.....	465
Figure VIIa-12:	Effect of delay time on the bandwidth of the phosphorescence emission spectra of erythrosin B dispersed in amorphous α -lactalbumin film at -20°C (◆), 0°C (■), 20°C (▲), 40°C (●), 60°C (▲) and 80°C (●) determined from time resolved emission spectra; peak frequency was calculated from analysis of emission spectra using a log-normal function.....	466
Figure VIIb-1:	Delayed emission spectra of tryptophan in amorphous α -lactalbumin films as a function of temperature (excitation	

	at 280 nm). The spectra were collected at 10°C intervals from -20°C to 60°C (the curves follow this order from high to low intensity at ~450 nm).....	493
Figure VIIb-2a:	The effect of temperature on the phosphorescence emission intensity of tryptophan in amorphous α -lactalbumin films as a function of temperature equilibrated against nitrogen. Intensity (I_p) was determined from analysis of the phosphorescence emission band (Figure VIIb-2) using a log-normal function (eq. (1), Materials and Methods). The intensity was normalized to -10°C.....	494
Figure VIIb-2b:	The effect of temperature on the phosphorescence emission intensity of tryptophan in amorphous α -lactalbumin films as a function of temperature equilibrated against nitrogen. Intensity (I_p) was determined from analysis of the phosphorescence emission band (Figure VIIb-2) using a log-normal function (eq. (1), Materials and Methods).....	495
Figure VIIb-3a:	Peak energy ν_p (♦, left hand scale) and bandwidth (■, right hand scale) for phosphorescence emission from tryptophan in α -lactalbumin films as a function of temperature.....	496
Figure VIIb-3b:	Peak energy ν_p (♦, left hand scale) and bandwidth (■, right hand scale) for phosphorescence emission from tryptophan in α -lactalbumin films as a function of temperature.....	497
Figure VIIb-4:	(a) Normalized phosphorescence intensity decay [$I(t)/I(0)$] of tryptophan in amorphous α -lactalbumin film at 20°C in the presence of nitrogen (♦). The solid lines through the data are fits using a multi-exponential function. (b) The modified residuals [(Data-Fit)/Data ^{1/2}] for these fits to data in the presence of nitrogen (dotted line).....	498
Figure VIIb-5a:	Lifetime components τ_1 (♦), τ_2 (■), τ_3 (▲), τ_4 (●) obtained from a multi-exponential model fit (Eq. (3), Materials and Methods) to phosphorescence intensity decay data from tryptophan in amorphous α -lactalbumin films equilibrated against nitrogen as a function of temperature. The data was calculated every 10°C from -20°C to 100°C..	499
Figure VIIb-5b:	Log plot of lifetime components τ_1 (♦), τ_2 (■), τ_3 (▲), τ_4 (●) obtained from a multi-exponential model fit (Eq. (3), Materials and Methods) to phosphorescence intensity decay data from tryptophan in amorphous α -lactalbumin films equilibrated against nitrogen as a function of temperature. The data was calculated every 10°C from -20°C to 100°C.....	500
Figure VIIb-6:	Intensity decay fit parameters amplitude for tryptophan in amorphous α -lactalbumin films in nitrogen as a function of temperature. The data was calculated every 10°C from -	

	20°C to 100°C. The amplitudes a_1 (◆) and a_2 (■) correspond to the longer life time components (τ_1 , τ_2) and a_3 (▲) and a_{14} (●) correspond to the shorter lifetime components (τ_3 , τ_4). The amplitudes were obtained from a multi exponential model fit (Eq. (3), Materials and Methods) to phosphorescence intensity decay data from tryptophan in amorphous α -lactalbumin films equilibrated against nitrogen as a function of temperature...	501
Figure VIIb-7:	Average lifetime from a multi-exponential model fit (Eq. (4), Materials and Methods) to phosphorescence intensity decay data from tryptophan in amorphous α -lactalbumin films equilibrated against nitrogen as a function of temperature. The data was calculated every 10°C from -20°C to 100°C.....	502
Figure VIIb-8a:	The Arrhenius plot of the individual lifetime component τ_1 (◆), τ_2 (■), τ_3 (▲) and τ_4 (●) of tryptophan in amorphous α -lactalbumin as a function of inverse of temperature.....	503
Figure VIIb-8b:	The Arrhenius plot of the average lifetime of tryptophan in amorphous α -lactalbumin as a function of inverse of temperature.....	504
Figure VIIb-9:	Temperature dependence of the total non-radiative decay rate of the triplet state k_{NR} ($k_p = k_{RP} + k_{NR}$) to So of tryptophan in amorphous α -lactalbumin film over the temperature range from -20°C to 100°C, values were calculated from the lifetime data.....	505
Figure VIIb-10:	The Arrhenius plot of the total non-radiative decay rate of the triplet state k_{NR} ($k_p = k_{RP} + k_{NR}$) to So of tryptophan in amorphous α -lactalbumin film as function of inverse of temperature.....	506
Figure VIIb-11:	The structure of α -lactalbumin showing positions of tryptophan residues (Pymol)	507
Figure VIIb-12:	The surface accessible area of tryptophan residues (Pymol).	508
Figure VIIb-13:	The distance calculation between tryptophan residues and disulphide bond (Pymol).	509
Figure VIIc-1:	Delayed emission spectra of vanillin in amorphous α -lactalbumin films as a function of temperature (excitation at 320 nm). The spectra were collected at 10°C intervals from -20°C to 100°C (the curves follow this order from high to low intensity at ~490 nm).	529
Figure VIIc-2:	The effect of temperature on the phosphorescence emission intensity of vanillin in amorphous α -lactalbumin films as a function of temperature equilibrated against nitrogen. Intensity (I_P) was determined from analysis of the	

	phosphorescence emission band (Figure VIIc-1) using a log-normal function (eq. (1), Materials and Methods). The data was normalized to -20°C.	530
Figure VIIc-3:	Peak energy ν_p (◆, left hand scale) and bandwidth (■, right hand scale) for phosphorescence emission from vanillin in α -lactalbumin films as a function of temperature.	531
Figure VIIc-4:	(a) Normalized phosphorescence intensity decay $[I(t)/I(0)]$ of vanillin dispersed in amorphous α -lactalbumin film at 20°C in the presence of nitrogen (◆). The solid lines through the data are fits using a multi-exponential function. (b) The modified residuals $[(Data-Fit)/Data^{1/2}]$ for these fits to data in the presence of nitrogen (dotted line).	532
Figure VIIc-5a:	Lifetime components τ_1 (◆), τ_2 (■), τ_3 (▲), τ_4 (●) obtained from a multi-exponential model fit (Eq. (3), Materials and Methods) to phosphorescence intensity decay data from vanillin dispersed in amorphous α -lactalbumin films equilibrated against nitrogen as a function of temperature. The data was calculated every 10°C from -20°C to 100°C...	533
Figure VIIc-5b:	The log plot of lifetime components τ_1 (◆), τ_2 (■), τ_3 (▲), τ_4 (●) obtained from a multi-exponential model fit (Eq. (3), Materials and Methods) to phosphorescence intensity decay data from vanillin dispersed in amorphous α -lactalbumin films equilibrated against nitrogen as a function of temperature. The data was calculated every 10°C from -20°C to 100°C.	534
Figure VIIc-6:	Intensity decay fit parameters amplitude for vanillin in amorphous α -lactalbumin films in nitrogen as a function of temperature. The data was calculated every 10°C from -20°C to 100°C. The amplitudes a_1 (◆) and a_2 (■) correspond to the longer life time components (τ_1 , τ_2) and a_3 (▲) and a_{14} (●) correspond to the shorter lifetime components (τ_3 , τ_4). The amplitudes were obtained from a multi exponential model fit (Eq. (3), Materials and Methods) to phosphorescence intensity decay data from vanillin dispersed in amorphous α -lactalbumin films equilibrated against nitrogen as a function of temperature...	535
Figure VIIc-7:	Average lifetime from a multi-exponential model fit (Eq. (4), Materials and Methods) to phosphorescence intensity decay data from vanillin dispersed in amorphous α -lactalbumin films equilibrated against nitrogen as a function of temperature. The data was calculated every 10°C from -20°C to 100°C.	536
Figure VIIc-8a:	The Arrhenius plot of the individual lifetime component τ_1 (◆), τ_2 (■), τ_3 (▲) and τ_4 (●) of vanillin in amorphous α -lactalbumin as a function of inverse of temperature.	537

Figure VIIc-8b:	The Arrhenius plot of the average lifetime of vanillin in amorphous α -lactalbumin as a function of inverse of temperature.....	538
Figure VIIc-9:	Temperature dependence of the total non-radiative decay rate of the triplet state k_{NR} ($k_p = k_{RP} + k_{NR}$) to So of vanillin in amorphous α -lactalbumin film over the temperature range from -20°C to 100°C, values were calculated from the lifetime data.	539
Figure VIIcb-10:	The Arrhenius plot of the total non-radiative decay rate of the triplet state k_{NR} ($k_p = k_{RP} + k_{NR}$) to So of vanillin in amorphous α -lactalbumin film as function of inverse of temperature.	540
Figure VIId-1a:	Comparison of average lifetime of erythrosin B (single stretch exponential fit), vanillin (multi exponential fit) and tryptophan (multi exponential fit) dispersed in amorphous films of α -lactalbumin equilibrated against nitrogen as a function of temperature. The data was calculated every 10°C from -20°C to 100°C.	547
Figure VIId-1b:	Comparison of log plot of average lifetime of erythrosin B (single stretch exponential fit), vanillin (multi exponential fit) and tryptophan (multi exponential fit) dispersed in amorphous films of α -lactalbumin equilibrated against nitrogen as a function of temperature. The data was calculated every 10°C from -20°C to 100°C.....	548
Figure VIId-2a:	Comparison of k_p of erythrosin B, vanillin and tryptophan in amorphous films of α -lactalbumin equilibrated against nitrogen as a function of temperature.	549
Figure VIId-2b:	Comparison of $\ln(k_p)$ of erythrosin B, vanillin and tryptophan in amorphous films of α -lactalbumin equilibrated against nitrogen as a function of temperature.	550
Figure VIId-3a:	Comparison of k_{NR} of average lifetime of erythrosin B (single stretch exponential fit), vanillin (multi exponential fit) and tryptophan (multi exponential fit) dispersed in amorphous films of α -lactalbumin equilibrated against nitrogen as a function of temperature. The data was calculated every 10°C from -20°C to 100°C.	551
Figure VIId-3b:	Comparison of Arrhenius plot of $\ln k_{NR}$ for erythrosin B, vanillin and tryptophan in amorphous films of α -lactalbumin equilibrated against nitrogen as a function of temperature.	552
Figure VIII-1a:	Delayed emission spectra of erythrosin B dispersed in amorphous films of sucrose (referred as ES matrix) as a function of temperature (excitation at 500 nm). The spectra	

	were collected at 10°C intervals from -20°C to 100°C (the curves follow this order from high to low intensity at ~690 nm).	583
Figure VIII-1b:	Delayed emission spectra of erythrosin B dispersed in amorphous films of sucrose also containing vanillin (referred as EVS matrix) as a function of temperature (excitation at 500 nm). The spectra were collected at 10°C intervals from -20°C to 100°C (the curves follow this order from high to low intensity at ~690 nm).	584
Figure VIII-2:	Peak energy ν_p (left hand scale) and bandwidth FWHM (right hand scale) for phosphorescence emission from erythrosin B in amorphous EVS and ES films as a function of temperature. The spectra were collected every 10°C from -20 to 100°C. The frequency is given by in (Δ) EVS matrix and by (\blacktriangle) in ES matrix. The FWHM is given by (\diamond) in EVS matrix and by (\blacklozenge) in ES matrix.	585
Figure VIII-3:	Normalized phosphorescence intensity decay $[I(t)/I(0)]$ of Ery B dispersed in amorphous EVS films at 20°C in the presence of nitrogen. The solid lines through the data are fits using a stretched-exponential function. Below is the plot of modified residuals $[(Data-Fit)/Data^{1/2}]$ for these fits to data plotted in the presence of nitrogen.	586
Figure VIII 4a-4b:	Intensity decay fit parameters for erythrosin B in amorphous sucrose film ES (\blacksquare) and EVS (\blacklozenge). The values were measured every 10°C from -20°C to 100°C. The measurements were made in the absence of oxygen. (a) Stretched exponential lifetimes in nitrogen as a function of temperature. (b) Stretched exponential fitting parameter β as a function of temperature.	587
Figure VIII-5a:	Delayed emission spectra of vanillin in amorphous sucrose films (referred as VS) as a function of temperature (excitation at 320 nm). The spectra were collected at 10°C intervals from -20°C to 100°C (the curves follow this order from high to low intensity at ~490 nm).	588
Figure VIII-5b:	Delayed emission spectra of vanillin in amorphous sucrose films also containing erythrosin B (referred as EVS) as a function of temperature (excitation at 320 nm). The spectra were collected at 10°C intervals from -20°C to 100°C (the curves follow this order from high to low intensity at ~490 nm).	589
Figure VIII-6:	Peak energy ν_p (left hand scale) and bandwidth FWHM (right hand scale) for phosphorescence emission from vanillin in amorphous EVS and VS films as a function of temperature. The spectra were collected every 10°C from -20 to 100°C. The frequency is given by in (Δ) EVS matrix	

	and by (▲) in VS matrix. The FWHM is given by (◇) in EVS matrix and by (◆) in VS matrix.	590
Figure VIII-7:	Normalized phosphorescence intensity decay $[I(t)/I(0)]$ of methyl vanillin dispersed in amorphous EVS films at 20°C in the presence of nitrogen. The solid lines through the data are fits using a multi-exponential function. Below is the plot of modified residuals $[(Data-Fit)/Data^{1/2}]$ for these fits to data plotted in the presence of nitrogen.	591
Figure VIII-8a:	Lifetime components τ_1 (◆), τ_2 (■), τ_3 (▲) and τ_4 (●) obtained from a multi-exponential model fit (Eq. (8), Materials and Methods) to phosphorescence intensity decay data from vanillin dispersed in amorphous EVS films equilibrated against nitrogen as a function of temperature. The data was calculated every 10°C from -20°C to 100°C.	592
Figure VIII-8b:	Comparison of longer lifetime components τ_1 (◆) and τ_2 (■) obtained from a multi-exponential model fit (Eq. (8), Materials and Methods) to phosphorescence intensity decay data from vanillin dispersed in amorphous EVS or VS films equilibrated against nitrogen as a function of temperature. The data was calculated every 10°C from -20°C to 100°C.	593
Figure VIII-8c:	Comparison of shorter lifetime components τ_1 (◆) and τ_2 (■) obtained from a multi-exponential model fit (Eq. (8), Materials and Methods) to phosphorescence intensity decay data from vanillin dispersed in amorphous EVS or VS films equilibrated against nitrogen as a function of temperature. The data was calculated every 10°C from -20°C to 100°C.	594
Figure VIII-9:	The average lifetime of vanillin in EVS (◆) and VS (■) films obtained from a multi-exponential model fit equilibrated against nitrogen as a function of temperature. The data were collected every 10°C from -20°C to 100°C..	595
Figure VIII-10:	Intensity decay fit parameters amplitude for vanillin in amorphous EVS film in nitrogen as a function of temperature. The data was calculated every 10°C from -20°C to 90°C. The amplitudes a_1 (◆) and a_2 (■) correspond to the longer life time components (τ_1 , τ_2) and a_3 (▲) and a_4 (●) correspond to the shorter lifetime components (τ_3 , τ_4). The amplitudes were obtained from a multi exponential model fit (Eq. (8), Materials and Methods) to phosphorescence intensity decay data from vanillin dispersed in amorphous sucrose films equilibrated against nitrogen as a function of temperature...	596
Figure VIII-10a-d:	Comparison of intensity decay fit amplitudes for vanillin in	

	amorphous EVS and VS film in nitrogen as a function of temperature.	597
Figure VIII-11:	The Arrhenius plot of natural log of k_p for average lifetime as function of inverse of temperature for vanillin and erythrosin B dispersed in EVS films.	599
Figure VIII-12a-b:	Comparing the Ratio A and Ratio B corresponding to phosphorescence and delayed fluorescence of erythrosin B, respectively, as a function of temperature in absence of oxygen.	600
Figure VIII-13:	Comparing the delayed fluorescence lifetime of erythrosin B in EVS (♦) and ES (■) films. The values were measured every 10°C from -20°C to 100°C. The measurements were made in the absence of oxygen.	601
Figure IX-1a:	Delayed emission spectra of erythrosin B dispersed in amorphous films of sucrose (referred as ES matrix) as a function of temperature (excitation at 500 nm). The spectra were collected at 10°C intervals from -10°C to 100°C (the curves follow this order from high to low intensity at ~690 nm).	627
Figure IX-1b:	Delayed emission spectra of erythrosin B dispersed in amorphous films of sucrose also containing tryptophan (referred as TES matrix) as a function of temperature (excitation at 500 nm). The spectra were collected at 10°C intervals from -10°C to 100°C (the curves follow this order from high to low intensity at ~690 nm).	628
Figure IX-2:	Peak energy ν_p (left hand scale) and bandwidth FWHM (right hand scale) for phosphorescence emission from erythrosin B in amorphous TES and ES films as a function of temperature. The spectra were collected every 10°C from -10°C to 100°C. The frequency is given by in (Δ) TES matrix and by (▲) in ES matrix. The FWHM is given by (◇) in TES matrix and by (◆) in ES matrix.	629
Figure IX-3:	Normalized phosphorescence intensity decay $[I(t)/I(0)]$ of erythrosin B dispersed in amorphous TES films at 20°C in the presence of nitrogen. The solid lines through the data are fits using a stretched-exponential function. Below is the plot of modified residuals $[(Data-Fit)/Data^{1/2}]$ for these fits to data plotted in the presence of nitrogen.	630
Figure IX 4a-4b:	Intensity decay fit parameters for erythrosin B in amorphous sucrose film ES and TES. The values were measured every 10°C from -10°C to 100°C. The measurements were made in the absence of oxygen. (a) Stretched exponential lifetimes in nitrogen as a function of temperature. (b) Stretched exponential fitting parameter β as a function of temperature.	631

Figure IX-5a:	Delayed emission spectra of tryptophan dispersed in amorphous films of sucrose (referred as TS) as a function of temperature (excitation at 280 nm). The spectra were collected at 10°C intervals from -10°C to 80°C (the curves follow this order from high to low intensity at ~455 nm).	632
Figure IX-5b:	Delayed emission spectra of tryptophan dispersed in amorphous films of sucrose also containing erythrosin B (referred as TES matrix) as a function of temperature (excitation at 280 nm). The spectra were collected at 10°C intervals from -0°C to 70°C (the curves follow this order from high to low intensity at ~455 nm).....	633
Figure IX-6a-6b:	Peak energy ν_p (6a) and bandwidth (6b) for phosphorescence emission from tryptophan in amorphous films of TS and TES as a function of temperature. The delayed emission spectra collected as a function of temperature (Figure 5a and 5b) were analyzed using lognormal functions as described in Materials and Methods using eq. (1) and (2).	634
Figure IX-7:	Normalized phosphorescence intensity decay $[I(t)/I(0)]$ of tryptophan dispersed in amorphous TES films at 20°C in the presence of nitrogen. The solid lines through the data are fits using a multi-exponential function. Below is the plot of modified residuals $[(Data-Fit)/Data^{1/2}]$ for these fits to data plotted in the presence of nitrogen.....	635
Figure IX-8a:	Lifetime components τ_1 (◆), τ_2 (■), τ_3 (▲) and τ_4 (●) obtained from a multi-exponential model fit to phosphorescence intensity decay data from tryptophan dispersed in amorphous films of TES equilibrated against nitrogen as a function of temperature. The data was calculated every 10°C from -10°C to 100°C.....	636
Figure IX-8b:	Comparison of longer lifetime components τ_1 (◆) and τ_2 (■) obtained from a multi-exponential model fit (Eq. (3), Materials and Methods) to phosphorescence intensity decay data from tryptophan dispersed in amorphous TES or TS films equilibrated against nitrogen as a function of temperature. The data was calculated every 10°C from -10°C to 100°C.	637
Figure IX-8c:	Comparison of shorter lifetime components τ_1 (◆) and τ_2 (■) obtained from a multi-exponential model fit (Eq. (3), Materials and Methods) to phosphorescence intensity decay data from tryptophan dispersed in amorphous TES or TS films equilibrated against nitrogen as a function of temperature. The data was calculated every 10°C from -10°C to 100°C.	638
Figure IX-9:	The average lifetime of tryptophan in TES and TS films obtained from a multi-exponential model fit equilibrated	

	against nitrogen as a function of temperature. The data were collected every 10°C from -10°C to 100°C.....	639
Figure IX-10:	Intensity decay fit parameters amplitude for tryptophan in amorphous TES film in nitrogen as a function of temperature. The data was calculated every 10°C from -10°C to 100°C. The amplitudes a_1 (♦) and a_2 (■) correspond to the longer life time components (τ_1 , τ_2) and a_3 (▲) and a_4 (●) correspond to the shorter lifetime components (τ_3 , τ_4). The amplitudes were obtained from a multi exponential model fit (Eq. (3), Materials and Methods) to phosphorescence intensity decay data from tryptophan dispersed in TES films equilibrated against nitrogen as a function of temperature.	640
Figure IX-10a-10d:	Comparing the intensity decay fit amplitudes for tryptophan in amorphous TES and TS film in nitrogen as a function of temperature.	641
Figure IX-11:	The Arrhenius plot of natural log of k_p for average lifetime as function of inverse of temperature for tryptophan and erythrosin B dispersed in TES films.	643
Figure X-1a:	Delayed emission spectra of vanillin dispersed in amorphous films of sucrose (referred as VS matrix) as a function of temperature (excitation at 320 nm). The spectra were collected at 10°C intervals from -10°C to 100°C (the curves follow this order from high to low intensity at ~490 nm).	663
Figure X-1b:	Delayed emission spectra of vanillin dispersed in amorphous films of sucrose containing tryptophan (referred as TVS matrix) as a function of temperature (excitation at 320 nm). The spectra were collected at 10°C intervals from 0°C to 100°C (the curves follow this order from high to low intensity at ~490 nm).	664
Figure X-2:	Peak energy ν_p (left hand scale) and bandwidth FWHM (right hand scale) for phosphorescence emission from vanillin in amorphous TVS and VS films as a function of temperature. The spectra were collected every 10°C from -10°C to 100°C. The frequency is given by in (Δ) TVES matrix and by (▲) in VS matrix. The FWHM is given by (◇) in TVS matrix and by (◆) in VS matrix.....	665
Figure X-3:	Normalized phosphorescence intensity decay $[I(t)/I(0)]$ of vanillin dispersed in amorphous TVS films at 20°C in the presence of nitrogen. The solid lines through the data are fits using a stretched-exponential function. Below is the plot of modified residuals $[(Data-Fit)/Data^{1/2}]$ for these fits to data plotted in the presence of nitrogen.	666
Figure X-4a:	Lifetime components τ_1 (♦), τ_2 (■), τ_3 (▲) and τ_4 (●)	667

	obtained from a multi-exponential model fit to phosphorescence intensity decay data from vanillin dispersed in amorphous films of TVS equilibrated against nitrogen as a function of temperature. The data was calculated every 10°C from -10°C to 100°C.....	
Figure X-4b:	Comparison of longer lifetime components τ_1 (♦) and τ_2 (■) obtained from a multi-exponential model fit (Eq. (3), Materials and Methods) to phosphorescence intensity decay data from vanillin dispersed in amorphous TVS or VS films equilibrated against nitrogen as a function of temperature. The data was calculated every 10°C from -10°C to 100°C.	668
Figure X-4c:	Comparison of shorter lifetime components τ_1 (♦) and τ_2 (■) obtained from a multi-exponential model fit (Eq. (3), Materials and Methods) to phosphorescence intensity decay data from vanillin dispersed in amorphous TVS or VS films equilibrated against nitrogen as a function of temperature. The data was calculated every 10°C from -10°C to 100°C.	669
Figure X-5:	The average lifetime of vanillin in TVS (■) and VS (♦) films obtained from a multi-exponential model fit equilibrated against nitrogen as a function of temperature. The data were collected every 10°C from -10°C to 100°C...	670
Figure X-6:	Intensity decay fit parameters amplitude for vanillin in amorphous TVS film in nitrogen as a function of temperature. The data was calculated every 10°C from -10°C to 100°C. The amplitudes a_1 (♦) and a_2 (■) correspond to the longer life time components (τ_1 , τ_2) and a_3 (▲) and a_4 (●) correspond to the shorter lifetime components (τ_3 , τ_4). The amplitudes were obtained from a multi exponential model fit (Eq. (3), Materials and Methods) to phosphorescence intensity decay data from vanillin dispersed in TVS films equilibrated against nitrogen as a function of temperature.	671
Figure X-7a:	Delayed emission spectra of tryptophan dispersed in amorphous films of sucrose (referred as TS) as a function of temperature (excitation at 280 nm). The spectra were collected at 10°C intervals from -10°C to 80°C (the curves follow this order from high to low intensity at ~455 nm)....	672
Figure X-7b:	Delayed emission spectra of tryptophan dispersed in amorphous films of sucrose also containing vanillin (referred as TVS) as a function of temperature (excitation at 280 nm). The spectra were collected at 10°C intervals from 0°C to 100°C (the curves follow this order from high to low intensity at ~455 nm).	673

Figure X-8:	Normalized phosphorescence intensity decay $[I(t)/I(0)]$ of tryptophan dispersed in amorphous TVS films at 20°C in the presence of nitrogen. The solid lines through the data are fits using a multi-exponential function. Below is the plot of modified residuals $[(Data-Fit)/Data^{1/2}]$ for these fits to data plotted in the presence of nitrogen. The data was collected at 405 nm.	674
Figure X-9a:	Lifetime components τ_1 (◆), τ_2 (■), τ_3 (▲) and τ_4 (●) obtained from a multi-exponential model fit to phosphorescence intensity decay data from tryptophan dispersed in amorphous films of TVS equilibrated against nitrogen as a function of temperature. The data was calculated every 10°C from -10°C to 100°C.....	675
Figure X-10a:	Comparison of longer lifetime component τ_1 obtained from a multi-exponential model fit (Eq. (3), Materials and Methods) to phosphorescence intensity decay data from tryptophan dispersed in amorphous TVS (◇) (emissions at ~ 405 nm) or TS a (◇) (emissions at ~ 455 nm) or TS b (◇) (emissions at ~ 405 nm) films equilibrated against nitrogen as a function of temperature. The data was calculated every 10°C from -10°C to 100°C.....	676
Figure X-10b:	Comparison of longer lifetime component τ_2 obtained from a multi-exponential model fit (Eq. (3), Materials and Methods) to phosphorescence intensity decay data from tryptophan dispersed in amorphous TVS (□) (emissions at ~ 405 nm) or TS a (□) (emissions at ~ 455 nm) or TS b (□) (emissions at ~ 405 nm) films equilibrated against nitrogen as a function of temperature. The data was calculated every 10°C from -10°C to 100°C.....	677
Figure X-10c:	Comparison of shorter lifetime component τ_3 obtained from a multi-exponential model fit (Eq. (3), Materials and Methods) to phosphorescence intensity decay data from tryptophan dispersed in amorphous TVS (Δ) (emissions at ~ 405 nm) or TS a (Δ) (emissions at ~ 455 nm) or TS b (Δ) (emissions at ~ 405 nm) films equilibrated against nitrogen as a function of temperature. The data was calculated every 10°C from -10°C to 100°C.....	678
Figure X-10d:	Comparison of shorter lifetime component τ_4 obtained from a multi-exponential model fit (Eq. (3), Materials and Methods) to phosphorescence intensity decay data from tryptophan dispersed in amorphous TVS (○) (emissions at ~ 405 nm) or TS a (○) (emissions at ~ 455 nm) or TS b (○) (emissions at ~ 405 nm) films equilibrated against nitrogen as a function of temperature. The data was calculated every 10°C from -10°C to 100°C.....	679

Figure X-11:	The average lifetime of tryptophan in TVS 405 nm (■), TS 455 nm (◆) and TS 405 nm (▲) films obtained from a multi-exponential model fit equilibrated against nitrogen as a function of temperature. The data were collected every 10°C from -10°C to 100°C.	680
Figure X-12:	Intensity decay fit parameters amplitude for tryptophan in amorphous TVS film in nitrogen as a function of temperature. The data was calculated every 10°C from -10°C to 80°C. The amplitudes a1 (◆) and a2 (■) correspond to the longer life time components (τ_1 , τ_2) and a3 (▲) and a4 (●) correspond to the shorter lifetime components (τ_3 , τ_4). The amplitudes were obtained from a multi exponential model fit (Eq. (3), Materials and Methods) to phosphorescence intensity decay data from tryptophan dispersed in TVS films equilibrated against nitrogen as a function of temperature.....	681
Figure X-13a:	Comparison of longer lifetime amplitude a1 obtained from a multi-exponential model fit (Eq. (3), Materials and Methods) to phosphorescence intensity decay data from tryptophan dispersed in amorphous TVS (◇) (emissions at ~ 405 nm) or TS a (◇) (emissions at ~ 455 nm) or TS b (◇) (emissions at ~ 405 nm) films equilibrated against nitrogen as a function of temperature. The data was calculated every 10°C from -10°C to 80°C.....	682
Figure X-13b:	Comparison of longer lifetime amplitude a2 obtained from a multi-exponential model fit (Eq. (3), Materials and Methods) to phosphorescence intensity decay data from tryptophan dispersed in amorphous TVS (□) (emissions at ~ 405 nm) or TS a (□) (emissions at ~ 455 nm) or TS b (□) (emissions at ~ 405 nm) films equilibrated against nitrogen as a function of temperature. The data was calculated every 10°C from -10°C to 80°C.....	683
Figure X-13c:	Comparison of shorter lifetime amplitude a3 obtained from a multi-exponential model fit (Eq. (3), Materials and Methods) to phosphorescence intensity decay data from tryptophan dispersed in amorphous TVS (Δ) (emissions at ~ 405 nm) or TS a (Δ) (emissions at ~ 455 nm) or TS b (Δ) (emissions at ~ 405 nm) films equilibrated against nitrogen as a function of temperature. The data was calculated every 10°C from -10°C to 80°C.....	684
Figure X-13d:	Comparison of shorter lifetime component a4 obtained from a multi-exponential model fit (Eq. (3), Materials and Methods) to phosphorescence intensity decay data from tryptophan dispersed in amorphous TVS (○) (emissions at ~ 405 nm) or TS a (○) (emissions at ~ 455 nm) or TS b (○)	

	(emissions at ~ 405 nm) films equilibrated against nitrogen as a function of temperature. The data was calculated every 10°C from -10°C to 80°C	685
Figure X-14a:	The Arrhenius plot of natural log of k_p for average lifetime as function of inverse of temperature for tryptophan dispersed in TVS (emissions at 405 nm), TS a (emissions at 455nm) and b (emissions at 405 nm) films.....	686
Figure X-14b:	The Arrhenius plot of natural log of k_p for average lifetime as function of inverse of temperature for tryptophan and vanillin dispersed in TVS films.	687

Chapter I:

Introduction

Amorphous Solids Amorphous solids have disordered molecular arrangement compared to their crystalline form (Hancock and Zografi, 1997; Walstra, 2003). The amorphous state is considered to be a non-equilibrium state (Fennema, 1996). The most common way of forming amorphous solid is by rapid cooling of liquid melt, but there are many other routes to an amorphous state such as spray drying, freeze drying, extrusion, grinding, milling, etc, (Liu et al., 2006). Amorphous state exists in many foods (e.g., hard boiled candy), pharmaceuticals (e.g., lyophilized drugs) and biological materials (e.g., seeds) (Slade and Levine, 1991; Tolstoguzov, 2000; Walters, 2004).

Amorphous solids are glassy (rigid solid) at low temperatures and rubbery (in case of polymers) or super cooled melt (in case of low molecular weight materials) at high temperature. The transition from glass to liquid is termed as glass transition and occurs at a defined temperature called T_g . Molecules are considered to be rigid and less mobile at low temperature in glass and gain motion as temperature increases through the glass transition into the rubber/melt state.

Stability (physical, chemical and biological) is shown to be highly governed by moisture content (Labuza, 1970) and on the other hand glass transition temperature T_g has been shown to be critically affected by water content and based on this stability has been linked to T_g . Amorphous solids are considered be stable at $T < T_g$ and unstable at $T > T_g$.

As one compiles the literature to date, physical, chemical and biological changes (Ross, 2003) have been observed in amorphous solids both in glass and melt state. These changes are observed not only above T_g but also below T_g with differing rate (Bell and Hageman, 1994; Bell and Hageman, 1996; Buera et al., 1995; Buera and Karel, 1995)

So T_g cannot be considered as an index temperature for stability. For example, the kinetics of aspartame degradation in PVP (polyvinyl pyrrolidine) have been shown to differ with water activity rather than T_g (Bell and Hageman, 1994) and, rate of the degradation has been shown to change four fold on either side of T_g with no distinct break. This reaction is known to require rearrangement of aspartame for degradation to occur, which demands mobility, and hence the conclusion was made, due to no major changes in rates below and above T_g , that the free volume in the glass state of PVP is large enough for aspartame to rearrange.

Physical changes such as crystallization, collapse, caking and agglomeration can be predicted using T_g as a reference temperature (Le Meste et al., 2002) as these changes are dependent on flow rate. Viscosity influences diffusion, and viscosity by itself is influenced by temperature, so there is a link between temperature and diffusion and hence T_g , and thus T_g can be used to predict rates of diffusion controlled reactions (Champion et al., 2000).

Some reactions, for example, acid-catalyzed sucrose hydrolysis in amorphous PVP, were shown to be influenced by a_w , rather than T_g (Buera and Karel, 1995). On the other hand

thiamin stability in amorphous PVP was more influenced by the glass transition (Bell and White, 2000).

Thus, glass transition can explain kinetics of reactions requiring diffusion and collisions but not rearrangements. Low mobility in glassy state due to high viscosity is thought to restrict the reactions, but as shown in following examples that is not the case. There are several chemical/biochemical reactions shown to occur below, at and above T_g with different rates. Non-enzymatic browning in model food systems has been shown to occur at slower rates at low temperatures below T_g and at higher rates above T_g (Buera and Karel, 1995; Craig et al., 2001; Karmas et al., 1992). Similar is the case observed for oxidation reactions, where rates of oxidation were shown to increase with $T-T_g$ (Shimada et al). Sucrose hydrolysis has been shown to occur in glassy state (Chen et al., 1999). Thus one can conclude that these reactions did occur in the glassy state.

Retrogradation rates at storage temperatures above T_g were higher than at storage below T_g in normal rice (Hsu and Heldman, 2005). Retrogradation is diffusion limited. Molecular mobility above T_g is higher and causes higher rates of water diffusion and accelerated reaction rates. Molecular mobility dictated by T_g was shown to influence tyrosinase storage stability (Chen et al., 1999), loss of activity was faster in rubbery system of PVP than the glassy system suggesting mobility might be affecting tyrosinase stability and combination of porosity and matrix mobility associated with rubbery state maximize the rate constants of tyrosinase inactivation.

Though molecular mobility is expected to be restricted below T_g in the viscous glass, the above reactions do not support suggesting molecular mobility does occur above and below T_g and the rates differ. The overall conclusion one can make is that physical, chemical and biological changes cannot be predicted just by T_g , and they occur both below T_g in glass and above T_g in rubber/melt (depending on which reactions we are talking about). An important point to also note is that the rates of these changes observed differed. Thus to predict stability (chemical, physical or biological) related to molecular mobility, one must consider matrix mobility above, below and at T_g .

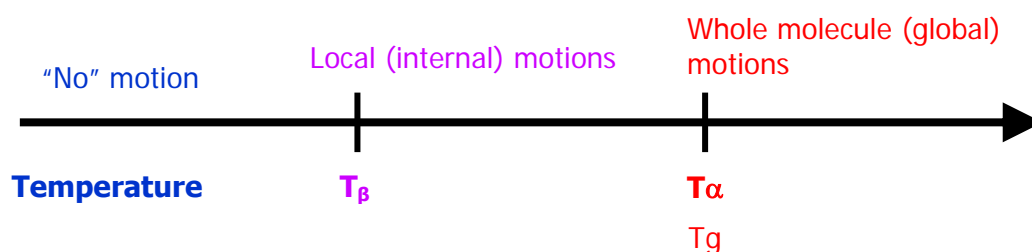
Molecular Mobility: The physical change in terms of molecular mobility occurring in glass and rubber/melt are very important in defining the shelf-life and quality of food, pharmaceuticals and biological materials that are amorphous solids (Roos, 1995; Hancock and Zografi, 1997; Sun et al., 1998; Buitink et al., 1998). Kinetics of physical, chemical and biochemical processes are affected by degree of molecular mobility in the amorphous solids. Molecular mobility could represent different types of motions (Figure 1), vibrations of atoms or bonds, reorientations of small groups of atoms, or translational motion of molecules or segments of polymers (Le Meste et al., 2002) that are activated at specified conditions (Ludescher et al., 2001). Vibration, reorientation of small groups of atoms, are considered local and do not involve the surrounding atoms or molecules, but these motions are sensitive to packing of surrounding matrix. In glasses, based on its density of packing, vibrations could be greater contributors to molecular mobility. On the other hand, translational motions are long range and are strongly affected by the ability to deform or displace the surrounding atoms or molecules.

An asymmetric molecule with N atoms has three modes of translational mobility (along the three Cartesian axes), three modes of rotational mobility (about the three Cartesian axes), and $3N-6$ modes of internal vibrational mobility (Castellan, 1983). Sucrose ($N=45$) thus has 129 vibrational modes while even small proteins or carbohydrates ($N>1500$) have over 4500 vibrational modes (Ludescher et al., 2001). But not all the possible modes of motion will be able to quench the probe lifetime

Figure I-1

Molecular mobility

- Motion of entire molecule (Translation & Rotation)
- Motion within the molecule (Vibration)



(Modified from Roudaut et al., 2000).

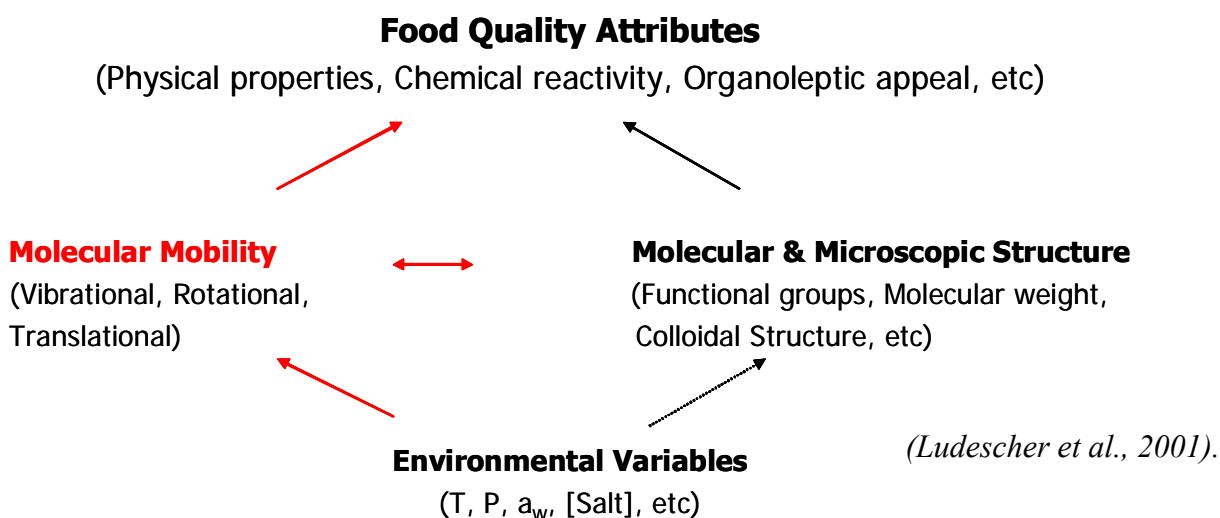
Amorphous glasses have extremely high viscosity and so are expected to have loss of molecular mobility. But molecular motions have been shown to occur in glass even below 50°C below T_g (Hancock et al., 1995), it's just that they are slow. Molecular mobility has been shown to be present in partially dried seeds (amorphous aqueous matrix) even at cryogenic temperatures (Walters, 2004). In glass, motions are mainly local (vibrations of atoms, reorientation of small groups of atoms) and in rubber/melt these motions could be long range translational and rotational (Le Meste et al., 2002; Liu

et al., 2006; Schmidt, 2004). Due to high viscosity and dense packing of glass, translational and rotational motions are thought to be restricted but vibrational motions are present (Craig et al., 1999; Schmidt, 2004), so storage below T_g is useful due to slower molecular mobility but is not an assurance, of stability.

Molecular mobility is strongly affected by temperature and water besides other factors and extent of mobility is dependent also on state of material glass or rubber/melt. Figure 2 shows a schematic model for the role that environmental variables, molecules and microscopic structure, and molecular mobility play in modulating food quality (Ludescher et al., 2001).

Figure I-2

A schematic model of variables playing role in modulating food quality



Protein motions: Stability of solid proteins (Lai and Topp, 1999) is strongly affected by temperature, water, pH, presence of any protectants, etc., as these factors are known to affect dynamics of proteins (molecular mobility). Residual water has significant effect on

solid state stability of proteins (Towns, 1995). As compiled by Hill et al., proteins show many degrees of molecular motions like molecular vibrations, rotation of amino acid side chains, to more global larger scale motions of entire protein segments depending on internal and external environmental conditions (Hill et al., 2005; Brooks et al., 1998). Thus proteins have several degrees of motions; these motions are desirable to keep protein flexible enough to perform lots of functions but in cases where motions lead to unfolding causing loss of its functionality it is highly undesirable.

For example, proteins are thought to lose stability (Vanderheeren and Hansoms, 1994) due to preferential orientation of amino acids when exposed to air-water or liquid-water interfaces (Hill et al., 2005). Thus proteins stability is affected by both internal and external environmental factors. Proteins show broad distribution of motions ranging from 10^{-15} to 10^4 s in solution. Proteins are shown to exhibit dynamic transition T_d (similar to T_g) at low temperature; above T_d the dynamic behavior is thought to be highly temperature dependent and shows an-harmonic vibrations and below T_d harmonic vibrations (e.g., localized amino acid fluctuations) (Hill et al., 2005).

Although there are other methods to study protein dynamics, fluorescence and phosphorescence spectroscopy with the help of intrinsic (e.g., tryptophan) probes or extrinsic covalently attached organic dye (e.g., erythrosin) has being widely used to study their dynamics in solution and in solid state (McGown and Nithipatikom, 2000).

Carbohydrate motions: Amorphous carbohydrates are very widely used in foods and pharmaceuticals and are important components of biological materials. Water is a strong plasticizer of amorphous carbohydrates and has a strong influence on the glass transition temperature (Roos, 1995; Slade and Levine, 1988). As water content and temperature increases, mobility of water is shown to increase by ^1H NMR, and at T_g mobility of water shows a break indicating more the water content stronger is its plasticizing effect (Van den Dries et al., 1998). The T_g of dry amorphous sucrose at 57°C decreased to -46°C due to plasticizing effect of water (Roos and Karel, 1991). Small sugars may also have plasticizing effect and are thought to do so by reducing the molecular entanglement (Kilburn et al., 2005). At low temperature and low plasticizer concentration only vibrational motions are present in carbohydrates. This could include localized bond vibrations in small molecules and more bond vibrations and side group rotations for larger molecules. At high temperature translational mobility becomes activated and glass transition occurs (Champion et al., 2000; Zallen, 1998). If only vibrational motions are considered monosaccharide glucose could have 66 normal modes, disaccharide sucrose 129, oligosaccharide raffinose 192 and polysaccharide amylose more than 3×10^5 (Ludescher et al., 2001).

Glass and Sub-Glass Relaxations: A glass is considered to be not in equilibrium but to exist in a metastable state (Fennema, 1996; Slade and Levine, 1988). Glass transition temperature is defined at the temperature range corresponding to glass-liquid transitions. When a molecule is perturbed the time it takes to come to equilibrium is defined as the relaxation time and process is referred as a relaxation process. In glasses due to slow

motions of molecules the relaxation times are longer compared to rubber/melt where molecules are moving faster, relaxation times vary from $>10^8$ s in glass to 10^{-9} s in melt, such increase is associated with reduction of translational and rotational motions of molecules (Hill et al., 2005). Molecular relaxations have been observed both below and above T_g with different amplitude and co-operativity thus indicating presence of molecular motions (Bidault et al., 2005; Chung and Lim, 2004; Kim et al., 2003; Noel et al., 2000).

These relaxation processes are classified α , β , γ etc., and these are sensitive to temperature and dependent on motions that are concerned. Some sugars and their relaxation temperatures are compiled in Table 1. In glass to liquid transition, molecular mobility is presented as α relaxation in the T_g zone; as temperature is lowered below T_g molecular mobility is presented as β and γ (in some cases δ) relaxations also called secondary relaxations (Ediger et al., 1996; Hancock and Zografi, 1997; Vyazovkin and Dranca, 2006). The α relaxation corresponds to translational and rotational motion of molecules that support flow. Sub- T_g relaxations have being reported in biopolymers and low molecular weight sugars (β, γ, δ) (Le Meste et al., 2002; Wagner and Richert, 1998, 1999). As described these relaxations correspond to rotations of lateral groups (γ relaxation at very low temperature) or to local conformations changes of the main chain in polysaccharides (Le Meste et al., 2002; Montes et al., 1998). Some associate β relaxation with localized movement of whole molecule.

Loss of crispy texture is attributed to sub-T_g relaxations associated with motions preceding the onset of α -relaxations (Champion et al., 2000). As compiled in Hill et al., (2005) the thermal stability of proteins is governed by connectivity and co-operativity between β -like motions that control α -like motions.

Thus, molecular motions persist below and above T_g. In glass to liquid transitions relaxation time of material is considered to be similar to experimental time scale and changes are observed, but in sub-T_g these relaxation times are very long and demand special consideration (Le Meste et al., 2002). As these motions affect stability of amorphous solids they are of concern.

Table I-1

Various transitions in carbohydrates (T_g, T _{α} , T _{β}) & proteins (T_d).

	T _g / K	T _{α} / K	T _{β} / K	T _d / K
Carbohydrates				
D-Glucose	312	333	211	
Maltose	370	376	223	
D-Mannose	311	333	210	
Sucrose	338			
Protein				
Wet Lysozyme				200
50% w/w glycerol: lysozyme				270
Dry Lysozyme				No Apparent Value

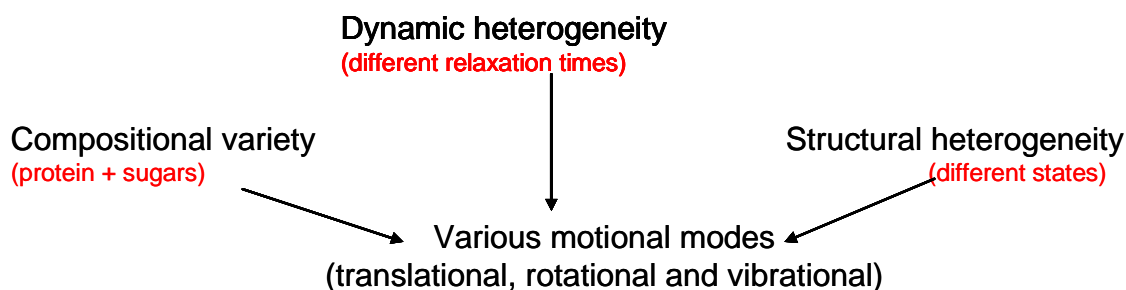
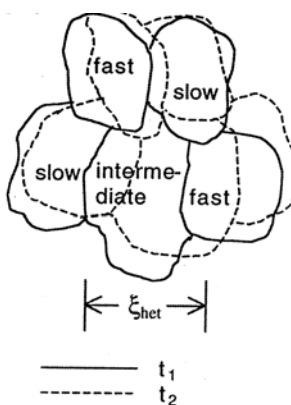
(Noel et al., 2000 and Hill et al., 2005)

Heterogeneity of amorphous solids: Another issue with amorphous solids is they show (Figure 3) dynamic heterogeneity (Ediger et al., 1996; Sillescu, 1999). Schematic

representation of spatial heterogeneity near glass transition temperature is shown in Figure 4. Amorphous solids due to heterogeneous nature may have distinct regions (high density or low density) and show different relaxation times (Liu et al., 2006; Shamblin et al., 1999). In a study dual glass transitions observed in normal rice starch were attributed to heterogeneous regions in the amorphous state of the normal rice starch (Chung and Lim, 2004). Sillescu, (1999) has extensively reviewed existence of heterogeneity in glass forming liquids and polymers, by compiling different experimental techniques like NMR, dielectric and optical experiments which indicate the presence of dynamical heterogeneity (Sillescu, 1999; Richert, 1997, 2001).

Dynamic site heterogeneity has been studied by Ludescher and colleagues using phosphorescence spectroscopy in various amorphous solids. Phosphorescence emission from erythrosin B has been shown to be distributed among dynamically distinct sites in different amorphous matrices like gelatin (Simon-Lukasik and Ludescher, 2006), maltose and maltitol (Shirke and Ludescher, 2005), lactose and lactitol (Shirke and Ludescher, 2006), sucrose (Pravinata et al., 2005), and bovine serum albumin (Nack and Ludescher, 2006). It has been shown that in these amorphous solids different sites vary in overall molecular mobility indicating the presence of dynamic heterogeneity.

Numerous experimental techniques are used to characterize molecular mobility of amorphous solids like NMR, dielectric spectroscopy, differential scanning calorimetry, and luminescence spectroscopy. My research focuses on using phosphorescence spectroscopy to characterize molecular mobility in amorphous solids.

Figure I-3**Molecular mobility and Heterogeneity****Figure I-4****Spatially Heterogeneity Dynamics****Figure I-4:** Schematic representation of spatial heterogeneity near glass transition temperature at time t_1 and t_2 (Ediger, 2000).

Luminescence Spectroscopy: Luminescence is the emission of light from any substance and occurs from an electronically excited state and is categorized as fluorescence or phosphorescence depending on the nature of the excited state (Lakowicz, 1999). Phosphorescence is the emission of light from an excited triplet state and fluorescence

occurs from an excited singlet state. Phosphorescence can be distinguished from fluorescence based on the kinetics of the excited state once absorption has occurred. The emission rates of fluorescence are 10^8s^{-1} and that of phosphorescence are $10^3\text{-}10^0\text{s}^{-1}$ (Lakowicz, 1999). The lifetime of the excited electronic state dictates the timescale of the molecular events that engage themselves in the excited state properties. Due to the timescale of excited singlet state, fluorescence spectroscopy responds to molecular events in the range of $10^{-6}\text{-}10^{-11}$ s and those of excited triplet state in case of phosphorescence spectroscopy respond to molecular event in the ms to s time scale (Lakowicz, 1999; Parker, 1968).

Due to the longer lifetimes of the triplet state, phosphorescence is more sensitive than fluorescence to deactivation by collisions with solvent molecules, quenchers and energy transfer processes and hence is strongly observed in rigid media (e.g., glass) where diffusional quenching is absent (Parker, 1968). Phosphorescence or fluorescence spectroscopy do not directly provide information about molecular motions, the dynamic information is obtained from the kinetics of the excited state. Phosphorescence spectroscopy has being shown to be sensitive to molecular mobility (Ludescher, 1990; Shah and Ludescher, 1993). This research will be focusing on using phosphorescence spectroscopy to study molecular mobility. Phosphorescence spectroscopy uses optical spectroscopic probes that report on properties of the molecular environment around the probe (Slavik, 1994).

Molecular Probes: Phosphorescence can be obtained from probes that can be divided into two categories: intrinsic or extrinsic probes. Extrinsic probes could be either covalently attached (e.g., erythrosin isothiocyanate attached to a protein surface; (Simon-Lukasik and Ludescher, 2004) or dispersed (e.g., erythrosin B dispersed in sucrose matrix; Pravinata et al., 2005). The intrinsic probe could be naturally occurring amino acid residue in proteins (e.g., tryptophan: Mazhul et al., 2002) and thus could provide site specific dynamic information (Hurtubise, 1990, 1997). The different time scales of motions demand different probes; for example slower motions like the ones that occur in viscous glass demand using long-lifetime chromophores as compared to say if the medium was water (Lakowicz, 1999).

A probe observes molecular mobility during its excited state lifetime, and for slower motions (Craig et al., 1999) longer lifetime probes are more suitable and the opposite is true for faster motions. A probe should have high quantum yield of phosphorescence emission and the lifetime of emission should be within the timescale for monitoring motions (Lettinga et al., 2000). Organic dyes having easily populated stable triplet states offer good choice as probes and are referred to as “triplet probes” (Parker, 1968). The lifetime of some common triplet state probes is shown in Table 2 (Adapted from Thomas, 1986).

Table I-2**Spectroscopic properties of some triplet state probes**

Triplet Probes	Lifetime / ms	Absorbance nm
Eosin	1-2	530
Erythrosin B	0.3-0.4	530
Di-iodofluorescein	0.5	502
Di-bromofluorescein	0.9	514
Tryptophan	1000	280

(Thomas, 1986).

A commonly used organic dye, eosin, has 70% of excited molecules converted to triplet state and has lifetimes of several ms in which the heavy bromine atoms facilitate intersystem crossing increasing the quantum yield and offering long lived triplet state (Thomas, 1986). Erythrosin B has 98% of excited molecules converting to triplet state and has higher quantum yield than eosin (Garland and Moore., 1979) and is considered as an ideal probe for phosphorescence studies. The phosphorescence of erythrosin B is due to the xanthene ring with four iodine atoms. Erythrosin B has phosphorescence emission time scale of 10^{-5} to 10^{-3} s corresponding to motion in glassy environment and is sensitive to oxygen (Lam et al., 2001). Numerous studies in our lab have used erythrosin B and shown it to be sensitive in monitoring molecular mobility in many simple model amorphous systems and thus it definitely offers a good choice as a probe. However the

maximum excited state lifetime of erythrosin B is approximately ~ 1 ms thus restricting its application to longer time range (Thomas, 1986).

Tryptophan has been shown to exhibit strong room temperature phosphorescence emission after excluding oxygen in many proteins (Vanderkooi et al., 1987). Tryptophan is the most commonly used intrinsic probe in study of protein dynamics (Lakowicz, 1999). Its phosphorescence lifetime at 77K is 5-6s (Strambini and Gonnelli, 1995). Tryptophan phosphorescence can be as long as 1-2 s in proteins and thus could measure slower motions that are un-measurable with most other triplet probes (Thomas, 1986).

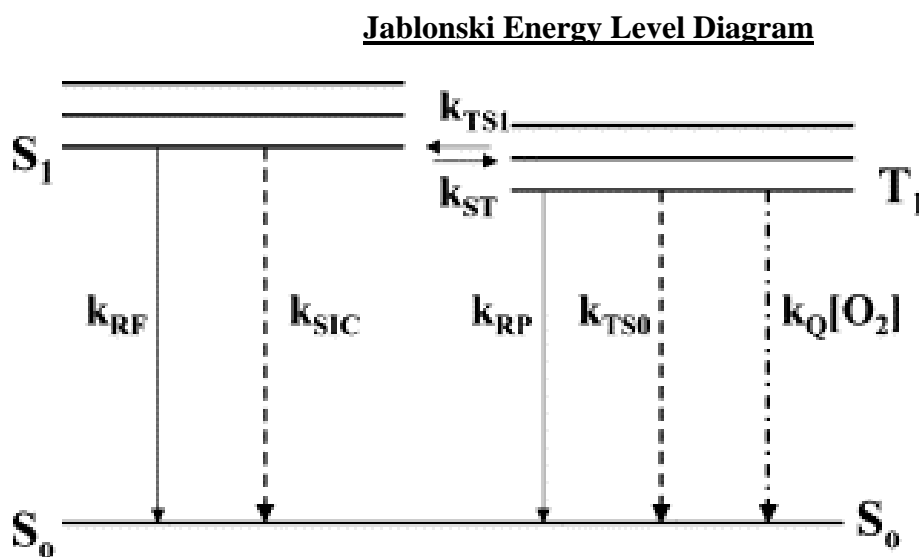
Phosphorescence emission from intrinsic tryptophan has been used to monitor the effect of hydration on the internal molecular mobility of the protein lysozyme (Shah and Ludescher, 1992, 1993; Subramaniam et al., 2006). Tryptophan has also been used as a dispersed probe in studying molecular mobility in amorphous sucrose (McCaul and Ludescher, 1999; Shah and Ludescher, 1995). However tryptophan as a probe for protein dynamic study has several disadvantages: a) Most proteins have several tryptophans making it difficult to study site selectively; b) Tryptophan may not be present in a protein; c) Tryptophan has to be buried in a rigid environment for phosphorescence in solution; d) The tryptophan signal could be quenched by several quenchers (e.g., disulfide), and energy transfer among chromophores can complicate the interpretations, etc. (Vanderkooi et al., 1990).

Vanillin has been one of the most exciting flavor compounds for ages. In this research it is being looked at in a fresh perspective. Its phosphorescence properties have been characterized, but vanillin has not yet being explored as triplet probe to date. Vanillin has being shown to exhibit room temperature phosphorescence (Nishigaki et al., 1996). However there is no data currently available in the literature where vanillin has been used for monitoring molecular mobility in amorphous systems. And as vanillin is an important component found widely in food it offers a great inspiration to study its use as a triplet probe.

Basic photophysics: Figure 5 gives the Jablonski energy level diagram with appropriate rate constants for the various photophysical events occurring during luminescence. Following light absorption the ground state molecule makes an essentially instantaneous transition to one of the many vibrational levels of the first excited state (S_1); excess vibrational energy is rapidly dissipated to the solvent matrix to relax to lowest vibrational level of S_1 . Along with fluorescence (rate k_{RF}), the excited state may engage in several de-excitation processes including non-radiative decay to S_0 through exchange of vibrational energy to the matrix (rate constant k_{SIC}), intersystem crossing from S_1 to T_1 (rate k_{ST}) and collisional quenching (rate $k_Q[Q]$). Along with phosphorescence (rate k_{RP}) other de-excitation processes that occur include non-radiative decay from T_1 to S_0 (rate k_{TS0}), collisional quenching (rate $k_Q[Q]$). The above photophysical events are common to erythrosin B, tryptophan and vanillin; but in case of erythrosin B in addition to all the above events reverse intersystem crossing from T_1 to S_1 (rate k_{TS1}) is also observed

giving rise to delayed fluorescence. The rate constants k_{RF} and k_{RP} are fixed by the probe structure and are unaffected by the environment (Birks, 1970; Turro, 1991).

Figure I-5



Abbreviations Used:

- k_{RF} : Rate constant for fluorescence decay S_1 to S_0
- k_{SIC} : Rate constant for non-radiative decay rate S_1 to S_0
- k_{ST} : Rate constant for intersystem crossing S_1 to T_1
- $k_q[Q]$: Rate constant for quenching of excited singlet state
- k_{RP} : Rate constant for phosphorescence decay
- k_{TS0} : Rate constant for non-radiative decay from T_1 to S_0
- $k_Q[Q]$: Rate constant for quenching of excited triplet state
- k_{TS1} : Rate constant for reverse intersystem crossing T_1 to S_1
- k_{NR} : Rate constant for total nonradiative decay $k_{TS0} + k_Q[Q]$: phosphorescence

For a phosphor once luminescence quantum yield and luminescence lifetimes are acquired it is possible to employ fundamental photophysical equations to calculate rate constants for the excited state processes (Duchowicz et al., 1998; Hurtubise, 1997; Parker, 1968).

Emission Intensity: Quantum yield (Φ) is define as the ratio of photons emitted to photon absorbed. Emission intensity is directly proportional to quantum yield. The quantum yield for fluorescence is given by the following ratio of rate constants (Lakowicz, 1999).

$$\Phi_F = k_{RF} / (k_{RF} + k_{SIC} + k_{ST} + k_Q [Q]) \quad (1)$$

In the absence of a specific quencher Equation 1 simplifies to.

$$\Phi_F = k_{RF} / (k_{RF} + k_{SIC} + k_{ST}) \quad (2)$$

In case of phosphorescence the quantum yield for phosphorescence (Φ_P) is the product of the quantum yield for T_1 formation (Φ_T) times the probability of emission from T_1 (q_P) (Hurtubise, 1990, 1997).

In the case of erythrosin B, due to reverse intersystem crossing the Φ_P is given as follows.

$$\Phi_P = \Phi_{TQP} = \{k_{ST} / (k_{RF} + k_{SIC} + k_{ST} + k_q [Q])\} \{k_{RP} / (k_{RP} + k_{TS0} + k_{TS1} + k_Q [Q])\} \quad (3)$$

In case of tryptophan and vanillin due to absence of reverse intersystem crossing the Φ_P is given as follows.

$$\Phi_P = \Phi_{TP} = \{k_{ST}/(k_{RF} + k_{SIC} + k_{ST} + k_q [Q])\} \{k_{RP}/(k_{RP} + k_{TS0} + k_Q [Q])\} \quad (4)$$

The quantum yield for delayed fluorescence in the absence of oxygen is the product of the quantum yield of fluorescence and the probabilities of intersystem crossing from S_1 to T_1 and also from T_1 to S_1 (Duchowicz et al., 1998). In absence of quencher molecule.

$$\Phi_{DF} = \Phi_F \{k_{ST}/k_{RF} + k_{SIC} + k_{ST}\} \{k_{TS1}/k_{RP} + k_{TS0} + k_{TS1}\} \quad (5)$$

Phosphorescence intensity can be monitored by measuring the intensity decay as function of time. The phosphorescence lifetime can be expressed in terms of the de-excitation rate constants. In case of erythrosin B it is given as shown in Equation 6 and for tryptophan and vanillin is given as shown in Equation 7 in absence of any external quenchers.

$$k_P(T) = k_{RP} + k_{TS0}(T) + k_{TS1}(T) \quad (6)$$

$$k_P(T) = k_{RP} + k_{TS0}(T) \quad (7)$$

In a complex amorphous matrix, there may be several different environments and hence several different lifetimes of the triplet probe. The phosphorescence intensity decay could be fitted with either stretched exponential function or multi-exponential functions (Chen,

2003; Shamblin et al., 2000). For example, if two different species (in different environments) of the emitting chromophore remain independent of each other, the decay will be biexponential. In a multi-exponential model the intensity is assumed to be decaying as the sum of individual single-exponential decays. The multi-exponential model is as show in Equation 8; τ_i are decay times, α_i represent the amplitudes of the components at $t = 0$ and n is the number of decay times.

$$I(t) = \sum_{i=1}^n \alpha_i \exp(-t/\tau_i) \quad (8)$$

In many cases one does not expect a limited number of discrete decays times, but rather a distribution of decay times (Lakowicz, 1999). In such cases the intensity decays are typically analyzed in terms of a lifetime distribution. Phosphorescence intensity decays are often non-exponential and a stretched exponential decay function has being shown to describe the wide distribution of relaxation times (Champion et al., 2000, Lee et al., 2001). The stretched exponential equation is given as shown in Equation 9, where $I(t)$ is the intensity as a function of time following pulsed excitation, $I(0)$ is the initial intensity at time zero, τ is the lifetime, and β is the stretching exponent which characterizes the distribution of the decay times, KWW.

$$I(t) = I(0) \exp[-(t/\tau)^\beta] \quad (9)$$

Emission Energy: Both absorption and emission are distributed over a large range of energies, and the energetic interactions between the polar chromophore and the immediate environment are sensitive to dipolar interactions (Ludescher et al., 2001). When the molecule is excited it can be stabilized by dipolar relaxation, molecular motion in the local matrix which has a dramatic effect on the emission energy. The dipolar relaxation can influence emission energy only if it is on the same time scale as the excited lifetime, making the slower process of phosphorescence (10^{-6} to 1s) more desirable for studies of amorphous solids. In amorphous rubbery and glassy matrices the solvent relaxation is slow ($>>10^{-6}$ s) due to limited molecular mobility, and the emission does not occur from the excited state while fully surround by a relaxed solvent shell, but rather from a non-equilibrium state undergoing relaxation (Ludescher et al., 2001). Thus phosphorescence spectroscopy offers an effective tool to study dipolar relaxation (Ludescher et al., 2001).

Oxygen Quenching: The process of quenching causes reduction in the quantum yield. Oxygen is the most effective quencher of the triplet state and hence it is necessary to remove during phosphorescence measurements (Vanderkooi et al., 1987). Measurements of +/- oxygen thus can be used to monitor the extent of oxygen diffusion through the matrix.

Hypothesis: Vanillin can be used as a triplet state probe to measure molecular mobility in amorphous materials below glass transition temperature.

The physical properties of amorphous solids are modulated by specific modes of molecular mobility above and below the glass transition temperature which are responsible for physical and chemical changes. Luminescence spectroscopy uses optical probes that can report on the properties of the molecular environment around the probe. Depending upon the specific luminescent probe, the triplet lifetime ranges from microseconds to seconds, thus providing a sensitive signal on timescale suitable for study of matrices in either glass or the rubber/melt state.

We hypothesize that molecular mobility measurements should not be restricted to a single probe as different molecular probes could provide different information with respect to mobility on different time scales. This project will provide insight into the way different probes report molecular mobility in the same matrix. The use of the novel probe vanillin would open a great potential towards molecular mobility measurements. The possibility of using multiple probes will offer a new dimension into molecular mobility measurements. A more thorough understanding generated from molecular mobility maps using different probes about the amorphous system characteristics will ultimately lead to successful predictions of physical stability of amorphous solids.

Research Objective: The objectives of this research are as follows.

Objective 1: Characterize the luminescence properties and photophysical events of vanillin as a triplet state probe in amorphous sucrose films as a function of temperature.

Objective 2: Understand the mechanism of environmental sensitivity of vanillin to molecular motions using different analogs of vanillin in amorphous sucrose films.

Objective 3: Study the effect of molecular weight and glass transition temperature on sensitivity of vanillin using glucose homologous series.

Objective 4: Characterize the molecular mobility of different amorphous matrices (excipients) used for various controlled release application as a function of temperature using phosphorescence of vanillin.

Objective 5: Understand molecular mobility in amorphous sucrose films using phosphorescence of Erythrosin B, Tryptophan and Vanillin (having varied intrinsic lifetimes) as a triplet state probe.

Objective 6: Investigate molecular mobility in amorphous protein films using phosphorescence of extrinsic probes (Erythrosin B and Vanillin) and intrinsic probe (Tryptophan) (having varied intrinsic lifetimes) as a function of temperature.

Objective 7: Investigate the potential of using multiple probe combinations (Erythrosin B and Vanillin, Vanillin and Tryptophan or Erythrosin B and Tryptophan) in amorphous sucrose films to report molecular mobility.

References

- Bell, L.N. and Hageman, M.J. Differentiating between the effect of water activity and glass transition dependent mobility on solid state chemical reaction: aspartame degradation. *Journal of Agricultural and Food Chemistry*. 42 (1994). 2398-2401.
- Bell, L.N. and Hageman, M.J. Glass transition explanation for effect of polyhydroxy compounds on protein denaturation in dehydrated solids. *Journal of Food Science*. 61 (1996). 372-375.
- Bell, L.N. and White, K.L. Thiamin stability in solids as affected by the glass transition. *Journal of Food Science*. 65 (2000). 498-501.
- Bidault, O., Assifaoui, A., Champion D. and Le Meste, M. Dielectric spectroscopy measurements of the sub-T_g relaxations in amorphous ethyl cellulose: a relaxation magnitude study. *Journal of Non-crystalline Solids*. 351 (2005). 1167-1178.
- Birks, J.B. *Photophysics of Aromatic Molecules*. John Wiley and Sons, New York (1970).
- Brooks, C.L. III, Gruebele, M., Onuchic, J.N. and Wolynes, P.G. Chemical physics of protein folding. *Proceedings of National Academy of Sciences of USA*. 95 (1998). 11037-11038.
- Buera, M.P. and Karel, M. Effect of physical changes on the rates of non enzymatic browning and related reactions. *Food Chemistry* 52 (1995). 167-173.
- Buera, M.P., Chirife, J. and Karel, M. A study of acid catalyzed sucrose hydrolysis in an amorphous polymer matrix at reduced moisture content. *Food Research International*. 28 (1995). 359-365.
- Buitink, L. and Leprince, O. Glass formation in plant anhydrobiotes: survival in the dry state. *Cryobiology*. 48 (2004). 215-228.
- Castellan, G.W. *Physical Chemistry*. The Benjamin/Cummings Publishing, Menlo Park (1983).
- Champion, D., Le Meste, M. and Simatos, D. Towards an improved understanding of glass transition and relaxations in foods: molecular mobility in the glass transition range. *Trends in Food Science and Technology*. 11 (2000). 41-55.
- Champion, D., Le Meste, M. and Simatos, D. Towards an improved understanding of glass transition and relaxations in foods: molecular mobility in the glass transition range. *Trends in Food Science and Technology*. 11 (2000). 41-55.
- Chen, R. Apparent stretched exponential luminescence decay in crystalline solids. *Journal of Luminescence*. 102 (2003). 510-518.

- Chen, Y, Aull, J.L. and Bell, L.N. Invertase storage stability and sucrose hydrolysis in solids as affected by water activity and glass transition. *Journal of Agricultural and Food Chemistry*. 47 (1999). 504-509.
- Chen, Y., Aull, J.L. and Bell, L.N. Solid-state tyrosinase stability as affected by water activity and glass transition. *Food Research International*. 32 (1999). 467-472.
- Chung, H. and Lim, S. Physical aging of glassy normal and waxy rice starches: thermal and mechanical characterization. *Carbohydrate Polymers*. 57 (2004). 15-21.
- Craig, D.Q., Royall, P.G., Kett, V.L. and Hopton, M.L. The relevance of the amorphous state of pharmaceutical dosage forms: glassy drugs and freeze dried systems. *International Journal of Pharmaceutics*. 179 (1999). 179-207.
- Craig I.D, Parker R, Rigby N.M, Cairns P, and Ring S.G. Maillard reaction kinetics in model preservation systems in the vicinity of the glass transition: Experiment and theory. *Journal of Agricultural and Food Chemistry*. 49 (2001). 4706-4712.
- Duchowicz, R., Ferrer, M.L. and Acuna, A.U. Kinetic spectroscopy of erythrosin phosphorescence and delayed fluorescence in aqueous solution at room temperature. *Photochemistry and Photobiology*. 68 (1998). 494-501.
- Ediger, M.D., Angell, C.A. and Nagel, S.R. Supercooled Liquids and Glasses. *Journal of Physical Chemistry*. 100 (1996). 13200-13212
- Fennema, O. *Water and Ice*. Marcel Dekker Inc, New York (1996).
- Garland, P.B. and Moore, C.H. Phosphorescence of protein-bound eosin and erythrosin: A possible probe for measurements of slow rotational mobility. *Biochemistry Journal*. 183 (1979). 561-572.
- Hancock, B.C, and Zografi, G. Characteristics and significance of amorphous state in pharmaceutical systems. *Journal of Pharmaceutical Sciences*. 86 (1997). 1-12.
- Hancock, B.C., Shamblin S.L. and Zografi, G. Molecular mobility of amorphous pharmaceutical solids below their glass transition temperatures. *Pharmaceutical Research*. 12 (1995). 799-806.
- Hill J.J, Shalaev E.Y. and Zografi, G. Thermodynamic and dynamic factors involved in the stability of native proteins structure in amorphous solids in relation to levels of hydration. *Journal of Pharmaceutical Sciences*. 94 (2005). 1636-1667.
- Hsu, C. and Heldman, D.R. Influence of glass transition temperature on rate of rice starch retrogradation during low temperature storage. *Journal of Food Process Engineering*. 28 (2005). 506-525.

- Hurtubise, R.J. Phosphorimetry: Theory Instrumentation, and Applications. VCH Publishers, Inc, New York (1990).
- Hurtubise, R.J. Solid matrix luminescence analysis: photophysics, physicochemical interactions and applications. *Analytica Chimica Acta*. 351 (1997). 1-22.
- Karmas, R., Buera, M.P. and Karel, M. Effect of glass transition on rates of non enzymatic browning in foods. *Journal of Agricultural and Food Chemistry*. 40 (1992). 873-679.
- Kilburn, D., Claude, J., Schweizer, T., Alam, A. and Ubbink, J. Carbohydrate polymers in amorphous states: An integrated thermodynamic and nanostructural investigation. *Biomacromolecules*. 6 (2005). 864-879.
- Kim, Y.J., Hagiwara, T., Kawai, K., Suzuki, T. and Takai, R. Kinetic process of enthalpy relaxation of glassy starch and effect of physical aging upon its water vapor permeability property. *Carbohydrate Polymers*. 53 (2003). 289-296.
- Labuza, T.P. Properties of water as related to the keeping quality of foods. *Proceedings of the third International Congress of Food Science and Technology* (1970). 618-35.
- Lai, M.C. and Topp, E.M. Solid state chemical stability of protein and peptides. *Journal of Pharmaceutical Sciences*. 88 (1999). 489-500.
- Lakowicz, J.R. Principles of Fluorescence Spectroscopy, Second Edition. Kluwer Academic/Plenum Press, New York (1999).
- Lam, S.K., Chan, M.A. and Lo, D. Characterization of phosphorescence oxygen sensor based on erythrosin B in sol-gel silica in wide pressure and temperature ranges. *Sensors and Actuators. B* 73 (2001). 135-141.
- Le Meste, M., Champion, D., Roudaut G., Blond, G. and Simatos, D. Glass transition and food technology: A critical appraisal. *Journal of Food Science*. 67 (2002). 2444-2458.
- Lee, K.C.B., Siegel, J., Webb, S.E.D., Leveque-Fort, S., Cole, M.J., Jones, R., Dowling, K., Leve, M.J. and French, P.M.W. Applications of the stretched exponential function to fluorescence lifetime imaging. *Biophysical Journal*. 81 (2001). 1265-1274.
- Lettinga, M.P., Zuilhof, H. and van Zandvoort, M.A. Phosphorescence and fluorescence characterization of fluorescein derivatives immobilized in various polymers matrices. *Physical Chemistry Chemical Physics*. 2 (2000). 3697-3707.

- Liu, Y., Bhandari, B. and Zhou, W. Glass transition and enthalpy relaxation of amorphous food saccharides: A review. *Journal of Agricultural and Food Chemistry*. 54 (2006). 5701-5717.
- Ludescher, R.D., Shah, N.K., McCaul, C.P. and Simon, K.V. Beyond T_g: optical luminescence measurements of molecular mobility in amorphous solid foods. *Food Hydrocolloids*. 15 (2001). 331-339.
- Ludescher, R.D. Molecular dynamics of food proteins: Experimental techniques and observations. *Trends in Food Science and Technology*. 1 (1990). 145-149.
- Mazhul, V.M., Zaitseva, E.M. and Shcherbin, D.G. Phosphorescence of tryptophan residues of proteins at room temperature. *Journal of Applied Spectroscopy*. 69 (2002). 213-219.
- McCaul, C.P. and Ludescher, R.D. Room temperature phosphorescence from tryptophan and halogenated tryptophan analogs in amorphous sucrose. *Photochemistry and Photobiology*. 70 (1999). 166-171.
- McGown, L.B. and Nithipatikom, K. Molecular fluorescence and phosphorescence. *Applied Spectroscopy Reviews*. 35 (2000). 353-393.
- Montes, H., Mazeau, K. and Cavaille, J.Y. The mechanical beta relaxation in amorphous cellulose. *Journal of Non-crystalline Solids*. 235-237 (1998). 416-421.
- Nack, T.J. and Ludescher, R.D. Molecular mobility and oxygen permeability in amorphous bovine serum albumin films. *Food Biophysics*. 1 (2006). 151-162.
- Nishigaki, A., Ngashima, U., Uchida, A., Oonishi, I. and Oshima, S. Hysteresis in the temperature dependence of phosphorescence of 4-Hydroxy-3-Methoxybenzaldehyde (vanillin) in Ethanol. *Journal of Physical Chemistry*. 102 (1998). 1106-1111.
- Noel, T.R., Parker, R. and Ring, S.G. Effect of molecular structure and water content on the dielectric relaxation behavior of amorphous low molecular weight carbohydrates above and below their glass transition. *Carbohydrate Research*. 329 (2000). 839-845.
- Parker, C.A. *Photoluminescence of Solutions*. Elsevier Pub Co., Amsterdam (1968).
- Pravinata, L.V., You, Y. and Ludescher, R.D. Erythrosin B phosphorescence monitors molecular mobility and dynamic heterogeneity in amorphous sucrose. *Biophysical Journal*. 88 (2005). 3551-3561.
- Richert, R. Spectral selectivity in the slow beta relaxation of a molecular glass. *Europhysics Letters*. 54 (2001). 767-773.

- Roos, Y. and Karel, M. Phase transitions of amorphous sucrose and frozen sucrose solutions. *Journal of Food Science*. 56 (1991). 266-267.
- Roos, Y. *Phase Transitions in Foods*. Academic Press, San Diego, California (1995).
- Roos, Y.H. Thermal analysis, state transition and food quality. *Journal of Thermal Analysis and Calorimetry*. 71 (2003). 197-203.
- Schmidt, S.J. Water and solids mobility in foods. *Advances in Food and Nutrition Research*. 48 (2004). 1-101.
- Shah, N.K. and Ludescher, R.D. Hydration and the internal dynamics of hen egg white lysozyme. *Proceedings of SPIE* 1640 (1992). 174-179.
- Shah, N.K. and Ludescher, R.D. Influence of hydration on the internal dynamics of hen egg white lysozyme in the dry state. *Photochemistry and Photobiology*. 58 (1993). 169-174.
- Shah, N.K. and Ludescher, R.D. Phosphorescence of probes of the glassy state in amorphous sucrose. *Biotechnology Progress*. 11 (1995). 540-544.
- Shamblin, S., Hancock, B.C., Dupuis, Y. and Pikal, M.J. Interpretation of relaxation time constants for amorphous pharmaceutical systems. *Journal of Pharmaceutical Sciences*. 89 (2000). 417-427.
- Shamblin, S.L., Tang, X.L., Chang, L.Q., Hancock, B.C. and Pikal, M.J. Characterization of the time scales of molecular motion in pharmaceutically important glasses. *Journal of Physical Chemistry*. 103 (1999). 4113-4121.
- Shirke, S. and Ludescher, R.D. Dynamic site heterogeneity in amorphous maltose and maltitol from spectral heterogeneity in erythrosin B phosphorescence. *Carbohydrate Research*. 340 (2005). 2661-2669.
- Shirke, S. and Ludescher, R.D. Dynamic site heterogeneity in amorphous lactose and lactitol from spectral heterogeneity in erythrosin B phosphorescence. *Biophysical Chemistry*. 123 (2006). 122-133.
- Sillescu, H.J. Heterogeneity at the glass transition: a review. *Journal of Non-Crystalline Solids*. 243 (1999). 81-108.
- Simon-Lukasik, K.V. and Ludescher, R.D. Effect of plasticizer on dynamic site heterogeneity in cold-cast gelatin films. *Food Hydrocolloids*. 20 (2006). 88-95.
- Simon-Lukasik, K.V. and Ludescher R.D. Erythrosin B phosphorescence as a probe of oxygen diffusion in amorphous gelatin films. *Food Hydrocolloids*. 18 (2004). 621-630.

- Slade, L. and Levine, H. A Food Polymer Science approach to structure interactions. *Advances in experimental medicine and biology*. 302 (1991). 29-101.
- Slade, L. and Levine, H. Non-equilibrium behavior of small carbohydrate water systems. *Pure and Applied Chemistry*. 60 (1988). 1841-1864.
- Slavik, J. *Fluorescent Probes in Cellular and Molecular Biology*. CRC Press, Boca Raton, FL (1994).
- Strambini, G.B. and Gonnelli, M. Tryptophan phosphorescence in fluid solution. *Journal of American Chemical Society*. 117 (1995). 7646-7651.
- Subramaniam, V., Gafni, A. and Steel, D.G. Time-resolved tryptophan phosphorescence spectroscopy: A sensitive probe of protein folding and structure. *IEEE Journal of Selected Topics in Quantum Electronics*. 2 (2006). 1107-1114.
- Sun, W.Q. and Davidson, P. Protein inactivation in amorphous sucrose and trehalose matrices: effects of phase separation and crystallization. *Biochimica Biophysica Acta*. 1425 (1998) 235-244.
- Thomas, D. *Rotational Diffusion of Membranes*. Ragan, C.I. and Cherry, R.J. *Techniques for Analysis of membrane proteins*. Chapman and Hall, London. (1986). 377-394.
- Tolstoguzov, V.B. The importance of glassy biopolymer components in food. *Nahrung*. 44 (2000). 76-84.
- Towns, J.K. Moisture content in proteins: its effect and measurements. *Journal of Chromatography*. 705 (1995). 115-127.
- Turro, N. *Modern Molecular Photochemistry*. University Science Books, Sausalito, CA (1991).
- van den Dries, I.J., van Dusschoten, D. and Hemminga, M.A. Mobility in maltose-water glasses studied with ¹H NMR. *Journal of Physical Chemistry*. 102 (1998). 10483-10489.
- Vanderheeren, G. and Hanssens, I. Thermal unfolding of bovine alpha lactalbumin. *The Journal of Biological Chemistry*. 269 (1994). 7090-7094.
- Vanderkooi, J.M., Englander, S.W., Papp, S., Wright, W.W. and Owen, C.S. Long range electron exchange measured in proteins by quenching of tryptophan phosphorescence. *Proceedings of National Academy of Sciences of USA*. 87 (1990). 5099-5103.

- Vanderkooi, J. M., Maniara, G., Green, T. J. and Wilson, D. F. An optical method for measurement of dioxygen concentration based upon quenching of phosphorescence. *Journal of Biological Chemistry*. 262 (1987). 5476-5482.
- Vyazovkin, S. and Dranca, I. Probing beta relaxations in pharmaceutically relevant glasses by using DSC. *Pharmaceutical Research*. 23 (2006). 422-428.
- Wagner, H. and Richert, R. Equilibrium and non-equilibrium type beta relaxations: D-Sorbitol versus o-Terphenyl. *Journal of Physical Chemistry*. 103 (1999). 4071-4077.
- Walstra, P. *Physical Chemistry of Foods*. Marcel Dekker Inc, New York (2003).
- Walters, C. Temperature dependency of molecular mobility in preserved seeds. *Biophysical Journal*. 86 (2004). 1253-1258.
- Zallen, R. *The Physics of Amorphous Solids*. John Wiley and Sons, New York (1998).

Chapter II: Vanillin phosphorescence as a triplet state probe to monitor molecular mobility in amorphous sucrose.

Introduction

In amorphous solid foods and pharmaceuticals, shelf-life is influenced by modes of molecular mobility which influence the kinetics of physical and chemical processes. Molecular mobility is strongly affected by temperature and water (Roos and Karel, 1990, 1991a, 1991b). Changes in molecular mobility are thus important in defining the shelf-life and quality of amorphous solid foods, pharmaceuticals, and other biomaterials. Molecular motions have been shown to occur in glass even 50°C below T_g (Hancock et al., 1995) and in partially dried seeds at cryogenic temperatures (Walters, 2004). Predictions of stability must consider matrix mobility above and below T_g (the glass transition temperature); measurement of molecular mobility in amorphous solids over time scales ranging from $< 10^{-9}$ ns to $> 10^8$ s at temperatures above and below T_g requires specialized methods. In glass, motions are mainly local (vibrations of atoms, reorientation of small groups of atoms) (Craig et al., 1999; Schmidt, 2004) and in rubber/melt these motions could be long range translational and rotational (Schmidt, 2004; Le Meste et al., 2002; Liu et al., 2006). These motions are strong concern to us as they affect rates of molecular diffusion, and thus chemical reaction rate in amorphous solid foods, as well as the rates of other physical processes. In glass to liquid transitions relaxation time of material is considered to be similar to experimental time scale and changes are observed, but in sub-T_g these relaxation times are very long and demand special consideration (Le Meste et al., 2002).

Phosphorescence spectroscopy is a sensitive, site-specific method that can be used to detect molecular mobility in the environment of a probe embedded within an amorphous matrix. Phosphorescence is more sensitive than fluorescence to deactivation by collisions with solvent molecules, quenchers and energy transfer processes and hence is strongly observed in rigid media (e.g. glass) where diffusional quenching is absent (Parker, 1968). Phosphorescence spectroscopy has been shown to be sensitive to molecular mobility (Ludescher, 1990; Shah and Ludescher, 1993). Due to the timescale of excited triplet state, phosphorescence spectroscopy responds to molecular event in the ms to s time scale (Parker, 1968; Lakowicz, 1999). Molecular mobility can be detected within the local environment of a probe using phosphorescence spectroscopy as it is a sensitive site specific method (Simon-Lukasik and Ludescher, 2004; Simon-Lukasik and Ludescher, 2006a, 2006b, Ludescher et al., 2001; Shirke and Ludescher, 2006a, 2006b).

Solid-surface room-temperature phosphorescence has been observed from a wide variety of conjugated organic compounds (e.g., vanillin) (Schulman and Parker, 1977). Molecules exhibit the phenomena when adsorbed on a suitable solid surface. Strong phosphorescence of organic compounds has been observed in gas phase, rigid media or at cryogenic temperature (Schulman and Walling, 1972, 1973). The rigid matrix prevents the non-radiative decay of the triplet state by collisional energy transfer (internal conversion processes) and by inhibiting quenching by ground state triplet oxygen when sample is dried (Schulman and Walling 1972). Surfaces such as paper, sucrose and starch have provided excellent supports for observing room temperature phosphorescence of organic compounds (Schulman and Parker, 1977).

Vanillin has been shown to exhibit phosphorescence at cryogenic and room temperature when adsorbed on a substrate such as filter paper (Schulman and Walling, 1973; Nishigaki et al., 1998). Vanillin is one of the most exciting flavor compounds for ages, and has found numerous applications in food and pharmaceuticals, and is very commonly added as a flavoring in these applications. In this research it is being looked at in a fresh perspective. This research focuses on exploring the potential of using vanillin as a triplet state probe to monitor molecular mobility in amorphous solids.

This research investigated how the steady-state and time-resolved emission and intensity of phosphorescence from vanillin (4-hydroxy-3-methoxy benzaldehyde), a commonly used flavor compound, can be used to probe molecular mobility when dispersed within amorphous pure sucrose films. There are not studies where vanillin phosphorescence has been used to monitor molecular mobility in amorphous solids. And as vanillin is an important component found widely it offers potential for use as a triplet probe in amorphous biomaterials. This would be the first study which will characterize the luminescence properties of phosphorescence of vanillin in amorphous sucrose films and investigate the potential of using vanillin phosphorescence to monitor molecular mobility in simple amorphous matrices.

Materials and Methods

Materials: Water was deionized and then glass distilled. Glycerol (Spectral Grade) was Sigma-Aldrich Chemical Company (St. Louis, MO), isopentane (Baker grade) was from J. T. Baker Chem. Co., Phillipsburg, NJ, Ethyl ether (anhydrous) was from Fisher Scientific, Fair Lawn NJ, and ethanol (anhydrous) was from Parmco Products, Inc, Brookfield, CT). Sucrose was from (99.5% pure) Sigma Chemical, St. Louis, MO. The probe vanillin (3-methoxy-4-hydroxy benzaldehyde: Figure 1a) was from Sigma-Aldrich, Milwaukee, WI.

Sucrose Solution: Sucrose solution was made as described in Pravinata et al., 2005. Approximately 20 g of sucrose (99.5% pure; Sigma Chemical, St. Louis, MO) were dissolved in 100 mL of deionized water containing 0.5 g of activated charcoal to remove luminescent impurities. After stirring overnight, the charcoal was removed by vacuum filtration using ashless filter paper (Whatman No. 40, Whatman International, Maidstone, UK), additional charcoal was added, and the process repeated. Sucrose solution was made to a final concentration of 65–67 wt % sucrose; concentration was confirmed using a refractometer (NSG Precision Cells, Farmingdale, NY). This sucrose solution was filtered through a 0.2 μ m membrane to remove particulates.

Vanillin: A 66mM stock solution of vanillin (Sigma-Aldrich, Milwaukee, WI) was prepared in distilled deionized water. This concentration was selected to simplify the addition of the probe to the sucrose solution. For absorbance, fluorescence and phosphorescence measurements the 66mM stock was diluted to 50 μ M in distilled deionized water. For measuring absorbance and phosphorescence in amorphous solid,

vanillin was added to the sucrose solution at a molar ratio of $1:10^3$ (dye: sucrose). Other ratios $3:10^4$, $5:10^4$ and $2:10^3$ were also tested to study the effect of probe concentration. The ratio $1:10^3$ (dye: sucrose) was chosen as at this concentration it was determined that the probe does not aggregate, existing only as individual molecules monitoring the molecular mobility of the sucrose.

Sucrose films: To produce glassy sucrose films containing vanillin, 20 μL of a sucrose solution containing vanillin were spread on a quartz slide ($30 \times 13.5 \times 0.6$ mm; custom made by NSG Precision Cells, Farmingdale, NY). After spreading the solutions on the slides were then dried under a heat gun (Vidal Sassoon) for 5 min to a maximum temperature of $\sim 88^\circ\text{C}$ (measured using a thermocouple probe) and the final thickness was ~ 0.05 mm. The slides were stored at room temperature against P_2O_5 and Drierite, protected from the light to prevent any photo bleaching, for at least 7 days before any phosphorescence measurements were made. The desiccant was refreshed as needed to maintain a relative humidity close to 0%.

Sample preparation for measurement at 77K: Solutions of vanillin were prepared at 20 mM concentration in a glycerol/water (60/40, v/v) or in EPA (ethyl ether/isopentane/ethanol 5/5/2, v/v). For measurements in amorphous sucrose films vanillin was added to the sucrose solution at a molar ratio of $1:10^3$ (dye: sucrose) and films were prepared as described above. The liquid solution/slide was placed in a quartz cylindrical cell with 4 mm inner diameter (National Scientific Company, Quakertown PA) for measurement at room temperature and at 77 K. At 77 K the tube was immersed in

liquid N₂ using a finger type Dewar obtained from Jobin-Yvon Spex. Ninety-degree geometry was used for these measurements. Sugar glasses doped with vanillin derivatives were prepared by plating sucrose solution on quartz plates followed by evaporation. The quartz plates were placed in the sample compartment and front-face geometry was used for measurement.

Instrumentation: For measurements at 77K emission intensity and spectra were measured with a Fluorolog-3-21 Jobin-Yvon Spex Instrument SA (Edison, NJ) equipped with a 450 W Xenon lamp for excitation and a cooled R2658P Hamamatsu photomultiplier tube for detection. At room temperature absorption measurements were recorded in a Cary Eclipse spectrophotometer and fluorescence and phosphorescence measurements were made on a Cary Eclipse fluorescence spectrophotometer (Varian Instruments, Walnut Creek, CA). For measurements at -20°C to 100°C phosphorescence measurements were made on a Cary Eclipse fluorescence spectrophotometer (Varian Instruments, Walnut Creek, CA). The solution or quartz slides were placed in a standard 1cm x 1cm x 1cm quartz fluorescence cuvette, which was capped with a lid having inlet and outlet ports for gas lines. The cuvette was flushed with a gentle stream of nitrogen for 15 minutes to eliminate oxygen. An oxygen free nitrogen stream was generated by passage of high purity nitrogen through a Supelco (Bellefonte, PA) gas purifier. The temperature was controlled by using a TLC 50 thermoelectric heating/cooling system (Quantum Northwest, Spokane, WA). The TLC-50 sample compartment was fitted with a jacketed cover and the temperature of the cuvette was monitored directly using a thermocouple in the cuvette. The film was equilibrated for 15 minutes at each temperature before

collecting the data. The Cary Eclipse uses a pulsed lamp and collects emission intensity in analog mode; data were not collected within the first 0.1-0.2 ms to suppress fluorescence coincident with the lamp pulse.

Spectroscopic Measurements: For measurements at 77K in glycerol: water, EPA and amorphous sucrose films vanillin was excited at 340 nm. Emission spectra were scanned in the 330 nm – 560 nm range. Slit width was set to provide a band-pass 2 nm for excitation and 1 nm for emission. For time-dependent intensity measurements for lifetime determination the band-pass for excitation was 5 nm and for emission band-path 5 nm at 475 nm wavelength. The excitation shutter was closed and the emission photons were counted at 0.1 sec intervals. The data were digitized and transferred to Excel (Microsoft) for analysis of exponential decay.

Absorbance spectra of vanillin (50 μ M) were collected in aqueous solution from 250 nm to 400 nm at 20°C. Luminescence emission spectra (fluorescence and phosphorescence) of vanillin in aqueous solution were collected at 20°C at 320 nm.

Phosphorescence of vanillin in amorphous sucrose were collected from 400 to 800 nm (10 nm bandwidth) using excitation at 320 nm (20 nm bandwidth) over the temperature range from –20°C to 100°C. Each data point was collected from a single flash with 0.2 ms delay, 100 ms gate time, and 0.12 s total decay time. Lifetime measurements were made as a function of temperature. The samples were excited at 320 nm (20 nm bandwidth) and emission transients collected at 490 nm (20 nm bandwidth) at

temperature ranging from -20°C to 100°C . Each decay was the average of 50 cycles, and for each cycle data was collected from a single flash with a delay of 0.2 ms, windows for gate time and total decay time were varied at each temperature. All measurements were made in quadruplicate.

Data Analysis

Emission Energy as a function of temperature: Emission spectra were fit using the program Igor (Wavemetrics, Inc., Lake Oswego, OR) to a log-normal function Equation 1 over the temperature range -20°C to 100°C .

$$I(\nu) = I_0 \exp \left\{ -\ln(2) \left(\frac{\ln[1 + 2b(\nu - \nu_p) / \Delta]}{b} \right)^2 \right\} \quad (1)$$

In this equation I_0 is the maximum intensity of the emission spectra, ν_p is the frequency (in cm^{-1}) of the emission maximum, Δ is a line width parameter, and b is an asymmetry parameter. The bandwidth of the emission, the full width at half maximum (Γ), is related to b and Δ Equation 2.

$$\Gamma = \Delta \left(\frac{\sinh(b)}{b} \right) \quad (2)$$

Photophysical Scheme: The phosphorescence intensity decays were collected as described above and were fitted using a multi-exponential functions (Chen, 2003; Shamblin et al., 2000). The multi-exponential model is as show in Equation 3. τ_i are decay times, α_i represent the amplitudes of the components at $t = 0$ and n is the number of decay times. Phosphorescence lifetimes were determined with the statistical program Igor (Wavemetrics, Inc., Lake Oswego, OR). Fits were judged satisfactory if the R^2 values

were in the range of 0.995-1.0 and the modified residuals $((\text{data} - \text{fit})/\text{data}^{1/2})$ varied randomly about zero. The average lifetime was calculated using Equation 4.

$$I(t) = \sum_{i=1}^n \alpha_i \exp(-t/\tau_i) \quad (3)$$

$$\tau_{\text{Avg}} = \sum_{i=1}^n \alpha_i \tau_i / \sum_{i=1}^n \alpha_i \quad (4)$$

The phosphorescence lifetimes were used to calculate the rate constants associated with the various processes that depopulate the excited triplet state. The lifetime τ is related to the rate constants for de-excitation of the triplet excited state of the probe according to the following Equation 5 (Papp and Vanderkooi, 1989).

$$1/\tau = k_{\text{RP}} + k_{\text{NR}}(T) + k_{\text{Q}}[\text{O}_2] = k_{\text{P}} \quad (5)$$

Here $k_{\text{P}} (=1/\tau)$ is the total decay rate, k_{RP} is the rate of radiative decay of the ground state (2.69 s^{-1} , measured in this study), k_{NR} is the rate of non-radiative decay to the singlet state followed by vibrational relaxation to S_0 due to collisional quenching. The magnitude of k_{NR} reflects factors associated with the mechanism by which the excited T_1 state of methyl vanillin is coupled to highly excited vibrations of the S_0 ground state as well as external factors associated with the mechanism by which the ground state vibrational energy can dissipate from the excited state into the surrounding matrix (Fischer et al., 2002; Vanderkooi and Berger, 1989). As the efficiency of external vibrational dissipation

is related to overall mobility of the matrix, the magnitude of k_{NR} provides a measure of matrix mobility. One common method for restricting the collisional deactivation is to super cool analyte solutions with liquid nitrogen to a rigid glass. The term $k_Q [O_2]$ refers to the collisional quenching due to interaction between the excited chromophore and triplet state oxygen.

Results

Luminescence Emission Spectra: Figure 1b shows the absorption spectra of vanillin at room temperature in aqueous solution and in amorphous sucrose film. The excitation spectrum for vanillin phosphorescence at 490 nm in amorphous sucrose film is shown in Figure 1c. Vanillin shows room temperature phosphorescence (RTP) when embedded in amorphous sucrose matrix. The delayed emission spectra from vanillin in amorphous sucrose show a phosphorescence band at longer wavelength corresponding to $S_0 \leftarrow T_1$ transitions.

Vanillin phosphorescence emission spectra appear with maximum at ~490 nm. Vanillin phosphorescence was found to be temperature dependent (Figure 2) over the temperature range from -20°C to 100°C in amorphous sucrose films. The decrease in phosphorescence intensity with increasing temperature results from a thermally stimulated process (Parker, 1968). The normalized phosphorescence intensity plot is shown in Figure 3. The Arrhenius plot of inverse phosphorescence intensity ($1/I_p$) is shown in Figure 4. I_p was determined by fitting the phosphorescence emission spectra to a log-normal function. This plot exhibited a triphasic decrease in phosphorescence intensity as the temperature increased. The plot was nonlinear displaying upward curvature. Break point temperatures determined from intersection of trendline to points at low, intermediate and high temperature were estimated to be about ~40°C and ~80°C (Figure 4). The activation energies for phosphorescence quenching calculated from the slopes at low, intermediate and high temperatures were 7.8 kJ mol⁻¹, 54.0 kJ mol⁻¹ and 93.7 kJ mol⁻¹ respectively. The slope at low temperature is ~12 times smaller than the

slope at higher temperature for amorphous sucrose, indicating high sensitivity of the matrix to temperature. The break point is around $\sim 20^{\circ}\text{C}$ below the glass transition temperature for sucrose. The decrease in phosphorescence intensity (with temperature) is due to an increase in k_{NR} . This decrease in the glass and in the melt indicates the presence of mobility both below and above T_g .

The emission energy (ν_p) and bandwidth (Γ) were determined by fitting the phosphorescence emission spectra to a log-normal function (equation 1, Materials and Methods). The values of the emission energy and bandwidth as a function of temperature are shown in Figure 5a. There was a gradual, linear decrease in the emission energy at low temperature (-20°C to 40°C) followed by steeper decrease at higher temperatures. The decrease in emission energy indicates an increase in the average extent of matrix dipolar relaxation around the excited triplet state. A break point temperature determined from intersection of trendline to points at low and high temperature was estimated to be about $\sim 40^{\circ}\text{C}$ (Figure 5b). The phosphorescence bandwidth (equation 2, Materials and Methods) increased gradually at low temperature in the glass and then increased at higher temperature in the melt, reflecting a large increase in the range of energetically distinct matrix environments in amorphous sucrose below and above T_g (Figure 5a). The bandwidth increased linearly and gradually with temperature up to $\sim 50^{\circ}\text{C}$ (Figure 5c) and quiet dramatically at higher temperatures about T_g (65°C).

Phosphorescence Intensity Decays: Vanillin phosphorescence decay kinetics were studied as a function of temperature in the absence of oxygen. Decay of the

phosphorescence intensity of vanillin at 77K in degassed glycerol water and EPA are shown in Figure 6a and for amorphous sucrose films is shown in Figure 6b. These decays were fitted to single exponential functions and the lifetimes obtained are compiled in the Table 1. The lifetime at 77K in glycerol water ($\tau = 372$ ms) was used to calculate k_{RP} , because glycerol water represents the amorphous sucrose structure.

Time-resolved phosphorescence intensity decays of vanillin in amorphous sucrose films were measured over the temperature range from -20°C to 100°C . The decay intensity was fitted using both stretched and multi-exponential functions, but the best fit was obtained with a four-exponential function. Fits were judged satisfactory if the modified residuals $((\text{data} - \text{fit})/\text{data}^{1/2})$ varied randomly about zero. The phosphorescence intensity decay of vanillin in amorphous sucrose film at 20°C in the presence of nitrogen is plotted in Figure 7 along with the modified residuals for a fit using a four component multi-exponential function (equation 3, Materials and Methods).

All intensity decays over the temperature interval from -20°C to 80°C were well fit using a four-exponential function and those at 90°C and 100°C were well fit using a two-exponential function. This analysis indicated that the probe had multiple lifetimes in the amorphous sucrose matrix at all temperatures. The phosphorescence lifetime decreased with increasing temperature indicating an increase in the triplet state quenching rates with temperature; the results of these analyses are plotted in Figure 7a. The four lifetimes were 184.4 ms, 76.7 ms, 18.2 ms and 2.6 ms at 20°C , thus demonstrating the presence of local environments with ~ 70 fold differences in mobility. The decrease in lifetime as a function

of temperature was dramatic both below and above T_g , indicating the presence of a range of molecular motions both below and above T_g . The plot of the amplitudes of each lifetime component as a function of temperature is as shown in Figure 8. The amplitudes of longer lifetime components (τ_1, τ_2) a_1 and a_2 decreased and that of shorter lifetime components (τ_3, τ_4) a_3 and a_4 increased as a function of temperature.

The average lifetime (calculated using eq. 4, Material and Methods) is shown in Figure 9a as a function of temperature. The average lifetime varied from 156.4 ms at -20°C to 0.5 ms at 100°C , indicating an ~ 300 -fold difference in mobility. For vanillin the decrease in lifetime as a function of temperature corresponds to an increase with temperature in the non-radiative decay process k_{NR} (eq. 5, Materials and Methods). The average lifetime as a function of $T-T_g$ showed that the lifetime decreased dramatically in the glass and melt state (Figure 9b). The non-radiative decay rate k_{NR} reflects the sum of all collisional interactions between the matrixes and the probe and is sensitive to the molecular environment. An Arrhenius plot of k_p calculated from the average lifetime is shown in Figure 10. The plot was nonlinear displaying upward curvature. Break point temperatures determined from intersection of trendline to points at low and high temperature were estimated to be about $\sim 40^\circ\text{C}$. The activation energies calculated from the slopes at low and high temperatures were 9.64 kJ mol^{-1} and 74.1 kJ mol^{-1} respectively. Arrhenius plots of k_p for individual lifetime components are shown in Figure 11. The break point temperatures (Figure 12a-12d) determined from intersection of trendline to points at low and high temperature and the activation energies for individual lifetime component are compiled in Table 2. The longest lifetime component (τ_1) showed transition temperatures

of 60°C with activation energies at low and high temperatures of 4.1 kJ mol⁻¹ and 110.0 kJ mol⁻¹, respectively (Figure 12a). The second longest lifetime component showed transition temperatures of 55°C with activation energies at low and high temperature of 9.6 kJ mol⁻¹ and 112 kJ mol⁻¹, respectively (Figure 12b). The shortest lifetime component showed single transition temperature at 42°C with activation energies at low and high temperature as 13.6 kJ mol⁻¹ and 49.03 kJ mol⁻¹ respectively (Figure 12c). The second shortest lifetime component showed single transition temperature of 50°C with activation energies at low and high temperature as 11.3 kJ mol⁻¹ and 68.2 kJ mol⁻¹ respectively (Figure 12d). The two longer lifetime components exhibited triphasic behavior as a function of temperature whereas the two shorter lifetime components showed biphasic behavior.

Data for sample with probe: sucrose ratio of 3:10⁴, 5:10⁴, 1:10³ and 2:10³ were compared. There was no effect observed with change in probe concentration.

Photophysical rate constants: Analysis of lifetimes in terms of the underlying photophysical rate constant for de-excitation of the triplet state provides additional insights into the effect of temperature on matrix mobility in amorphous sucrose films. The k_{NR} term is a rate constant for non-radiative decay; it is the actual measure of the effect of the motions that quenches probes excited triplet state and was obtained from eq. 5. The magnitude of k_{NR} reflects the internal and external factors associated with the mechanism by which the excited T₁ state of vanillin is coupled to highly excited vibrational states of the S₀ ground state as well as external factors associated with the

mechanisms by which the ground state vibrational energy can dissipate from the excited probe into the surrounding matrix (Fischer et al., 2002; Vanderkooi and Berger, 1989). The efficiency of this vibrational dissipation is related to the overall mobility of the matrix, and hence the magnitude of k_{NR} provides a measure of molecular mobility.

The k_{NR} values were calculated by subtracting the radiative decay rate ($1/\tau = 2.69 \text{ s}^{-1}$ at 77K from vanillin lifetime in glycerol: water) from the inverse of the lifetime. A plot of k_{NR} as a function of temperature is represented in Figure 13a. An Arrhenius plot of k_{NR} is as shown in Figure 13b. Break point temperatures determined from intersection of trendline to points at low and high temperature were estimated to be about $\sim 40^\circ\text{C}$ (Figure 13b). The activation energies calculated from the slopes at low, intermediate and high temperatures were 13.8 kJ mol^{-1} and 72.3 kJ mol^{-1} , respectively. These are the activation energies of the motions which quench vanillin's excited triplet state. The non-radiative quenching rate varied almost ~ 500 -fold from -20°C ($k_{\text{NR}} = 3.7 \pm 0.5$) to 100°C ($k_{\text{NR}} = 1893.3 \pm 100$). This analysis thus suggests that sucrose glass is mobile below T_g and this mobility is enhanced as a function of temperature. The non-radiative decay rate k_{NR} for individual lifetime component is shown in Figure 14a. An Arrhenius plot of k_{NR} calculated from the individual lifetime component is shown in Figure 14b.

Discussion

Vanillin phosphorescence provides a long-lived optical signal whose lifetime and quantum yield are sensitive to the local environment. Vanillin phosphorescence provides insight into the solid-state luminescence of amorphous sucrose. Phosphorescence emission spectra and time-resolved intensity decays, measured in sucrose as a function of temperature in the absence of oxygen, were strongly modulated by matrix molecular mobility. The two important measurements, emission spectra and emission intensity decay with time, are modulated by matrix molecular mobility. Temperature had a large effect on vanillin phosphorescence intensity and lifetime both in the glass and in the melt.

Matrix Mobility: Emission energy (inverse of wavelength) reveals the solvent dipolar relaxation around the excited triplet state. Dipolar relaxation modulates the excited state energy because matrix molecules reorient around the excited probe molecules and lower the energy by stabilizing the excited state. The rate of relaxation is facilitated by temperature. Dipolar relaxation causes the vanillin phosphorescence spectra to red shift, i.e., lower energy. The emission energy decreased with increase in temperature. The peak frequency of the phosphorescence emission decreased $\sim 947\text{ cm}^{-1}$ over a temperature range from -20°C to 100°C . At low temperatures the rate of dipolar relaxation, due to slower molecular motions in the non equilibrium solvent shells, is low, and so emission energy is higher. But as the temperature increases the rates of dipolar relaxation increases causing a decrease in emission energy.

Temperature had a large effect on the emission energy of vanillin in the glass and at T_g in the melt. The glass transition temperature of sucrose is reported to $\sim 65^\circ\text{C}$ (Roos, 1993). The emission energy decreased gradually below and drastically above T_g with temperature, due to activation of translational motion corresponding to α -relaxation. Such behavior has also been reported in amorphous sucrose using erythrosin B as a triplet state probe (Pravinata et al., 2005). However in case of vanillin the decrease in emission energy showed a transition temperature of $\sim 40^\circ\text{C}$, which is $\sim 20^\circ\text{C}$ below T_g (65°C) of sucrose, which could be attributed to high sensitivity of vanillin. As vanillin has longer lifetime ($\tau_{77\text{K}} = 372$ ms) whereas erythrosin B has much shorter lifetime ($\tau_{77\text{K}} = 24.3$ ms (Duchowicz et al, 1998) it gives a longer time window for vanillin to see longer relaxation processes. Thus vanillin as a triplet state probe indicates that the amorphous sucrose matrix gains mobility much below T_g of sucrose.

The FWHM is a measure of width of the peak at half of the peak height and tells us about site heterogeneity within the matrix. The increase in FWHM indicated increase in inhomogeneous broadening indicating that there is a corresponding increase in the range of energetically distinct matrix environments in amorphous sucrose. This increase was gradual at low temperatures and increased with increasing temperature indicating that the increase in dipolar relaxation rate was accompanied by an increase in the width of the distribution of energetically distinct environments. Similar trends have been observed in amorphous sucrose (Pravinata et al., 2005), maltose and maltitol (Shirke and Ludescher, 2006) and lactose and lactitol (Shirke and Ludescher, 2006) around their glass transition temperature. Amorphous solids show dynamic heterogeneity and exhibit a range of

structural features due to local differences in packing density (Ediger et al., 1996; Sillescu, 1999). Sillescu, (1999) has extensively reviewed existence of heterogeneity in glass forming liquids and polymers, by compiling different experimental techniques like NMR, dielectric and optical experiments which indicate the presence of dynamical heterogeneity (Sillescu 1999; Richert, 1997, 2001) both through space and time: the molecular mobility in the amorphous matrix could differ significantly at any given time, while the molecular mobility can fluctuate significantly through time at any give site. Amorphous solids due to heterogeneous nature may have distinct regions (high density or low density) and show different relaxation times (Liu et al., 2006; Shamblin et al., 1999). It has been shown using phosphorescence spectroscopy that in these amorphous solids different sites vary in overall molecular mobility indicating the presence of dynamic heterogeneity (Simon-Lukasik K and Ludescher, 2006a, 2006b: Shirke and Ludescher, 2005; Shirke and Ludescher 2006a, 2006b; Pravinata et al., 2005; Nack and Ludescher, 2006). The increase in bandwidth showed a transition temperature of $\sim 55^{\circ}\text{C}$, 10°C below T_g (65°C) of sucrose.

Time-resolved phosphorescence intensity decays from vanillin were multiexponential both below and above the glass transition temperature, indicating that the pure (single component) amorphous matrix was dynamically heterogeneous on the molecular level. These data show that vanillin is a promising probe to measure molecular mobility and dynamic heterogeneity in amorphous solid foods, indicating how an intrinsic component like a flavor compound can be used to report on the molecular mobility in foods. Vanillin lifetime data show local environment in amorphous sucrose to be extremely variable.

Vanillin was found to be sensitive to molecular changes below and above T_g of sucrose as seen from the lifetime data.

In a complex amorphous matrix, there may be several different environments and hence several different lifetimes of the triplet probe. The four lifetime components of vanillin in amorphous sucrose films were $\tau_1 = 186.4$ ms, $\tau_2 = 76.7$ ms, $\tau_3 = 18.8$ ms, and $\tau_4 = 2.6$ ms at 20°C, thus demonstrating the presence of local environments with ~70 fold differences in mobility. The different lifetimes observed are due to different locations of the probes in different environments in the amorphous sucrose matrix that differ in molecular mobility. The two longer lifetime component τ_1 and τ_2 indicate that about 68% of the probes are located in the less mobile environment at 20°C, and the two shorter lifetime components τ_3 and τ_4 indicate that about 32%, of the probes are located in the more mobile environments

This is in agreement with the previous studies reported in the literature. Previous studies have been conducted where phosphorescence from the luminescent chromophores tryptophan (McCaul and Ludescher, 1999), N-acetyltryptophanamide (NATA) (Shah and Ludescher 1995) and erythrosin B (Ery B) (Shah and Ludescher, 1995; Pravinata 2003), was used to probe the molecular dynamics of the glassy state and the glass-to-rubber transition in amorphous sucrose. Tryptophan and four halogenated tryptophan analogs dispersed in freeze-dried sucrose showed three phosphorescence lifetimes ranging from about 10ms to over 1s in glassy sucrose at 20°C. Time-resolved phosphorescence intensity decays from NATA and Erythrosin B were multiexponential both above and

below the glass transition temperature, indicating that the sucrose matrix is heterogeneous on the molecular level. Another xanthene dye, Eosin Y, incorporated in sucrose film also provided similar information about molecular mobility and site heterogeneity (Pravinata et al., 2005).

Vanillin exhibited multiple phosphorescence lifetimes in the sucrose glass. The lifetime data of vanillin in amorphous sucrose indicate that the glassy state is a dynamically heterogeneous state and so is the melt state. Temperature had a large effect on the phosphorescence lifetime of vanillin both below T_g in the glass and above T_g in the melt. The phosphorescence lifetime decreased drastically below and above T_g with temperature, due to an increase in the ability of the excited vanillin to dissipate vibrational energy into the matrix. This dissipation is facilitated by β -relaxation (corresponding to more localized motions) below T_g and α -relaxation above T_g (corresponding to translation or rotational motion).

Dipolar relaxation originates from dipolar groups like hydroxyl groups in sucrose (Stratt and Maroncelli, 1996), and reflects mobility of sugars hydroxyl groups. In glass, solvent relaxation is slow because molecular mobility is slow whereas in melt the solvent relaxation is fast due to increase in molecular mobility. In glasses due to slow motions of molecules the relaxation times are longer compared to rubber/melt where molecules are moving faster, relaxation time vary from $>10^8$ s in glass to 10^{-9} s in melt, such increase is associated with reduction of translational and rotational motions of molecules (Hill et al, 2005).

In sugars two relaxation processes have been reported (Moran et al., 2000; Gangasharan and Murthy., 1993; Chan et al., 1986; Tombari et al., 2001; Noel et al., 1996; Gangasharan and Murthy., 1995; Champion et al., 2003; Kaminski et al 2008). These relaxation processes are classified α , β , γ etc., in amorphous sucrose (Kaminski K et al., 2008). The glass transition marks the onset of the structural α -relaxation (slower). Below the normal T_g amorphous or partially crystalline polymers also exhibit secondary relaxations (faster). These are given by β , γ etc in decreasing order of occurrence. These sub T_g relaxations have amplitudes smaller than the α relaxations associated with major backbone chain movement (i.e. the primary glass transition). The existence of secondary relaxations is indicative of mobility at temperatures below T_g . The α relaxation is the slowest relaxation process related to loss of translational motion (Ediger et al., 1996, Noel et al., 1996). This structural relaxation is arrested at the T_g (Moran et al., 2000). The α -relaxation above T_g involves motions due to local rotation of $-\text{OH}$ group or even rotation of the entire molecules.

Secondary relaxation process β occurs at sub- T_g temperatures. There have been many different interpretations for origins of secondary relaxation suggesting they occur due to segmental rotation of the linear chain of the monosugars (Gangasharan and Murthy., 1995) intra and intermolecular interactions (Champion et al., 2003), rotation of the hydroxymethyl groups attached to the sugar ring (Noel et al., 1996). The slow β process (also called Johari-Goldstein process) is also thought to occur from motion of the entire molecules (Kaminski et al., 2006). Studies suggest that this process may be dependent on

structural factors such as the size of the molecule. The fast β process is thought to occur because of anharmonic cage rattling i.e. complex vibrational motions. The physical reason or origin of a particular secondary relaxation however remains unclear. The faster γ processes is considered to be local motion involving intramolecular degrees of freedom, originating from the hydrogen bonding.

At high temperature translational mobility becomes activated and glass transition occurs (Champion et al., 2000; Zallen, 1998). In amorphous sucrose, glass to liquid transition, molecular mobility is presented as α relaxation in the T_g zone. The α relaxation corresponds to translational and rotational motion of molecules that support flow in the melt. As temperature is lowered below T_g molecular mobility is presented as β and γ relaxations also called secondary relaxations (Ediger et al., 1996; Hancock and Zografi, 1997; Vyazovkin and Dranca, 2006) (19: 2008 paper). In the glass the local vibrational and rotational motions help hydroxyl groups reorient around the probe molecules. The sub- T_g relaxations (β, γ) have been reported in amorphous sucrose due to localized motions (Le Meste et al., 2002; Wagner and Richert, 1998, 1999). A recent study by Kaminski et al in addition to commonly observed primary and secondary relaxation, have reported presence of slower secondary relaxation lying in between the two (Kaminski et al., 2008). The β relaxation in sucrose is considered to be the universal Johari-Goldstein. β relaxation observed in other sugars too (Ngai and Paluch, 2004; Johari and Goldstein, 1970; Ngai, 1998; 2003; Ngai et al., 2006; Capaccioli et al., 2006; Bohmer et al., 2006, Kaminski et al., 2006), which involves rotation of both monosaccharide (glucose and fructose) rings and is coupled with possible translational motion of the entire molecule

(Poppe and Van Halbeek, 1992). The rotation of the two rings round each other is also considered to be one of possibility of β relaxation in sucrose. The γ relaxation is being found to be result of internal motion (backbone rotation) within the monosaccharide (glucose and fructose) presence in the sucrose.

The Arrhenius plot of $\ln k_p$ for average lifetime showed transition temperature of $\sim 40^\circ\text{C}$, $\sim 20^\circ\text{C}$ below T_g (65°C) of sucrose. The k_{NR} increases gradually in the glass and much more dramatically in the melt, indicating that the non-radiative quenching rate can sense the molecular mobility activated below and at the glass transition. Compared to α relaxation with higher activation energy ($E_a = 72.4 \text{ kJ mol}^{-1}$) which is usually associated with the cooperative global translational motion of the matrix molecules, β relaxation is a secondary relaxation which requires less activation energy ($E_a = 13.8 \text{ kJ mol}^{-1}$) (Champion et al., 2003).

As vanillin has longer lifetime ($\tau_{77K} = 372 \text{ ms}$) it gives a longer time window to vanillin to see longer relaxation processes. All the spectroscopic measures of molecular mobility in amorphous sucrose films using vanillin as a triplet state probe, emission intensity, emission energy, and emission lifetime, indicate presence of transition points in sucrose films at $\sim 40^\circ\text{C}$. The bandwidth indicated presence of break point at $\sim 55^\circ\text{C}$. In sucrose (using dielectric spectroscopy) three relaxation processes have being reported at temperatures 126°C to 74°C (α -relaxation), 72°C to 12°C (β -relaxation) and 6°C to -145°C (γ -relaxation) (Kaminski et al., 2008).

Thus vanillin as a triplet state probe indicates that the amorphous sucrose matrix gain mobility much below T_g of sucrose which is much enhanced at T_g . Vanillin thus provides a way to monitor the molecular dynamics of the sugar matrix in the glassy and the melt state. Vanillin does provide a very novel insight into the molecular dynamics of amorphous sucrose, indicating that the local environments are extremely variable not only in the melt state but also the glassy state. Vanillin is extremely sensitive molecular motions due to longer lifetime window.

In vanillin various conformations results from rotations of methoxyl group about the C-O bond here (Nishigaki et al., 1998). Conformation of vanillin is conserved during the photophysical processes due to the matrix stiffness, but as the matrix mobility changes, vanillin conformation changes which results in spectral changes due to rotation of methoxyl group. So we hypothesize that movement of methoxyl group could be sensitive to matrix mobility. The rotation of methoxyl group in glassy state could be well supported based on free volume theory (FVT). Free volume in an amorphous system is geometrically interpreted as a continuous network of lakes and channels which permits the diffusive motion of its molecules (Miller et al., 1997).

WLF (Williams-Landel-Ferry) and VTF (Vogel-Fulcher-Tamman-Hesse) commonly used equation to predict temperature dependence of viscosity for super cooled liquids. The free volume based WLF theory has been shown to be more applicable in predicting temperature dependent mechanical properties of amorphous materials (Oversteegen and

Roth, 2005; Kilburn et al 2006; Kasapis, 2008). FVT assumes that temperature dependence of viscosity is related to free volume (Dolittle, 1951). The FVT is based on change in volume expansion coefficient at glass transitions and assumes that molecular motions depend on the presence of holes or voids (Roos, 1995) and thus allowing the molecular movement to take place. These holes between molecules provide the free volume that is needed for molecular rearrangements. Our studies using different analogs of vanillin (Chapter III) supports this interpretation. Thus vanillin could also indicate increase in free volume in amorphous sucrose matrix as a function of temperature.

Conclusions

Characterization of vanillin luminescence (as triplet state probe) demonstrates that it can emit RTP in amorphous solids, which changes as a function of temperature. The peak energy, bandwidth and lifetime data suggest that it is sensitive to molecular mobility and can be used monitor molecular mobility in amorphous sucrose films. The decay of phosphorescence of vanillin in amorphous sucrose is strictly multi-exponential indicating presence of site dynamics. These properties warrant the application of vanillin phosphorescence intensity to probe μs -ms dynamics of amorphous solids in glass and in the melt. Also vanillin makes an excellent probe to study molecular mobility below T_g in the glassy state due to high sensitivity. Vanillin is able to detect mobility in the glass where β and γ relaxations have been reported. The variation in the four lifetime components of vanillin provide detailed information of site dynamics.

It's usage as a molecular probe opens a great potential where a component like a flavor compound can be used to report about molecular mobility in actual amorphous systems. Thus vanillin is a promising probe to measure molecular mobility and is highly sensitive due to longer lifetime.

Figure II-1a

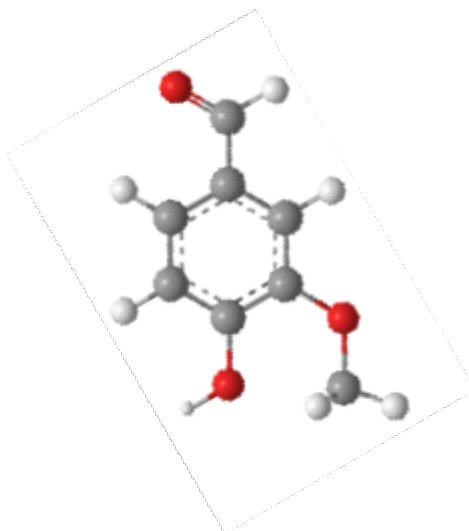


Figure II-1a: Structure of 4-hydroxy-3-methoxy-benzaldehyde (vanillin or methyl vanillin).

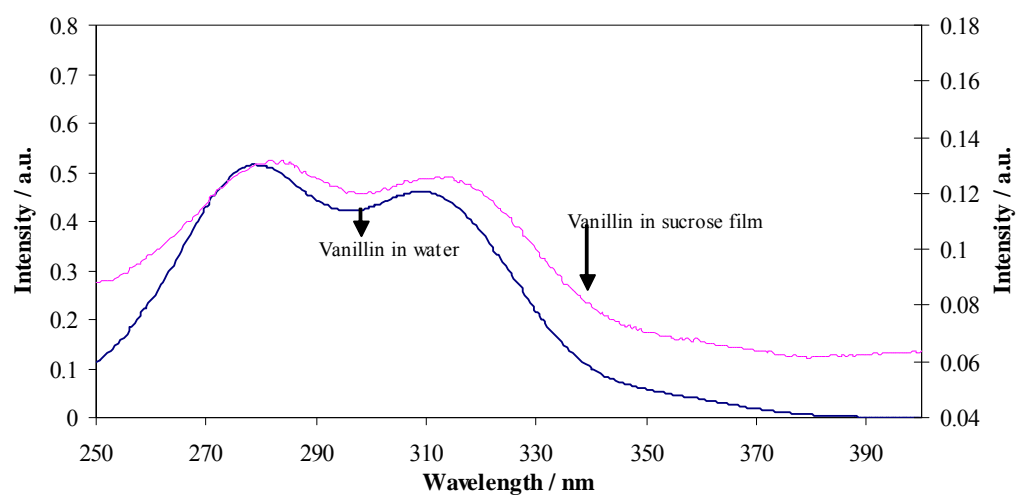
Figure II-1b

Figure II-1b: Absorption spectra of vanillin in aqueous solution (50 μ M) and amorphous sucrose (1:10³: dye: sucrose) at 20°C.

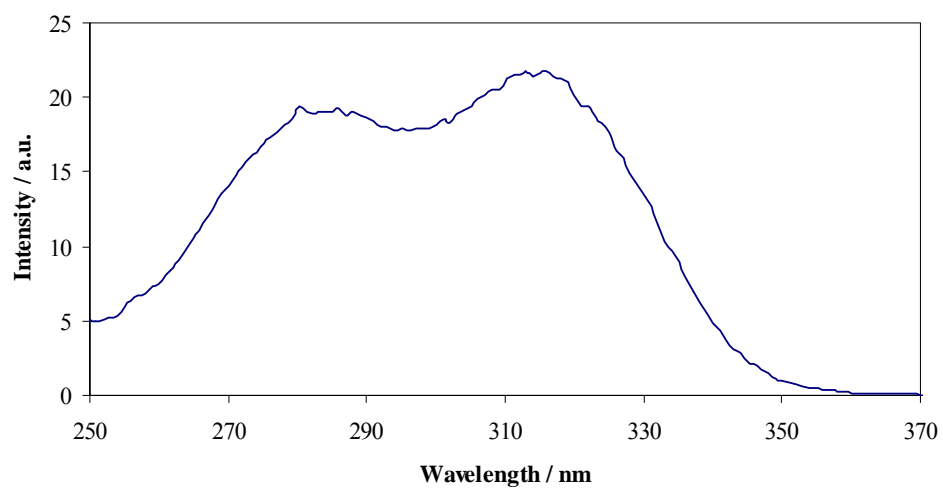
Figure II-1c

Figure II-1c: Excitation spectra for vanillin phosphorescence at 490 nm in amorphous sucrose ($1:10^3$: dye: sucrose) films ($-O_2$) at 20°C.

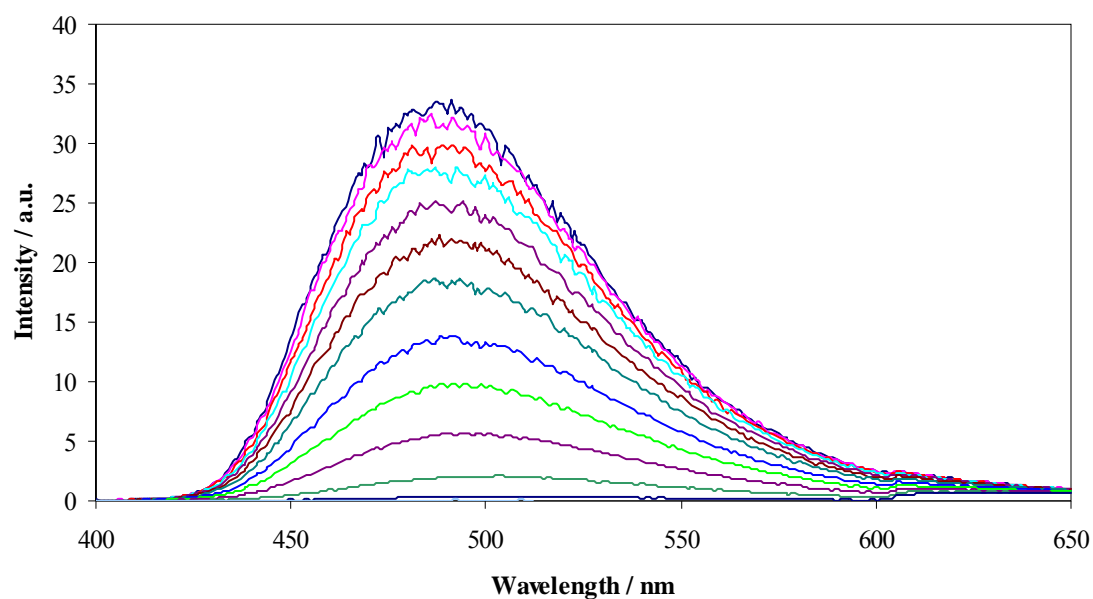
Figure II-2

Figure II-2: Delayed emission spectra of vanillin in amorphous sucrose films as a function of temperature (excitation at 320 nm). The spectra were collected at 10°C intervals from -20°C to 100°C (the curves follow this order from high to low intensity at ~490 nm).

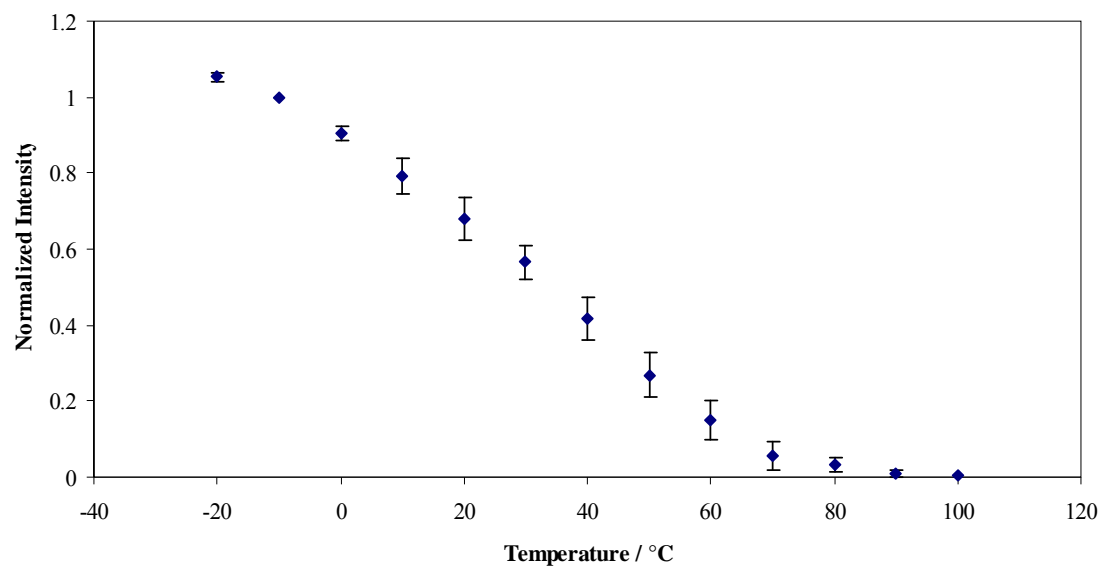
Figure II-3

Figure II-3: The effect of temperature on the phosphorescence emission intensity of vanillin in amorphous sucrose films as a function of temperature equilibrated against nitrogen. Intensity (I_P) was determined from analysis of the phosphorescence emission band (Figure 2) using a log-normal function (eq. (1), Materials and Methods).

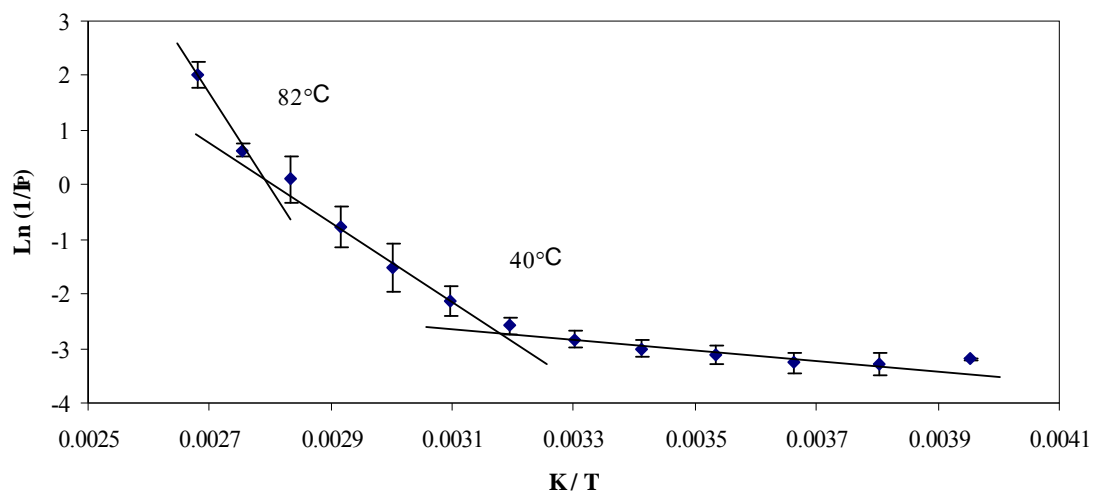
Figure II-4

Figure II-4: Arrhenius plot of the effect of temperature on the phosphorescence emission intensity I_P of vanillin in amorphous sucrose films. Lines drawn over the data points indicate slopes at low and high temperatures.

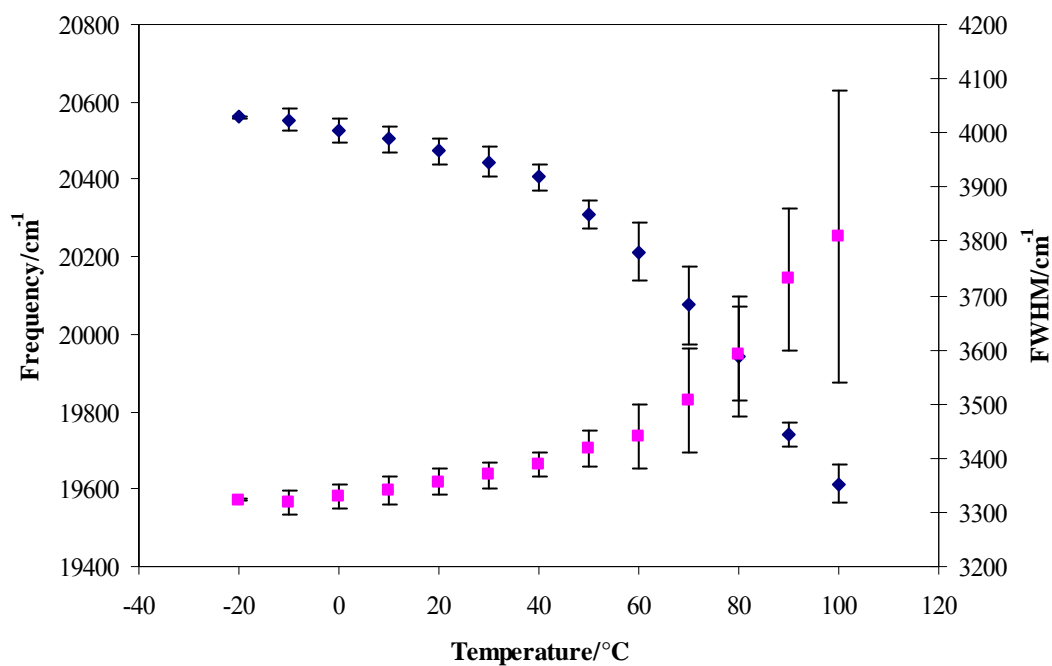
Figure II-5a

Figure II-5a: Peak energy ν_p (♦, left hand scale) and bandwidth (■, right hand scale) for phosphorescence emission from vanillin in amorphous sucrose films as a function of temperature. The delayed emission spectra collected as a function of temperature (Figure II-2) were analyzed using log-normal function.

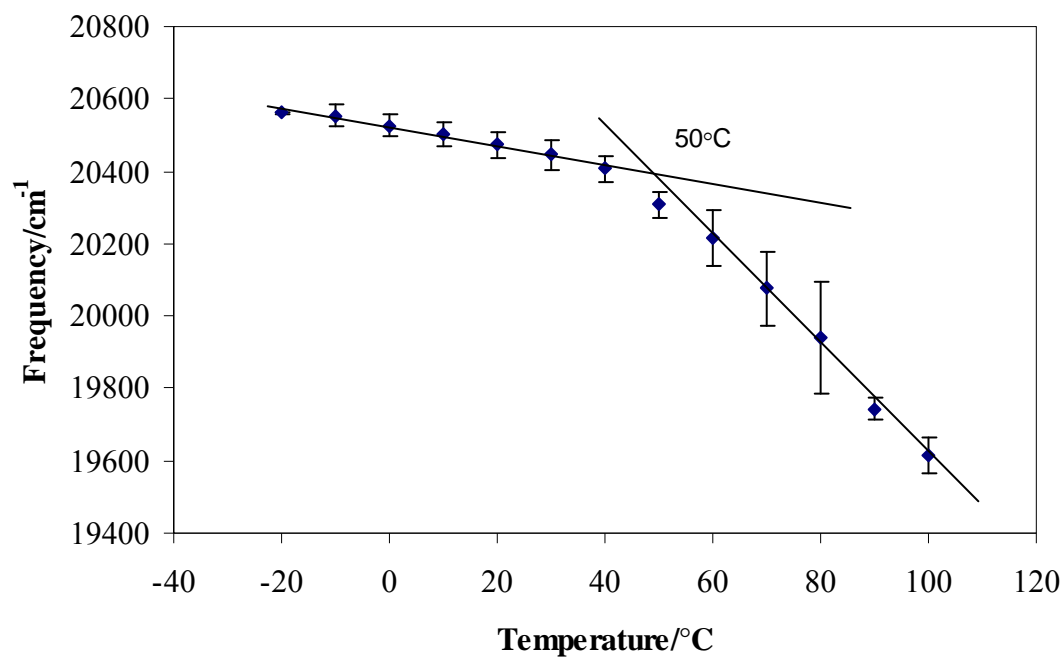
Figure II-5b

Figure II-5b: Peak frequency of phosphorescence emission spectra of vanillin in amorphous sucrose films plotted against temperature. Lines drawn over the data points indicate slopes at low and high temperatures.

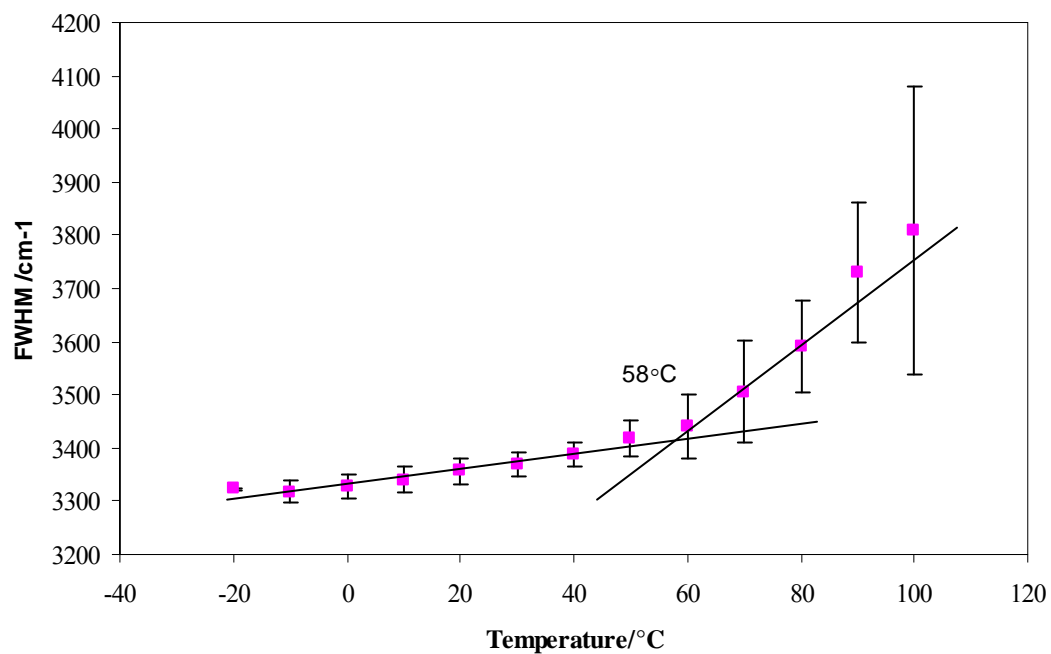
Figure II-5c

Figure II-5c: FWHM of phosphorescence emission spectra of vanillin in amorphous sucrose films plotted against temperature. Lines drawn over the data points indicate slopes at low and high temperatures.

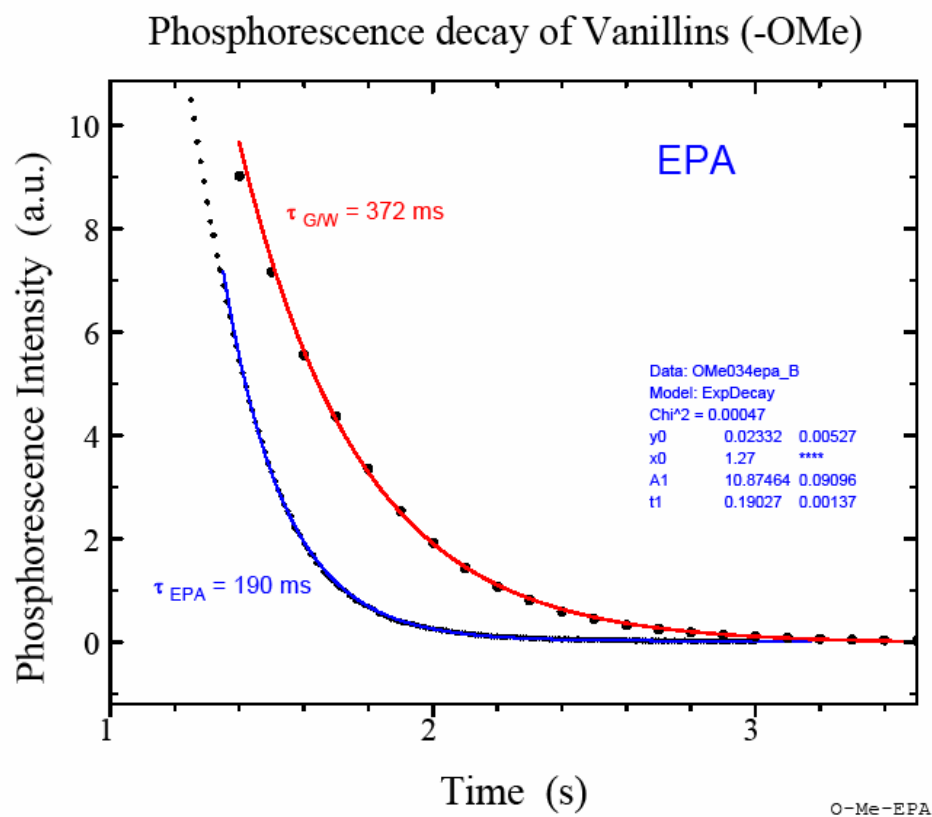
Figure II-6a

Figure II-6a: Decay of the phosphorescence intensity of vanillin in degassed glycerol water (6/4 v/v) and EPA at 77K, $\lambda_{\text{excitation}} = 350\text{nm}$, $\lambda_{\text{emission}} = 490\text{nm}$.

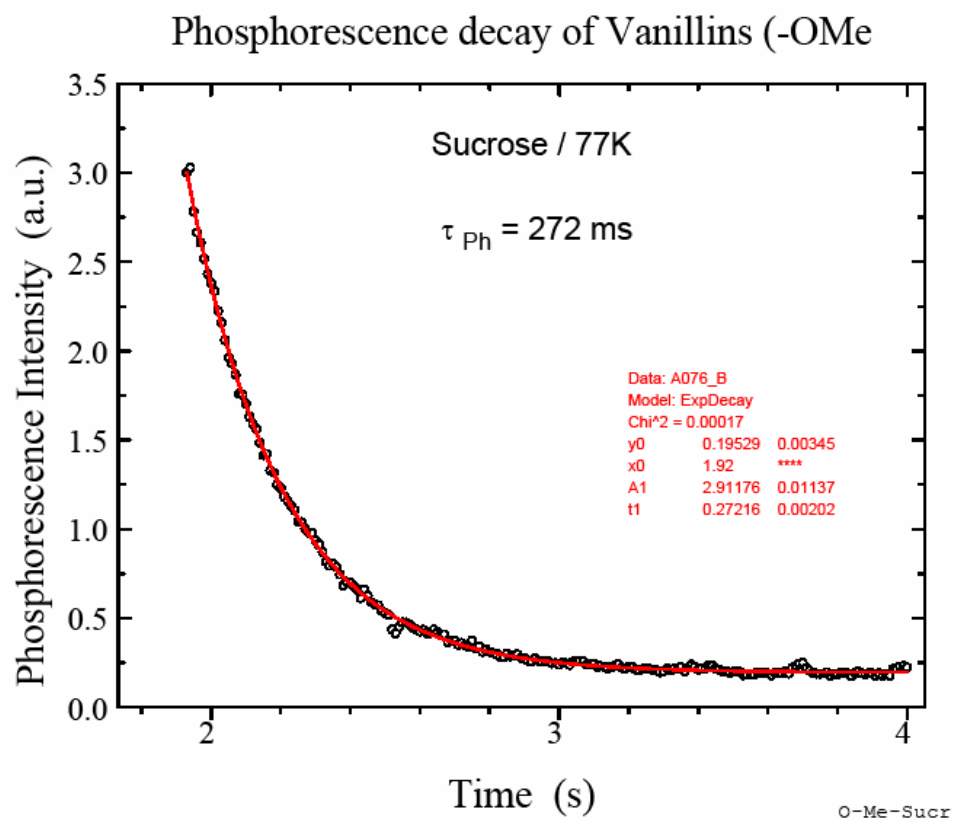
Figure II-6b

Figure II-6b: Decay of the phosphorescence intensity of vanillin in degassed amorphous sucrose (1:1000 vanillin: sucrose) film at 77K, $\lambda_{excitation} = 350\text{nm}$, $\lambda_{emission} = 490\text{nm}$.

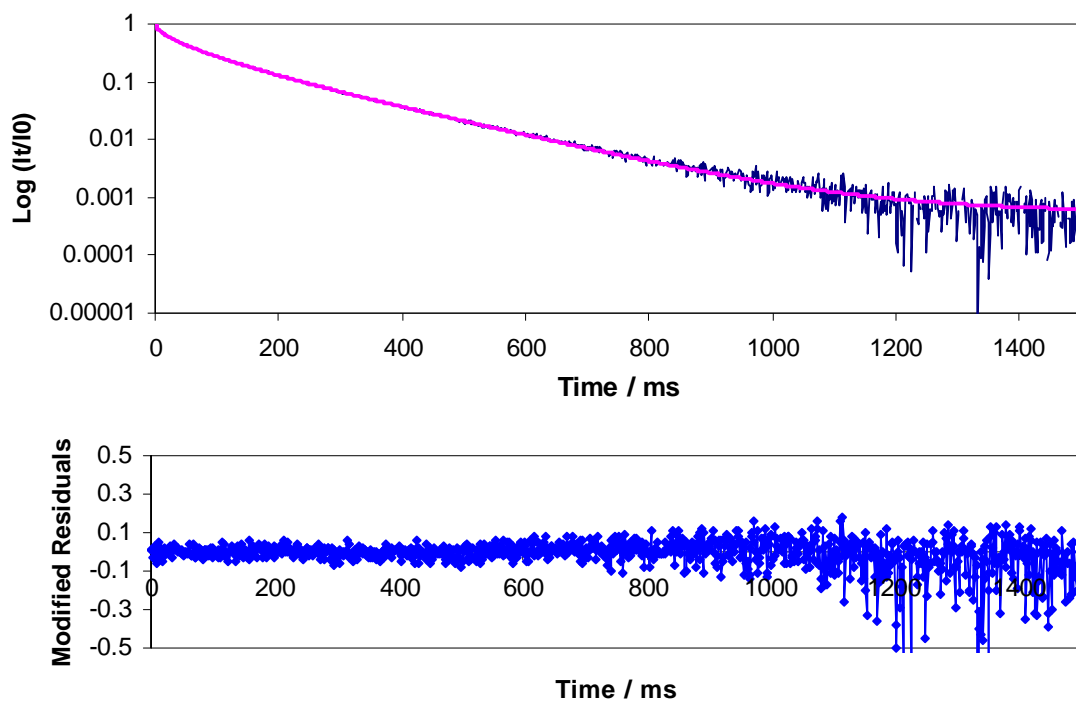
Figure II-7

Figure II-7: Normalized phosphorescence intensity decay $[I(t)/I(0)]$ of vanillin dispersed in amorphous sucrose film at 20°C in the presence of nitrogen (\diamond). The solid line through the data is a fit using a multi-exponential function. (b) A plot of modified residuals $[(\text{Data}-\text{Fit})/\text{Data}^{1/2}]$ for this fit.

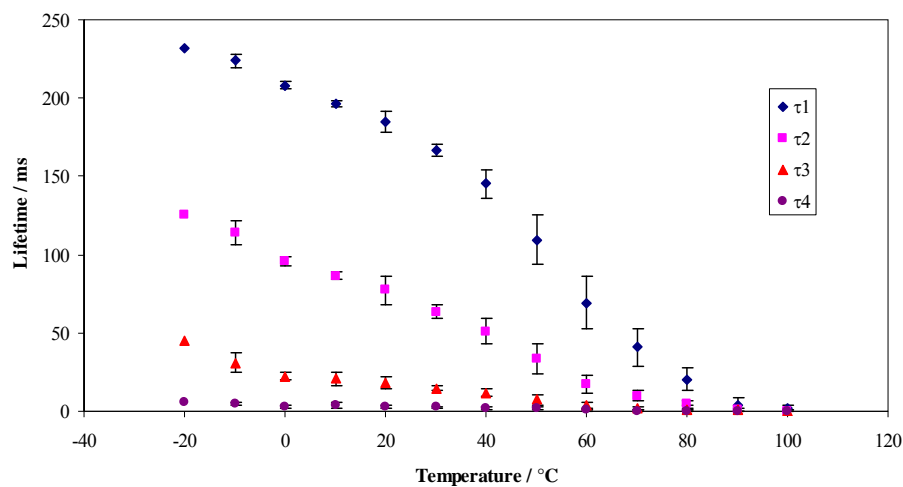
Figure II-7a

Figure II-7a: Lifetime components τ_1 (◆), τ_2 (■), τ_3 (▲), τ_4 (●) obtained from a multi-exponential model fit (Eq. (3), Materials and Methods) to phosphorescence intensity decay data from vanillin dispersed in amorphous sucrose films equilibrated against nitrogen as a function of temperature. The data was measured every 10°C from -20°C to 100°C.

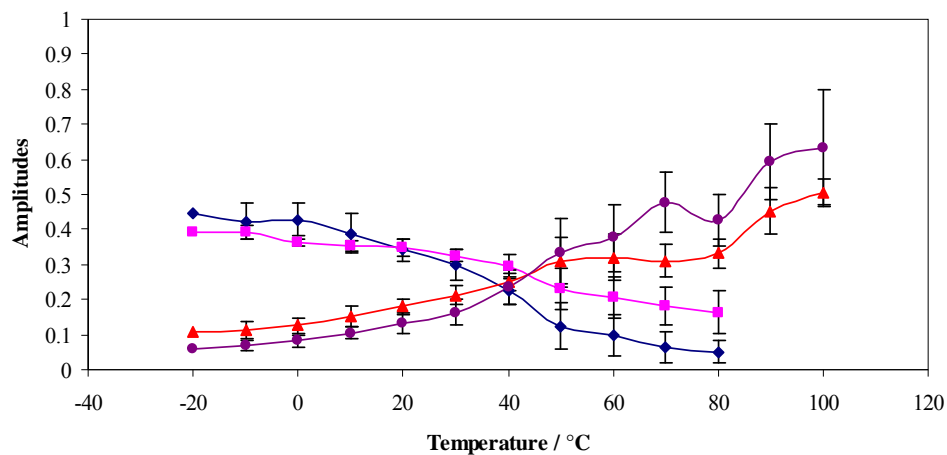
Figure II-8

Figure II-8: Intensity decay fit amplitudes for vanillin in amorphous sucrose films in nitrogen as a function of temperature. The data were calculated every 10°C from -20°C to 100°C. The amplitudes a_1 (♦) and a_2 (■) correspond to the longer life time components (τ_1 , τ_2), and a_3 (▲) and a_4 (●) correspond to the shorter lifetime components (τ_3 , τ_4). The amplitudes were obtained from a multi exponential model fit (Eq. (3), Materials and Methods) to phosphorescence intensity decay data from vanillin dispersed in amorphous sucrose films equilibrated against nitrogen as a function of temperature

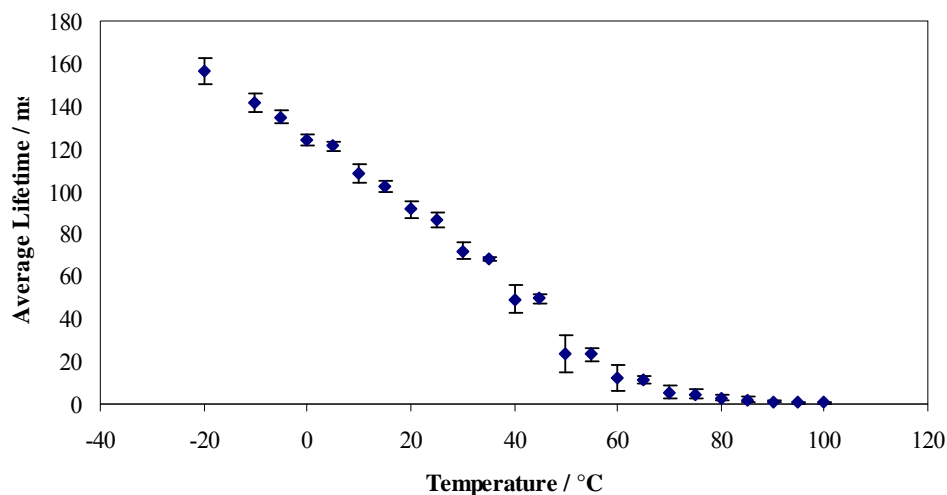
Figure II-9a

Figure II-9a: Average lifetime from a multi-exponential model fit (Eq. (4), Materials and Methods) to phosphorescence intensity decay data from vanillin dispersed in amorphous sucrose films equilibrated against nitrogen as a function of temperature. The data were calculated every 5°C from -20°C to 100°C.

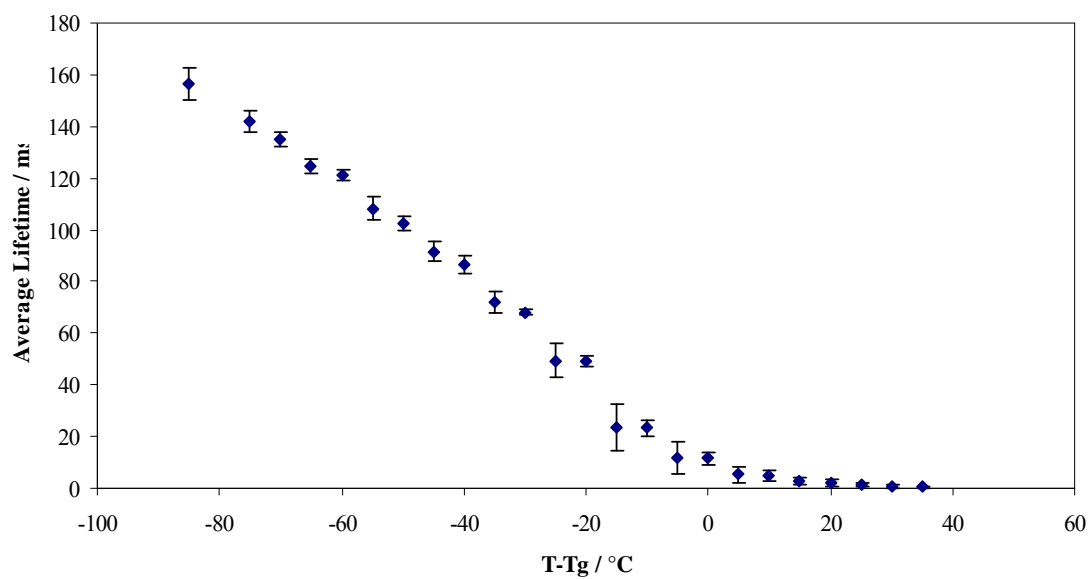
Figure II-9b

Figure II-9b: Average lifetime of vanillin dispersed in amorphous sucrose films equilibrated against nitrogen as a function of T-Tg. The data were calculated every 5°C from -20°C to 100°C. The Tg value used was 65°C.

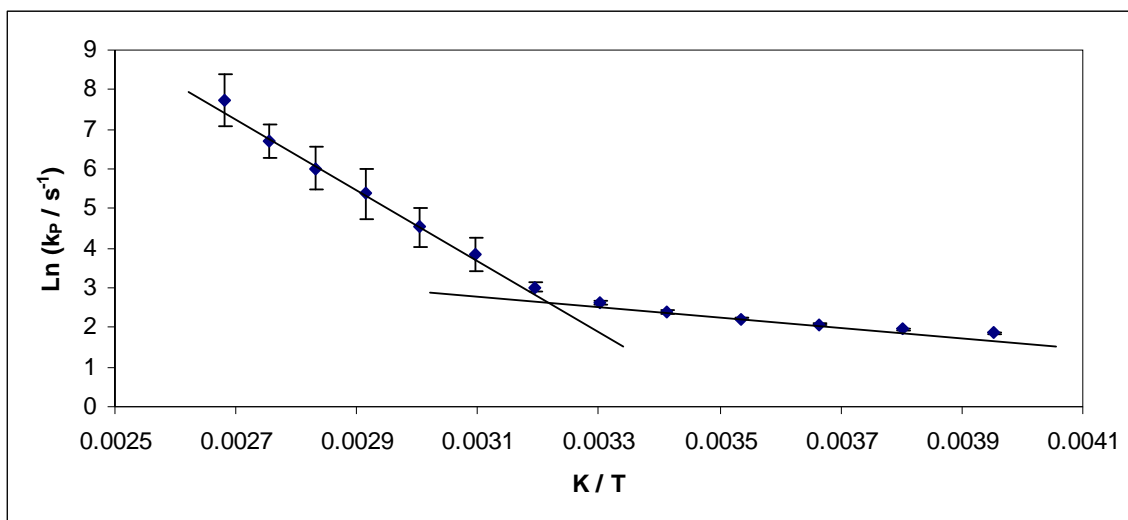
Figure II-10

Figure II-10: An Arrhenius plot of k_p calculated from the average lifetime of vanillin in amorphous sucrose.

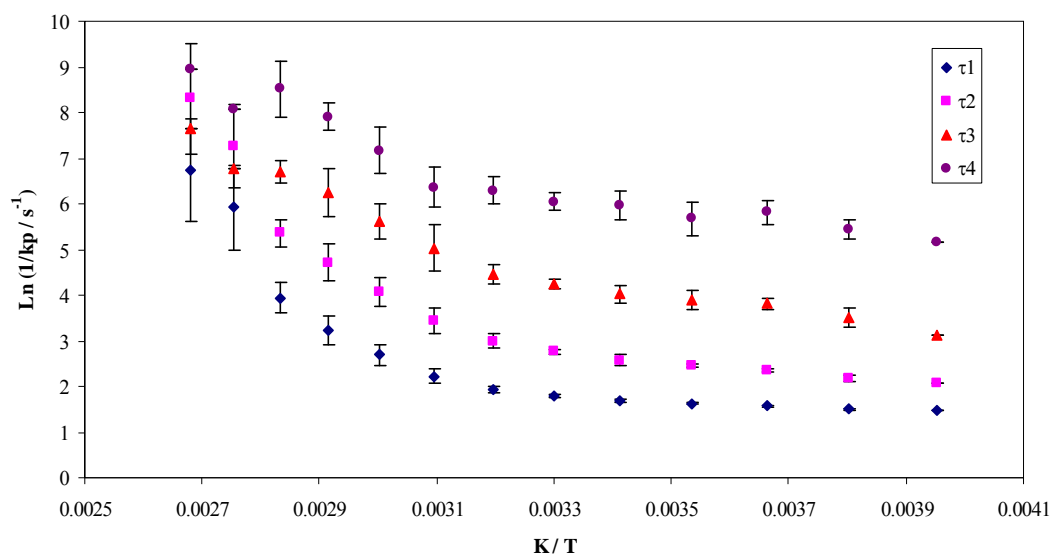
Figure II-11

Figure II-11: An Arrhenius plot of k_p calculated from the individual lifetime components τ_1 (◆), τ_2 (■), τ_3 (▲) and τ_4 (●).

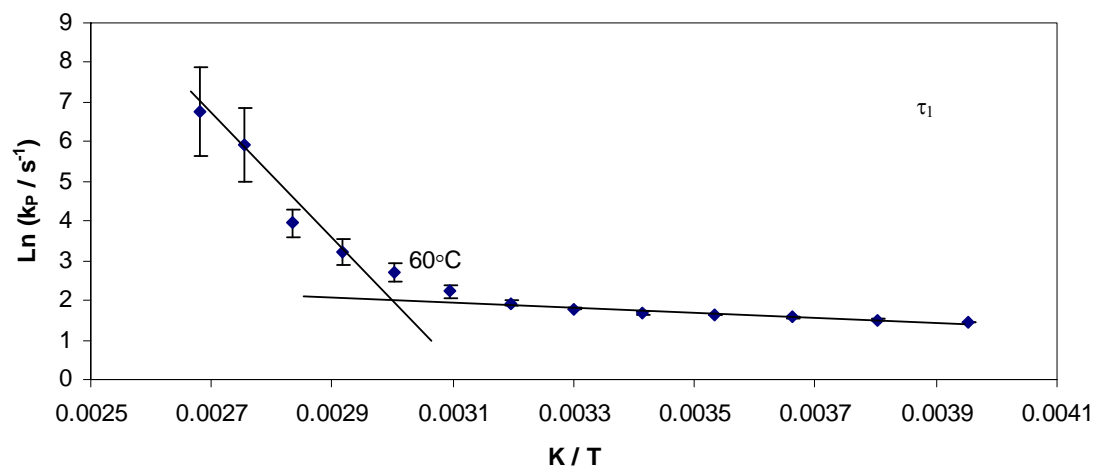
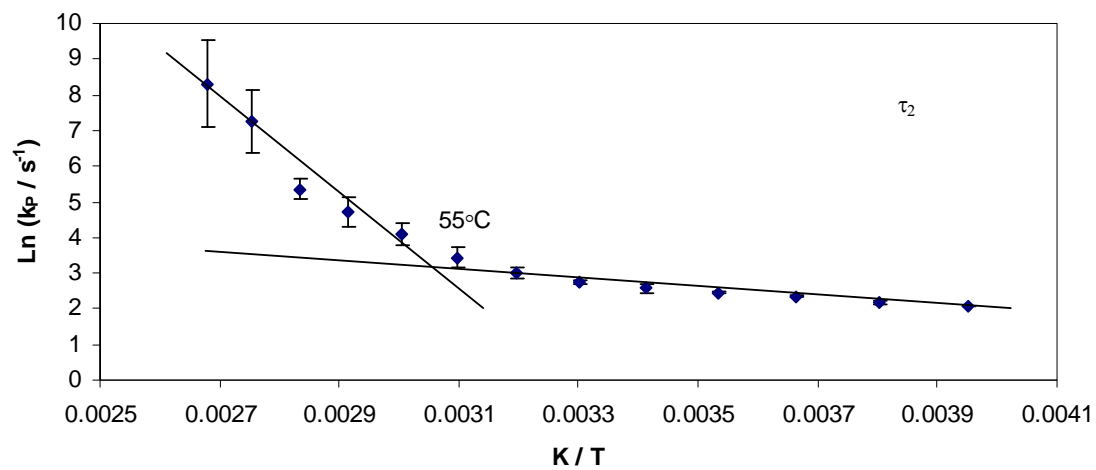
Figure II-12a*Figure II-12b*

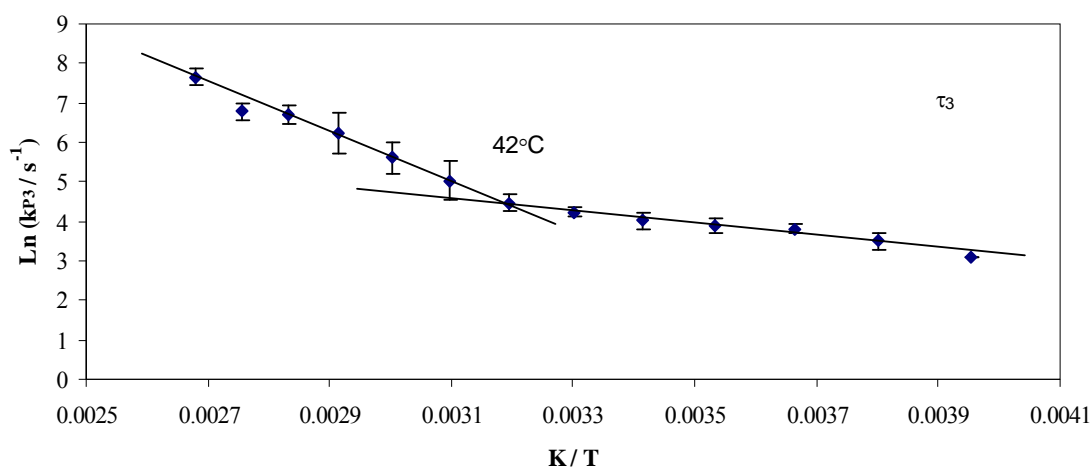
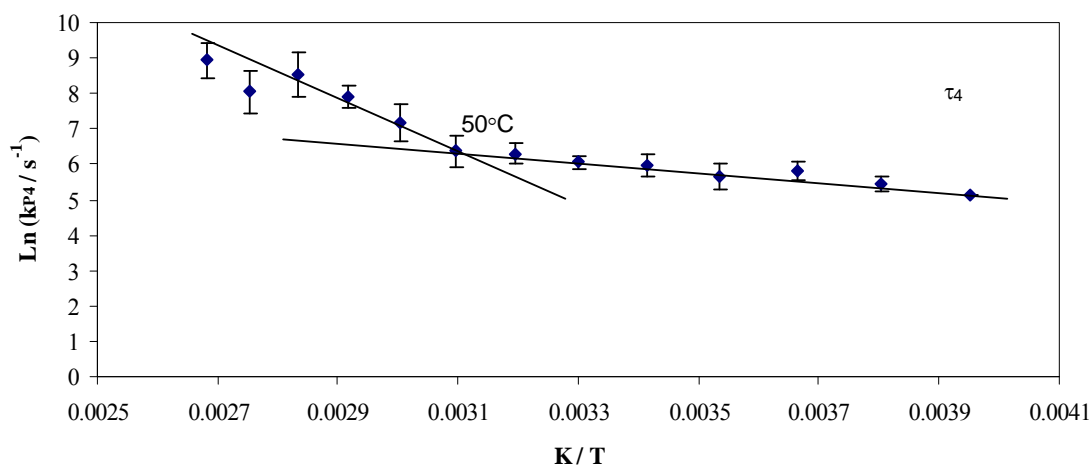
Figure II-12c**Figure II-12d**

Figure II-12a to 12d: Arrhenius plots of k_p for individual lifetime components τ_1 (12a), τ_2 (12b), τ_3 (12c) and τ_4 (12d) of vanillin in amorphous sucrose as a function of inverse of temperature. Lines drawn through the data points indicate slopes at low and high temperatures for each lifetime component.

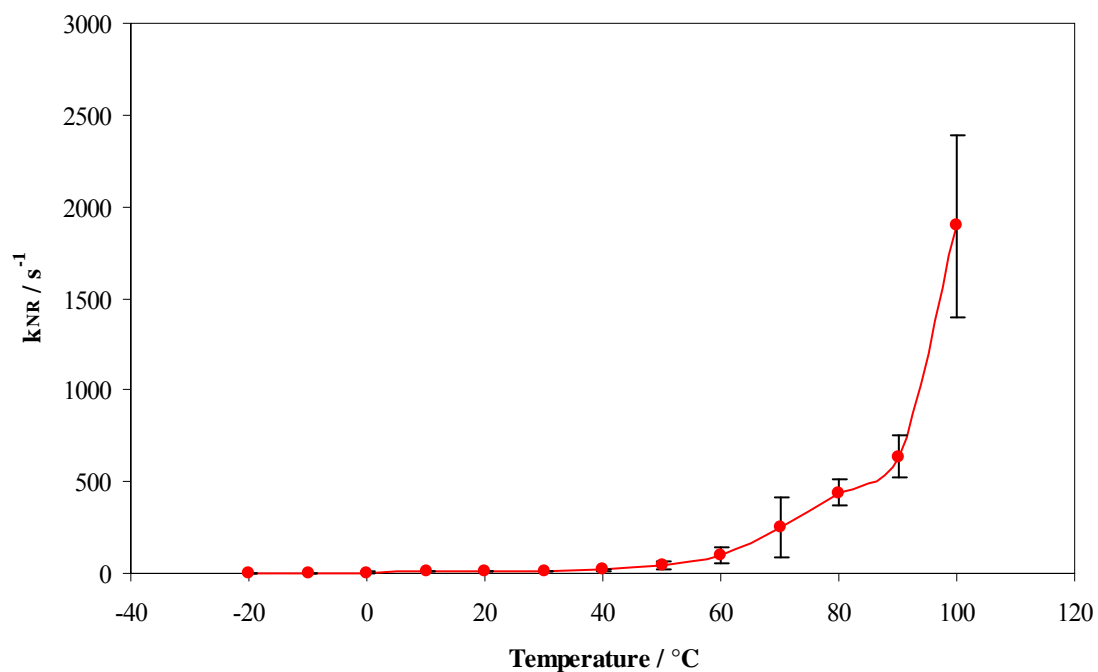
Figure II-13a

Figure II-13a: Temperature dependence of the total non-radiative decay rate of the triplet state k_{NR} ($k_p = k_{RP} + k_{NR}$) to S_0 of methyl vanillin in amorphous sucrose film over the temperature range from -20°C to 100°C; values were calculated from the average lifetime data.

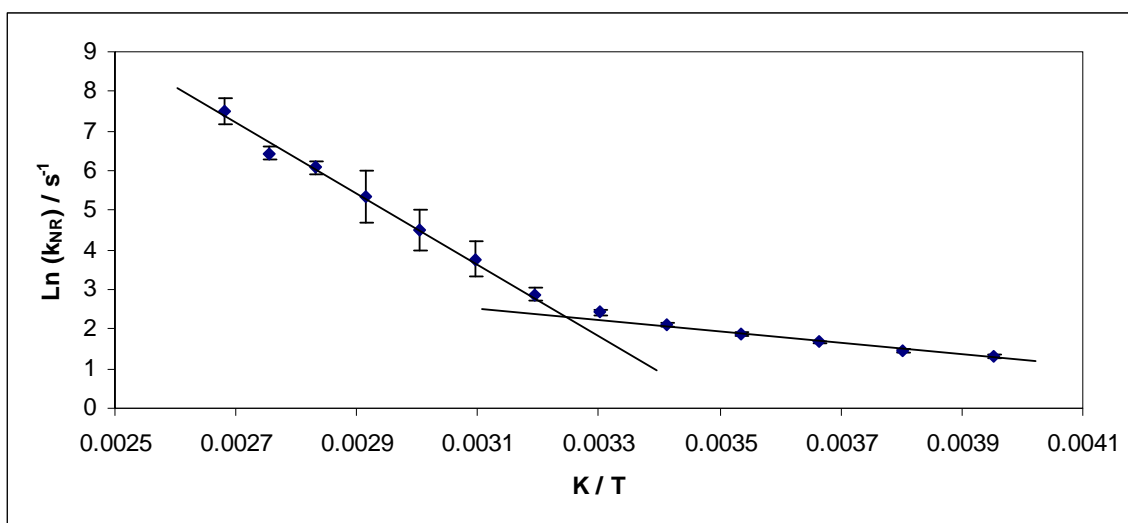
Figure II-13b

Figure II-13b: An Arrhenius plot of the total non-radiative decay rate of the triplet state k_{NR} ($k_{\text{p}} = k_{\text{RP}} + k_{\text{NR}}$) to S_0 of vanillin in amorphous sucrose film.

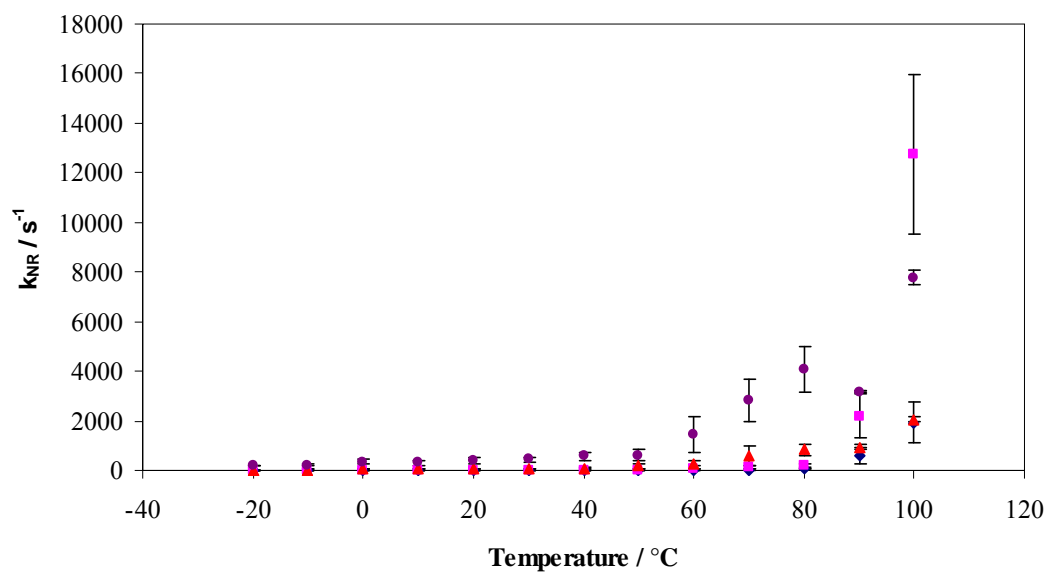
Figure II-14a

Figure II-14a: Temperature dependence of the total non-radiative decay rate of the triplet state k_{NR} ($k_p = k_{RP} + k_{NR}$) to S_0 for individual lifetime components of vanillin in amorphous sucrose film over the temperature range from -20°C to 100°C; values were calculated from the individual lifetime data.

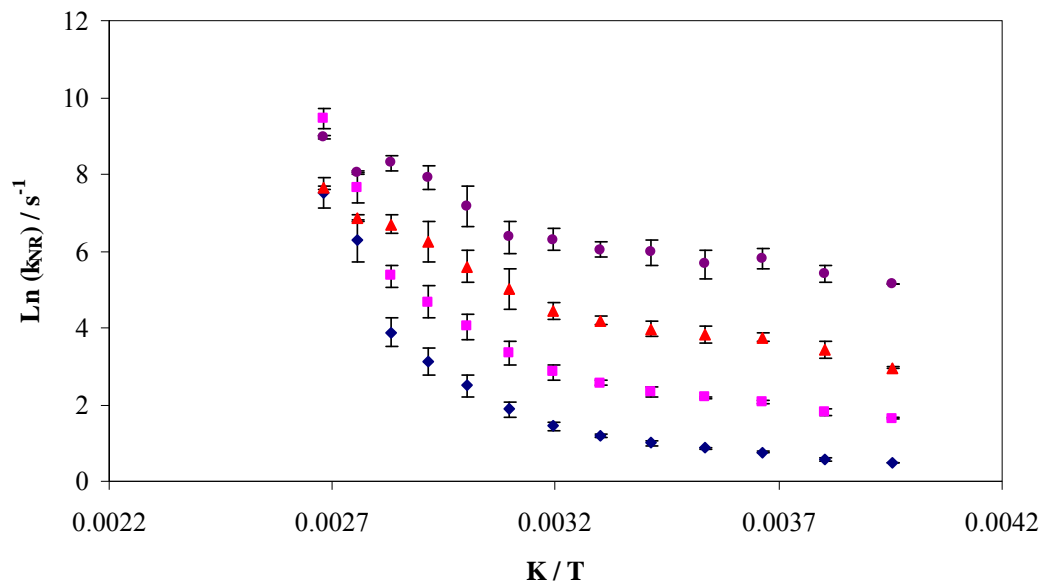
Figure II-14b

Figure II-14b: An Arrhenius plot of the total non-radiative decay rate of the triplet state k_{NR} ($k_p = k_{RP} + k_{NR}$) to S_0 for individual lifetime components of vanillin in amorphous sucrose film.

Table II-1

Table II-1: Excitation and emission wavelength and phosphorescence lifetime of vanillin in glycerol water, EPA and amorphous sucrose film at 77K after degassing.

Medium	$\lambda_{\text{Excitation}} / \text{nm}$	$\lambda_{\text{Fluorescence}} / \text{nm}$	$\lambda_{\text{Phosphorescence}} / \text{nm}$	$\tau^0_{\text{Phosphorescence}} / \text{ms}$
Glycerol water (6/4v/v)	350	400	480	372
EPA	350	400	480	190
Sucrose Film	320	400	480	272

Table II-2

Table II-2: Calculated activation energy E_a for each individual lifetime components τ_1 , τ_2 , τ_3 and τ_4 and average lifetime at low (LT) and high temperature (HT).

Methyl Vanillin			
Lifetime		Ea kJ / mol	Transition Temperatures °C
τ_1	LT	4.14	60
	HT	110.00	
τ_2	LT	9.60	55
	HT	112.00	
τ_3	LT	13.63	42
	HT	49.03	
τ_4	LT	11.33	50
	HT	68.21	
τ_{Avg}	LT	9.64	40
	HT	76.34	
k_{NR}	LT	13.84	40
	HT	72.32	

References

- Bell, L. N. and Hageman, M. J. Differentiating between the effect of water activity and glass transition dependent mobility on solid state chemical reaction: aspartame degradation. *Journal of Agricultural and Food Chemistry*, 42 (1994). 2398 -2401.
- Bell, L. N. and Hageman, M. J. Glass transition explanation for effect of polyhydroxy compounds on protein denaturation in dehydrated solids. *Journal of Food Science* 61 (1996). 372-375.
- Bohmer, R., Diezemann, G., Geil, B., Hinze, G., Nowaczyk, A. and Winterlich, A. correlation of primary and secondary relaxations in a supercooled liquid. *Physical Review Letter*. 97 (2006). 135701:1-135701:2.
- Buera, M. P. and Karel, M. Effect of physical changes on the rates of non enzymatic browning and related reactions. *Food Chemistry*. 52 (1995). 167-173.
- Buera, M. P., Chirife, J. and Karel, M. A study of acid catalyzed sucrose hydrolysis in an amorphous polymer matrix at reduced moisture content. *Food Research International*. 28 (1995). 359-365.
- Capaccioli, S., Kessairi, K., Prevosto, D., Lucchesi, M. and Ngai, K. L. Genuine Johari-Goldstein β -relaxations in glass-forming binary mixtures. *Journal of Non Crystalline Solids*. 352 (2006). 4643-4648.
- Champion, D., Le Meste, M. and Simatos, D. Towards an improved understanding of glass transition and relaxations in foods: molecular mobility in the glass transition range. *Trends in Food Science and Technology*. 11 (2000). 41-55.
- Champion, D., Maglione, M., Niquet, G., Simatos, D. and Le Meste, M. Study of α - and β - relaxation processes in supercooled sucrose liquids. *Journal of Thermal Analysis and Calorimetry*. 71 (2003). 249-261.
- Chan, R. K., Pathmanathan, K. and Johari, G. P. Dielectric relaxations in the liquid and glassy states of glucose and its water mixtures. *Journal of Physical Chemistry*. 90 (1986). 6358-6362.
- Chen, R. Apparent stretched exponential luminescence decay in crystalline solids. *Journal of Luminescence*. 102-103 (2003). 510-18.
- Craig, D.Q., Royall, P. G., Kett, V. L. and Hopton, M. L. The relevance of the amorphous state of pharmaceutical dosage forms: glassy drugs and freeze dried systems. *International Journal of Pharmaceutics*. 179 (1999). 179-207.

- Doolittle, A. K. and Doolittle, D. B. Studies in Newtonian flow. V. Further verification of free space viscosity equation. *Journal of Applied Physics*. 28 (1957). 901-905.
- Ediger, M.D., Angell, C.A. and Nagel, S. R. Supercooled Liquids and Glasses. *Journal of Physical Chemistry*. 100 (1996). 13200-13212.
- Fischer, C. J., Gafni, A., Steel, D. G. and Schauerte, J. A. The triplet-state lifetime of indole in aqueous and viscous environments: significance to the interpretation of room temperature phosphorescence in proteins. *Journal of the American Chemical Society*. 124 (2004). 10359-10266.
- Gangasharan, Murthy, S. S. N. Study of α , β , and γ -relaxation processes in some supercooled liquids and supercooled plastic crystals. *Journal of Chemical Physics*. 99 (1993). 9865-9873.
- Hancock, B. C. and Zografi, G. Characteristics and significance of amorphous state in pharmaceutical systems. *Journal of Pharmaceutical Sciences*. 86 (1997). 1-12.
- Hancock, B. C., Shamblin, S. L. and Zografi, G. Molecular mobility of amorphous pharmaceutical solids below their glass transition temperatures. *Pharmaceutical Research*. 12 (1995). 799-806.
- Hill, J. J., Shalaev, E. Y. and Zografi, G. Thermodynamic and dynamic factors involved in the stability of native proteins structure in amorphous solids in relation to levels of hydration. *Journal of Pharmaceutical Sciences*. 94 (2005). 1636-1667.
- Johari, G. P and Goldstein, M. Viscous liquids and the glass transition. II. Secondary relaxations in glasses of rigid molecules. *Journal of Chemical Physics*. 53 (1970). 2372-2388.
- Kaminski, K., Kaminski, E., Hensel-Bielowka, S., Chelmecka, E., Paluch, M., Ziolo, J., Wlodarczyk, P. and Ngai, K. L. Identification of the molecular motions responsible for the slower secondary (β) relaxation in sucrose. *Journal of Physical Chemistry*. Xxx (2008). A-G.
- Kaminski, K., Kaminski, E., Paulch. M., Ziolo, J. and Ngai, K. L. The true Johari-Goldstein β -relaxation of monosaccharides. *Journal of Physical Chemistry*. 110 (2006). 25045-25049.
- Kasapis, D. Beyond the free volume theory: Introduction of the concept of cooperativity to the chain dynamics of biopolymers during vitrification. *Food Hydrocolloids*. 22 (2008). 84-90.

- Kilburn, D., Dlubek, G., Pionteck, J. and Alam, M. A. Free volume in poly (n-alkyl methacrylate)s from positron lifetime and PVT experiments and its relation to the structural relaxation. *Polymer*. 47 (2006). 7774-7785.
- Lakowicz, J. R. *Principles of Fluorescence Spectroscopy*. Second ed. New York: Kluwer Academic/Plenum Press. (1999).
- Le Meste, M., Champion, D., Roudaut, G., Blond, G. and Simatos, D. Glass transition and food technology: A critical appraisal. *Journal of Food Science*. 67 (2002). 2444-2458.
- Liu, Y., Bhandari, B. and Zhou, W. Glass transition and enthalpy relaxation of amorphous food saccharides: A review. *Journal of Agricultural and Food Chemistry*. 54 (2006). 5701-5717.
- Ludescher, R.D., Shah, N. K., McCaul, C. P. and Simon, K. V. Beyond Tg: optical luminescence measurements of molecular mobility in amorphous solid foods. *Food Hydrocolloids*. 15 (2001). 331-339.
- Ludescher, R. D. Molecular dynamics of food proteins: Experimental techniques and observations. *Trends in Food Science and Technology*. 1 (1990). 145-149.
- McCaul, C. P. and Ludescher, R. D. Room temperature phosphorescence from tryptophan and halogenated tryptophan analogs in amorphous sucrose. *Photochemistry and Photobiology* 70 (1999). 166-171.
- Miller, D. P. and Krochta, J. M. Oxygen and aroma barrier properties of edible films: a review. *Trends in Food Science and Technology*. 8 (1997). 228-237.
- Moran, G. R., Jeffrey, K. R., Thomas, J. M. and Stevens, J. R. A dielectric analysis of liquid and glassy solid of glucose/water solutions. *Carbohydrate Research*. 328 (2000). 573-584.
- Nack, T. J. and Ludescher, R. D. Molecular mobility and oxygen permeability in amorphous bovine serum albumin films. *Food Biophysics*. 1 (2006). 151-162.
- Ngai, K. L. and Paluch, M. J. Classification of secondary relaxation in glass-formers based on dynamic properties. *Journal of Chemical Physics*. 120 (2004). 857-873.
- Ngai, K. L. Relation between some secondary relaxations and the α relaxations in glass-forming materials according to the coupling model. *Journal of Chemical Physics*. 109 (1998). 6982-6994.
- Ngai, K. L. An extended coupling model description of the evolution of dynamics with time in supercooled liquids and ionic conductors. *Journal of Physics: Condensed Matter*. 15 (2003). S1107-S1125.

- Ngai, K. L., Casalini, R., Capaccioli, S., Paluch, M and Roland, C. M. Advanced Chemical Physics. 133B (2006). 497.
- Nishigaki, Ngashima, U., Uchida, A., Oonishi, I. and Oshima, S. Hysteresis in the temperature dependence of phosphorescence of 4-Hydroxy-3-Methoxybenzaldehyde (vanillin) in ethanol. Journal of Physical Chemistry. 102 (1998). 1106-1111.
- Noel, T. R., Parker, R. and Ring, S. G. A comparative study of the dielectric relaxation behavior of glucose, maltose and their mixtures with water in the liquid and glassy states. Carbohydrate Research. 282 (1996). 193-206.
- Oversteegen, S. M. and Roth, R. General methods of free volume theory. The Journal of Chemical Physics. 122 (2005). 1-12.
- Papp, S. and Vanderkooi, J. M. Tryptophan phosphorescence at room temperature as a tool to study protein structure and dynamics. Photochemistry and Photobiology. 49 (1989). 775-784.
- Parker, C. A. Photoluminescence of Solutions. Amsterdam: Elsevier Pub Co., (1968).
- Poppe, L. and Van Halbeek, H. The rigidity of sucrose: just an illusion? Journal American Chemical Society. 114 (1992). 1092-1094.
- Pravinata, L.V., You, Y. and Ludescher, R. D. Erythrosin B phosphorescence monitors molecular mobility and dynamic heterogeneity in amorphous sucrose. Biophysical Journal. 88 (2005). 3551-3561.
- Pravinata, L. C. Molecular mobility of amorphous sucrose detected by phosphorescence of erythrosin B and eosin. Master Thesis. Rutgers University, New Brunswick, NJ. (2003).
- Richert, R. Evidence of dynamic heterogeneity near T_g from the time resolved inhomogeneous broadening of optical line shapes. Journal of Physical Chemistry 101 (1997). 6323-6326.
- Richert, R. Spectral selectivity in the slow beta relaxation of a molecular glass. Europhysics Letters. 54 (2001). 767-773.
- Roos, Y. Phase Transitions in Foods. San Diego, California: Academic Press, (1995).
- Roos, Y. H. Thermal analysis, state transition and food quality. Journal of Thermal Analysis and Calorimetry. 71 (2003). 197-203.

- Roos, Y. and Karel, M. Differential scanning calorimetry study of phase transitions affecting the quality of dehydrated materials. *Biotechnology Progress*. 6 (1990). 159–163.
- Roos, Y. and Karel, M. Plasticizing effect of water on thermal behavior and crystallization of amorphous food models. *Journal of Food Science*. 34 (1991a). 324–329.
- Roos, Y. and Karel, M. Phase transitions of mixtures of amorphous polysaccharides and sugars. *Biotechnology Progress*. 7 (1991b). 49–53.
- Roos, Y. Melting and glass transitions of low molecular weight carbohydrates. *Carbohydrate Research*. 238 (1993). 39-48.
- Schmidt, S. J. Water and solids mobility in foods. *Advance Food and Nutrition Research*. 48 (2004). 1-101.
- Schulman, E. M. and Parker, R. T. Room temperature phosphorescence of organic compounds. The effects of moisture, oxygen and the nature of the support-phosphor interactions. *The Journal of Physical Chemistry*. 81 (1977). 1932-1939.
- Schulman, E. M. and Walling, C. Phosphorescence of adsorbed ionic organic molecules at room temperature. *Science*. 178 (1972). 52-54.
- Schulman, E. M. and Walling C. Triplet state phosphorescence of adsorbed ionic organic molecules at room temperature. *Journal of Physical Chemistry* 77, 902-05. 1973.
- Shah, N. K. and Ludescher, R. D. Influence of hydration on the internal dynamics of hen egg white lysozyme in the dry state. *Photochemistry and Photobiology*. 58 (1993). 169-174.
- Shah, N. K. and Ludescher, R. D. Phosphorescence of probes of the glassy state in amorphous sucrose. *Biotechnology Progress*. 11 (1995). 540-544.
- Shamblin, S., Hancock, B. C., Dupuis, Y. and Pikal, M. J. Interpretation of relaxation time constants for amorphous pharmaceutical systems. *Journal of Pharmaceutical Sciences*. 89 (2000). 417-427.
- Shamblin, S. L., Tang, X. L., Chang, L. Q., Hancock, B. C. and Pikal, M. J. Characterization of the time scales of molecular motion in pharmaceutically important glasses. *Journal of Physical Chemistry*. 103 (1999). 4113-41121.
- Shirke, S. and Ludescher, R. D. Dynamic site heterogeneity in amorphous maltose and maltitol from spectral heterogeneity in erythrosin B phosphorescence. *Carbohydrate Research*. 340 (2005). 2661-2669.

- Shirke, S. and Ludescher, R. D. Dynamic site heterogeneity in amorphous lactose and lactitol from spectral heterogeneity in erythrosin B phosphorescence. *Biophysical Chemistry*. 123 (2006a). 122-133.
- Shirke, S. and Ludescher, R. D. Molecular mobility and glass transition in amorphous glucose, maltose and maltotriose. *Carbohydrate Research*. 340 (2006b). 2654-2660.
- Sillescu, H. J. Heterogeneity at the glass transition: a review. *Journal of Non-Crystalline Solids*. 243 (1999). 81-108.
- Simon-Lukasik, K. V. and Ludescher, R. D. Effect of plasticizer on dynamic site heterogeneity in cold-cast gelatin films. *Food Hydrocolloids*. 20 (2006a). 88-95.
- Simon-Lukasik, K. V. and Ludescher, R. D. Molecular mobility in water and glycerol plasticized cold and hot cast gelatin films. *Food Hydrocolloids*. 20 (2006b). 96-105.
- Stratt, R. M. and Maroncelli, M. Nonreactive dynamics in solution: the emerging molecular view of solvation dynamics and vibrational relaxations. *Journal of Physical Chemistry*. 100 (1996). 12981-12996.
- Tombari, E., Cardelli, C., Salvetti, G. and Johari, G. P. Dielectric relaxation and the conformer equilibrium in the liquid and glassy states of β -D-fructose. *Journal of Molecular Structure*. 559 (2001). 245-254.
- Vanderkooi, J. M. and Berger, J. W. Excited triplet state used to study biological macromolecules at room temperature. *Biochimica et Biophysica Acta: Bioenergetics*. 976 (1989). 1-27.
- Vyazovkin, S. and Dranca, I. Probing beta relaxations in pharmaceutically relevant glasses by using DSC. *Pharmaceutical Research*. 23 (2006). 422-428.
- Wagner, H. and Richert, R. Equilibrium and non-equilibrium type beta relaxations: D-Sorbitol versus o-Terphenyl. *Journal of Physical Chemistry*. 103 (1999). 4071-4077.
- Wagner, H. and Richert, R. Spatial uniformity of the beta relaxation in D-sorbitol. *Journal of Non-crystalline Solids*. 242 (1998). 19-24.
- Walters, C. Temperature dependency of molecular mobility in preserved seeds. *Biophysical Journal*. 86 (2004). 1253-1258.
- Zallen, R. *The Physics of Amorphous Solids*. New York: John Wiley and Sons. (1998).

Chapter III: Investigating the mechanism of environmental sensitivity of vanillin to molecular motions using vanillin analogs in amorphous sucrose films.

Introduction

Strong phosphorescence is observed at room temperature from organic compounds adsorbed on rigid surfaces (Schulman and Walling, 1973; Zander, 1968; Hurtubise 1981). We have shown in chapter II that vanillin (3-methoxy-4-hydroxy benzaldehyde) can be used as a triplet state probe to monitor molecular mobility in amorphous solids. Vanillin phosphorescence lifetime and quantum yield were found to be extremely sensitive to the local environment in the amorphous solids in the glassy state and the glass-to-rubber transition into the melt. Vanillin is a promising probe to measure molecular mobility and is highly sensitive and has a long lifetime ($\tau^0 = 372$ ms). The mechanism of vanillin sensitivity to molecular mobility is unclear. This study intends to clarify the mechanism of vanillin sensitivity by using different analogs of vanillin.

In vanillin, various conformations results from rotations of methoxyl group about the C-O bond (Nishigaki et al., 1998). The stiffness of matrix structure immobilizes vanillin but as the matrix become more mobile vanillin can rearrange. Conformation of vanillin is conserved during the photophysical processes due to the matrix stiffness, but as the matrix becomes more mobile it gives room for rotation of methoxyl group which results in conformation changes in vanillin.

The rotational motion of molecules in viscous environment generally occurs on a millisecond to second time scale (Turro, 1978). The capability of being able to rotate or

not rotate about the C-O bond could be governed by two factors. The first factor is the presence of a smaller group (H) instead of a bulkier group (CH_3 or C_2H_5) could make the rotation of the group easier and affect the phosphorescence; the other factor being changes in the matrix mobility creating free volume. The FVT (free volume theory) is based on change in volume expansion coefficient at glass transitions and assumes that molecular motions depend on the presence of holes or voids (Roos, 1995)) and thus allowing the molecular movement to take place. These holes between molecules provide the free volume that is needed for molecular rearrangements.

So we hypothesized that probably movement of methoxyl group about the C-O bond could be sensitive to matrix mobility. To test this hypothesis we selected different analogs of vanillin (3-methoxy-4-hydroxy benzaldehyde, referred as methyl vanillin) Figure III-1 where the methoxy group was (a) absent (4-hydroxy benzaldehyde, referred as hydroxy vanillin), (b) replaced with a hydroxy group (3, 4-dihydroxyl benzaldehyde referred as dihydroxy vanillin) or (c) replaced with ethoxy group (3-ethoxy-4-hydroxy benzaldehyde, referred as ethyl vanillin). Some of these probes have been shown to have room temperature phosphorescence when adsorbed on a solid substrate such as filter paper, etc. (Schulman, 1972). Some of these probes with RTP have mainly used in the field of environmental research, forensic science, pharmaceutical analysis, biochemistry, etc. (Hurtubise, 1981; vo-Dinh, 1984; Gunshefski and Santana, 1992). Rigidity is required for RTP which is provided by hydrogen bonding but there is also a packing effect that can affect the movement of the molecules entrapped in cages made by cellulose chains of filter paper (McAleese and Dunlap, 1984; Wright, 1987).

However none of these probes have being utilized to study molecule mobility in amorphous solids. This study will use vanillin and its analogs to monitor dynamics in amorphous sucrose in the glassy or rubbery state giving site specific dynamic information.

Amorphous sucrose glasses provide a rigid environment for phosphorescence measurement and hence were used in the current study (Shah and Ludescher, 1995; Fister and Harris, 1996; Wang and Hurtubise, 1997). Amorphous sucrose provides rigid condition, and hence phosphorescence signals of vanillin and its analogs are intense and are characterized by longer lifetime. In the present study we measured the phosphorescence emission and lifetime of vanillin and its analogs dispersed in amorphous sucrose film as a function of temperature. For a comparison, the same measurements were also made for each analog in glycerol: water, EPA and sucrose films at 77K.

Materials and Methods

Materials: Water was deionized and then glass distilled. Glycerol (Spectral Grade) was from Sigma-Aldrich Chemical Company (St. Louis, MO), isopentane (Baker grade) was from J. T. Baker Chem. Co. (Phillipsburg, NJ), ethyl ether (anhydrous) was from Fisher Scientific (Fair Lawn NJ), and ethanol (anhydrous) was from Parmco Products, Inc (Brookfield, CT). Sucrose (99.5% pure) was from Sigma Chemical. The probes 4-hydroxy benzaldehyde (hydroxyl vanillin), 3, 4-dihydroxyl benzaldehyde (dihydroxy vanillin), 3-methoxy-4-hydroxy benzaldehyde (methyl vanillin) and 3-ethoxy-4-hydroxy benzaldehyde (ethyl vanillin), were from Sigma-Aldrich (Milwaukee, WI). The structures of vanillin and its analogs are shown in Figure 1.

Sucrose Solution: Sucrose solution was made as described in Pravinata et al., 2005. Approximately 20 g of sucrose were dissolved in 100 mL of deionized water containing 0.5 g of activated charcoal to remove luminescent impurities. After stirring overnight, the charcoal was removed by vacuum filtration using ashless filter paper (Whatman No. 40, Whatman International, Maidstone, UK), additional charcoal was added, and the process repeated. Sucrose solution was made to a final concentration of 65–67 wt % sucrose; concentration was confirmed using a refractometer (NSG Precision Cells, Farmingdale, NY). This sucrose solution was filtered through a 0.2 μm membrane to remove particulates.

Vanillin: A 66mM stock solution of either ethyl, methyl, dihydroxy or hydroxy vanillin was prepared in distilled deionized water. This concentration was selected to simplify the

addition of the probe to the sucrose solution. For absorbance, fluorescence and phosphorescence measurements in solution the 66mM stock was diluted to 50 μ M in distilled deionized water. For measuring absorbance and phosphorescence in amorphous solid, probes were added to the sucrose solution at a molar ratio of 1:10³ (dye: sucrose). The ratio 1:10³ was chosen as at this concentration it was determined that the probe does not aggregate, existing only as individual molecules monitoring the molecular mobility of the sucrose.

Sucrose films: To produce glassy sucrose films containing probes, 20 μ L of a sucrose solution containing probe were spread on a quartz slide (30 \times 13.5 \times 0.6 mm; custom made by NSG Precision Cells, Farmingdale, NY). After spreading the solutions, the slides were then dried under a heat gun (Vidal Sassoon) for 5 min to a maximum temperature of \sim 88°C (measured using a thermocouple probe) and the final thickness was \sim 0.05 mm. The slides were stored at room temperature against P₂O₅ and Drierite, protected from the light to prevent any photobleaching, for at least 7 days before any phosphorescence measurements were made. The desiccant was refreshed as needed to maintain a relative humidity close to 0%.

Sample preparation for measurement at 77K: Solutions of methyl vanillin and analogs were prepared at 20 mM concentration in a glycerol/water (60/40, v/v) or in EPA (ethyl ether/isopentane/ethanol 5/5/2, v/v). The liquid solutions were placed in a quartz cylindrical cell with 4 mm inner diameter (National Scientific Company, Quakertown PA) for measurement at room temperature and at 77 K. At 77 K the tube was immersed in

liquid N₂ using a finger type Dewar obtained from Jobin-Yvon Spex. Ninety-degree geometry was used for these measurements. Sugar glasses doped with vanillin derivatives were prepared by plating sucrose solution on quartz plates followed by evaporation. The quartz plates were placed in the sample compartment and front-face geometry was used for measurement. All the measurement at 77K was done in Dr Jane Vanderkooi's lab at University of Pennsylvania with the help of Dr Bogumil Zelent.

Instrumentation: For measurements at 77K emission intensity and spectra were measured with a Fluorolog-3-21 Jobin-Yvon Spex Instrument SA (Edison, NJ) equipped with a 450 W Xenon lamp for excitation and a cooled R2658P Hamamatsu photomultiplier tube for detection. At room temperature absorption measurements were recorded in a Cary Eclipse spectrophotometer and fluorescence and phosphorescence measurements were made on a Cary Eclipse fluorescence spectrophotometer (Varian Instruments, Walnut Creek, CA). For measurements at -20°C to 100°C phosphorescence measurements were made on a Cary Eclipse fluorescence spectrophotometer (Varian Instruments, Walnut Creek, CA). The quartz slides were placed in a standard 1cm x 1cm x 1cm quartz fluorescence cuvette, which was capped with a lid having inlet and outlet ports for gas lines. The cuvette was flushed with a gentle stream of nitrogen for 15 minutes to eliminate oxygen. An oxygen free nitrogen stream was generated by passage of high purity nitrogen through a Supelco (Bellefonte, PA) gas purifier. The temperature was controlled by using a TLC 50 thermoelectric heating/cooling system (Quantum Northwest, Spokane, WA). The TLC-50 sample compartment was fitted with a jacketed cover and the temperature of the cuvette was monitored directly using a thermocouple in

the cuvette. The film was equilibrated for 15 minutes at each temperature before collecting the data. The Cary Eclipse uses a pulsed lamp and collects emission intensity in analog mode; data were not collected within the first 0.1-0.2 ms to suppress fluorescence coincident with the lamp pulse.

Luminescence Measurements: For measurements at 77K in glycerol: water, EPA and amorphous sucrose films excitation wavelength was at 340 nm for methyl and ethyl vanillin. Other samples hydroxy and dihydroxy vanillin were excited at 320 nm. Emission spectra were scanned in the 330 nm – 560 nm range. Slit width was set to provide a band-pass 2 nm for excitation and 1 nm for emission. For time-dependent intensity measurements for lifetime determination the band-pass for excitation was 5 nm and for emission band-path 5 nm at 475 nm wavelength. The excitation shutter was closed and the emission photons were counted at 0.1 sec intervals. The data were digitized and transferred to Excel (Microsoft) for analysis of exponential decay.

For measurements at -20°C to 100°C delayed luminescence emission spectra (phosphorescence) of methyl vanillin and analogs in amorphous sucrose films were collected from 400 to 800 nm (10 nm bandwidth) using excitation at 320 nm (20 nm bandwidth) for ethyl, methyl and dihydroxy vanillin and 300 nm for hydroxy vanillin over the temperature range from -20°C to 100°C. Each data point was collected from a single flash with 0.2 ms delay, 100 ms gate time, and 0.12 s total decay time.

Lifetime measurements were made in presence of nitrogen as a function of temperature ranging from -20°C to 100°C . The samples were excited at 320 nm (20 nm bandwidth) for ethyl, methyl and dihydroxy vanillin and 300 nm for hydroxy vanillin and emission transients collected at 490 nm (20 nm bandwidth) and 450 nm (20 nm bandwidth) respectively. Each decay was average of 50 cycles, and for each cycle data was collected from a single flash with a delay of 0.2 ms, windows for gate time and total decay time was varied at each temperature. All measurements were made in quadruplicate.

Data Analysis

Emission Energy as a function of temperature: Emission spectra's were fitted using the program Igor (Wavemetrics, Inc., Lake Oswego, OR). The emission spectra were analyzed by fitting phosphorescence of ethyl, methyl, dihydroxy and hydroxy vanillin to a log-normal function Equation 1 over the temperature range of -20°C to 100°C .

$$I(\nu) = I_0 \exp \left\{ -\ln(2) \left(\frac{\ln[1 + 2b(\nu - \nu_p) / \Delta]}{b} \right)^2 \right\} \quad (1)$$

In this equation I_0 , is the maximum intensity value of the emission spectra, ν_p is the frequency in cm^{-1} of the emission maximum, Δ is the line width parameter, and b is the asymmetry parameter. The bandwidth of the emission, the full width at half maximum (Γ), is related to b and Δ Equation 2.

$$\Gamma = \Delta \left(\frac{\sinh(b)}{b} \right) \quad (2)$$

Photophysical Scheme: The phosphorescence intensity decay was collected as described above and was fitted using a multi-exponential function (Shamblin et al., 2000). The multi-exponential model is as show in Equation 3; τ_i are decay times, α_i represent the amplitudes of the components at $t = 0$ and n is the number of decay times. Phosphorescence lifetimes were determined with the statistical program Igor (Wavemetrics, Inc., Lake Oswego, OR). Fits were judged satisfactory if the R^2 values were in the range of 0.995-1.0 and the modified residuals $((\text{data} - \text{fit})/\text{data}^{1/2})$ varied randomly about zero. The average lifetime was calculated using Equation 4.

$$I(t) = \sum_{i=1}^n \alpha_i \exp(-t/\tau_i) \quad (3)$$

$$\tau_{\text{Avg}} = \frac{\sum_{i=1}^n \alpha_i \tau_i}{\sum_{i=1}^n \alpha_i} \quad (4)$$

The phosphorescence lifetimes were used to calculate the rate constants associated with the various processes that depopulate the excited triplet state. The lifetime τ is related to the rate constants for de-excitation of the triplet excited state of the probe according to the following equation 5 (Papp and Vanderkooi, 1989).

$$1/\tau = k_{\text{RP}} + k_{\text{NR}}(T) + k_{\text{Q}}[\text{O}_2] = k_{\text{P}} \quad (5)$$

Here k_p ($=1/\tau$) is the total decay rate, k_{RP} is the rate of radiative decay of the ground state (measured in this study for each probe), k_{NR} is the rate of non-radiative decay to the singlet state followed by vibrational relaxation to S_0 due to collisional quenching. The magnitude of k_{NR} reflects factors associated with the mechanism by which the excited T_1 state is coupled to highly excited vibrations of the S_0 ground state as well as external factors associated with the mechanism by which the ground state vibrational energy can dissipate from the excited state into the surrounding matrix (Fischer et al., 2004; Vanderkooi and Berger, 1989). As the efficiency of external vibrational dissipation is related to overall mobility of the matrix, the magnitude of k_{NR} provides a measure of matrix mobility. One common method for restricting the collisional deactivation is to supercool analyte solutions with liquid nitrogen to a rigid glass. The term $k_Q [O_2]$ refers to the collisional quenching due to interaction between the excited chromophore and triplet state oxygen.

Results

Luminescence emission spectra: Figure 2 shows the phosphorescence excitation spectra of ethyl, methyl, dihydroxy and hydroxy vanillin at room temperature in the amorphous sucrose film. The phosphorescence emission spectra of methyl vanillin and the three analogs hydroxy, dihydroxy and ethyl vanillin at 77K in glycerol: water, EPA and amorphous sucrose film are shown in Figure 3a, 3b and 3c respectively. Figure 4a, 4b, 4c and 4d show the phosphorescence emission spectra as a function of temperature of hydroxy (-20°C to 80°C), dihydroxy (-20°C to 80°C), methyl (-20°C to 100°C) and ethyl vanillin (-20°C to 100°C) dispersed in amorphous sucrose film. The emission maximum in sucrose film appears at ~450 nm for hydroxy vanillin and ~490 nm for dihydroxy, methyl and ethyl vanillin. The emission intensity was completely quenched by 80°C for hydroxy vanillin and 90°C for dihydroxy vanillin. However, in case of methyl and ethyl vanillin the emissions lasted up to 100°C. The various thermally stimulated processes cause decrease in phosphorescence intensity (I_p) with increase in temperature (Parker, 1968).

A comparison plot of normalized phosphorescence intensity is shown in Figure 5. Plots (Figure 6) of $\ln (1/I_p)$ vs. K/T (using the maximum intensity determined from fitting the spectra to a log-normal function, Eq. 1 Materials and Methods), were used to calculate the transition temperature and activation energy (E_a). The transition temperature was calculated from the Arrhenius plot by fitting each temperature region with a straight line. Break point temperatures were determined from intersection of trendline to points at low, intermediate and high temperature. The plot was biphasic in hydroxy (Figure 6a) and

dihydroxy (Figure 6b) vanillin and triphasic in methyl (Figure 6c) and ethyl (Figure 6d) vanillin. The temperature at the intersection point of trend lines for the high, intermediate and low temperature regions, representing the transition temperatures, are compiled in Table 1. Hydroxy vanillin showed a transition at 25°C, dihydroxy vanillin at 22°C, methyl vanillin at 36°C and 80°C and ethyl vanillin at 40°C and 75°C.

The activation energies obtained from the slopes of fit line are as compiled in Table 1. The activation energy is the energy for the motions which quench the excited triplet state. There was not much of a difference in activation energy at low temperature (E_{aL}) and high temperature (E_{aH}) regions for hydroxy ($E_{aL} = 21.82 \pm 1 \text{ kJ / mol}^{-1}$ and $E_{aH} = 77 \pm 2.1 \text{ kJ / mol}^{-1}$) and dihydroxy vanillin ($E_{aL} = 24.16 \pm 1 \text{ kJ / mol}^{-1}$ and $E_{aH} = 79.68 \pm 2.1 \text{ kJ / mol}^{-1}$). The activation energies at low and intermediate temperatures (E_{aI}) were not very different for methyl vanillin ($E_{aL} = 7.76 \pm 1 \text{ kJ / mol}^{-1}$ and $E_{aI} = 53.96 \pm 2.1 \text{ kJ / mol}^{-1}$) and ethyl vanillin ($E_{aL} = 8.48 \pm 1 \text{ kJ / mol}^{-1}$ and $E_{aI} = 42.6 \pm 2.1 \text{ kJ / mol}^{-1}$), but at high temperature ethyl vanillin ($E_{aH} = 139.85 \pm 1 \text{ kJ / mol}^{-1}$) had much higher activation energy compared to methyl vanillin ($E_{aH} = 93.7 \pm 1 \text{ kJ / mol}^{-1}$).

Peak frequencies were obtained by fitting the phosphorescence intensity data to a log-normal function (Materials and Methods, Eq. 1). Peak frequencies of the phosphorescence of hydroxy vanillin in amorphous sucrose film as a function of temperature are shown in Figure 7. Peak frequencies of the phosphorescence of dihydroxy, methyl and ethyl vanillin in amorphous sucrose film as function of temperature are shown in Figure 8a. The phosphorescence emission peak frequency of

vanillin and its analogs varied systematically with temperature below and above the glass transition temperature of sucrose ($T_g = 65^\circ\text{C}$).

In the case of hydroxy vanillin the peak frequency varied between 22,675 to 22,584.5 cm^{-1} ($\Delta\nu = 90.5 \text{ cm}^{-1}$) throughout the temperature range from -20°C to 60°C (decrease in intensity above 60°C prevented any further measurements to be taken). In case of dihydroxy, methyl and ethyl vanillin, peak frequency varied between 20,341 to 19,674.5 cm^{-1} ($\Delta\nu = 666.5 \text{ cm}^{-1}$), 20,561 to 19,675 cm^{-1} ($\Delta\nu = 886 \text{ cm}^{-1}$) and 20,462.75 to 19,275 cm^{-1} ($\Delta\nu = 1188 \text{ cm}^{-1}$) respectively throughout the temperature range from -20°C to 100°C . The emission energy for hydroxy vanillin decreases noticeably below the glass transition temperature. However in the case of dihydroxy, methyl and ethyl vanillin the emission energy decrease gradually at low temperature in the glass but decreased dramatically at higher temperatures in the melt. The decrease in peak frequency as a function of temperature indicated an increase in dipolar relaxation (Lackowicz, 1999; Richert, 2000). The emission energy was highest for ethyl vanillin followed by methyl and dihydroxy vanillin. Considering that the only difference in structure among dihydroxy, methyl and ethyl vanillin is the side group R attached to the O-R where $R = \text{C}_2\text{H}_5$, CH_3 or H the difference seen could be attributed to this structural difference. Hydroxy vanillin is ~ 10 times smaller in $\Delta\nu$ than the others. The significant difference in emission properties at 77K and in sucrose at room temperature indicates that hydroxy vanillin does not respond to environment in the same way as others.

Full width at half maxima (FWHM) is the width of the spectra at half maximum and is calculated using Eq. 2 (Materials and Methods). The emission bandwidth is a measure of the extent of inhomogeneous broadening due to the presence of probes in multiple sites with different emission energies. The plot of FWHM of hydroxy vanillin in amorphous sucrose films as a function of temperature is shown in Figure 7. Comparison plots of FWHM for dihydroxy, methyl and ethyl vanillin are shown in Figure 8b. Dihydroxy vanillin had much higher FWHM values than methyl and ethyl vanillin. The increase was gradual at low temperature and dramatic at higher temperature for all the four probes indicating that the increase in dipolar relaxation rate was accompanied by an increase in the width of the distribution of energetically distinct environments. The bandwidth increased dramatically at temperatures approaching the sucrose glass transition indicating that the distribution of site energies was significantly broadened due to the onset of α -relaxation process.

The ability to monitor molecular mobility is attributed to the sensitivity of hydroxy, dihydroxy, methyl and ethyl vanillin's emission to dipolar relaxation of solvent molecules around its polar singlet excited state. The decrease in emission energy and the broadening of emission spectra with an increase in temperature can be explained with a solvent relaxation mechanism.

Phosphorescence Intensity Decay: The phosphorescence decays of hydroxy, dihydroxy, methyl and ethyl vanillin in glycerol: water, EPA and amorphous sucrose films at 77K fitted to a simple single-exponential function. The decays in glycerol: water and EPA for hydroxy vanillin are shown in Figure 9a, dihydroxy vanillin in Figure 9b, methyl vanillin in Figure 9c and ethyl vanillin in Figure 9d. The decays in amorphous sucrose film at 77K are shown for hydroxy vanillin in Figure 10a, dihydroxy vanillin in Figure 10b, methyl vanillin in Figure 10c and ethyl vanillin in Figure 10d. In glycerol: water the lifetimes was longest for hydroxy vanillin ($\tau^\circ = 545$ ms), followed by methyl ($\tau^\circ = 372$ ms), ethyl ($\tau^\circ = 358$ ms) and dihydroxy ($\tau^\circ = 352$ ms) vanillin. These values at 77K in glycerol: water was used to calculate k_{RP} (Eq. 5). In amorphous sucrose films at 77K hydroxy vanillin had the longest lifetime ($\tau = 403$ ms) whereas dihydroxy ($\tau = 330$ ms), methyl ($\tau = 272$ ms) and ethyl ($\tau = 286$ ms) vanillin had very similar lifetimes.

Time-resolved phosphorescence intensity decays of vanillin and analogs in amorphous sucrose films were also measured over the temperature range from -20°C to 100°C. The hydroxy vanillin was excited at 300 nm and emission collected at 450 nm, whereas dihydroxy, methyl and ethyl vanillin molecules were excited at 320 nm and emission was collected at 490 nm. The decays were fitted using a multi-exponential function (Eq. 3, Materials and Methods) where hydroxy vanillin was fitted to a five-exponential function whereas dihydroxy, methyl and ethyl fitted to a four-exponential function. Fits were judged satisfactory if the modified residuals $((\text{data-fit})/\text{data}^{1/2})$ varied randomly about zero. The phosphorescence intensity decays of hydroxy, dihydroxy, methyl and ethyl vanillin in amorphous sucrose film at 20°C in the presence of nitrogen are plotted in

Figure 11a, 11b, 11c and 11d, respectively, along with the modified residuals for a fit using a multi-exponential function.

The lifetimes as a function of temperature for hydroxy, dihydroxy, methyl and ethyl vanillin are shown in Figure 12a1, 12b1, 12c1 and 12d1, respectively. The log plots for hydroxy, dihydroxy, methyl and ethyl lifetime is shown in Figure 12a2, 12b2, 12c2 and 12d2, respectively. The lifetime is the average time a molecule spends in the excited state and is an indicator of the rigidity of the matrix. In case of hydroxy vanillin the five lifetime components at 20°C were $\tau_1 = 171.6$ ms, $\tau_2 = 54.1$ ms, $\tau_3 = 15.9$ ms, $\tau_4 = 4.2$ ms and $\tau_5 = 0.87$ ms indicating the presence of local environments with ~200 fold differences in mobility. In case of dihydroxy vanillin the four lifetime components at 20°C were $\tau_1 = 84.62$ ms, $\tau_2 = 20.71$ ms, $\tau_3 = 4.3$ ms and $\tau_4 = 0.73$ ms indicating the presence of local environments with ~100 fold difference in mobility. In case of methyl vanillin the four lifetime components at 20°C were $\tau_1 = 184.4$ ms, $\tau_2 = 76.7$ ms, $\tau_3 = 18.2$ ms and $\tau_4 = 2.7$ ms indicating the presence of local environments with ~70 fold difference in mobility. In case of ethyl vanillin the four lifetime components at 20°C were $\tau_1 = 189.4$ ms, $\tau_2 = 89.0$ ms, $\tau_3 = 23.4$ ms and $\tau_4 = 3.2$ ms indicating the presence of local environment with ~60 fold difference in mobility.

All the lifetime components decreased drastically with increase in temperature from -20°C to 100°C. The decrease in lifetime occurs because of an increase in the rate of collisional quenching from interaction of the probe with the sugar matrix and/or increase of vibrational relaxation. The different lifetimes observed are due to different locations of

the probes in different environments in the amorphous sucrose matrix that differ in molecular mobility. In environments with more mobility, the probe has a shorter lifetime (Strambini and Gonnelli, 1985) as a result of quenching. In the environments with higher lifetimes, probes sense lower mobility and are less easily quenched.

The plot of amplitudes of each lifetime component for hydroxy, dihydroxy, methyl and ethyl vanillin as a function of temperature are shown in Figures 13a, 13b, 13c and 13d, respectively. The amplitudes of longer lifetime components decreased and that of shorter lifetime components increased as a function of temperature. The fractional amplitudes in case of hydroxy vanillin at 20°C for longer lifetime components were $a_1 = 0.0351$ and $a_2 = 0.1021$ and for shorter lifetime components were $a_3 = 0.1813$, $a_4 = 0.2818$ and $a_5 = 0.4421$. The fractional amplitudes in case of dihydroxy vanillin at 20°C for longer lifetime components were $a_1 = 0.0752$ and $a_2 = 0.1665$ and for shorter lifetime components were $a_3 = 0.2737$ and $a_4 = 0.4845$. The fractional amplitudes in case of methyl vanillin at 20°C for longer lifetime components were $a_1 = 0.3418$ and $a_2 = 0.3477$ and for shorter lifetime components were $a_3 = 0.1791$ and $a_4 = 0.1314$. The fractional amplitudes in case of ethyl vanillin at 20°C for longer lifetime components were $a_1 = 0.3411$ and $a_2 = 0.3687$ and for shorter lifetime components were $a_3 = 0.1713$ and $a_4 = 0.1189$.

Thus, at 20°C in case of hydroxy vanillin only ~ 13.5% of the probes were in less mobile environment and the rest (86.5%) of the probes were in mobile environments. In case of dihydroxy vanillin ~ 24% of probes were in less mobile environment and the rest (76%)

of the probes were in mobile environments. For methyl vanillin (68.95%) of probes were in less mobile environment and the rest (31.05%) of the probes were in mobile environments. And lastly in case of ethyl vanillin (70.98%) of probes were in less mobile environment and the rest (29.02%) of the probes were in mobile environments. Comparing the amplitudes among all the probes in the same amorphous sucrose matrix at the same temperature (20°C), indicate that the majority (~80%) of the hydroxy and dihydroxy vanillin probes were located in mobile environment whereas in the case of methyl and ethyl vanillin the majority (~70%) were located in the less mobile environment. This difference could be attributed to the structural variations among vanillin and each of the analogs. This difference could also be attributed to the ability of the probe to form hydrogen bond with the matrix.

The average lifetime was calculated using Eq. 4. A comparison plot of average lifetime as a function of temperature is shown in Figure 14a. The average lifetime of hydroxy vanillin varied from 67.5 ms at -20°C to 0.12 ms at 90°C, indicating ~562-fold difference in average mobility. The average lifetime of dihydroxy vanillin varied from 56.8 ms at -20°C to 0.54 ms at 90°C, indicating ~105-fold difference in average mobility. The average lifetime of methyl vanillin varied from 156.4 ms at -20°C to 0.5 ms at 100°C, indicating ~300-fold difference in average mobility. The average lifetime of ethyl vanillin varied from 162.1 ms at -20°C to 0.24 ms at 100°C, indicating ~675-fold difference in average mobility. The decrease in lifetime as a function of temperature corresponds to an increase with temperature in the non-radiative decay process k_{NR} (eq. 5, Materials and Methods). The differences in the mobility detected by each of the probe could be

attributed to the structural variations among the probes. In the glass the average lifetime followed the order of ethyl > methyl > hydroxy > dihydroxy vanillin. In the melt at temperatures above 60°C ethyl and methyl vanillin had longer lifetimes compared to hydroxy and dihydroxy vanillin. However, lifetimes overlapped between the ethyl and methyl pair and also between the hydroxy and dihydroxy pair above 60°C.

The Arrhenius plot of $\ln(k_p)$ for average lifetime for hydroxy, dihydroxy, methyl and ethyl vanillin is shown in Figure 14b. Arrhenius plots of $\ln(k_{pi})$ for individual lifetime components were also plotted for hydroxy (Figure 15a), dihydroxy (Figure 15b), methyl (Figure 15c) and ethyl (Figure 15d) vanillin. Break point temperatures and activation energies determined from intersection of trendline to points at low, intermediate and high temperature for individual lifetime components and average lifetimes are as compiled in Table 2, 3, 4 and 5 for hydroxy, dihydroxy, methyl and ethyl vanillin, respectively.

The hydroxy vanillin average lifetime showed transition temperatures of 35°C with activation energies at low and high temperature of 30.9 kJ mol⁻¹ and 87.1 kJ mol⁻¹, respectively (Table 2). The dihydroxy vanillin average lifetime showed a transition temperature of 30°C with activation energies at low and high temperature of 26.8 kJ mol⁻¹ and 51.0 kJ mol⁻¹, respectively (Table 3). The methyl vanillin average lifetime showed transition temperatures of ~40°C with activation energies at low, intermediate and high temperature of 9.64 kJ mol⁻¹ and 76.34 kJ mol⁻¹, respectively (Table 4). The ethyl vanillin average lifetime showed transition temperatures of 40°C and 76°C with activation energies at low and high temperature of 9.03 kJ mol⁻¹ and 143.02 kJ mol⁻¹, respectively

(Table 5). The activation energies at high temperature in the melt were significantly different among vanillin and the analogs following the order of ethyl > methyl > hydroxy > dihydroxy.

Rate Constants: Analysis of lifetimes in terms of underlying photophysical rate constants for de-excitation of the triplet state provides additional insights into the effect of temperature on matrix mobility in amorphous sucrose films. The k_{NR} term is a rate constant for non-radiative decay; it is the actual measure of the effect of the motion that quenches probes excited triplet state and is obtained from eq. 5. The k_{NR} values were calculated by subtracting the phosphorescence emission rate constant ($1/\tau$ at 77K in glycerol: water) from the inverse of the lifetime. Plots of k_{NR} as a function of temperature are represented in Figure 16a and 16b for hydroxy, dihydroxy, methyl and ethyl vanillin. The rate for dihydroxy vanillin was the highest followed by hydroxy, methyl and ethyl vanillin up to 40°C in the glass, but above 40°C in the melt the order was hydroxy > dihydroxy > methyl > ethyl vanillin.

The respective Arrhenius plots of k_{NR} for hydroxy, dihydroxy, methyl and ethyl vanillin are shown in Figures 17a, 17b, 17c and 17d. The activation energy obtained from the slope trendline in this plot is the activation energy of the motions which quench probes excited triplet state. The E_a values and transition temperatures for each probe are tabulated in Table 6. At high temperature the activation energy followed the order ethyl > methyl > hydroxy > dihydroxy vanillin.

Discussion

The two general modes of matrix molecular mobility; dipolar relaxation and collisional quenching modulate the emission energy and lifetime of the excited triplet state (Pravinata et al., 2005; Shirke et al 2005, 2006). The phosphorescence of vanillin and its analogs was found to be extremely sensitive to the local environment in the amorphous sucrose in the glassy state and at the glass-to-rubber transition into the melt. The emission energy decreased gradually in the glass and more dramatically in the melt for all four probes, reflecting the effect of temperature on the rate of dipolar relaxation around the excited triplet state. The change in emission energy as a function of temperature was ~ 10 times smaller in hydroxy vanillin compared to the other probes, this probably is related to the size of the dipole that exists in the molecule in the excited triplet state. The emission energy was lower for dihydroxy vanillin as compare to methyl and ethyl vanillin, whereas FWHM was much higher in dihydroxy vanillin as compared to methyl and ethyl vanillin. The increase in dipolar relaxation rate was accompanied by an increase in the width of the distribution of energetically distinct environments. The ability to monitor molecular mobility is attributed to the sensitivity of the emission of hydroxy, dihydroxy, methyl and ethyl vanillin to dipolar relaxation of solvent molecules around its polar triplet excited state. The decrease in emission energy and the broadening of emission spectra with an increase in temperature can be explained with a solvent relaxation mechanism (Ludescher et al., 2001).

The phosphorescence decays at 77K fitted to a single exponential function. There was no significant difference in the lifetime among dihydroxy ($\tau = 352$ ms), methyl ($\tau = 372$ ms)

and ethyl ($\tau = 358$ ms) vanillin in glycerol: water at 77K; however the lifetime of hydroxy ($\tau = 545$ ms) vanillin was significantly larger. All four probes at 77K in EPA had lower lifetimes compared to glycerol: water, dihydroxy ($\tau = 215$ ms), methyl ($\tau = 190$ ms), ethyl ($\tau = 189$ ms) and hydroxy ($\tau = 255$ ms) vanillin, thus indicating the effect of solvent on lifetime. Vanillin has been reported to have lifetime ($\tau = 172$ ms) at 77K in ethanol. In amorphous sucrose films at 77K the lifetimes were intermediate between those observed in glycerol: water and EPA, dihydroxy ($\tau = 330$ ms), methyl ($\tau = 272$ ms), ethyl ($\tau = 286$ ms) and hydroxy ($\tau = 403$ ms) vanillin. At τ_{77K} in glycerol: water the lifetime differs from that of the sucrose for two reasons one been the different nature of the two solvent and thus different hydrogen bond networks. The other reason was presence of more mobility in sucrose at 77K than in glycerol: water. Thus, comparing the above data indicated that hydroxy vanillin has lifetime values significantly different than dihydroxy, methyl and ethyl vanillin. This difference could be attributed to structural variation between hydroxy vanillin and the other three probes where the $-OR$ group is absent in hydroxy vanillin. Thus hydroxy vanillin differs from other probes where at τ_{77K} it has longer lifetime, phosphorescence emission is blue shifted at 293K in sucrose, phosphorescence excitation is blue shifted at 293K (and only one band), phosphorescence emission is not affected by the solvent at 77K (compared to other probes), and has small $\Delta\nu(T)$. All this suggest that hydroxy vanillin is in by itself.

For dihydroxy, methyl and ethyl vanillin (where the only structural variation is in the R group attached to the oxygen) there was no significant difference in the lifetimes indicating that the structural variation had no effect on the intrinsic phosphorescence

lifetime. Although there was no significant difference in the lifetime's values among dihydroxy, methyl and ethyl vanillin at 77K, the average lifetimes at 20°C were distinctly different for the three probes where lifetimes were dihydroxy ($\tau = 12.2$ ms), methyl ($\tau = 92.0$ ms), ethyl ($\tau = 108.2$ ms). In case of hydroxy vanillin at 20°C, $\tau = 16.2$ ms. This decrease in lifetime from 77K to room temperature among all the probes is due to increase in matrix molecular mobility. The phosphorescence lifetimes of hydroxy, dihydroxy, methyl and ethyl embedded in amorphous sucrose films were thus strongly modulated by matrix mobility. All analogs exhibited complex decay pattern and were fitted to a multi-exponential function.

At 77K in amorphous sucrose films the decays were fitted to a single exponential function but at 293K the decays were multi-exponential ($n = 4, 5$). This indicates narrow distribution of environments at 77K and broad distribution at 293K. Comparing the lifetimes τ_{77K} in sucrose to τ_{293K} in sucrose indicates presence of broad distribution of environment at 293K.

The variation in the lifetime components of each probe indicated that the local environment in amorphous sucrose films has either ~ 200 (hydroxy vanillin), ~ 100 (dihydroxy vanillin), ~ 70 (methyl vanillin) or ~ 60 (ethyl vanillin) fold difference in mobility. It is worth noting that some of the environments in sucrose at 253K are nearly as immobile (have similar lifetimes) as at 77K; ~ 240 ms vs. 272 ms in case of methyl vanillin and ~ 240 ms vs. 286 ms in case of ethyl vanillin. The transition temperature calculated from the Arrhenius plot of k_p (average lifetime) showed variation with the R

group where hydroxyl vanillin (35°C), dihydroxy vanillin (30°C), methyl vanillin (40°C) and ethyl vanillin (60°C). Even individual lifetime components showed variation in transition temperature for each probe.

The amplitudes indicate that a majority (~80%) of the hydroxy and dihydroxy vanillin probes are located in a mobile environment whereas in case of methyl and ethyl vanillin (~70%) a majority is located in a less mobile environment. The amplitudes also varied as function of temperature in hydroxy, dihydroxy, methyl and ethyl vanillin. As a function of temperature from -20°C to 100°C the order of average lifetime was ethyl vanillin > methyl vanillin > hydroxyl vanillin > dihydroxy vanillin. The activation energy phosphorescence quenching (from $\ln k_p$ for average lifetime) at high temperature also followed the same order ethyl vanillin ($E_{aH} = 137.3 \text{ kJ mol}^{-1}$) > hydroxyl vanillin ($E_{aH} = 74.37 \text{ kJ mol}^{-1}$) > methyl vanillin ($E_{aH} = 72.32 \text{ kJ mol}^{-1}$) > dihydroxy vanillin ($E_{aH} = 51.64 \text{ kJ mol}^{-1}$). The activation energies (for collisional quenching) also differed among the four probes in the same temperature region in amorphous sucrose films.

These differences could be attributed to the structural differences in the vanillin and its analogs. Vanillin and its analogs have exactly the same structure except the R group attached to the C-R bond that varied in molecular size, where R = -OC₂H₅ (ethyl vanillin) > R = -OCH₃ (methyl vanillin) > R = -OH (dihydroxy vanillin) > R = -H (CO-R is absent) in case of hydroxy vanillin. The longer lifetimes and higher activation energies in ethyl vanillin is due to the effect of larger molecular size group (-C₂H₅) as compared to the others. The nonradiative decay rate for dihydroxy vanillin was the highest followed by

hydroxy, methyl and ethyl vanillin up to 40°C in the glass, but above 40°C in the melt the order was hydroxy > dihydroxy > methyl > ethyl vanillin. The activation energy for collisional quenching followed the order where at low temperature dihydroxy > hydroxy > methyl > ethyl and at high temperature ethyl > methyl > hydroxy > dihydroxy.

A study (Nishigaki et al., 1998) looked at molecules with different size (vanillin, 4-hydroxy benzaldehyde, tobias acid, 2-napthoic acid and 9-anthracenemethanol adsorbed on filter paper (Nishigaki et al., 1996). They found that 9-anthracenmethanol had relatively high activation energy though it has only one adsorption site and this behavior was thought to be effect of molecular size. Filter paper have cages, when small molecules are adsorbed on it , they still have large space for movement, but larger molecules are held tight in the cage and escape from the collisional radiationless deactivation. Our study shows similar observation where bigger molecule ethyl vanillin is held rigid in the amorphous sucrose film and escape from the collisional radiationless deactivation (showing longer lifetime) as compared to methyl, dihydroxy and hydroxyl vanillin.

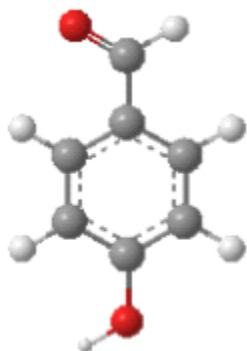
At low temperatures the amorphous sucrose films is rigid and hence restricts any movements of the molecules. But at higher temperate amorphous sucrose films have free volume, where small molecules like hydroxy and dihydroxy vanillin are adsorbed in it they still have large space for movement, but larger molecules like methyl and ethyl vanillin are held tight in the cage and escape from the collisional radiationless deactivation, thus showing longer lifetimes.

WLF (Williams-Landel-Ferry) and VTF (Vogel-Fulcher-Tamman-Hesse) commonly used equation to predict temperature dependence of viscosity for super cooled liquids. The free volume based WLF theory has been shown to be more applicable in predicting temperature dependent mechanical properties of amorphous materials. FVT assumes that temperature dependence of viscosity is related to free volume (Dolittle, 1951). The FVT is based on change in volume expansion coefficient at glass transitions and assumes that molecular motions depend on the presence of holes or voids (Roos, 1995) and thus allowing the molecular movement to take place. These holes between molecules provide the free volume that is needed for molecular rearrangements. Our studies using different analogs of vanillin (Chapter III) supports this interpretation. Thus vanillin could also indicate increase in free volume in amorphous sucrose matrix as a function of temperature. Thus based on this we conclude that movement of methoxyl group about the C-O bond could be sensitive to matrix mobility.

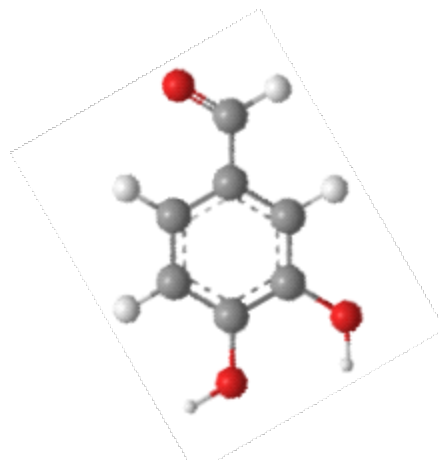
There is one more possibility that the effect is not that of larger group but rather that of group not able to hydrogen bond to matrix. As dihydroxy vanillin is capable of hydrogen bonding with the matrix which is not the case with methyl and ethyl vanillin. Thus there is a possibility that there is the effect of the substituent on coupling the probe vibrations to the matrix. This study provides useful insight about the mechanism of vanillin sensitivity to molecular mobility in amorphous sucrose films by using analogs of vanillin.

Conclusion

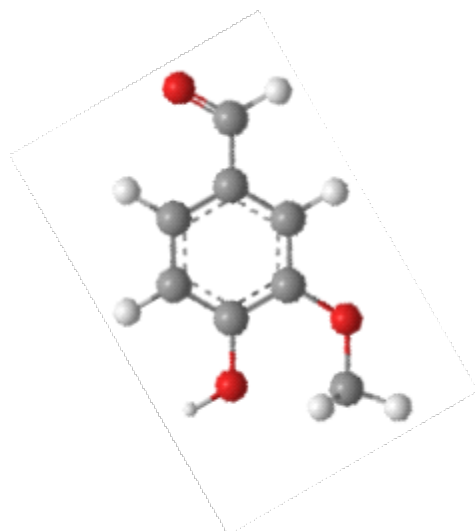
Hydroxy, dihydroxy, methyl and ethyl vanillin phosphorescence lifetime were found to be extremely sensitive to the local environment in the amorphous sucrose in the glassy state and at the glass-to-rubber transition into the melt. Phosphorescence emission spectra and time-resolved intensity decays, measured in sucrose as a function of temperature in the absence of oxygen, were strongly modulated by matrix molecular mobility for vanillin and its analogs. At low temperatures the amorphous sucrose films are rigid and hence restrict any movements of the molecules. But at higher temperature amorphous sucrose films have free volume, when small molecules like hydroxy and dihydroxy vanillin are adsorbed in it, they still have large space for movement, but larger molecules like methyl and ethyl vanillin are held tight in the cage and escape from the collisional radiationless deactivation, thus showing longer lifetimes. The only structural variation among the four probes is the presence of different molecular size R groups attached to the O-R bond (in case of dihydroxy, methyl and ethyl vanillin) or absence of O-R group (in case of hydroxy vanillin). Thus based on this we conclude that capability of movement of methoxyl group about the C-O bond could be a contributor to sensitivity of vanillin to matrix molecular mobility. The other possibility could be that there is the effect of the substituent on coupling the probe vibrations to the matrix based on ability to form hydrogen bond with the matrix. This study provides useful insight about the mechanism of vanillin sensitivity to molecular mobility in amorphous sucrose films by using analogs of vanillin.

Figure III-1

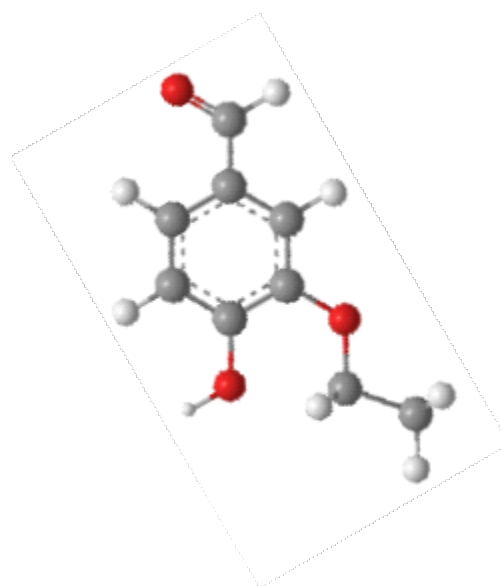
4-Hydroxybenzaldehyde



3, 4-Dihydroxybenzaldehyde



4-Hydroxy-3-methoxybenzaldehyde



4-Hydroxy-3-ethoxybenzaldehyde

Figure III-1: Structure of hydroxy vanillin (4-hydroxy-benzaldehyde), dihydroxy vanillin (3, 4-dihydroxy-benzaldehyde), methyl vanillin (4-hydroxy-3-methoxy-benzaldehyde) and ethyl vanillin (4-hydroxy-3-ethoxy-benzaldehyde).

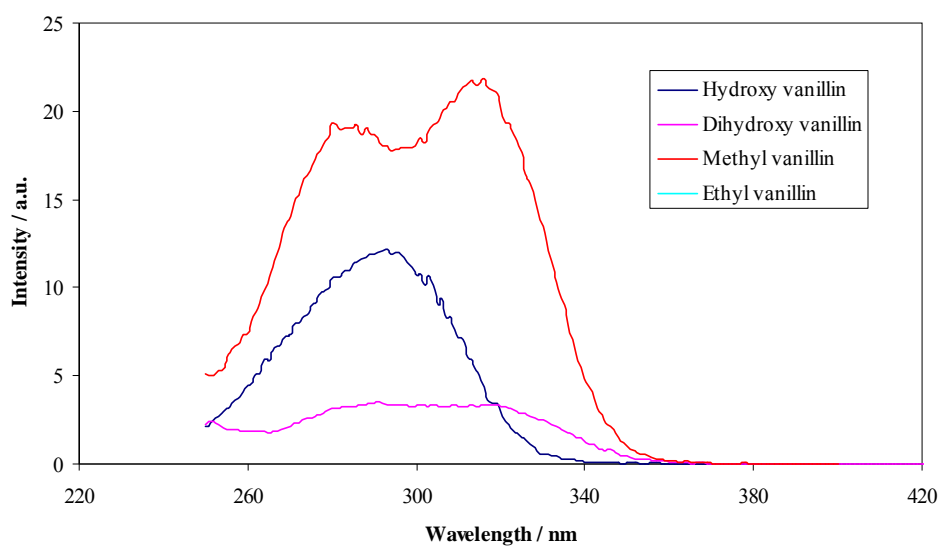
Figure III-2

Figure III-2: Phosphorescence excitation spectra for hydroxy, dihydroxy, methyl and ethyl vanillin phosphorescence in amorphous sucrose films ($1:10^3$: dye: sucrose) ($-O_2$) at 20°C . Emissions were collected for hydroxy (450 nm), dihydroxy (490 nm), methyl (490 nm) and ethyl vanillin (490 nm).

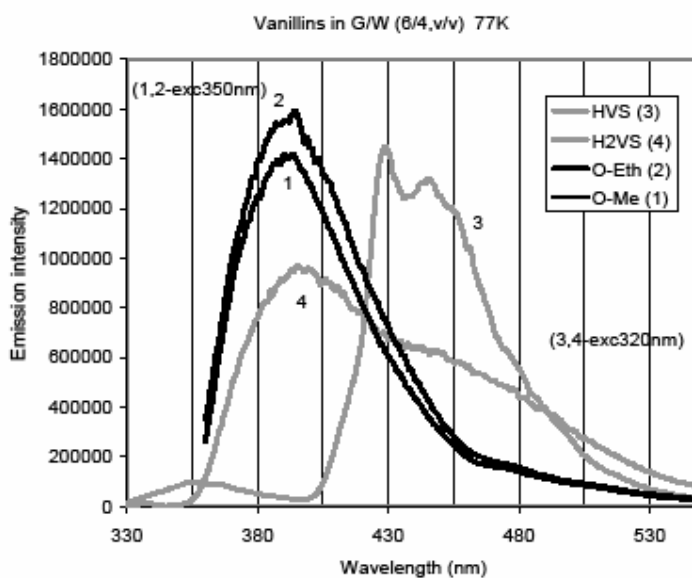
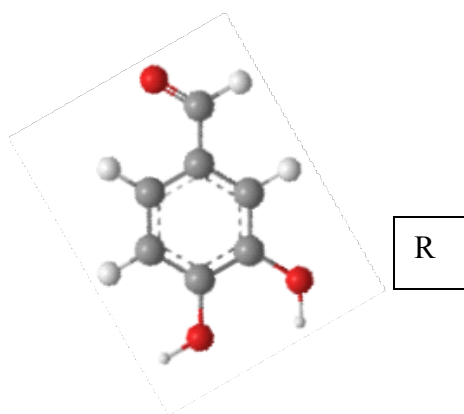
Figure III-3a

Figure III-3a: The phosphorescence emission spectra of methyl vanillin (1) and the three analogs hydroxy (3), dihydroxy (4) and ethyl (2) vanillin at 77K in glycerol: water. Excitations were hydroxy (320 nm), dihydroxy (320 nm), methyl (350 nm) and ethyl vanillin (350 nm).



R

- = H (hydroxy: HVS)
- = OH (dihydroxy: H2VS)
- = OCH₃ (methyl: O-Me)
- = OC₂H₅ (ethyl: O-Eth)

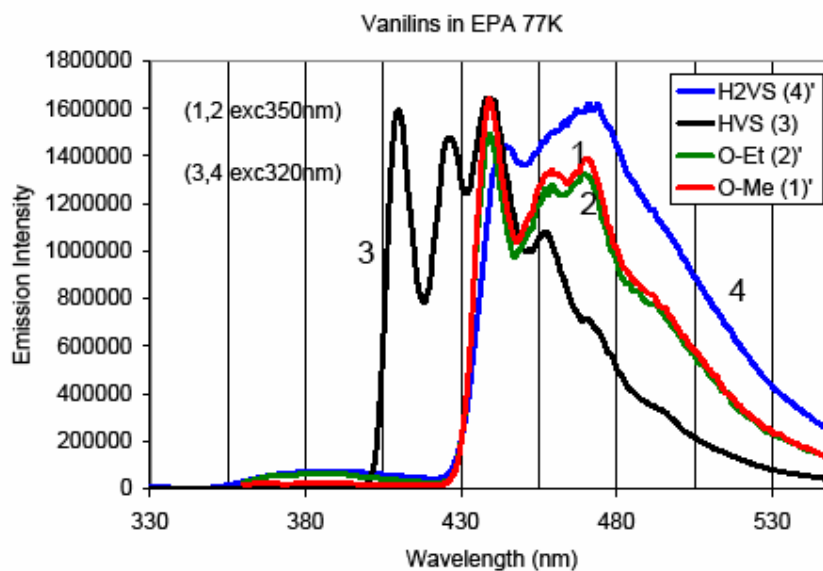
Figure III-3b

Figure III-3b: The phosphorescence emission spectra of methyl vanillin (1) and the three analogs hydroxy (3), dihydroxy (4) and ethyl (2) vanillin at 77K in EPA solvent. Excitations were hydroxy (320 nm), dihydroxy (320 nm), methyl (350 nm) and ethyl vanillin (350 nm).

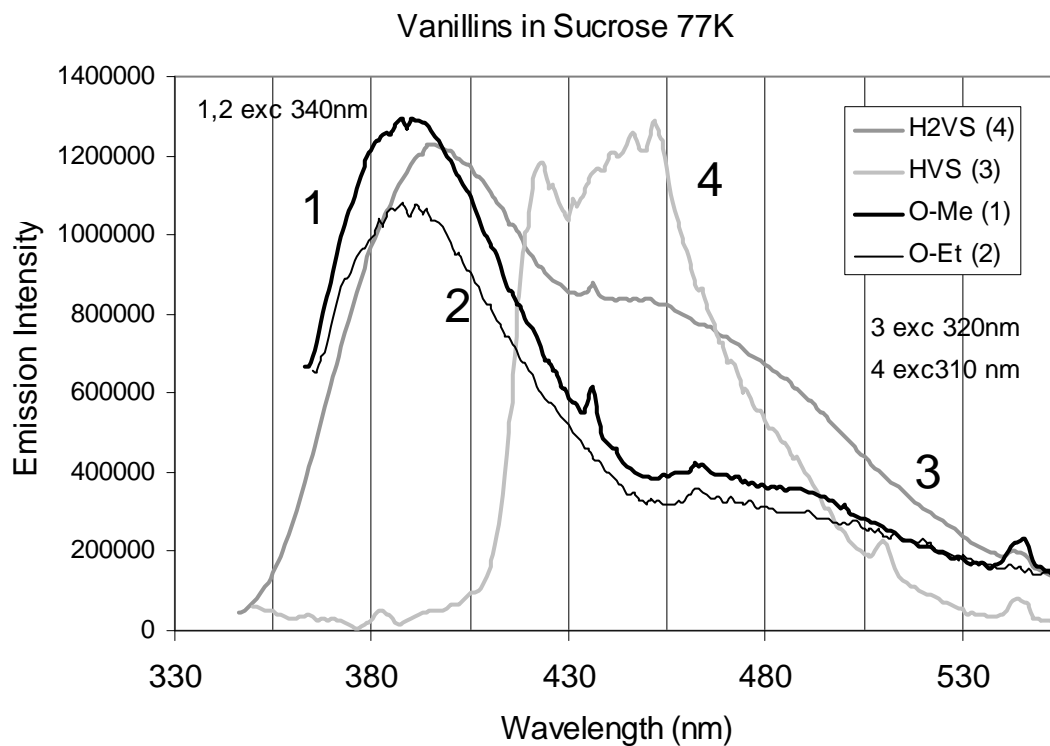
Figure III-3c

Figure III-3c: The phosphorescence emission spectra of methyl vanillin (1) and the three analogs hydroxy (3), dihydroxy (4) and ethyl (2) vanillin at 77K in amorphous sucrose films. Excitations were hydroxy (320 nm), dihydroxy (320 nm), methyl (350 nm) and ethyl vanillin (350 nm).

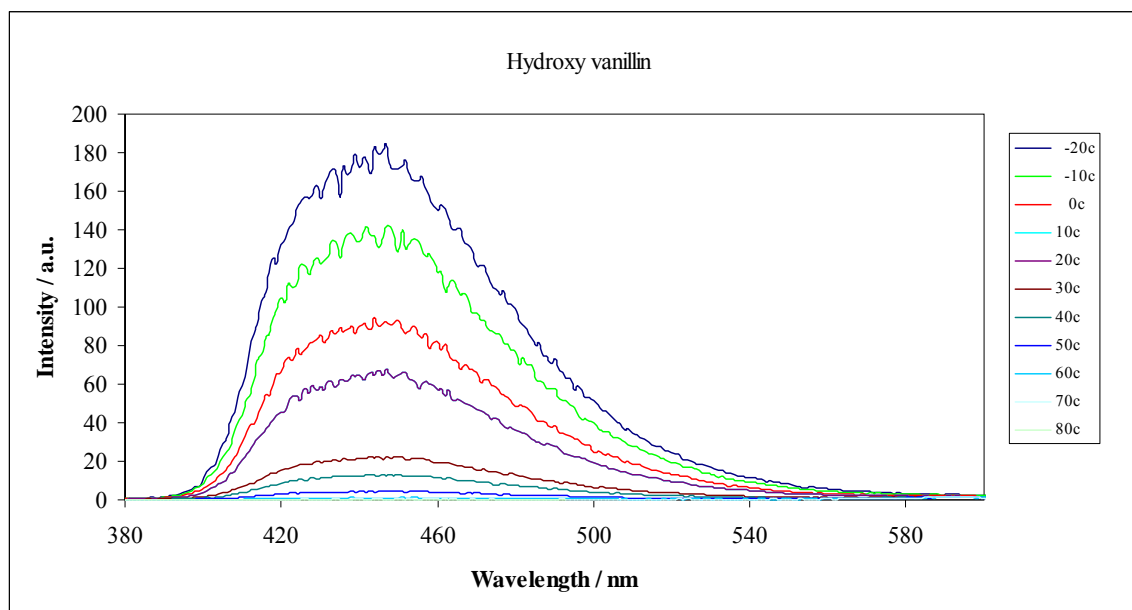
Figure III-4a

Figure III-4a: Delayed emission spectra of hydroxy vanillin in amorphous sucrose films as a function of temperature (excitation at 300 nm). The spectra were collected at 10°C intervals from -20°C to 80°C (the curves follow this order from high to low intensity at ~450 nm).

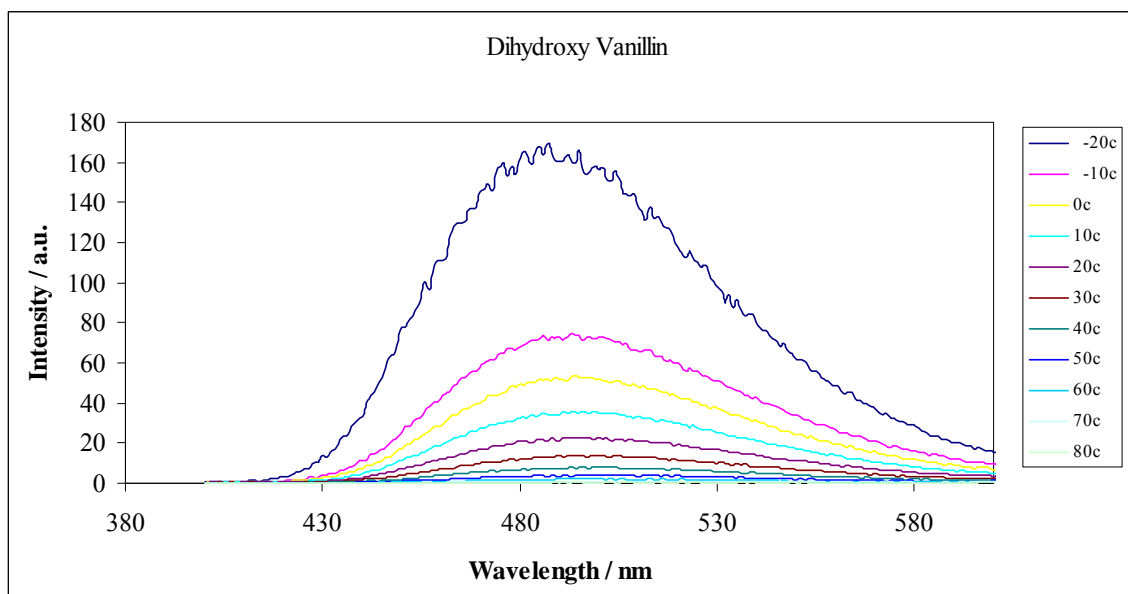
Figure III-4b

Figure III-4b: Delayed emission spectra of dihydroxy vanillin in amorphous sucrose films as a function of temperature (excitation at 320 nm). The spectra were collected at 10°C intervals from -20°C to 80°C (the curves follow this order from high to low intensity at ~490 nm).

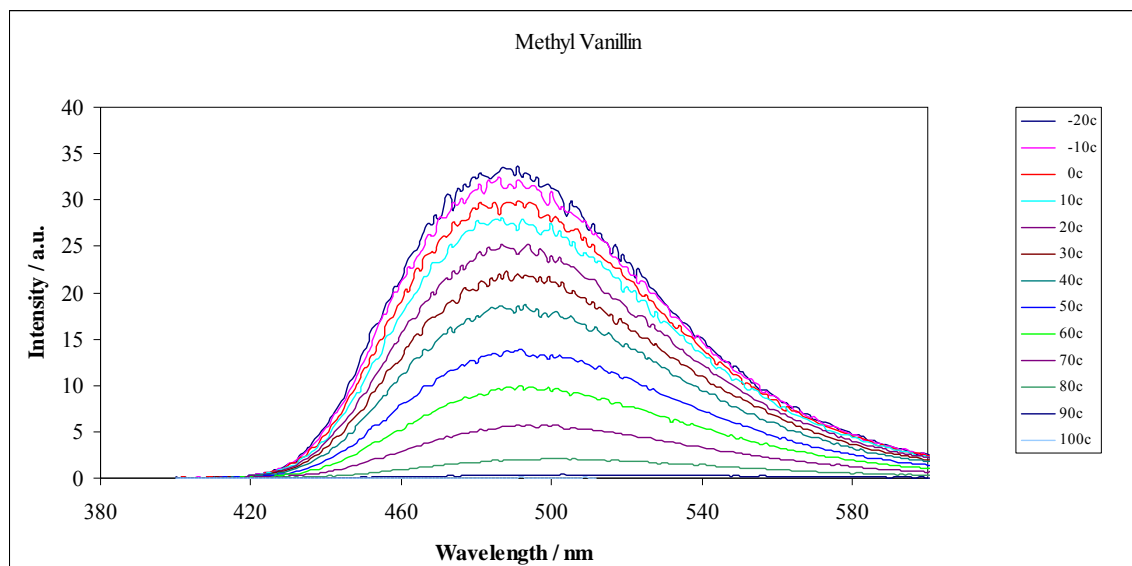
Figure III-4c

Figure III-4c: Delayed emission spectra of methyl vanillin in amorphous sucrose films as a function of temperature (excitation at 320 nm). The spectra were collected at 10°C intervals from -20°C to 100°C (the curves follow this order from high to low intensity at ~490 nm).

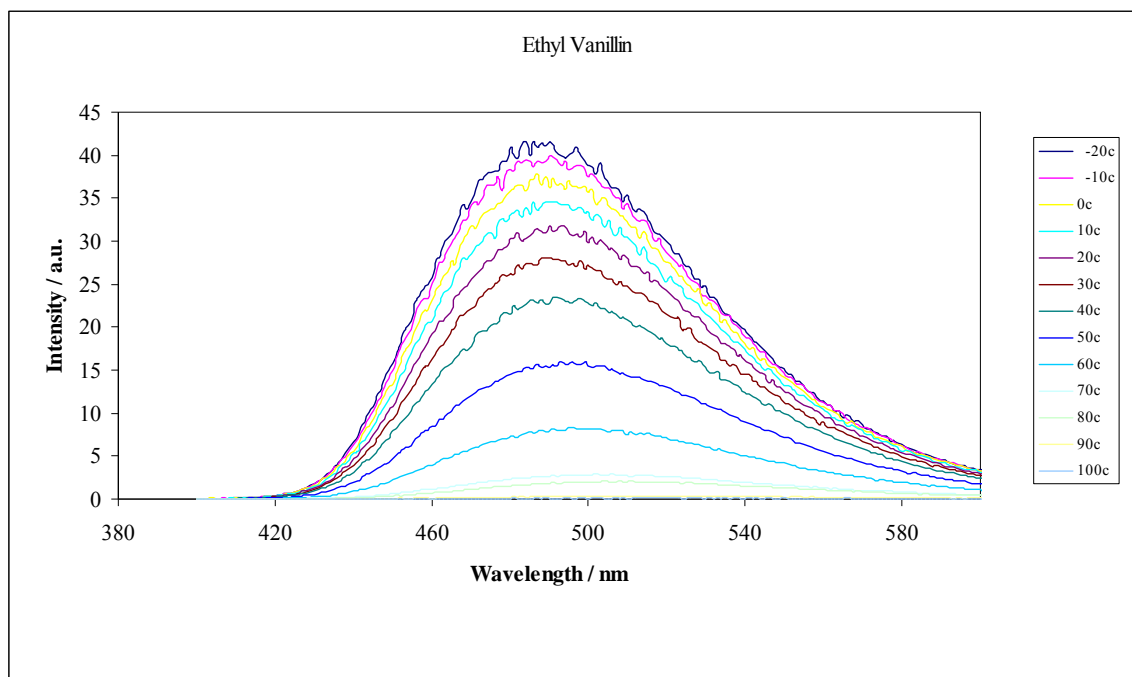
Figure III-4d

Figure III-4d: Delayed emission spectra of ethyl vanillin in amorphous sucrose films as a function of temperature (excitation at 320 nm). The spectra were collected at 10°C intervals from -20°C to 100°C (the curves follow this order from high to low intensity at ~490 nm).

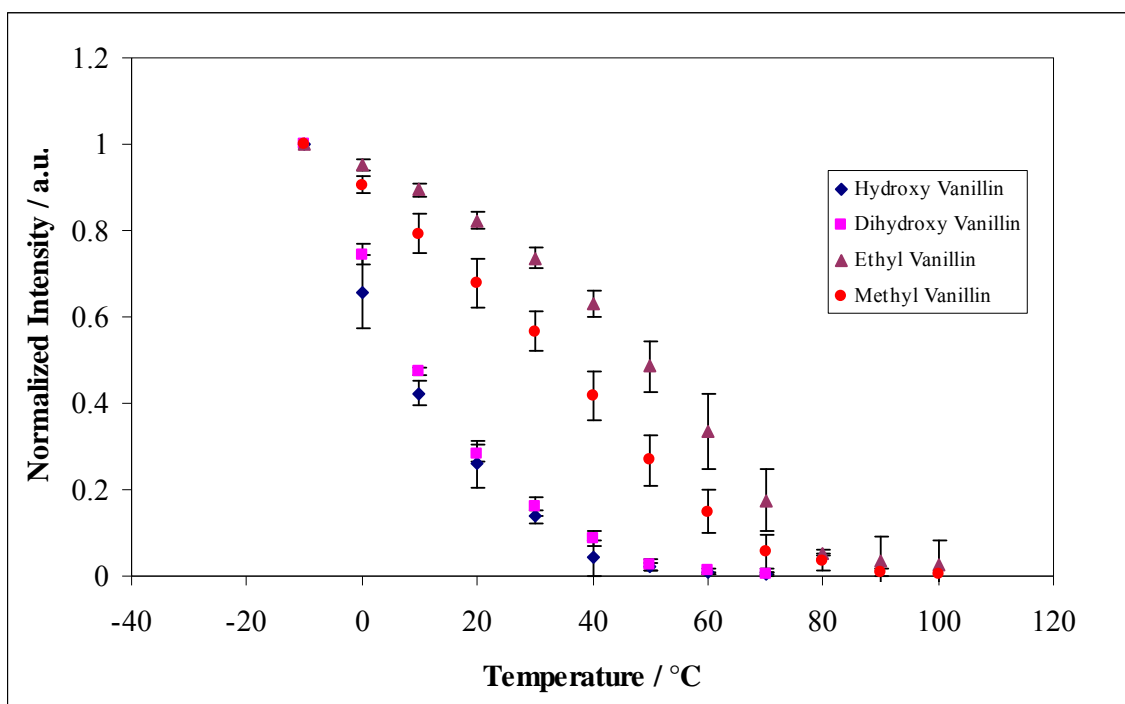
Figure III-5

Figure III-5: The effect of temperature on the phosphorescence emission intensity of hydroxy, dihydroxy, methyl and ethyl vanillin in amorphous sucrose films as a function of temperature equilibrated against nitrogen. The curves were normalized to -20°C. Intensity (I_p) was determined from analysis of the phosphorescence emission band (Figure III-4a, 4b, 4c, 4d) using a log-normal function (Eq. (1), Materials and Methods).

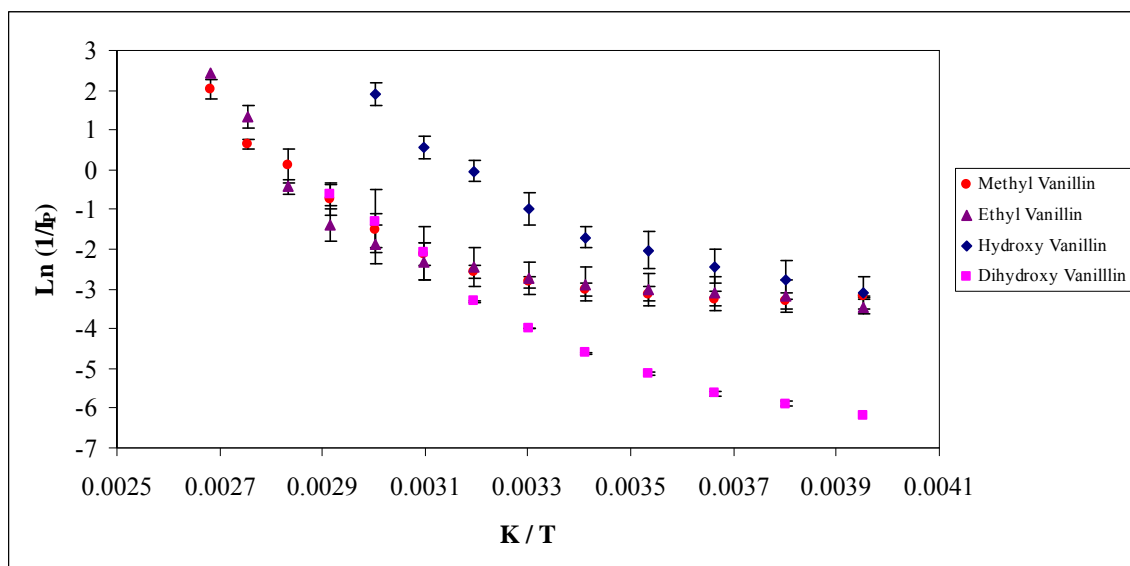
Figure III-6

Figure III-6: Arrhenius plot ($1/I_p$) of the effect of temperature on the phosphorescence emission intensity I_p of hydroxy, dihydroxy, methyl and ethyl vanillin in amorphous sucrose films.

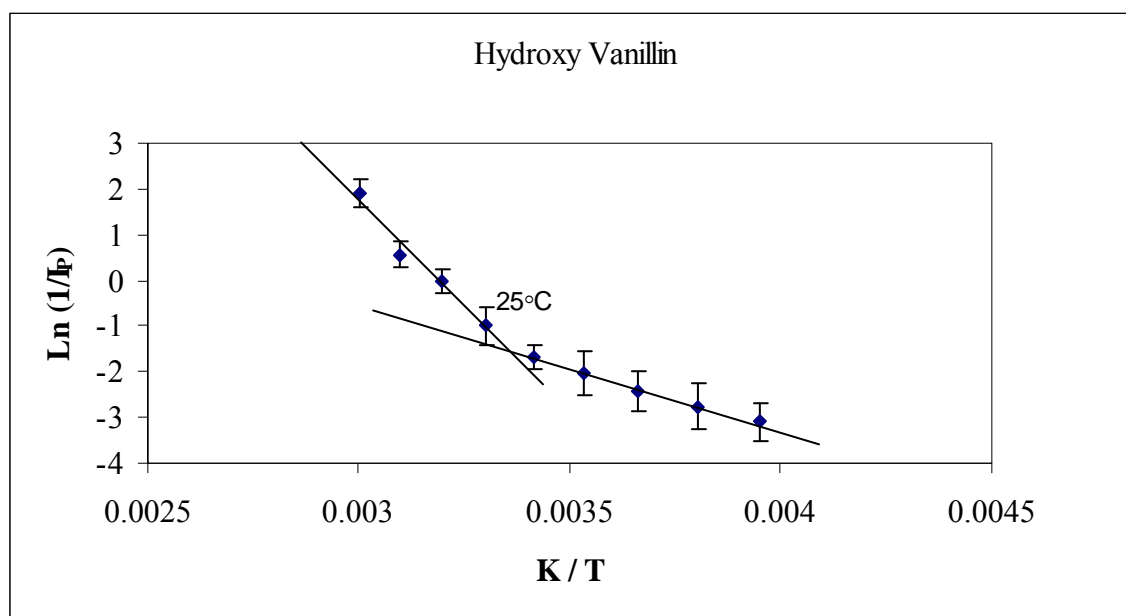
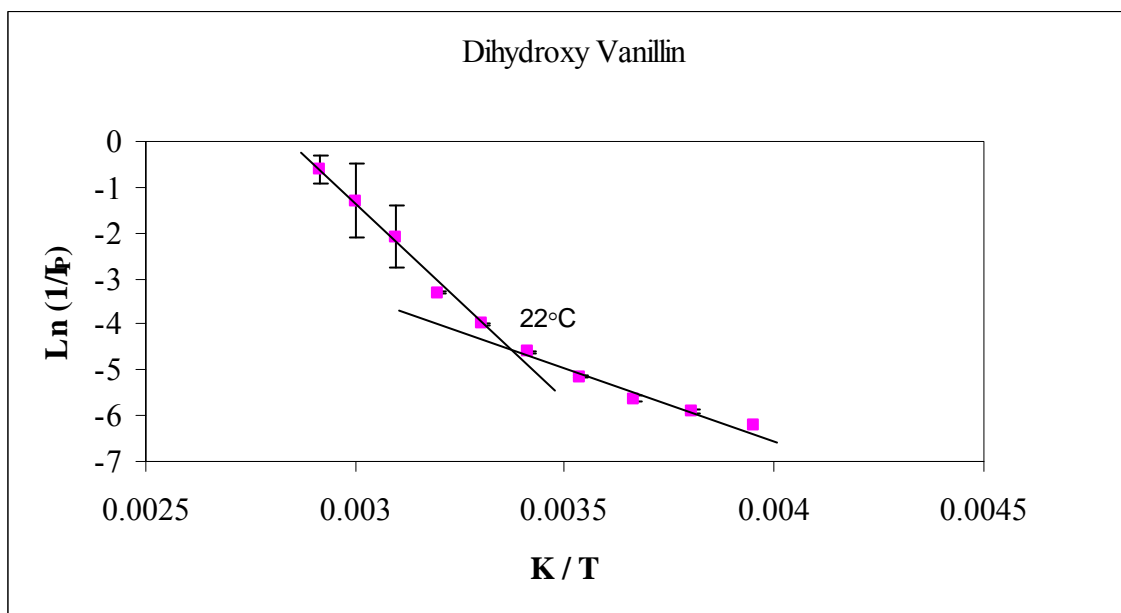
Figure III-6a*Figure III-6b*

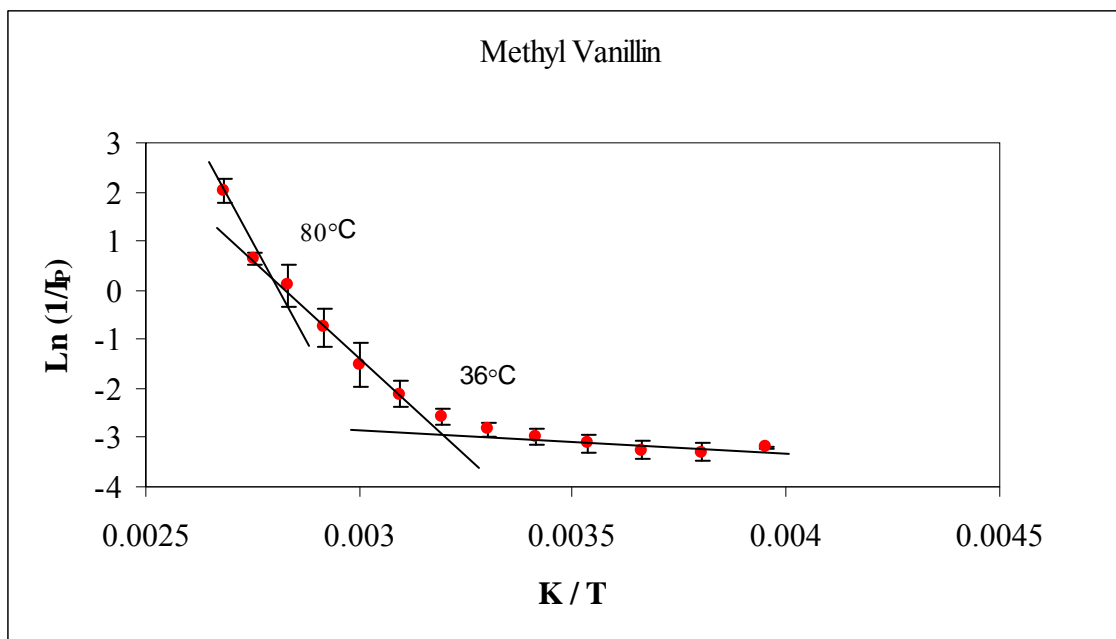
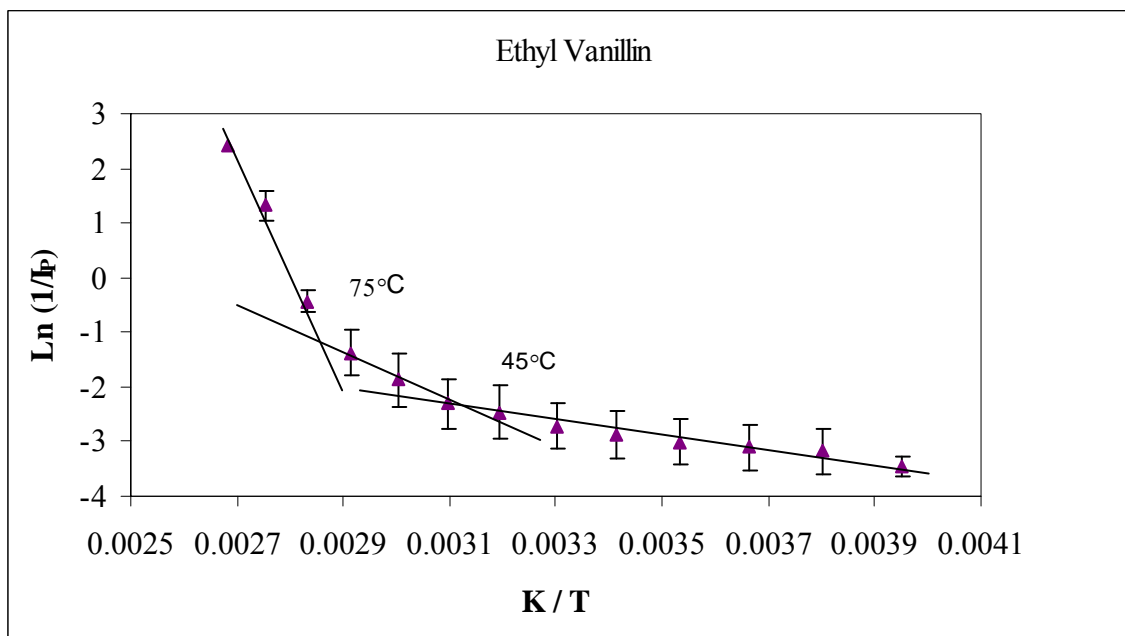
Figure III-6c**Figure III-6d**

Figure III-6a-6d: Arrhenius plot of the effect of temperature on the phosphorescence emission intensity $1/I_p$ of hydroxy, dihydroxy, methyl and ethyl vanillin in amorphous sucrose films. Lines drawn over the data points indicate slopes at low, intermediate and high temperatures hydroxy (6a), dihydroxy (6b), methyl (6c) and ethyl (6d) vanillin.

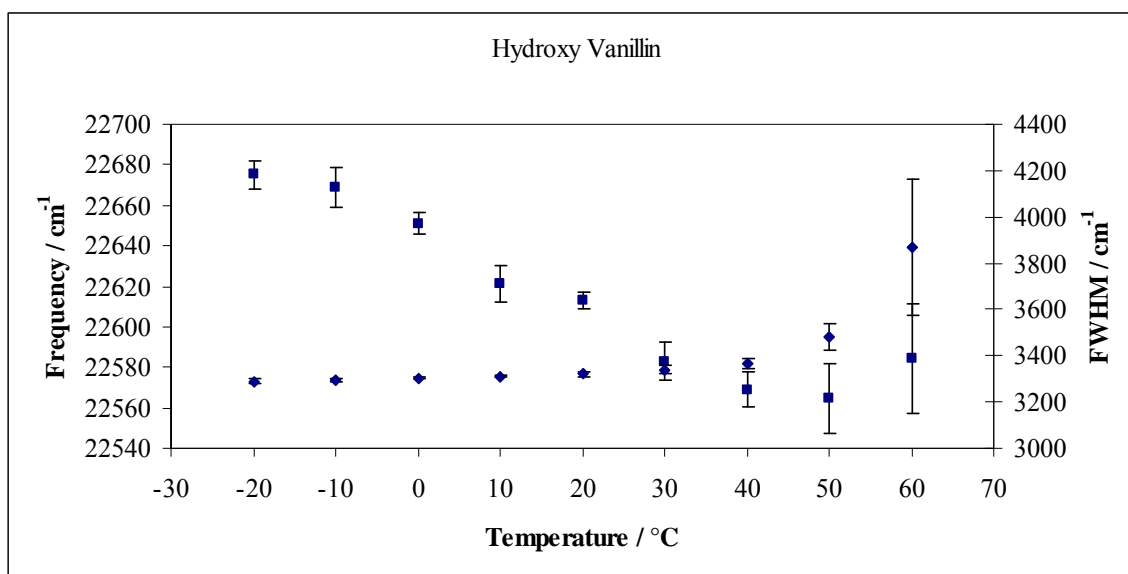
Figure III-7

Figure III-7: Peak energy ν_p (■, left hand scale) and bandwidth (◆, FWHM right hand scale) for phosphorescence emission from hydroxy vanillin in amorphous sucrose films as a function of temperature. The delayed emission spectra collected as a function of temperature (Figure III-4a) were analyzed using log-normal function as described in Materials and Methods using eq. (1) and (2).

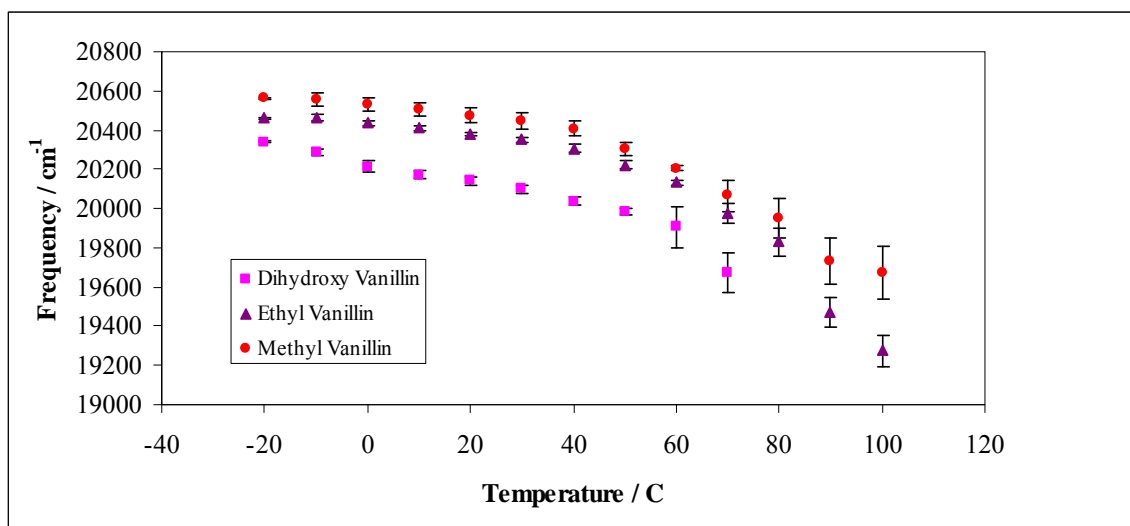
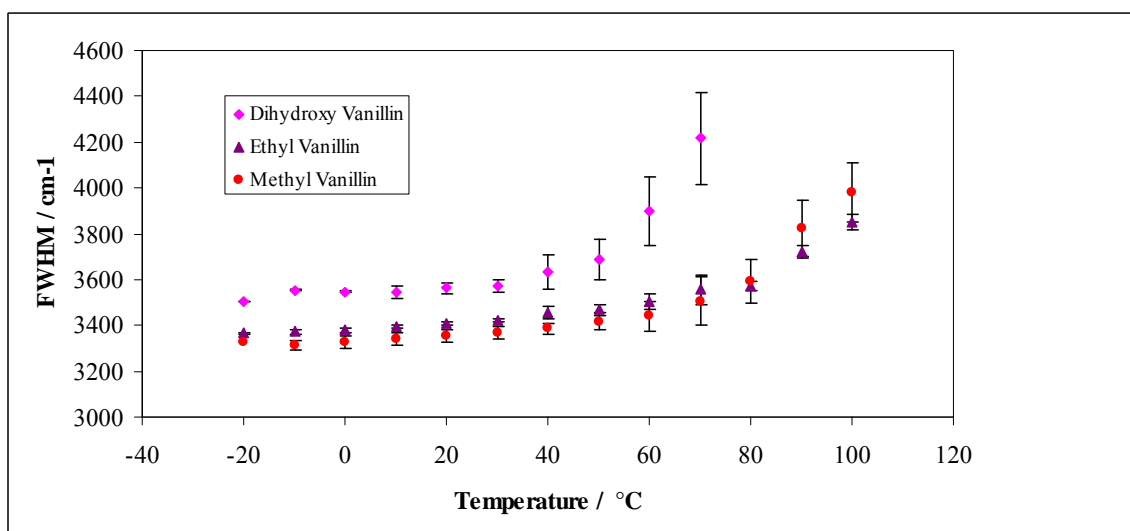
Figure III-8a**Figure III-8b**

Figure III-8a and 8b: Peak energy ν_p for phosphorescence emission from dihydroxy (■), methyl (●) and ethyl (▲) vanillin in amorphous sucrose films as a function of temperature (a). Bandwidth for phosphorescence emission from dihydroxy (■), methyl (●) and ethyl (▲) vanillin in amorphous sucrose films as a function of temperature (b). The delayed emission spectra collected as a function of temperature (Figure III) were analyzed using log-normal function as described in Materials and Methods using eq. (1) and (2).

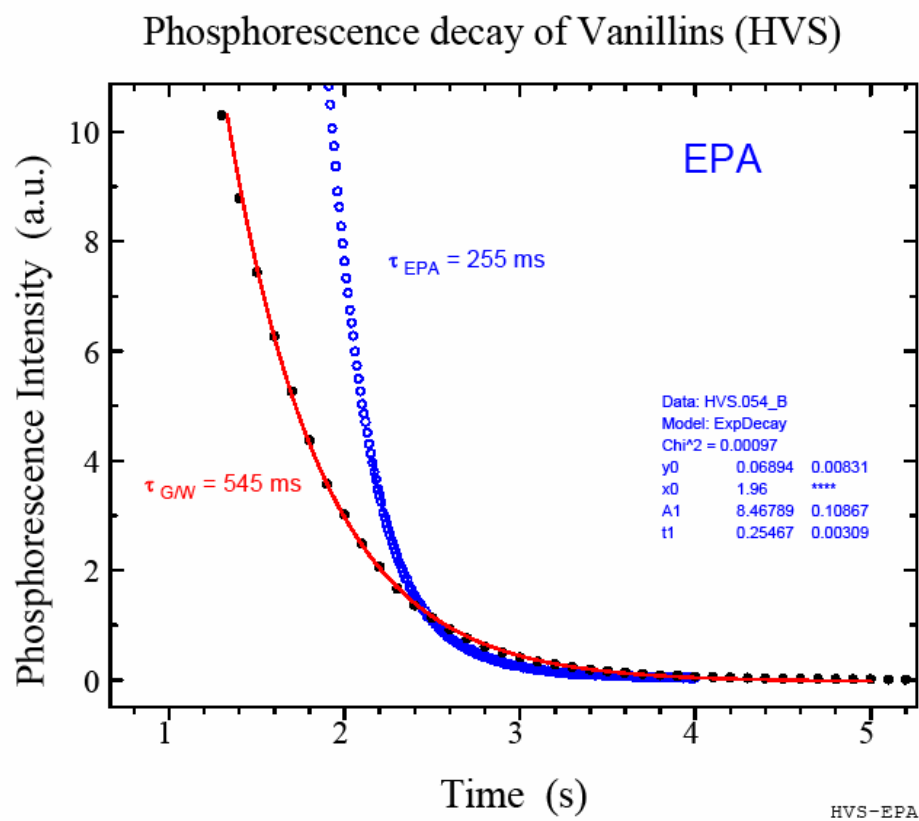
Figure III-9a

Figure III-9a: Lifetime obtained from a single-exponential model fit to phosphorescence intensity decay data from hydroxy vanillin dissolved in glycerol: water or EPA at 77K.

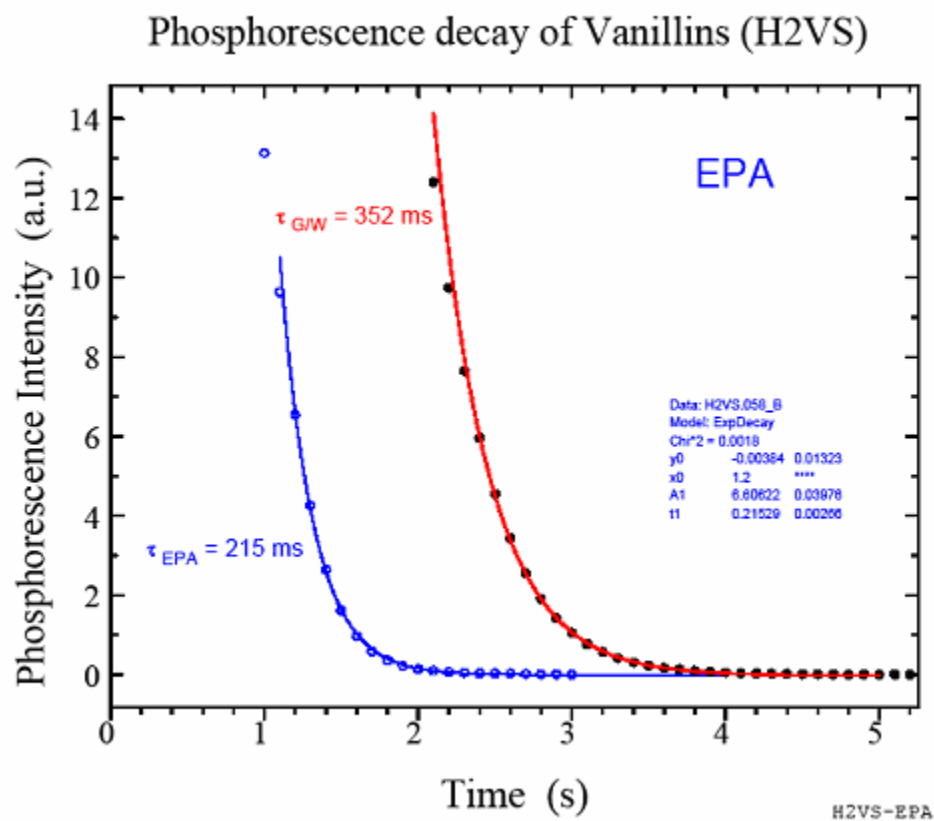
Figure III-9b

Figure III-9b: Lifetime obtained from a single-exponential model fit to phosphorescence intensity decay data from dihydroxy vanillin dissolved in glycerol: water or EPA at 77K.

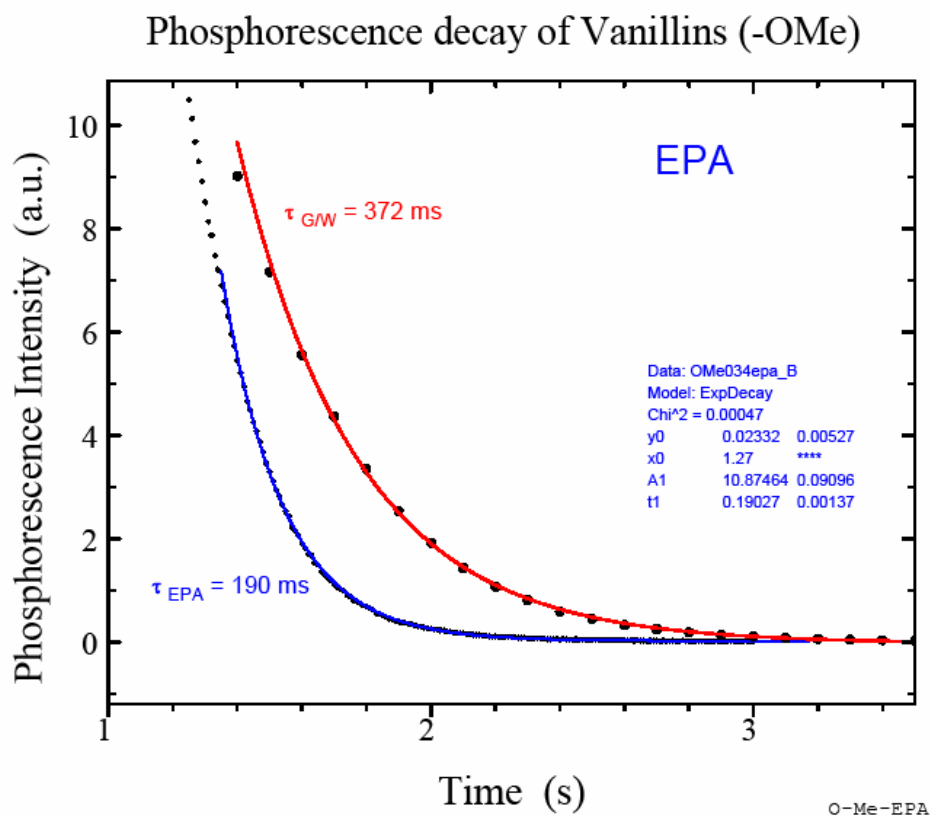
Figure III-9c

Figure III-9c: Lifetime obtained from a single-exponential model fit to phosphorescence intensity decay data from methyl vanillin dissolved in glycerol: water or EPA at 77K.

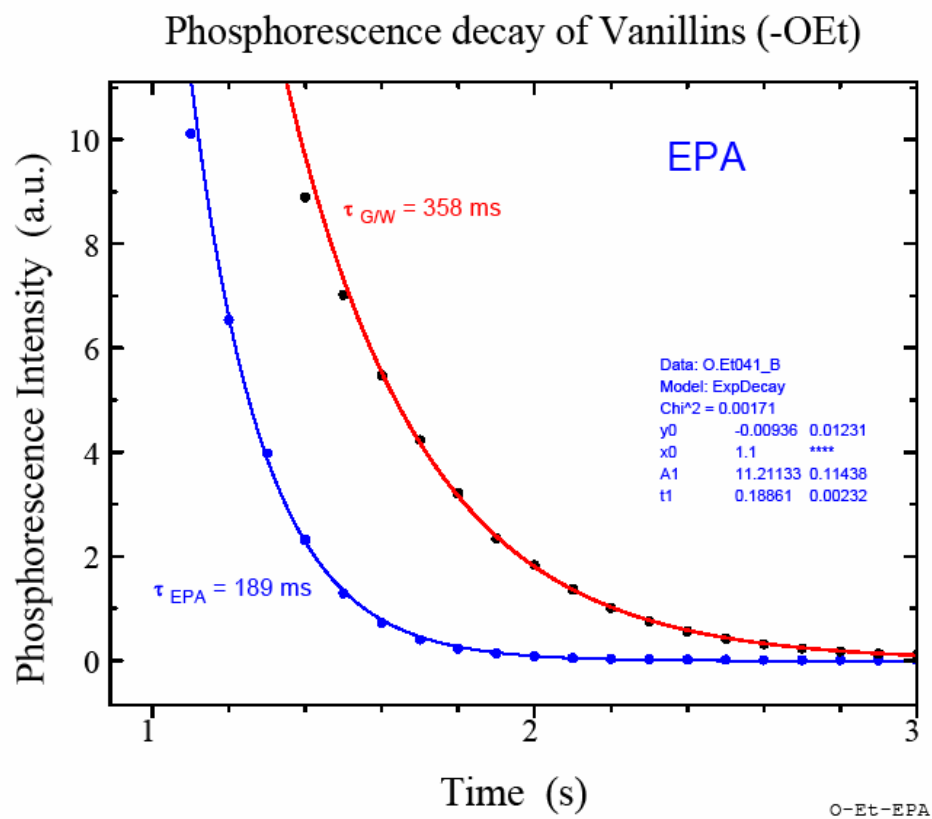
Figure III-9d

Figure III-9d: Lifetime obtained from a single-exponential model fit to phosphorescence intensity decay data from ethyl vanillin dissolved in glycerol: water or EPA at 77K.

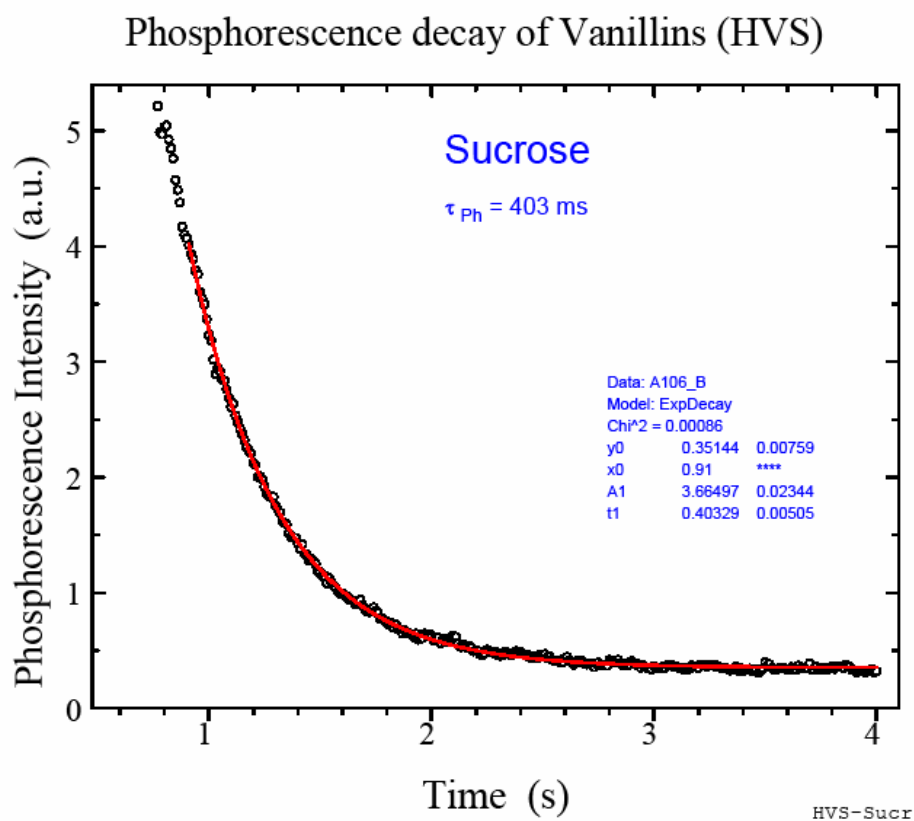
Figure III-10a

Figure III-10a: Lifetime obtained from a single-exponential model fit to phosphorescence intensity decay data from hydroxy vanillin dispersed in amorphous sucrose film at 77K.

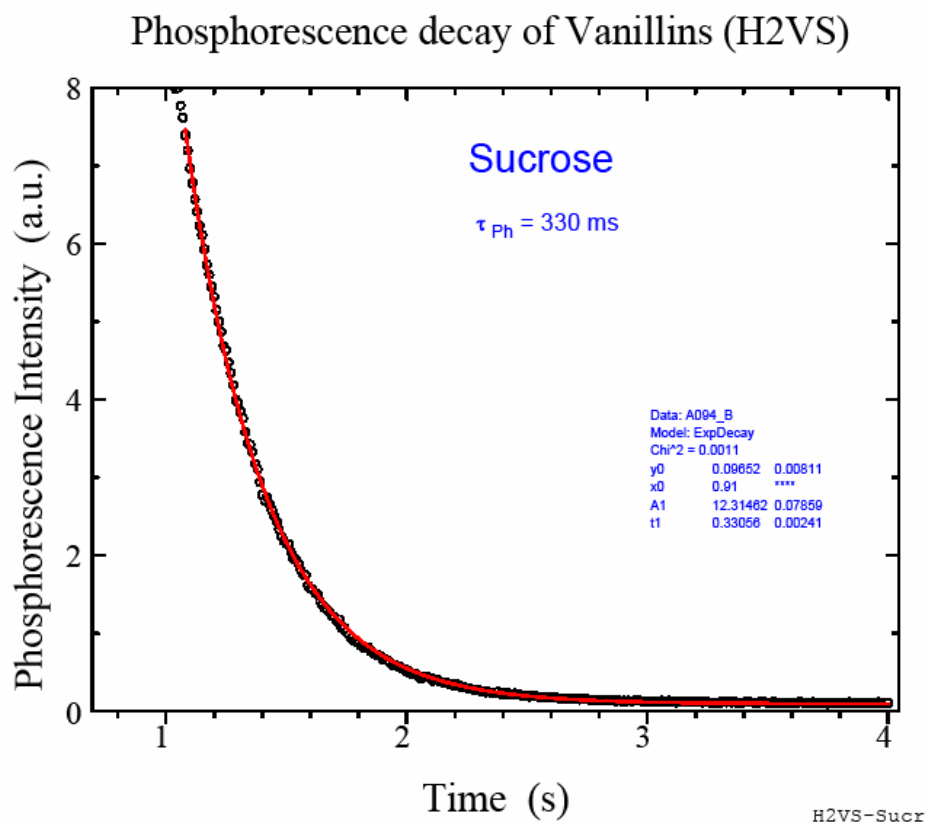
Figure III-10b

Figure III-10b: Lifetime obtained from a single-exponential model fit to phosphorescence intensity decay data from dihydroxy vanillin dispersed in amorphous sucrose film at 77K.

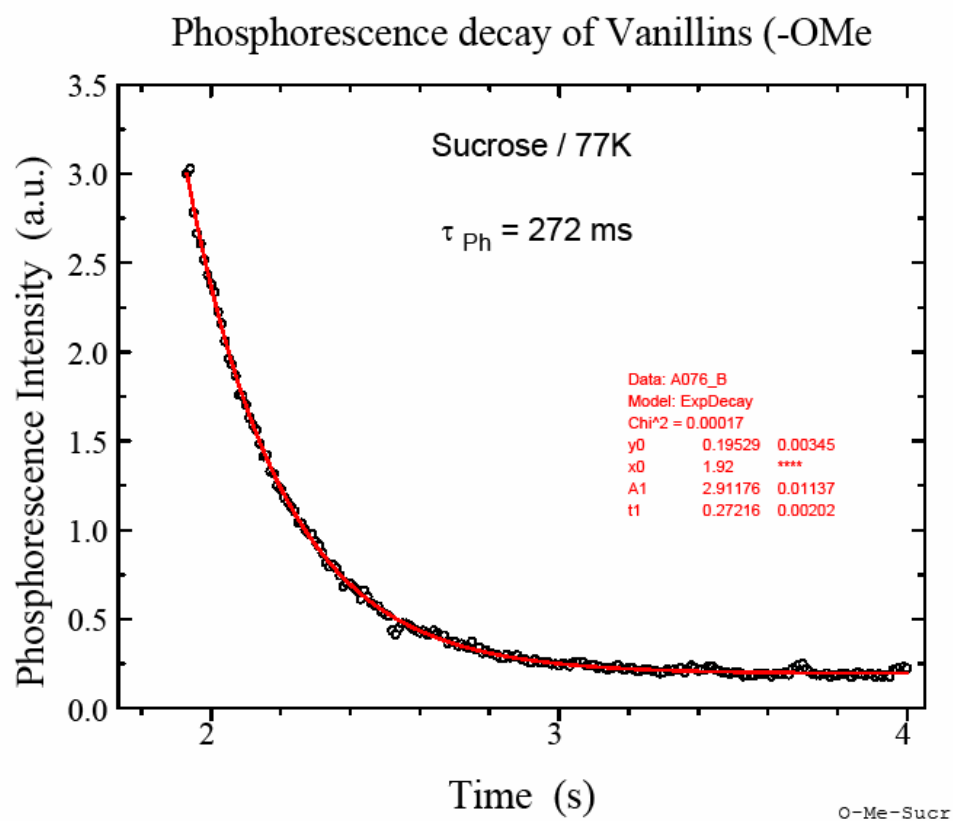
Figure III-10c

Figure III-10c: Lifetime obtained from a single-exponential model fit to phosphorescence intensity decay data from methyl vanillin dispersed in amorphous sucrose film at 77K.

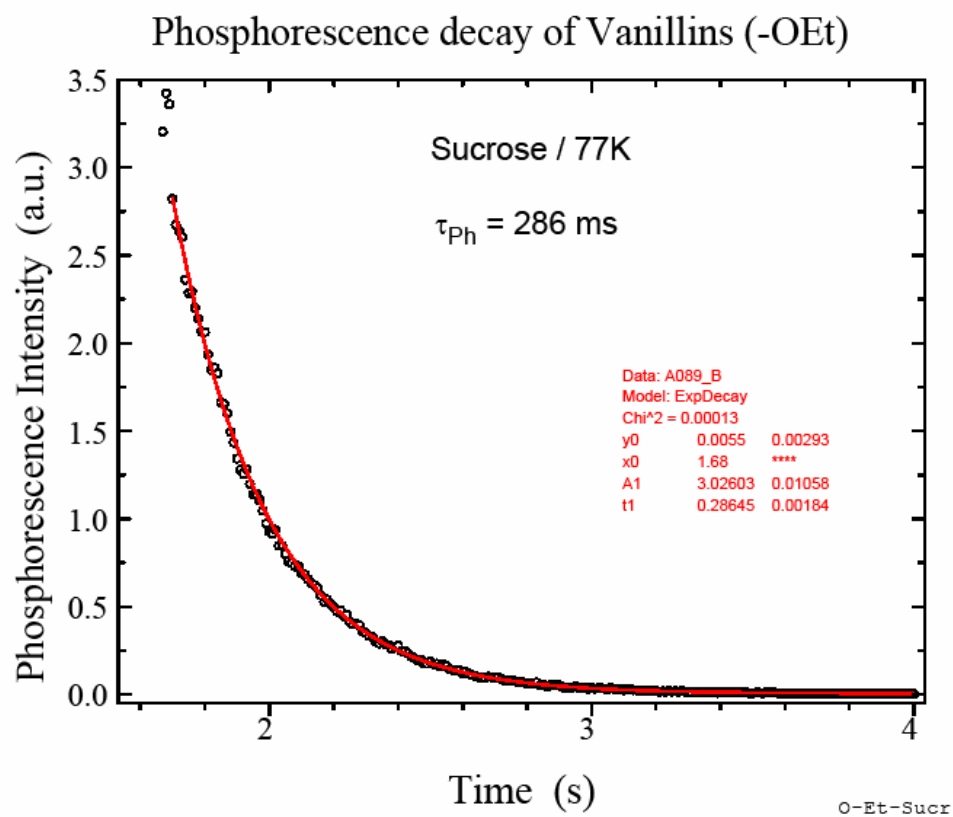
Figure III-10d

Figure III-10d: Lifetime obtained from a single-exponential model fit to phosphorescence intensity decay data from ethyl vanillin dispersed in amorphous sucrose film at 77K.

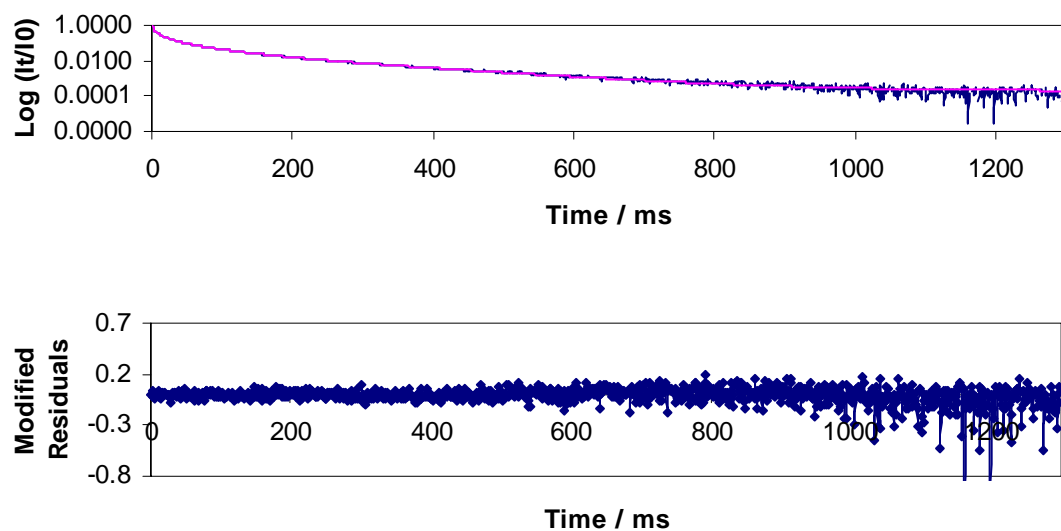
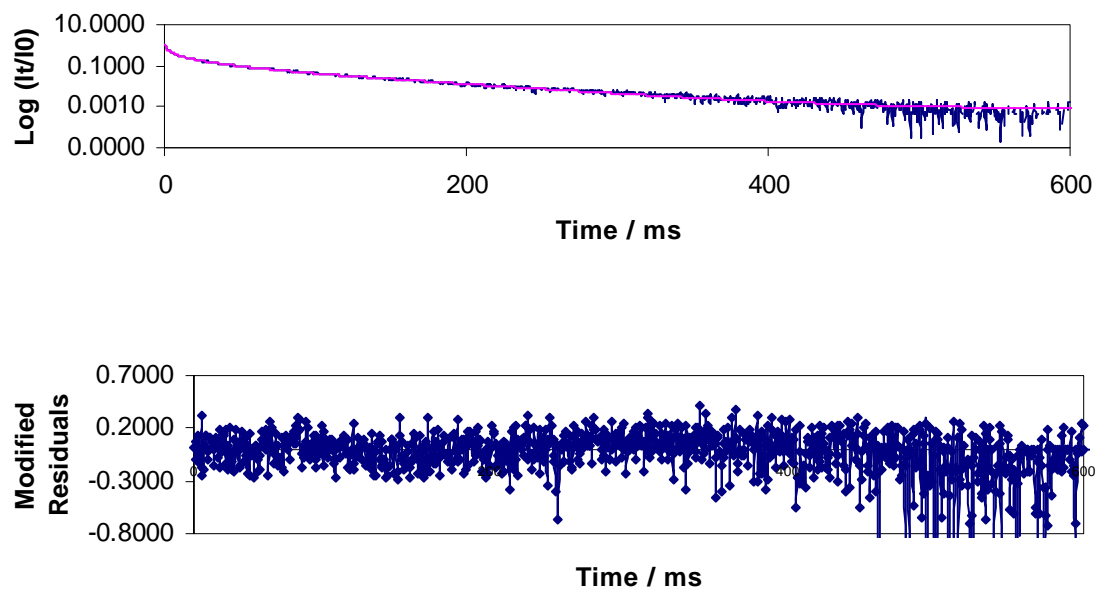
Figure III-11a*Figure III-11b*

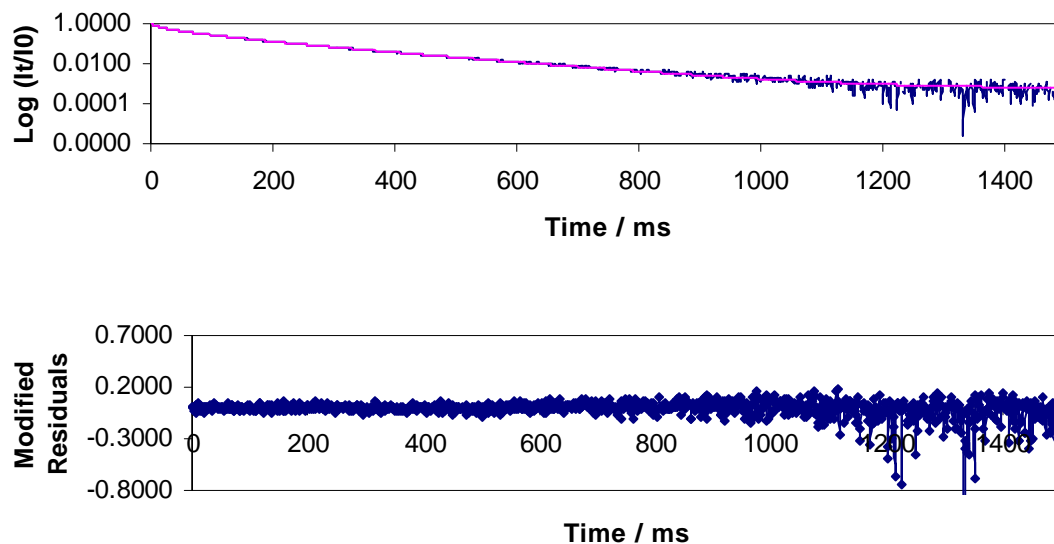
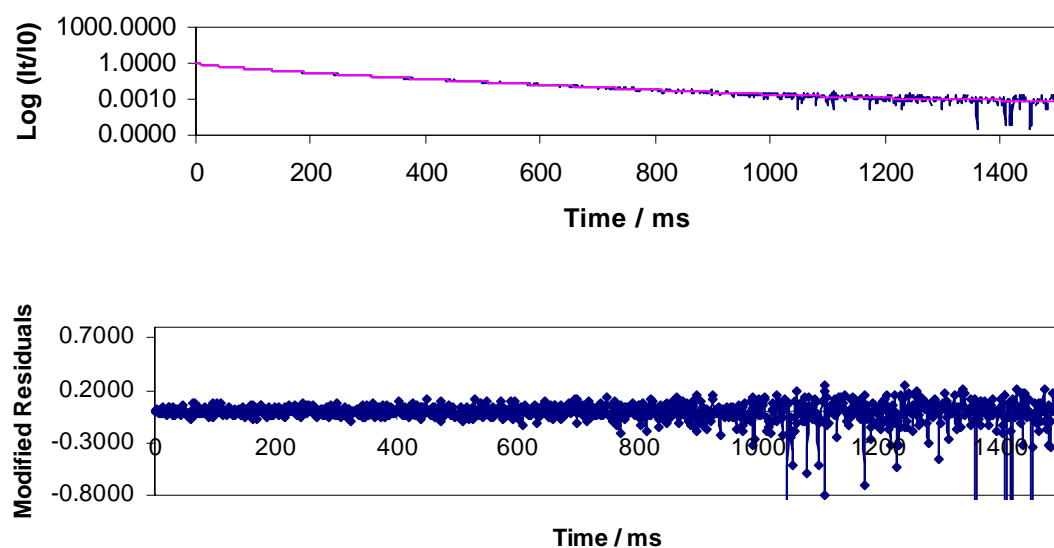
Figure III-11c*Figure III-11d*

Figure III-11a, 11b, 11c and 11d: Normalized phosphorescence intensity decays $[I(t)/I(0)]$ of hydroxy (4a), dihydroxy (4b), methyl (4c) and ethyl (4d) vanillin dispersed in amorphous sucrose films at 20°C in the presence of nitrogen. The solid lines through the data are fits using a multi-exponential function (Eq. (3), Materials and Methods). A plot of modified residuals $[(\text{Data-Fit})/\text{Data}]^{1/2}$ for these are shown in the bottom graph.

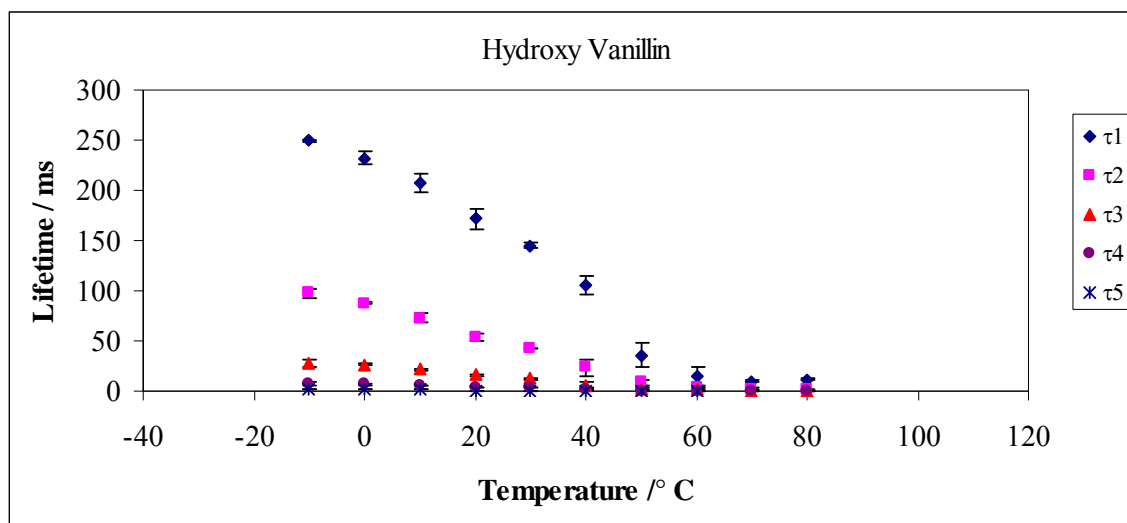
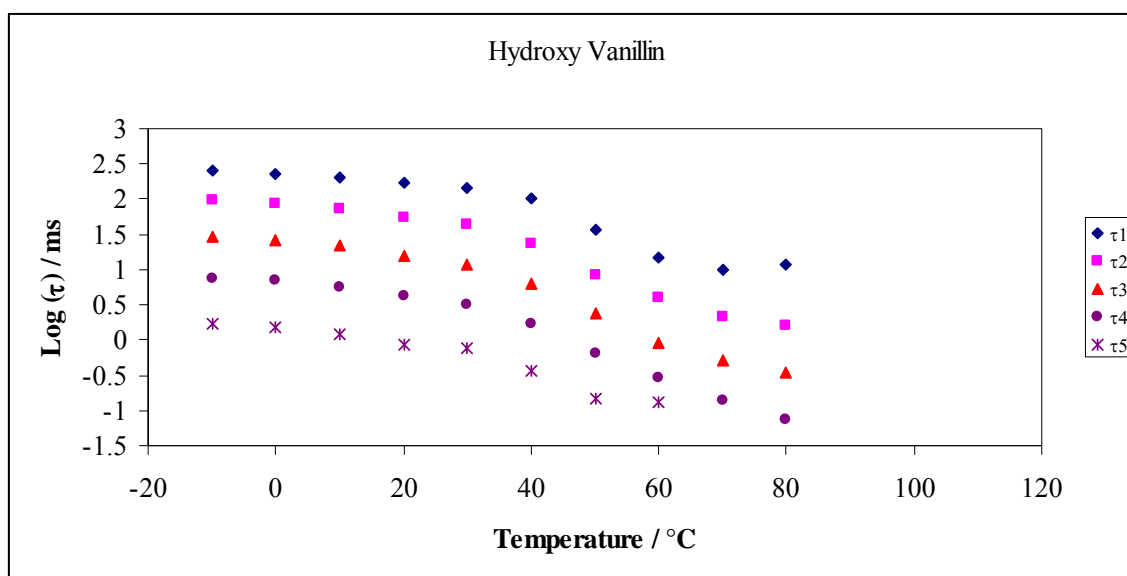
Figure III-12a1**Figure III-12a2**

Figure III-12a1 and 12a2: Lifetime components τ_1 (\blacklozenge), τ_2 (\blacksquare), τ_3 (\blacktriangle), τ_4 (\bullet) and τ_5 (\times) obtained from a multi-exponential model fit (Eq. (3), Materials and Methods) to phosphorescence intensity decay data from hydroxy vanillin dispersed in amorphous sucrose films equilibrated against nitrogen as a function of temperature. The data were measured every 10°C from -20°C to 80°C. The lifetime vs. temperature (12a1) and log (lifetime) vs. temperature (12a2)

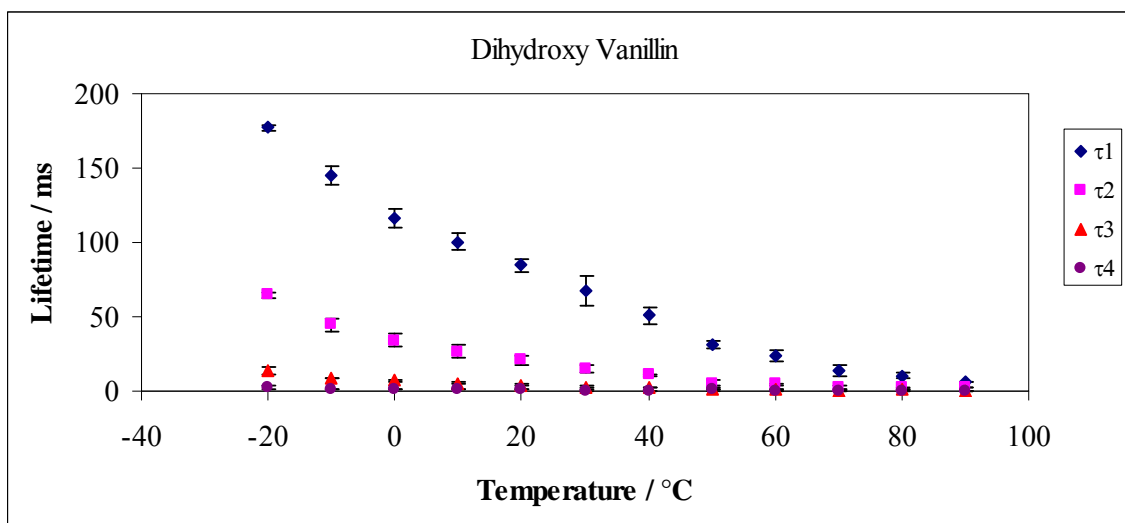
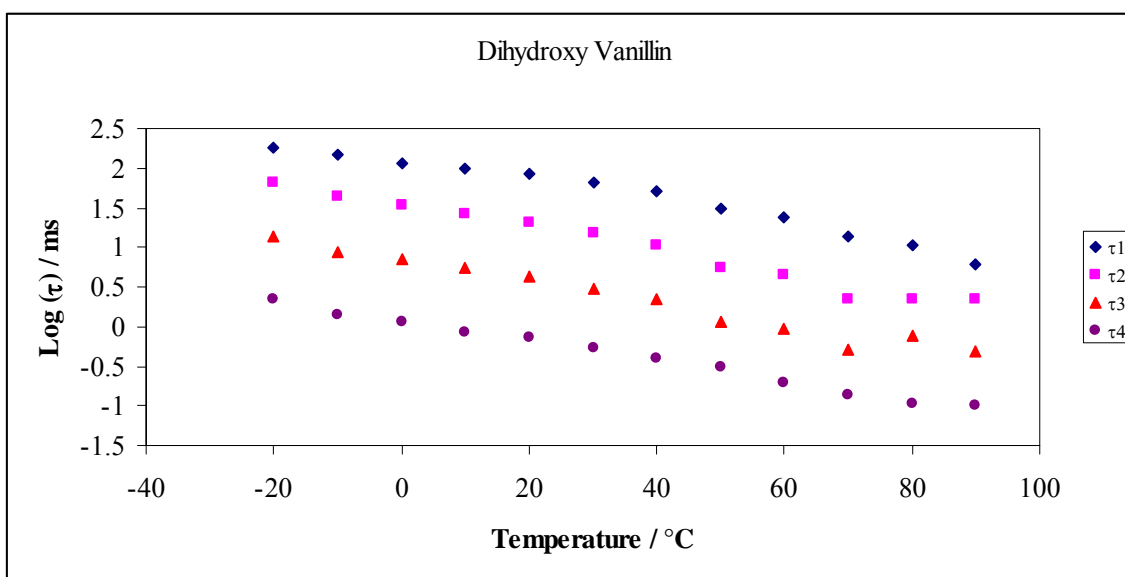
Figure III-12b1**Figure III-12b2**

Figure III-12b1 and 12b2: Lifetime components τ_1 (\blacklozenge), τ_2 (\blacksquare), τ_3 (\blacktriangle) and τ_4 (\bullet) obtained from a multi-exponential model fit (Eq. (3), Materials and Methods) to phosphorescence intensity decay data from dihydroxy vanillin dispersed in amorphous sucrose films equilibrated against nitrogen as a function of temperature. The data were measured every 10°C from -20°C to 90°C. The lifetime vs. temperature (12b1) and log (lifetime) vs. temperature (12b2)

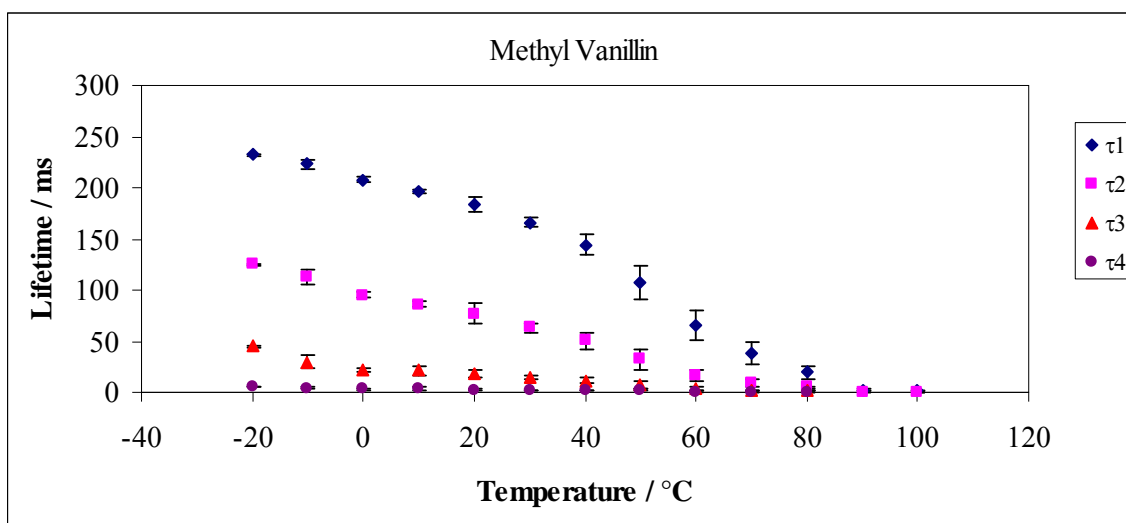
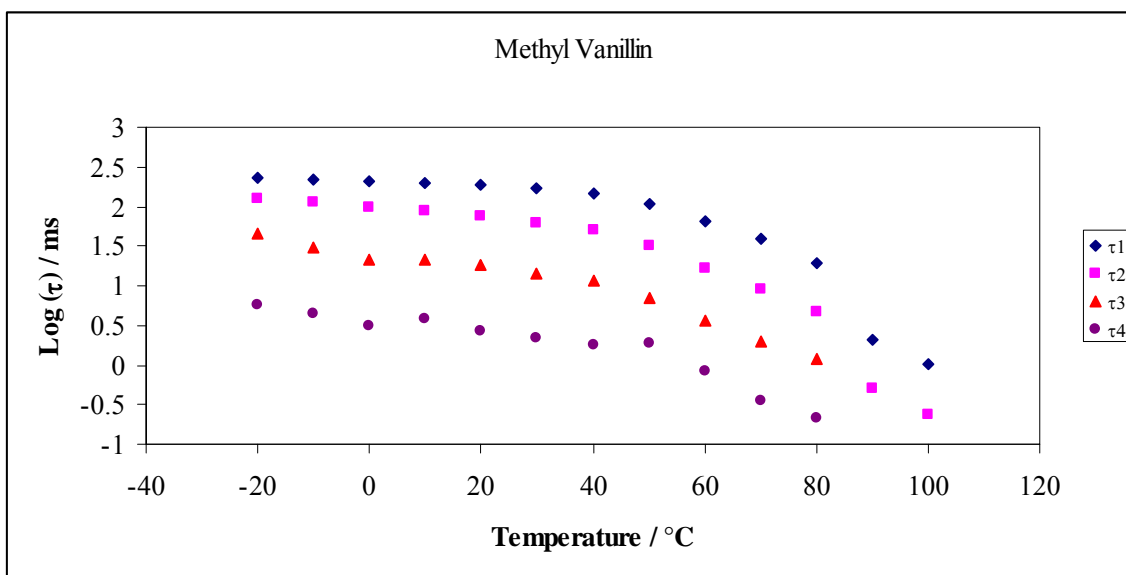
Figure III-12c1**Figure III-12c2**

Figure III-12c1 and 12c2: Lifetime components τ_1 (\blacklozenge), τ_2 (\blacksquare), τ_3 (\blacktriangle) and τ_4 (\bullet) obtained from a multi-exponential model fit (Eq. (3), Materials and Methods) to phosphorescence intensity decay data from methyl vanillin dispersed in amorphous sucrose films equilibrated against nitrogen as a function of temperature. The data were measured every 10°C from -20°C to 100°C. The lifetime vs. temperature (12c1) and log (lifetime) vs. temperature (12c2)

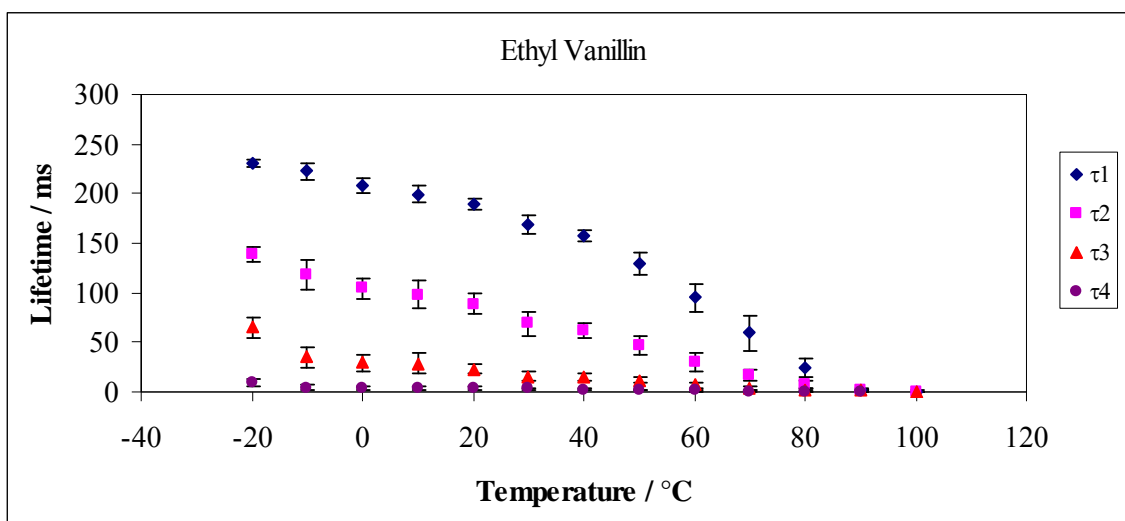
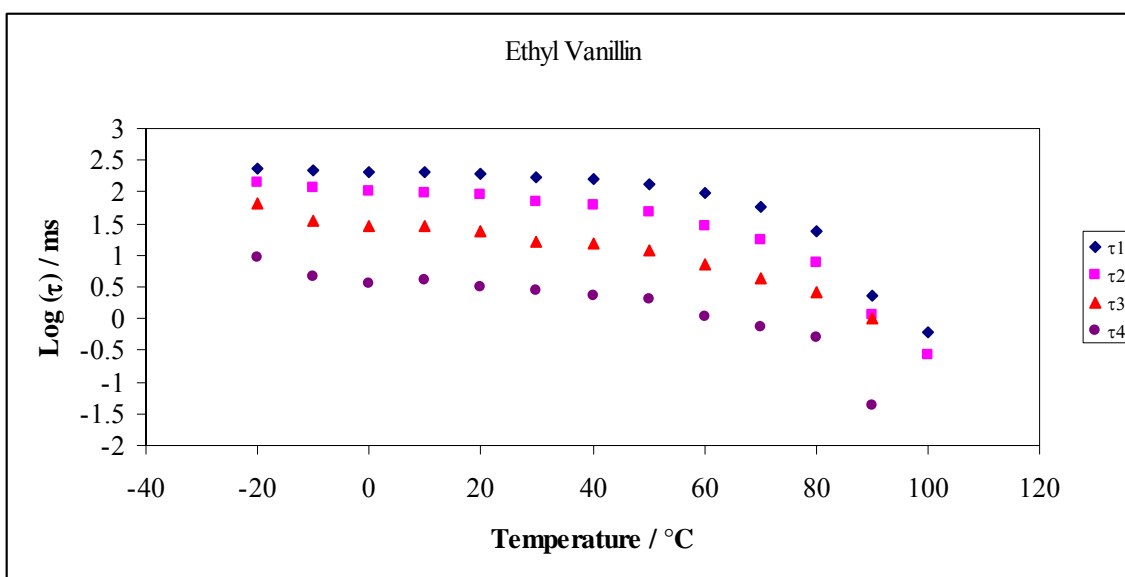
Figure III-12d1**Figure III-12d2**

Figure III-12d1 and 12d2: Lifetime components τ_1 (\blacklozenge), τ_2 (\blacksquare), τ_3 (\blacktriangle) and τ_4 (\bullet) obtained from a multi-exponential model fit (Eq. (3), Materials and Methods) to phosphorescence intensity decay data from ethyl vanillin dispersed in amorphous sucrose films equilibrated against nitrogen as a function of temperature. The data were measured every 10°C from -20°C to 100°C. The lifetime vs. temperature (12d1) and log (lifetime) vs. temperature (12d2)

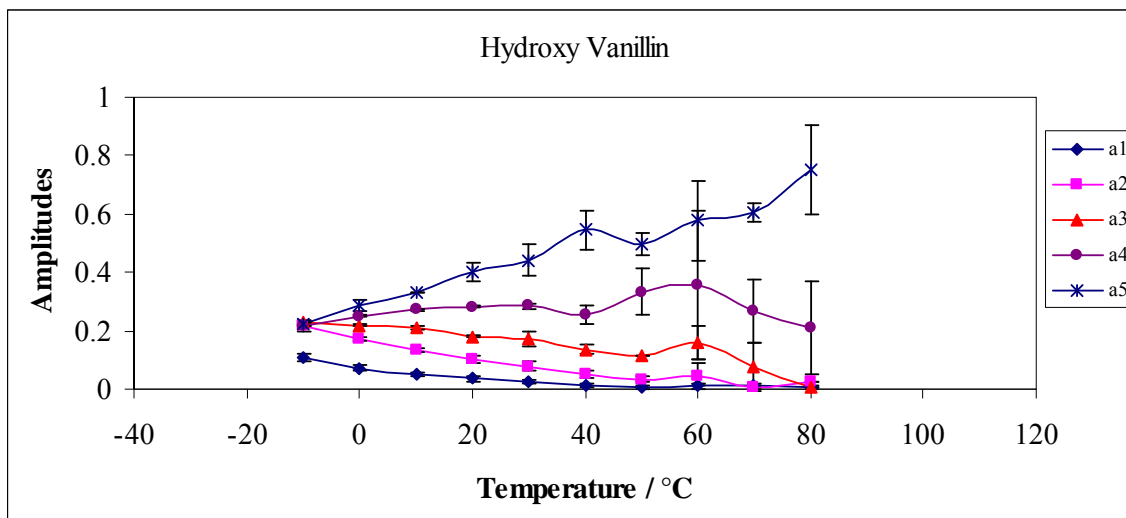
Figure III-13a

Figure III-13a: Intensity decay fit amplitudes for hydroxy vanillin in amorphous sucrose films in nitrogen as a function of temperature. The data were measured every 10°C from -20°C to 80°C. The amplitudes a_1 (♦) and a_2 (■) correspond to the longer life time components (τ_1 , τ_2) and a_3 (▲), a_4 (●) and a_5 (x) correspond to the shorter lifetime components (τ_3 , τ_4 , τ_5). The amplitudes were obtained from a multi exponential model fit (Eq. (3), Materials and Methods) to phosphorescence intensity decay data from hydroxy vanillin dispersed in amorphous sucrose films equilibrated against nitrogen as a function of temperature.

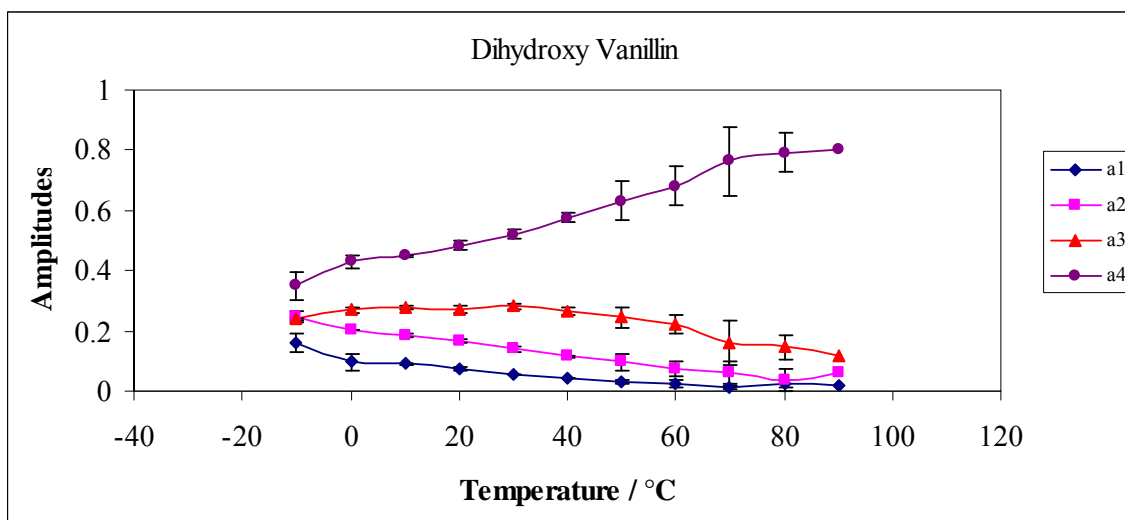
Figure III-13b

Figure III-13b: Intensity decay fit amplitudes for dihydroxy vanillin in amorphous sucrose films in nitrogen as a function of temperature. The data were measured every 10°C from -20°C to 80°C. The amplitudes a_1 (♦) and a_2 (■) correspond to the longer life time components (τ_1 , τ_2) and a_3 (▲) and a_4 (●) correspond to the shorter lifetime components (τ_3 , τ_4). The amplitudes were obtained from a multi exponential model fit (Eq. (3), Materials and Methods) to phosphorescence intensity decay data from dihydroxy vanillin dispersed in amorphous sucrose films equilibrated against nitrogen as a function of temperature.

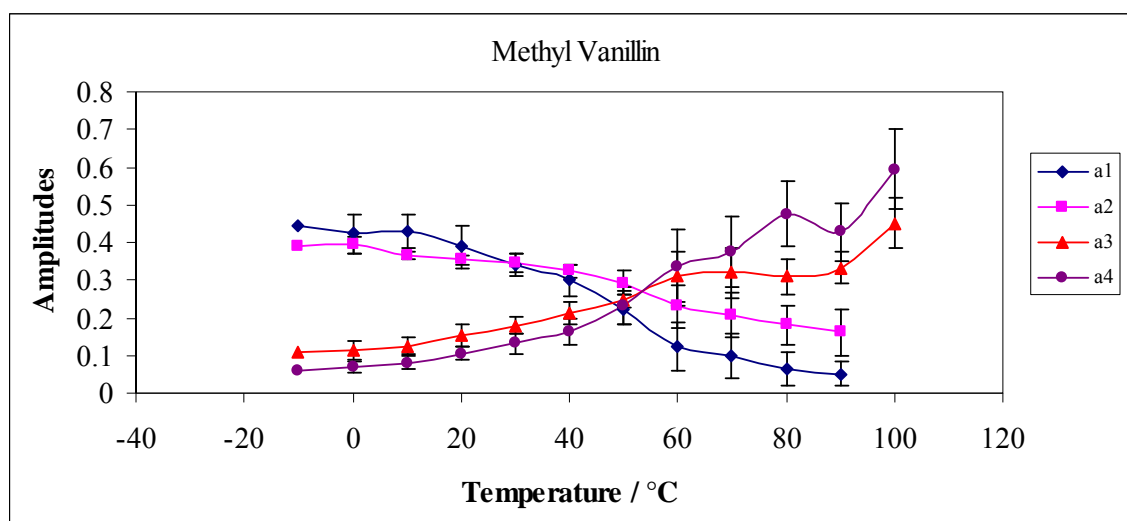
Figure III-13c

Figure III-13c: Intensity decay fit amplitudes for methyl vanillin in amorphous sucrose films in nitrogen as a function of temperature. The data were measured every 10°C from -20°C to 80°C. The amplitudes a_1 (♦) and a_2 (■) correspond to the longer life time components (τ_1 , τ_2) and a_3 (▲) and a_4 (●) correspond to the shorter lifetime components (τ_3 , τ_4). The amplitudes were obtained from a multi exponential model fit (Eq. (3), Materials and Methods) to phosphorescence intensity decay data from methyl vanillin dispersed in amorphous sucrose films equilibrated against nitrogen as a function of temperature.

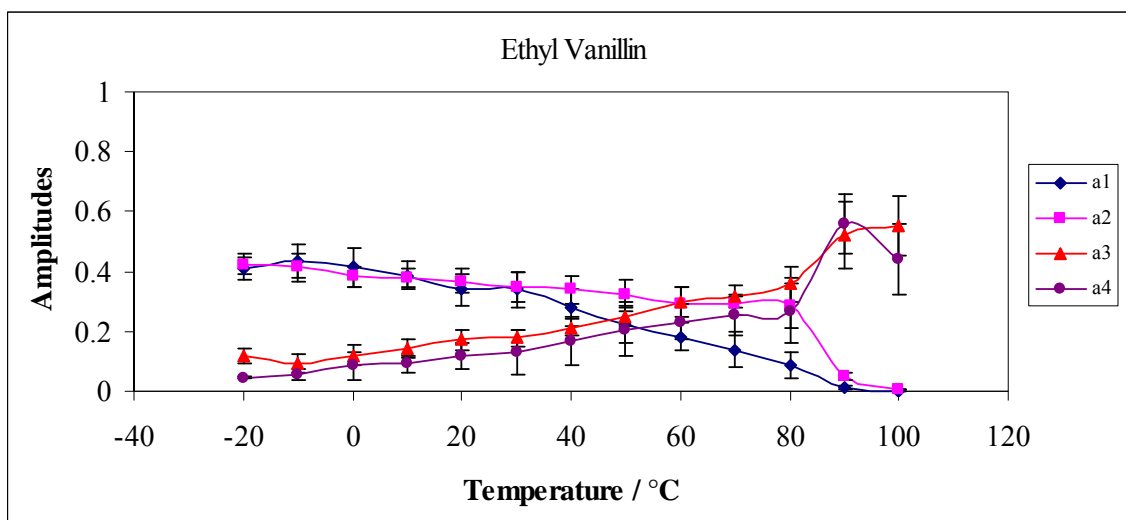
Figure III-13d

Figure III-13d: Intensity decay fit amplitudes for ethyl vanillin in amorphous sucrose films in nitrogen as a function of temperature. The data were measured every 10°C from -20°C to 80°C. The amplitudes a_1 (♦) and a_2 (■) correspond to the longer life time components (τ_1 , τ_2) and a_3 (▲) and a_4 (●) correspond to the shorter lifetime components (τ_3 , τ_4). The amplitudes were obtained from a multi exponential model fit (Eq. (3), Materials and Methods) to phosphorescence intensity decay data from ethyl vanillin dispersed in amorphous sucrose films equilibrated against nitrogen as a function of temperature.

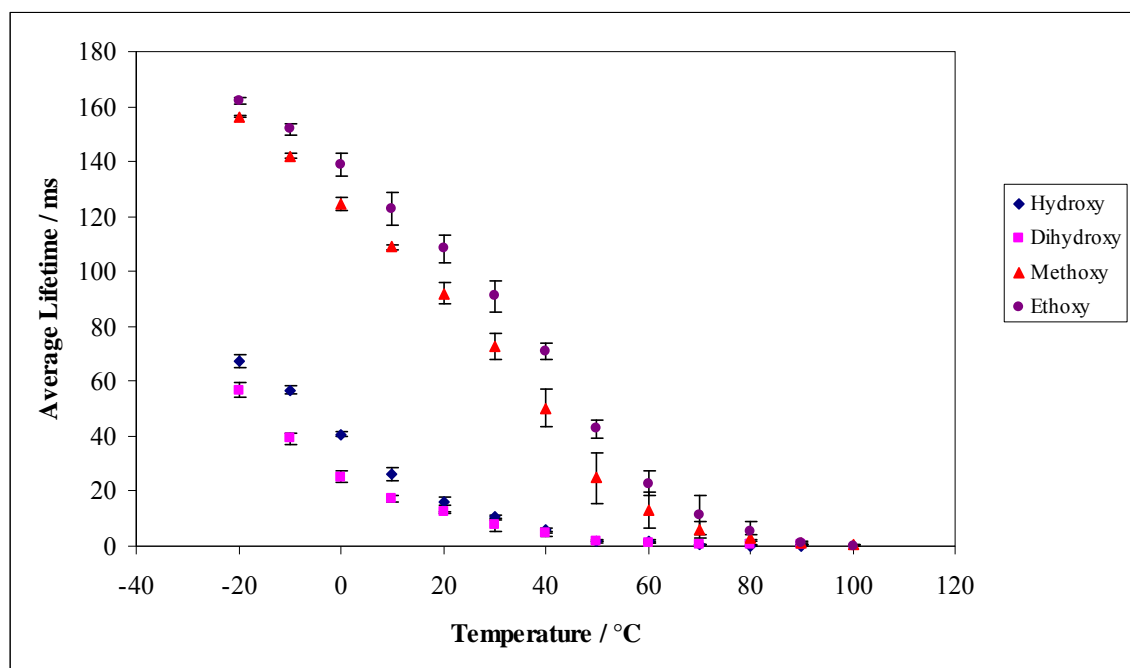
Figure III-14a

Figure III-14a: Average lifetime from a multi-exponential model fit (Eq. (4), Materials and Methods) to phosphorescence intensity decay data from hydroxy (♦), dihydroxy (■), methyl (●) and ethyl (▲) vanillin dispersed in amorphous sucrose films equilibrated against nitrogen as a function of temperature. The data were measured every 10°C from -20°C to 100°C.

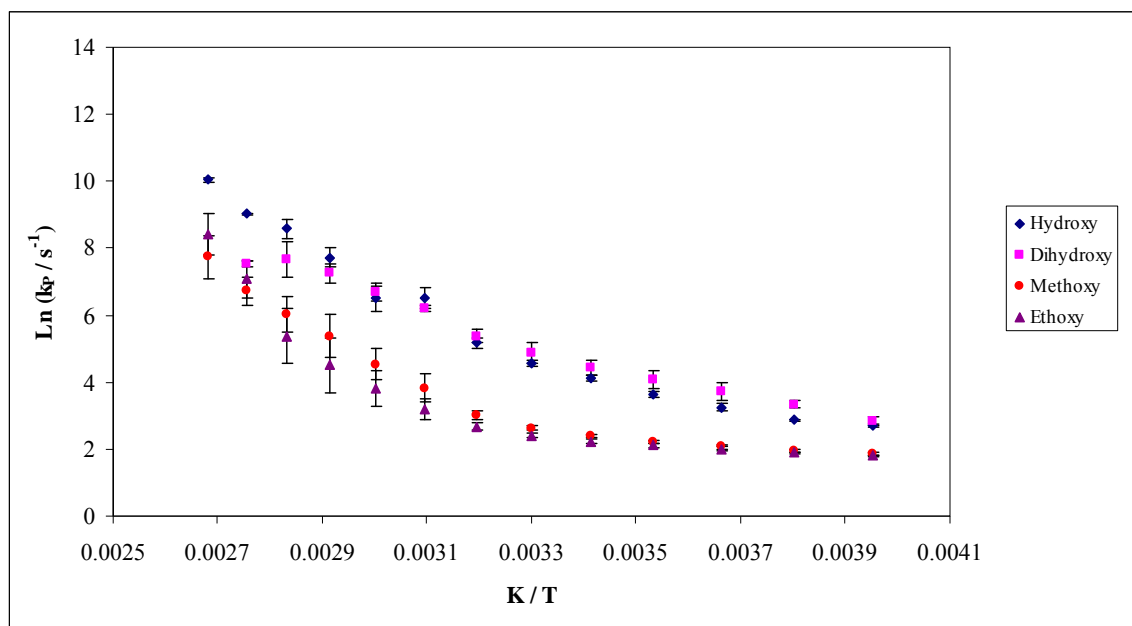
Figure III-14b

Figure III-14b: Arrhenius plots of the average lifetime of hydroxy, dihydroxy, methyl and ethyl vanillin in amorphous sucrose as a function of inverse of temperature.

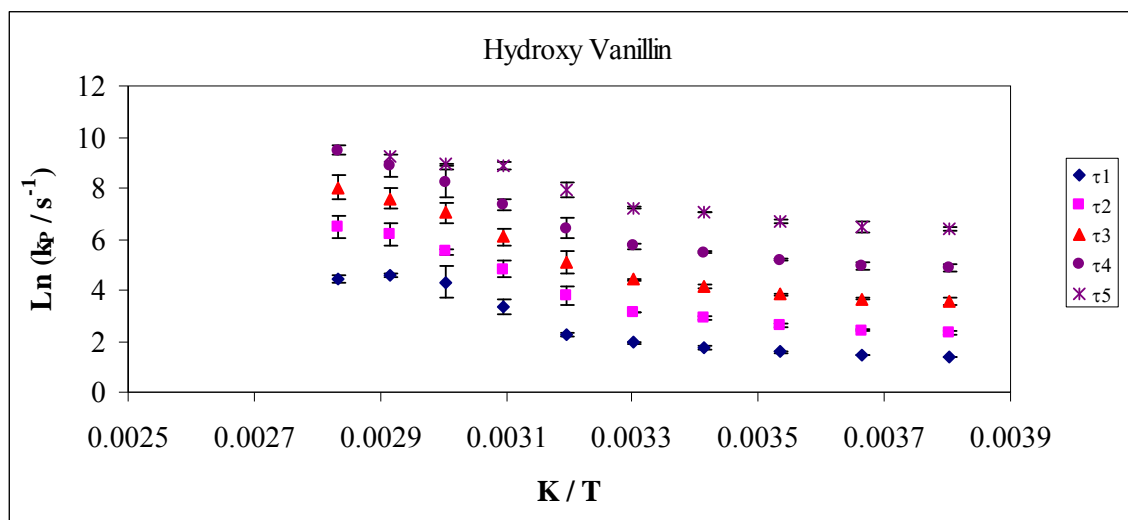
Figure III-15a

Figure III-15a: The Arrhenius plot of the individual lifetime component τ_1 (\blacklozenge), τ_2 (\blacksquare), τ_3 (\blacktriangle), τ_4 (\bullet) and τ_5 (\times) of hydroxy vanillin in amorphous sucrose as a function of inverse of temperature.

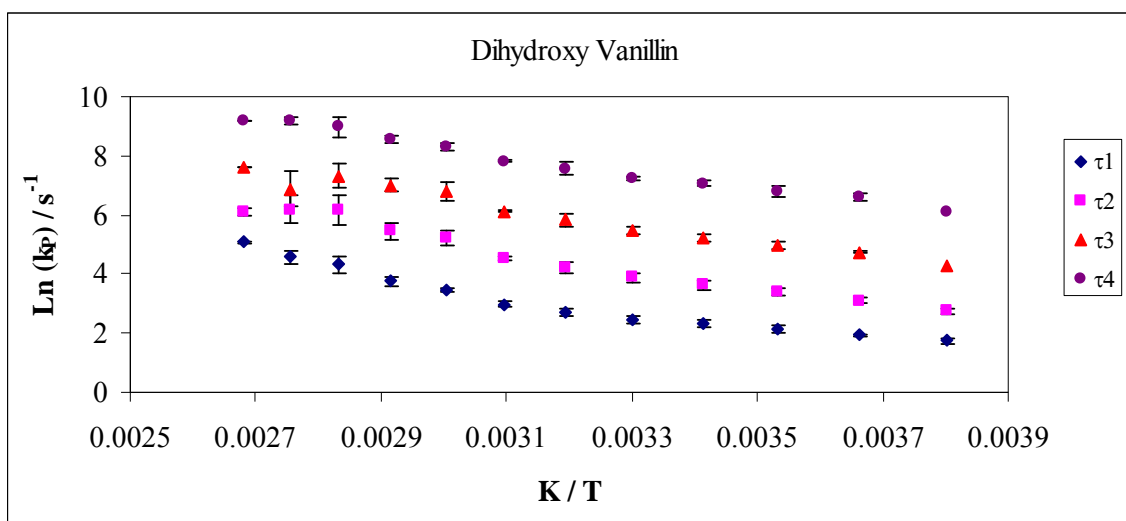
Figure III-15b

Figure III-15b: The Arrhenius plot of the individual lifetime component τ_1 (\blacklozenge), τ_2 (\blacksquare), τ_3 (\blacktriangle) and τ_4 (\bullet) dihydroxy vanillin in amorphous sucrose as a function of inverse of temperature.

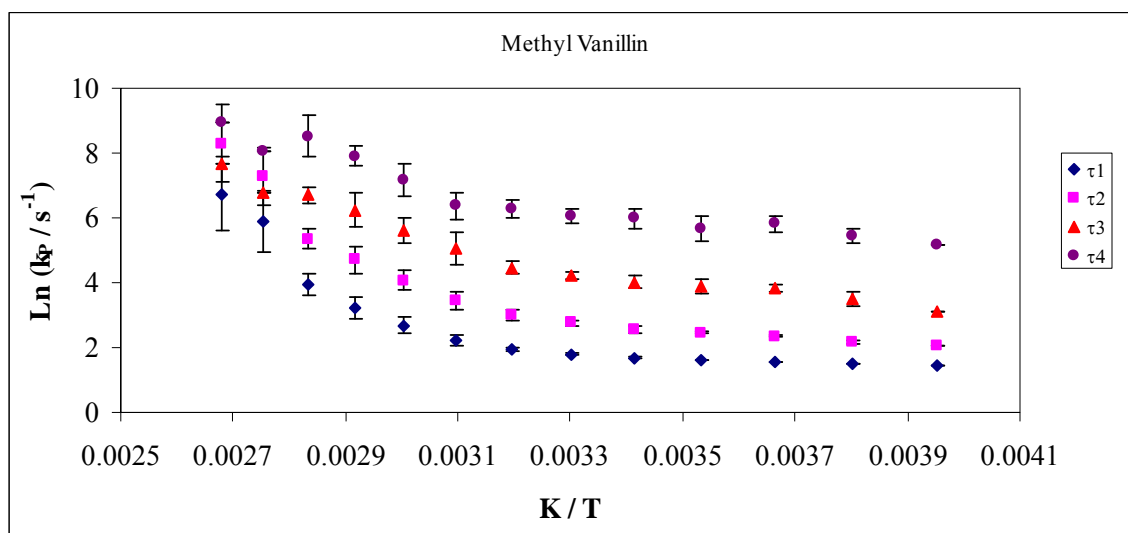
Figure III-15c

Figure III-15c: The Arrhenius plot of the individual lifetime component τ_1 (\blacklozenge), τ_2 (\blacksquare), τ_3 (\blacktriangle) and τ_4 (\bullet) methyl vanillin in amorphous sucrose as a function of temperature.

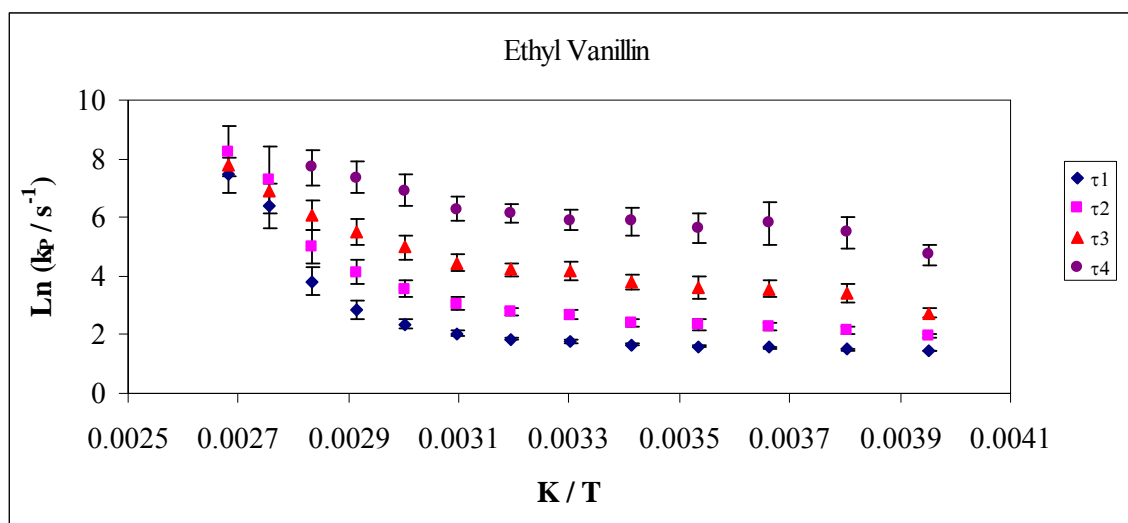
Figure III-15d

Figure III-15d: The Arrhenius plot of the individual lifetime component τ_1 (\blacklozenge), τ_2 (\blacksquare), τ_3 (\blacktriangle) and τ_4 (\bullet) ethyl vanillin in amorphous sucrose as a function of inverse of temperature.

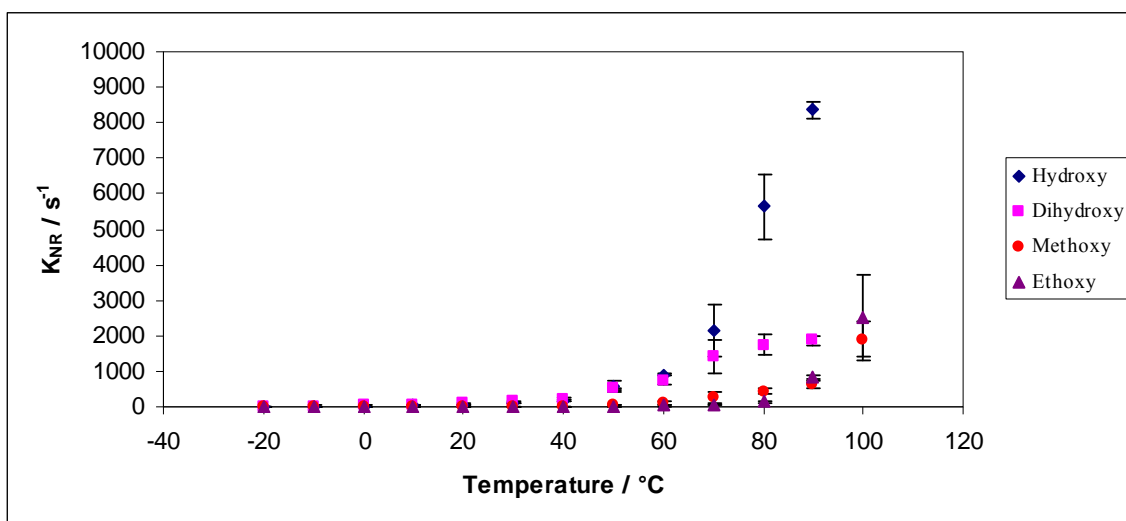
Figure III-16a

Figure III-16a: Temperature dependence of the total non-radiative decay rate of the triplet state k_{NR} ($k_p = k_{RP} + k_{NR}$) to S_0 of hydroxy, dihydroxy, methyl and ethyl vanillin in amorphous sucrose film over the temperature range from $-20^{\circ}C$ to $100^{\circ}C$.

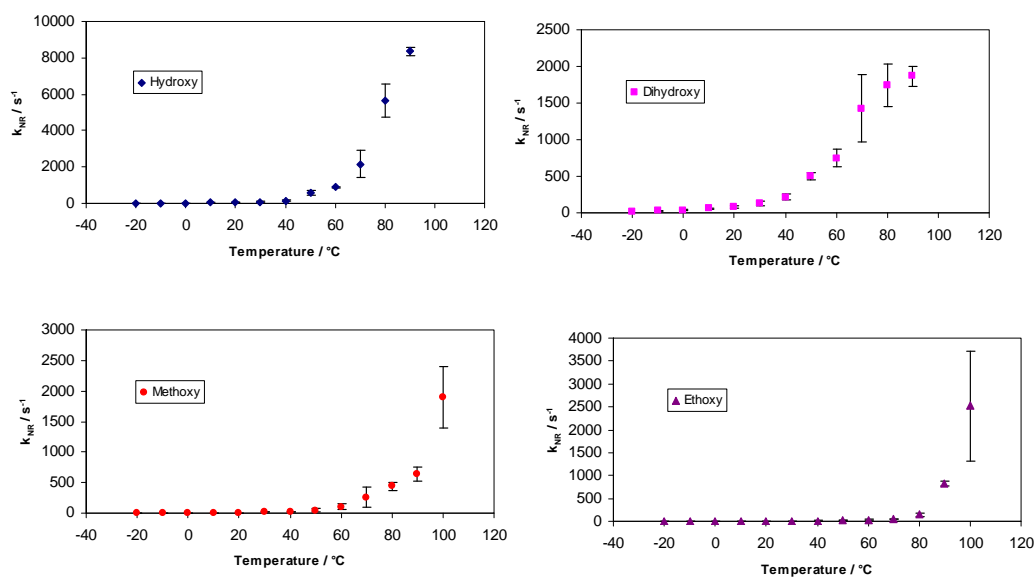
Figure III-16b

Figure III-16b: Temperature dependence of the total non-radiative decay rate of the triplet state k_{NR} ($k_p = k_{RP} + k_{NR}$) to S_0 of hydroxy, dihydroxy, methyl and ethyl vanillin in amorphous sucrose film over the temperature range from -20°C to 100°C.

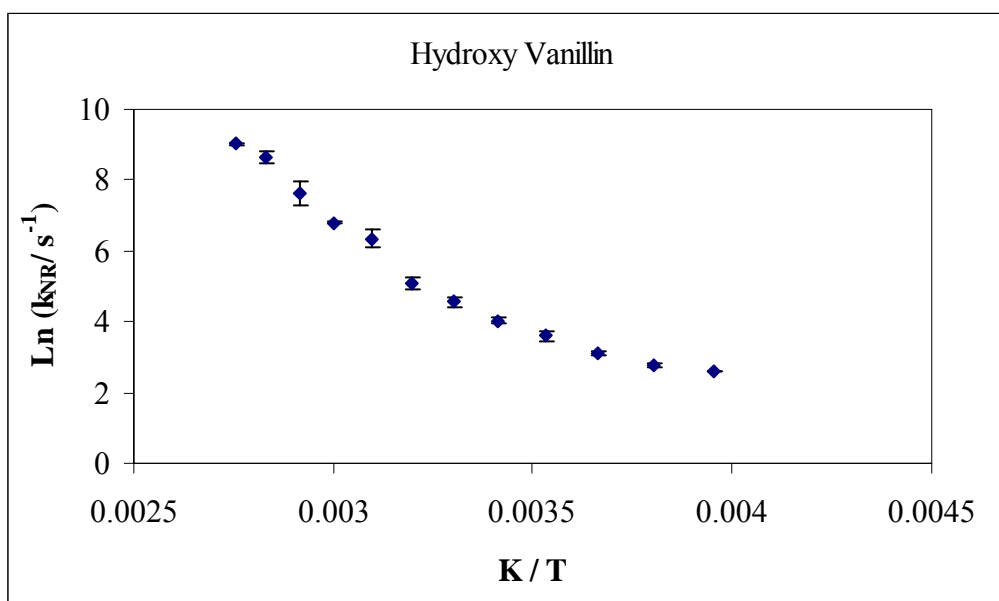
Figure III-17a

Figure III-17a: Arrhenius plot of the total non-radiative decay rate of the triplet state k_{NR} ($k_p = k_{RP} + k_{NR}$) to S_0 of hydroxy vanillin in amorphous sucrose film as function of inverse of temperature.

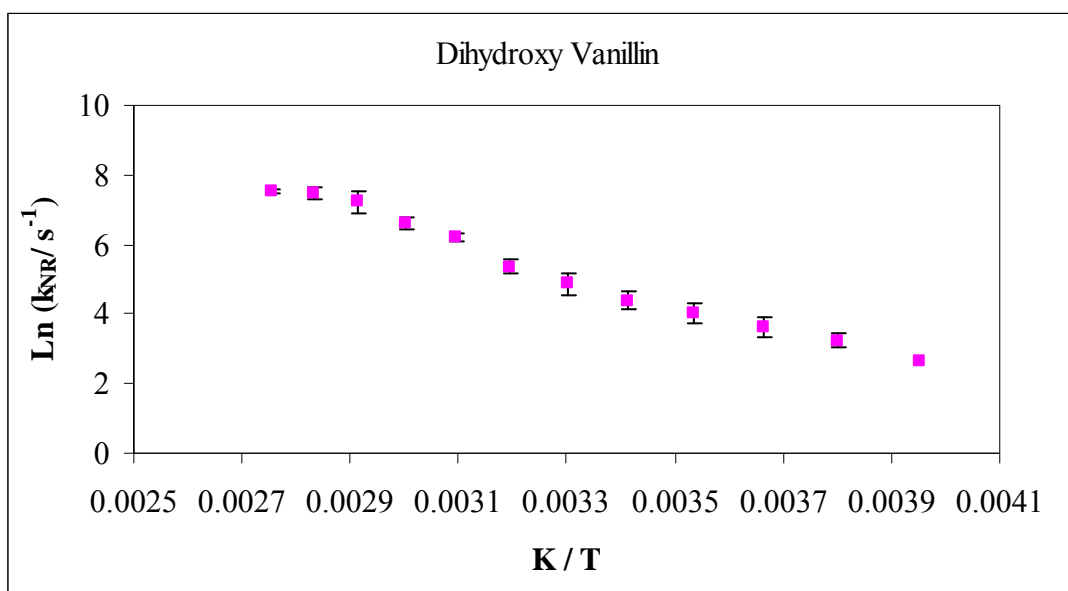
Figure III-17b

Figure III-17b: Arrhenius plot of the total non-radiative decay rate of the triplet state k_{NR} ($k_p = k_{RP} + k_{NR}$) to S_0 of dihydroxy vanillin in amorphous sucrose film as function of inverse of temperature.

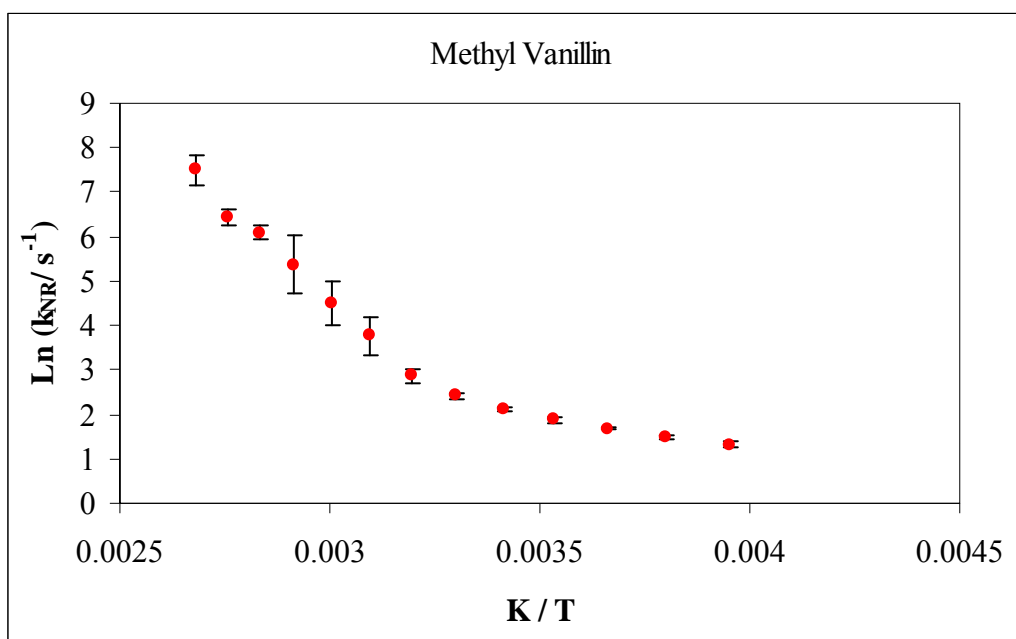
Figure III-17c

Figure III-17c: Arrhenius plot of the total non-radiative decay rate of the triplet state k_{NR} ($k_p = k_{RP} + k_{NR}$) to S_0 of methyl vanillin in amorphous sucrose film as function of inverse of temperature.

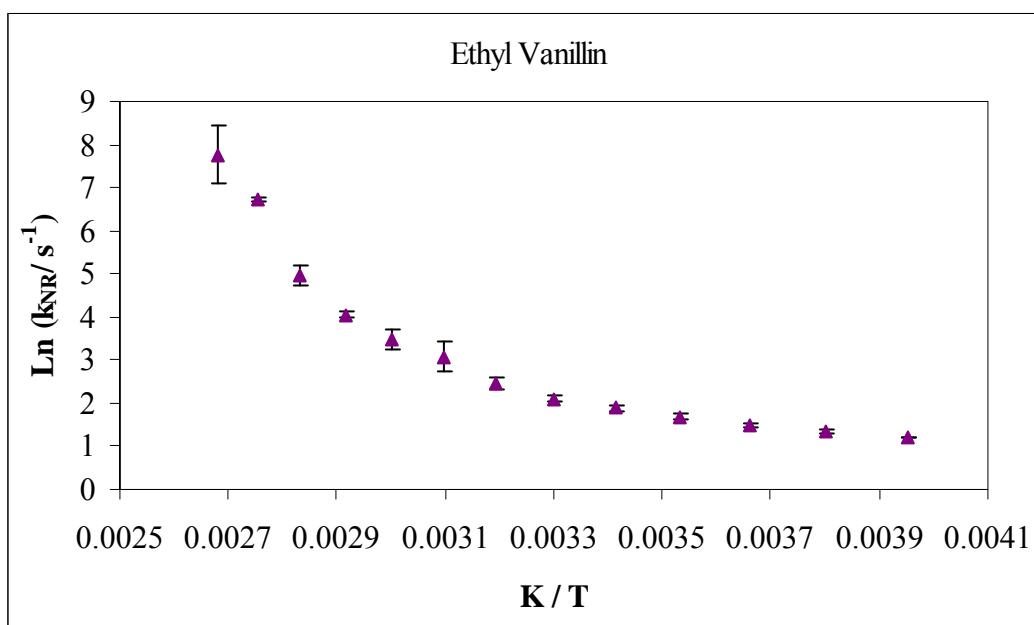
Figure III-17d

Figure III-17d: Arrhenius plot of the total non-radiative decay rate of the triplet state k_{NR} ($k_p = k_{RP} + k_{NR}$) to S_0 of ethyl vanillin in amorphous sucrose film as function of inverse of temperature.

Table III-1

Table III-1: Calculated activation energy E_a and transition temperatures for hydroxy, dihydroxy, methyl and ethyl vanillin in amorphous sucrose films at low (LT) and high temperature (HT). These values were obtained from $\ln(1/I_p)$ vs. K/T .

Vanillin		Equation	R^2	E_a KJ / mol	Transition temperature / °C
Hydroxy	LT	$y = -2624.3x + 7.2358$	0.99	21.82	25
	HT	$y = -9366.9x + 29.856$	0.97	77.88	
Dihydroxy	LT	$y = -2906.2x + 8.4625$	0.97	24.16	22
	HT	$y = -9584.2x + 27.246$	0.99	79.68	
Methyl	LT	$y = -932.89x + 0.2056$	0.95	7.76	36
	IT	$y = -6490.5x + 18.065$	0.98	53.96	80
	HT	$y = -11270x + 32.011$	0.96	93.70	
Ethyl	LT	$y = -1019.8x + 0.6236$	0.97	8.48	45
	IT	$y = -5123.7x + 13.539$	1.00	42.60	75
	HT	$y = -16821x + 47.515$	0.99	139.85	

Table III-2

Table III-2: Calculated activation energy E_a for each individual lifetime components τ_1 , τ_2 , τ_3 , τ_4 and τ_5 and average lifetime at low (LT) and high temperature (HT) for hydroxy vanillin in amorphous sucrose films.

Hydroxy Vanillin			
Lifetime	Temperature	E_a KJ / mol	Transition Temperatures °C
τ_1	LT	9.16	37
	HT	89.60	
τ_2	LT	14.02	30
	HT	62.33	
τ_3	LT	14.58	30
	HT	67.80	
τ_4	LT	18.09	30
	HT	70.36	
τ_5	LT	14.29	30
	HT	78.38	
τ_{Avg}	LT	30.93	35
	HT	87.06	

Table III-3

Table III-3: Calculated activation energy E_a for each individual lifetime components τ_1 , τ_2 , τ_3 and τ_4 and average lifetime at low and high temperature for dihydroxy vanillin in amorphous sucrose films.

Dihydroxy Vanillin			
Lifetime	Temperature	E_a KJ / mol	Transition Temperatures °C
τ_1	LT	12.10	30
	HT	37.02	
τ_2	LT	18.10	50
	HT	46.33	
τ_3	LT	18.26	35
	HT	19.42	
τ_4	LT	17.94	30
	HT	28.81	
τ_{Avg}	LT	26.84	30
	HT	51.05	

Table III-4

Table III-4: Calculated activation energy E_a for each individual lifetime components τ_1 , τ_2 , τ_3 and τ_4 and average lifetime at low and high temperature for methyl vanillin in amorphous sucrose films.

Methyl Vanillin			
Lifetime		E_a kJ / mol	Transition Temperatures °C
τ_1	LT	4.14	60
	HT	110.00	
τ_2	LT	9.60	55
	HT	112.00	
τ_3	LT	13.63	42
	HT	49.03	
τ_4	LT	11.33	50
	HT	68.21	
τ_{Avg}	LT	9.64	40
	HT	76.34	

Table III-5

Table III-5: Calculated activation energy E_a for each individual lifetime components τ_1 , τ_2 , τ_3 and τ_4 and average lifetime at low and high temperature for ethyl vanillin in amorphous sucrose films.

Ethyl Vanillin			
Lifetime	Temperature	E_a KJ / mol	Transition Temperatures °C
τ_1	LT	4.25	63
	HT	173.47	
τ_2	LT	8.61	60
	HT	179.93	
τ_3	LT	12.00	55
	HT	72.67	
τ_4	LT	11.35	55
	HT	44.13	
τ_{Avg}	LT	9.03	60
	HT	143.02	

Table III-6

Table III-6: Calculated activation energy E_a for non-radiative decay rate at low and high temperature for hydroxy, dihydroxy, methyl and ethyl vanillin in amorphous sucrose films.

Lifetime	Temperature	Equation	R^2	E_a KJ / mol	Transition Temperatures °C
Hydroxy	LT	$y = -3345.7x + 15.5$	0.96	27.82	35
	IT	$y = -8945.5x + 33$	0.98	74.37	
Dihydroxy	LT	$y = -3260.1x + 15.57$	1.00	27.10	30
	HT	$y = -6211.3x + 25.32$	0.99	51.64	
Methyl	LT	$y = -1164.2x + 7.8$	0.99	13.84	40
	HT	$y = -8698.2x + 30$	0.98	72.32	
Ethyl	LT	$y = -1367.7x + 6.11$	0.98	11.37	60
	HT	$y = -16511x + 52.036$	0.98	137.27	

References

- Fischer, C. J., Gafni, A., Steel, D. G. and Schauerte, J. A. The triplet-state lifetime of indole in aqueous and viscous environments: significance to the interpretation of room temperature phosphorescence in proteins. *Journal of the American Chemical Society*. 124 (2004). 10359-10266.
- Fister, J. C. and Harris, J. M. Time and Wavelength-Resolved Delayed-Fluorescence Emission from Acridine Yellow in an Inhomogeneous Saccharide Glass. *Analytical chemistry*. 68 (1996). 639-646.
- Gunshefski, M., Santana, J. J., Stephenson, J. and Winefordnert, J.D. Solid-Surface Room Temperature Phosphorescence. *Applied spectroscopy Reviews*. 27 (1992). 143-144.
- Hurtubise, R. J. Solid surface luminescence analysis. Marcel Dekker Inc., New York. (1981).
- Hurtubise, R. J. Solid surface luminescence analysis. Marcel Dekker, New York. (1981).
- Lakowicz, J.R. Principles of Fluorescence Spectroscopy, Second Edition.: Kluwer Academic/Plenum Press, New York (1999).
- Ludescher, R.D., Shah, N.K., McCaul, C.P and Simon, K.V. Beyond Tg: optical luminescence measurements of molecular mobility in amorphous solid foods. *Food Hydrocolloids*. 15 (2001). 331-339.
- McAleese, D. L and Dunlap, R. B. Matrix isolation mechanism for solid surface room-temperature phosphorescence induction. *Analytical Chemistry*. 56 (1984). 2244.
- Nishigaki, A., Uchida, A., Oonishi, I and Oshima, S. Characteristics of phosphorescence of ionic organic compounds adsorbed on filter paper. Polycyclic aromatic compounds. 9 (1996). 323-330.
- Nishigaki, A., Ngashima, U., Uchida, A., Oonishi, I. and Oshima, S. Hysteresis in the temperature dependence of phosphorescence of 4-Hydroxy-3-Methoxybenzaldehyde (vanillin) in ethanol. *Journal of Physical Chemistry*. 102 (1998) 1106-1111.
- Papp, S. and Vanderkooi, J.M. Tryptophan phosphorescence at room temperature as a tool to study protein structure and dynamics. *Photochemistry and Photobiology*. 49 (1989). 775-84.
- Parker, C.A. Photoluminescence of Solutions. Elsevier Pub Co., Amsterdam (1968).

- Pravinata, L.V., You, Y. and Ludescher, R.D. Erythrosin B phosphorescence monitors molecular mobility and dynamic heterogeneity in amorphous sucrose. *Biophysical Journal*. 88 (2005). 3551-3561.
- Richert, R. Triplet state salvation dynamics: Basics and applications. *Journal of Chemical Physics*. 113 (2000). 8404-8429.
- Roos, Y. *Phase Transitions in Foods*. Academic Press, San Diego, California (1995).
- Schulman, E.M. and Parker, R.T. Room temperature phosphorescence of organic compounds. The effects of moisture, oxygen and the nature of the support-phosphor interactions. *The Journal of Physical Chemistry*. 81 (1977). 1932-1939.
- Schulman, E.M. and Walling, C. Triplet state phosphorescence of adsorbed ionic organic molecules at room temperature. *Journal of Physical Chemistry*. 77 (1973). 902-905.
- Shah, N.K. and Ludescher, R.D. Phosphorescence of probes of the glassy state in amorphous sucrose. *Biotechnology Progress*. 11 (1995). 540-544.
- Shamblin, S., Hancock, B.C, Dupuis, Y. and Pikal, M.J. Interpretation of relaxation time constants for amorphous pharmaceutical systems. *Journal of Pharmaceutical Sciences*. 89 (2000). 417-427.
- Shirke, S. and Ludescher, R.D. Dynamic site heterogeneity in amorphous maltose and maltitol from spectral heterogeneity in erythrosin B phosphorescence. *Carbohydrate Research* 340 (2005). 2661-2669.
- Shirke, S. and Ludescher, R.D. Dynamic site heterogeneity in amorphous lactose and lactitol from spectral heterogeneity in erythrosin B phosphorescence. *Biophysical Chemistry* 123 (2006). 122-133.
- Strambini, G.B. and Gonnelli, M. The indole nucleus triplet-state lifetime and its dependence on solvent microviscosity. *Chemical Physics Letters*. 115 (1985). 196-200.
- Turro, N. J. *Modern Molecular Photochemistry*. The Benjamin/Cummings Publishing, Menlo Park, CA. (1978).
- Vanderkooi, J. M. and Berger, J. W. Excited triplet state used to study biological macromolecules at room temperature. *Biochimica et Biophysica Acta: Bioenergetics*. 976 (1989). 1-27.
- Vo-Dinh, T. *Room temperature phosphorimetry for chemical analysis*. Wiley-Interscience, New York. (1984).

- Wang, J. and Hurtubise, R. J. Solid matrix luminescence from trace organic compounds in glasses prepared from sugars. *Applied Spectroscopy*. 50 (1996). 53-58.
- Wright, J. D. *Molecular Crystals*. Cambridge University Press: Cambridge. (1987). 27-31.
- Zander, A. *Phosphorimetry*. Academic Press, New York, NY. (1968). 117-120.

Chapter IV: Vanillin sensitivity to molecular mobility as a function of molecular weight and glass transition temperature in glucose homologous series.

Introduction

Vitrification of sugars and other carbohydrates from melt or from concentrated aqueous solution plays a major role in the confectionary industry, in stabilizing dried and frozen foods and also provides desiccant tolerance to spores, seeds and even whole organisms (Roos, 1995; Fennema 1996; Le Meste et al., 2002; Crowe and Carpenter, 1998; Buitink and Leprince, 2004). The physical, chemical and biological changes in amorphous sugars and carbohydrates occur both below T_g in glass and above T_g in rubber/melt (Roos, 2003). The physical change (in terms of molecular mobility) occurring in glass and rubber/melt are very important in defining the shelf-life and quality of food, pharmaceuticals and biological materials that are amorphous in nature (Bell and Hageman, 1994, 1996; Buera and Karel, 1995; Buera et al., 1995; Roos, 1995, 2003). These motions are strong concern to us as they affect rates of molecular diffusion, and thus chemical reaction rate as well as the rates of other physical processes in amorphous foods and pharmaceuticals (Ludescher et al., 2001).

The glass transition temperature of sugars has being shown to be more dependent on molecular weight than on the structure (Orford et al., 1990). The glass transition temperature has being shown to increase with molecular weight: in the homologous series, the T_g of glucose (311K) < maltose (366K) < maltotriose (407K) < maltotetraose (406K) < maltopentaose (411K) < maltohexaose (420K) < maltoheptaose (427K) (Slade and Levine, 1991).

A number of techniques are used to measure molecular mobility of amorphous materials such as NMR (Karger and Ludermann, 1991, Hills and Pardoe, 1995; van den Dries et al., 2000; Hill et al., 2000; Margulies et al., 2000; Richert, 2001; Suhiko et al., 2000), FTIR (Wolkers et al., 1997; Ottenhof et al., 2003), electron spin resonance (ESR) (Contreras-Lopez et al., 2000) etc. They are used to determine T_g , molecular relaxation times, and the percent of amorphous content, and different modes of motions. DSC is used to measure T_g and other thermodynamic properties (e.g. enthalpy changes and heat capacity) (Shamblin et al., 1999; Baek et al., 2004). Thermo mechanical analysis uses to study relaxation processes. Dielectric relaxation and dynamic mechanical spectroscopy are widely used to study T_g and secondary thermal transitions because of their sensitivity to low order molecular mobility (Noel et al., 1996, 2000; Champion et al 2003). Recently TSDC has been used to resolve a broad global relaxation into its different individual components fractions or segments (Correia et al., 2000, 2001). The phosphorescence intensity decays of erythrosin B embedded in amorphous sugars has being shown to be sensitive to molecular mobility in the glassy state (Pravinata et al., 2005; Shirke, and Ludescher, 2005; Shirke and Ludescher, 2006).

The phosphorescence intensity decay of vanillin embedded in amorphous sucrose has recently been shown to be sensitive to the molecular mobility in the glassy state and changes in mobility at the glass transition temperature (Chapter II). We report here mobility measurements in amorphous thin films of the glucose homologous series glucose, maltose, maltotriose, maltotetraose, maltopentaose, maltohexaose and

maltoheptaose as a function of temperature using vanillin phosphorescence as triplet state probe.

Materials and Methods

Sample Preparation: Glucose, maltose, maltotriose, maltotetraose, maltopentaose, maltohexaose and maltoheptaose were purchased from Sigma-Aldrich (St. Louis, MO) with minimum purity of 98% and were used without further purification. These components were dissolved to near saturation in deionized water at room temperature. The vanillin was dissolved in distilled deionized water to make a 66mM solution, an aliquot from this solution was added to each of the sugars solutions to obtain a solution with dye: sugar molar ratio of $\sim 1:10^3$. An aliquot (20 μ l) of the dye- containing sugar solution was spread on a quartz slide 3 cm x 1.35 cm (NSG Precision Cells, Hicksville, NY). After spreading (~ 0.05 mm) the solutions on the slides were then dried under a heat gun (Vidal Sassoon) for 5 min to a maximum temperature of 88°C (measured using a thermocouple probe). The slides were stored at room temperature against P₂O₅ and DrieRite protecting from the light to prevent any photo bleaching for at least 7 days before any phosphorescence measurements were made. The desiccant was refreshed as needed to maintain a relative humidity close to 0%. The glass transition temperatures were determined from the literature and are as glucose (311K), maltose (366K), maltotriose (407K), maltotetraose (406K), maltopentaose (411K), maltohexaose (420K), maltoheptaose (427K) (Slade and Levine, 1991).

Instrumentation: All phosphorescence measurements were made on a Cary Eclipse fluorescence spectrophotometer (Varian Instruments, Walnut Creek, CA). The quartz slides were placed in a standard 1cm x 1cm x 1cm quartz fluorescence cuvette, which was capped with a lid having inlet and outlet ports for gas lines. The cuvette was flushed

with a gentle stream of nitrogen for 15 minutes to eliminate oxygen. An oxygen free nitrogen stream was generated by passage of high purity nitrogen through a Supelco (Bellefonte, PA) gas purifier. The temperature was controlled by using a TLC 50 thermoelectric heating/cooling system (Quantum Northwest, Spokane, WA). The TLC-50 sample compartment was fitted with a jacketed cover and the temperature of the cuvette was monitored directly using a thermocouple in the cuvette. The film was equilibrated for 15 minutes at each temperature before collecting the data. The Cary Eclipse uses a pulsed lamp and collects emission intensity in analog mode; data were not collected within the first 0.1-0.2 ms to suppress fluorescence coincident with the lamp pulse.

Luminescence measurement: Delayed luminescence emission (10 nm bandwidth) spectra of vanillin in amorphous sugars were collected from 400 nm to 800 nm using excitation at 320 nm (20 nm bandwidth) over the temperature range from -10°C to 150°C . Each data point was collected from a single flash with 0.2ms delay, 100ms gate time, and 0.12s total decay time.

Lifetime measurements were made in presence of nitrogen as a function of temperature. The samples were excited at 320 nm (20 nm bandwidth) and emission transients collected at 490nm (20 nm bandwidth) at temperature ranging from -10°C to 150°C . Each decay was average of 50 cycles, and for each cycle data was collected from a single flash with a delay of 0.2 ms, windows for gate time and total decay time was varied at each temperature. All measurements were made in quadruplicate.

Data Analysis

Emission Energy as a function of temperature: Emission spectra's were fitted using the program Igor (Wavemetrics, Inc., Lake Oswego, OR). The emission spectra were analyzed by fitting phosphorescence of vanillin to a log-normal function Equation 1 over the temperature range.

$$I(\nu) = I_0 \exp \left\{ - \ln(2) \left(\frac{\ln[1 + 2b(\nu - \nu_p) / \Delta]}{b} \right)^2 \right\} \quad (1)$$

In this equation I_0 , is the maximum intensity value of the emission spectra, ν_p is the frequency in cm^{-1} of the emission maximum, Δ is the line width parameter, and b is the asymmetry parameter. The bandwidth of the emission, the full width at half maximum (Γ), is related to b and Δ Equation 2.

$$\Gamma = \Delta \left(\frac{\sinh(b)}{b} \right) \quad (2)$$

Photophysical Scheme: The phosphorescence intensity decay were collected as described above and were fitted using a multi-exponential functions (Shamblin et al., 2000). The multi-exponential model is as show in Equation 3. τ_i are decay times, α_i represent the amplitudes of the components at $t = 0$ and n is the number of decay times. Phosphorescence lifetimes were determined with the statistical program Igor (Wavemetrics, Inc., Lake Oswego, OR). Fits were judged satisfactory if the R^2 values were in the range of 0.995-1.0 and the modified residuals $((\text{data} - \text{fit})/\text{data}^{1/2})$ varied randomly about zero. The average lifetime was calculated using Equation 4.

$$I(t) = \sum_{i=1}^n \alpha_i \exp(-t/\tau_i) \quad (3)$$

$$\tau_{\text{Avg}} = \sum_{i=1}^n \alpha_i \tau_i / \sum_{i=1}^n \alpha_i \quad (4)$$

The phosphorescence lifetimes were used to calculate the rate constants associated with the various processes that depopulate the excited triplet state. The lifetime τ is related to the rate constants for de-excitation of the triplet excited state of the probe according to the following Equation 5 (Papp and Vanderkooi, 1989).

$$1/\tau = k_{\text{RP}} + k_{\text{NR}}(T) + k_{\text{Q}}[\text{O}_2] = k_{\text{P}} \quad (5)$$

Here $k_{\text{P}} (=1/\tau)$ is the total decay rate, k_{RP} is the rate of radiative decay of the ground state (2.69 s^{-1} , measured in this study), k_{NR} is the rate of non-radiative decay to the singlet state followed by vibrational relaxation to S_0 due to collisional quenching. The magnitude of k_{NR} reflects factors associated with the mechanism by which the excited T_1 state of vanillin is coupled to highly excited vibrations of the S_0 ground state as well as external factors associated with the mechanism by which the ground state vibrational energy can dissipate from the excited state into the surrounding matrix (Fischer et al., 2002; Vanderkooi and Berger 1989). As the efficiency of external vibrational dissipation is related to overall mobility of the matrix, the magnitude of k_{NR} provides a measure of matrix mobility (Strambini and Gonnelli, 1985). One common method for restricting the

collisional deactivation is to super cool analyte solutions with liquid nitrogen to a rigid glass. The term $k_Q [O_2]$ refers to the collisional quenching due to interaction between the excited chromophore and triplet state oxygen.

Results

Scan: Delayed phosphorescence emission spectra of vanillin dispersed in glucose (Figure 1a), maltose (Figure 1b), maltotriose (Figure 1c), maltotetraose (Figure 1d), maltopentaose (Figure 1e), maltoheaxaose (Figure 1f) and maltoheptaose (Figure 1g) were measured as a function of temperature. Emission was collected between -10°C to 150°C based on the sugar until the emission was quenched. The emission peak in all the sugars was at ~ 490 nm. Phosphorescence intensity of vanillin was obtained from the delayed phosphorescence spectra fitted to the log-normal function (Eq. 1 of Materials and Methods). The emission intensity decreased with increase in temperature. A comparison plot of normalized phosphorescence intensity for all sugars is shown in Figure 2.

Peak frequency of the phosphorescence spectra of vanillin for glucose (Figure 3a), maltose (Figure 3b), maltotriose (Figure 3c), maltotetraose (Figure 3d), maltopentaose (Figure 3e), maltoheaxaose (Figure 3f) and maltoheptaose (Figure 3g) are plotted as a function of temperature. A comparison plot of peak frequency in all sugars is shown in Figure 4a. The peak frequency decreases with increase in temperature corresponding to a change in molecular environment due to matrix relaxation. At low temperature in the glass the peak frequency decreased gradually in case of glucose, and much more sharply at high temperature in the melt. However for maltose, maltotriose, maltotetraose, maltopentaose, maltohexaose and maltoheptaose there was a gradual decrease in peak frequency in the glass all the way into the melt. Figure 5a is a plot of peak frequency against T-T_g for the glucose homologous series. In glucose glass peak frequencies were

almost constant, whereas in case of maltose, maltotriose, maltotetraose, maltopentaose, maltohexaose and maltoheptaose there was a gradual decrease in peak frequency.

FWHM of the phosphorescence spectra of vanillin for glucose (Figure 3a), maltose (Figure 3b), maltotriose (Figure 3c), maltotetraose (Figure 3d), maltopentaose (Figure 3e), maltoheaxaose (Figure 3f) and maltoheptaose (Figure 3g) are plotted as a function of temperature. A comparison plot of FWHM is shown in Figure 4b. The FWHM increases with increase in temperature reflecting an increase in inhomogeneous broadening of the spectra due to interaction of vanillin molecules with the matrix of surrounding molecules. The FWHM increased gradually at low temperature in the glass and much more dramatically at higher temperature in the melt for the entire glucose series. Figure 5b is a plot of peak frequency against T-T_g for the glucose homologous series.

Lifetime: Lifetimes were measured by exciting vanillin at 320 nm and collecting the transient emission decay at 490 nm as a function of temperature from -10°C to 150°C. The decays were fitted using a multi-exponential function where glucose, maltose and maltotriose fitted to a four-exponential function whereas maltotetraose, maltopentaose, maltohexaose and maltoheptaose were fitted to a three-exponential function (Eq. 3, Materials and Methods). Fits were judged satisfactory if the modified residuals ((data-fit)/data^{1/2}) varied randomly about zero. The phosphorescence intensity decays of vanillin in amorphous films of glucose, maltose, maltotriose, maltotetraose, maltopentaose, maltohexaose and maltoheptaose at 20°C in the presence of nitrogen are plotted in Figure

6a, 6b, 6c, 6d, 6e, 6f and 6g, respectively, along with the modified residuals for a fit using a multi-exponential function.

The lifetimes of vanillin dispersed in amorphous films of glucose, maltose, maltotriose, maltotetraose, maltopentaose, maltohexaose and maltoheptaose as a function of temperature are shown in Figure 7a, 7b, 7c, 7d, 7e, 7f and 7g, respectively. The lifetime is the average time a molecule spends in the excited state and is an indicator of the rigidity of the matrix. All the lifetime components decreased with increase in temperature from -10°C to 150°C. The decrease in lifetime occurs because of an increase in the rate of collisional quenching (k_{NR}) from interaction of the probe with the sugar matrix and increase of vibrational relaxation. In environments with more mobility, the probe has a shorter lifetime (Strambini and Gonnelli, 1985) as result of quenching. In the environments with higher lifetimes, the probe senses lower mobility and is less easily quenched. Lifetimes are higher at low temperature indicating lower quenching in the glass. At high temperature lifetimes are much shorter comparatively indicating higher quenching in the melt. Comparing the individual lifetimes of vanillin in the glassy state (defined as below T_g) of each sugar indicated that each lifetime component decreased in sugars with increasing molecular weight and T_g following sequence, where lifetimes were glucose > maltose > maltotriose > maltotetraose > maltopentaose > maltohexaose > maltoheptaose. This trend suggested that the rate of molecular collisional quenching is greater in sugars with higher T_g and molecule weight.

The plots of the amplitudes of each lifetime component for vanillin dispersed in amorphous films of glucose, maltose, maltotriose, maltotetraose, maltopentaose, maltohexaose and maltoheptaose as a function of temperature are shown in Figure 8a, 8b, 8c, 8d, 8e, 8f and 8g, respectively. The amplitudes of the longer lifetime component(s) decreased and that of the shorter lifetime component(s) increased as a function of temperature in all sugar matrices. The different lifetimes observed are due to different locations of the probes in different environments in the amorphous sucrose matrix that differ in molecular mobility. In each sugar at 20°C, 80% of the probes were present in less mobile environment and the rest 20 % of the probes were in mobile environments.

The average lifetime was calculated using Eq. 4. A comparison plot of average lifetimes as a function of temperature is shown in Figure 9a. The plot of lifetime versus $T-T_g$ (Figure 9b), shows that the lifetime of vanillin is highest in glucose > maltose > maltotriose > maltotetraose > maltopentaose > maltohexaose > maltoheptaose over the entire range of ΔT . This indicates that quenching due to molecular collision in glucose is lower than the other sugars. Thus glucose matrix is less mobile as compared to the rest of the homologous series. Similarly maltose has higher lifetime as compared to the rest of the homologous series indicating it to be less mobile as compared to the rest. Thus the sequence of matrix mobility with temperature is as follows glucose < maltose < maltotriose < maltotetraose < maltopentaose < maltohexaose < maltoheptaose. This is also an increasing sequence for T_g .

The average lifetime in case of glucose varied from 165.5 ms at -10°C to 1.1 ms at 70°C , indicating ~ 147 -fold difference in mobility. The average lifetime in case of maltose varied from 134.2 ms at -10°C to 0.81 ms at 120°C , indicating ~ 165 -fold difference in mobility. The average lifetime in case of maltotriose varied from 132.4 ms at -10°C to 0.38 ms at 150°C , indicating ~ 348 -fold difference in mobility. The average lifetime in case of maltotetraose varied from 117.68 ms at -10°C to 0.68 ms at 150°C , indicating ~ 172 -fold difference in mobility. The average lifetime in case of maltopentaose varied from 118.7 ms at -10°C to 0.7 ms at 150°C , indicating ~ 168 -fold difference in mobility. The average lifetime in case of maltohexaose varied from 124.6 ms at -10°C to 0.55 ms at 150°C , indicating ~ 228 -fold difference in mobility. The average lifetime in case of maltoheptaose varied from 122.8 ms at -10°C to 0.56 ms at 150°C , indicating ~ 217 -fold difference in mobility.

An Arrhenius plots of $\ln(k_p)$ for the individual lifetime components as a function of inverse temperature are shown for glucose (Figure 10a), maltose (Figure 10b), maltotriose (Figure 10c), maltotetraose (Figure 10d), maltopentaose (Figure 10e), maltohexaose (Figure 10f) and maltoheptaose (Figure 10g). Break point temperatures and activation energies determined from intersection of trendline to points at low, intermediate and high temperature for individual lifetime components are compiled in Tables 1, 2, 3, 4, 5, 6 and 7 for glucose, maltose, maltotriose, maltotetraose, maltopentaose, maltohexaose and maltoheptaose, respectively. An Arrhenius plot of $\ln k_p$ for the average lifetime for each sugar is shown in Figure 11a. The plot of $\ln(k_p)$ as a function of T_g/T is shown in Figure 11b. Break point temperatures and activation

energies determined from intersection of trendline to points at low, intermediate and high temperature for the average lifetime for each sugar are compiled in Table 8.

The values of k_{NR} were calculated as shown in equation 5 in Materials and Methods. The values of k_{NR} represent the matrix mobility; the higher the k_{NR} the higher the matrix mobility. Figure 12 is a plot of k_{NR} as function of temperature for each individual sugar matrix. Figure 13a is a plot of k_{NR} as a function of $T-T_g$. There was a significant increase in k_{NR} both below and above T_g in all the sugars. In the glass (below T_g) the increase in k_{NR} followed the order glucose < maltose < maltotriose < maltotetraose < maltopentaose < maltohexaose < maltoheptaose (Figure 13b). This indicates that matrix mobility increased with an increase in molecular weight and T_g of sugars. The same trend existed above T_g with the exception that maltose < glucose < maltotriose < maltotetraose < maltopentaose < maltohexaose < maltoheptaose (Figure 13c). Thus, it could be concluded that in the entire glucose homologous series the matrix mobility increases with increase in molecular weight and T_g of the sugar molecule. The glucose matrix (lowest molecular weight sugar) is least mobile and maltoheptaose matrix (highest molecular weight sugar) is most mobile.

An Arrhenius plot for $\ln k_{NR}$ for each sugar is shown in Figure 14. Break point temperature and activation energies determined from intersection of trendline to points at low, intermediate and high temperature for average lifetime for each sugar are compiled in Table 9. At low temperature the activation energy is (E_{a1}) were among the sugars, glucose (10.2 kJ mol⁻¹), maltose (16 kJ mol⁻¹), maltotriose (20 kJ mol⁻¹), maltotetraose

(17 kJ mol⁻¹), maltopentaose (19 kJ mol⁻¹), maltohexaose (21 kJ mol⁻¹) and maltoheptaose (22 kJ mol⁻¹). Comparing the high temperature zone activation energy (E_{a2}) the value were glucose (120 kJ mol⁻¹), maltose (66.3 kJ mol⁻¹), maltotriose (68.2 kJ mol⁻¹), maltotetraose (60.7 kJ mol⁻¹), maltopentaose (54.9 kJ mol⁻¹), maltohexaose (56.9 kJ mol⁻¹) and maltoheptaose (57.4 kJ mol⁻¹).

Discussion

We have used phosphorescence of vanillin to evaluate how changes in molecular weight modulate molecular mobility in amorphous solids of the glucose homologous series glucose, maltose, maltotriose, maltotetraose, maltopentaose, maltohexaose and maltoheptaose. The phosphorescence emission in each sugar matrix were fitted to a log normal function which provided two important parameters, peak frequency and FWHM. The peak frequencies (plotted against T-T_g) in the glass followed the sequence glucose > maltose > maltotriose > maltotetraose ≥ maltopentaose ≥ maltohexaose ≥ maltoheptaose. Thus there was a decrease in peak frequency in the glass with an increase in molecular weight and T_g of the sugar. For example, glucose showed higher peak frequencies in the glass regions as compared to rest of the series indicating a larger extent of solvent relaxation in maltose, maltotriose, maltotetraose, maltopentaose, maltohexaose and maltoheptaose (sugars with higher molecular weight and T_g) making them more mobile than glucose in glass.

The FWHM (plotted against T-T_g) in the glass followed the same order glucose < maltose < maltotriose < maltotetraose ≤ maltopentaose ≤ maltohexaose ≤ maltoheptaose. Thus, there was an increase in FWHM in the glass with increase in molecular weight and T_g of sugars. For example, glucose showed lower FWHM (having narrowed distribution of different environments) in the glassy regions as compared to rest of the series indicating presence of larger number of different environments in maltose, maltotriose, maltotetraose, maltopentaose, maltohexaose and maltoheptaose (sugars with higher molecular weight and T_g) making them more mobile than glucose. The dipolar relaxation

rate was accompanied by an increase in the width of the distribution of energetically distinct environments in all the entire homologous series.

The phosphorescence intensity decay of vanillin has been shown to fit to multi-exponential functions (Chapter II). In a complex amorphous matrix, there may be several different environments and hence several different lifetimes of the triplet probe. In a multi-exponential model the intensity is assumed to be decaying as the sum of individual single-exponential decays. Phosphorescence intensity decays for the temperature range -10°C to 150°C were fitted using a multi-exponential function to obtain lifetimes and amplitudes. The lifetime provided the rate constant for de-excitation of the excited triplet state. The lifetime data showed that the rate constant for collisional quenching k_{NR} is sensitive to the physical state of amorphous matrix. The magnitude of k_{NR} is sensitive to internal factors related to vibrational coupling between the excited state and the ground state as well as external factors related to dissipation of the vibrational energy of the excited probe into the surrounding matrix. Since the efficiency of this vibrational coupling is related to the overall mobility of the matrix, the magnitude of k_{NR} provides a direct measure of matrix mobility.

Matrix mobility increased with molecular size in both the glass and melt in the entire glucose homologous series. The sequence of matrix mobility with temperature was glucose > maltose > maltotriose > maltotetraose > maltopentaose > maltohexaose > maltoheptaose; this is also an increasing sequence for molecular weight and T_g . A study by Shirke et al., 2006 using erythrosin B phosphorescence has also shown that matrix

molecular mobility varies in the order of glucose < maltose < maltotriose indicating that molecular mobility is higher in sugars with higher molecular weights and thus higher glass transition temperatures. And other study has drawn a similar conclusion using tryptophan phosphorescence to show that sucrose < maltose < trehalose, where increased mobility was observed with increase in T_g and molecular weight (Zunic, 2004).

This correlation of matrix mobility with molecular size (and thus T_g) is well supported with the FTIR studies by Wolkers and co-workers. They used FTIR to characterize hydrogen bonding network of amorphous carbohydrates of different chain length. They indicated that with increase in molecular weight in sugars there is increase in the slope of the plot of vibrational frequency of the OH stretch versus temperature (Wolkers 1998, 2004). The positive correlation between the stretching band of νOH and T_g, indicated increase in hydrogen bond length with T_g, and on the other hand increase in wavenumber-temperature coefficient of νOH with T_g indicated decrease in strength of hydrogen bond with increase in T_g. The increase in molecular mobility with increase in molecular weight could be attributed to increase in hydrogen bond length (in the glucose homologous series from glucose to maltoheptaose) which decreases the hydrogen bond strength and hence exhibiting higher rates of molecular mobility (Jeffrey, 1997). Faster rotational mobility of spin probes has been observed in sugars with higher molecular weight (Dzuba et al., 1993).

Conclusion

Phosphorescence emission and intensity decay of the triplet probe vanillin dispersed in amorphous glucose homologous series (glucose, maltose, maltotriose, maltotetraose, maltopentaose, maltohexaose and maltoheptaose) were measured to monitor molecular mobility of the sugar matrix in the glass and melt around the glass transitions temperature (T_g). The emission spectra were fitted to a log-normal function and all sugars exhibited complex decay pattern and were fitted to a multi-exponential function. The decays for glucose, maltose and maltotriose were fitted to a four exponential function and those for maltotetraose, maltopentaose, maltohexaose and maltopentaose were fitted to a three exponential function in which lifetime and amplitudes are the physically meaningful parameters. When normalized to glass-transition temperature, vanillin lifetime decreased in the order of glucose > maltose > maltotriose > maltotetraose > maltopentaose > maltohexaose > maltoheptaose. The collisional quenching rate constant k_{NR} as a function of $T-T_g$ followed the order maltoheptaose > maltohexaose > maltopentaose > maltotetraose > maltotriose > maltose > glucose, indicating higher mobility in higher molecular weight sugar.

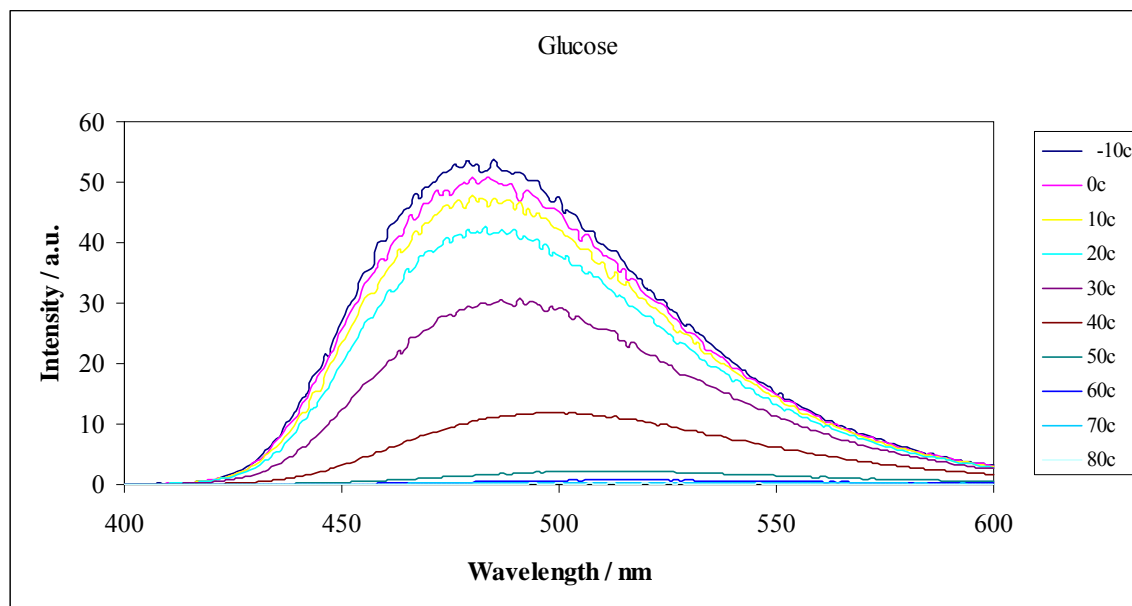
Figure IV-1a

Figure IV-1a: Delayed emission spectra of vanillin dispersed in amorphous films of glucose as a function of temperature (excitation at 320 nm). The spectra were collected at 10°C intervals from -10°C to 80°C (the curves follow this order from high to low intensity at ~490 nm).

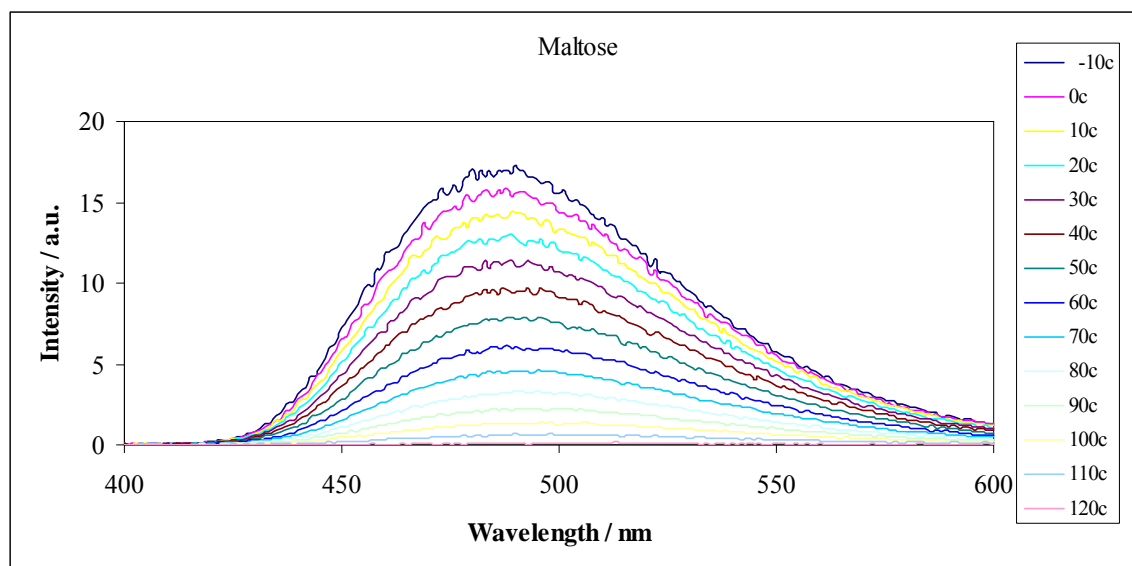
Figure IV-1b

Figure IV-1b: Delayed emission spectra of vanillin dispersed in amorphous films of maltose as a function of temperature (excitation at 320 nm). The spectra were collected at 10°C intervals from -10°C to 120°C (the curves follow this order from high to low intensity at ~490 nm).

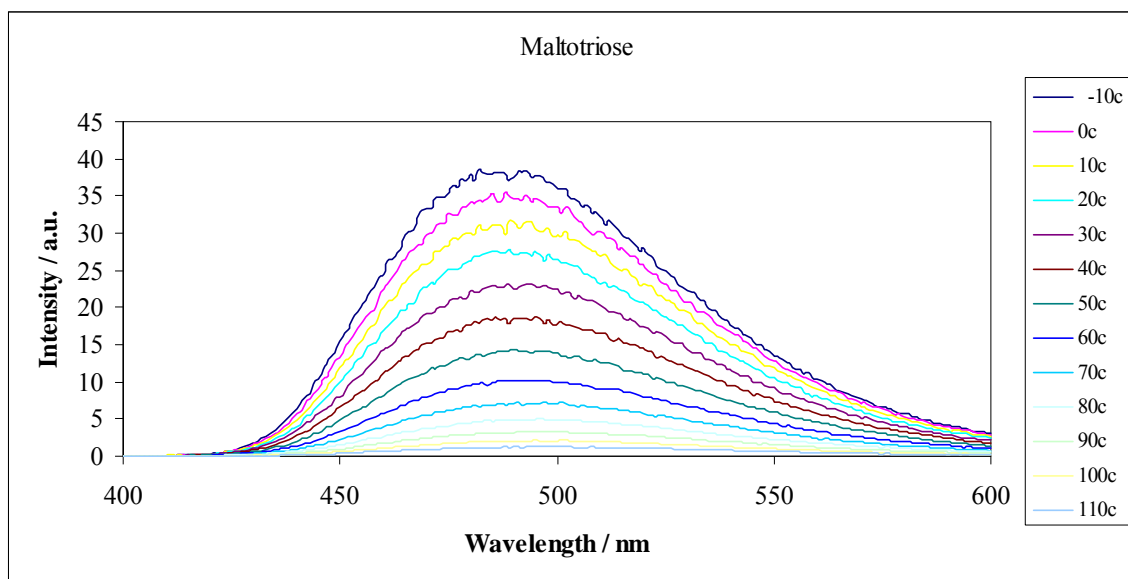
Figure IV-1c

Figure IV-1c: Delayed emission spectra of vanillin dispersed in amorphous films of maltotriose as a function of temperature (excitation at 320 nm). The spectra were collected at 10°C intervals from -10°C to 110°C (the curves follow this order from high to low intensity at ~490 nm).

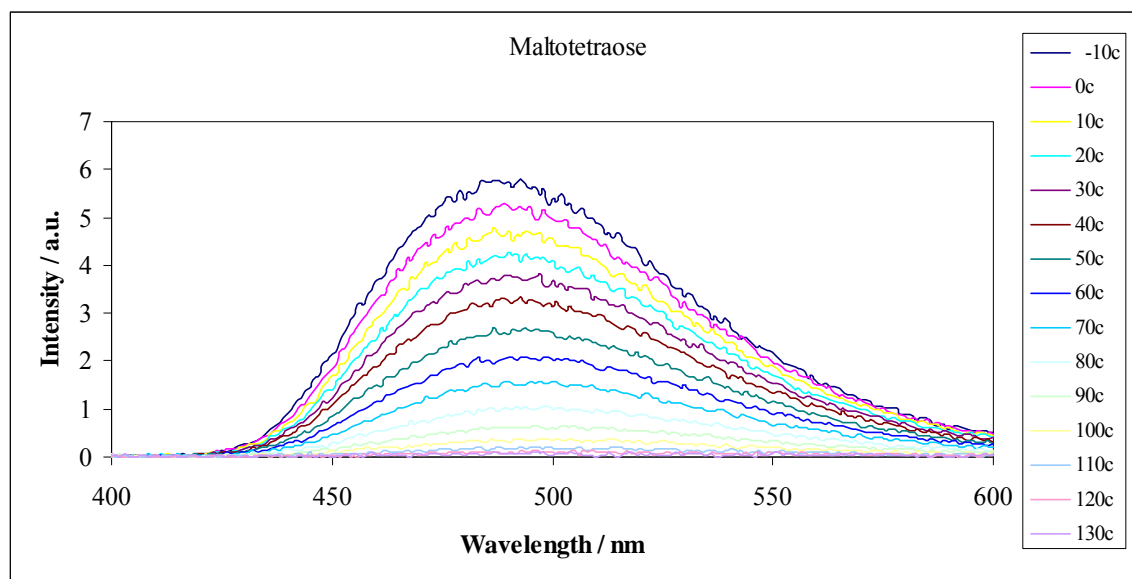
Figure IV-1d

Figure IV-1d: Delayed emission spectra of vanillin dispersed in amorphous films of maltotetraose as a function of temperature (excitation at 320 nm). The spectra were collected at 10°C intervals from -10°C to 130°C (the curves follow this order from high to low intensity at ~490 nm).

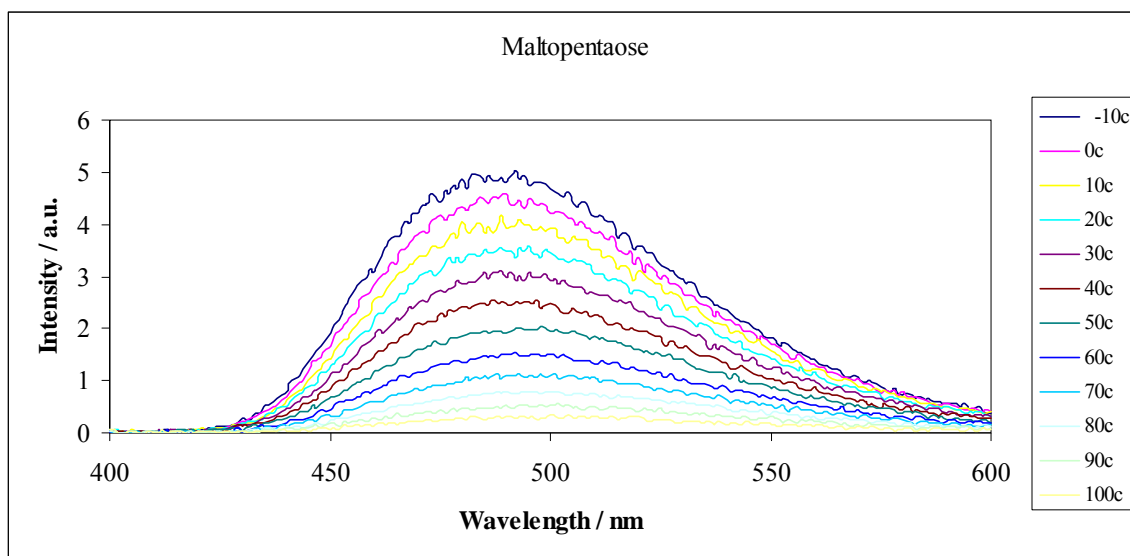
Figure IV-1e

Figure IV-1e: Delayed emission spectra of vanillin dispersed in amorphous films of maltopentaose as a function of temperature (excitation at 320 nm). The spectra were collected at 10°C intervals from -10°C to 100°C (the curves follow this order from high to low intensity at ~490 nm).

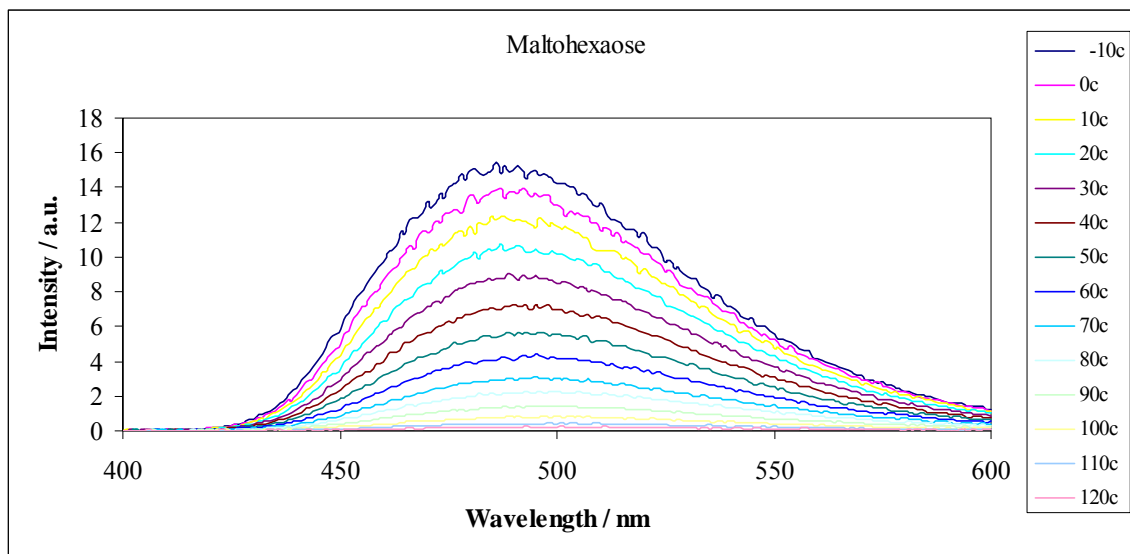
Figure IV-1f

Figure IV-1f: Delayed emission spectra of vanillin dispersed in amorphous films of maltohexaose as a function of temperature (excitation at 320 nm). The spectra were collected at 10°C intervals from -10°C to 120°C (the curves follow this order from high to low intensity at ~490 nm).

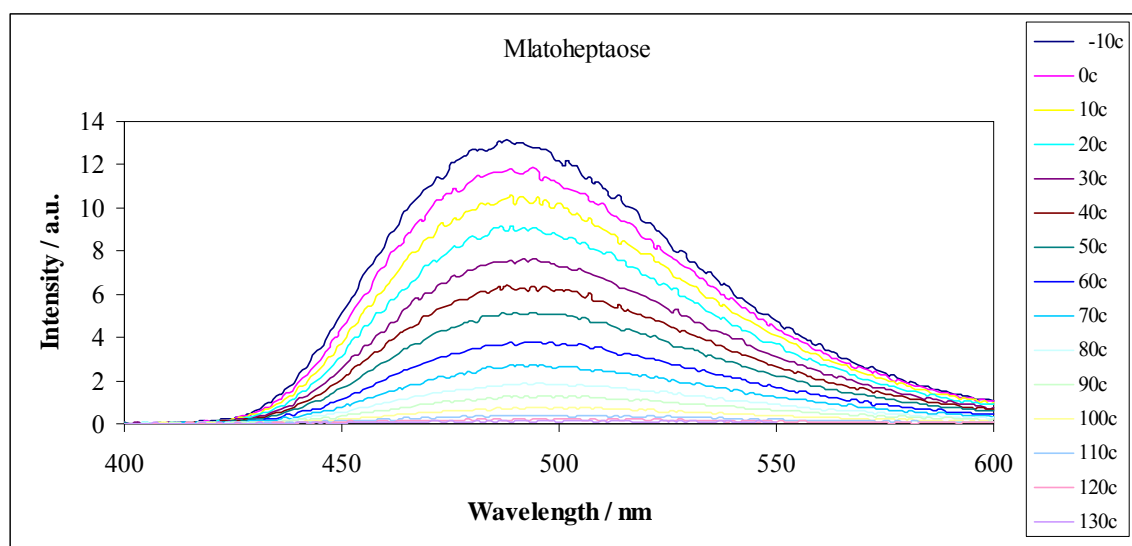
Figure IV-1g

Figure IV-1g: Delayed emission spectra of vanillin dispersed in amorphous films of maltoheptaose as a function of temperature (excitation at 320 nm). The spectra were collected at 10°C intervals from -10°C to 130°C (the curves follow this order from high to low intensity at ~490 nm).

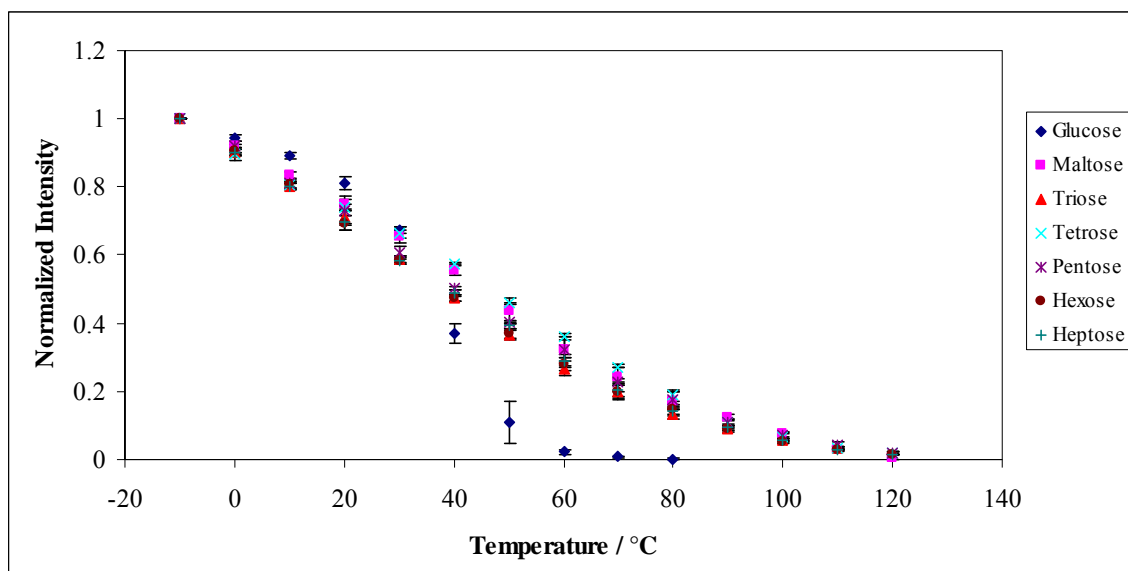
Figure IV-2

Figure IV-2: Intensity (I_p) was determined from analysis of the phosphorescence emission band (Figures IV-1 a, b, c, d, e, f, g) using a log-normal function (eq. (1), Materials and Methods). The effect of temperature on the phosphorescence emission intensity of vanillin in amorphous films of glucose (♦), maltose (■), maltotriose (▲), maltotetraose (×), maltopentaose (*), maltohexaose (●) and maltoheptaose (+) as a function of temperature equilibrated against nitrogen. Intensity normalized to value at -10°C for each sample.

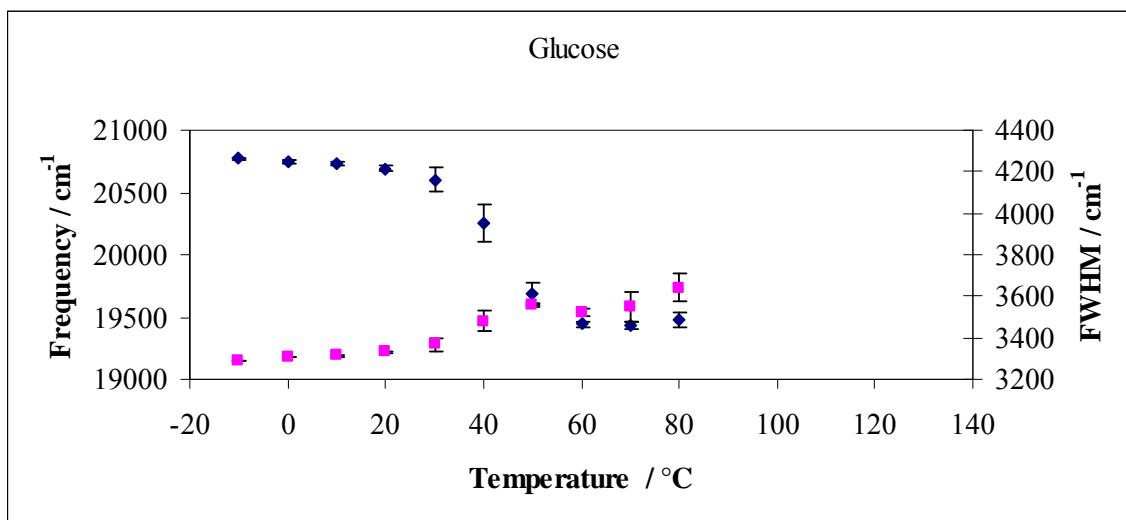
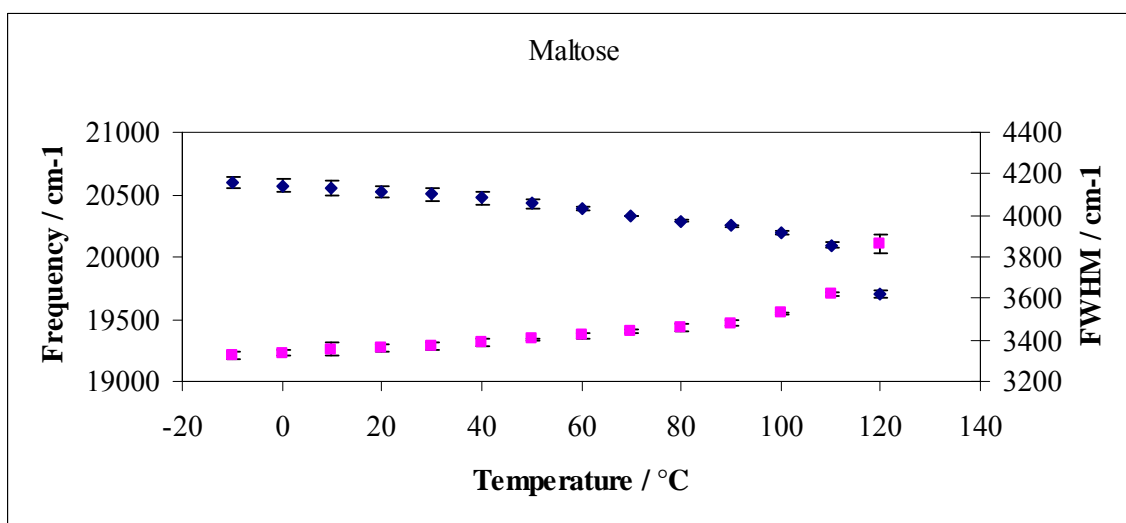
Figure IV-3a*Figure IV-3b*

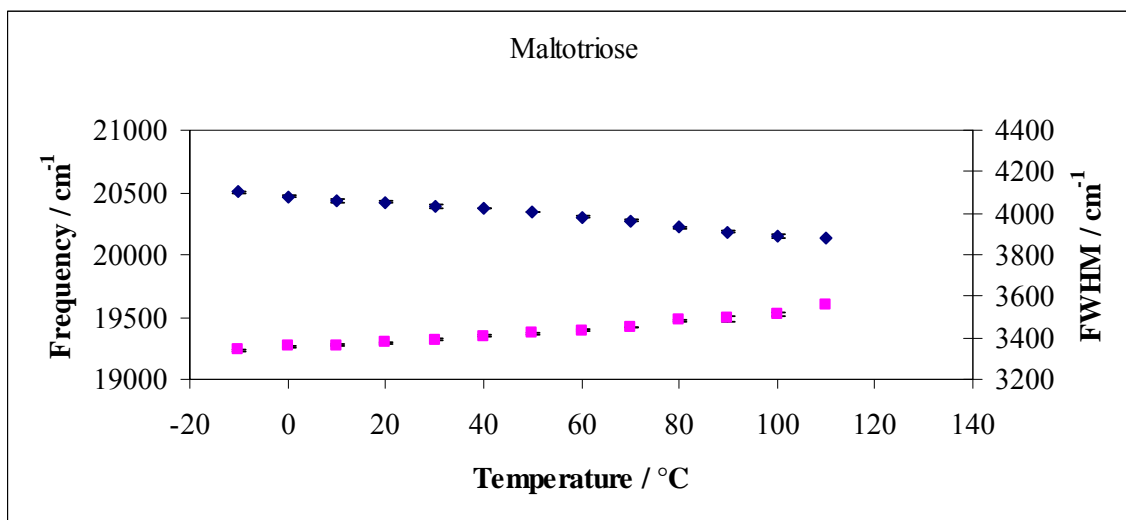
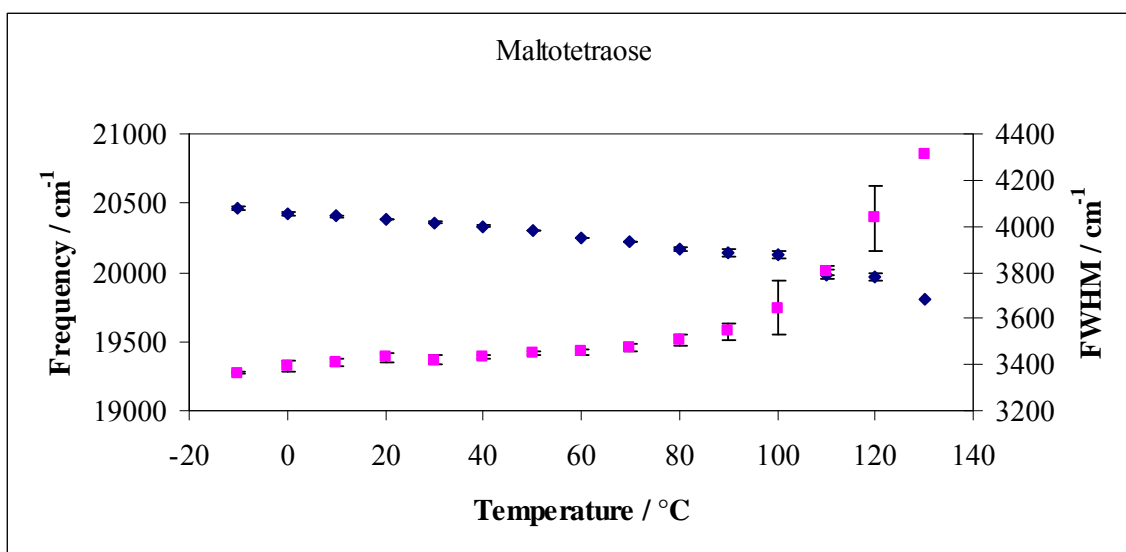
Figure IV-3c*Figure IV-3d*

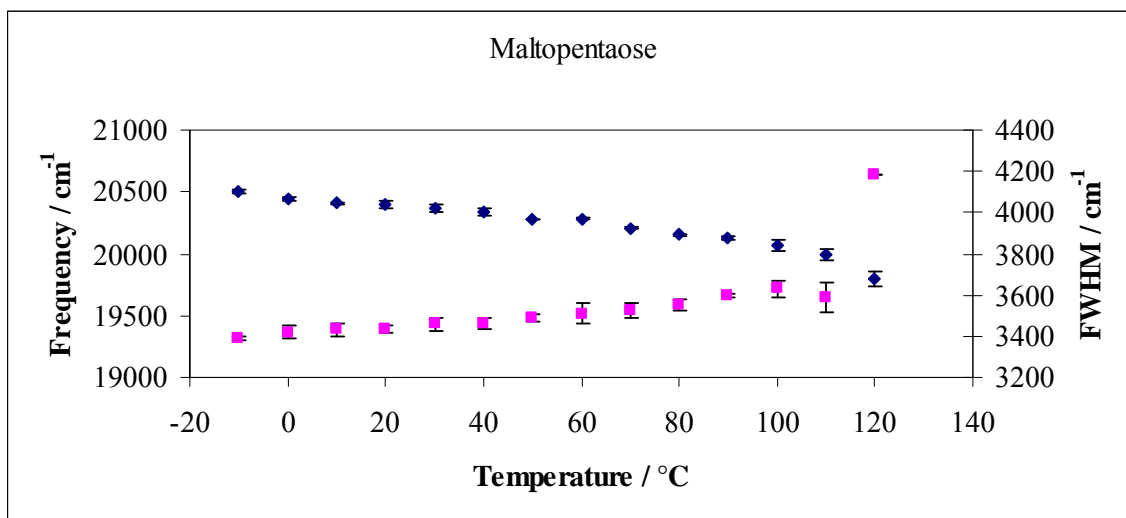
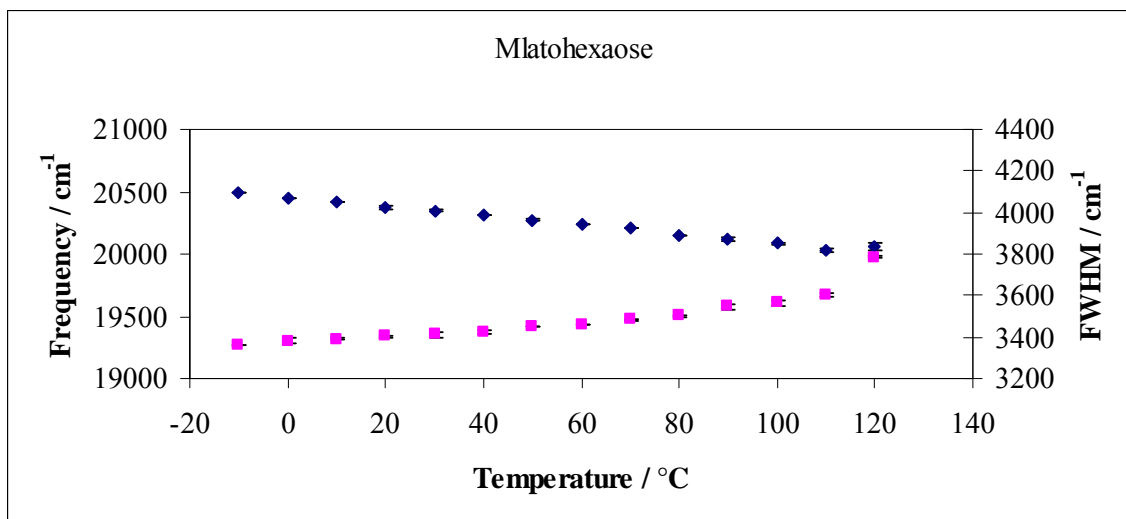
Figure IV-3e*Figure IV-3f*

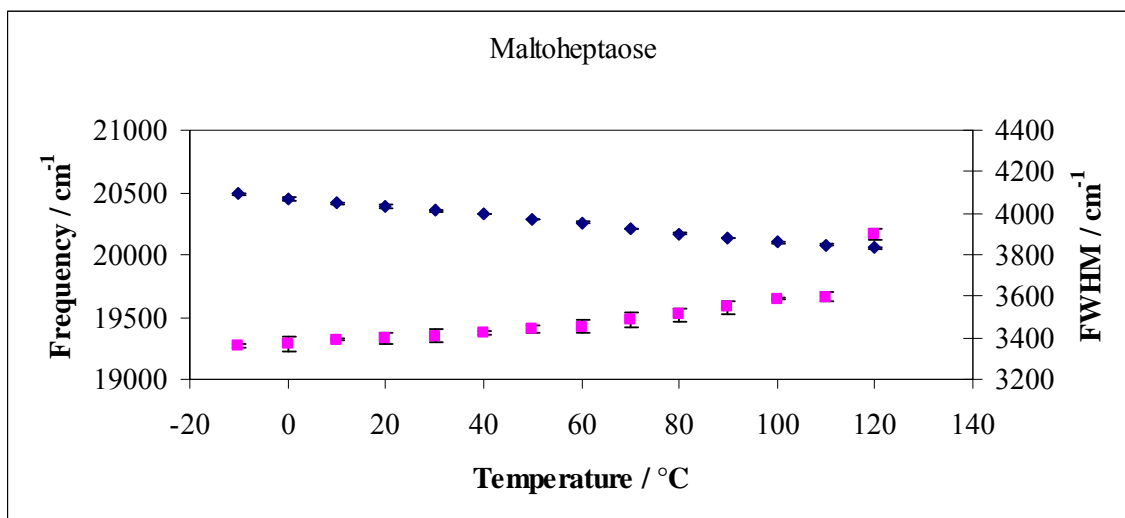
Figure IV-3g

Figure IV-3a to 3g: Peak energy ν_p and bandwidth for phosphorescence emission from vanillin in amorphous films of glucose (3a), maltose (3b), maltotriose (3c), maltotetraose (3d), maltopentaose (3e), maltohexaose (3f) and maltoheptaose (3g) as a function of temperature. The delayed emission spectra collected as a function of temperature (Figure IV-1a to 1g) were analyzed using log-normal function as described in Materials and Methods using eq. (1) and (2).

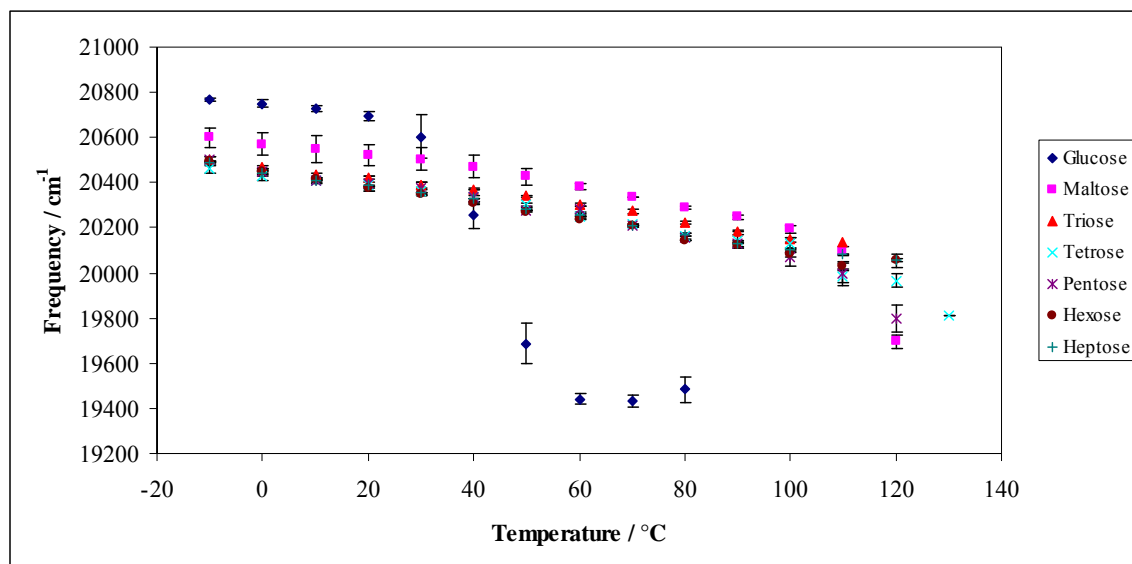
Figure IV-4a

Figure IV-4a: Comparison of peak energy ν_p for phosphorescence emission from vanillin in amorphous films of glucose (\blacklozenge), maltose (\blacksquare), maltotriose (\blacktriangle), maltotetraose (\times), maltopentaose ($*$), maltohexaose (\bullet) and maltoheptaose ($+$) as a function of temperature.

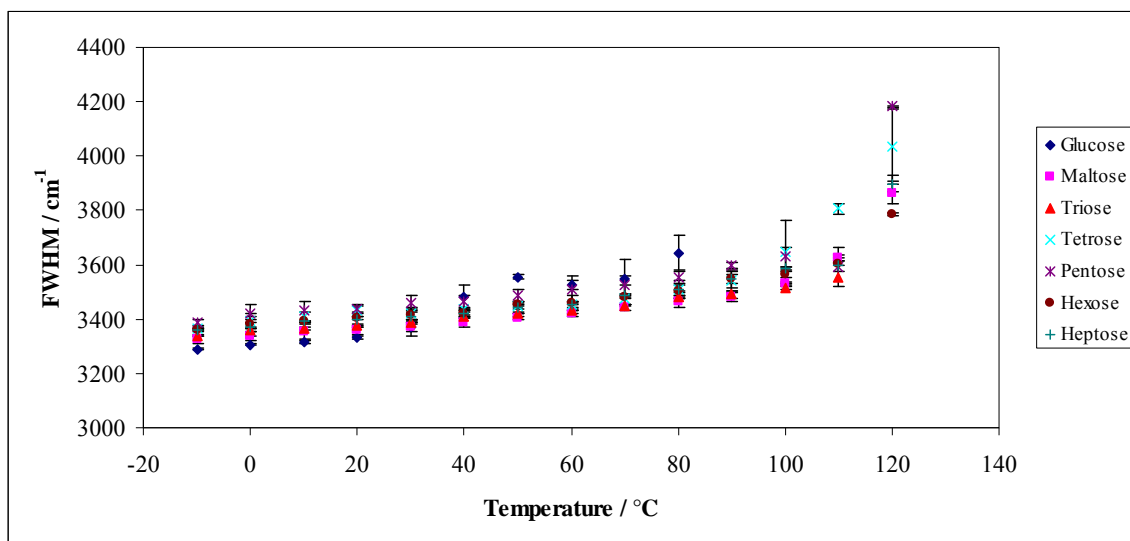
Figure IV-4b

Figure IV-4b: Comparison of bandwidth for phosphorescence emission from vanillin in amorphous films of glucose (♦), maltose (■), maltotriose (▲), maltotetraose (×), maltopentaose (*), maltohexaose (●) and maltoheptaose (+) as a function of temperature.

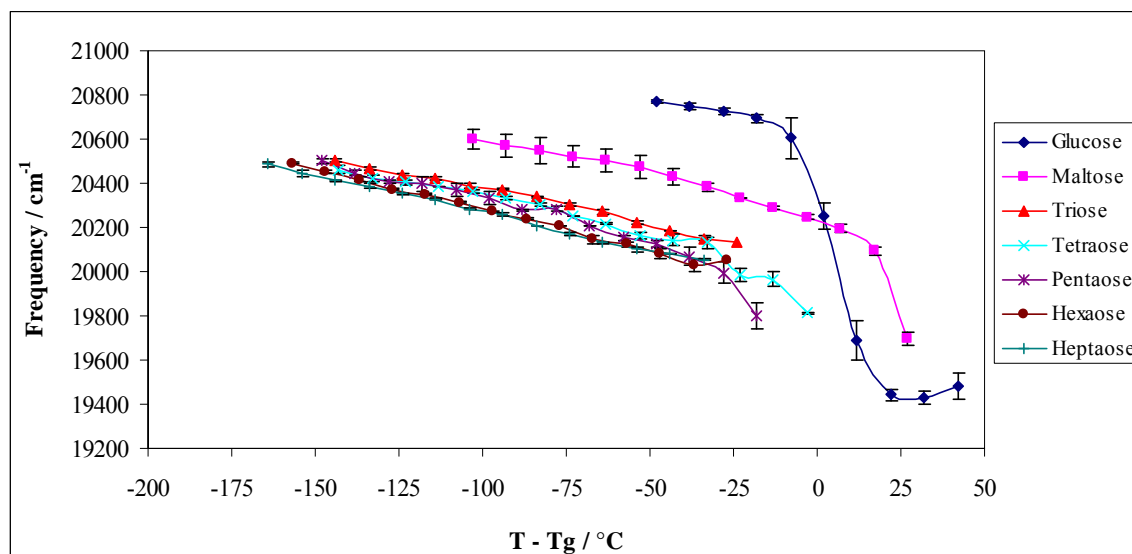
Figure IV-5a

Figure IV-5a: Comparison of peak energy ν_p for phosphorescence emission from vanillin in amorphous films of glucose (\blacklozenge), maltose (\blacksquare), maltotriose (\blacktriangle), maltotetraose (\times), maltopentaose ($*$), maltohexaose (\bullet) and maltoheptaose ($+$) as a function of $T-T_g$.

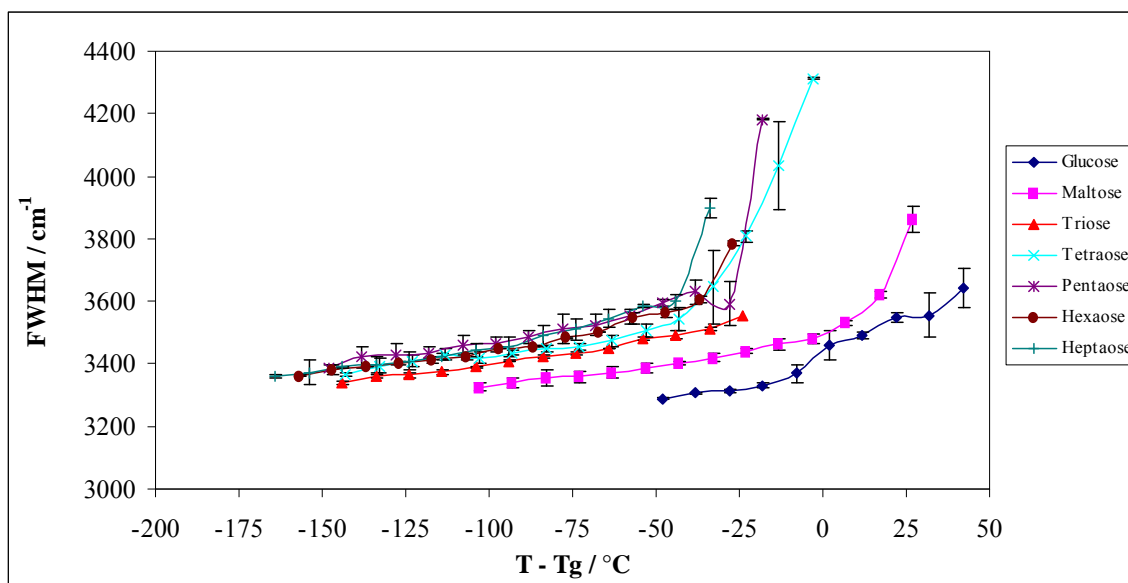
Figure IV-5b

Figure IV-5b: Comparison of FWHM for phosphorescence emission from vanillin in amorphous films of glucose (♦), maltose (■), maltotriose (▲), maltotetraose (×), maltopentaose (*), maltohexaose (●) and maltoheptaose (+) as a function of T-T_g.

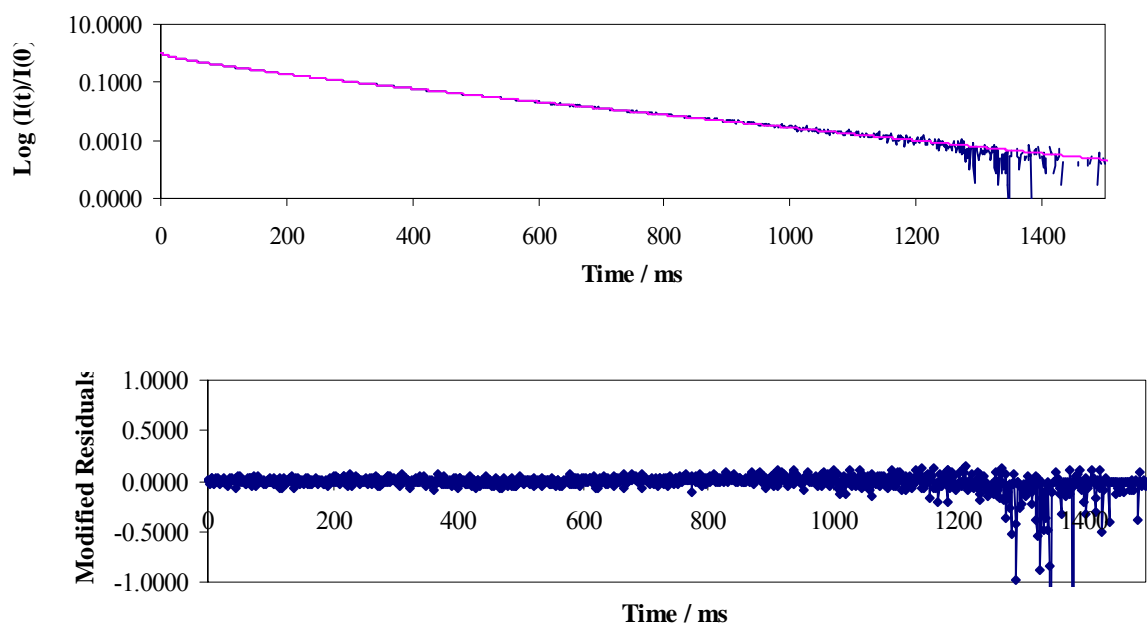
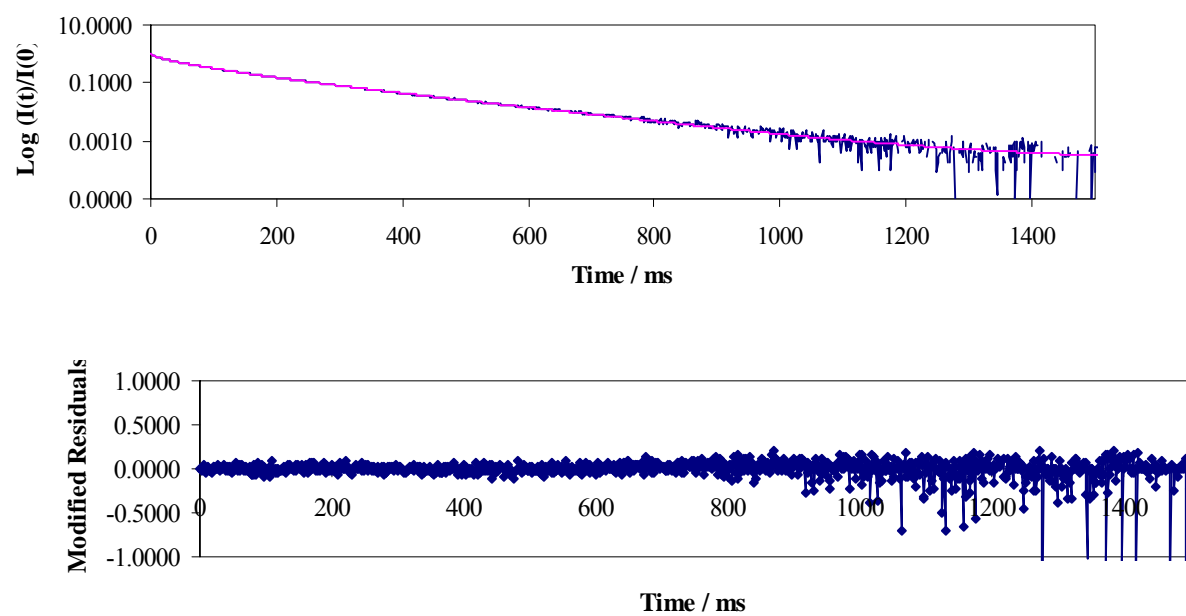
Figure IV-6a: Glucose*Figure IV-6b: Maltose*

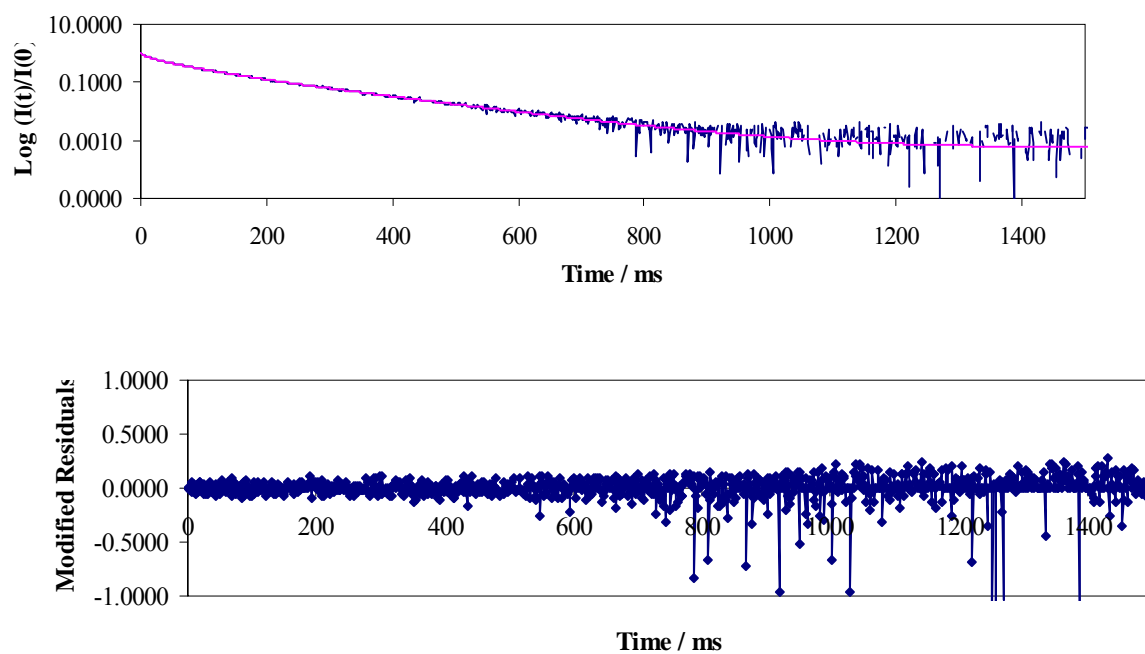
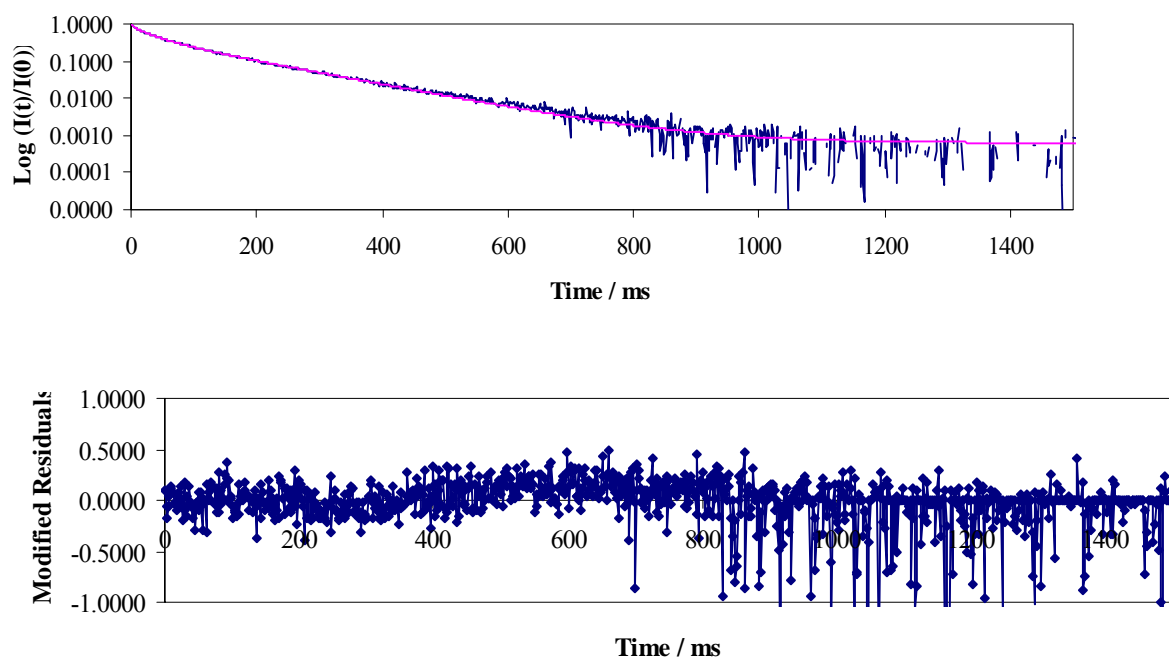
Figure IV-6c: Maltotriose*Figure IV-6d: Maltotetraose*

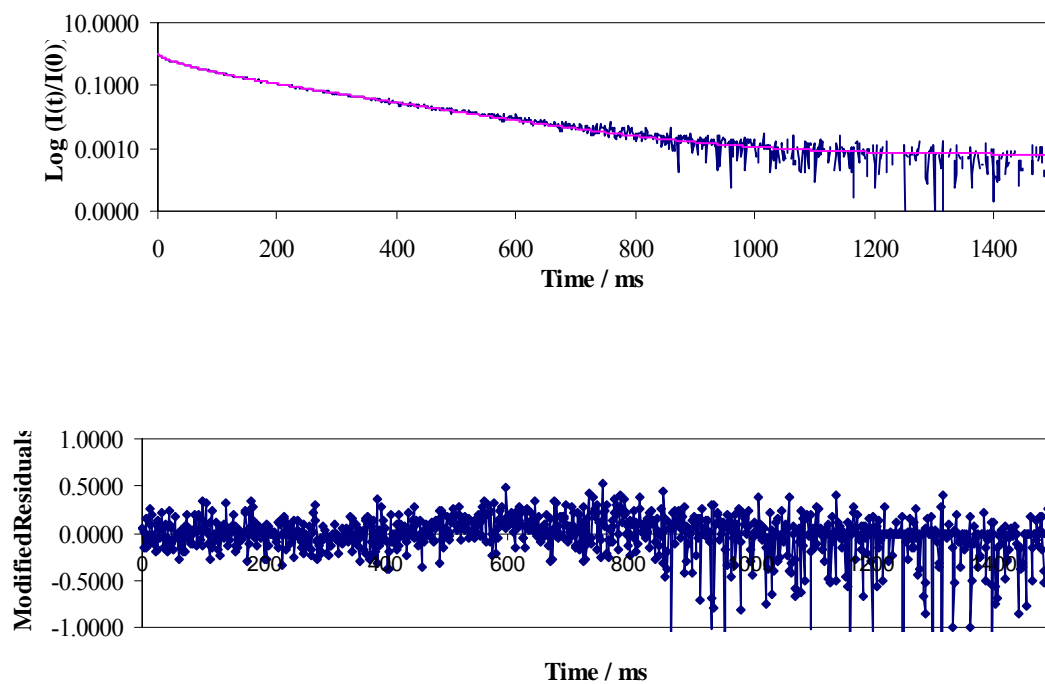
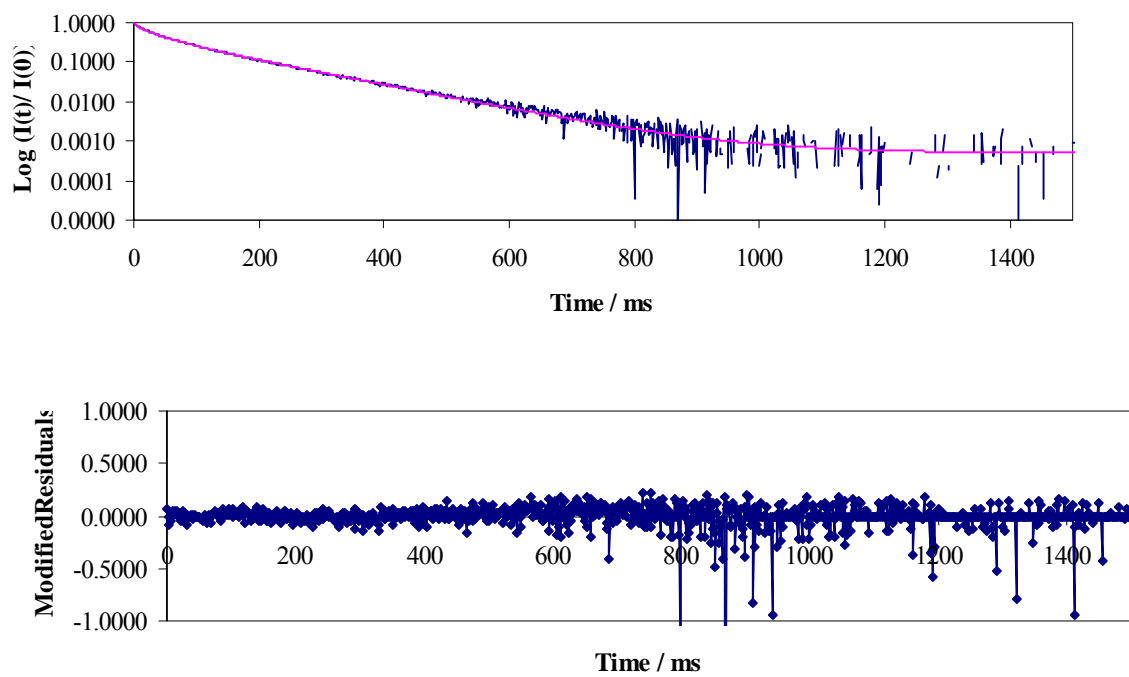
Figure IV-6e: Maltopentaose*Figure IV-6f: Mlatohexaose*

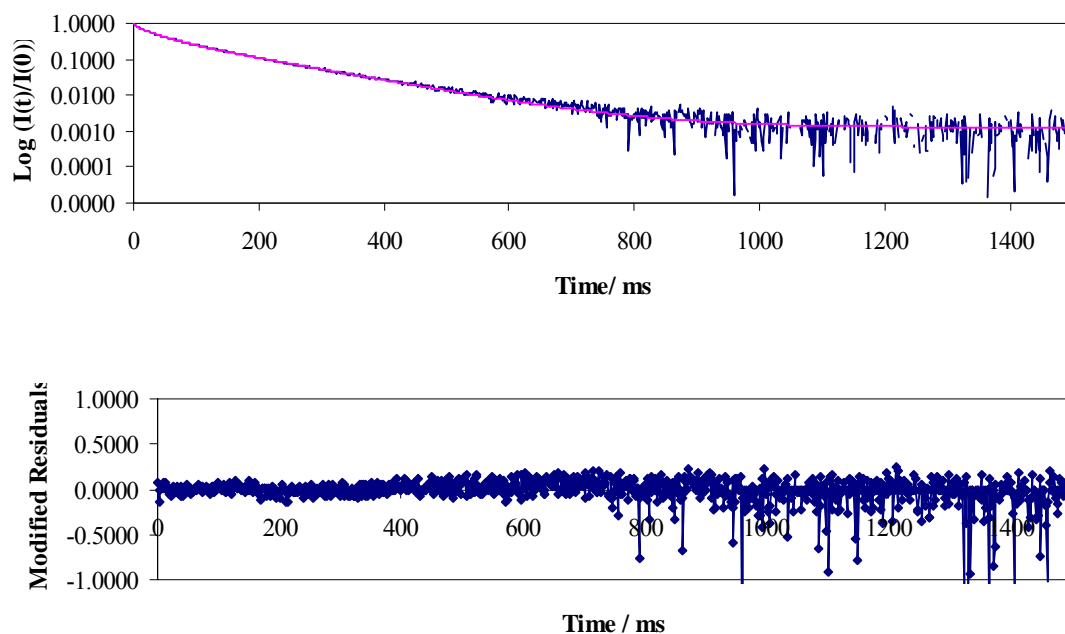
Figure IV-6g: Maltoheptaose

Figure IV-6a-6g: Normalized phosphorescence intensity decays $[I(t)/I(0)]$ of methyl vanillin dispersed in amorphous films of glucose (6a), maltose (6b), maltotriose (6c), maltotetraose (6d), maltopentaose (6e), maltohexaose (6f) and maltoheptaose (6g) at 20°C in the presence of nitrogen. The solid lines through the data are fits using a multi-exponential function (Eq. (3), Materials and Methods). A plot of modified residuals $[(\text{Data}-\text{Fit})/\text{Data}]^{1/2}$ for these fits are shown in the bottom graphs.

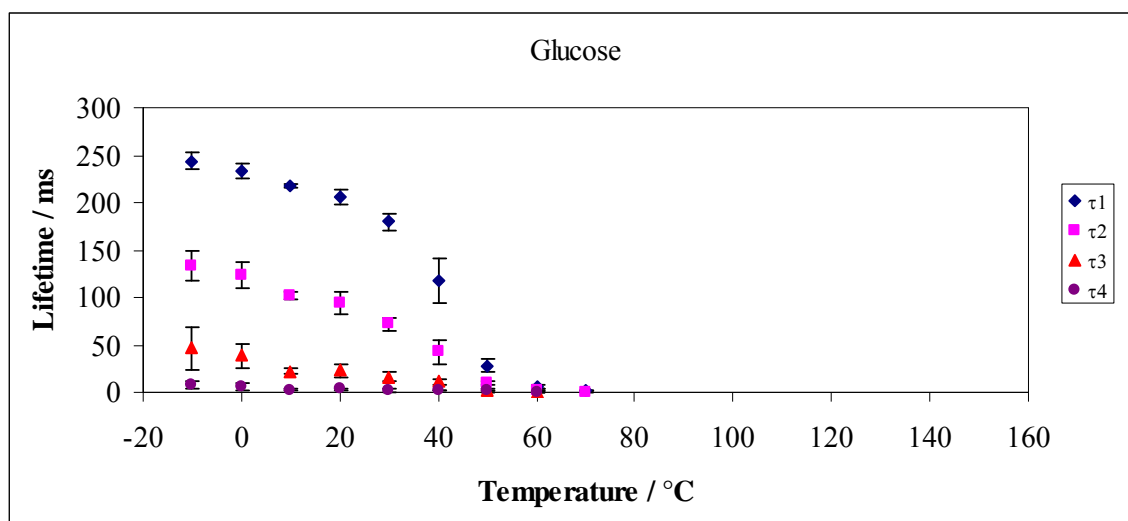
Figure IV-7a

Figure IV-7a: Lifetime components τ_1 (\blacklozenge), τ_2 (\blacksquare), τ_3 (\blacktriangle) and τ_4 (\bullet) obtained from a multi-exponential model fit (Eq. (3), Materials and Methods) to phosphorescence intensity decay data from vanillin dispersed in amorphous films of glucose equilibrated against nitrogen as a function of temperature. The data were calculated every 10°C from -10°C to 70°C.

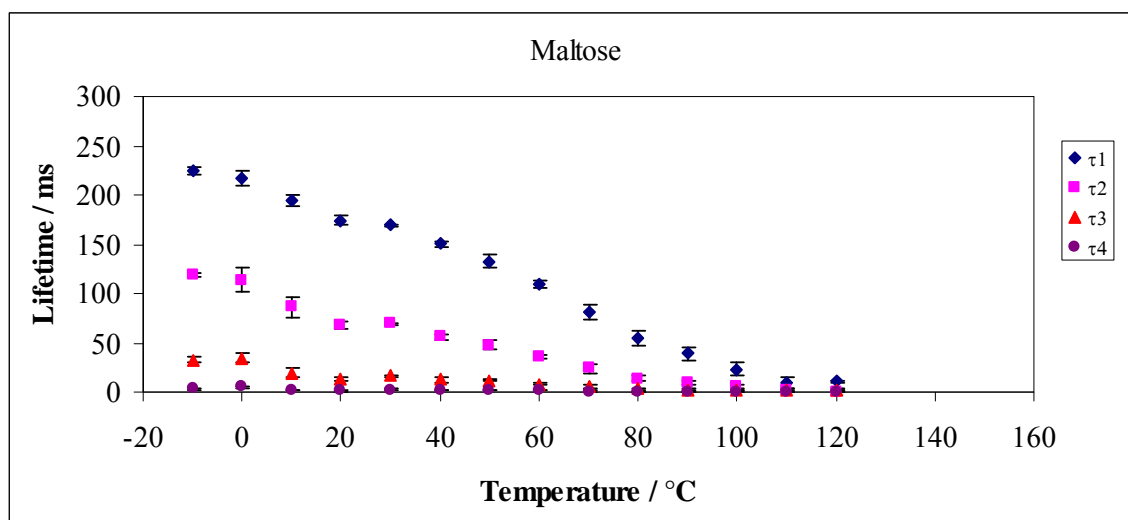
Figure IV-7b

Figure IV-7b: Lifetime components τ_1 (\blacklozenge), τ_2 (\blacksquare), τ_3 (\blacktriangle) and τ_4 (\bullet) obtained from a multi-exponential model fit (Eq. (3), Materials and Methods) to phosphorescence intensity decay data from vanillin dispersed in amorphous films of maltose equilibrated against nitrogen as a function of temperature. The data were calculated every 10°C from -10°C to 120°C.

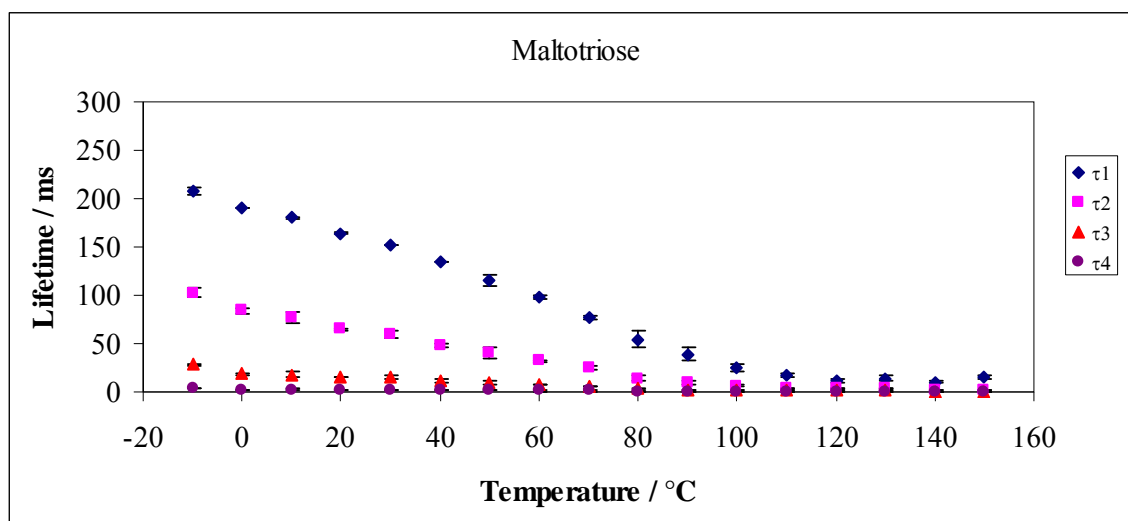
Figure IV-7c

Figure IV-7c: Lifetime components τ_1 (◆), τ_2 (■), τ_3 (▲) and τ_4 (●) obtained from a multi-exponential model fit (Eq. (3), Materials and Methods) to phosphorescence intensity decay data from methyl vanillin dispersed in amorphous films of maltotriose equilibrated against nitrogen as a function of temperature. The data were calculated every 10°C from -10°C to 150°C.

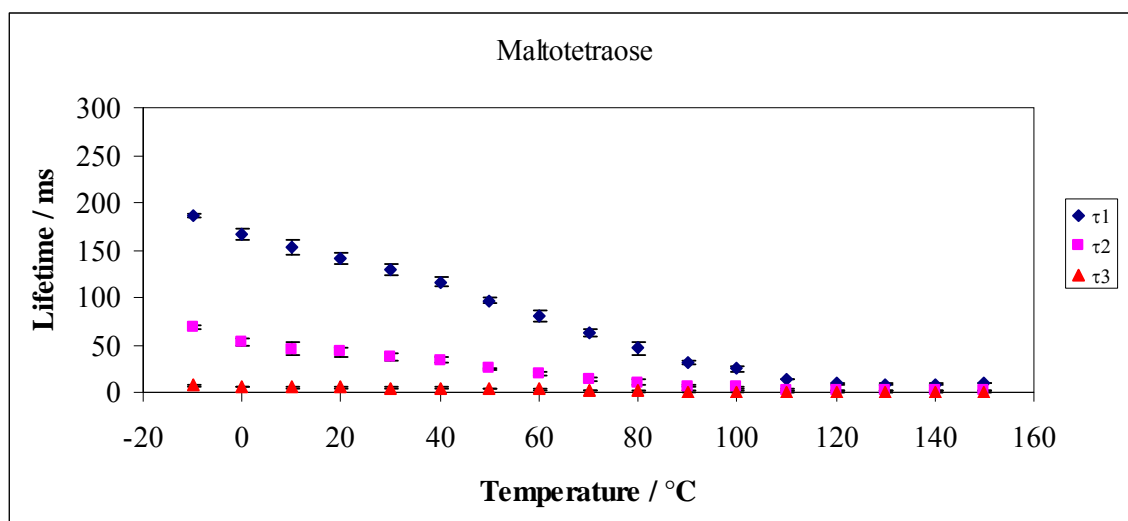
Figure IV-7d

Figure IV-7d: Lifetime components τ_1 (\blacklozenge), τ_2 (\blacksquare) and τ_3 (\blacktriangle) obtained from a multi-exponential model fit (Eq. (3), Materials and Methods) to phosphorescence intensity decay data from vanillin dispersed in amorphous films of maltotetraose equilibrated against nitrogen as a function of temperature. The data were calculated every 10°C from -10°C to 150°C.

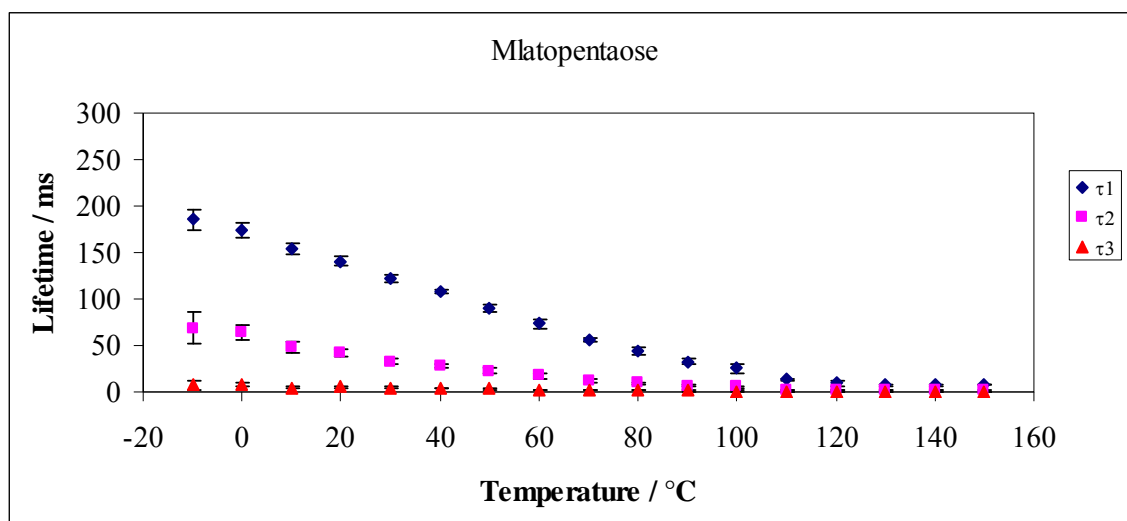
Figure IV-7e

Figure IV-7e: Lifetime components τ_1 (\blacklozenge), τ_2 (\blacksquare) and τ_3 (\blacktriangle) obtained from a multi-exponential model fit (Eq. (3), Materials and Methods) to phosphorescence intensity decay data from vanillin dispersed in amorphous films of maltopentaose equilibrated against nitrogen as a function of temperature. The data were calculated every 10°C from -10°C to 150°C.

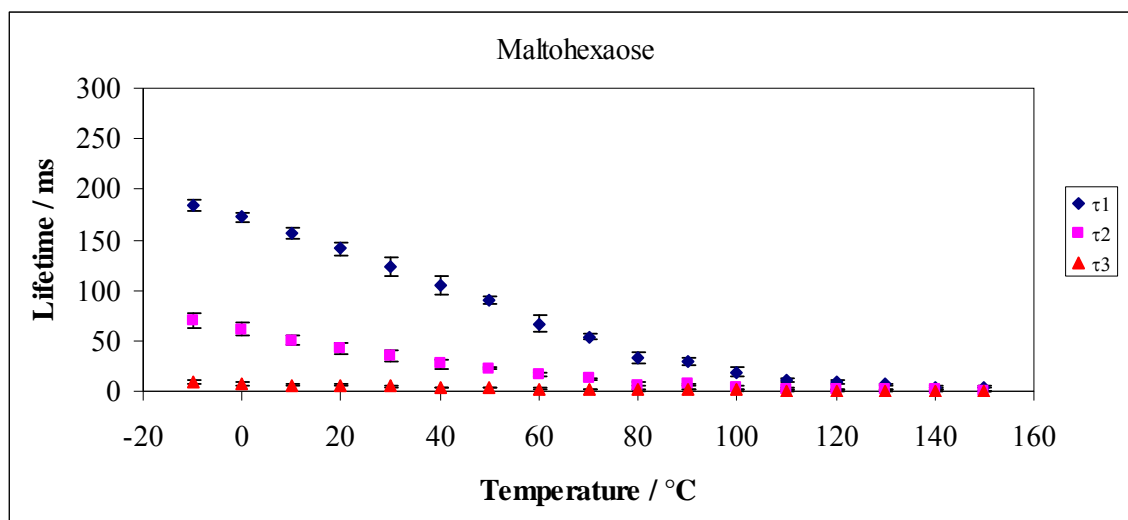
Figure IV-7f

Figure IV-7f: Lifetime components τ_1 (\blacklozenge), τ_2 (\blacksquare) and τ_3 (\blacktriangle) obtained from a multi-exponential model fit (Eq. (3), Materials and Methods) to phosphorescence intensity decay data from vanillin dispersed in amorphous films of maltohexaose equilibrated against nitrogen as a function of temperature. The data were calculated every 10°C from -10°C to 150°C.

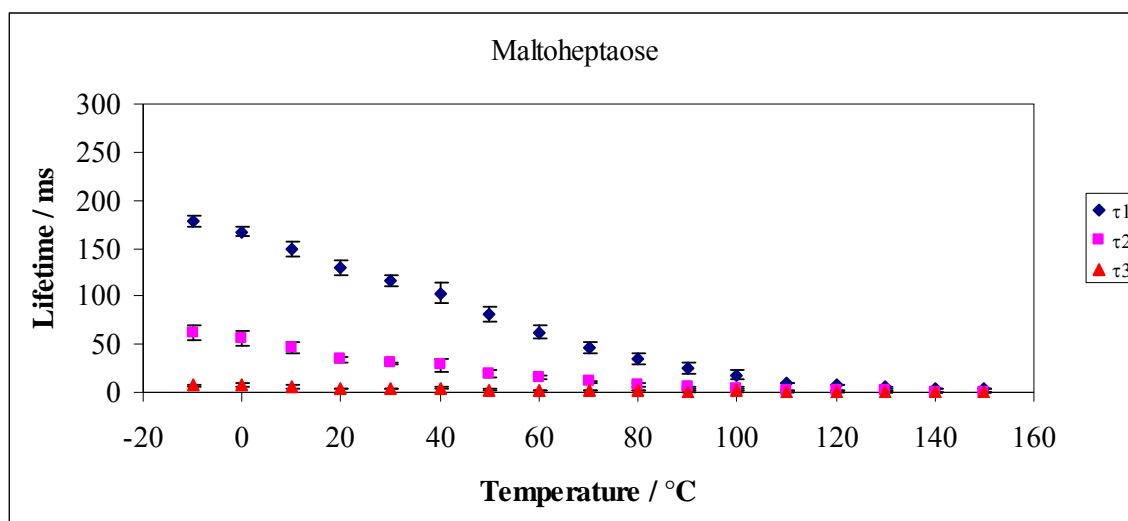
Figure IV-7g

Figure IV-7g: Lifetime components τ_1 (\blacklozenge), τ_2 (\blacksquare) and τ_3 (\blacktriangle) obtained from a multi-exponential model fit (Eq. (3), Materials and Methods) to phosphorescence intensity decay data from vanillin dispersed in amorphous films of maltoheptaose equilibrated against nitrogen as a function of temperature. The data was calculated every 10°C from -10°C to 150°C.

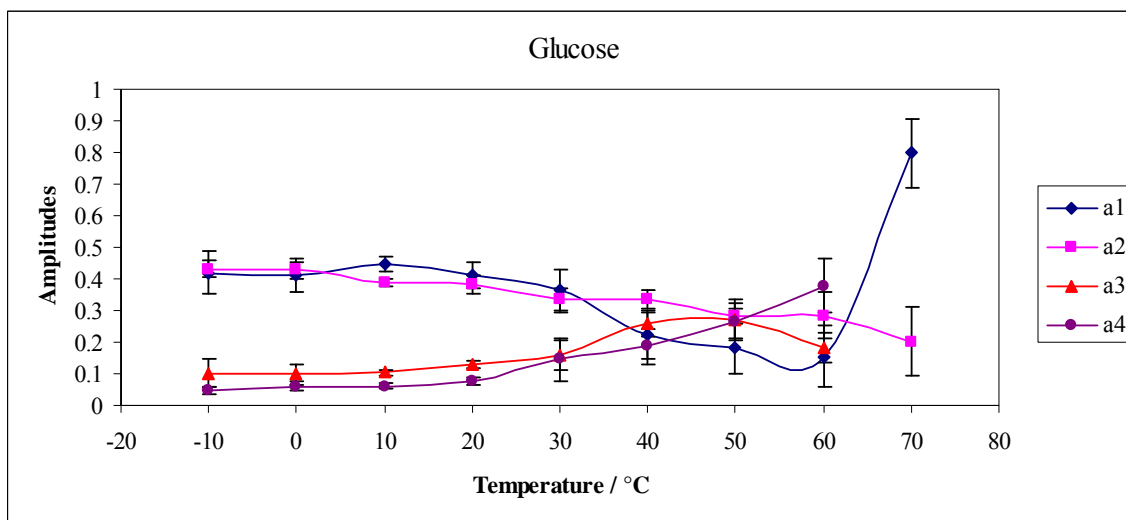
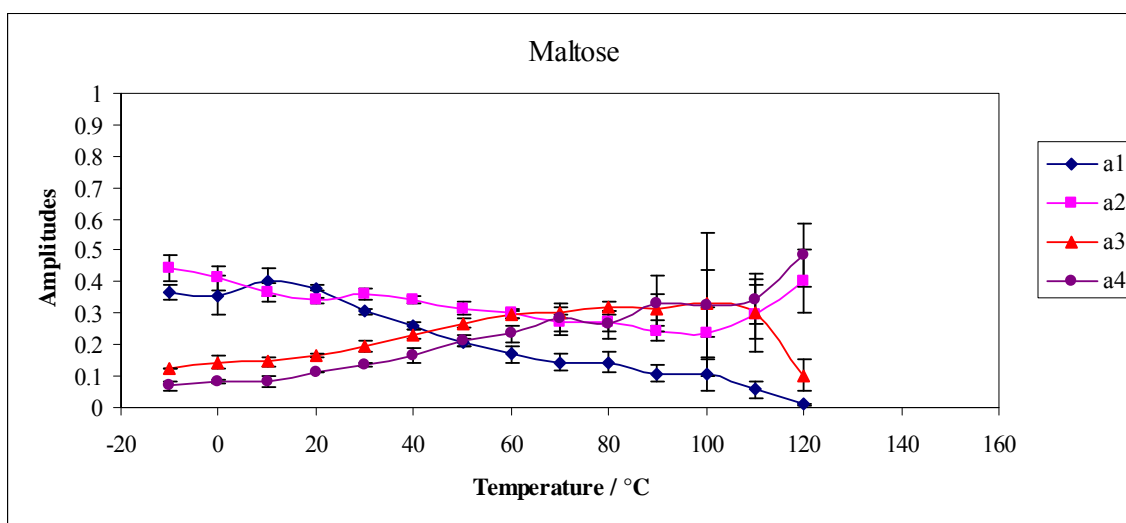
Figure IV-8a*Figure IV-8b*

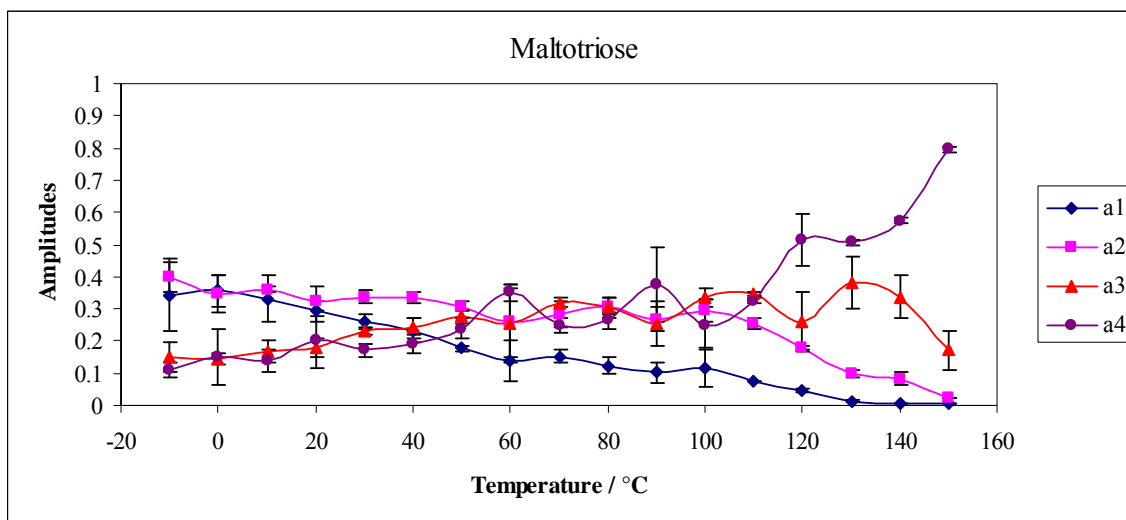
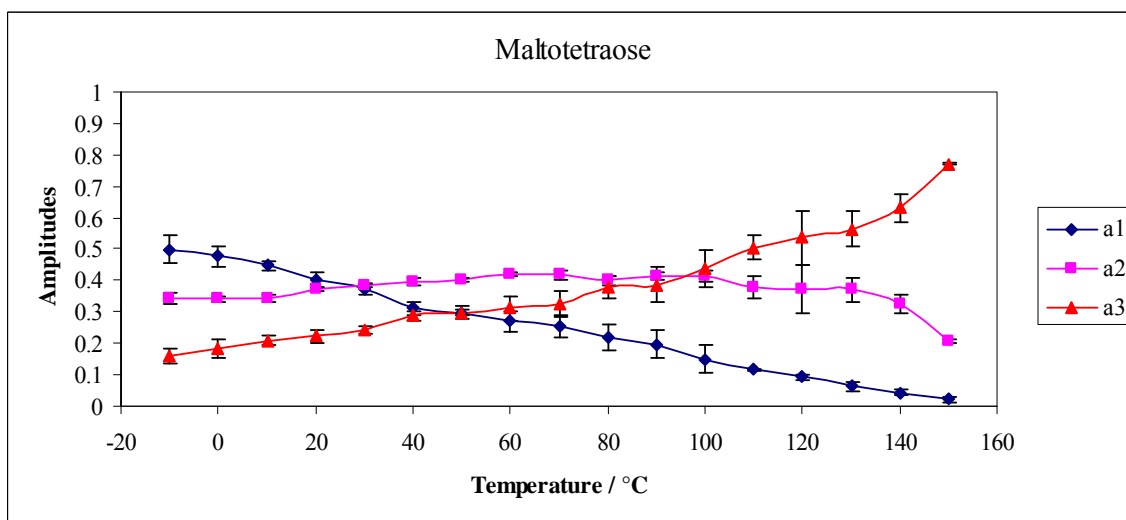
Figure IV-8c*Figure IV-8d*

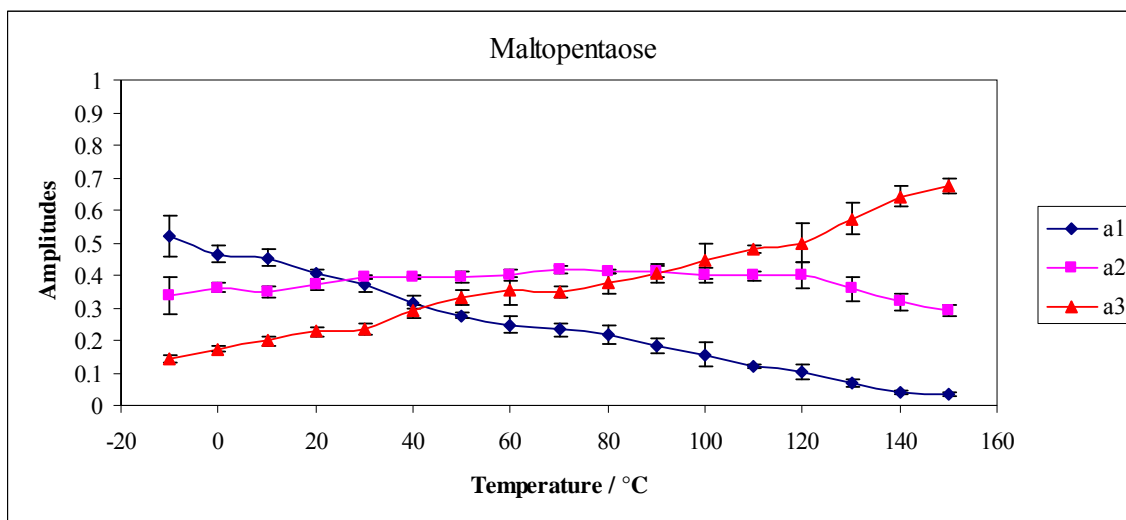
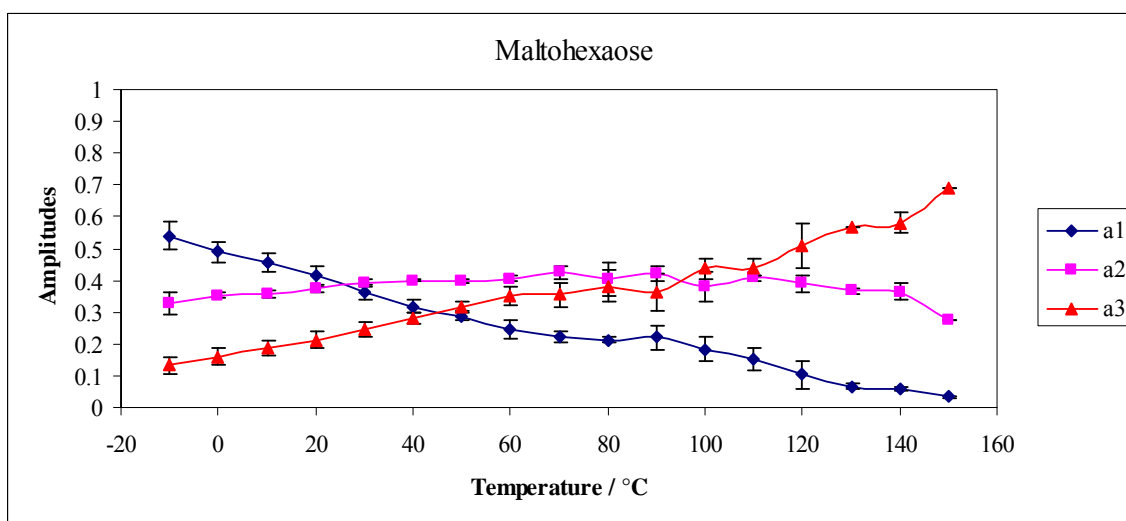
Figure IV-8e*Figure IV-8f*

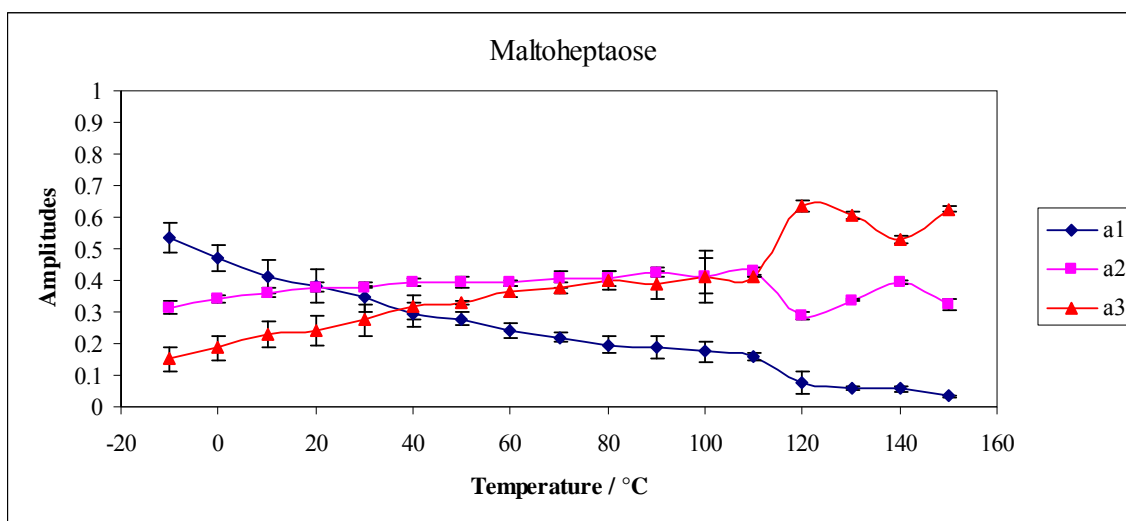
Figure IV-8g

Figure IV-8a-8g: Intensity decay fit amplitudes for vanillin in amorphous films of glucose (8a), maltose (8b), maltotriose (8c), maltotetraose (8d), maltopentaose (8e), maltohexaose (8f) and maltoheptaose (8g) in nitrogen as a function of temperature. The data were calculated every 10 °C from -10 °C to 150 °C. The amplitudes a_1 (♦) and a_2 (■) correspond to the longer life time components (τ_1 , τ_2) and a_3 (▲) and a_4 (●) correspond to the shorter lifetime components (τ_3 , τ_4). The amplitudes were obtained from a multi exponential model fit (Eq. (3), Materials and Methods) to phosphorescence intensity decay data from vanillin dispersed in amorphous films equilibrated against nitrogen as a function of temperature

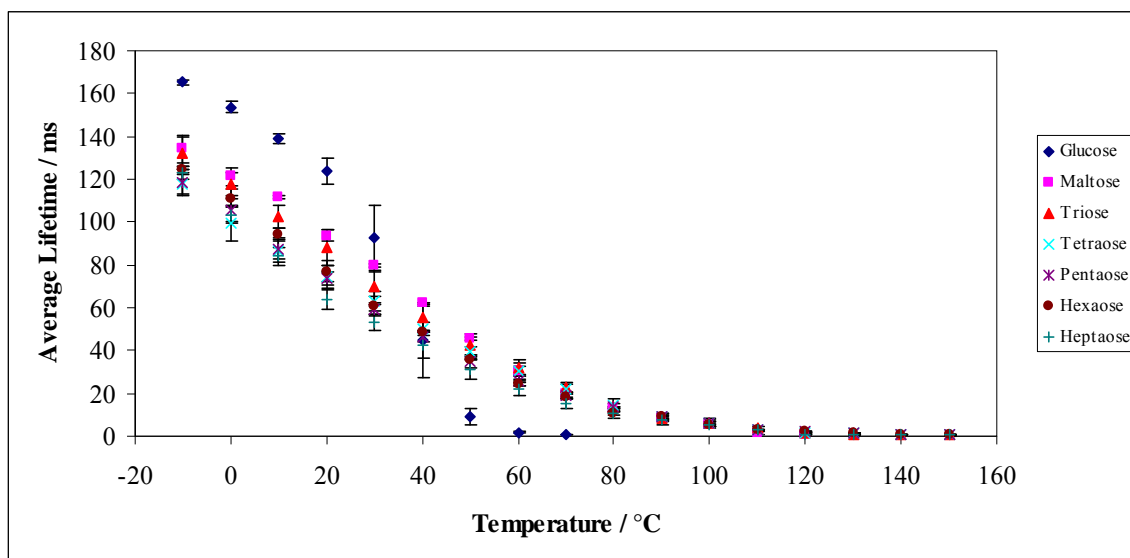
Figure IV-9a

Figure IV-9a: Average lifetime from a multi-exponential model fit (Eq. (4), Materials and Methods) to phosphorescence intensity decay data from vanillin dispersed in amorphous films of glucose (♦), maltose (■), maltotriose (▲), maltotetraose (×), maltopentaoase (*), maltohexaoase (●) and maltoheptaose (+) equilibrated against nitrogen as a function of temperature. The data were calculated every 10°C from -10°C to 150°C.

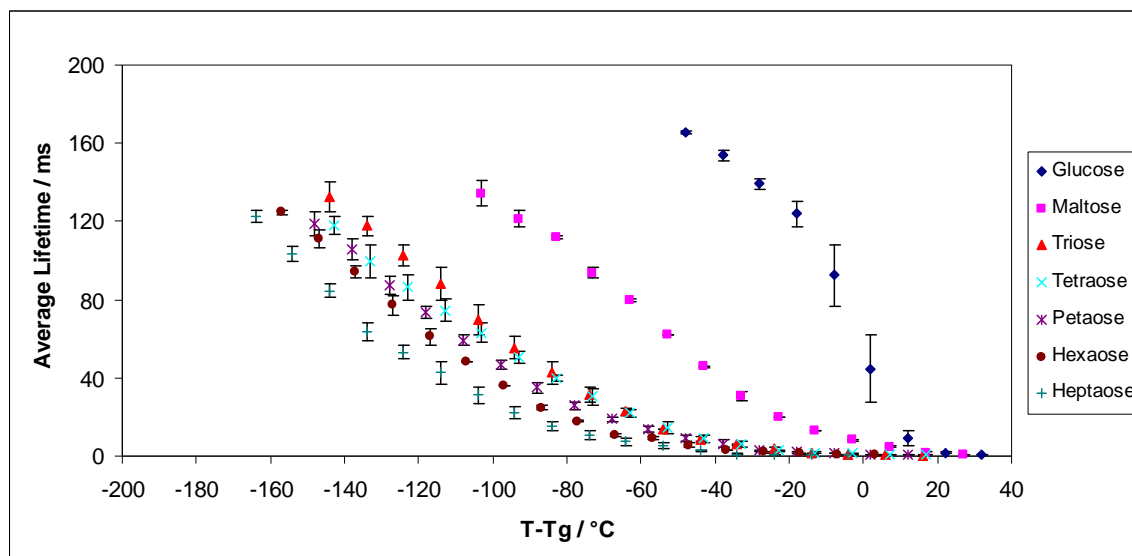
Figure IV-9b

Figure IV-9b: Average lifetime from a multi-exponential model fit (Eq. (4), Materials and Methods) to phosphorescence intensity decay data from vanillin dispersed in amorphous films of glucose (♦), maltose (■), maltotriose (▲), maltotetraose (×), maltopentaose (*), maltohexaose (●) and maltoheptaose (+) equilibrated against nitrogen as a function of T-Tg. The data were calculated every 10°C from -10°C to 150°C.

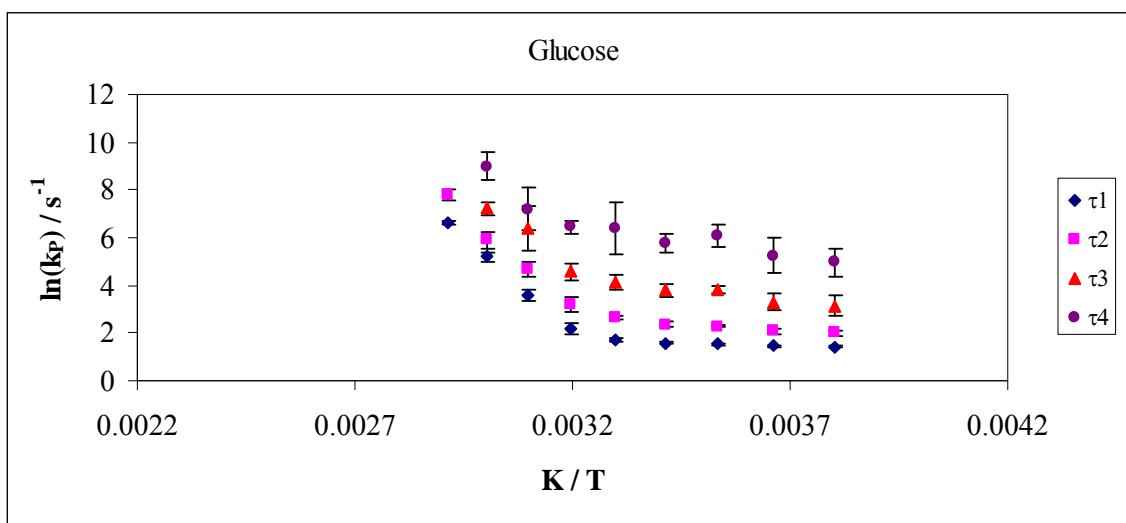
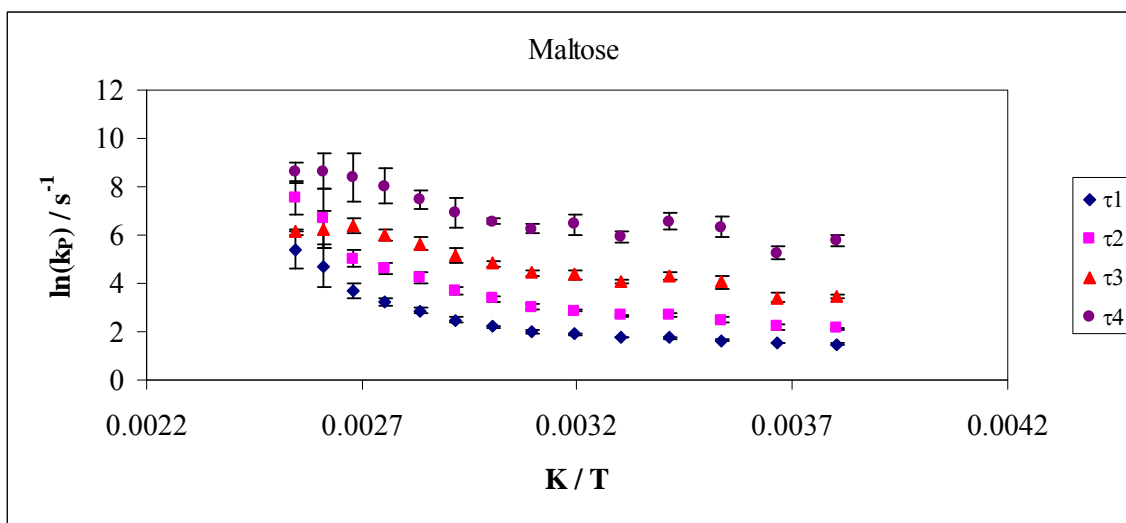
Figure IV-10a*Figure IV-10b*

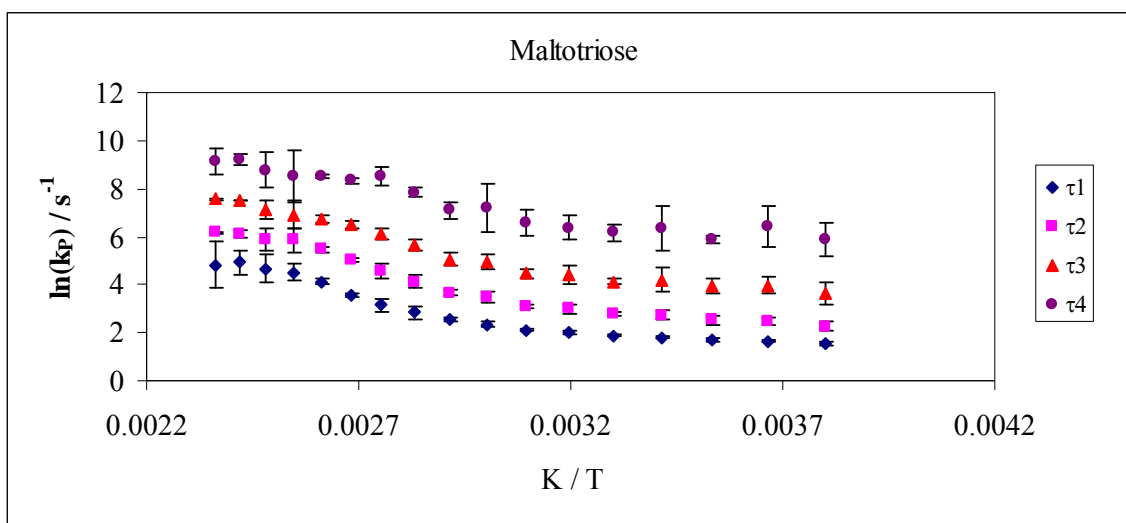
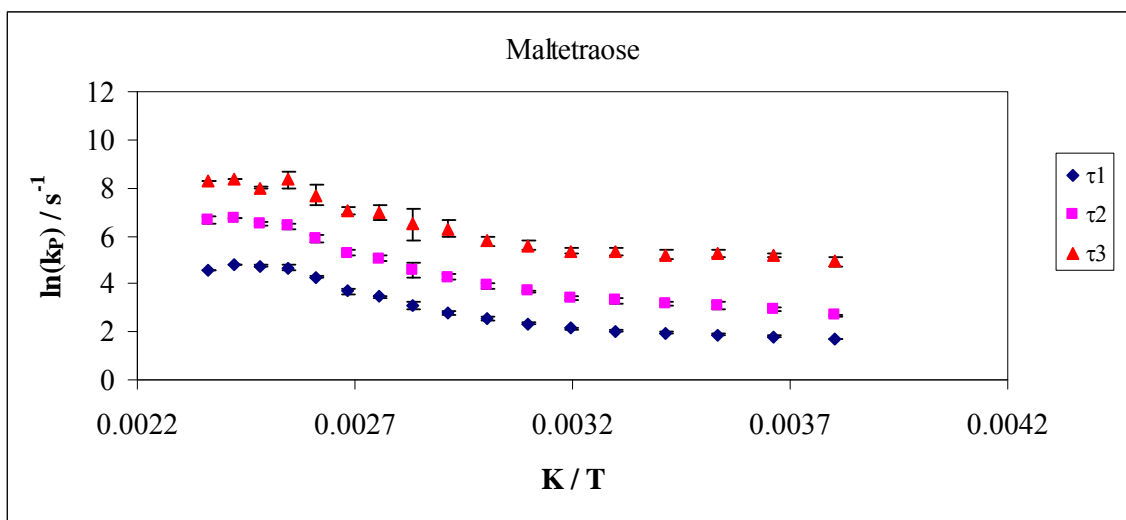
Figure IV-10c*Figure IV-10d*

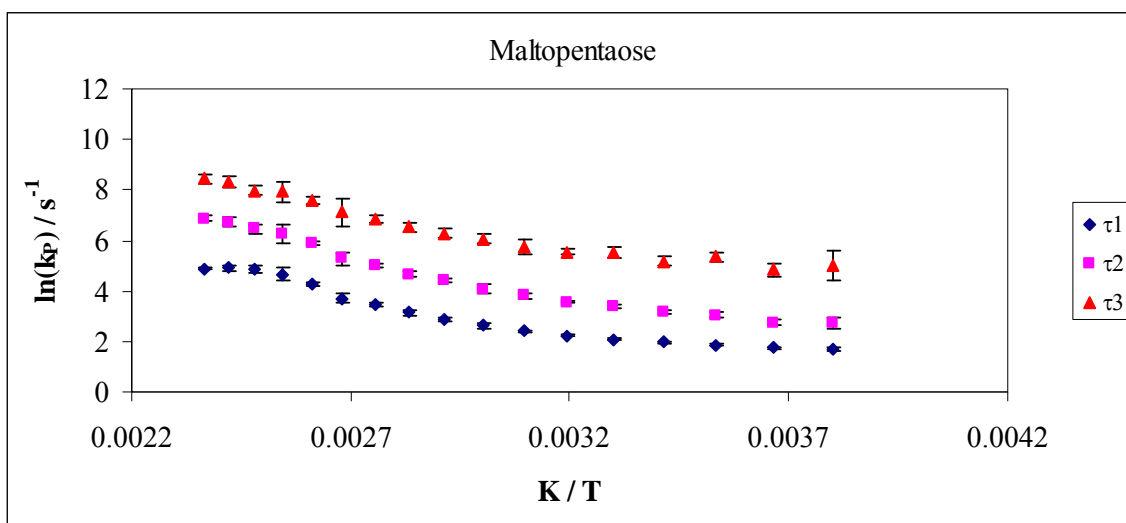
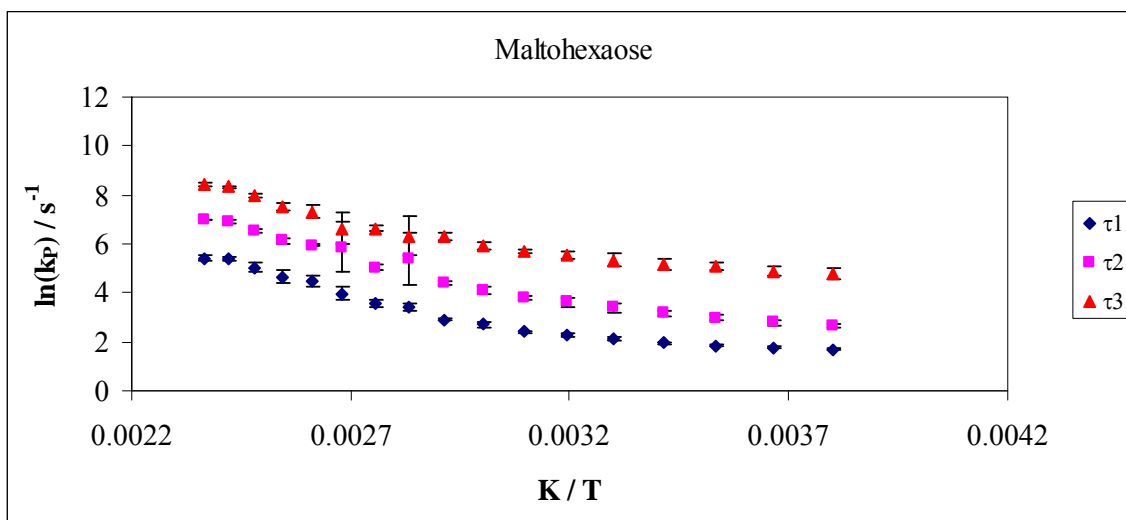
Figure IV-10e*Figure IV-10f*

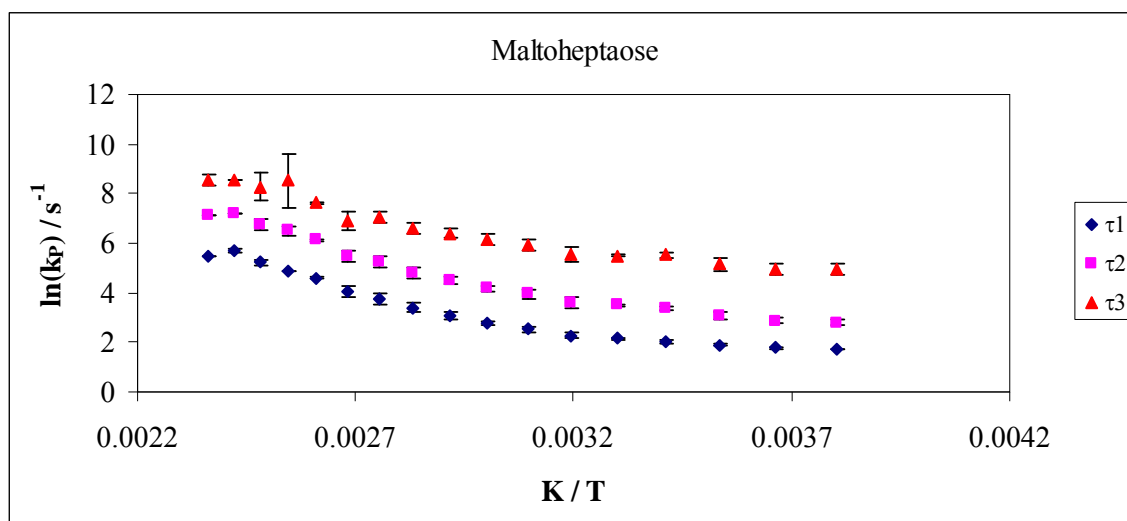
Figure IV-10g

Figure IV-10a to 10g: Arrhenius plots of the inverse of individual lifetime component τ_1 , τ_2 , τ_3 and τ_4 of vanillin in amorphous films of glucose (10a), maltose (10b), maltotriose (10c), maltotetraose (10d), maltopentaose (10e), maltohexaose (10f) and maltoheptaose (10g) as a function of inverse of temperature.

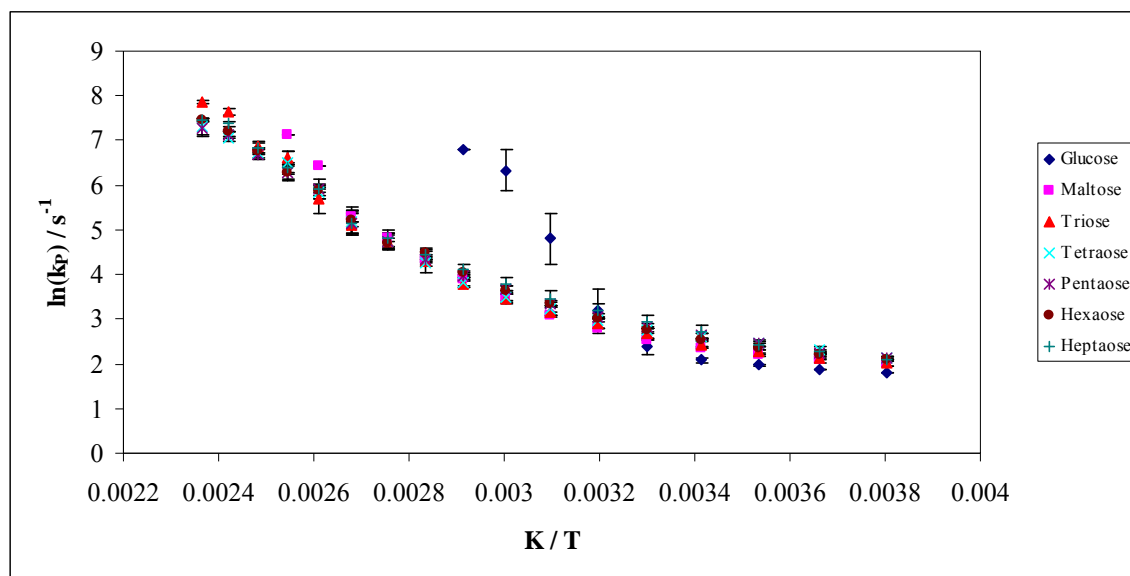
Figure IV-11a

Figure IV-11a: Arrhenius plot of the average lifetime of vanillin in amorphous films of glucose (\blacklozenge), maltose (\blacksquare), maltotriose (\blacktriangle), maltotetraose (\times), maltopentaose ($*$), maltohexaose (\bullet) and maltoheptaose ($+$) as a function of inverse of temperature.

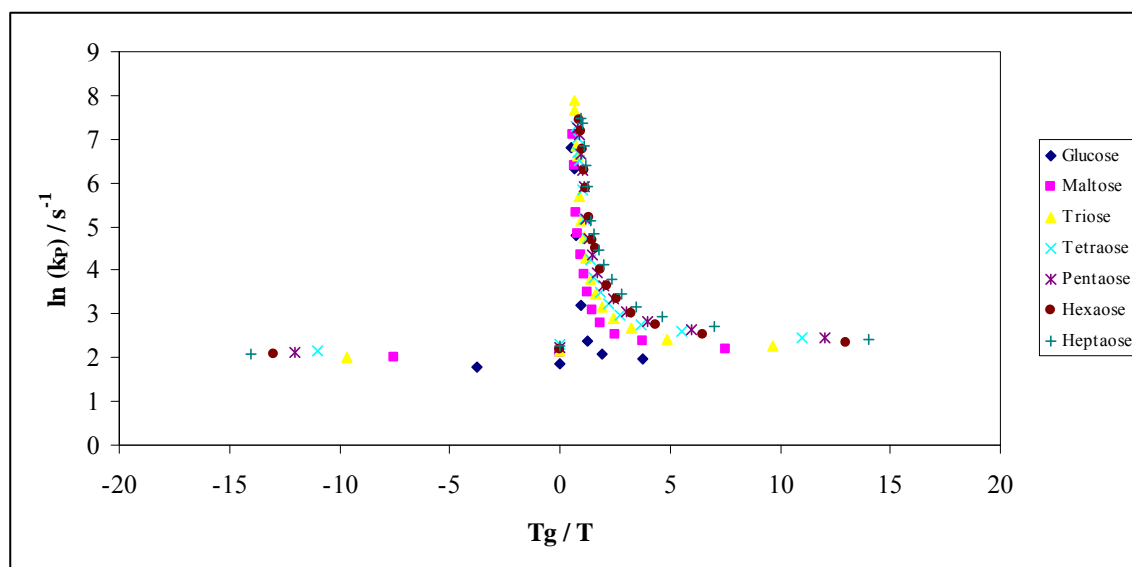
Figure IV-11b

Figure IV-11b: Arrhenius plot of the average lifetime of vanillin in amorphous films of glucose (◆), maltose (■), maltotriose (▲), maltotetraose (×), maltopentose (*), maltohexaose (●) and maltoheptaose (+) as a function of T_g/T .

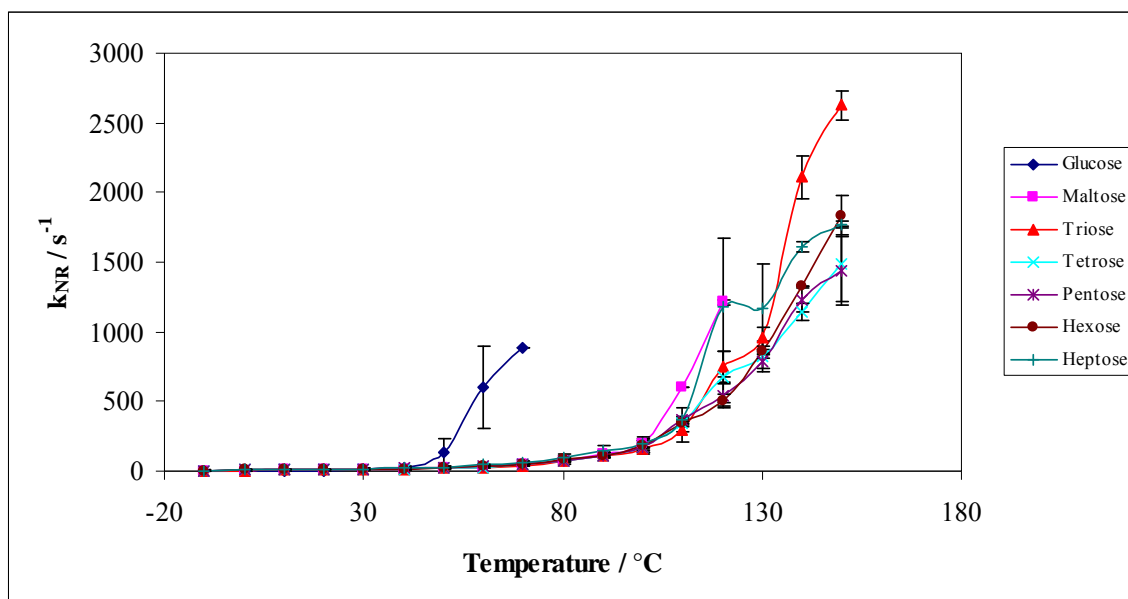
Figure IV-12

Figure IV-12: Temperature dependence of the total non-radiative decay rate of the triplet state k_{NR} ($k_p = k_{RP} + k_{NR}$) to S_0 of vanillin in amorphous glucose, maltose, maltotriose, maltotetraose, maltopentaose, maltohexaose and maltoheptaose film over the temperature range from -10°C to 150°C , values were calculated from the lifetime data in Figures IV-7a to 7g and amplitude data in Figures IV-8a to 8g.

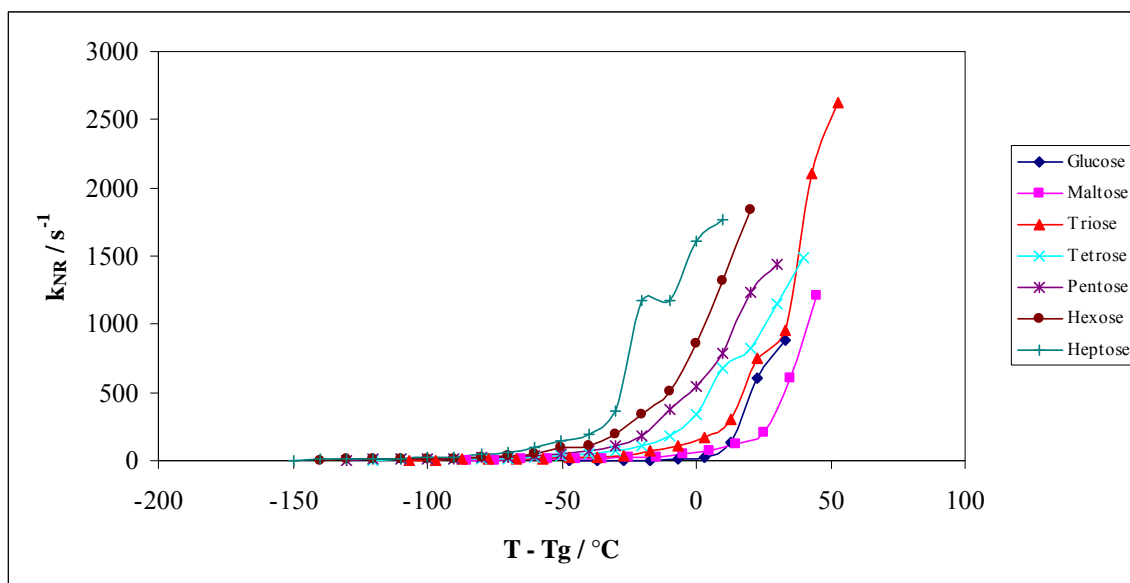
Figure IV-13a

Figure IV-13a: Temperature dependence of the total non-radiative decay rate of the triplet state k_{NR} ($k_p = k_{RP} + k_{NR}$) to S_0 of vanillin in amorphous glucose, maltose, maltotriose, maltotetraose, maltopentaose, maltohexaose and maltoheptaose film plotted as a function of $T - T_g$; values were calculated from the lifetime data in Figure IV-7a to 7g.

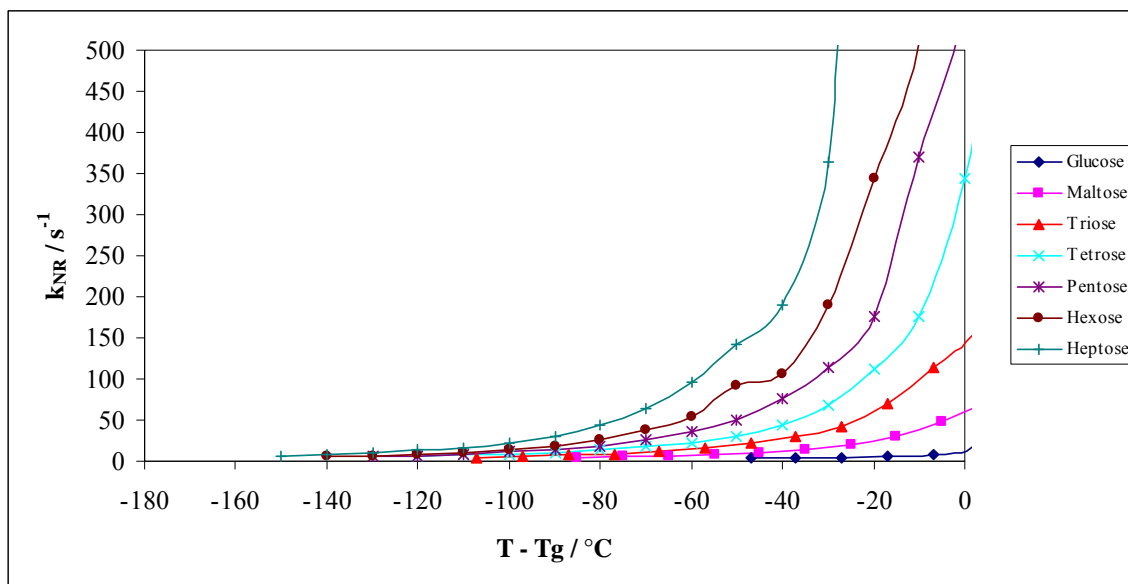
Figure IV-13b

Figure IV-13b: Temperature dependence of the total non-radiative decay rate of the triplet state k_{NR} ($k_p = k_{RP} + k_{NR}$) to S_0 of vanillin in amorphous glucose, maltose, maltotriose, maltotetraose, maltopentaose, maltohexaose and maltoheptaose film plotted as a function of $T - T_g$ (expanded for below T_g).

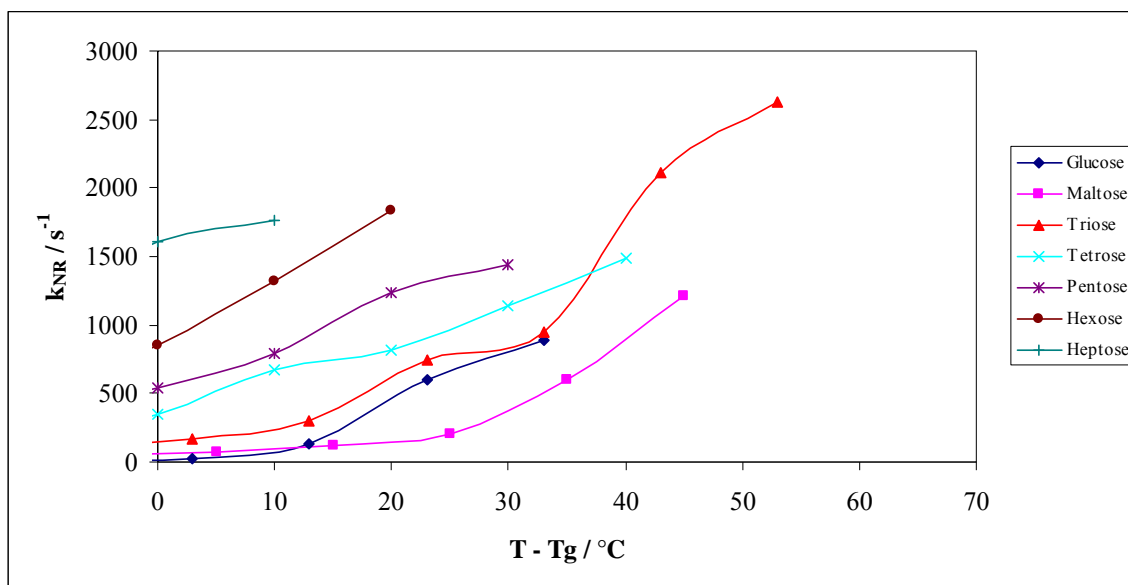
Figure IV-13c

Figure IV-13c: Temperature dependence of the total non-radiative decay rate of the triplet state k_{NR} ($k_p = k_{RP} + k_{NR}$) to S_0 of vanillin in amorphous glucose, maltose, maltotriose, maltotetraose, maltopentaose, maltohexaose and maltoheptaose film plotted as a function of $T - T_g$ (expanded for above T_g).

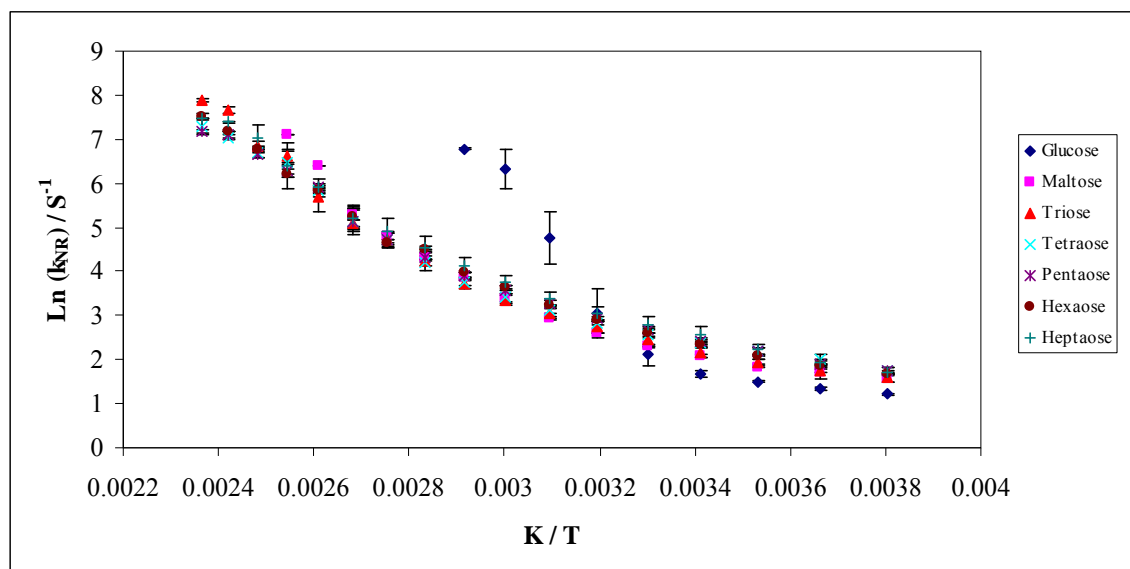
Figure IV-14a

Figure IV-14a: The Arrhenius plot of the total non-radiative decay rate of the triplet state k_{NR} ($k_p = k_{RP} + k_{NR}$) to S_0 of vanillin in amorphous glucose, maltose, maltotriose, maltotetraose, maltopentaose, maltohexaose and maltoheptaose film as function of inverse of temperature.

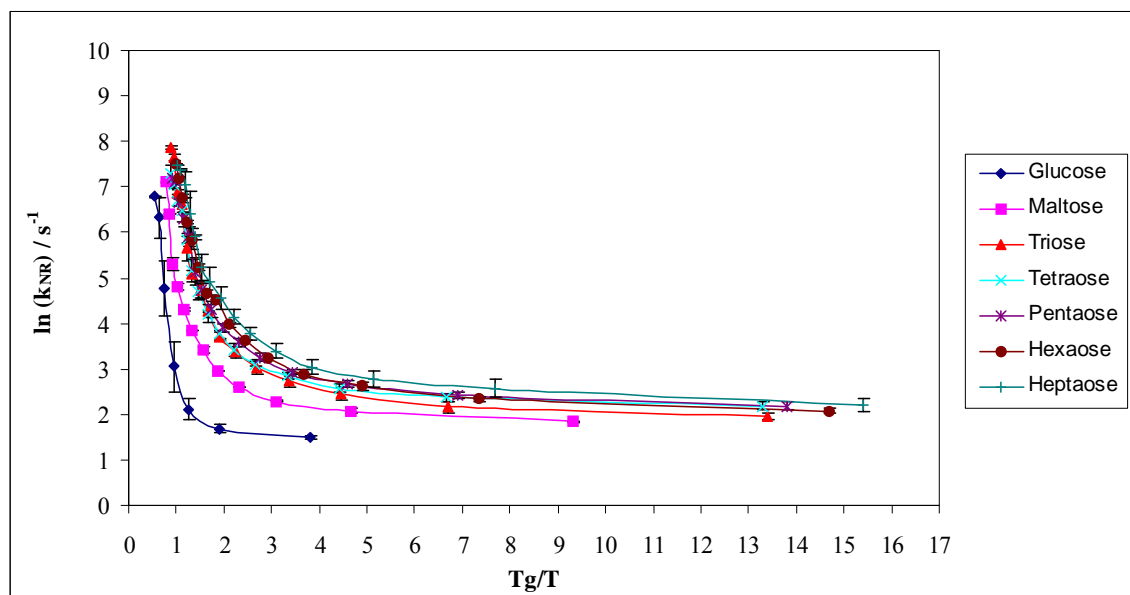
Figure IV-14b

Figure IV-14b: The Arrhenius plot of the total non-radiative decay rate of the triplet state k_{NR} ($k_p = k_{RP} + k_{NR}$) to S_0 of vanillin in amorphous glucose, maltose, maltotriose, maltotetraose, maltopentaose, maltohexaose and maltoheptaose film as function of T_g/T .

Table IV-1

Table IV-1: Calculated activation energy E_a for individual k_p at low and high temperature for vanillin in amorphous films of glucose.

Glucose			
Lifetime component		E_a KJ/ mol	Transition temperature / °C
τ_1	LT	3.70	35
	HT	134.32	
τ_2	LT	7.94	35
	HT	133.60	
τ_3	LT	16.44	35
	HT	115.27	
τ_4	LT	16.92	35
	HT	159.21	

Table IV-2

Table IV-2: Calculated activation energy E_a for individual k_p at low, intermediate and high temperature for vanillin in amorphous films of maltose.

Maltose			
Lifetime component		E_a KJ/ mol	Transition temperature / °C
τ_1	LT	5.44	52
	IT	34.69	98
	HT	101.83	
τ_2	LT	10.67	52
	IT	39.05	100
	HT	152.82	
τ_3	LT	12.56	50
	HT	41.48	
τ_4	LT	9.21	55
	HT	46.50	

Table IV-3

Table IV-3: Calculated activation energy E_a for individual k_p at low and high temperature for vanillin in amorphous films of maltotriose.

Maltotriose			
Lifetime component		E_a KJ/ mol	Transition temperature / °C
τ_1	LT	5.90	70
	HT	50.35	
τ_2	LT	9.79	62
	HT	49.90	
τ_3	LT	9.10	60
	IT	55.42	
	HT	29.57	
τ_4	LT	7.35	60
	HT	25.29	

Table IV-4

Table IV-4: Calculated activation energy E_a for individual k_p at low and high temperature for vanillin in amorphous films of maltotetraose.

Maltotetraose			
Lifetime component		E_a KJ/ mol	Transition temperature / °C
τ_1	LT	5.90	75
	HT	59.84	
τ_2	LT	9.33	72
	HT	67.62	
τ_3	LT	5.22	60
	HT	36.52	

Table IV-5

Table IV-5: Calculated activation energy E_a for individual k_p at low and high temperature for vanillin in amorphous films of maltopentaose.

Maltopentaose			
Lifetime component		E_a KJ/ mol	Transition temperature / °C
τ_1	LT	9.41	78
	HT	59.36	
τ_2	LT	14.18	80
	HT	52.73	
τ_3	LT	7.96	60
	HT	32.20	

Table IV-6

Table IV-6: Calculated activation energy E_a for individual k_p at low and high temperature for vanillin in amorphous films of maltohexaose.

Maltohexaose			
Lifetime component		E_a KJ/ mol	Transition temperature / °C
τ_1	LT	8.50	75
	HT	44.75	
τ_2	LT	13.61	70
	HT	38.18	
τ_3	LT	8.29	80
	HT	45.07	

Table IV-7

Table IV-7: Calculated activation energy E_a for individual k_p at low and high temperature for vanillin in amorphous films of and maltoheptaose.

Maltoheptaose			
Lifetime component		E_a KJ/ mol	Transition temperature / °C
τ_1	LT	7.70	60
	HT	44.28	
τ_2	LT	11.83	68
	HT	27.13	
τ_3	LT	14.23	60
	HT	45.78	

Table IV-8

Table IV-8: Calculated activation energy E_a for average k_p at low, intermediate and high temperature for methyl vanillin in amorphous films of glucose, maltose, maltotriose, maltotetraose, maltopentaose, maltohexaose and maltoheptaose.

Lifetime	Temperature	R^2	E_a KJ / mol	Transition Temperatures °C
Glucose	LT	0.98	6.21	32
	HT	0.97	103.26	
Maltose	LT	0.93	12.21	70
	HT	0.96	81.86	
Maltotriose	LT	0.95	16.30	72
	HT	0.98	67.56	
Maltotetraose	LT	0.96	13.64	65
	HT	0.99	55.65	
Maltopentaose	LT	0.97	15.70	70
	HT	0.99	53.49	
Maltohexaose	LT	0.95	16.19	70
	HT	0.99	56.60	
Maltoheptaose	LT	0.97	18.88	75
	HT	0.99	58.37	

Table IV-9

Table IV-9: Calculated activation energy E_a for k_{NR} at low and high temperature for methyl vanillin in amorphous films of glucose, maltose, maltotriose, maltotetraose, maltopentaose, maltohexaose and maltoheptaose.

Sugar	Temperature	E_a KJ / mol	Transition Temperatures°C	Tg°C
Glucose	LT	10.15	32	38
	HT	120.21		
Maltose	LT	15.96	60	93
	HT	66.27		
Maltotriose	LT	19.95	70	134
	HT	68.18		
Maltotetraose	LT	16.66	65	133
	HT	60.66		
Maltopentaose	LT	19.03	70	138
	HT	54.88		
Maltohexaose	LT	21.57	70	147
	HT	56.92		
Maltoheptaose	LT	22.42	72	154
	HT	57.44		

References

- Baek, M. H., Yoos, B. and Lim, S.T. Effects of sugar alcohols on thermal transitions and cold stability of corn starch gel. *Food Hydrocolloids*. 18 (2003). 133-142.
- Bell, L. N. and Hageman, M. J. Differentiating between the effect of water activity and glass transition dependent mobility on solid state chemical reaction: aspartame degradation. *Journal of Agricultural and Food Chemistry*. 42 (1994). 2398-2401.
- Bell, L. N. and Hageman, M. J. Glass transition explanation for effect of polyhydroxy compounds on protein denaturation in dehydrated solids. *Journal of Food Science*. 61 (1996). 372-375.
- Buera, M. P. and Karel, M. Effect of physical changes on the rates of non enzymatic browning and related reactions. *Food Chemistry*. 52 (1995). 167-173.
- Buera, M. P., Chirife, J. and Karel, M. A study of acid catalyzed sucrose hydrolysis in an amorphous polymer matrix at reduced moisture content. *Food Research International*. 28 (1995). 359-365.
- Buitink, L. and Leprince, O. Glass formation in plant anhydrobiotes: survival in the dry state. *Cryobiology*. 48 (2004). 215-228.
- Champion, D., Maglione, M., Niquet, G., Simatos, D. and Le Meste, M. Study of α - and β - relaxation processes in supercooled sucrose liquids. *Journal of Thermal Analysis and Calorimetry*. 71 (2003). 249-261.
- Chan, R. K., Pathmanathan, K. and Johari, G. P. Dielectric relaxations in the liquid and glassy states of glucose and its water mixtures. *Journal of Physical Chemistry*. 90 (1986). 6358-6362.
- Contreras-Lopez, E., Champion, D., Herves, H., Blond, G. and Le Meste, M. Rotational and translational mobility of small molecules in sucrose plus polysaccharide solutions. *Journal of Agricultural Food Chemistry*. 48 (2000). 1009-1015
- Correia, N. T., Alvarez, C. and Ramos, J. J. M. The β - α branching in D-sorbitol as studied by thermally stimulated depolarization currents. *Journal of Physical Chemistry*. 105 (2001). 5663-5669.
- Crowe, J. H., Carpenter, J. F. and Crowe, L. M. The role of vitrification in anhydrobiosis. *Annual Review Physiology*. 60 (1998). 73-103.
- Dzuba, S. A., Golovina, Y. A. and Tsevetkov, Y. D. Echo-Induced EPR Spectra of Spin Probes as a Method for Identification of Glassy States in Biological Objects. *Journal of Magnetic Resonance*. 101 (1993). 134-138.

- Fennema O. Water and Ice. New York: Marcel Dekker Inc. (1996).
- Fischer, C. J., Gafni, A., Steel, D. G. and Schauerte, J. A. The triplet-state lifetime of indole in aqueous and viscous environments: significance to the interpretation of room temperature phosphorescence in proteins. *Journal of the American Chemical Society*. 124 (2002). 10359-10266.
- Hill, B. P., and Pardoe, K. Proton and deuterium NMR studies of the glass transition in a 10% water-maltose solution. *Journal of Molecular Liquids*. 63 (1995). 229-237.
- Jeffrey, G. A. An introduction to hydrogen bonding; Oxford University Press: NY and Oxford. (1997).
- Le Meste, M., Champion, D., Roudaut G., Blond G. and Simatos, D. Glass transition and food technology: A critical appraisal. *Journal of Food Science*. 67 (2002). 2444-2458.
- Ludescher, R. D., Shah, N. K., McCaul, C. P. and Simon, K. V. Beyond Tg: optical luminescence measurements of molecular mobility in amorphous solid foods. *Food Hydrocolloids*. 15 (2001). 331-339.
- Margulies, M. M., Sixou, B., David, L., Vigier, G., Dolmazon, R., and Albrand, M. Molecular mobility of sorbitol and maltitol: A ¹³C NMR and molecular dynamic approach. *European Physical Journal E*. 3 (2000). 55-62.
- Noel, T.R., Parker, R. and Ring, S. G. Effect of molecular structure and water content on the dielectric relaxation behavior of amorphous low molecular weight carbohydrates above and below their glass transition. *Carbohydrate Research*. 329 (2000). 839-845.
- Noel, T. R., Ring, S. G. and Whittam, M. A. Dielectric relaxations of small carbohydrate molecules in the liquid and glassy states. *Journal of Physical Chemistry*. 96 (1992). 5662-5667.
- Orford, P.D., Parker, R. and Ring, S. G. Aspects of the glass transition behavior of mixtures of carbohydrates of low molecular weight. *Carbohydrate Research*. 196 (1990). 11-18.
- Ottenof, M., MacNaughtan, W. and Farhat, I. A. FTIR study of state and phase transitions of low moisture sucrose and lactose. *Carbohydrate Research*. 338 (2003). 2195-2202.
- Papp, S. and Vanderkooi, J. M. Tryptophan phosphorescence at room temperature as a tool to study protein structure and dynamics. *Photochemistry and Photobiology*. 49 (1989). 775-784.

- Pravinata, L.V., You, Y. and Ludescher, R. D. Erythrosin B phosphorescence monitors molecular mobility and dynamic heterogeneity in amorphous sucrose. *Biophysical Journal*. 88 (2005). 3551-3561.
- Richert, R. Spectral selectivity in the slow beta relaxation of a molecular glass. *Europhysics Letters*. 54 (2001). 767-73.
- Roos, Y. H. *Phase Transitions in Foods*. San Diego, California: Academic Press, (1995).
- Roos, Y. H. Thermal analysis, state transition and food quality. *Journal of Thermal Analysis and Calorimetry*. 71 (2003). 197-203.
- Shamblin, S., Hancock, B. C., Dupuis, Y. and Pikal, M. J. Interpretation of relaxation time constants for amorphous pharmaceutical systems. *Journal of Pharmaceutical Sciences*. 89 (2000). 417-427.
- Shamblin, S. L., Tang, X. L., Chang, L. Q., Hancock, B. C. and Pikal M. J. Characterization of the time scales of molecular motion in pharmaceutically important glasses. *Journal of Physical Chemistry*. 103 (1999). 4113-4121.
- Shirke, S. and Ludescher, R. D. Dynamic site heterogeneity in amorphous maltose and maltitol from spectral heterogeneity in erythrosin B phosphorescence. *Carbohydrate Research*. 340 (2005). 2661-2669.
- Shirke, S. and Ludescher, R. D. Molecular mobility and glass transition in amorphous glucose, maltose and maltotriose. *Carbohydrate Research*. 340 (2006). 2654-260.
- Slade, L. and Levine, H. Beyond water activity: recent advances based on an alternative approach to the assessment of food quality and safety. *Critical Review in Food Science and Nutrition*. 30 (1991). 115-360.
- Strambini, G. B. and Gonnelli, M. The indole nucleus triplet-state lifetime and its dependence on solvent microviscosity. *Chemical Physics Letters*. 115 (1985). 196-200.
- Suihko, E. J., Forbes, R. T., and Apperley, D. C. A solid state NMR study of molecular mobility and phase separation in co-spray-dried-protein-sugar particles. *European Journal of Pharmaceutical Sciences*. 25 (2005). 1005-112.
- van den Dries I. J., van Dusschoten, D. and Hemminga, M. A. Mobility in maltose-water glasses studied with ^1H NMR. *Journal of Physical Chemistry*. 102 (1998). 10483-89.

- van den Dries, I. J., Besseling, N. A. M., van Dusschoten, D., Hemminga, M. A., and van der Linden, E. Relation between a transition in molecular mobility and collapse phenomena in glucose-water system. *Journal of Physical Chemistry*. 1004 (2000). 9260-9266.
- Vanderkooi, J. M and Berger, J. W. Excited triplet state used to study biological macromolecules at room temperature. *Biochimica et Biophysica Acta: Bioenergetics*. 976 (1989). 1-27.
- Wagner, H. and Richert, R. Equilibrium and non-equilibrium type beta relaxations: D-Sorbitol versus o-Terphenyl. *Journal of Physical Chemistry*. 103 (1999). 4071-4077.
- Wagner, H. and Richert, R. Spatial uniformity of the beta relaxation in D-sorbitol. *Journal of Non-crystalline Solids*. 242 (1998). 19-24.
- Wolkers, W.F., and Oliver, A. E., Tablin, F., Crowe, J. H. A Fourier-transform infrared spectroscopy study of sugar glasses. *Carbohydrate Research*. 339 (2004). 1077-1085.
- Wolkers, W.F., Oldenhof, H., Alberda, M., Hoekstra, F. A. A Fourier transform infrared micro spectroscopy study of sugar glasses: application to anhydrobiotic higher plant cells. *Biochimica Biophysica Acta*. 1379 (1998). 83-96.
- Zunic, A. Molecular mobility of amorphous disaccharide studied by tryptophan luminescence. Master Thesis. Rutgers University. New Brunswick, NJ. (2004).

Chapter V: Characterizing molecular mobility of different amorphous excipients used for various controlled release applications.

Introduction

Pharmaceutical formulations are generally produced by lyophilization or spray-drying (Zallen, 1998; Hancock and Zografi, 1997). In pharmaceutical formulations an active pharmaceutical ingredient is combined with varying number of excipients (Taylor and Zografi 1998, Constantino et al., 1998, Khiugaz and Clas, 2000; Gupta et al., 2004). Pharmaceutical excipients are substances other than the pharmacologically active component (e.g., protein or peptides) which are included in the manufacturing process or are contained in a finished pharmaceutical product dosage form. Some of the commonly used excipients are amorphous sugars (sucrose, trehalose, etc.), maltodextrins, and polymers e.g. poly vinyl pyrrolidone (PVP). The function of the excipient is to define a formulation that is physically and chemically stable, manufacturable and bioavailable (Joshi, 2004). An excipient provides protection to drug candidates that exhibit poor solubility and stability (Crowley, 1999). Incorporating sugars or polymers into the formulation provided physical and/or chemical stabilization both during and after the drying process. Most of these excipients are used because of their ability to maintain the amorphous state. For example, maltodextrins are used as potential protectants during lyophilization for labile protein components due to their higher T_g and their ability to maintain the amorphous state (Lim and Reid, 1991; Corveleyn and Remon, 1996). Excipients are considered to be inert in therapeutic or biological actions; and they should hinder unwanted phase transitions (due to their amorphous nature) and ensure the

required stability of the drug in the formulation during the manufacturing process and storage.

Stabilizing excipients such as amorphous sugars can prevent physical and chemical degradation of protein formulations by the establishment of hydrogen bonds between protein and excipients and by forming an amorphous glassy matrix around the protein (Carpenter and Crowe, 1989; Arakawa et al., 1993; Angel, 1995; Allison et al., 1999). The addition of amorphous sugars to protein has being shown to be very beneficial as they can serve as plasticizers, stabilizers and/or protectants (Kaushik and Bhat, 2003). Proteins embedded in amorphous sugars are protected (Imamamura et al., 2003; Eriksson et al., 2002; Hinrichs et al., 2001; Suzuki et al., 1998). Sucrose ($T_g = 65^\circ\text{C}$) is known to protect protein against the deleterious effects of harsh environmental conditions (Yancey et al., 1982; Borowitzka, 1985) and is commonly used in protein formulations to protect labile proteins (Chang et al., 2005), and hence was selected in this study. Similarly, trehalose, due to its high T_g , is thought to have superior stabilizing ability compared to other carbohydrates (Green and Angel, 1989; Kaushik and Bhat, 2003). Trehalose ($T_g = 110^\circ\text{C}$) glasses have shown greater ability to resist phase separation and crystallization due to restricted molecular motions (Sun and Davidson, 1998) and hence was selected. Poly vinyl pyrrolidone (PVP) is another commonly used as excipient (Fisher et al., 1992). PVP has being shown to inhibit crystallization in amorphous solid dispersions (Frank, 1987; Sochava et al., 1985). PVP, which has a high T_g ($T_g = 177^\circ\text{C}$), will raise the T_g of the mixture and decrease the mobility of the phase reducing its tendency to crystallize (Green and Angell, 1989; Slade et al., 1989).

The stability of the active components in an amorphous solid matrix is strongly influenced by many factors such as residual water content, temperature, viscoelastic state of the amorphous solid, the excipients present, pH, etc. But the major factor contributing to stability of protein/carbohydrate glasses is molecular mobility (Yoshioka et al., 1997), as it influences conformational flexibility of proteins even well below T_g (Hancock et al., 1995; Oksanen and Zografi, 1993; Lai et al., 1999). Crystallization from the amorphous state is related to molecular mobility (Hancock et al., 1995; Oksanen and Zografi, 1993). Both the water substitution theory and the glassy state theory consider the glass transition phenomena and the T_g of excipients as essentials in determining the effectiveness of those excipients in protein stabilization (Green and Angell, 1989; Mazzobre et al., 1997; Crystall et al., 1997; Carpenter and Crowe, 1989). Physical changes in the formulation can lead to altered dissolution or other delivery properties of the final dosage form.

The glass transition and molecular mobility are thus two phenomena very important to excipients functionality. For example, collapse phenomena are important for protection (Johnson et al., 2002) and have been directly related to the molecular mobility of amorphous sugars (van den Dries et al., 2000). Thus it is very important to characterize molecular mobility of these excipients in the glassy state. The objective of this research is to study molecular mobility of the excipients sucrose, trehalose and PVP using a novel sensitive technique of luminescence spectroscopy as a function of temperature. The mobility data is compared among the three excipients and correlated to their stability data available in the literature. We have recently shown vanillin phosphorescence to be sensitive to molecular mobility in amorphous solids (Chapter II). In this research the

molecular mobility of amorphous films of sucrose, trehalose and PVP is studied using vanillin as a triplet state probe. Understanding the molecular mobility of these amorphous excipients will provide knowledge toward developing matrices, for example, for controlled release applications. They will provide an in depth understanding about molecular mobility below and above T_g of the selected excipients.

Materials and Methods

Sample Preparation: Sucrose, trehalose and PVP (K-30) were purchased from Sigma-Aldrich (St. Louis, MO) with minimum purity of 98%. The trehalose and PVP were used without further purification, whereas sucrose was purified as described in Pravinata et al 2005. These components were dissolved to near saturation in deionized water at room temperature. The vanillin was dissolved in distilled deionized water to make a 66mM solution, an aliquot from this solution was added to each of the sugars solutions to obtain a solution with dye: sugar molar ratio of $1:10^3$ in case of sucrose and trehalose, whereas in case of PVP dye:PVP molar ratio was 1:4. An aliquot (20 μ l) of the dye- containing solution was spread on a quartz slide 3 cm x 1.35 cm (NSG Precision Cells, Hicksville, NY). After spreading (\sim 0.05 mm) the solutions on the slides were then dried under a heat gun (Vidal Sassoon) for 5 min to a maximum temperature of 88°C (measured using a thermocouple probe). The slides were stored at room temperature against P_2O_5 and Drierite protecting from the light to prevent any photo bleaching for at least 7 days before any phosphorescence measurements were made. The desiccant was refreshed as needed to maintain a relative humidity close to 0%. The glass transition temperatures were determined from the literature and were sucrose ($T_g = 65^\circ\text{C}$), trehalose ($T_g = 110^\circ\text{C}$) and PVP ($T_g = 177^\circ\text{C}$) (Roos, 1993; Green and Angel, 1989; Roe and Labuza, 2005; Slade et al., 1989).

Instrumentation: All phosphorescence measurements were made on a Cary Eclipse fluorescence spectrophotometer (Varian Instruments, Walnut Creek, CA). The quartz slides were placed in a standard 1cm x 1cm x 1cm quartz fluorescence cuvette, which

was capped with a lid having inlet and outlet ports for gas lines. The cuvette was flushed with a gentle stream of nitrogen for 15 minutes to eliminate oxygen. An oxygen free nitrogen stream was generated by passage of high purity nitrogen through a Supelco (Bellefonte, PA) gas purifier. The temperature was controlled by using a TLC 50 thermoelectric heating/cooling system (Quantum Northwest, Spokane, WA). The TLC-50 sample compartment was fitted with a jacketed cover and the temperature of the cuvette was monitored directly using a thermocouple in the cuvette. The film was equilibrated for 15 minutes at each temperature before collecting the data. The Cary Eclipse uses a pulsed lamp and collects emission intensity in analog mode; data were not collected within the first 0.1-0.2 ms to suppress fluorescence coincident with the lamp pulse.

Luminescence measurement: Delayed luminescence emission (10 nm bandwidth) spectra of vanillin in amorphous sugars were collected from 400 nm to 800 nm using excitation at 320 nm (20 nm bandwidth) over the temperature range from -10°C to 120°C . Each data point was collected from a single flash with 0.2ms delay, 100ms gate time, and 0.12s total decay time. Lifetime measurements were made in presence of nitrogen as a function of temperature. The samples were excited at 320 nm (20 nm bandwidth) and emission transients collected at 490nm (20 nm bandwidth) at temperature ranging from -10°C to 120°C . Each decay was average of 50 cycles, and for each cycle data was collected from a single flash with a delay of 0.2 ms, windows for gate time and total decay time was varied at each temperature. All measurements were made in quadruplicate.

Data Analysis

Emission Energy as a function of temperature: Emission spectra's were fitted using the program Igor (Wavemetrics, Inc., Lake Oswego, OR). The emission spectra were analyzed by fitting phosphorescence of vanillin to a log-normal function Equation 1 over the temperature range.

$$I(\nu) = I_0 \exp \left\{ - \ln(2) \left(\frac{\ln[1 + 2b(\nu - \nu_p) / \Delta]}{b} \right)^2 \right\} \quad (1)$$

In this equation I_0 , is the maximum intensity value of the emission spectra, ν_p is the frequency in cm^{-1} of the emission maximum, Δ is the line width parameter, and b is the asymmetry parameter. The bandwidth of the emission, the full width at half maximum (Γ), is related to b and Δ Equation 2.

$$\Gamma = \Delta \left(\frac{\sinh(b)}{b} \right) \quad (2)$$

Photophysical Scheme: The phosphorescence intensity decay were collected as described above and were fitted using a multi-exponential functions (Shamblin et al., 2000). The multi-exponential model is as show in Equation 3. τ_i are decay times, α_i represent the amplitudes of the components at $t = 0$ and n is the number of decay times. Phosphorescence lifetimes were determined with the statistical program Igor (Wavemetrics, Inc., Lake Oswego, OR). Fits were judged satisfactory if the R^2 values were in the range of 0.995-1.0 and the modified residuals $((\text{data} - \text{fit})/\text{data}^{1/2})$ varied randomly about zero. The average lifetime was calculated using Equation 4.

$$I(t) = \sum_{i=1}^n \alpha_i \exp(-t/\tau_i) \quad (3)$$

$$\tau_{\text{Avg}} = \sum_{i=1}^n \alpha_i \tau_i / \sum_{i=1}^n \alpha_i \quad (4)$$

The phosphorescence lifetimes were used to calculate the rate constants associated with the various processes that depopulate the excited triplet state. The lifetime τ is related to the rate constants for de-excitation of the triplet excited state of the probe according to the following Equation 5 (Papp and Vanderkooi, 1989).

$$1/\tau = k_{\text{RP}} + k_{\text{NR}}(T) + k_{\text{Q}}[\text{O}_2] = k_{\text{P}} \quad (5)$$

Here $k_{\text{P}} (=1/\tau)$ is the total decay rate, k_{RP} is the rate of radiative decay of the ground state (2.69 s^{-1} , measured in this study), k_{NR} is the rate of non-radiative decay to the singlet state followed by vibrational relaxation to S_0 due to collisional quenching. The magnitude of k_{NR} reflects factors associated with the mechanism by which the excited T_1 state of vanillin is coupled to highly excited vibrations of the S_0 ground state as well as external factors associated with the mechanism by which the ground state vibrational energy can dissipate from the excited state into the surrounding matrix (Fischer et al., 1992; Vanderkooi and Berger, 1989). As the efficiency of external vibrational dissipation is related to overall mobility of the matrix, the magnitude of k_{NR} provides a measure of matrix mobility. One common method for restricting the collisional deactivation is to

super cool analyte solutions with liquid nitrogen to a rigid glass. The term $k_Q [O_2]$ refers to the collisional quenching due to interaction between the excited chromophore and triplet state oxygen.

Results

Delayed emission spectra: Delayed phosphorescence emission of vanillin dispersed in sucrose (Figure 1a), trehalose (Figure 1b) and PVP (Figure 1c) was measured as a function of temperature. The emission was collected between -10°C to 100°C in case of sucrose and PVP and from -10°C to 120°C in case of trehalose, until the emission lasted. The emission peak in sucrose and trehalose was at ~ 490 nm. The emission peak in PVP was shifted by ~10nm and appeared at ~480 nm. Phosphorescence intensity of vanillin was obtained from the delayed phosphorescence spectra fitted to the log-normal function (Eq. 1 of Materials and Methods). The emission intensity decreased with increase in temperature. A comparison plot of normalized phosphorescence intensity for sucrose, trehalose and PVP is shown in Figure 2. An Arrhenius plot of the effect of temperature on the phosphorescence emission intensity of vanillin in amorphous films of sucrose, trehalose and PVP is shown in Figure 3. Break point temperatures determined from intersection of trendline to points at low, intermediate and high temperature for sucrose, trehalose and PVP are shown in Figures 4a, 4b and 4c, respectively.

The emission energy (ν_p) and bandwidth (Γ), determined by fitting the phosphorescence emission spectra to a log-normal function (equation 1, Materials and Methods), are shown in Figure 5a, 5b and 5c for sucrose, trehalose and PVP, respectively. The peak frequency decreased with increase in temperature in sucrose, trehalose and PVP corresponding to a change in molecular environment due to matrix relaxation. Trehalose showed approximately linear decrease with temperature in emission energy both in the glass and melt. However, sucrose and PVP showed a gradual decrease in emission energy

in glass but much dramatic decrease at high temperature. The decrease in emission energy indicates an increase in the average extent of matrix dipolar relaxation around the excited triplet state. A comparison plot for peak frequency as a function of temperature is shown in Figure 6a. A comparison of peak frequency among the three excipients showed that values were highest in PVP followed by sucrose and trehalose (at least at low temperature).

The phosphorescence bandwidth increased gradually at low temperature in the glass and then increased sharply at higher temperature in the melt, reflecting a large increase in the range of energetically distinct matrix environments in amorphous sucrose, trehalose and PVP. A comparison plot for bandwidth as a function of temperature is shown in Figure 6b. At low temperature in the glass trehalose had the highest values for FWHM followed by sucrose and PVP; however at high temperature PVP showed higher values followed by sucrose and trehalose.

Phosphorescence Lifetime: Lifetimes were measured by exciting vanillin at 320 nm and collecting the emission at 490 nm in case of sucrose and trehalose and 480 nm for PVP as a function of temperature from -10°C to 120°C. The decays were fitted using a four-exponential function (Eq. 3, Materials and Methods). Fits were judged satisfactory if the modified residual $((\text{data-fit})/\text{data}^{1/2})$ varied randomly about zero. The phosphorescence intensity decay of vanillin in amorphous films of sucrose, trehalose and PVP at 20°C in the presence of nitrogen are plotted in Figure 7a, 7b and 7c, respectively, along with the modified residuals for a fit using a multi-exponential function.

The phosphorescence lifetime decreased with increasing temperature indicating an increase in the triplet state quenching rate with temperature; the results of these analyses are plotted in Figure 8a, 8b and 8c for sucrose, trehalose and PVP, respectively. The four lifetimes in sucrose were $\tau_1 = 184.4$ ms, $\tau_2 = 76.7$ ms, $\tau_3 = 18.2$ ms and $\tau_4 = 2.6$ ms at 20°C, thus demonstrating the presence of local environments with ~70 fold differences in trehalose mobility. The four lifetimes in trehalose were $\tau_1 = 183.0$ ms, $\tau_2 = 80.6$ ms, $\tau_3 = 19.3$ ms and $\tau_4 = 2.3$ ms at 20°C, thus demonstrating the presence of local environments with ~81 fold differences in mobility. The four lifetimes in PVP were $\tau_1 = 81.1$ ms, $\tau_2 = 24.3$ ms, $\tau_3 = 5.5$ ms and $\tau_4 = 0.92$ ms at 20°C, thus demonstrating the presence of local environments with ~88 fold differences in mobility. The lifetime is the average time a molecule spends in the excited state and is an indicator of the rigidity of the matrix.

A plot of the amplitudes of each lifetime component as a function of temperature is shown in Figure 9a, 9b and 9c for sucrose, trehalose and PVP, respectively. In general the amplitudes of the longer lifetime (τ_1, τ_2) components a_1 and a_2 decreased and that of the shorter lifetime (τ_3, τ_4) components a_3 and a_4 increased as a function of temperature. At 20°C In sucrose and trehalose almost ~65 % of the probes were in immobile environments (with longer lifetime) and the remaining ~35% were in mobile environment (shorter lifetimes). But in the case of PVP ~45% of probes were in immobile environments and the remaining ~55% were in mobile environments. A comparison of the amplitude for sum of longer and shorter lifetimes is shown in Figure 10a and 10b. Throughout the temperature range from -10°C to 120°C, trehalose showed higher

percentage of probes to be present in rigid environments as compared to PVP and also lower number of probes to be present in mobile environments as compared to PVP. Below T_g sucrose also showed higher percentage of probes to be present in rigid environments as compared to PVP and also lower percentage of probes to be present in mobile environments as compared to PVP. But above T_g sucrose showed more number of probes to be present in the mobile environment as compared to PVP. A comparison between sucrose and trehalose below T_g of sucrose revealed no difference in percentage of probes present in rigid and mobile environments as shown in Figure 10a and 10b. But above T_g of sucrose, trehalose showed much higher number of probes in rigid environments and much lower percentage in the mobile environments as compared to sucrose.

An Arrhenius plots of $\ln k_p$ for individual lifetime components are shown in Figure 11a, 11b and 11c for sucrose, trehalose and PVP, respectively. The break point temperatures determined from intersection of trendline to points at low and high temperature and the activation energies for individual lifetime component for each amorphous matrix are as compiled in Table 1a, 1b and 1c.

The average lifetime was calculated using Eq. 4. A comparison plot of average lifetime as a function of temperature is shown in Figure 12a. The average lifetime as a function of $T - T_g$ is shown in Figure 12b. The average lifetime in case of sucrose varied from 142.1 ms at -10°C to 0.50 ms at 100°C , indicating ~ 282 -fold difference in mobility. The average lifetime in case of trehalose varied from 134.4 ms at -10°C to 2.46 ms at 120°C ,

indicating ~55-fold difference in mobility. The average lifetime in case of PVP varied from 44.9 ms at -10°C to 0.19 ms at 120°C, indicating ~242-fold difference in mobility. Below T_g of sucrose the average lifetimes were much lower in PVP as compared to sucrose, indicating PVP to be more mobile than sucrose. However, above the T_g of sucrose there was no significant difference in lifetimes of PVP and sucrose. There was no significant difference in lifetimes of sucrose and trehalose below T_g of sucrose. But the lifetime varied significantly above T_g of sucrose, with trehalose showing higher lifetime as compared to sucrose.

An Arrhenius plot of $\ln k_p$ for the average lifetime component is shown in Figure 12c for sucrose, trehalose and PVP. An Arrhenius plot of $\ln k_p$ for the average lifetime component as function of T_g/T is shown in Figure 12d for sucrose, trehalose and PVP. The break point temperature determined from intersection of trendline to points at low and high temperature and the activation energies for average lifetime for each amorphous matrix are as compiled in Table 2. The activation energy for sucrose $E_a = 9.64 \text{ kJ mol}^{-1}$, and $f E_a = 74.1 \text{ kJ mol}^{-1}$. The activation energy for trehalose $E_a = 12.7 \text{ kJ mol}^{-1}$ and $E_a = 47.1 \text{ kJ mol}^{-1}$. The activation energy for PVP $E_a = 21.7 \text{ kJ mol}^{-1}$ and $E_a = 57 \text{ kJ mol}^{-1}$. PVP shows higher activation energy as compared to trehalose in all the temperature zones. Trehalose has higher activation energy as compared to sucrose at low temperature, and lower activation energy at high temperature. Sucrose has lower activation energy than PVP at low temperature, but higher activation energy at high temperature.

The plot of lifetime versus $T-T_g$ (Figure 12b), shows that the lifetimes of vanillin are highest in sucrose > trehalose > PVP over the entire temperature range of ΔT . This indicates that quenching due to molecular collision in sucrose glass is lower than the other two excipients. Thus sucrose glass is less mobile as compared to trehalose and PVP. And PVP is the most mobile matrix in comparison to sucrose and trehalose.

The values of k_{NR} were calculated as shown in equation 5 in Materials and Methods. The values of k_{NR} represent the matrix mobility; the higher the k_{NR} the higher the matrix mobility. Figure 13a is a plot of k_{NR} as function of temperature for sucrose, trehalose and PVP. The values of k_{NR} are significantly higher in PVP as compared to sucrose (Figure 13b), but as the T_g of sucrose approaches the rate constant for non-radiative decay increases significantly in sucrose as compared to PVP (Figure 13c). The values of k_{NR} are not significantly different in trehalose as compared to sucrose (Figure 13b), but as the T_g of sucrose approaches the rate constant for non-radiative decay increases significantly in sucrose as compared to trehalose (Figure 13c). A comparison of k_{NR} between PVP and trehalose indicates that rates were significantly higher in trehalose as compared to PVP throughout the temperature range from -10°C to 120°C (Figure 13a and 13b). Temperature dependence of the total non-radiative decay rate of the triplet state k_{NR} ($k_p = k_{RP} + k_{NR}$) to S_0 of vanillin in amorphous sucrose, trehalose and PVP film are plotted as a function of $T-T_g$ (Figure 13d).

An Arrhenius plot for $\ln k_{NR}$ for each matrix is shown in Figure 14. Break point temperatures and activation energies determined from intersection of trendline to points

at low, intermediate and high temperature for each excipient are compiled in Table 3. The activation energy obtained is the energy for the motion which quenches vanillin's excited triplet state. At low temperature the activation energies followed the order PVP ($E_a = 23 \text{ kJ mol}^{-1}$) > trehalose ($E_a = 16 \text{ kJ mol}^{-1}$) > sucrose ($E_a = 13 \text{ kJ mol}^{-1}$). At high temperature sucrose ($E_a = 72.3 \text{ kJ mol}^{-1}$) > PVP ($E_a = 57.27 \text{ kJ mol}^{-1}$) > trehalose ($E_a = 48.7 \text{ kJ mol}^{-1}$).

The $\ln k_{NR}$ term is lowest for trehalose and highest for PVP with sucrose overlapping with trehalose at low temperature and with PVP at high temperature. Thus the order at low temperature is trehalose = sucrose < PVP and at high temperature trehalose < sucrose = PVP. As the temperature increases the $\ln k_{NR}$ terms increases faster for sucrose compared to trehalose. Throughout the temperature zone $\ln k_{NR}$ term for trehalose < PVP.

Discussion

We have used vanillin phosphorescence to study molecular mobility in three commonly used stabilizing excipients sucrose, trehalose and PVP. These excipients have varied T_g values ranging from sucrose ($T_g = 65^\circ\text{C}$), trehalose ($T_g = 110^\circ\text{C}$) and PVP ($T_g = 177^\circ\text{C}$). The molecular weight of PVP (m.w. = 30 kDa) is much higher than sucrose and trehalose, whereas sucrose (m.w. = 342.2 g) and trehalose (m.w. = 342.2 g) have the same molecular size.

The higher peak frequencies in PVP in the glass region as compared to sucrose and trehalose indicate a larger extent of solvent relaxation in sucrose and trehalose. Trehalose shows larger extent of solvent relaxation as compared to sucrose below 50°C , but above 60°C the emission energy of sucrose is much significantly reduced as compared to trehalose. Trehalose showed broader distribution of energetically distinct environments as compared to sucrose and PVP.

The individual lifetime components in trehalose and sucrose were significantly higher than in PVP indicating that sucrose and trehalose are more rigid matrices as compared to PVP. Below $\sim 50^\circ\text{C}$, the lifetimes of sucrose and trehalose were similar but above $\sim 60^\circ\text{C}$ trehalose showed significantly higher lifetimes values compared to sucrose. Thus below $\sim 50^\circ\text{C}$ both sucrose and trehalose have the same rigidity as measure by vanillin phosphorescence, but above $\sim 50^\circ\text{C}$ trehalose is more rigid than sucrose. A comparison of average lifetimes revealed the same details among the three excipients. Thus, though PVP

has the highest T_g ($\sim 177^\circ\text{C}$), shows more mobility in this data compared to sucrose with $T_g \sim 65^\circ\text{C}$ and trehalose with $T_g \sim 110^\circ\text{C}$. In the temperature range from -10°C to 50°C there is no significant difference in mobility between sucrose and trehalose. But above 60°C trehalose shows lower mobility as compared to sucrose. The data indicate that at temperature from -10°C to 40°C sucrose and trehalose are the least mobile sugars compared to PVP. This means that on an average sucrose and trehalose molecules are more tightly packed around the vanillin and the rate of vibrational relaxation is the least in sucrose and trehalose. As the temperature increases above 50°C (towards the T_g of sucrose) the tightness of packing of sucrose drops more significantly than that of trehalose and PVP, which is accompanied by the greater rate of vibrational relaxation for sucrose than PVP followed by trehalose. On the other hand, the data indicate that at temperature from -10°C to 120°C trehalose is the least mobile sugar compared to PVP. This means that on average trehalose molecules are more tightly packed around the vanillin and the rate of vibrational relaxation is the least in trehalose.

The phosphorescence lifetime at each T- T_g point is higher for sucrose followed by trehalose and then PVP indicating that sucrose has the least mobile matrix among the three excipients with respect to T_g . A study by Zunic (2004) using tryptophan phosphorescence revealed that mobility was higher in trehalose as compared to sucrose with respect to T_g . The protein stability in sucrose and trehalose glasses was compared and found that the mobility in trehalose below T_g is greater than that in sucrose glass although trehalose has higher T_g than sucrose (Duddu and Dal Monte, 1997; Duddu et al., 1997). T_g of trehalose is higher than sucrose and hence has much decreased relaxation

rates (Sun and Davidson, 1998). Sucrose shows mobility in glass at Tg-50K from enthalpy relaxation (Hancock et al., 1995). Its zero mobility temperature (T_0), estimated as 3.5°C from width of glass transition, is much lower than Tg 64°C. Similarly trehalose has T_0 estimated as 44°C a value lower than Tg 101°C (Hatley et al., 1997).

The values of k_{NR} represent the matrix mobility; higher the k_{NR} the higher the matrix mobility. In summary a comparison between sucrose and PVP indicates that amorphous sucrose has lower molecular mobility below ~50°C (close to Tg of sucrose) and could be a better stabilizer than PVP (Figure 13a). But above ~50°C close to the Tg of sucrose, sucrose shows higher rates of collisional quenching compared to PVP, and hence PVP is a better stabilizer above ~50°C. Whereas a comparison between trehalose and PVP indicates that trehalose has lower molecular mobility than PVP and is a better stabilizer in the temperature range between -10°C to 120°C. Comparing sucrose and trehalose shows no significant difference in matrix mobility below ~50°C (close to Tg of sucrose) but once glass transition approaches in sucrose, sucrose shows higher molecular mobility as compared to trehalose. Thus below 50°C the mobility sequence is PVP > sucrose = trehalose above 50°C PVP > sucrose > trehalose.

Thus trehalose is a less mobile matrix than PVP and could be a better protein stabilizer. This is well supported with data available in the literature where trehalose is thought to have superior stabilizing ability compared to other carbohydrates (Green and Angell, 1989; Kaushik and Bhat, 2003; Miller et al., 1999). Trehalose could also be a better stabilizer as it has highest potential for hydrogen bonding to biomaterials (Sun and

Davidson, 1998). It is also thought that trehalose could form hydrated crystal above T_g and hence reducing the initial moisture content of the remaining amorphous phase (Aldous et al., 1995; Crowe et al., 1996). Trehalose has been shown to have a very specific interaction with proteins (Branca et al., 1999; Crowe et al., 1994, 1998; Green and Angell, 1989). Trehalose has high H-bonding affinity, thus may replace the water molecules close to protein surface.

Sucrose does not differ in mobility with respect to trehalose below 50°C and could offer similar stability, but above 50°C it is the most mobile matrix as compared to trehalose and PVP. PVP is the most mobile matrix as compared to sucrose (below 50°C) and trehalose (-10°C to 120°C). Glassy Trehalose is thought to be an effective stabilizer compared to sucrose, maltose and glucose (Kawai et al., 2005). Trehalose with much lower T_g than maltodextrin or PVP is shown to be more effective in preserving proteins due to its glass forming ability, restricted mobility (Sun and Davidson, 1998). Sucrose and Trehalose are found to be more protecting compared to dextrans (Gabellieri and Strambini, 2001). A study on maltodextrin and PVP with much higher T_g have being shown to have less stabilizing effect on membranes and protein (Crowe et al., 1994; Mazzobre et al., 1997). This could be well explained by the observation made in this study where PVP which has the highest T_g showed higher mobility compared to sucrose and trehalose with respect to T_g . Thus indicating PVP to be an unstable excipient (in terms of higher molecular mobility) among the three excipients with respect to T_g .

This study also supports the fact that higher mobility is seen in matrices with higher Tg and molecular weight. A study by Sonali et al showed increase in molecular mobility with increase in molecular weight and Tg (Shirke and Ludescher, 2006). A similar observation was made by us in the glucose homologous series where mobility was found to increase with increase in molecular weight and Tg of the sugar molecule (Chapter IV).

Wolker et al., used FTIR to characterize hydrogen bonding network of amorphous glasses of different chain length and reported increase in molecular mobility with increase in molecular weight, attributed the increase to increase in hydrogen bond length (in the sugar glasses) which decreases the hydrogen bond strength and hence exhibiting higher rates of molecular mobility (Wolker et al., 1998, 2004).

Conclusion

A comparison of molecular mobility as a function of temperature was made between the three commonly used excipients sucrose, trehalose and PVP using vanillin phosphorescence. These excipients are known for their stabilizing effect and show varied glass transition temperatures; sucrose ($T_g = 65^\circ\text{C}$), trehalose ($T_g = 110^\circ\text{C}$) and PVP ($T_g = 177^\circ\text{C}$). The study indicates that below 50°C PVP is the most mobile matrix as compared to trehalose and sucrose (which have similar mobility below 50°C). Above 50°C , once the T_g of sucrose is approached, sucrose is the most mobile matrix followed by PVP and trehalose. Sucrose showed least mobility among the three excipients with respect to T_g , whereas PVP showed the maximum mobility. Overall trehalose showed the least mobility compared to the three excipients.

These excipients also follow the order for molecular mobility which increases with increasing molecular weight and T_g . Thus PVP with highest molecular weight and T_g is seen to be most mobile as compared to sucrose (below 50°C) and trehalose (below and above 50°C). Sucrose ($T_g = 65^\circ\text{C}$) and trehalose ($T_g = 110^\circ\text{C}$) have same molecular weight but different T_g , show no difference in mobility below 50°C but above trehalose shows lower mobility as compared to sucrose. The phosphorescence lifetime at each T_g point is higher for sucrose followed by trehalose and then PVP indicating that sucrose has the least mobile matrix among the three excipients with respect to T_g . These results are well supported by stabilizing effects known for these excipients in the literature.

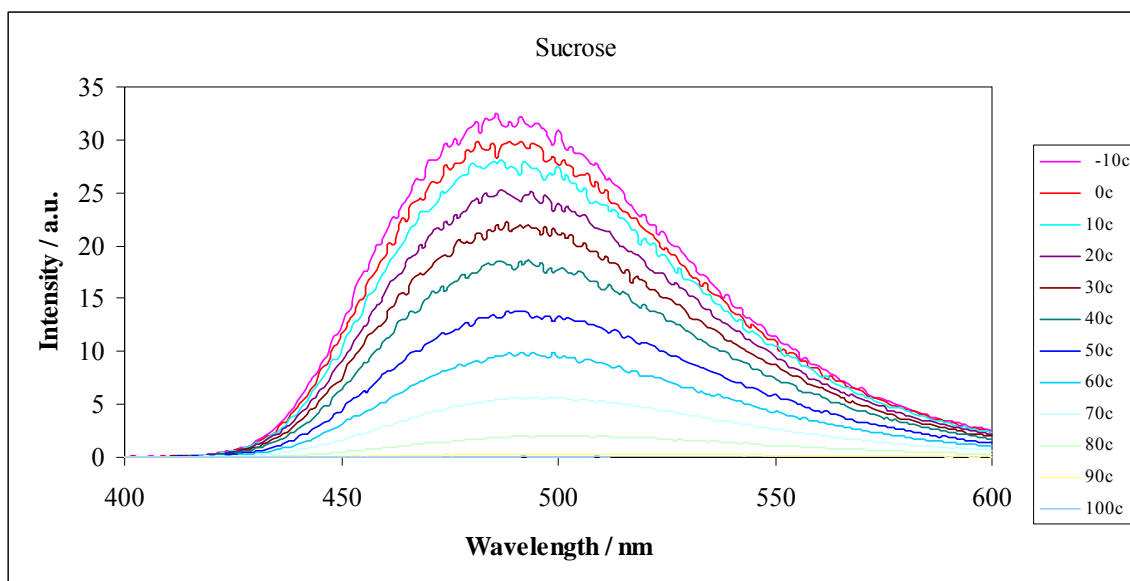
Figure V-1a

Figure V-1a: Delayed emission spectra of vanillin dispersed in amorphous films of sucrose as a function of temperature (excitation at 320 nm). The spectra were collected at 10°C intervals from -10°C to 100°C (the curves follow this order from high to low intensity at ~490 nm).

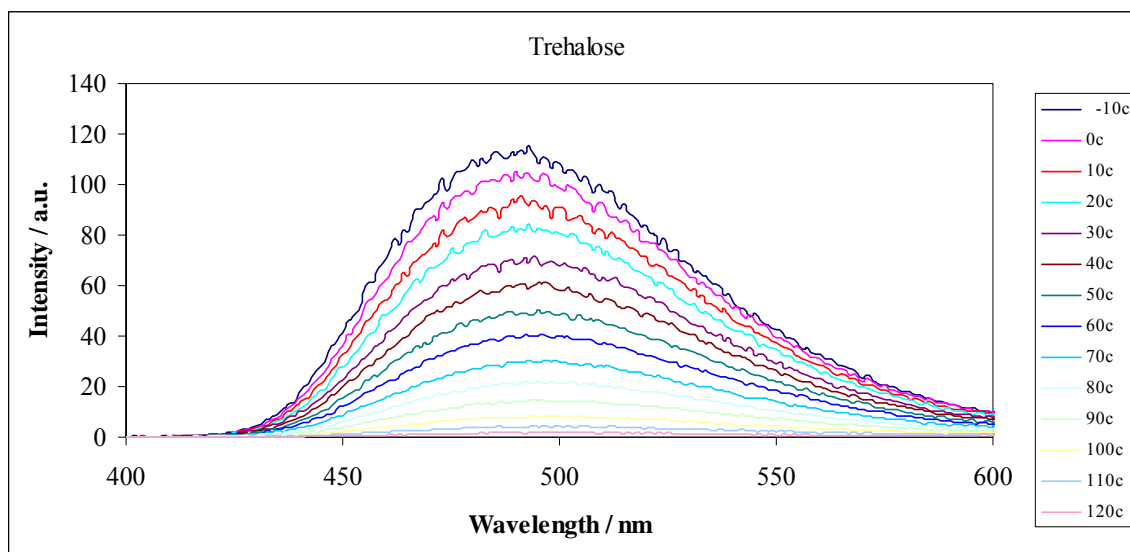
Figure V-1b

Figure V-1b: Delayed emission spectra of vanillin dispersed in amorphous films of trehalose as a function of temperature (excitation at 320 nm). The spectra were collected at 10°C intervals from -10°C to 120°C (the curves follow this order from high to low intensity at ~490 nm).

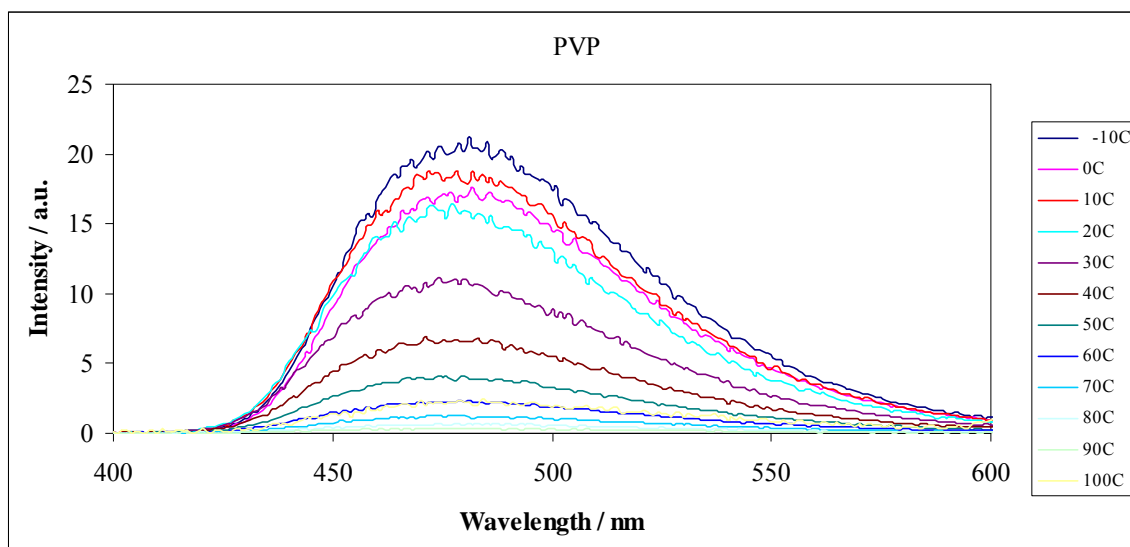
Figure V-1c

Figure V-1c: Delayed emission spectra of vanillin dispersed in amorphous films of PVP as a function of temperature (excitation at 320 nm). The spectra were collected at 10°C intervals from -10°C to 100°C (the curves follow this order from high to low intensity at ~480 nm).

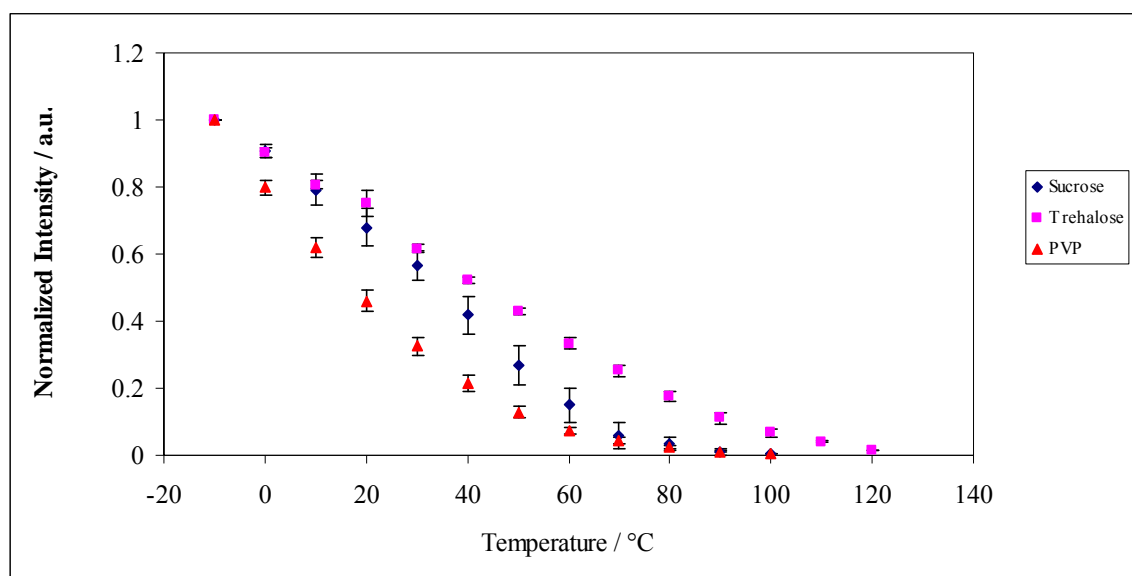
Figure V-2

Figure V-2: Intensity (I_p) was determined from analysis of the phosphorescence emission band (Figure V-1a, 1b, 1c) using a log-normal function (eq. (1), Materials and Methods). The effect of temperature on the phosphorescence emission intensity of vanillin in amorphous films of sucrose, trehalose and PVP as a function of temperature equilibrated against nitrogen.

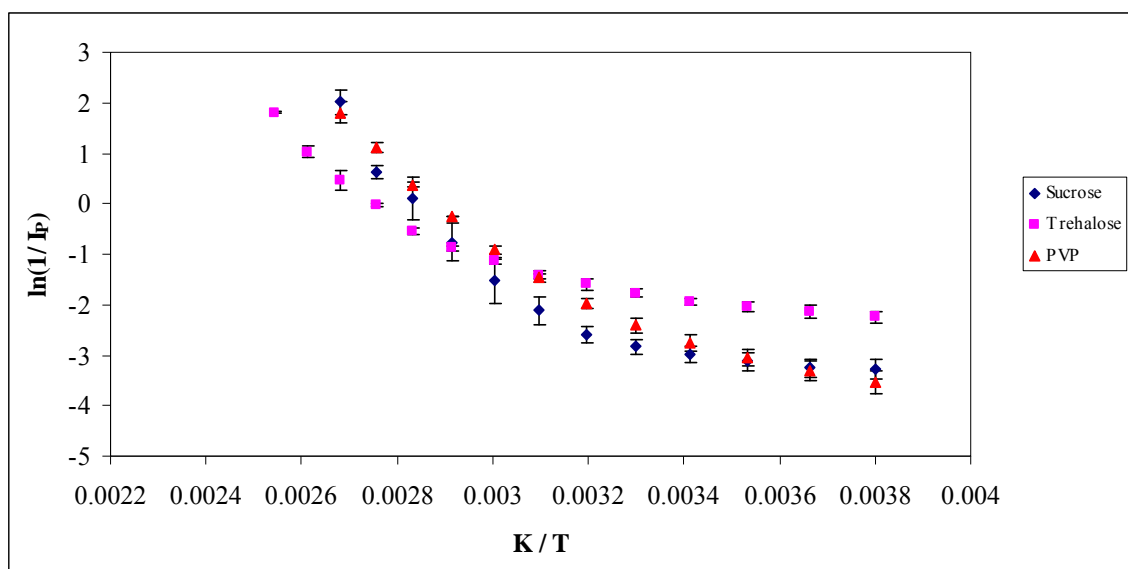
Figure V-3

Figure V-3: Arrhenius plot of the effect of temperature on the phosphorescence emission intensity ($1/I_p$) of vanillin in amorphous films of sucrose, trehalose and PVP.

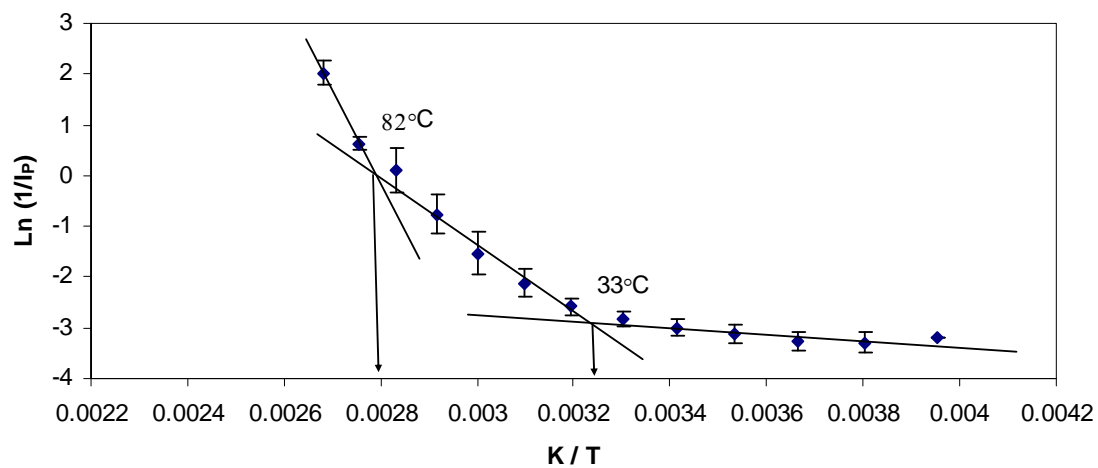
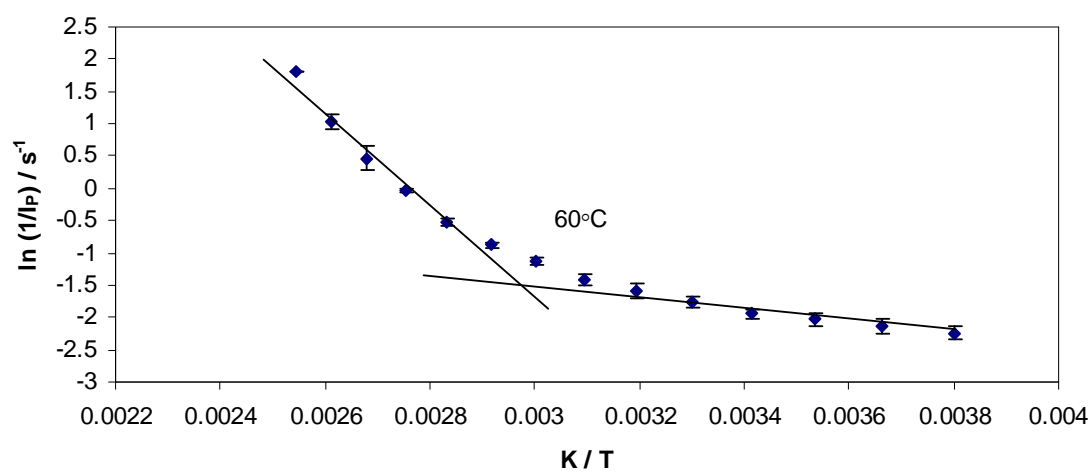
Figure V-4a*Figure V-4b*

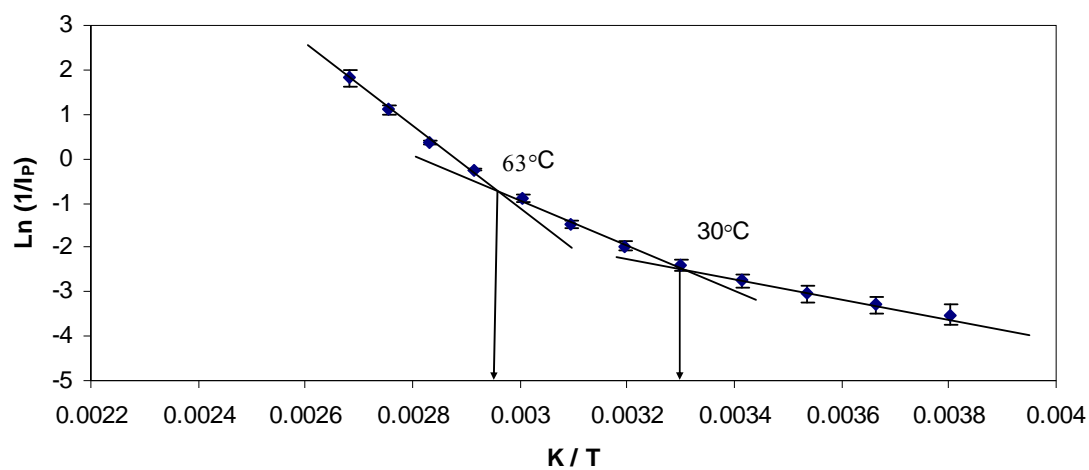
Figure V-4c

Figure V-4a-4c: Arrhenius plot of the effect of temperature on the phosphorescence emission intensity I_p of vanillin in amorphous films of sucrose, trehalose and PVP. Lines drawn over the data points indicate slopes at low and high temperatures sucrose, trehalose and PVP.

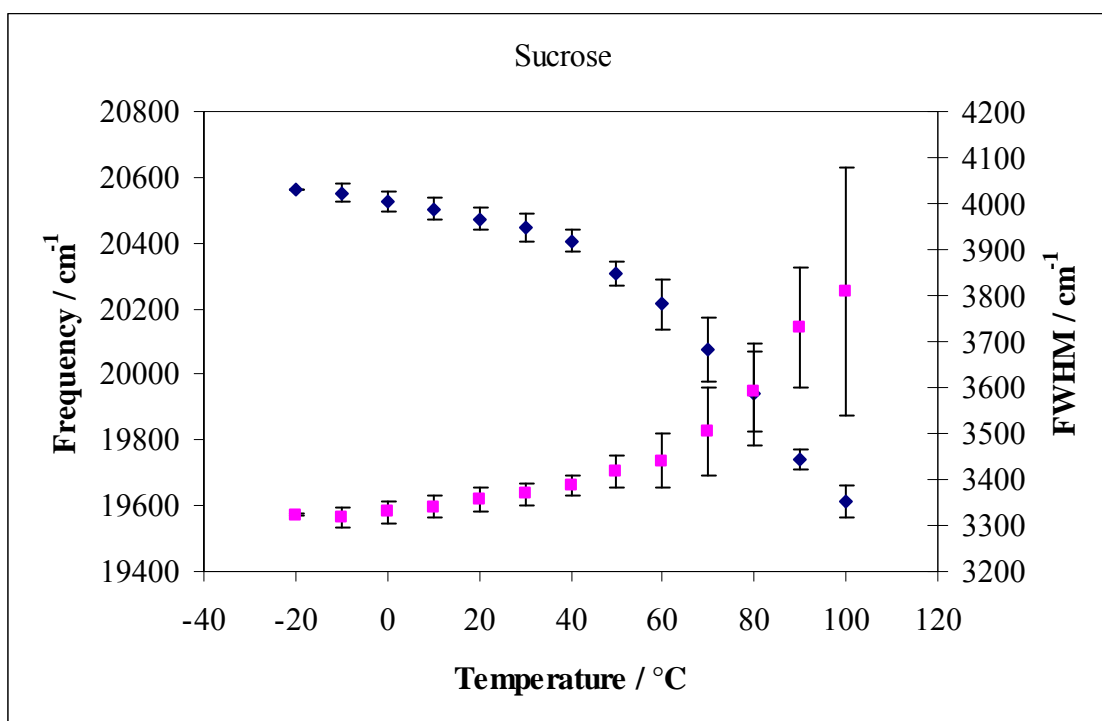
Figure V-5a

Figure V-5a: Peak energy ν_p and bandwidth for phosphorescence emission from vanillin in amorphous films of sucrose as a function of temperature. The delayed emission spectra collected as a function of temperature (Figure V-1a) were analyzed using log-normal function as described in Materials and Methods using eq. (1) and (2).

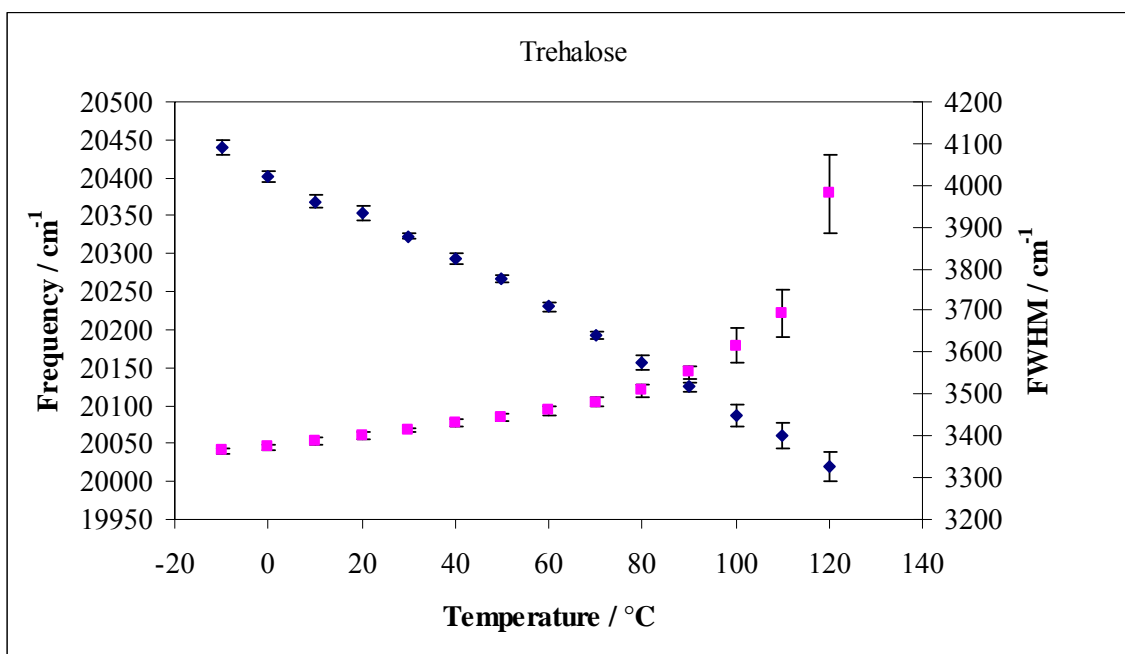
Figure V-5b

Figure V-5b: Peak energy ν_p and bandwidth for phosphorescence emission from vanillin in amorphous films of trehalose as a function of temperature. The delayed emission spectra collected as a function of temperature (Figure V-1b) were analyzed using log-normal function as described in Materials and Methods using eq. (1) and (2).

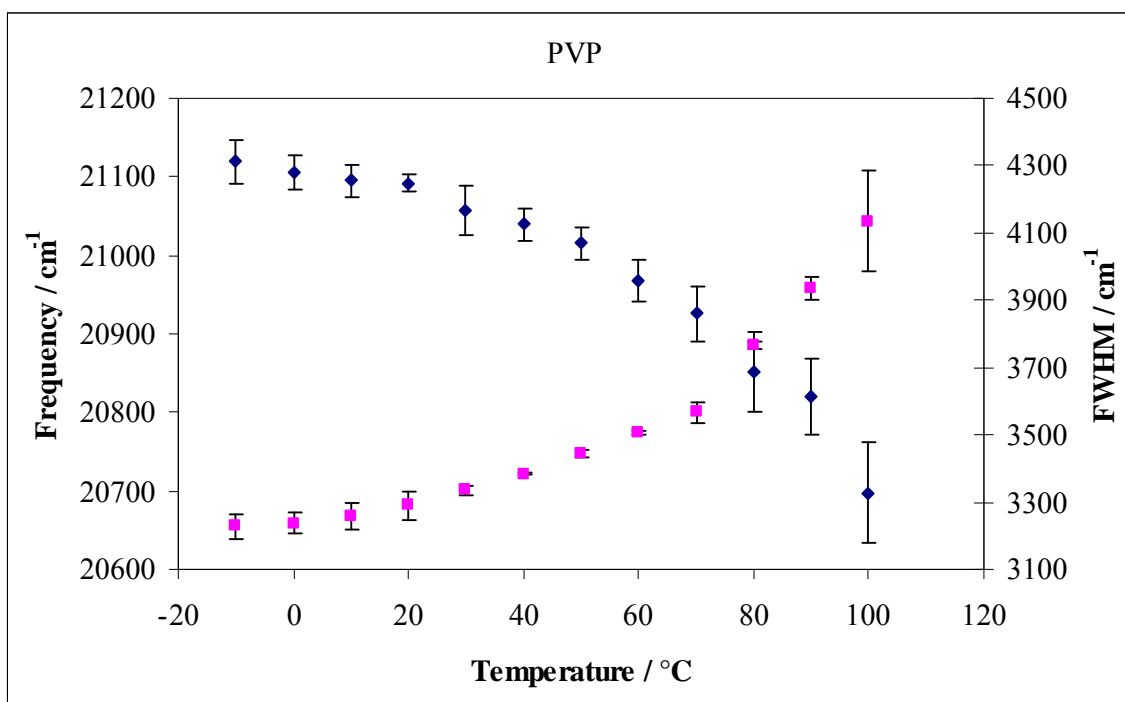
Figure V-5c

Figure V-5c: Peak energy ν_p and bandwidth for phosphorescence emission from vanillin in amorphous films of PVP as a function of temperature. The delayed emission spectra collected as a function of temperature (Figure V-1c) were analyzed using log-normal function as described in Materials and Methods using eq. (1) and (2).

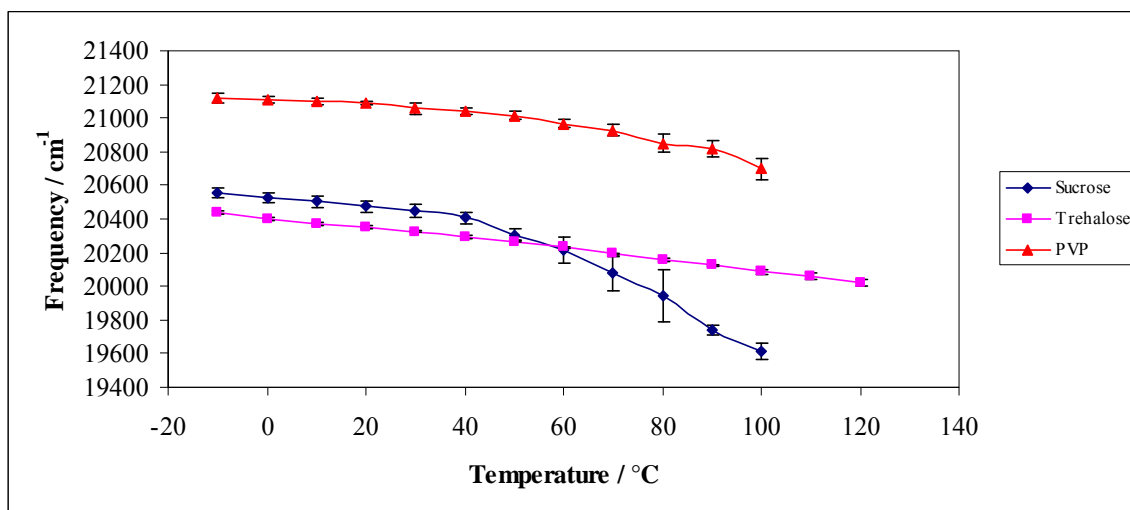
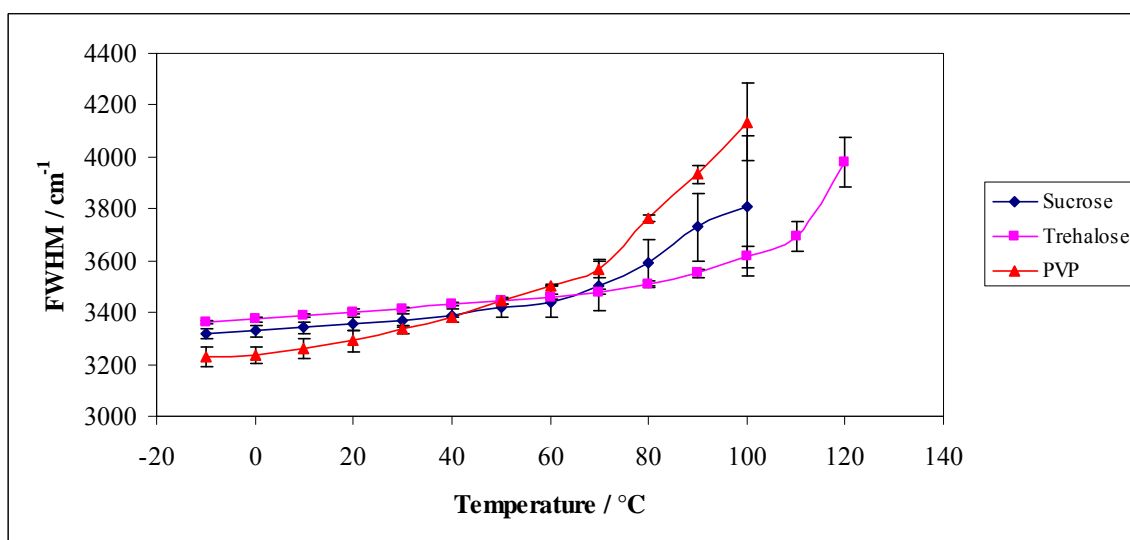
Figure V-6a*Figure V-6b*

Figure V-6a and 6b: Peak energy ν_p (6a) and bandwidth (6b) for phosphorescence emission from vanillin in amorphous films of sucrose (\blacklozenge), trehalose (\blacksquare) and PVP (\blacktriangle) as a function of temperature.

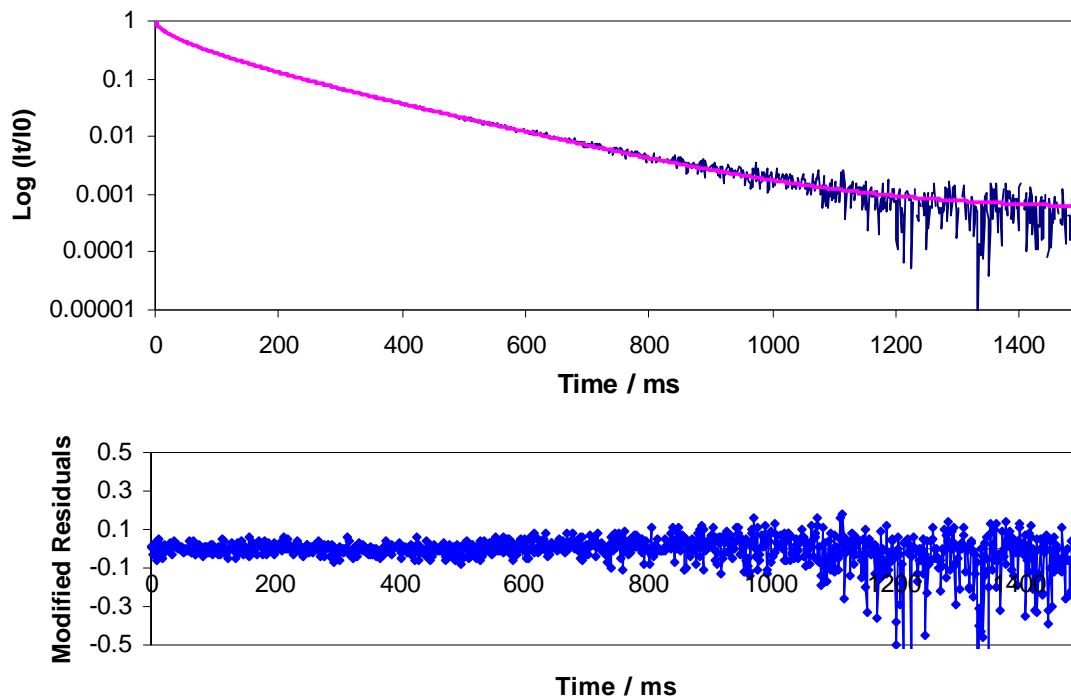
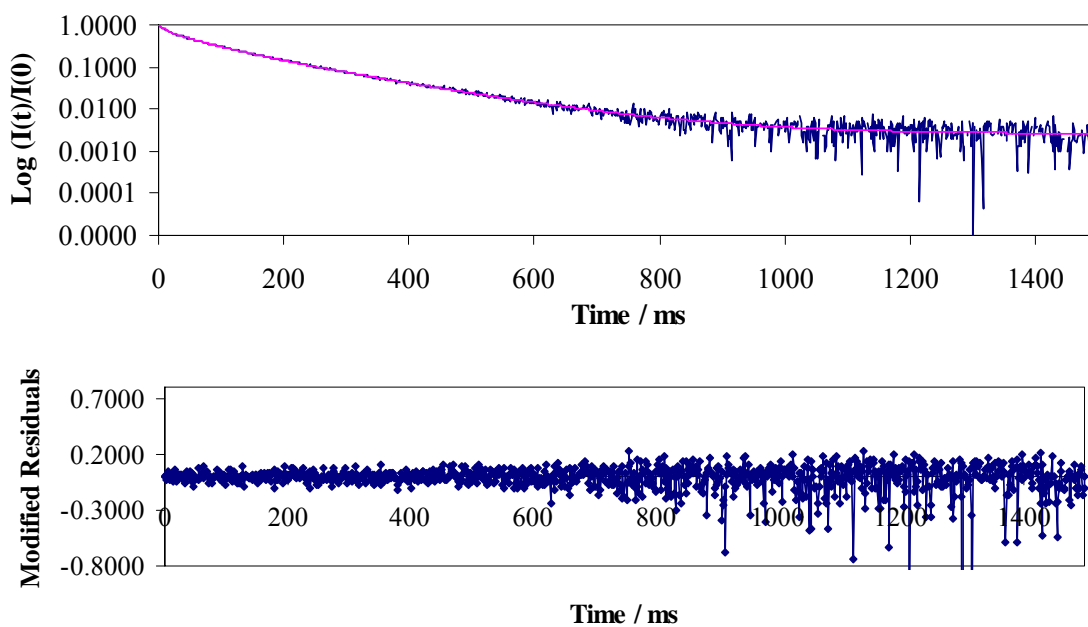
Figure V-7a*Figure V-7b*

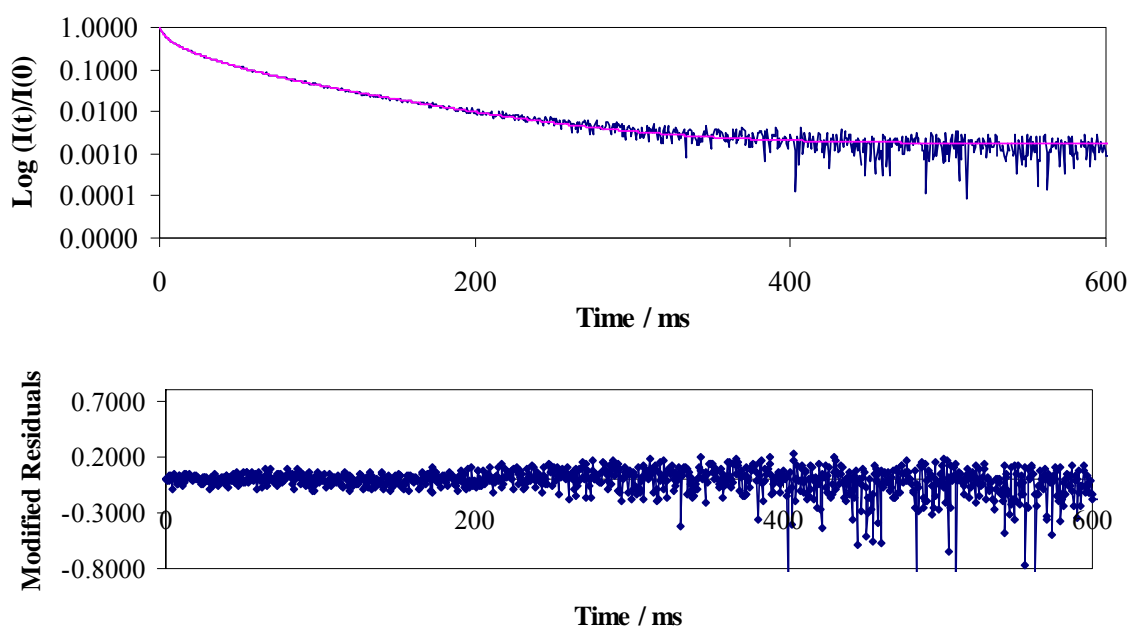
Figure V-7c

Figure V-7a, 7b and 7c: Normalized phosphorescence intensity decay $[I(t)/I(0)]$ of vanillin dispersed in amorphous films of sucrose (7a), trehalose (7b) and PVP (7c) at 20°C in the presence of nitrogen. The solid lines through the data are fits using a multi-exponential function (Eq. (3), Materials and Methods). A plot of modified residuals $[(\text{Data-Fit})/\text{Data}^{1/2}]$ for these fits is shown in the bottom graph.

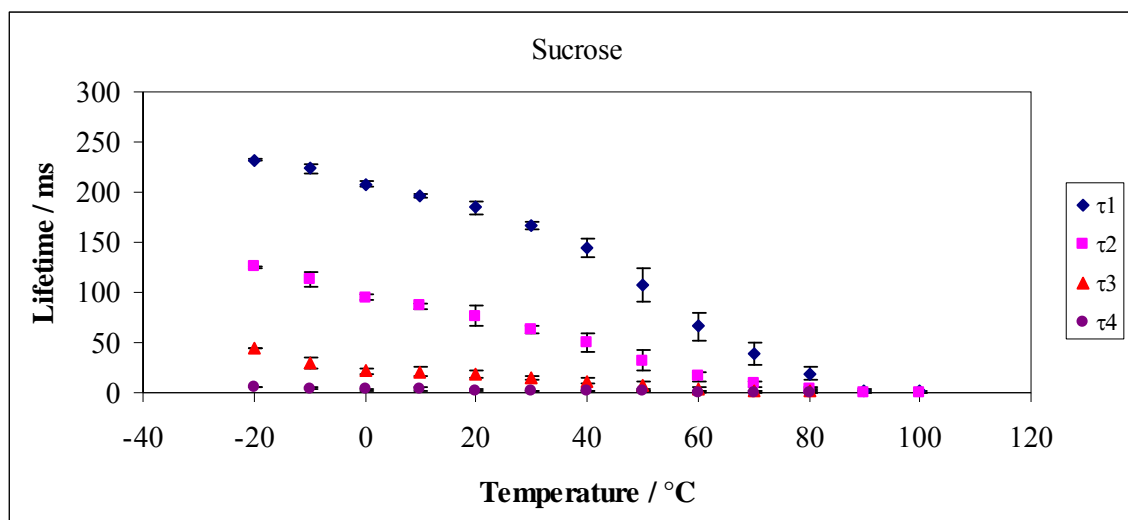
Figure V-8a

Figure V-8a: Lifetime components τ_1 (\blacklozenge), τ_2 (\blacksquare), τ_3 (\blacktriangle) and τ_4 (\bullet) obtained from a multi-exponential model fit (Eq. (3), Materials and Methods) to phosphorescence intensity decay data from vanillin dispersed in amorphous films of sucrose equilibrated against nitrogen as a function of temperature. The data were calculated every 10°C from -10°C to 100°C.

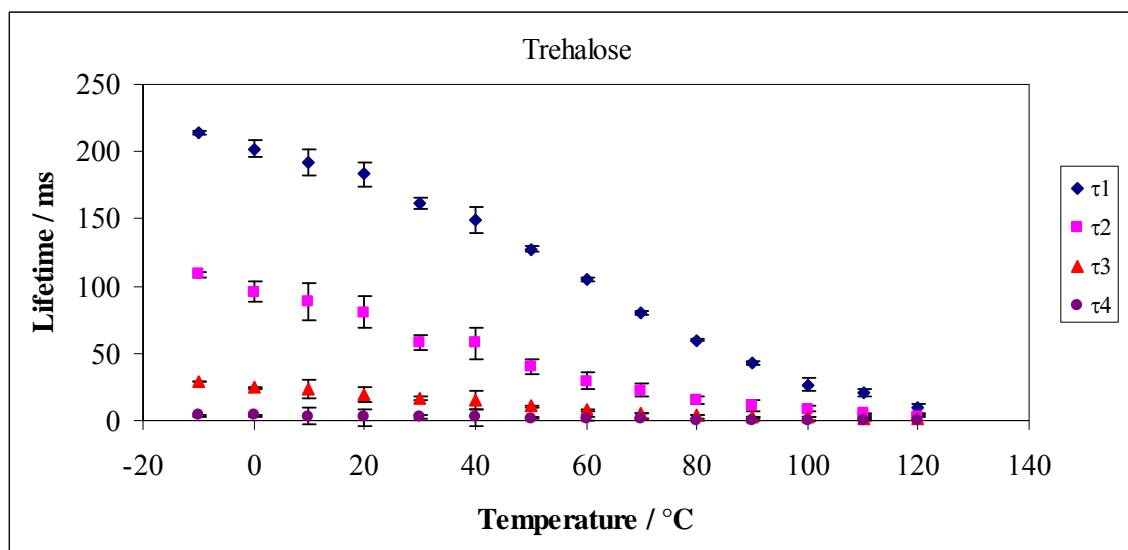
Figure V-8b

Figure V-8b: Lifetime components τ_1 (\blacklozenge), τ_2 (\blacksquare), τ_3 (\blacktriangle) and τ_4 (\bullet) obtained from a multi-exponential model fit (Eq. (3), Materials and Methods) to phosphorescence intensity decay data from vanillin dispersed in amorphous films of trehalose equilibrated against nitrogen as a function of temperature. The data were calculated every 10°C from -10°C to 120°C.

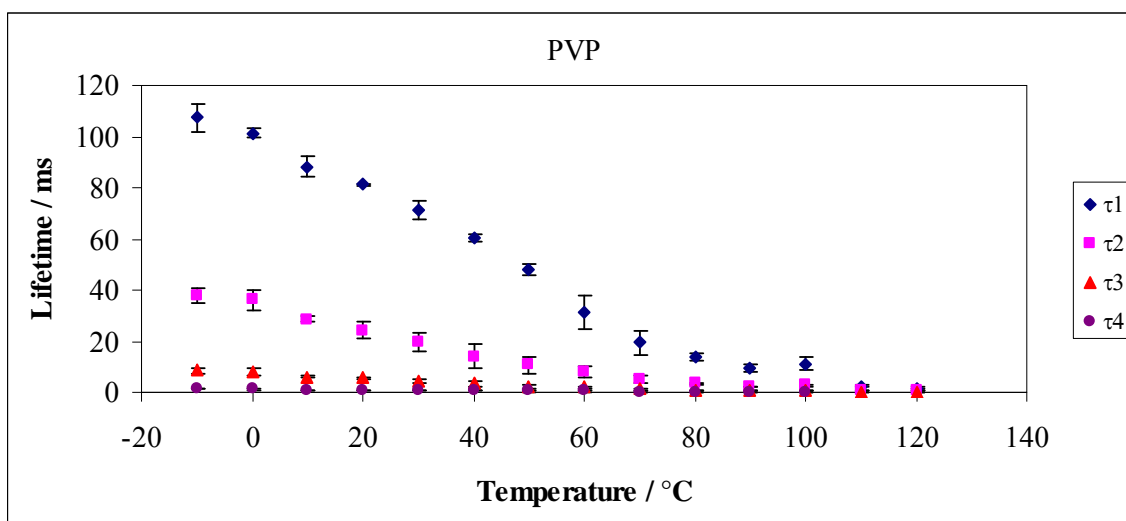
Figure V-8c

Figure V-8c: Lifetime components τ_1 (\blacklozenge), τ_2 (\blacksquare), τ_3 (\blacktriangle) and τ_4 (\bullet) obtained from a multi-exponential model fit (Eq. (3), Materials and Methods) to phosphorescence intensity decay data from vanillin dispersed in amorphous films of PVP equilibrated against nitrogen as a function of temperature. The data were calculated every 10°C from -10°C to 120°C.

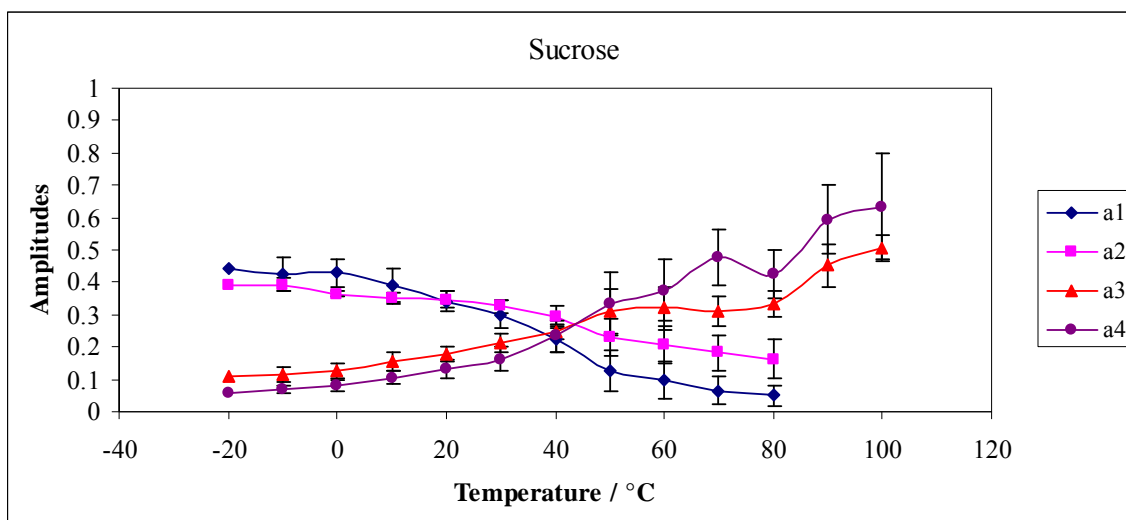
Figure V-9a

Figure V-9a: Intensity decay fit amplitudes for vanillin in amorphous films of sucrose in nitrogen as a function of temperature. The data were calculated every 10°C from -10°C to 100°C. The amplitudes a_1 (♦) and a_2 (■) correspond to the longer life time components (τ_1 , τ_2) and a_3 (▲) and a_4 (●) correspond to the shorter lifetime components (τ_3 , τ_4). The amplitudes were obtained from a multi exponential model fit (Eq. (3), Materials and Methods) to phosphorescence intensity decay data from vanillin dispersed in amorphous sucrose films equilibrated against nitrogen as a function of temperature

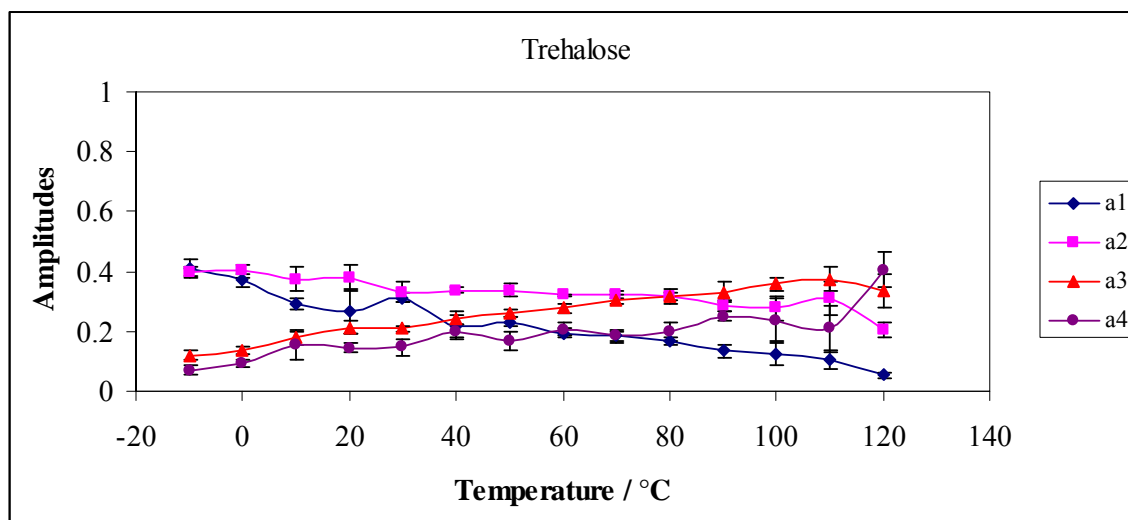
Figure V-9b

Figure V-9b: Intensity decay fit amplitudes for vanillin in amorphous films of trehalose in nitrogen as a function of temperature. The data were calculated every 10°C from -10°C to 120°C. The amplitudes a_1 (♦) and a_2 (■) correspond to the longer life time components (τ_1 , τ_2), and a_3 (▲) and a_4 (●) correspond to the shorter lifetime components (τ_3 , τ_4). The amplitudes were obtained from a multi exponential model fit (Eq. (3), Materials and Methods) to phosphorescence intensity decay data from vanillin dispersed in amorphous trehalose films equilibrated against nitrogen as a function of temperature

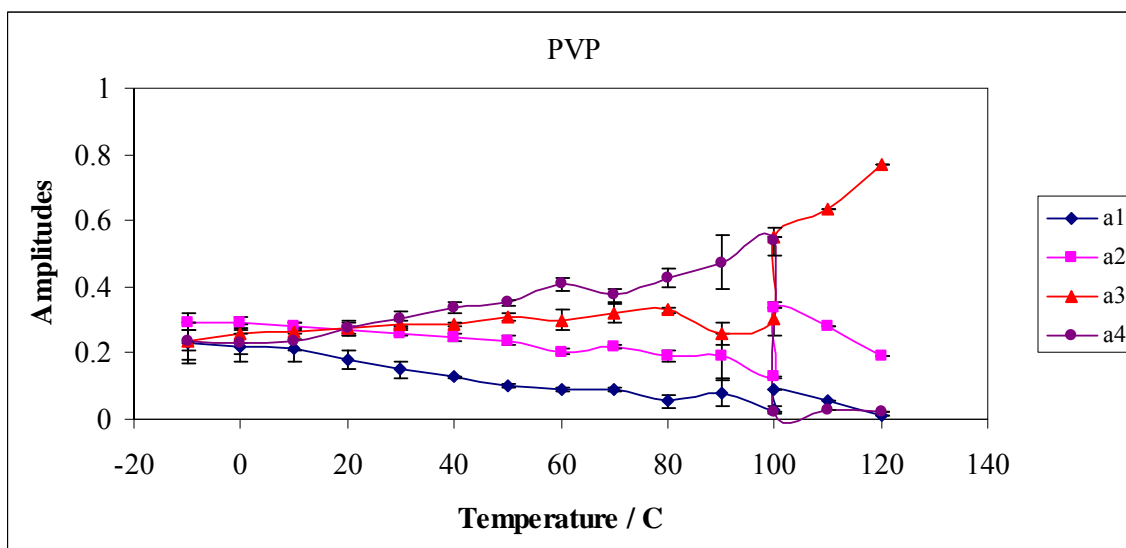
Figure V-9c

Figure V-9c: Intensity decay fit amplitudes for vanillin in amorphous films of PVP in nitrogen as a function of temperature. The data were calculated every 10°C from -10°C to 100°C. The amplitudes a_1 (♦) and a_2 (■) correspond to the longer life time components (τ_1 , τ_2) and a_3 (▲) and a_4 (●) correspond to the shorter lifetime components (τ_3 , τ_4). The amplitudes were obtained from a multi exponential model fit (Eq. (3), Materials and Methods) to phosphorescence intensity decay data from vanillin dispersed in amorphous PVP films equilibrated against nitrogen as a function of temperature.

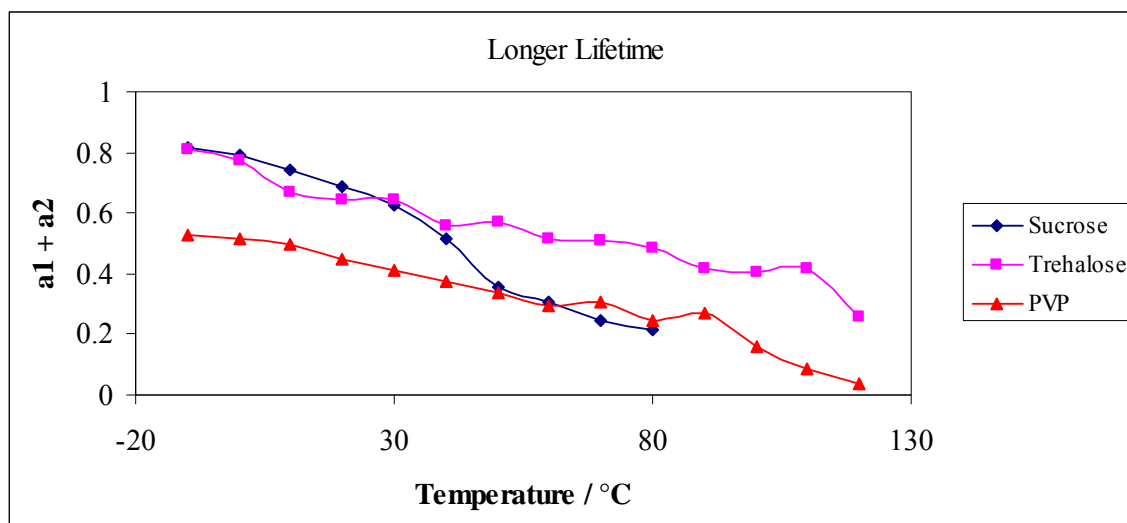
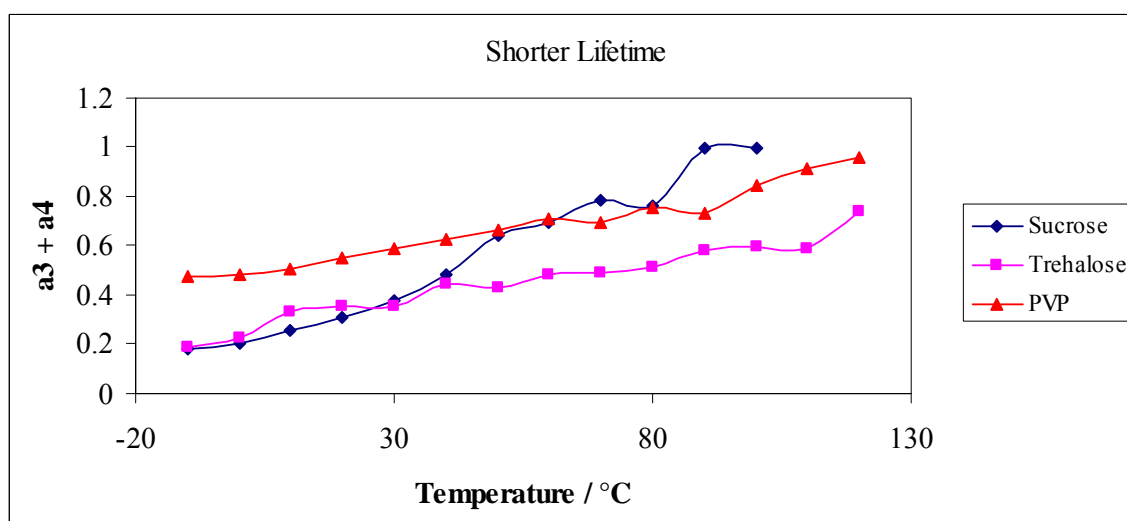
Figure V-10a*Figure V-10b*

Figure V-10a and 10b: Comparison of intensity decay fit amplitudes (for longer ($a_1 + a_2$) and shorter ($a_3 + a_4$) lifetime components) for vanillin in amorphous films of sucrose, trehalose and PVP in nitrogen as a function of temperature.

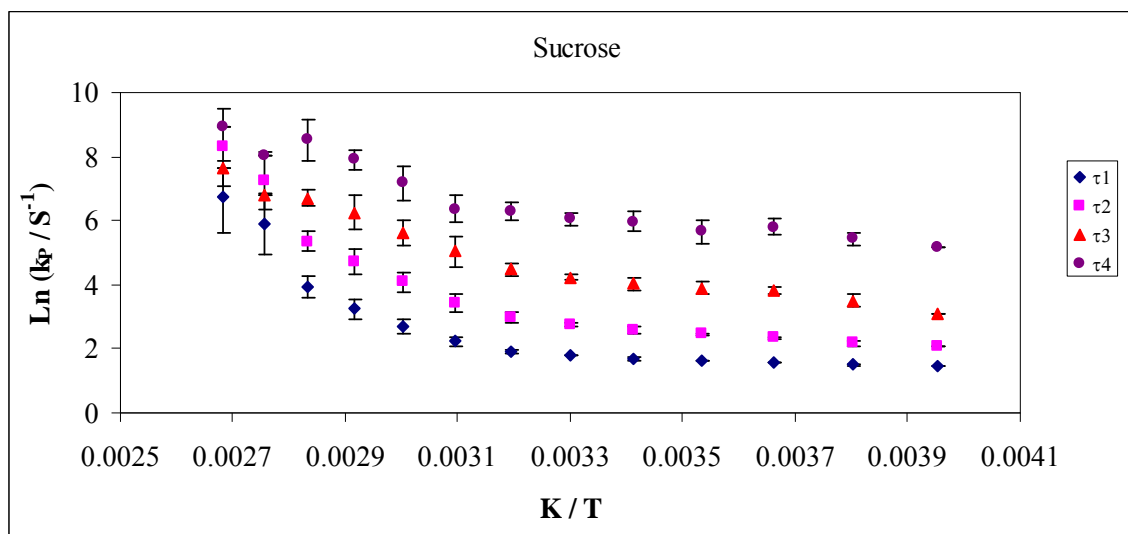
Figure V-11a

Figure V-11a: The Arrhenius plot of the individual lifetime component τ_1 (\blacklozenge), τ_2 (\blacksquare), τ_3 (\blacktriangle) and τ_4 (\bullet) of vanillin in amorphous films of sucrose as a function of inverse of temperature.

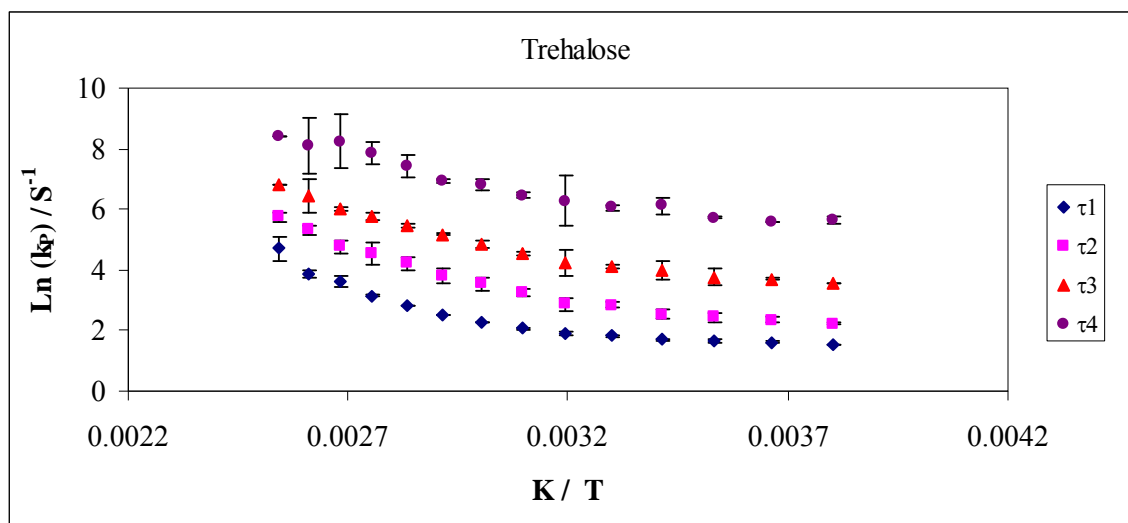
Figure V-11b

Figure V-11b: The Arrhenius plot of the individual lifetime component τ_1 (\blacklozenge), τ_2 (\blacksquare), τ_3 (\blacktriangle) and τ_4 (\bullet) of vanillin in amorphous films of trehalose as a function of inverse of temperature.

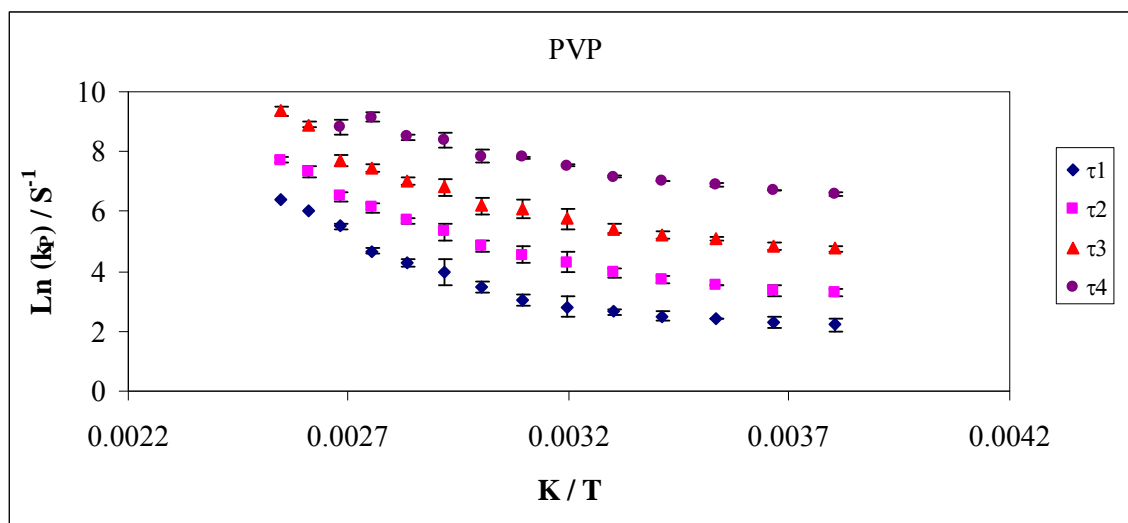
Figure V-11c

Figure V-11c: The Arrhenius plot of the individual lifetime component τ_1 (\blacklozenge), τ_2 (\blacksquare), τ_3 (\blacktriangle) and τ_4 (\bullet) of vanillin in amorphous films of PVP as a function of inverse of temperature.

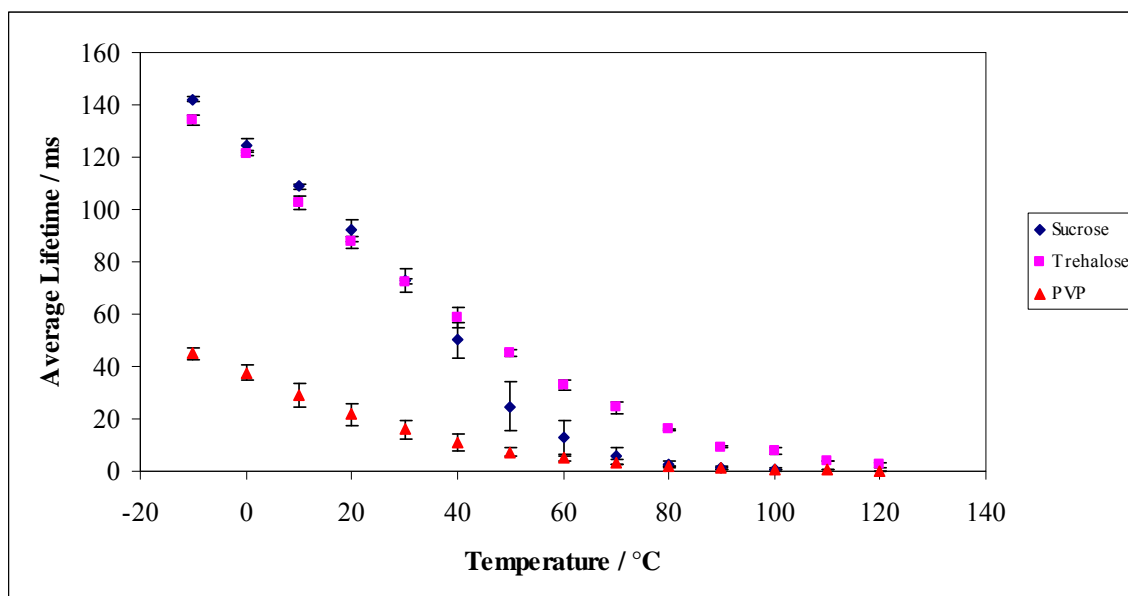
Figure V-12a

Figure V-12a: Average lifetime from a multi-exponential model fit (Eq. (4), Materials and Methods) to phosphorescence intensity decay data from vanillin dispersed in amorphous films of sucrose (♦), trehalose (■) and PVP (▲) equilibrated against nitrogen as a function of temperature.

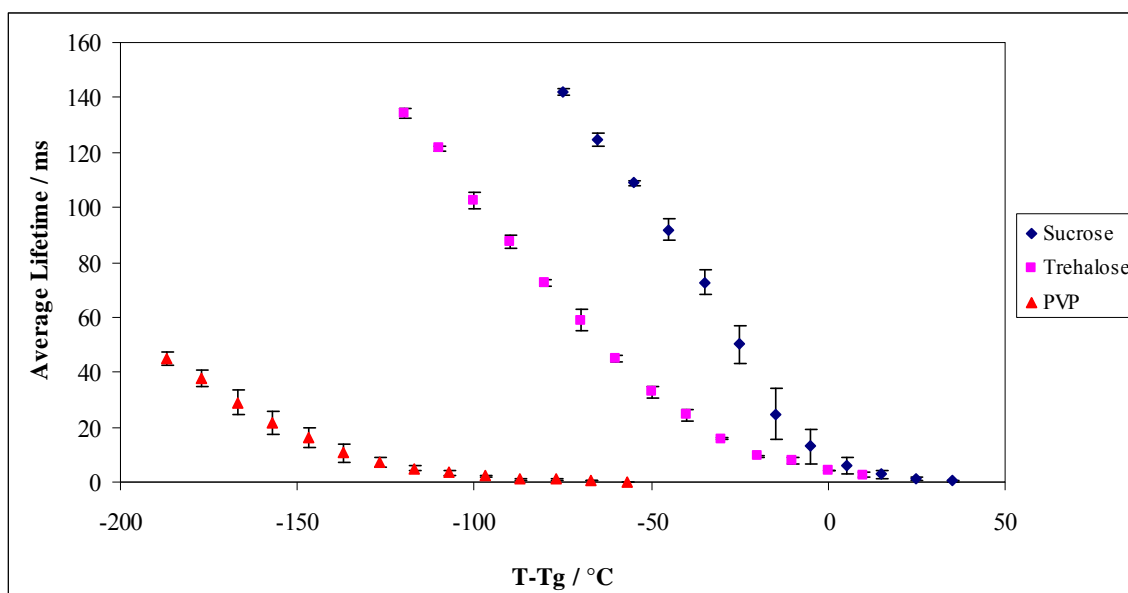
Figure V-12b

Figure V-12b: Average lifetime from a multi-exponential model fit (Eq. (4), Materials and Methods) to phosphorescence intensity decay data from vanillin dispersed in amorphous films of sucrose (♦), trehalose (■) and PVP (▲) equilibrated against nitrogen as a function of T-Tg.

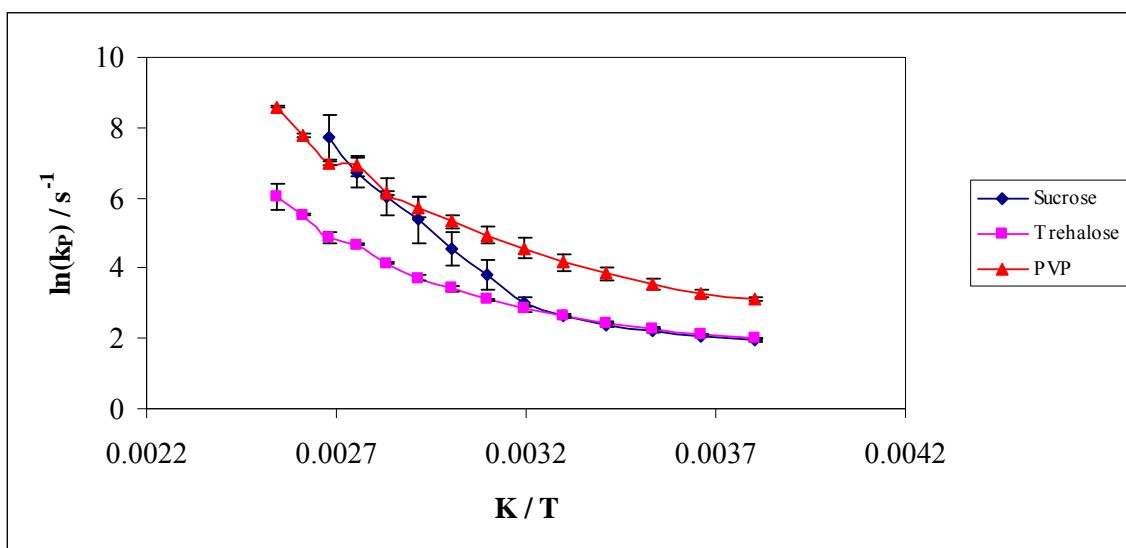
Figure V-12c

Figure V-12c: Arrhenius plot of the average lifetime of vanillin in amorphous films of sucrose (♦), trehalose (■) and PVP (▲) as a function of inverse temperature.

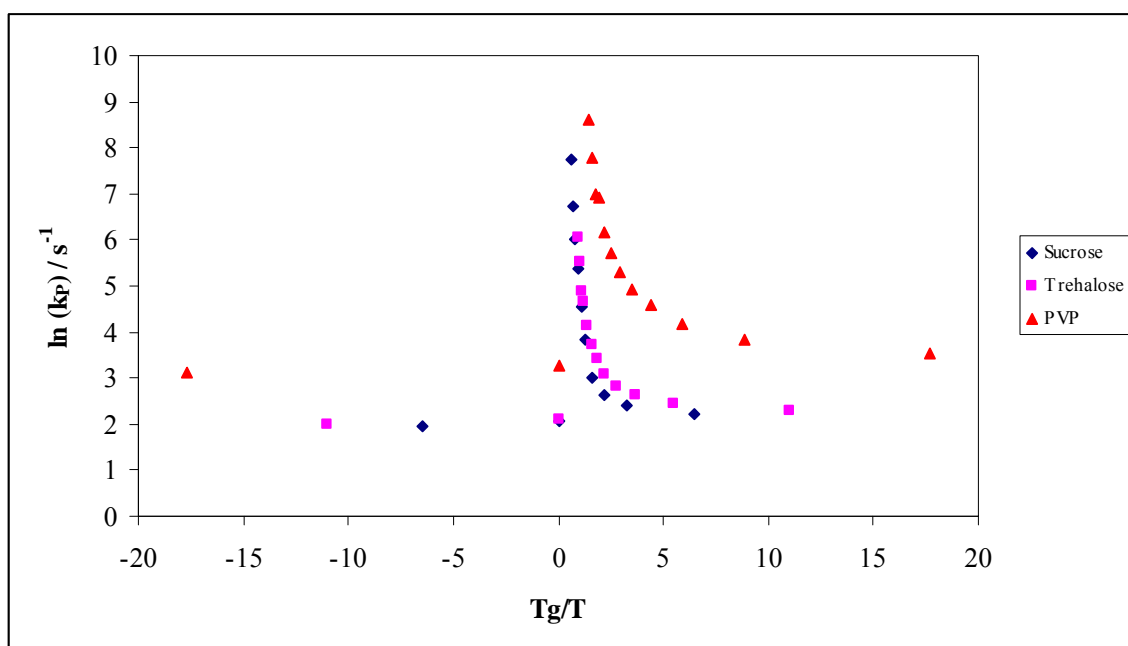
Figure V-12d

Figure V-12d: Arrhenius plot of the average lifetime of vanillin in amorphous films of sucrose (◆), trehalose (■) and PVP (▲) as a function of T_g/T .

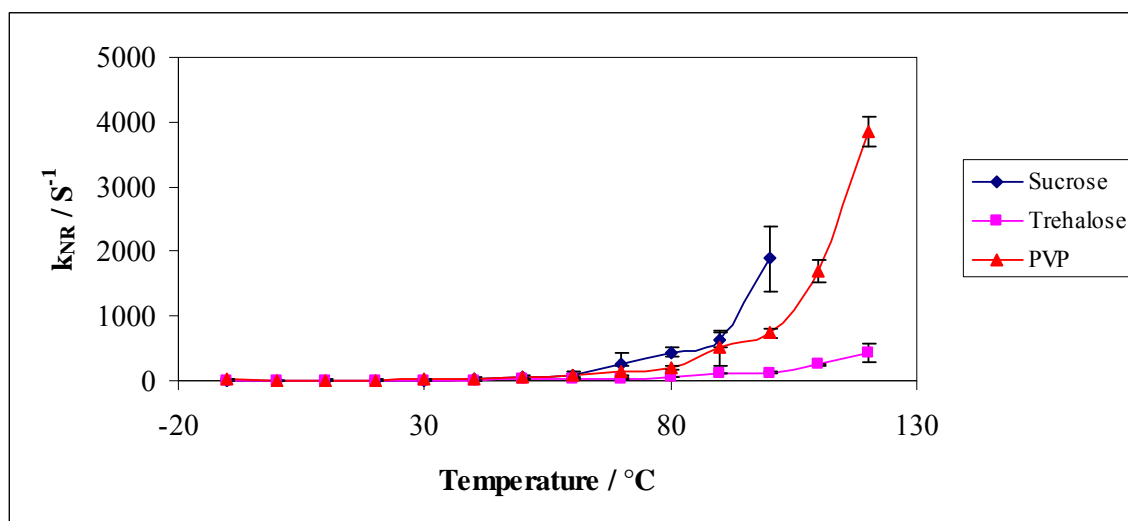
Figure V-13a

Figure V-13a: Temperature dependence of the total non-radiative decay rate of the triplet state k_{NR} ($k_p = k_{RP} + k_{NR}$) to S_0 of vanillin in amorphous sucrose, trehalose and PVP films.

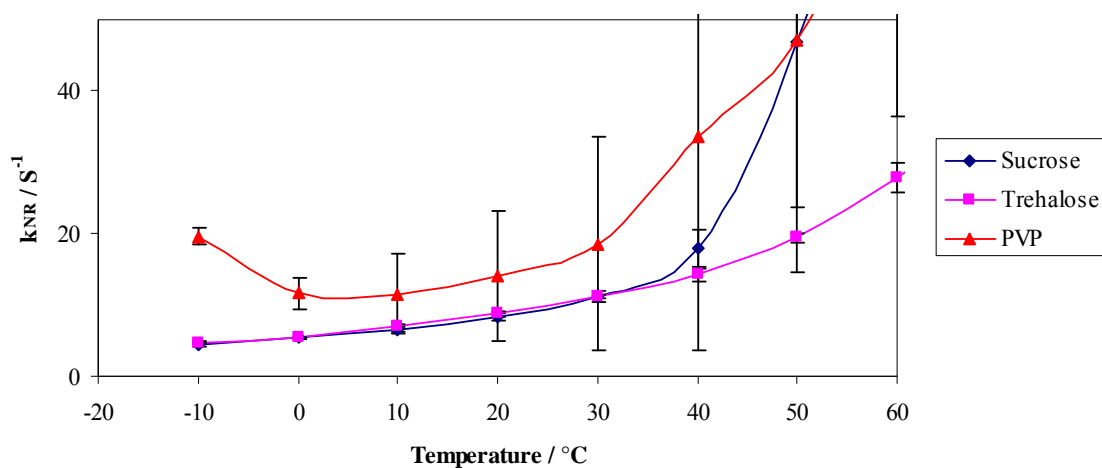
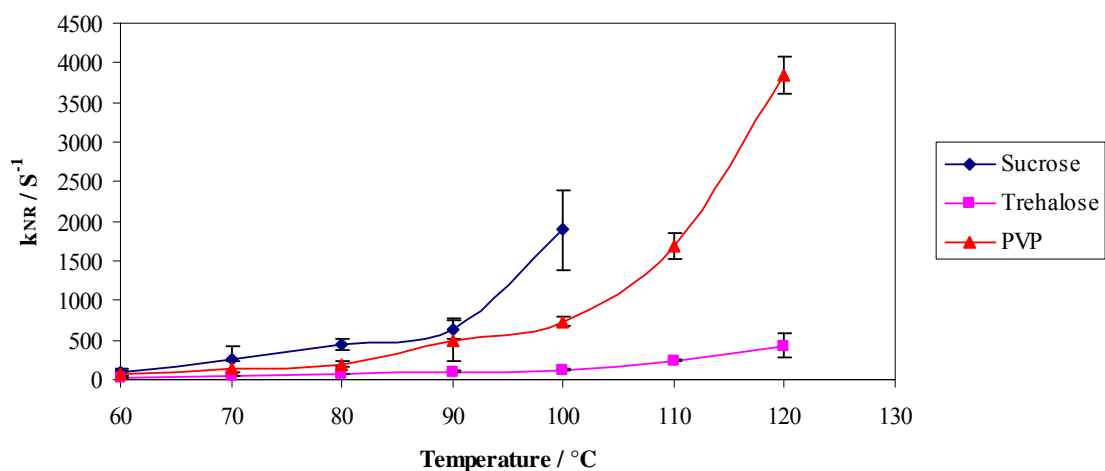
Figure V-13b**Figure V-13c**

Figure V-13b and 13c: Temperature dependence of the total non-radiative decay rate of the triplet state k_{NR} ($k_p = k_{RP} + k_{NR}$) to So of vanillin in amorphous sucrose, trehalose and PVP films. The graph is showing details below 60°C (13b) and above 60°C (13c).

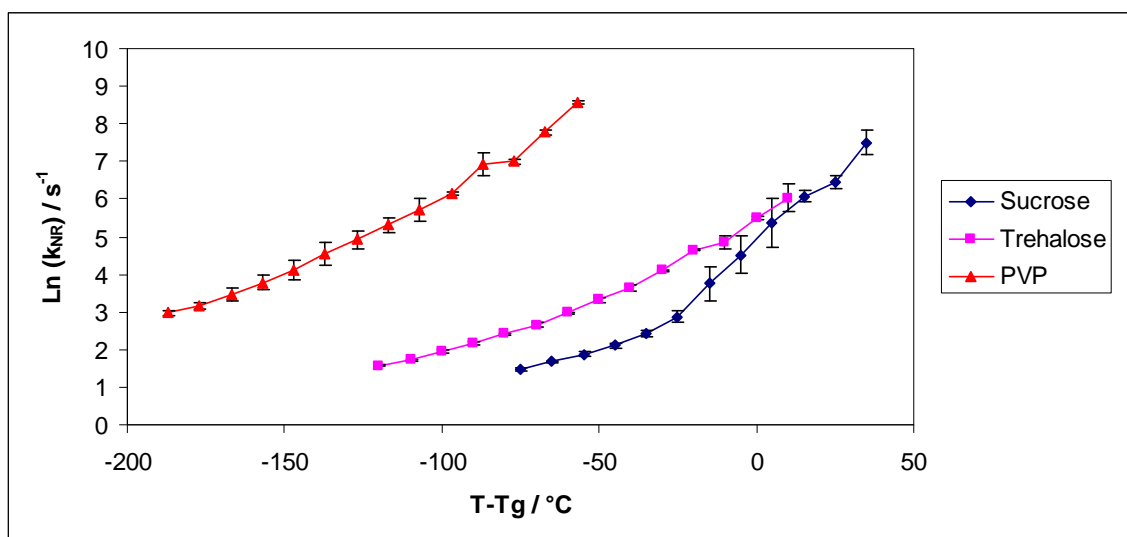
Figure V-13d

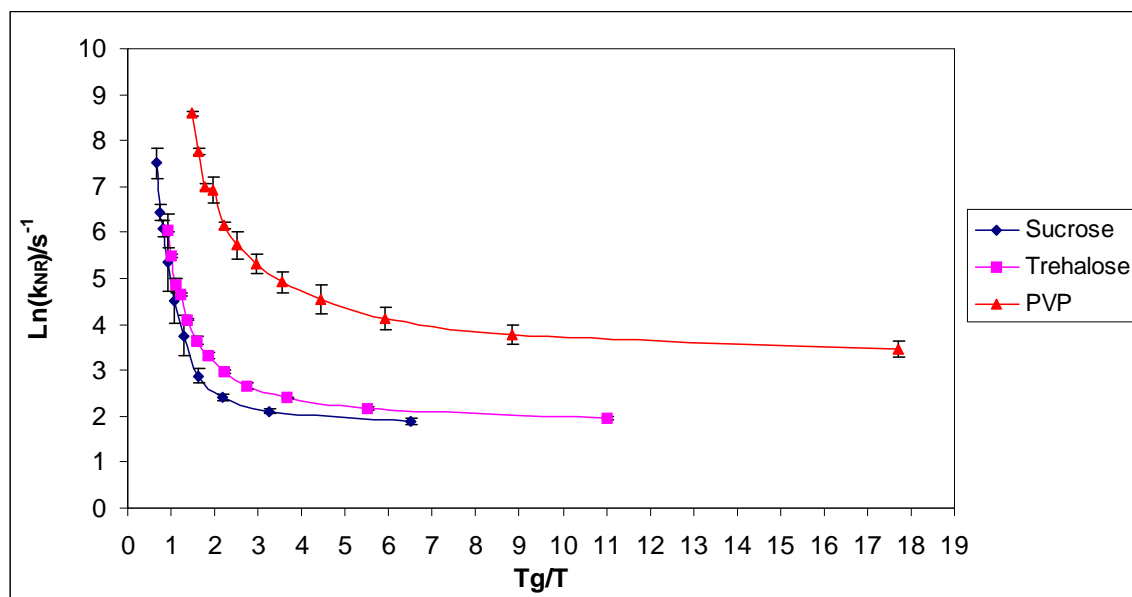
Figure V-14

Figure V-14: The Arrhenius plot of the total non-radiative decay rate of the triplet state k_{NR} ($k_p = k_{\text{RP}} + k_{\text{NR}}$) to So of vanillin in amorphous sucrose, trehalose and PVP films.

Table V-1a

Table V-1a: Calculated activation energy E_a for $\ln(k_p)$ for individual lifetime at low, intermediate and high temperature for vanillin in amorphous sucrose films.

Sucrose			
Lifetime		E_a kJ / mol	Transition Temperatures °C
τ_1	LT	4.14	60
	HT	110.00	
τ_2	LT	9.60	55
	HT	112.00	
τ_3	LT	13.63	42
	HT	49.03	
τ_4	LT	11.33	50
	HT	68.21	
τ_{Avg}	LT	9.64	40
	HT	76.34	

Table V-1b

Table V-1b: Calculated activation energy E_a for $\ln(k_p)$ for individual lifetime at low, intermediate and high temperature for vanillin in amorphous trehalose films.

Trehalose			
Lifetime	Temperature	E_a KJ / mol	Transition Temperatures °C
τ_1	LT	9.40	55
	HT	42.37	
τ_2	LT	4.93	60
	HT	35.11	
τ_3	LT	11.17	50
	HT	34.68	
τ_4	LT	14.31	60
	HT	35.91	
τ_{Avg}	LT	12.67	60
	HT	47.14	

Table V-1c

Table V-1c: Calculated activation energy E_a for $\ln(k_p)$ for individual lifetime at low, intermediate and high temperature for vanillin in amorphous PVP films.

PVP			
Lifetime	Temperature	E_a KJ / mol	Transition Temperatures °C
τ_1	LT	9.13	50
	HT	54.58	
τ_2	LT	16.76	60
	HT	55.41	
τ_3	LT	15.78	62
	HT	58.93	
τ_4	LT	9.61	30
	HT	25.28	
τ_{Avg}	LT	21.75	55
	HT	57.04	

Table V-2

Table V-2: Calculated activation energy E_a for $\ln(k_p)$ for average lifetime at low, intermediate and high temperature for vanillin in amorphous films of sucrose, trehalose and PVP.

$\ln(k_p)$	τ_{Avg}	Temperature	R^2	E_a KJ / mol	Transition Temperatures °C
Sucrose		LT	0.96	9.64	40
		HT	1.00	76.34	
Trehalose		LT	0.97	12.67	60
		HT	0.97	47.14	
PVP		LT	0.97	21.75	55
		HT	0.96	57.04	

Table V-3

Table V-3: Calculated activation energy E_a for $\ln(k_{NR})$ for average lifetime at low, intermediate and high temperature for vanillin in amorphous films of sucrose, trehalose and PVP.

	Temperature	Ea KJ / mol	Transition Temperatures °C	Tg°C
Sucrose	LT	13.84	40	65
	HT	72.32		110
Trehalose	LT	16.48	60	177
	HT	48.69		
PVP	LT	23.07	55	
	HT	57.27		

References

- Allison, S. D., Chang, B., Randolph, T. W. and Carpenter, J. F. Hydrogen bonding between sugars and protein is responsible for inhibition of dehydration-induced protein unfolding. *Archives of Biochemistry and Biophysics*. 365 (1999). 289-298.
- Angel, C. A. Formation of glasses from liquids and biopolymers. *Science*. 267 (1995). 1924-1935.
- Arakawa, T., Prestrelski, S. J., Kenney, W.C. and Carpenter, J. F. Factors affecting short-term and long-term stabilities of proteins. *Advanced Drug Delivery Reviews*. 10 (1993). 1-28.
- Borowitzka, L. J. R. and Gilles-Baillien, M. Glycerol and other carbohydrate osmotic effectors. In *Transport Processes, Iono- and Osmoregulation*, Berlin. (1985).
- Branca, C., Magazu, S., Maisano, G. and Migiliardo, P. Anomalous cryoprotective effectiveness of trehalose: Raman scattering evidences. *Journal of Chemical Physics*. 111 (1999). 281-287.
- Carpenter, J. F. and Crowe, J. H. An infrared spectroscopic study of the interactions of carbohydrates with dried proteins. *Biochemistry*. 28 (1989). 3916-3922.
- Chang, L., Shepherd, D., Sun, J., Ouellette, D., Grant, K. L. M., Tang, X. and Pikal, M. J. Mechanism of protein stabilization by sugars during freeze drying and storage: Native structure preservation, specific interaction, and/or immobilization in a glassy matrix. *Journal of Pharmaceutical Sciences*. 94 (2005). 1427-1444.
- Constantino, H. R., Curley, J. G., Wu, S. and Hsu, C. C. Water sorption behavior of lyophilized protein-sugar systems and implications for solid-state interactions. *International Journal of Pharmaceutics*. 166 (1998). 211-221.
- Corveleyn, S. and Remon, J. Maltodextrin as lyoprotectants in the lyophilization of a model protein, LDH. *Pharmaceutical Research*. 13 (1996). 146-150.
- Crowe J. H., Carpenter, J. F. and Crowe L. M. The role of vitrification in anhydrobiosis. *Annual Review Physiology*. 60 (1998). 73-103.
- Crowe, J. H., Leslie, S. B. and Crowe, L. M. Is vitrification sufficient to preserve liposomes during freeze drying? *Cryobiology*. 31 (1994). 355-366.
- Crowley, P. J. Excipients as stabilizers. *PSTT* 2 (1999). 237-243.
- Crystall, B. Glass pharmacy. *New Scientist*. (1997). 24-27.

- Duddu, S. P. and Dal Monte, P. R. Effect of glass transition temperature on the stability of lyophilized formulations containing a chimeric therapeutic monoclonal antibody. *Pharmaceutical Research*. 14 (1997). 591-595.
- Duddu, S. P., Zhang, G. and Dal Monte, P. R. The relationship between protein aggregation and molecular mobility below the glass transition temperature of lyophilized formulations containing monoclonal antibody. *Pharmaceutical Research*. 14 (1997). 596-700.
- Eriksson, H. J. C., Hinrichs, W. L. J., Veen, B. Van., Somsen, G. W., Jong, G. J. De. and Frijlink, H. W. Investigations into stabilization of drugs by sugar glasses: I Tablets prepared from stabilized alkaline phosphatase. *International Journal of Pharmaceutics*. 249 (2002). 59-70.
- Fischer, C. J., Gafni, A., Steel, D. G. and Schauerte, J. A. The triplet-state lifetime of indole in aqueous and viscous environments: significance to the interpretation of room temperature phosphorescence in proteins. *Journal of the American Chemical Society*. 124 (2004). 10359-10266.
- Fischer, E. W., Donth, E. and Steffen, W. Temperature dependence of characteristic length for glass transition. *Physical Review Letter*. 68 (1992). 2344-2346.
- Franks, F. Review on protein stability and function at low temperature. *Cryo-Letter*. 8 (1987). 108.
- Green, J. L. and Angell, C. A. Phase relations and vitrification in saccharide-water solution and the trehalose anomaly. *Journal of Physical Chemistry*. 93 (1989). 2880-2882.
- Gupta, P. I., Kakumanu. and Bansal, A. K. Stability and solubility of celecoxib-PVP amorphous dispersions: a molecular perspective. *Pharmaceutical Research*. 21 (2004). 1762-1769.
- Hancock, B. C. and Zografi, G. Characteristics and significance of amorphous state in pharmaceutical systems. *Journal of Pharmaceutical Sciences*. 86 (1997): 1-12.
- Hancock, B. C., Shamblin, S. L. and Zografi, G. Molecular mobility of amorphous pharmaceutical solids below their glass transition temperatures. *Pharmaceutical Research*. 12 (1995): 799-806.
- Hinrichs, W. L. J., Prinsen, M. G. and Frijlink, H. W. Inulin glasses for the stabilization of therapeutic proteins. *International Journal of Pharmaceutics*. 215 (2001). 163-174.

- Immura, K., Ogawa, T., Sakiyama, T. and Nakanishi, K. Effects of types of sugar on the stabilization of protein in the dried state. *Journal of Pharmaceutical Sciences*. 92 (2003). 266-274.
- Johnson, R. E., Kirchhoff, C. F. and Gaud, H. T. Mannitol-sucrose mixtures versatile formulations for protein lyophilization. *Journal of Pharmaceutical Sciences*. 91 (2002). 914-922.
- Joshi, V. Excipient Choice in Solid Dosage Forms. *Drug Delivery Technology*. (2004).
- Kaushik, J. K. and Bhat, R. Why is Trehalose an exceptional protein stabilizer? An analysis of thermal stability of proteins in the presence of the compatible osmolyte trehalose. *Journal of Biological Chemistry*. 278 (2003). 26458-26465.
- Khougaz, K. and Clas, S. D. Crystallization inhibition in solid dispersion of MK-0591 and poly (vinyl-pyrrolidone) polymers. *Journal of Pharmaceutical Sciences*. 89 (2000). 1325-1334.
- Lai, M., Hageman, M. J., Schowen, R. L. and Topp, E. M. Chemical stability of peptides in polymers. 1. Effect of water on peptide deamidation in poly (vinyl alcohol) and poly (vinyl pyrrolidone) matrices. *Journal of Pharmaceutical Sciences*. 10 (1999). 1073-1080.
- Lim, M. H. and Reid, D. S. Studies of reaction kinetics in relation to the Tg of the polymers in frozen model systems. In H. Levine & L. Slade. *Water relationships in foods*. New York, Plenum Press. (1991). 103-122.
- Mazzobre, M. F., del Pilar Buera, M. and Chirife, J. Protective role of trehalose on thermal stability of lactase in relation to its glass and crystal forming properties and effect of delaying crystallization. *Lebensm-Wiss. U.-Technol.* 30 (1997). 324-329.
- Miller, D. P., De Pablo, J. J. and Corti, H. R. Viscosity and glass transition temperature of aqueous mixtures of trehalose with borax and sodium cholate. *Journal of physical Chemistry*. 103 (1999). 10243-10249.
- Oksanen C. A. and Zografi, G. Molecular mobility in mixtures of absorbed water and solid poly (vinyl pyrrolidone). *Pharmaceutical Research*. 10 (1993). 791-799.
- Papp, S. and Vanderkooi J. M. Tryptophan phosphorescence at room temperature as a tool to study protein structure and dynamics. *Photochemistry and Photobiology*. 49 (1989). 775-784.
- Roe, K. D. and Labuza, T. P. Glass transition and crystallization of amorphous trehalose-sucrose mixtures. *International Journal of Food Prop.* 8 (2005). 559-574.

- Roos, Y. Melting and glass transitions of low molecular weight carbohydrates. *Carbohydrate Research*. 238 (1993). 39-48.
- Shamblyn, S., Hancock, B. C., Dupuis, Y. and Pikal, M. J. Interpretation of relaxation time constants for amorphous pharmaceutical systems. *Journal of Pharmaceutical Sciences*. 89 (2000). 417-427.
- Shirke, S. and Ludescher, R. D. Molecular mobility and glass transition in amorphous glucose, maltose and maltotriose. *Carbohydrate Research*. 340 (2006). 2654-2660.
- Slade, L., Levine, H. and Finley, J. W. In protein quality and effects of processing; Phillips, R. D., Finley, J. W., eds., Marcel and Dekker Inc: New York. (1989).
- Sochava, I. V., Belopol'skaya, T. V. and Smirnova, O. I. Biophysical chemistry. 22 (1985). 232-336.
- Sun, W. Q., Davidson, P. and Chan, H. S. O. Protein stability in the amorphous carbohydrate matrix: relevance to anhydrobiosis. *Biochimica et Biophysica Acta-General Subjects*. 1425 (1998). 245-254.
- Sun, W. Q., Davidson, P. and Chan, H. S. O. Protein stability in the amorphous carbohydrate matrix: relevance to anhydrobiosis. *Biochimica et Biophysica Acta-General Subjects*. 1425 (1998). 245-254.
- Suzuki, T., Imamura, K., Fujimoto, H. and Okazaki, M. Relation between thermal stabilizing effect of sucrose on LDH and sucrose-LDH hydrogen bond. *Journal of Chemical Engineering of Japan*. 31 (1998). 565-570.
- Taylor, L. S. and Zografi, G. Sugar-polymer hydrogen bond interactions in lyophilized amorphous mixtures. *Journal of Pharmaceutical Sciences*. 87 (1998). 1615-1621.
- Van den Dries, I. J., Besseling, N. A. M., van Dusschoten, D., Hemminga, M. A. and van der linden, E. Relation between a transition in molecular mobility and collapse phenomena in glucose-water system. *Journal of Physical Chemistry*. 1004 (2000). 9260-9266.
- Vanderkooi, J. M. and Berger, J. W. Excited triplet state used to study biological macromolecules at room temperature. *Biochimica et Biophysica Acta: Bioenergetics*. 976 (1989). 1-27.
- Wolkers, W.F., and Oliver, A. E., Tablin, F., Crowe, J. H. A Fourier-transform infrared spectroscopy study of sugar glasses. *Carbohydrate Research*. 339 (2004). 1077-1085.

- Wolkers, W.F., Oldenhof, H., Alberda, M. and Hoekstra, F. A. A Fourier transform infrared microspectroscopy study of sugar glasses: application to anhydrobiotic higher plant cells. *Biochimica Biophysica Acta*. 1379 (1998). 83-96.
- Yancey, P. H., Clark, M. E., Hand, S. C., Browlus, R. D. and Somero, G. N. Living with water stress: evolution of osmolyte systems. *Science*. 217 (1982). 1214-1222.
- Yoshioka, S., Miyazaki, T. and Aso, Y. β -relaxation of insulin molecule in lyophilized formulations containing trehalose or dextran as a determinant of chemical reactivity. *Pharmaceutical Research*. 23 (2006). 961-966.
- Zallen, R. *The Physics of Amorphous Solids*. New York: John Wiley and Sons, (1998).
- Zunic, A. Molecular mobility of amorphous disaccharide studied by tryptophan luminescence. Master Thesis. Rutgers University. New Brunswick, NJ. (2004).

Chapter VI: Molecular mobility in amorphous sucrose films detected using phosphorescence of erythrosin B, tryptophan and vanillin.

Introduction

Amorphous sucrose is very widely used in foods and pharmaceuticals (Noel et al., 2000). It is also one of the very commonly used protectants for biological materials (Crowe et al., 1998). Sucrose has been shown to be responsible for many degradation phenomena in foods such as crystallization, caking/lumping, structural collapse and stickiness (Roos, 1995; Fennema, 1996; Goff and Sahagian, 1996; Labuza et al., 2004). The reason is that in most of its applications sucrose exists in an amorphous state, which is a metastable state which has shown presence of molecular mobility (Pravinata, 2003; Pravinata et al., 2005). Molecular mobility in amorphous sucrose contributes greatly in modulating physical and chemical properties that correlate with their stability and shelf life.

Molecular motions persist below and above T_g . The glassy state and glass transition greatly defines the physical state of amorphous sucrose. In glasses due to slow motions of molecules the relaxation times are longer compared to rubber/melt where molecules move faster, relaxation times vary from $>10^8$ s in glass to 10^{-9} s in melt; such increase is associated with activation of translational and rotational motions of molecules (Hill et al., 2005). In glass to liquid transition, molecular mobility is presented as α relaxation in the T_g zone; as temperature is lowered below T_g molecular mobility is presented as β and γ (in some cases δ) relaxations also called secondary relaxations (Ediger et al., 1996; Hancock and Zografi, 1997; Vyazovkin and Dranca, 2006). As these motions affect stability of amorphous sucrose they are of concern. In glass to liquid transitions

relaxation time of material is considered to be similar to experimental time scale and changes are observed, but in sub-T_g these relaxation times are very long and demand special consideration (Le Meste et al., 2002). On the other hand the different length scale of these motions present in the amorphous sucrose glass also demands special measurements.

Luminescence spectroscopy can provide site-specific information about molecular mobility in amorphous materials (Lakowicz, 1999) and is a noninvasive and sensitive tool that can be used to generate mobility maps. Phosphorescence spectroscopy uses optical spectroscopic probes that report on properties of the molecular environment around the probe (Slavik, 1994) and due to the timescale of excited triplet state responds to molecular events in the range of ms to s (Lakowicz, 1999; Parker, 1968). These molecular probes report on the structure, physical and chemical properties, and dynamics of their local environment (Slavik, 1994). Phosphorescence spectroscopy has been shown to be sensitive to molecular mobility in amorphous protein and sugars (Ludescher et al., 2001; Shah and Ludescher, 1993; Shirke and Ludescher 2005, 2006).

As a probe's excited triplet state could respond to molecular events in the range of ms to s time scale, different probes could cover this range at different time scales depending upon their excited state lifetime and the various quenching mechanisms that de-excite the triplet state. A probe observes molecular mobility during its excited state lifetime, and for slower motions (Craig et al., 1997) longer lifetime probes are more suitable and the opposite is true for faster motions. The lifetime of the excited electronic state dictates the

timescale of the molecular events that engage themselves in the excited state properties. The different time scales of motions demand different probes; for example, slower motions like the ones that occur in viscous glass demand using long-lifetime chromophores as compared to say if the medium was water (Lakowicz, 1999). Considering the two commonly used probes erythrosin B and tryptophan where unquenched lifetimes are 25 ms and 6.5 s and when embedded in a glassy matrix could provide different information based on the time window. Also the mechanism of quenching of the triplet state of each probe could affect what motions are detection.

The dynamic complexity of amorphous sucrose arises from many modes of molecular mobility occurring on different time scales. This research focuses on using three different probes erythrosin B ($\tau_{77K} = 25$ ms), tryptophan ($\tau_{77K} = 6$ s) and vanillin ($\tau_{77K} = 372$ ms) with varied excited state lifetime to study molecular mobility within glassy and melt state in amorphous sucrose films using phosphorescence spectroscopy. Thus phosphorescence from each probe is utilized to measure molecular mobility on three different time scales corresponding to each probe.

References

- Craig, D. Q., Royall, p. g., Kett, V. L. and Hopton, M. L. The relevance of the amorphous state of pharmaceutical dosage forms: glassy drugs and freeze dried systems. *International Journal of Pharmaceutics*. 179 (1999). 179-207.
- Crowe, J. H., Carpenter J. F. and Crowe, L. M. The role of vitrification in anhydrobiosis. *Annual Review Physiology*. 60 (1998). 73-103.
- Ediger, M. D., Angell, C. A. and Nagel, S. R. Supercooled Liquids and Glasses. *Journal of Physical Chemistry*. 100 (1996). 13200-13212.
- Fennema, O. *Water and Ice*. New York: Marcel Dekker Inc. (1996).
- Goff, H. D. and Sahagian, M. E. Glass transition in aqueous carbohydrate solutions and their relevance to frozen stability. *Thermochimica Acta*. 280/281 (1996). 449-464.
- Hancock, B. C. and Zografi, G. Characteristics and significance of amorphous state in pharmaceutical systems. *Journal of Pharmaceutical Sciences*. 86 (1997). 1-12.
- Hill, J. J., Shalaev, E. Y. and Zografi, G. Thermodynamic and dynamic factors involved in the stability of native proteins structure in amorphous solids in relation to levels of hydration. *Journal of Pharmaceutical Sciences*. 94 (2005). 1636-1667.
- Labuza, T., Roe, K., Payne, C., Panda, F., Labuza, T. J., Labuza, P. S. and Krusch, L. Storage stability of dry food systems: influence of state changes during drying and storage. *Proceedings of the 14th international drying symposium (IDS 2004) Sao Paulo Brazil. 22-25 Aug. A (2004). 48-68.*
- Lakowicz, J. R. *Principles of Fluorescence Spectroscopy*. Second ed. New York: Kluwer Academic/Plenum Press. (1999).
- Le Meste, M., Champion, D., Roudaut, G., Blond, G. and Simatos, D. Glass transition and food technology: A critical appraisal. *Journal of Food Science*. 67 (2002). 2444-2458.
- Ludescher, R. D. Molecular dynamics of food proteins: Experimental techniques and observations. *Trends in Food Science and Technology*. 1 (1990). 145-149. 1990.
- Noel, T. R., Parker, R. and Ring, S. G. Effect of molecular structure and water content on the dielectric relaxation behavior of amorphous low molecular weight carbohydrates above and below their glass transition. *Carbohydrate Research*. 329 (2000). 839-845.
- Parker, C. A. *Photoluminescence of Solutions*. Amsterdam: Elsevier Pub Co. (1968).

- Pravinata, L. C. Molecular Mobility of Amorphous Sucrose Detected by Phosphorescence of Erythrosin B and Eosin Y. Diss. Rutgers University, NJ. (2003).
- Pravinata, L. V., You, Y. and Ludescher, R. D. Erythrosin B phosphorescence monitors molecular mobility and dynamic heterogeneity in amorphous sucrose. *Biophysical Journal*. 88 (2005). 3551-3561.
- Roos, Y. Phase Transitions in Foods. San Diego, California: Academic Press. (1995).
- Shah, N. K. and Ludescher, R. D. Influence of hydration on the internal dynamics of hen egg white lysozyme in the dry state. *Photochemistry and Photobiology*. 58 (1993). 169-174..
- Shirke, S. and Ludescher, R. D. Dynamic site heterogeneity in amorphous maltose and maltitol from spectral heterogeneity in erythrosin B phosphorescence. *Carbohydrate Research*. 340 (2005). 2661-2669.
- Shirke, S. and Ludescher, R. D. Dynamic site heterogeneity in amorphous lactose and lactitol from spectral heterogeneity in erythrosin B phosphorescence. *Biophysical Chemistry*. 123 (2006). 122-133.
- Slavik, J. Fluorescent Probes in Cellular and Molecular Biology. Boca Raton, FL: CRC Press. (1994).
- Vyazovkin, S. and Dranca, I. Probing beta relaxations in pharmaceutically relevant glasses by using DSC. *Pharmaceutical Research* 23 (2006): 422-428.

Chapter VI a: Molecular mobility in amorphous sucrose films detected using phosphorescence of erythrosin B.

Introduction

Erythrosin B has 98% of excited molecules converting to triplet state and has high quantum yield (Garland and Moore, 1979) and is considered as an ideal probe for phosphorescence studies. The phosphorescence of erythrosin B is due to the xanthene ring with four iodine atoms. Erythrosin B has phosphorescence emission time scale of 10^{-5} to 10^{-3} s corresponding to motion in glassy environment and is sensitive to oxygen (Lam S.K et al 2001). Phosphorescence from Erythrosin B has been shown to be sensitive in monitoring molecular mobility in many simple model amorphous systems and thus it definitely offers a good choice as a probe (Pravinata et al., 2005; Shirke and Ludescher, 2005, 2006a, 2006b; Simon-Lukasik and Ludescher, 2006a, 2006b, 2004).

Erythrosin B (acid form) has been used to monitor molecular mobility in many simple amorphous systems such as sucrose (Pravinata et al., 2005; Shah and Ludescher, 1995), gelatin (Simon-Lukasik and Ludescher, 2006a, 2006b), bovine serum albumin (Nack and Ludescher, 2006), and glucose, maltose and maltotriose (Shirke and Ludescher, 2006a, 2006b). Measurements of phosphorescence emission and lifetime from erythrosin isothiocyanate-labeled gelatin in amorphous solid films have indicated its utility to monitor oxygen diffusion (Simon-Lukasik and Ludescher, 2006a, 2006b). Erythrosin B has also being used to study plasticizer effect on molecular mobility (Simon-Lukasik and Ludescher, 2006a) and dynamic site heterogeneity (Simon-Lukasik and Ludescher, 2006b) in amorphous gelatin films. Erythrosin B has also been used to detect dipolar

relaxation and dynamic site heterogeneity in sugars and sugar alcohols (Shirke and Ludescher, 2005).

The numerous studies in our lab have used erythrosin B free acid form which is soluble in DMF and sodium salt of erythrosin B which is soluble in water (Yumin You: Unpublished data); this research explores the potential of using sodium form of erythrosin B which is water soluble. This research is focused on generating mobility maps in amorphous sucrose films using phosphorescence of sodium form of erythrosin B and comparing it to similar measurements made using tryptophan and vanillin as molecular probes.

Materials and Methods

Sucrose Solution: Sucrose solution was made as described in Pravinata et al 2005. Approximately 20 g of sucrose (99.5% pure; Sigma Chemical, St. Louis, MO) were dissolved in 100 mL of deionized water containing 0.5 g of activated charcoal to remove luminescent impurities. After stirring overnight, the charcoal was removed by vacuum filtration using ashless filter paper (Whatman No. 40, Whatman International, Maidstone, UK), additional charcoal was added, and the process repeated. Sucrose solution was made to a final concentration of 65–67 wt % sucrose; concentration was confirmed using a refractometer (NSG Precision Cells, Farmingdale, NY). This sucrose solution was filtered through a 0.2 μm membrane to remove particulates.

Erythrosin B: A 50mM stock solution of erythrosin B (Molecular Probes, Inc., Eugene, OR) was prepared in distilled deionized water. This concentration was selected to simplify the addition of the probe to the sucrose solution. For measuring phosphorescence in amorphous sucrose films, erythrosin B was added to the sucrose solution at a molar ratio of 1:10⁴ (dye: sucrose). The ratio 1:10⁴ (dye: sucrose) was chosen as at this concentration it was determined that the probe does not aggregate, existing only as individual molecules monitoring the molecular mobility of the sucrose.

Sucrose films: To produce glassy sucrose films containing vanillin, 20 μL of a sucrose solution containing erythrosin B were spread on a quartz slide (30 \times 13.5 \times 0.6 mm; custom made by NSG Precision Cells, Farmingdale, NY). After spreading the solutions on the slides were then dried under a heat gun (Vidal Sassoon) for 5 min to a maximum

temperature of $\sim 88^{\circ}\text{C}$ (measured using a thermocouple probe) and the final thickness was ~ 0.05 mm. The slides were stored at room temperature against P_2O_5 and Drierite, protected from the light to prevent any photo bleaching, for at least 7 days before any phosphorescence measurements were made. The desiccant was refreshed as needed to maintain a relative humidity close to 0%.

Instrumentation: Measurements were made on a Cary Eclipse fluorescence spectrophotometer (Varian Instruments, Walnut Creek, CA). This instrument, which collects in analog mode, uses a high intensity pulsed lamp and a time delay was employed to avoid any fluorescence during the lamp pulse. The temperature was controlled by using a TLC 50 thermoelectric heating/cooling system (Quantum Northwest, Spokane, WA). The TLC-50 sample compartment was fitted with a jacketed cover. The measurements were made in absence of oxygen (Nitrogen was purged for 15 minutes). Nitrogen stream was generated by passage of high purity nitrogen through a Supelco (Bellefonte, PA) carrier gas purifier. Quartz slides were placed in the standard 1cm x 1cm x 1cm quartz fluorescence cuvette, which was capped with a lid having inlet and outlet ports of gas lines.

Luminescence Measurements: The Cary Eclipse uses a pulsed lamp and collects emission intensity in analog mode; data were not collected within the first 0.1-0.2 ms to suppress fluorescence coincident with the lamp pulse. Delayed luminescence emission spectra were collected from 535 to 800 nm (10 nm bandwidth) using excitation at 500 nm (20nm bandwidth) over the temperature range from -20°C to 100°C . Each data point was

collected from a single flash with 0.2 ms delay, 5 ms gate time, and 0.2 s total decay time. The phosphorescence spectra collected as a function of temperature in the presence of nitrogen, were converted to intensity versus frequency (cm^{-1}) and analyzed to obtain the peak frequency and spectral bandwidth using eq. (1) and (2) (Maroncelli and Fleming, 1987).

Lifetime measurements were made in the presence of nitrogen ($-\text{O}_2$) as a function of temperature. The samples were excited at 540 nm (20 nm bandwidth) and emission transients collected at 690 nm (20 nm bandwidth) at temperatures ranging from -20°C to 100°C . Each decay transient was the sum of 50 cycles, and for each cycle data was collected from a single lamp flash with a delay of 0.1 ms, 0.06 ms gate time and 6.0 ms total decay time. All measurements were made in quadruplicate.

Data Analysis

Emission Energy as a function of temperature: Delayed luminescence spectra collected were fitted to a sum of two log normal functions using the program Igor (Wavemetrics, Inc., Lake Oswego, OR). The emission peak energy (ν_p) and bandwidth (full-width-at-half-maximum, FWHM) of the emission bands were determined by fitting both delayed fluorescence and phosphorescence emission as a function of frequency (in cm^{-1}) to a log normal function Equation 1 (Maroncelli and Fleming, 1987).

$$I(\nu) = I_0 \exp \left\{ -\ln(2) \left[\ln(1 + 2b(\nu - \nu_p)/\Delta)/b \right]^2 \right\} \quad (1)$$

In this equation I_0 is the maximum emission intensity, ν_p is the peak energy (in cm^{-1}) of the emission maximum, Δ is a line width parameter, and b is an asymmetry parameter.

The FWHM is related to b and Δ (Maroncelli and Fleming, 1987) Equation 2.

$$\Gamma = \Delta \sinh(b)/b \quad (2)$$

Phosphorescence Intensity: Intensity decay transits were analyzed using a non-linear least squares iterative fitting procedure using the program Igor (Wavemetrics, Inc., Lake Oswego, OR). Fits were judged satisfactory if the r^2 values were in the range of 0.995-1.0, and the modified residual $[(\text{data-fit})/\text{data}^{1/2}]$ varied randomly about zero. Intensity decays were clearly non-exponential and were analyzed using a stretched exponential function or Kohlrausch-Williams-Watts (KWW) model. This model has being shown to be appropriate to describe the wide distribution of relaxation times (Champion et al., 2000) for the molecular processes that depopulate excited states in amorphous solids (Pravinata et al., 2005; Nack and Ludescher 2006; Sundaresan and Ludescher, 2007) Equation 3.

$$I(t) = I(0) \exp\{-(t/\tau)^\beta\} + C \quad (3)$$

Where $I(0)$ is the initial amplitude at time zero, τ is the Kohlrausch-Williams-Watt lifetime (Lindsey and Patterson, 1980), and β is the stretching exponent, which varies from 0 to 1 and quantifies the non-exponential nature of the decay, and C is a constant; β provides a measure of the width of the distribution of lifetimes required to fit the intensity decay; the smaller the value of β , the wider the distribution of lifetimes (Lindsey and Patterson, 1980).

Photo-physical Scheme: The phosphorescence lifetimes were interpreted in terms of the rate constants associated with the various processes that contribute to the de-excitation of the excited triplet state of the probe (Duchowicz et al., 1998) Equation 4.

$$\tau^{-1} = k_P = k_{RP} + k_{TS1} + k_{TS0} + k_Q [O_2] \quad (4)$$

In this expression, k_{RP} is the rate of radiative decay of the triplet state (phosphorescence) under anoxic condition; its value for erythrosin is $41s^{-1}$ (Lettinga et al., 2000; Duchowicz et al., 1998). The term k_{TS1} (Equation 5) is the rate for thermally activated reverse intersystem crossing from the triplet to the singlet excited state; it has an exponential dependence on the energy gap (ΔE_{TS}) between singlet and the triplet state:

$$k_{TS1}(T) = k_{TS1}^0 \exp(-\Delta E_{TS}/RT) \quad (5)$$

The value of ΔE_{TS} (Equation 6) was calculated from the slope of the natural logarithm of the ratio of the emission intensity due to delayed fluorescence (I_{DF}) and phosphorescence (I_P) plotted versus $1/T$; I_{DF} and I_P were determined from log normal analysis of the emission spectra.

$$d [\ln (I_{DF}/I_P)]/d(1/T) = \Delta E_{TS}/R \quad (6)$$

(Where $R = 8.314 \text{ J K}^{-1} \text{ mol}^{-1}$). The value of k_{TS1} was calculated from equation 5 using $k_{\text{TS1}}^0 = 3.0 \times 10^7 \text{ s}^{-1}$ and $\Delta E_{\text{TS}} = 31.9 \text{ kJ mol}^{-1}$. Intersystem crossing to the ground state S_0 , which reflects relaxation of the probe from the excited triplet state to the ground state without the emission of a photon, has rate k_{TS0} . The value of k_{TS0} was calculated from the lifetime in the presence of nitrogen ($-\text{O}_2$) (where $k_{\text{Q}} [\text{O}_2]$ is negligible) using Eq. 4. The rate of collisional quenching of the excited triplet state of the probe by oxygen is $k_{\text{Q}} [\text{O}_2]$.

Results

Delayed fluorescence and phosphorescence emission spectra: The delayed emission spectra of erythrosin B in amorphous films of sucrose at $1:10^4$ Ery B: sucrose mole ratio exhibited maxima at ~ 550 nm and 670 nm (Figure 1). Both the delayed fluorescence and phosphorescence bands shifted to longer wavelength (lower energy) at higher temperature. The delayed emission spectra were collected over the temperature range -20°C to 100°C. Delayed emission spectra showed a decrease in phosphorescence intensity as a function of temperature; the delayed fluorescence intensity increased continuously from -20°C to 100°C as expected from thermally stimulated processes (Parker, 1968). The effect of temperature on the phosphorescence emission intensity of erythrosin B in amorphous films of sucrose as a function of temperature is shown in Figure 2. The emission energy (Figure 4) decreased linearly in the glass at low temperature and the slope became more negative above the T_g of sucrose. This decrease is due to an increase in the average extent of matrix dipolar relaxation around the excited triplet state. The bandwidth increased gradually with temperature in the glass and much more dramatically in the melt, reflecting a large increase in the range of energetically distinct environments above T_g (Figure 4).

The intensity ratio when plotted as a Van't Hoff plot of $\ln(I_{DF}/I_P)$ vs. $1/T$ (using the maximum emission intensity determined from fitting spectra to a log-normal function) was linear over the entire range of measured temperature (with $R^2 > 0.995$ for all curves) with no systematic deviation (Figure 3), the slope provides an estimate of the energy gap, ΔE_{TS} , between the lowest triplet (T_1) and singlet state (S_1). The value of $\Delta E_{TS} = 33.3 \pm 0.4$

kJ mol^{-1} in presence of nitrogen in amorphous sucrose was significantly smaller than that measured in water ($36.9 \pm 0.6 \text{ kJ mol}^{-1}$) and 66wt % sucrose solution ($36.9 \pm 1 \text{ kJ mol}^{-1}$) (Pravinata et al., 2005). The value of $35.3 \pm 0.4 \text{ kJ mole}^{-1}$ in presence of nitrogen for ΔE_{TS} in amorphous sucrose films was significantly higher than for Ery B in ethanol (Duchowicz et al., 1998), $28.5 \text{ kJ mole}^{-1}$, suggesting solvent properties modulate the singlet-triplet energy gap. The value of $\Delta E_{\text{TS}} = 35.3 \pm 0.4 \text{ kJ mol}^{-1}$ of sodium form of Ery B (used in this work) in amorphous sucrose films was comparable to but slightly higher than the values for acid form of Ery B (Pravinata et al., 2005) in amorphous films of sucrose ($\Delta E_{\text{TS}} = 31.6 \pm 0.4 \text{ kJ mol}^{-1}$).

Phosphorescence intensity decay: Phosphorescence intensity decays in the presence of nitrogen for erythrosin B in amorphous films of sucrose were measured over the temperature range from -20°C to 100°C . The intensity decays are plotted in Figure 5 along with fits using a stretched exponential function. The modified residuals for these fits varied randomly around zero, indicating that the stretched exponential function provided a statistically satisfactory fit to these data. All intensity decay data over the temperature interval from -20°C to 100°C were well fitted using a stretched exponential function and two physically important parameter lifetime τ and stretching exponent β were obtained.

The stretched exponential lifetimes and exponent β are plotted as a function of temperature (Figure 6). The lifetime of erythrosin B decreased from 0.66 ms at -20°C to 0.011 ms at 100°C . These values are comparable ($\tau = 0.6$ up to 0°C and $\tau = 0.2$ at 100°C)

to the values for the acid form of erythrosin B in amorphous sucrose films (Pravinata et al., 2005). The lifetime decreased biphasically with increasing temperature, reflecting an increase in the rate of non-radiative decay of the excited triplet state T_1 due to an increase in both the rate of reverse intersystem crossing to S_1 (k_{TS1}) and the rate of non-radiative decay to the ground state S_0 (k_{TS0}). Lifetimes are higher at lower temperature indicating lower collisional quenching in the glass. At lower temperature the slope of lifetime versus temperature is small and at high temperature the slope increases, indicating small activation energy for quenching in the glass and large in the melt.

The stretching exponent β showed a similar trend as lifetime remaining constant at ~ 0.92 up to $\sim 60^\circ\text{C}$ and decreased at higher temperature to ~ 0.86 at 100°C (Figure 6). These values are comparable ($\beta = 0.92$ up to $\sim 50^\circ\text{C}$ and $\beta = 0.8$ at 100°C) to the values for the free acid form of erythrosin B in amorphous sucrose films (Pravinata et al., 2005). The decrease in β reflects a large increase in the width of the distribution of phosphorescence decay times and corresponding distribution of dynamically distinct probe environments.

Rate Constants: An Arrhenius plot of $\ln(k_p)$ as a function of inverse temperature (Figure 7) showed a distinct break at $\sim 60^\circ\text{C}$ in sucrose which is in close to T_g ($\sim 65^\circ\text{C}$) of sucrose. The slopes of the curve provide information about the activation (E_a) energy for collisional quenching processes in glass and melt. In the glass $E_a = 1.9 \text{ kJ mole}^{-1}$ and in the melt $E_a = 12.8 \text{ kJ mole}^{-1}$.

The values of k_{TS0} were calculated based on k_{RP} and k_{TS1} measure by Duchowick et al (1998) (Eq. 4 Materials and Methods). The k_{TS0} is a term that represents matrix mobility; the higher the k_{TS0} the higher the matrix mobility. The non radiative quenching rate was approximately constant at 1500 s^{-1} in the glass but increased dramatically in the melt, indicating that the non-radiative quenching rate can sense the large scale molecular mobility activated at the glass transition temperature. The magnitude of k_{TS0} , k_{RP} and k_P for Ery B in sucrose increased as shown in Figure 8. The Arrhenius plot of $\ln k_P$ shows a break at $\sim 60^\circ\text{C}$ suggesting a gain in mobility (Figure 7) The magnitude of k_{TS0} increased moderately at low and more dramatically at high temperature. The Arrhenius plot of $\ln k_{TS0}$ shows a break at $\sim 60^\circ\text{C}$ suggesting a gain in mobility (Figure 7). The slope of the Arrhenius plot provided information about the activation energy; the two activation energies E_A calculated were 1.2 kJ mol^{-1} at low and 10.2 kJ mol^{-1} at high temperature.

Discussion

The two general modes of matrix molecular mobility, dipolar relaxation and collisional quenching, modulate the emission energy and lifetime of the excited triplet state of erythrosin B (Pravinata et al., 2005; Simon-Lukasik and Ludescher, 2005; Shirke et al., 2005). The thermal response of the peak emission energy and bandwidth reflected the affect of temperature on the rate of dipolar relaxation around the excited triplet state of Ery B in amorphous sucrose films (Figure 4). In amorphous sucrose films the decrease in emission energy reflects an increase in the average extent of matrix dipolar relaxation around the excited triplet state. Temperature has a small effect on the emission energy in the glass as compared to the melt. The α -relaxation rate thus increases above T_g due to activation of translational motions. The large increase in FWHM at higher temperatures indicated inhomogeneous broadening corresponding to increase in the width of the distribution of energetically distinct matrix environments in the amorphous sucrose films.

The emission intensity and emission lifetime in absence of oxygen are directly modulated by the rates of radiative emission k_{RP} , of the reverse intersystem crossing to excited singlet state k_{TS1} , and of intersystem crossing to the ground state k_{TS0} . The value of k_{RP} is 41s^{-1} for Ery B, while k_{TS1} follows Arrhenius kinetics. The evaluation of various photophysical events in Ery B indicates decrease in lifetime with increase in temperature. This decrease is due to the increase in rate of molecular collision which results in increased quenching from interactions between the probe and the matrix (k_{TS0}) and by an increase in the rate of reverse intersystem crossing (k_{TS1}). The rate of intersystem crossing k_{TS0} which is modulated by the physical state of the amorphous matrix reflects

not only the way the excited triplet state is vibrationally coupled to the singlet ground state but also the way ground state vibrational energy is dissipated from the excited probe into the surrounding matrix.

The stretching exponent β is a measure of the dynamic heterogeneity of the matrix primarily due to variability in k_{TS0} . β remained constant at low temperatures suggesting that the distribution of dynamic environments in sucrose is fairly constant but at higher temperature the distribution broadened significantly as shown in Figure 6. The increase in lifetime distribution indicates the presence of dynamically distinct environments in amorphous sucrose upon heating above T_g .

The effect of temperature on the lifetime indicates that the non-radiative quenching rate increases dramatically in the melt above T_g which is due to an increase in the ability of the excited erythrosin B to dissipate vibrational energy into the matrix. This decrease is due to α -relaxations activated above T_g . The non radiative quenching rate varied from 1455.2 s^{-1} at -20°C to 3570.3 s^{-1} at 100°C . These values were comparable to those found for the acid form of erythrosin B dispersed in amorphous sucrose film (Pravinata et al., 2005). The non radiative quenching rate was approximately constant at 1500 s^{-1} in the glass which was much lower than for erythrosin B (acid form) in amorphous sucrose film (1600 s^{-1}) and much smaller than in water (3200 s^{-1}) (Duchowick et al., 1998). The constant value of the non radiative quenching rate in the glass indicates that erythrosin B indicates that amorphous sucrose films is less mobile in the glass, but the larger increase in the melt indicates that erythrosin B senses motions activated mainly at glass transition.

Conclusion

This study used steady-state and time-resolved phosphorescence of the sodium form of erythrosin B (water soluble) to monitor molecular mobility in thin films of amorphous sucrose as a function of temperature. The phosphorescence energy and intensity were all sensitive to localized molecular mobility on the microsecond timescales in the glass and to more global modes of mobility activated at the glass transition. The data was comparable with previous studies using acid form of erythrosin B (DMF soluble) dispersed in amorphous sucrose film. Erythrosin B as a triplet state probe indicates that the amorphous sucrose matrix gain mobility above T_g of sucrose.

The results from this research were used to make comparison with molecular mobility data from the probes tryptophan and vanillin dispersed in amorphous sucrose films. There data was also used to compare with the data on dual probes (Chapter VIII on erythrosin B and vanillin and Chapter IX erythrosin B and tryptophan) dispersed in amorphous sucrose films.

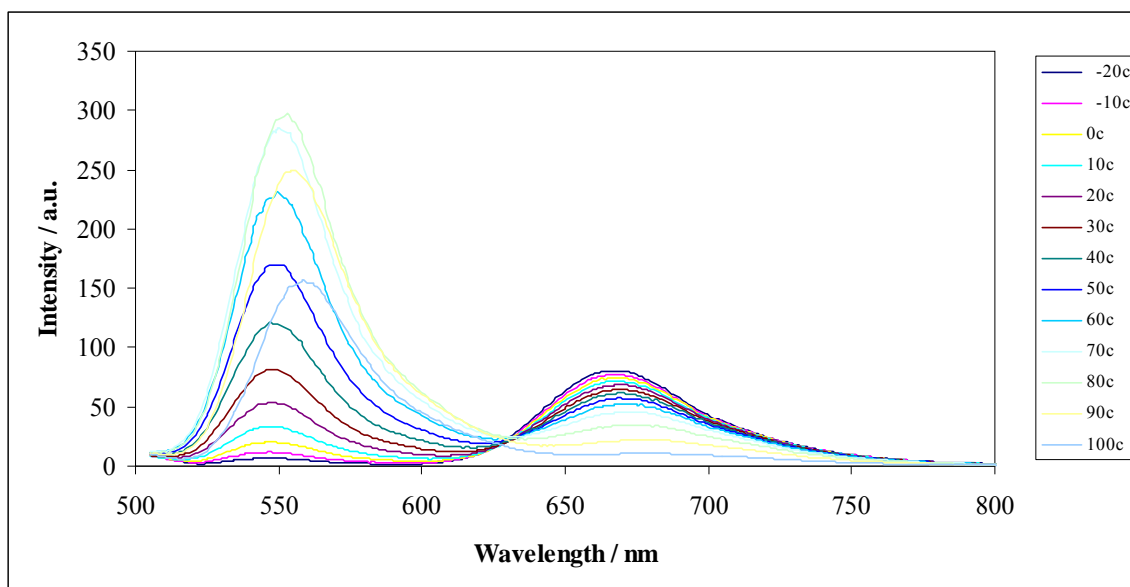
Figure VIa-1

Figure VIa-1: Delayed emission spectra of erythrosin B dispersed in amorphous films of sucrose as a function of temperature (excitation at 500 nm). The spectra were collected at 10°C intervals from -20°C to 100°C (the curves follow this order from high to low intensity at ~690 nm).

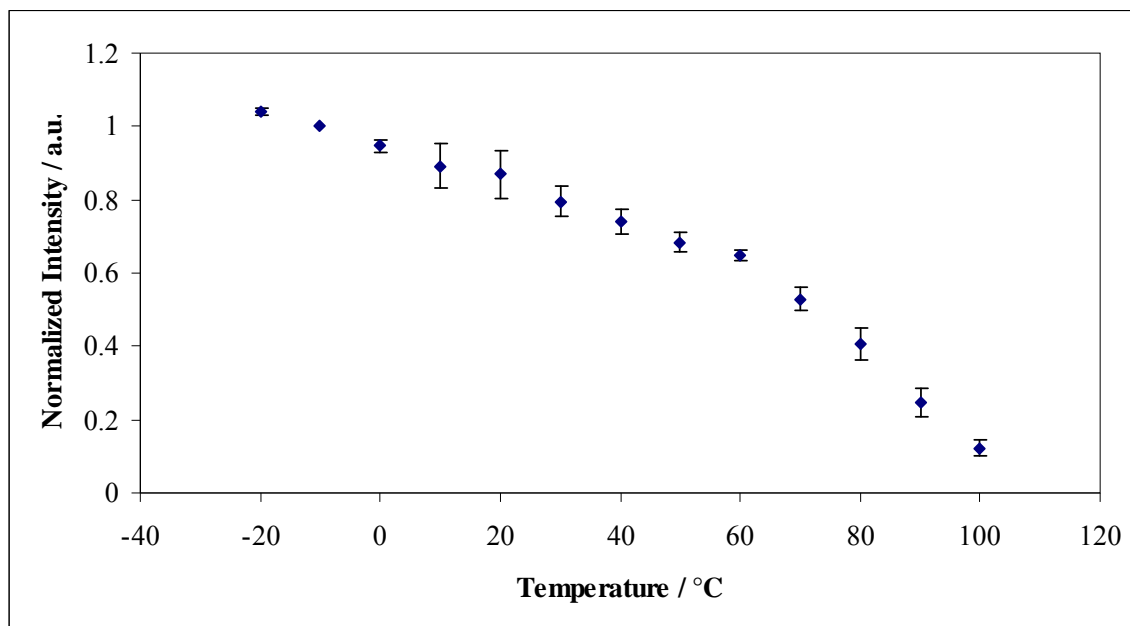
Figure VIa-2

Figure VIa-2: Intensity (I_p) was determined from analysis of the phosphorescence emission band (Figure 1) using a log-normal function (eq. (1), Materials and Methods). The effect of temperature on the phosphorescence emission intensity of erythrosin B in amorphous films of sucrose as a function of temperature equilibrated against nitrogen.

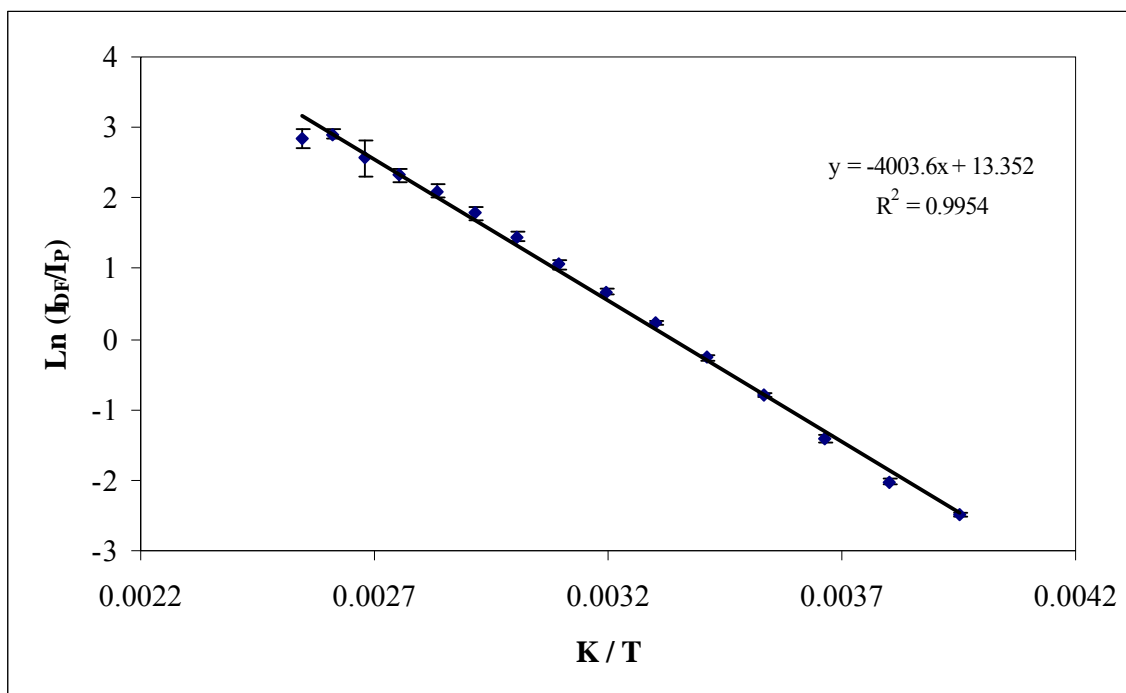
Figure VIa-3

Figure VIa-3: Plot of natural log of the intensity ratio between delayed fluorescence and phosphorescence in sucrose glass as a function of inverse temperature. $\Delta E_a = 33.29 \text{ KJ mol}^{-1}$.

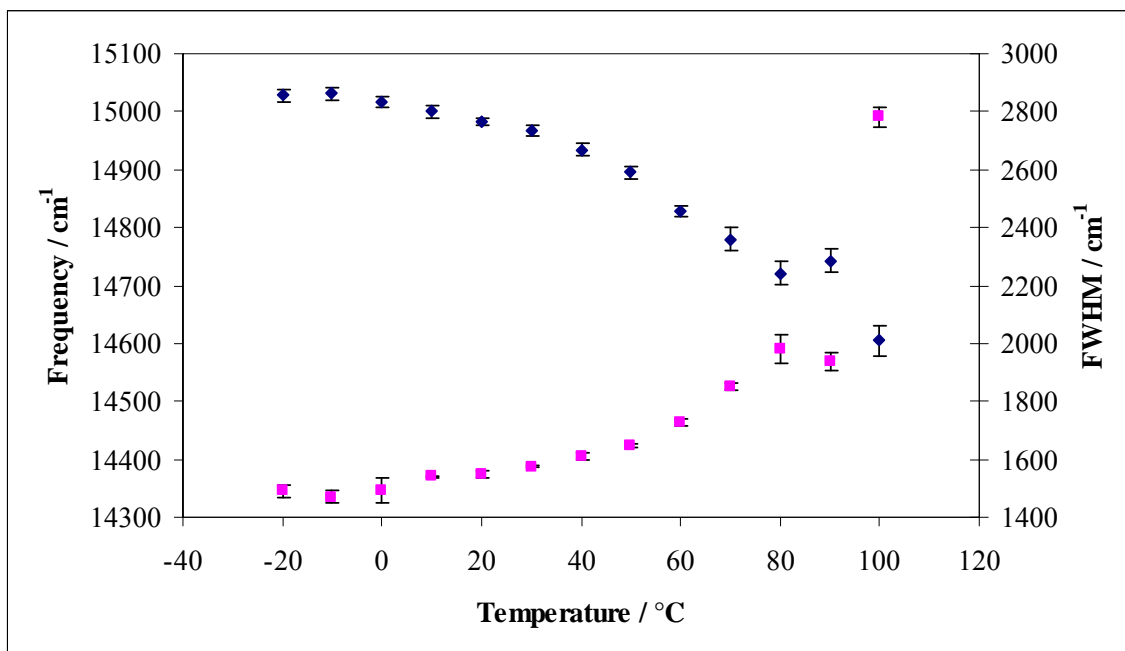
Figure VIa-4

Figure VIa-4: Peak energy ν_p (◆) and bandwidth (■) for phosphorescence emission from erythrosin B in amorphous films of sucrose as a function of temperature. The delayed emission spectra collected as a function of temperature (Figure 1) were analyzed using log-normal function as described in Materials and Methods using eq. (1) and (2).

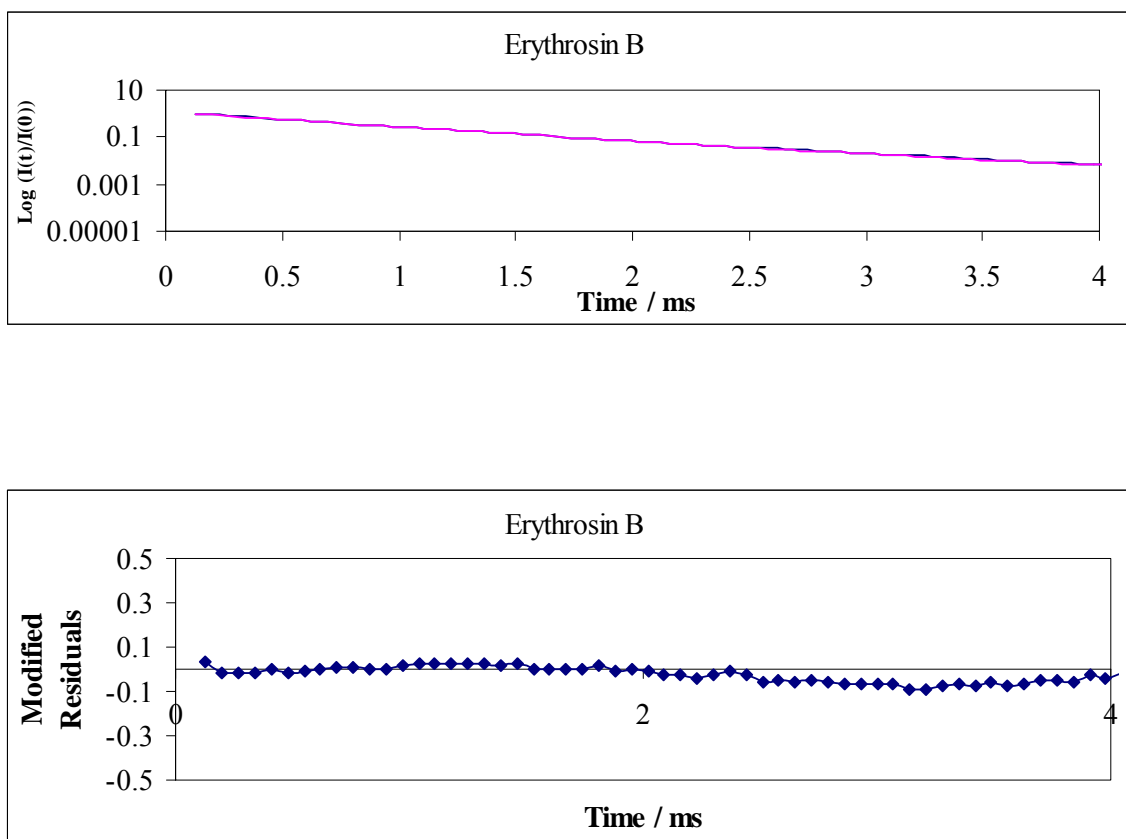
Figure VIa-5

Figure VIa-5: Normalized phosphorescence intensity decay $[I(t)/I(0)]$ of erythrosin B in dispersed in amorphous films of sucrose at 20°C in the presence of nitrogen. The solid line through the data is a fit using a stretch-exponential function (Eq. (3), Materials and Methods). A plot of modified residuals $[(\text{Data}-\text{Fit})/\text{Data}^{1/2}]$ for this fit is shown in the bottom graph.

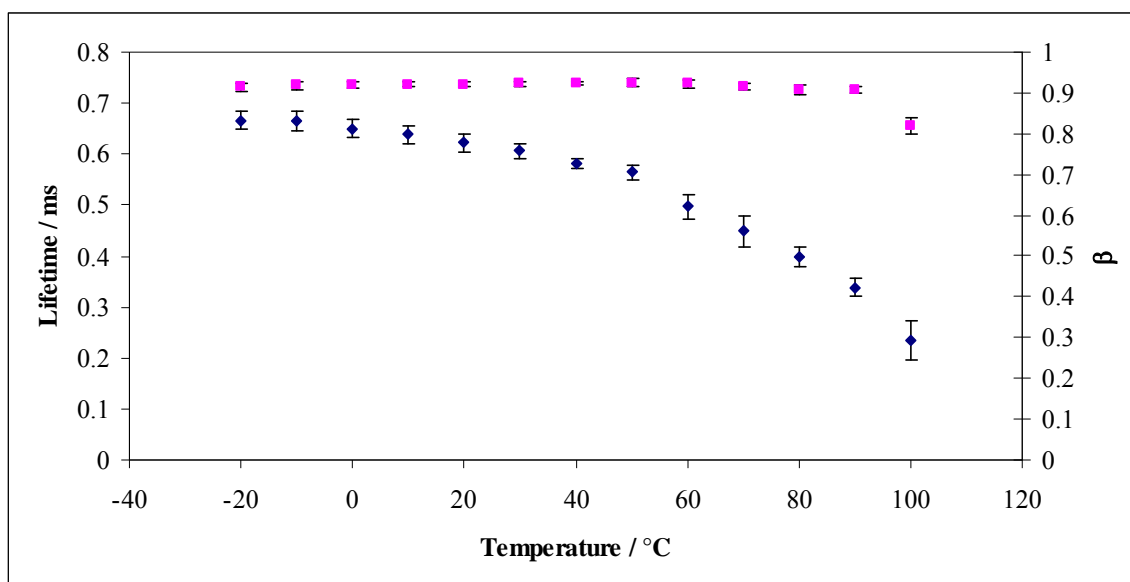
Figure VIa-6

Figure VIa-6: Temperature dependent of lifetime τ (\blacklozenge , left scale) and stretching exponent β (\blacksquare , right scale) from fits to a stretched exponential model of the intensity decay of erythrosin B in amorphous sucrose films.

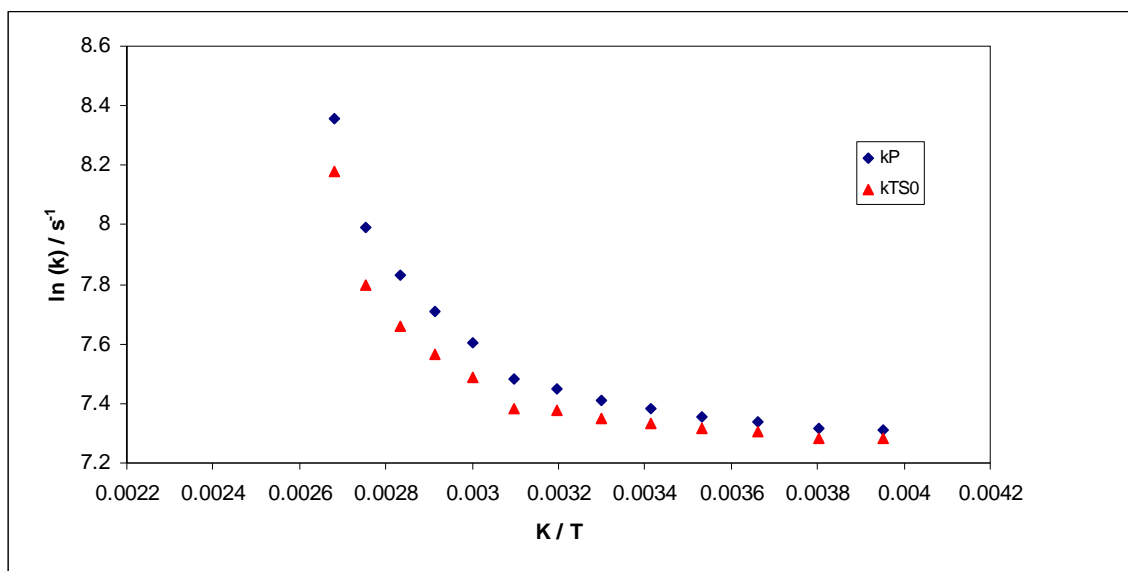
Figure VIa-7

Figure VIa-7: An Arrhenius plot of the lifetime τ of erythrosin B in amorphous films of sucrose as a function of inverse temperature. Lines drawn over the data points indicate slopes at low and high temperatures.

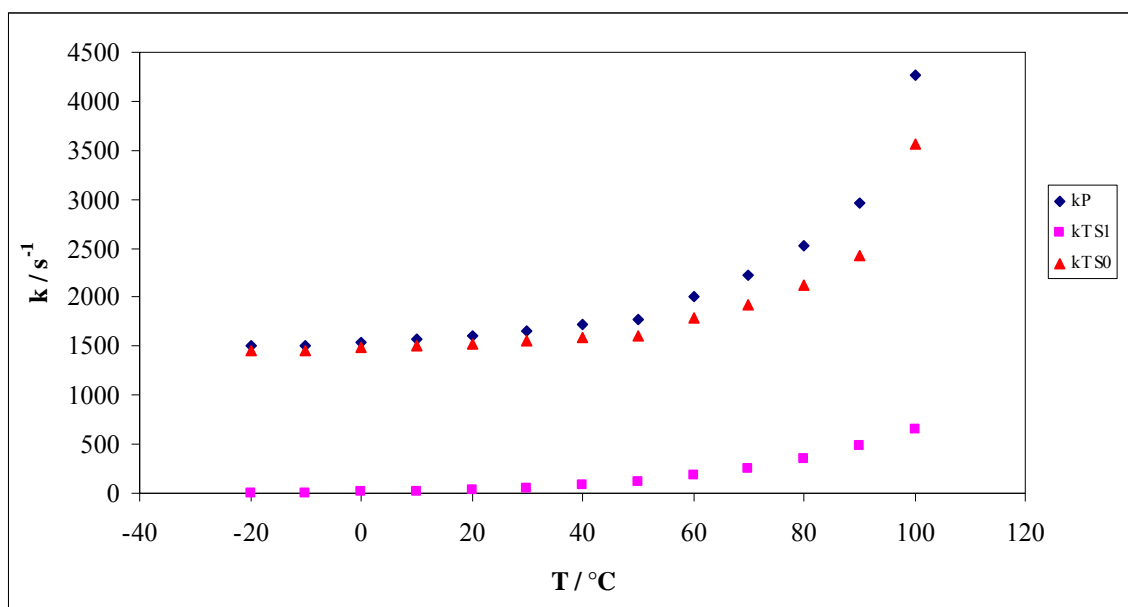
Figure VIa-8

Figure VIa-8: Temperature dependence of the total rate constant for non-radiative decay of the triplet state ($k = k_{RP} + k_{TS0} + k_{TS1}$, \blacklozenge), the rate of reverse intersystem crossing to S_1 (k_{TS1} , \blacksquare) and the rate of non-radiative decay to S_0 (k_{TS0} , \blacktriangle) of erythrosin B in amorphous sucrose over the temperature range from -20°C to 100°C : values were calculated from the lifetime data in Figure 6.

References

- Champion, D., Le Meste, M., and Simatos, D. Towards an improved understanding of glass transition and relaxations in foods: molecular mobility in the glass transition range. *Trends in Food Science and Technology*. 11 (2000). 41-55.
- Duchowicz, R., Ferrer, M.L. and Acuna, A.U. Kinetic spectroscopy of erythrosin phosphorescence and delayed fluorescence in aqueous solution at room temperature. *Photochemistry and Photobiology*. 68 (1998). 494-501.
- Fischer, C. J., Gafni, A., Steel, D. G. and Schauerte, J. A. The triplet-state lifetime of indole in aqueous and viscous environments: significance to the interpretation of room temperature phosphorescence in proteins. *Journal of the American Chemical Society*. 124 (2004). 10359-10266.
- Garland, P.B. and Moore, C.H. Phosphorescence of protein-bound eosin and erythrosin: A possible probe for measurements of slow rotational mobility. *Biochemistry Journal*. 183 (1979). 561-572.
- Lam, S.K., Chan, M.A. and Lo, D. Characterization of phosphorescence oxygen sensor based on erythrosin B in sol-gel silica in wide pressure and temperature ranges. *Sensors and Actuators. B* 73 (2001). 135-141.
- Lettinga, M.P., Zuilhof, H. and van Zandvoort, M.A. Phosphorescence and fluorescence characterization of fluorescein derivatives immobilized in various polymers matrices. *Physical Chemistry Chemical Physics*. 2 (2000). 3697-3707.
- Lindsey, C. P. and Patterson, G. D. Detailed comparison of the Williams-Watts and Cole-Davidson functions. *Journal of Chemical Physics*. 2 (1980). 3348-3357.
- Ludescher, R.D., Shah, N.K., McCaul, C.P. and Simon, K.V. Beyond T_g: optical luminescence measurements of molecular mobility in amorphous solid foods. *Food Hydrocolloids*. 15 (2001). 331-339.
- Maroncelli, M. and Fleming, G. R. Picosecond salvation dynamics of coumarin 153: The importance of molecular aspects of salvation. *Journal of Chemical Physics*. 86 (1987). 6221-6239.
- Nack, T.J. and Ludescher, R.D. Molecular mobility and oxygen permeability in amorphous bovine serum albumin films. *Food Biophysics*. 1 (2006). 151-162.
- Parker C.A. *Photoluminescence of Solutions*. Amsterdam: Elsevier Pub Co., 1968.
- Pravinata, L.C. *Molecular Mobility of Amorphous Sucrose Detected by Phosphorescence of Erythrosin B and Eosin Y*. Dissertation, Rutgers University, NJ, 2003.

- Pravinata, L.V., You, Y. and Ludescher, R.D. Erythrosin B phosphorescence monitors molecular mobility and dynamic heterogeneity in amorphous sucrose. *Biophysical Journal*. 88 (2005). 3551-3561.
- Shah, N.K. and Ludescher, R.D. Phosphorescence of probes of the glassy state in amorphous sucrose. *Biotechnology Progress*. 11 (1995). 540-544.
- Shirke, S. and Ludescher, R.D. Dynamic site heterogeneity in amorphous maltose and maltitol from spectral heterogeneity in erythrosin B phosphorescence. *Carbohydrate Research*. 340 (2005). 2661-2669.
- Shirke, S. and Ludescher, R.D. Dynamic site heterogeneity in amorphous lactose and lactitol from spectral heterogeneity in erythrosin B phosphorescence. *Biophysical Chemistry*. 123 (2006). 122-133.
- Shirke, S. and Ludescher, R.D. Molecular mobility and glass transition in amorphous glucose, maltose and maltotriose. *Carbohydrate Research*. 340 (2006). 2654-2660.
- Simon-Lukasik, K.V. and Ludescher, R.D. Effect of plasticizer on dynamic site heterogeneity in cold-cast gelatin films. *Food Hydrocolloids*. 20 (2006). 88-95.
- Simon-Lukasik, K.N. and Ludescher, R.D. Molecular mobility in water and glycerol plasticized cold and hot cast gelatin films. *Food Hydrocolloids*. 20 (2006). 96-105.
- Simon-Lukasik, K.V. and Ludescher, R.D. Erythrosin B phosphorescence as a probe of oxygen diffusion in amorphous gelatin films. *Food Hydrocolloids*. 18 (2004). 621-630.
- Sundaresan, K.V. and Ludescher, R. D. Molecular mobility and oxygen permeability in amorphous beta-lactoglobulin films. *Food Hydrochlorides*. 22 (2007). 403-413.
- Vanderkooi, J. M. and Berger, J. W. Excited triplet state used to study biological macromolecules at room temperature. *Biochimica et Biophysica Acta: Bioenergetics*. 976 (1989). 1-27.

Chapter VI b: Molecular mobility in amorphous sucrose films detected using phosphorescence of tryptophan.

Introduction

Tryptophan is a naturally occurring amino acid which has been shown to exhibit strong room temperature phosphorescence emission after excluding oxygen (Vanderkooi et al., 1987). Tryptophan phosphorescence has being found to be sensitive to the physical properties of the local environment (Ludescher, 2001; Strambini and Gonnelli, 1985). The long lifetime of this probe help detect molecular motions presence in the rigid, glassy regions within even fully hydrated proteins (Shah and Ludescher, 1992, 1993) Also the triplet state of indole has being shown to have a strong dependence on the radiation-less deactivation rate which depends on medium viscosity. The lifetime of tryptophan decreases from 6.5s in a glassy matrix at 77K to 1.2 ms in aqueous solutions at ambient temperature (Strambini and Gonnelli, 1995).

Tryptophan phosphorescence, for example, has been used to study the internal mobility of proteins in solution (Papp and Vanderkooi, 1989) and in the solid state (Shah and Ludescher, 1995) on the milliseconds to second timescale. Phosphorescence of tryptophan has being used to monitor molecular mobility of lysozyme (Shah and Ludescher 1992, 1993). Previous studies have being conducted where phosphorescence from the luminescent chromophores tryptophan (McCaul and Ludescher, 1999) and N-acetyltryptophanamide (NATA) (Shah and Ludescher, 1995) was used to probe the molecular dynamics of the glassy state and the glass-to-rubber transition in amorphous sucrose. Tryptophan has also being used to study molecular mobility in amorphous films

of sucrose, maltose and trehalose where sucrose was found to be the most mobile matrix among the three (Zunic, 2004).

This research focuses on the molecular mobility of amorphous sucrose using tryptophan as a molecular phosphorescence probe and compares it to similar measurements made in amorphous sucrose films using Erythrosin B and vanillin as molecular probes.

Materials and Methods

Sucrose Solution: Sucrose solution was made as described in Pravinata et al 2005. Approximately 20 g of sucrose (99.5% pure; Sigma Chemical, St. Louis, MO) were dissolved in 100 mL of deionized water containing 0.5 g of activated charcoal to remove luminescent impurities. After stirring overnight, the charcoal was removed by vacuum filtration using ashless filter paper (Whatman No. 40, Whatman International, Maidstone, UK), additional charcoal was added, and the process repeated. Sucrose solution was made to a final concentration of 65–67 wt % sucrose; concentration was confirmed using a refractometer (NSG Precision Cells, Farmingdale, NY). This sucrose solution was filtered through a 0.2 μm membrane to remove particulates.

Tryptophan: A 50mM stock solution of tryptophan (Sigma Chemical, St. Louis, MO) was prepared in distilled deionized water. This concentration was selected to simplify the addition of the probe to the sucrose solution. For measuring phosphorescence in amorphous sucrose films, tryptophan was added to the sucrose solution at a molar ratio of 1:500 (dye: sucrose). The ratio 1:500 (dye: sucrose) was chosen as at this concentration it was determined that the probe does not aggregate, existing only as individual molecules monitoring the molecular mobility of the sucrose.

Sucrose films: To produce glassy sucrose films containing vanillin, 20 μL of a sucrose solution containing tryptophan were spread on a quartz slide ($30 \times 13.5 \times 0.6$ mm; custom made by NSG Precision Cells, Farmingdale, NY). After spreading the solutions on the slides were then dried under a heat gun (Vidal Sassoon) for 5 min to a maximum

temperature of $\sim 88^{\circ}\text{C}$ (measured using a thermocouple probe) and the final thickness was ~ 0.05 mm. The slides were stored at room temperature against P_2O_5 and Drierite, protected from the light to prevent any photo bleaching, for at least 7 days before any phosphorescence measurements were made. The desiccant was refreshed as needed to maintain a relative humidity close to 0%.

Instrumentation: Measurements were made on a Cary Eclipse fluorescence spectrophotometer (Varian Instruments, Walnut Creek, CA). This instrument, which collects in analog mode, uses a high intensity pulsed lamp and a time delay was employed to avoid any fluorescence during the lamp pulse. The temperature was controlled by using a TLC 50 thermoelectric heating/cooling system (Quantum Northwest, Spokane, WA). The TLC-50 sample compartment was fitted with a jacketed cover. The measurements were made in absence of oxygen (Nitrogen was purged for 15 minutes). Nitrogen stream was generated by passage of high purity nitrogen through a Supelco (Bellefonte, PA) carrier gas purifier. Quartz slides were placed in the standard 1cm x 1cm x 1cm quartz fluorescence cuvette, which was capped with a lid having inlet and outlet ports of gas lines.

Luminescence Measurements: The Cary Eclipse uses a pulsed lamp and collects emission intensity in analog mode; data were not collected within the first 0.1-0.2 ms to suppress fluorescence coincident with the lamp pulse. Delayed luminescence emission spectra were collected from 350 to 600 nm (10 nm bandwidth) using excitation at 280 nm (20nm bandwidth) over the temperature range from -20°C to 100°C . Each data point was

collected from fifty flashes with 0.2 ms delay, 10 ms gate time, and 1.0 s total decay time. The phosphorescence spectra collected as a function of temperature in the presence of nitrogen, were converted to intensity versus frequency (cm^{-1}) and analyzed to obtain the peak frequency and spectral bandwidth using Eq. (1) and (2) (Maroncelli and Fleming 1987).

Lifetime measurements were made in the presence of nitrogen ($-\text{O}_2$) as a function of temperature. The samples were excited at 280 nm (20 nm bandwidth) and emission transients collected at 455 nm (20 nm bandwidth) at temperatures ranging from -20°C to 100°C . Each decay transient was the sum of 50 cycles and for each cycle data was collected from a single lamp flash with a delay of 0.2 ms. Windows for gate time and total decay time were varied at each temperature. All measurements were made in quadruplicate.

Data Analysis

Emission Energy as a function of temperature: Emission spectra were fit using the program Igor (Wavemetrics, Inc., Lake Oswego, OR) to a three log-normal function over the temperature range -10°C to 50°C and one log-normal function over the temperature range -60°C to 100°C Equation 1.

$$I(\nu) = I_0 \exp \left\{ -\ln(2) \left(\frac{\ln[1 + 2b(\nu - \nu_p) / \Delta]}{b} \right)^2 \right\} \quad (1)$$

In this equation I_0 is the maximum intensity of the emission spectra, ν_p is the frequency (in cm^{-1}) of the emission maximum, Δ is a line width parameter, and b is an asymmetry parameter. The bandwidth of the emission, the full width at half maximum (Γ), is related to b and Δ Equation 2.

$$\Gamma = \Delta \left(\frac{\sinh(b)}{b} \right) \quad (2)$$

Phosphorescence Intensity: Phosphorescence lifetimes were determined with the statistical program Igor (Wavemetrics, Inc., Lake Oswego, OR). The phosphorescence intensity decay were collected as described above and were fitted using a stretched exponential function and multi-exponential functions (Chen, 2003; Shamblin et al., 2000). Fits were judged satisfactory if the r^2 values were in the range of 0.995-1.0 and the modified residuals $((\text{data} - \text{fit})/\text{data}^{1/2})$ varied randomly about zero.

Multi-exponential function: The phosphorescence intensity decay were collected as described above and were also fitted using a multi-exponential functions. The multi-

exponential model is as show in Equation 3. τ_i are decay times, α_i represent the amplitudes of the components at $t = 0$ and n is the number of decay times. The average lifetime was calculated using Equation 4.

$$I(t) = \sum_{i=1}^n \alpha_i \exp(-t/\tau_i) \quad (3)$$

$$\tau_{\text{Avg}} = \sum_{i=1}^n \alpha_i \tau_i / \sum_{i=1}^n \alpha_i \quad (4)$$

Stretched exponential function: Intensity decays were analyzed using a stretched exponential function or Kohlrausch-Williams-Watts (KWW) model equation 5. This model has being shown to be appropriate to describe the wide distribution of relaxation times (Champion et al., 2000) for the molecular processes that depopulate excited states in amorphous solids (Pravinata et al., 2005; Nack and Ludescher, 2006; Sundaresan and Ludescher, 2007; Shirke and Ludescher, 2006a, 2006b). The average lifetime was calculated using Equation 6.

$$I(t) = I(0) \exp\{-(t/\tau_i)^{\beta_i}\} + C \quad (5)$$

$$\tau_{\text{Avg}} = \tau \cdot \Gamma(1/\beta)/\beta \quad (6)$$

Where $I(0)$ is the initial amplitude at time zero, τ is the Kohlrausch-Williams-Watt lifetime (Lindsey and Patterson, 1980), and β is the stretching exponent, which varies from 0 to 1 and quantifies the non-exponential nature of the decay, and C is a constant; β provides a measure of the width of the distribution of lifetimes required to fit the intensity decay; the smaller the value of β , the wider the distribution of lifetimes.

Photophysical Scheme: The lifetime is the average amount of time a molecule spends in the excited state. There are several different deactivation processes via phosphorescence emission (with rate constant k_{RP}), non-radiative relaxation (K_{TS0}) and collisional quenching ($k_{\text{Q}} [Q]$). The phosphorescence lifetimes were used to calculate the rate constants associated with the various processes that depopulate the excited triplet state. The lifetime τ is related to the rate constants for de-excitation of the triplet excited state of the probe according to the following Equation 7 (Papp and Vanderkooi, 1989).

$$1/\tau = k_{\text{RP}} + k_{\text{NR}} + k_{\text{Q}} [Q] = k_{\text{P}} \quad (7)$$

Here $k_{\text{P}} (=1/\tau)$ is the total decay rate. The rate of radiative decay k_{RP} of the ground state is fixed and not influenced by the matrix. k_{NR} is the rate of non-radiative decay to the singlet state followed by vibrational relaxation to S_0 due to collisional quenching. The magnitude of k_{NR} reflects factors associated with the mechanism by which the excited T_1 state is coupled to highly excited vibrations of the S_0 ground state as well as external

factors associated with the mechanism by which the ground state vibrational energy can dissipate from the excited state into the surrounding matrix (Fischer, 2002; Vanderkooi and Berger, 1989). As the efficiency of external vibrational dissipation is related to overall mobility of the matrix, the magnitude of k_{NR} provides a measure of matrix mobility. One common method for restricting the collisional deactivation is to super cool analyte solutions with liquid nitrogen to a rigid glass. The term $k_Q [Q]$ refers to the collisional quenching due to interaction between the excited chromophore and quencher. Oxygen is an efficient quencher of tryptophan phosphorescence i.e. it reduces the intensity and lifetime. Therefore the measurements were conducted under N_2 atmosphere. The collisional quenching rate constant can thus be excluded in the absence of a quencher molecule, and equation 7 simplified to.

$$1/\tau = k_{RP} + k_{NR} = k_P \quad (8)$$

The phosphorescence emission rate constant k_{RP} for tryptophan is known ($1/6 \text{ s}^{-1}$) (Bishai et al., 1967). It is obtained from the lifetime of tryptophan at temperature where non-radiative rates are negligible (77K).

Results

Phosphorescence emission spectra: Figure 1 is a plot of phosphorescence emission spectra of tryptophan in sucrose as a function of temperature ranging from -10°C to 80°C. The emission spectra were fitted using a three log-normal function (Equation 1, Materials and Methods).

The normalized plots of phosphorescence intensity versus temperature are shown in Figure 2. The plot shows that as the temperature increases the peak intensity of the emission spectra decreases. The decrease in intensity with increase in temperature is due to increase in mobility within the glassy matrix and in the melt above T_g of sucrose. The peak frequencies PF1, PF2 and PF3 (Figure 3) decreased very gradually in the glass at low temperature. Above 50°C the emission spectra broadened and was fitted to a log-normal one function (PF2). The PF2 shows dramatic decrease and the slope becomes more negative above T_g of sucrose. This decrease is due to increase in the average extent of matrix dipolar relaxation around the excited triplet state. The bandwidths FWHM1, FWHM2 and FWHM3 increased gradually with temperature in the glass and much more dramatically in the melt, reflecting a large increase in the range of energetically distinct environments above T_g (Figure 3). Thus the decrease in emission energy and the broadening of emission spectra with an increase in temperature can be explained with a solvent relaxation mechanism. With increase in temperature the reorientation of dipoles of sucrose molecules around tryptophan's excited state became faster.

Phosphorescence lifetime as a function of temperature: The phosphorescence intensity decays collected as a function of temperature were fitted using both multi-exponential and a sum of two stretched exponential functions (eq. 3 and 5 Materials and Methods). These lifetimes reflect the ensemble average because the peak excitation and peak emission wavelength were used. The intensity decays are plotted in Figure 4a and 4b along with fits using a multi-exponential or stretched exponential function, respectively. The modified residuals for these fits varied randomly around zero, indicating that these functions each provided a statistically satisfactory fit to these data (Figure 4a and 4b). The lifetime is the average time a molecule spends in the excited state and is the indicator of the rigidity of the matrix.

Multi-exponential fit: All intensity decay data over the temperature interval from -10°C to 100°C were well fitted using multi-exponential function and two physically important parameters lifetime τ and amplitude α were obtained. The lifetimes of tryptophan as a function of temperature are shown in Figure 5a. The log plots of lifetimes of tryptophan as a function of temperature are shown in Figure 5b. In case of multi-exponential function the four lifetime components at 20°C were $\tau_1 = 2587$ ms, $\tau_2 = 625.3$ ms, $\tau_3 = 118.84$ ms and $\tau_4 = 16.3$ ms indicating the presence of local environments with ~ 160 fold difference in mobility. A plot of the amplitudes of each lifetime component as a function of temperature is as shown in Figure 6a. The amplitudes of longer lifetime components decreased and that of shorter lifetime components increased as a function of temperature. The long lifetime components contributed 50-6% and the short components contributed 50-84% to the emission as a function of temperature. Above T_g ($\sim 65^{\circ}\text{C}$) a majority of the

contribution almost ~80% was from shorter lifetime whereas the rest ~20% was from longer lifetime component.

The average lifetime calculated using Eq. 4 is plotted in Figure 8a. An Arrhenius plot of the average lifetime, Figure 10a shows transition points at 30°C. An Arrhenius plot of the inverse of individual lifetime components τ_1 , τ_2 , τ_3 and τ_4 of tryptophan for multi-exponential function is shown in Figure 7a. The transition temperatures and activation energies from Arrhenius plot of individual lifetime components are compiled in Table 1a. Temperature dependence of the total rate constant for decay of the triplet state ($k_p = k_{RP} + k_{TS0} + k_{TS1}$) calculated from multi exponential function of tryptophan in amorphous sucrose over the temperature range from -10°C to 100°C is shown in Figure 9a.

The k_{NR} term is a rate constant for non-radiative decay; it is the actual measure of the effect of the motion that quenches the probe's excited triplet state and was obtained from Eq. 8. The k_{NR} values were calculated by subtracting the phosphorescence emission rate constant ($1/\tau$ at 77K) from the inverse of the lifetime. Plots of k_{NR} as a function of temperature are represented in Figure 9b. The Arrhenius plot of k_{NR} is shown in Figure 10b. The activation energy, obtained from the slope of fit line in this plot, is the activation energy of the motions which quench the probe's excited triplet state (Table 1a).

Stretched-exponential fit: All intensity decay data over the temperature interval from -10°C to 100°C were well fitted using a stretched exponential function and the physically important parameters lifetime τ and stretching exponent β were obtained. The stretched

exponential lifetimes (Figure 5c) and exponent β (Figure 6c) are plotted as a function of temperature. The log plots of lifetimes of tryptophan as a function of temperature are shown in Figure 5d. In case of stretched-exponential function the two lifetime components at 20°C were $\tau_1 = 1079$ ms and $\tau_2 = 7.7$ ms indicating the presence of local environments with ~ 140 fold difference in mobility. The stretching exponents β_1 and β_2 showed a dramatic decrease with increase in temperature. In case of stretched-exponential function the two stretching exponent at -10°C were $\beta_1 = 0.77$ and $\beta_2 = 0.3$ and decreased at 100°C to $\beta_1 = 0.24$ and $\beta_2 = 0.23$. The decrease in β reflects a large increase in the width of the distribution of phosphorescence decay times and corresponding distribution of dynamically distinct environments. A plot of the amplitudes of each lifetime component as a function of temperature is as shown in Figure 6b.

The average lifetime calculated using Eq. 6 is plotted in Figure 8b. The Arrhenius plot of average lifetime is shown in Figure 10a showing transition points at $\sim 30^\circ\text{C}$. An Arrhenius plot of the inverse of individual lifetime components τ_1 and τ_2 for two stretched exponential function is shown in Figure 7b. The k_{NR} term is a rate constant for non-radiative decay; it is the actual measure of the effect of the motion that quenches probes excited triplet state and was obtained from eq. 8. The k_{NR} values were calculated by subtracting the phosphorescence emission rate constant ($1/\tau$ at 77K) from the inverse of the lifetime. Plots of k_{NR} as a function of temperature are represented in Figure 9b. The Arrhenius plot of k_{NR} is shown in Figure 10b. The activation energy obtained from the slope of fit line in this plot is the activation energy of the motions which quench the

probe's excited triplet state. The E_a values and transition temperatures for each probe are tabulated in Table 1b.

Discussion

The phosphorescence emission spectra exhibited three peaks (from three different vibronic transitions 0-0, 0-1 and 0-2) up to 50°C and was fitted to a three log-normal function. At 20°C the three peak frequencies obtained were PF1 = 21066 cm⁻¹, PF2 = 22765 cm⁻¹ and PF3 = 24305 cm⁻¹. Above 50°C, the spectra reduced to a single peak due to broadening and were fitted to a one log-normal function. In amorphous sucrose films a decrease in emission energy reflects an increase in the average extent of matrix dipolar relaxation around the excited triplet state. Temperature had a small effect on the emission energy in the glass as compared to in the melt. The large increase in FWHM at higher temperatures indicated inhomogeneous broadening corresponding to increase in the width of the distribution of energetically distinct matrix environments in the amorphous sucrose films.

All the lifetime components decreased drastically with increase in temperature from -10°C to 100°C. The decrease in lifetime occurs because of an increase in the rate of collisional quenching from interaction of the probe with the sugar matrix which promotes an increase of vibrational relaxation to the matrix. In environments with more mobility, the probe has a shorter lifetime (Strambini and Gonnelli, 1985) as result of quenching. In the environments with higher lifetimes, probe senses lower mobility and is less easily quenched. The average lifetime varied from 1199 ms at -10°C to 0.33 ms at 100°C, indicating ~3600-fold difference in mobility. The Arrhenius plot of ln τ_p (average lifetime) showed transition temperatures of ~30°C with activation energies at low and high temperature of 21 kJ mol⁻¹ and 100 kJ mol⁻¹ respectively (Table 1a). The total quenching

rate showed a constant increase from 0.6 s^{-1} (-10°C) to 16 s^{-1} (-50°C) in the glass and increased dramatically in the melt ranging between 72 s^{-1} (600°C) to 3090 s^{-1} (100°C), indicating tryptophan can sense the molecular mobility below T_g and those activated at the glass transition temperature above T_g . The Arrhenius plot of $\ln k_{NR}$ showed transition temperatures of $\sim 30^{\circ}\text{C}$ with activation energies at low and high temperature as 23.9 kJ mol^{-1} and $107.4 \text{ kJ mol}^{-1}$ respectively.

In case of stretched-exponential function analysis the two lifetime components at 20°C were $\tau_1 = 1079 \text{ ms}$ and $\tau_2 = 7.7 \text{ ms}$ indicating the presence of local environments with ~ 140 fold difference in mobility. The stretching exponents β_1 and β_2 reflected a large increase in the width of the distribution of phosphorescence decay times and corresponding distribution of dynamically distinct environments. The average lifetime varied from 1151 ms at -10°C to 0.38 ms at 80°C , indicating ~ 3800 -fold difference in mobility. The Arrhenius plot of $\ln k_P$ (average lifetime) showed transition temperatures of $\sim 30^{\circ}\text{C}$ with activation energies at low and high temperature as 30.9 kJ mol^{-1} and $142.9 \text{ kJ mol}^{-1}$, respectively (Table 1b). The total quenching rate showed a constant increase from 0.7 s^{-1} (-10°C) to 55 s^{-1} (50°C) in the glass and increased dramatically in the melt ranging between 179.4 s^{-1} (60°C) to 5246 s^{-1} (80°C), indicating tryptophan can sense molecular motions below T_g and those activated at the glass transition temperature above T_g . The Arrhenius plot of $\ln k_{NR}$ showed transition temperatures of $\sim 30^{\circ}\text{C}$ with activation energies at low and high temperature as 33.9 kJ mol^{-1} and $132.9 \text{ kJ mol}^{-1}$ respectively.

Tryptophan and four halogenated tryptophan analogs dispersed in freeze-dried sucrose showed three phosphorescence lifetimes ranging from about 10ms to over 1s in glass sucrose at 20°C (McCaul and Ludescher, 1999). Time-resolved phosphorescence intensity decays from NATA were multiexponential both above and below the glass transition temperature, indicating that the sucrose matrix is heterogeneous on the molecular level (Shah and Ludescher, 1995). Tryptophan has also been used to study molecular mobility in amorphous films of sucrose, maltose and trehalose where sucrose was found to be the most mobile matrix among the three (Zunic, 2004).

There was no significant difference in the fits between multi and stretched exponential function. The results were comparable, where both fits showed transition temperature around 30°C. The activation energies obtained were higher in the stretched fit as compared to the multi-exponential fit. In the melt there was no difference in the value of k_{NR} but in the melt stretch function gave much higher values, but the trend still remained the same.

Conclusion

This study used steady-state and time-resolved phosphorescence of tryptophan (water soluble) to monitor molecular mobility in thin films of amorphous sucrose as a function of temperature. The phosphorescence energy and intensity were all very sensitive to localized molecular mobility on the microsecond timescales in the glass and to more global modes of mobility activated at the glass transition. The constant increase in non radiative quenching rate in the glass for tryptophan indicates that amorphous sucrose films is very mobile in the glass and in the melt. Thus tryptophan as a triplet state probe indicates that the amorphous sucrose matrix gain mobility much below T_g of sucrose.

There was no significant difference in the data interpretation between stretched fit and multi exponential fit.

The results from this research were used to make comparison of molecular mobility data from other probes erythrosin B and vanillin dispersed in amorphous sucrose films. This data was also used to compare the data on dual probes (Chapter 9 on erythrosin B and tryptophan and Chapter 10 vanillin and tryptophan) dispersed in amorphous sucrose films.

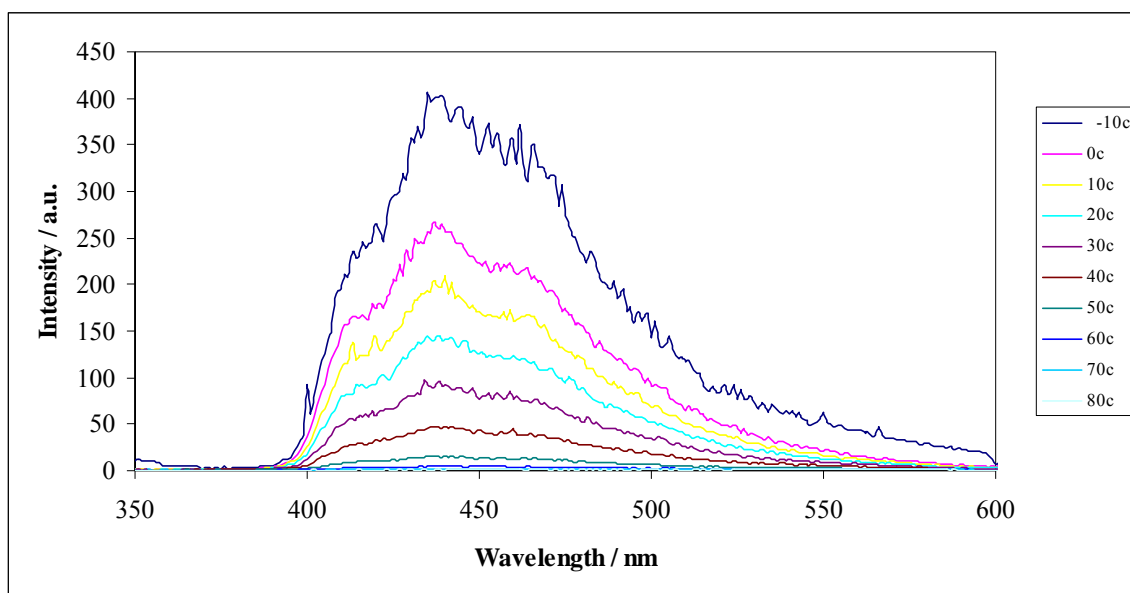
Figure VI b: 1

Figure VIb-1: Delayed emission spectra of tryptophan dispersed in amorphous films of sucrose as a function of temperature (excitation at 280 nm). The spectra were collected at 10°C intervals from -10°C to 80°C (the curves follow this order from high to low intensity at ~455 nm).

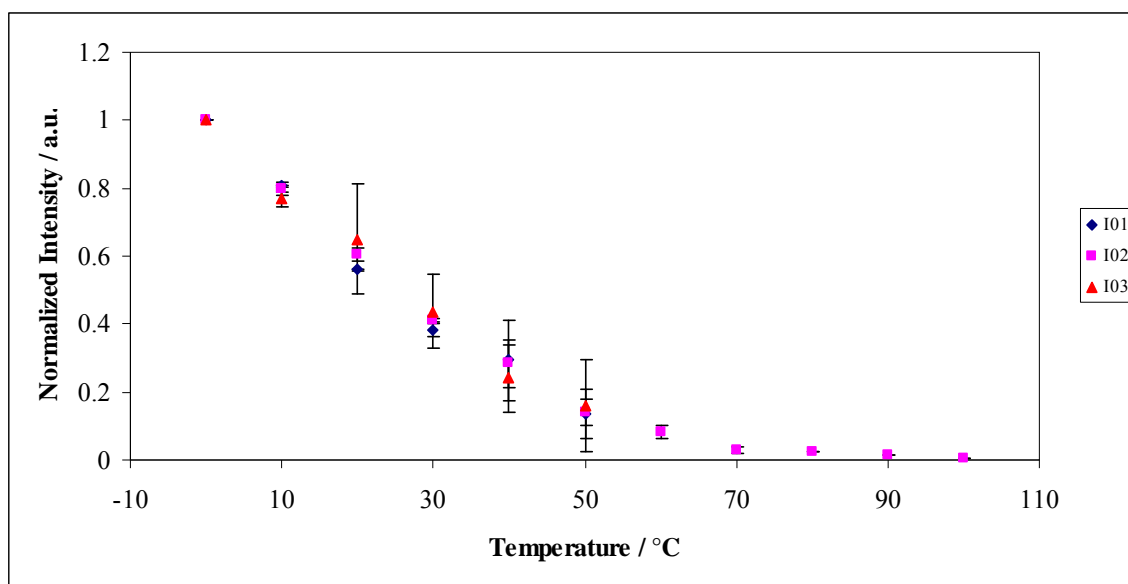
Figure VI b: 2

Figure VIb-2: Intensity (I_P) was determined from analysis of the phosphorescence emission band (Figure 1) using a log-normal three function (eq. (1), Materials and Methods). The effect of temperature on the phosphorescence emission intensity of tryptophan in amorphous films of sucrose as a function of temperature equilibrated against nitrogen. The spectra was fitted to a log-normal three function.

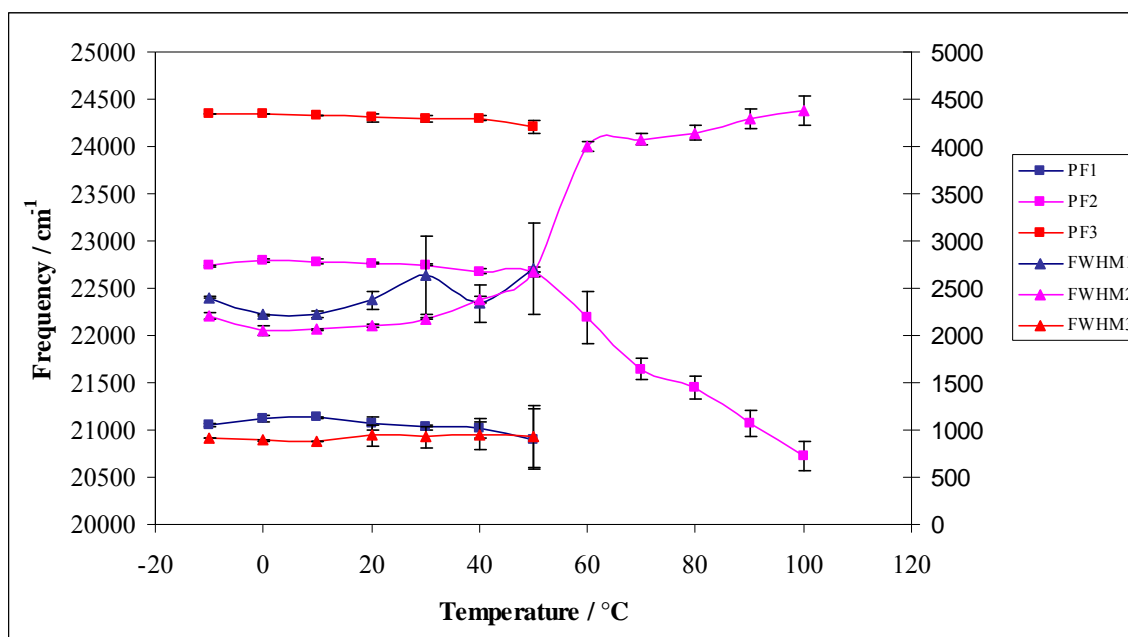
Figure VI b: 3

Figure VIb-3: Peak energy ν_p (■) and bandwidth (▲) for phosphorescence emission from tryptophan in amorphous films of sucrose as a function of temperature. The delayed emission spectra collected as a function of temperature (Figure 1) were analyzed using log-normal three function as described in Materials and Methods using eq. (1) and (2).

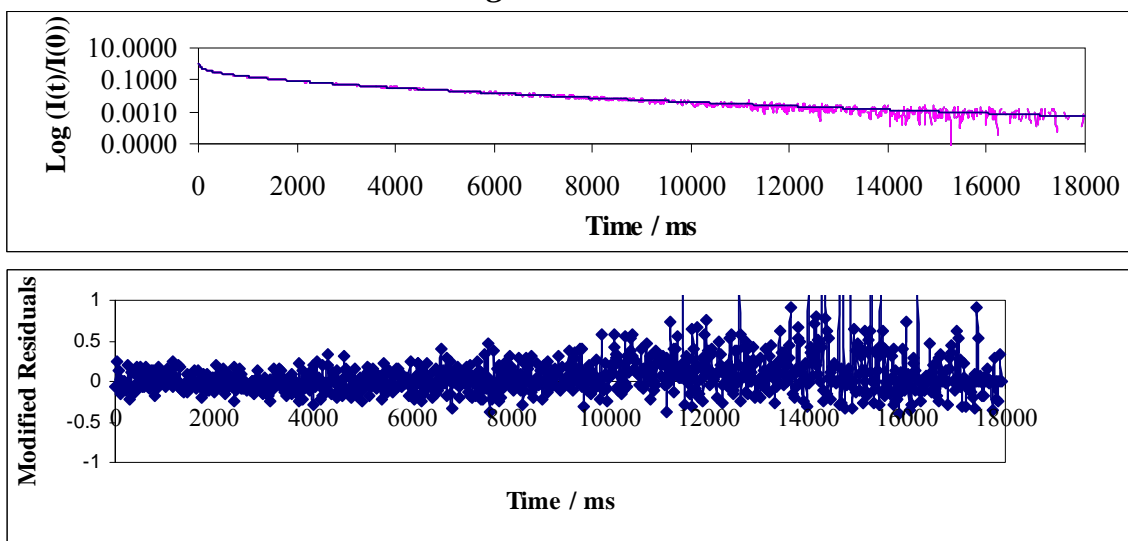
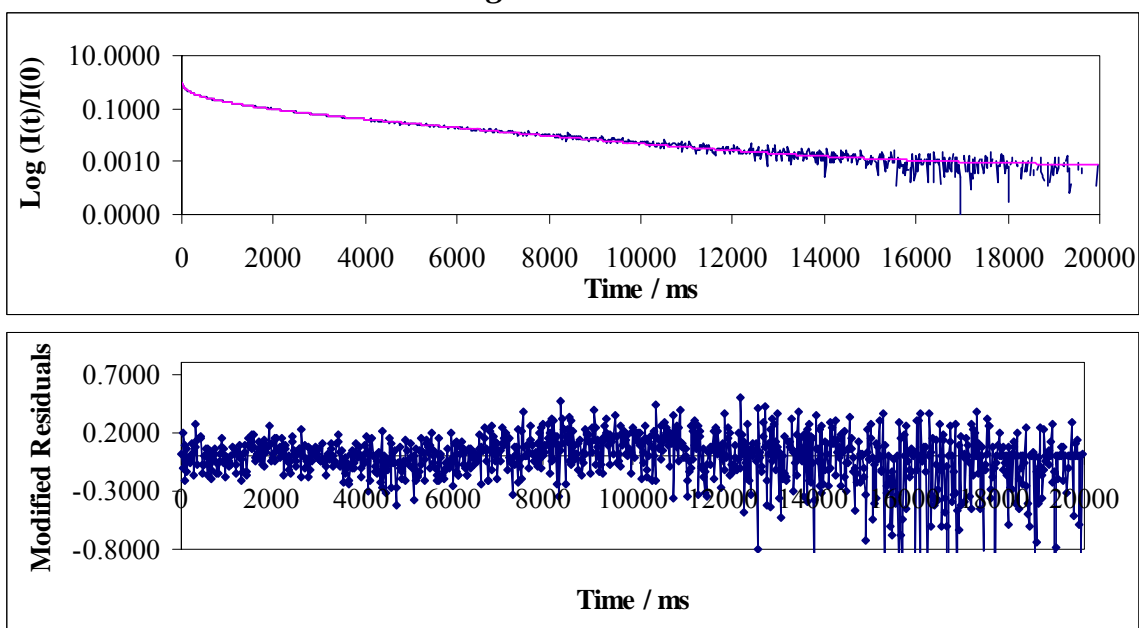
Figure VI b: 4a*Figure VI b: 4b*

Figure VIb-4a and 4b: Normalized phosphorescence intensity decay $[I(t)/I(0)]$ of tryptophan dispersed in amorphous films of sucrose at 20°C in the presence of nitrogen. The solid lines through the data are fits. A plot of modified residuals $[(\text{Data-Fit})/\text{Data}^{1/2}]$ for these fits is shown in the bottom graph. The decay was fitted using a multi-exponential function (3) and two stretch-exponential functions (5). The emissions were collected at 455nm.

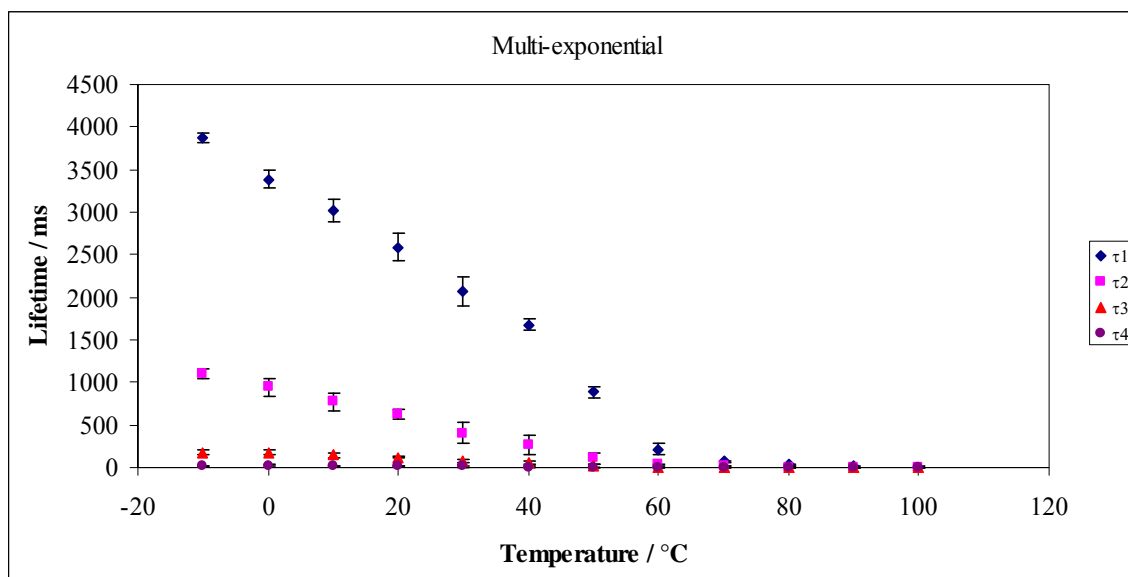
Figure VI b: 5a

Figure VIb-5a: Lifetime components τ_1 (\blacklozenge), τ_2 (\blacksquare), τ_3 (\blacktriangle) and τ_4 (\bullet) obtained from a multi-exponential model fit to phosphorescence intensity decay data from tryptophan dispersed in amorphous films of sucrose equilibrated against nitrogen as a function of temperature. The data was calculated every 10°C from -10°C to 100°C.

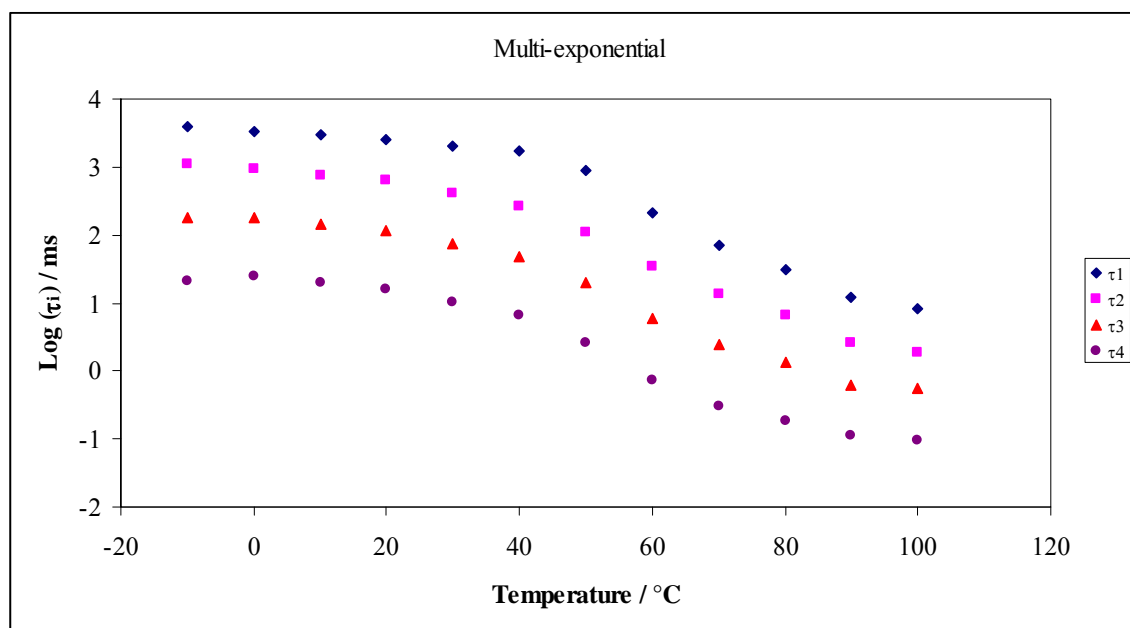
Figure VI b: 5b

Figure VIb-5b: The log plots of lifetime components τ_1 (\blacklozenge), τ_2 (\blacksquare), τ_3 (\blacktriangle) and τ_4 (\bullet) obtained from a multi-exponential model fit to phosphorescence intensity decay data from tryptophan dispersed in amorphous films of sucrose equilibrated against nitrogen as a function of temperature. The data was calculated every 10°C from -10°C to 100°C.

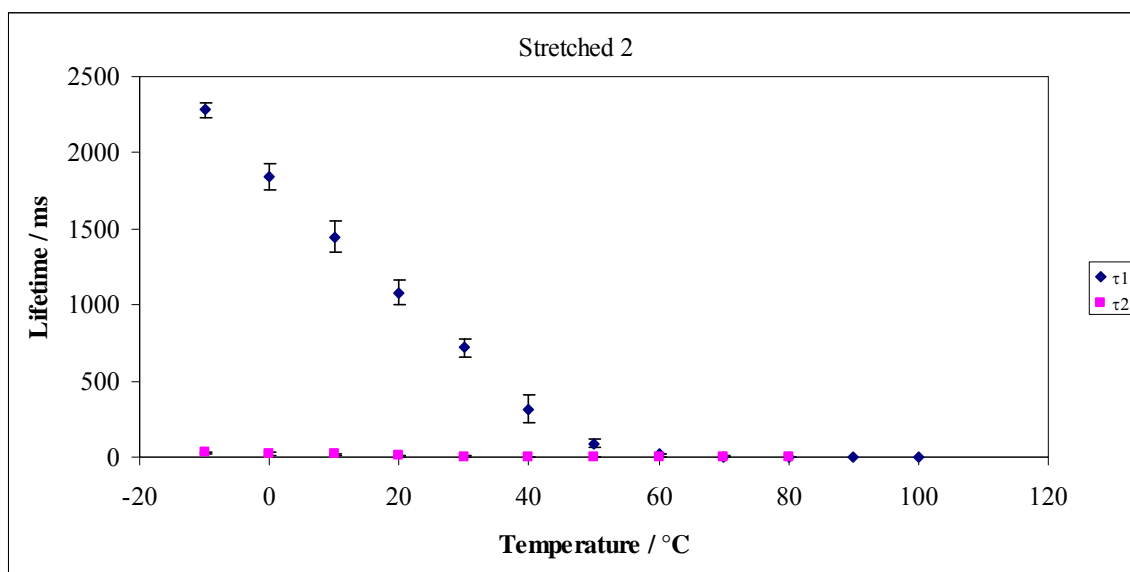
Figure VI b: 5c

Figure VIb-5c: Lifetime components τ_1 (◆) and τ_2 (■) obtained from a two stretch exponential function to phosphorescence intensity decay data from tryptophan dispersed in amorphous films of sucrose equilibrated against nitrogen as a function of temperature. The data was calculated every 10°C from -10°C to 100°C.

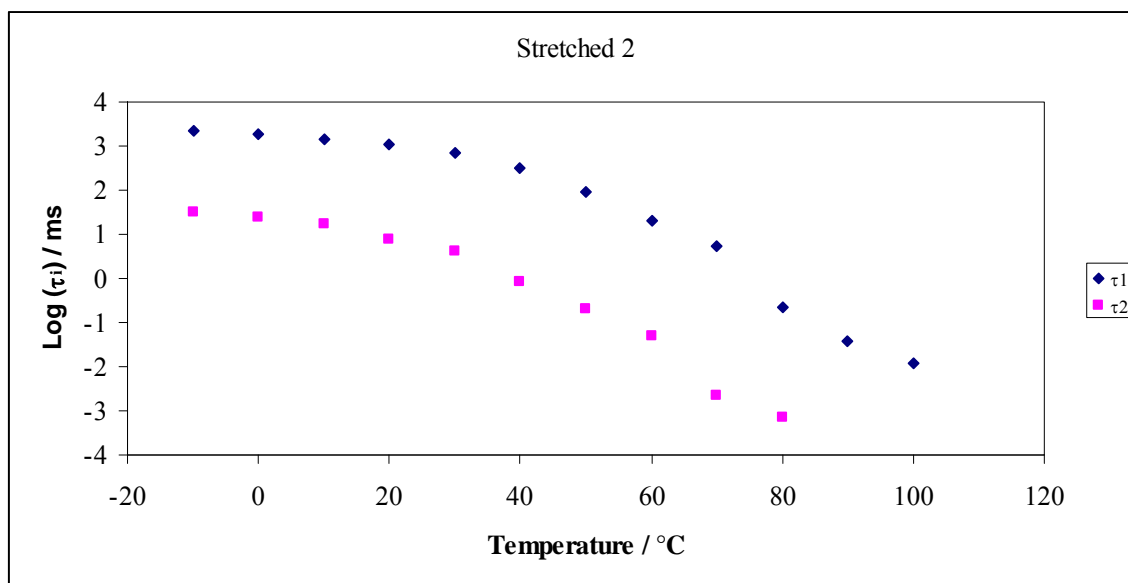
Figure VI b: 5d

Figure VIb-5d: The log plot of lifetime components τ_1 (◆) and τ_2 (■) obtained from a two stretch exponential function to phosphorescence intensity decay data from tryptophan dispersed in amorphous films of sucrose equilibrated against nitrogen as a function of temperature. The data was calculated every 10°C from -10°C to 100°C.

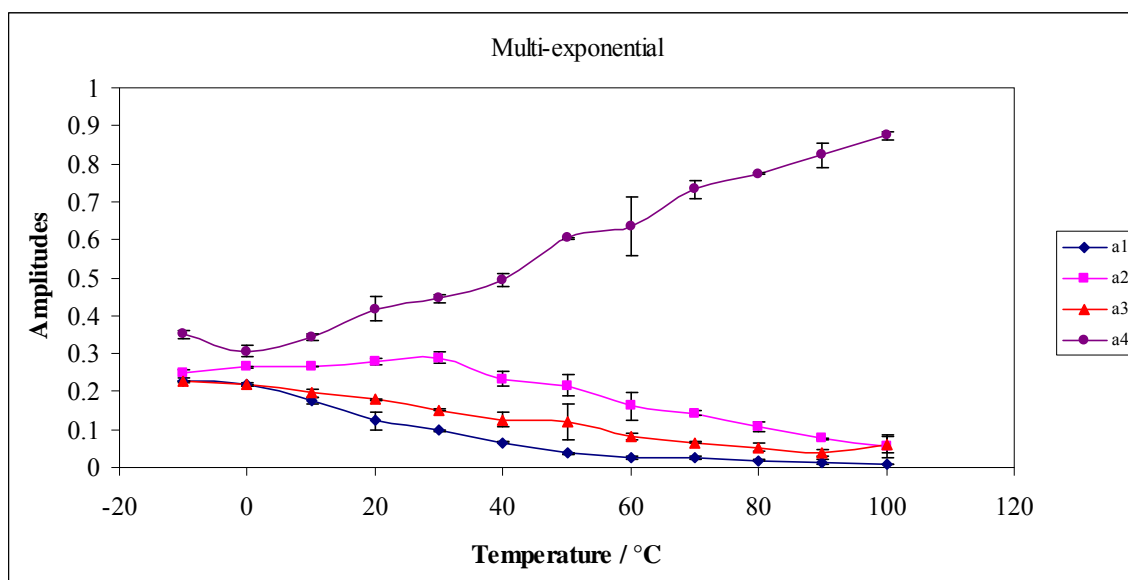
Figure VI b: 6a

Figure VIb-6a: Intensity decay fit parameters amplitude for tryptophan in amorphous films of sucrose in nitrogen as a function of temperature. The data was calculated every 10°C from -10°C to 100°C. The amplitudes a1 (♦) and a2 (■) correspond to the longer life time components (τ_1, τ_2) and a3 (▲) and a4 (●) correspond to the shorter lifetime components (τ_3, τ_4).

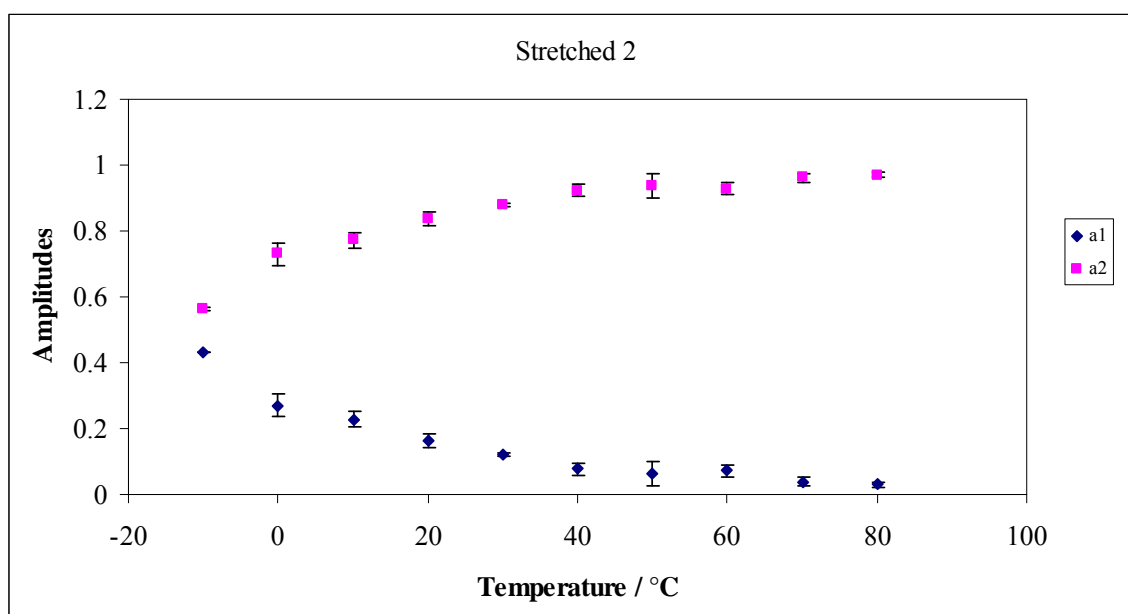
Figure VI b: 6b

Figure VIb-6b: Intensity decay fit amplitudes for stretched exponential fit to tryptophan in amorphous films of sucrose in nitrogen as a function of temperature. The data was calculated every 10°C from -10°C to 80°C. The amplitudes a_1 (♦) correspond to the longer life time components (τ_1) and a_2 (■) correspond to the shorter lifetime components (τ_2).

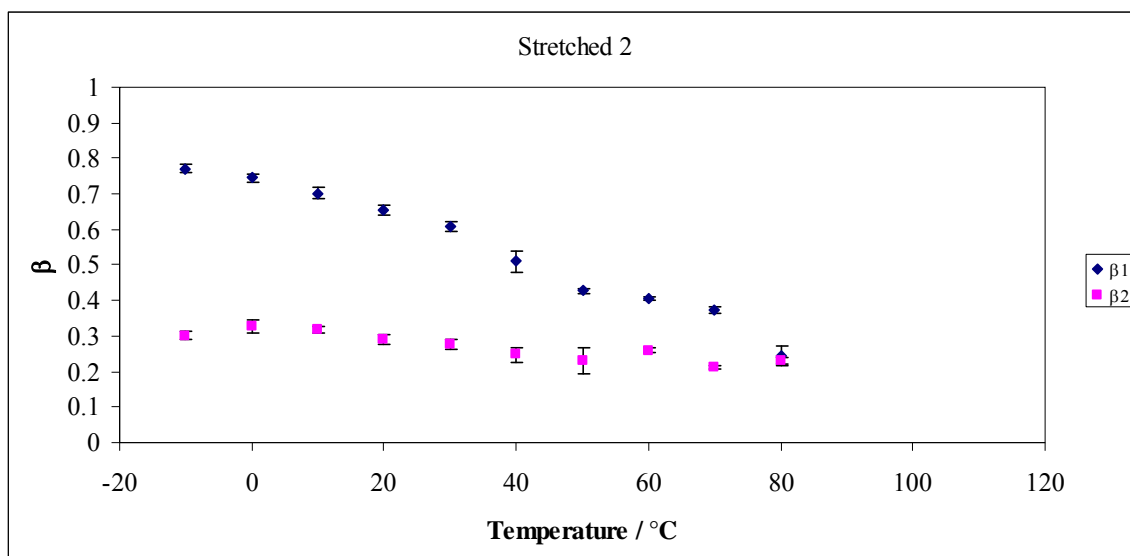
Figure VI b: 6c

Figure VIb-6c: Temperature dependent of stretching exponent β_1 (♦) and β_2 (■) from fits to a stretched exponential model of the intensity decay of tryptophan in amorphous sucrose films corresponding to τ_1 (long lifetime) and τ_2 (short lifetime).

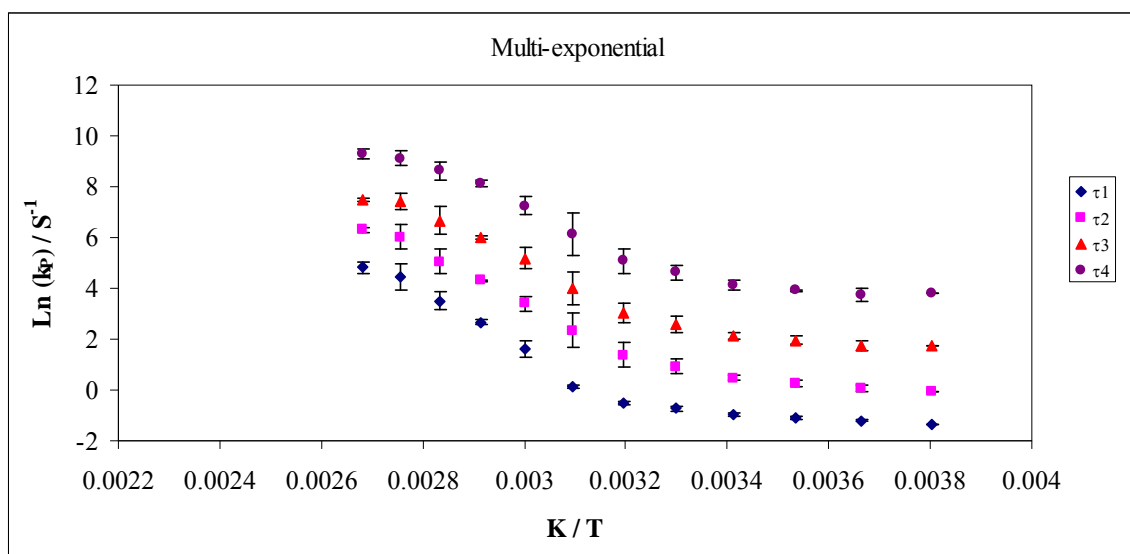
Figure VI b: 7a

Figure VIb-7a: The Arrhenius plot of the inverse of individual lifetime component τ_1 , τ_2 , τ_3 and τ_4 of tryptophan in amorphous films of sucrose as a function of inverse temperature. The Arrhenius plot is for multi-exponential function.

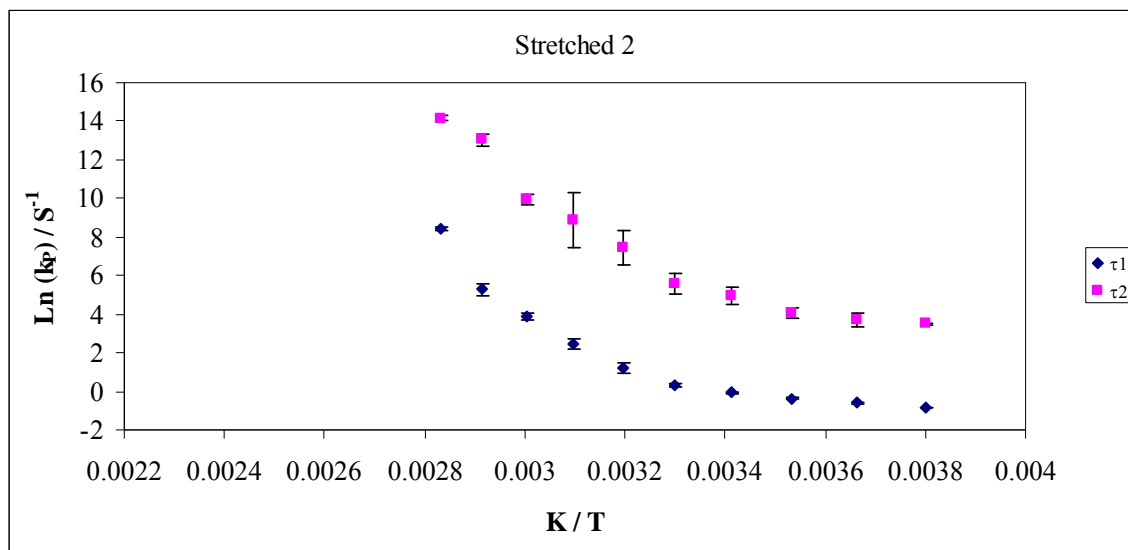
Figure VI b: 7b

Figure VIb-7b: The Arrhenius plot of the inverse of individual lifetime component τ_1 and τ_2 of tryptophan in amorphous films of sucrose as a function of inverse of temperature. The Arrhenius plot is for two stretched-exponential function.

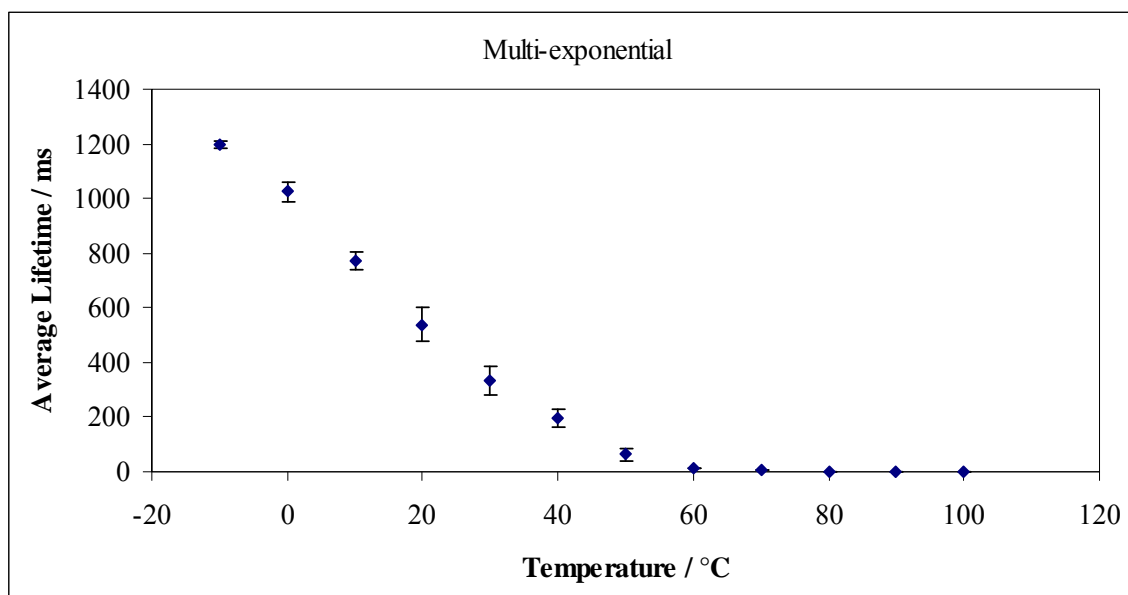
Figure VI b: 8a

Figure VIb-8a: Average Lifetime from a multi-exponential model fit to phosphorescence intensity decay data from tryptophan dispersed in amorphous films of sucrose equilibrated against nitrogen as a function of temperature. The data were calculated every 10°C from -10°C to 100°C.

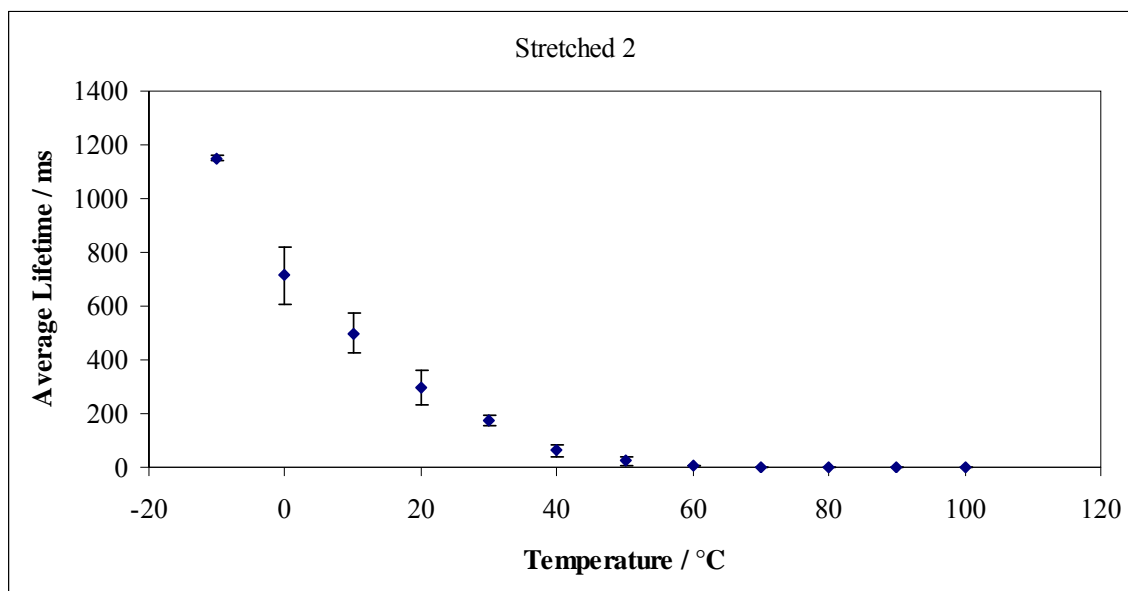
Figure VI b: 8b

Figure VIb-8b: Average Lifetime from a two stretched-exponential model fit to phosphorescence intensity decay data from tryptophan dispersed in amorphous films of sucrose equilibrated against nitrogen as a function of temperature. The data was calculated every 10°C from -10°C to 100°C.

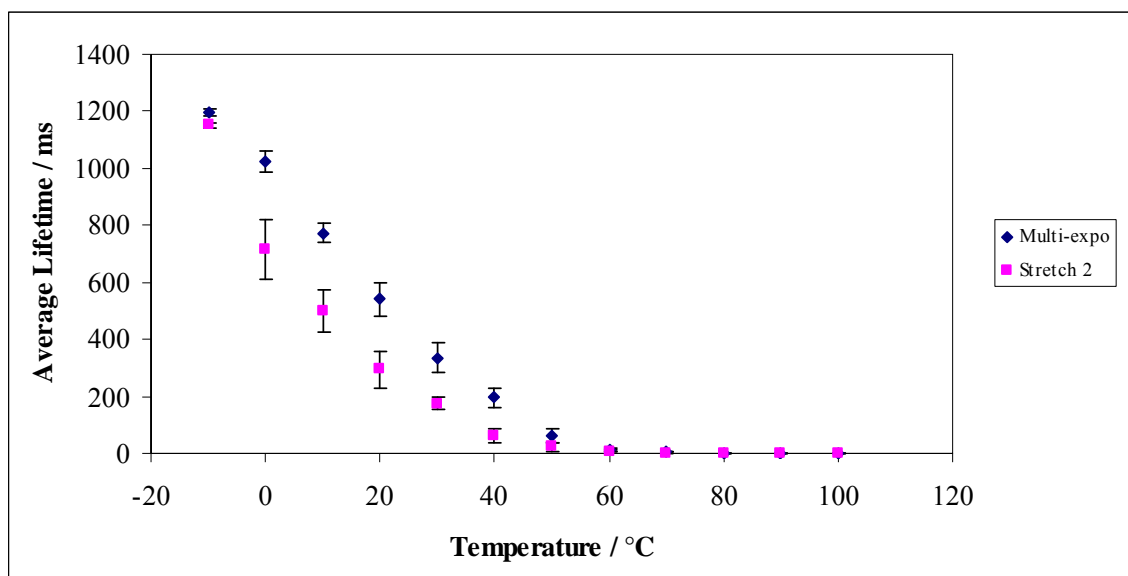
Figure VI b: 8c

Figure VIb-8c: Comparison of average lifetime between multi and a two stretched-exponential model fit to phosphorescence intensity decay data from tryptophan dispersed in amorphous films of sucrose equilibrated against nitrogen as a function of temperature. The data was calculated every 10°C from -10°C to 100°C.

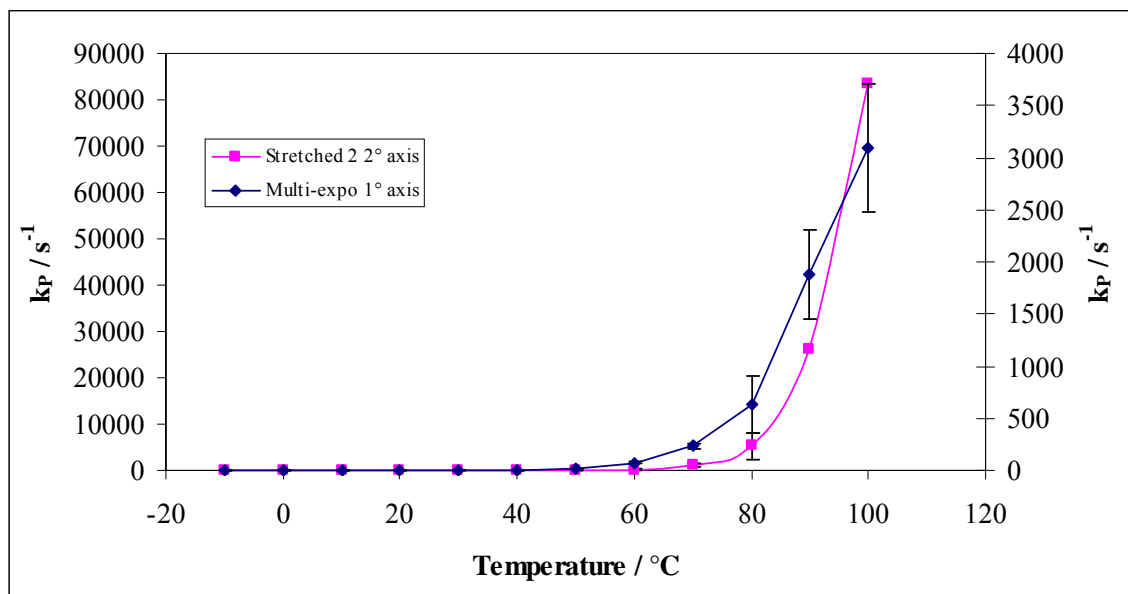
Figure VI b: 9a

Figure VIb-9a: Temperature dependence of the total rate constant for decay of the triplet state ($k_P = k_{RP} + k_{TS0} + k_{TS1}$) calculated from multi (◆) and two stretched exponential function (■) of tryptophan in amorphous sucrose over the temperature range from -10°C to 100°C; values were calculated from the lifetime data in Figure 8b.

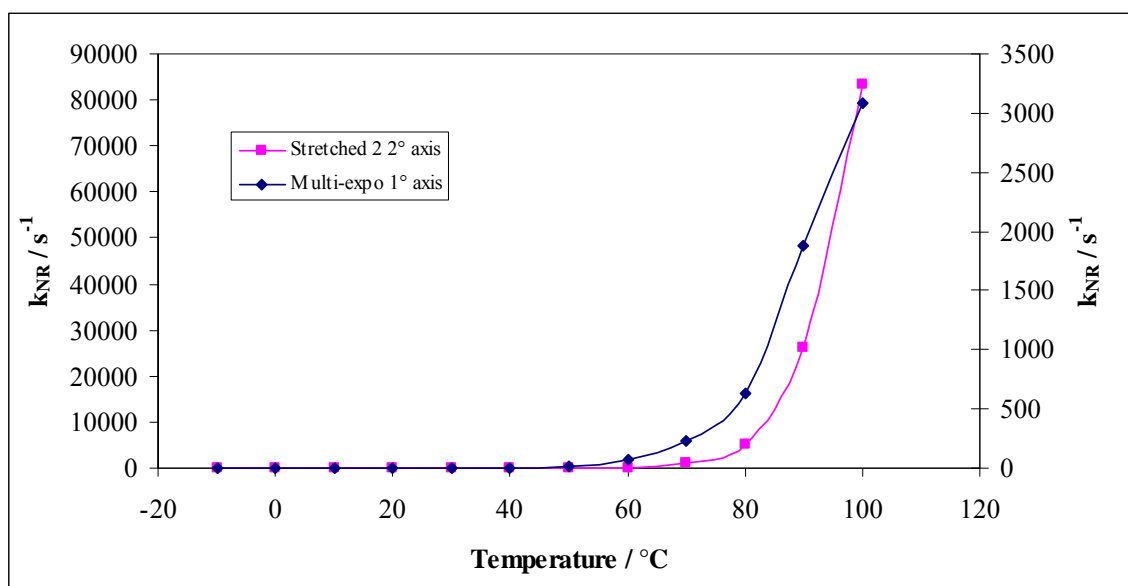
Figure VI b: 9b

Figure VIb-9b: Temperature dependence of the rate of non-radiative decay to S_0 (k_{NR}) calculated from multi (\blacklozenge) and two stretched exponential function (\blacksquare) of tryptophan in amorphous sucrose over the temperature range from -10°C to 100°C .

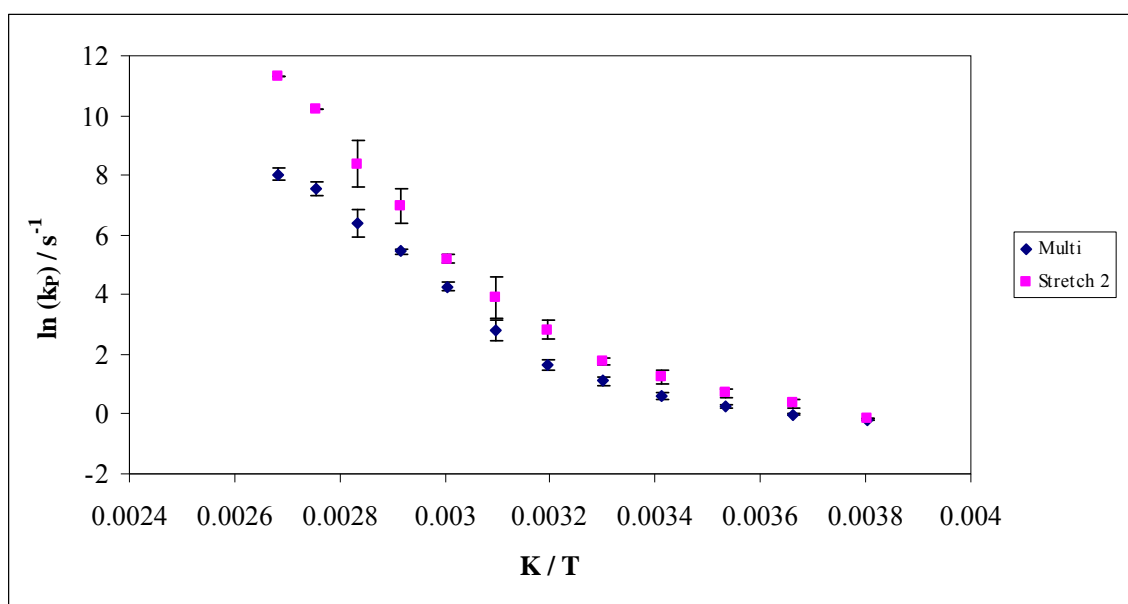
Figure VI b: 10a

Figure VIb-10a: The Arrhenius plot of the rate of (k_p) calculated from multi (♦) and two stretched exponential function (■) of tryptophan in amorphous sucrose over the temperature range from -10°C to 100°C .

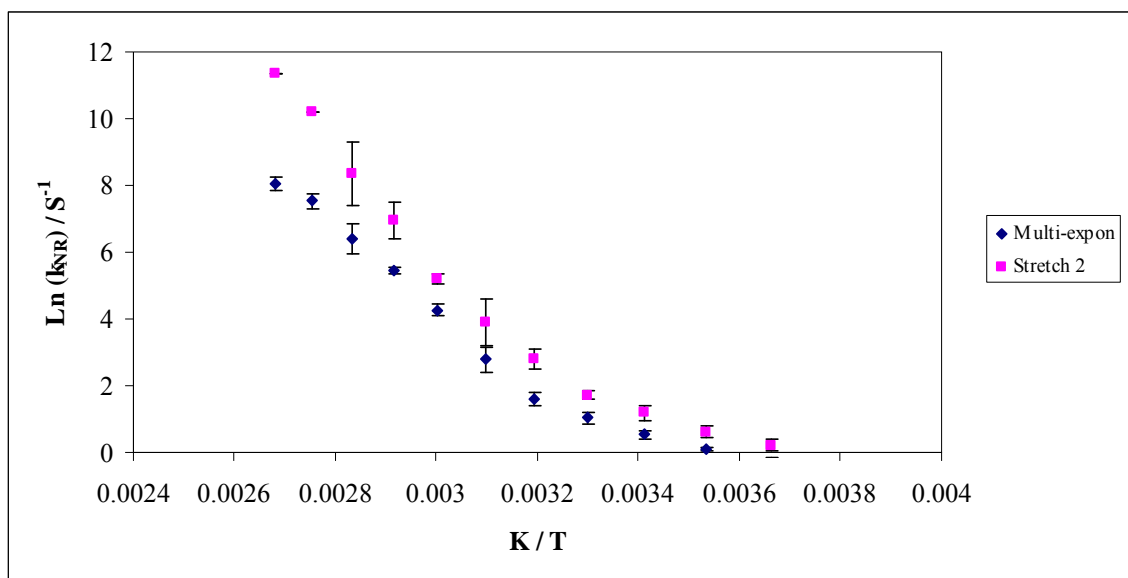
Figure VI b: 10b

Figure VIb-10b: The Arrhenius plot of the rate of non-radiative decay to S_0 (k_{NR}) calculated from multi (\blacklozenge) and two stretched exponential function (\blacksquare) of tryptophan in amorphous sucrose over the temperature range from -10°C to 100°C .

Table VI-1a

Table VIb-1a: Calculated activation energy E_a for k_p and k_{NR} at low, intermediate and high temperature for tryptophan in amorphous films of sucrose using multi-exponential function.

Component	Equation	R^2	E_a kJ mol ⁻¹	Transition Temperature °
Ln (k_{p1})	$y = -1205.3x + 3.1985$	0.97	10.02	42
	$y = -11129x + 34.936$	0.99	92.53	
Ln (k_{p2})	$y = -1463.1x + 5.4466$	0.99	12.16	32
	$y = -9414.7x + 31.697$	0.99	78.27	
Ln (k_{p3})	$y = -1647.3x + 7.7619$	1.00	13.70	32
	$y = -9306.8x + 33.044$	0.99	77.38	
Ln (k_{p4})	$y = -1641.9x + 9.7363$	0.99	13.65	32
	$y = -8894.3x + 33.796$	0.99	73.95	
Ln (k_{pAvg})	$y = -2534.1x + 9.3315$	0.95	21.07	30
	$y = -12102x + 40.622$	0.98	100.62	
Ln (k_{NR})	$y = -2872.8x + 10.391$	0.97	23.88	30
	$y = -12922x + 42.955$	0.99	107.43	

Table VI-1b

Table VIb-1b: Calculated activation energy E_a for k_p and k_{NR} at low, intermediate and high temperature for tryptophan in amorphous films of sucrose using two stretched-exponential function.

Component	Equation	R^2	E_a kJ mol ⁻¹	Transition Temperature °
Ln (k_{p1})	$y = -2253.5x + 7.6735$	0.97	18.74	35
	$y = -14690x + 48.026$	1.00	122.13	70
	$y = -38268x + 116.84$	1.00	318.16	
Ln (k_{p2})	$y = -2171.7x + 11.728$	0.99	18.06	20
	$y = -14768x + 54.453$	0.99	122.78	60
	$y = -24985x + 85.265$	0.94	207.73	
Ln (k_{pAvg})	$y = -3717.2x + 13.948$	0.99	30.90	30
	$y = -17188x + 57.244$	0.99	142.90	
Ln (k_{NR})	$y = -4073.7x + 15.11$	0.99	33.87	30
	$y = -15984x + 53.811$	0.98	132.89	

References

- Bishai, F., Kuntz, E. and Augenstein, L. Intra and intermolecular factors affecting the excited states of aromatic amino acids. *Biochimica et Biophysica Acta*. 140 (1967). 381-394.
- Champion, D., Le Meste, M. and Simatos, D. Towards an improved understanding of glass transition and relaxations in foods: molecular mobility in the glass transition range. *Trends in Food Science and Technology*. 11 (2000). 41-55.
- Garland, P.B. and Moore, C.H. Phosphorescence of protein-bound eosin and erythrosin: A possible probe for measurements of slow rotational mobility. *Biochemistry Journal*. 183 (1979). 561-572.
- Lettinga, M.P., Zuilhof, H. and van Zandvoort, M.A. Phosphorescence and fluorescence characterization of fluorescein derivatives immobilized in various polymers matrices. *Physical Chemistry Chemical Physics*. 2 (2000). 3697-3707.
- Lindsey, C. P. and Patterson, G. D. Detailed comparison of the Williams-Watts and Cole-Davidson functions. *Journal of Chemical Physics*. 2 (1980). 3348-3357.
- Ludescher, R.D., Shah, N.K., McCaul, C.P. and Simon, K.V. Beyond T_g: optical luminescence measurements of molecular mobility in amorphous solid foods. *Food Hydrocolloids*. 15 (2001). 331-339.
- Maroncelli, M. and Fleming, G. R. Picosecond salvation dynamics of coumarin 153: The importance of molecular aspects of salvation. *Journal of Chemical Physics*. 86 (1987). 6221-6239.
- McCaul, C.P. and Ludescher, R.D. Room temperature phosphorescence from tryptophan and halogenated tryptophan analogs in amorphous sucrose. *Photochemistry and Photobiology*. 70 (1999). 166-171.
- Nack, T.J. and Ludescher, R.D. Molecular mobility and oxygen permeability in amorphous bovine serum albumin films. *Food Biophysics*. 1 (2006). 151-162.
- Papp, S. and Vanderkooi, J.M. Tryptophan phosphorescence at room temperature as a tool to study protein structure and dynamics. *Photochemistry and Photobiology*. 49 (1989). 775-784.
- Pravinata, L.V., You, Y. and Ludescher, R.D. Erythrosin B phosphorescence monitors molecular mobility and dynamic heterogeneity in amorphous sucrose. *Biophysical Journal*. 88 (2005). 3551-3561.
- Shah, N.K. and Ludescher, R.D. Hydration and the internal dynamics of hen egg white lysozyme. *Proceedings of SPIE* 1640 (1992). 174-179.

- Shah, N.K. and Ludescher, R.D. Influence of hydration on the internal dynamics of hen egg white lysozyme in the dry state. *Photochemistry and Photobiology*. 58 (1993). 169-174.
- Shah, N.K. and Ludescher, R.D. Phosphorescence of probes of the glassy state in amorphous sucrose. *Biotechnology Progress*. 11 (1995). 540-544.
- Shirke, S. and Ludescher, R.D. Dynamic site heterogeneity in amorphous lactose and lactitol from spectral heterogeneity in erythrosin B phosphorescence. *Biophysical Chemistry*. 123 (2006). 122-133.
- Shirke, S. and Ludescher, R.D. Molecular mobility and glass transition in amorphous glucose, maltose and maltotriose. *Carbohydrate Research*. 340 (2006). 2654-2660.
- Simon-Lukasik, K.V. and Ludescher R.D. Erythrosin B phosphorescence as a probe of oxygen diffusion in amorphous gelatin films. *Food Hydrocolloids*. 18 (2004). 621-630.
- Strambini, G.B. and Gonnelli, M. Tryptophan phosphorescence in fluid solution. *Journal of American Chemical Society*. 117 (1995). 7646-7651.
- Strambini, G.B. and Gonnelli, M. The indole nucleus triplet-state lifetime and its dependence on solvent microviscosity. *Chemical Physics Letters*. 115 (1985). 196-200.
- Sundaresan, K.V. and Ludescher, R. D. Molecular mobility and oxygen permeability in amorphous beta-lactoglobulin films. *Food Hydrocolloids*. 22 (2007). 403-413.
- Vanderkooi, J. M., Maniara, G., Green, T. J. and Wilson, D. F. An optical method for measurement of dioxygen concentration based upon quenching of phosphorescence. *Journal of Biological Chemistry*. 262 (1987). 5476-5482.
- Zunic, A. Molecular mobility of amorphous disaccharide studied by tryptophan luminescence. Master Thesis. Rutgers University. New Brunswick, NJ. (2004).

Chapter VI c: Comparing molecular mobility in amorphous sucrose films detected using phosphorescence of erythrosin B, vanillin and tryptophan.

Discussion

Vanillin (Chapter II), tryptophan (Chapter VI b) and erythrosin B (Chapter VI a) have been used in amorphous sucrose to study molecular mobility as a function of temperature. This chapter aims at making a comparison among the three probes for molecular mobility measurements.

The phosphorescence lifetime of vanillin ($\tau_{77K} = 372$ ms) (Chapter II) and tryptophan ($\tau_{77K} = 6$ s) (Bishai et al., 1967) is considerably longer than that of erythrosin B ($\tau_{77K} = 25$ ms) (Duchowicz et al., 1998). Longer lived triplet probes (lifetimes of milliseconds to seconds) may help to access other modes of motion that affect the physical changes in the sucrose films. These probes could help detect slower molecular motions. The structural and dynamic heterogeneity that has been observed on the sub-millisecond time scale may be considerably different over milliseconds to seconds. The vanillin and tryptophan lifetime behavior is quite distinct and more dramatic than that seen with erythrosin B (Figure 1). As seen from the Figure 1a in the glassy region, vanillin and tryptophan show dramatic decrease in lifetime as compared to erythrosin B whose lifetime shows a gradual decrease. This difference may be attributed to longer lifetimes of vanillin and tryptophan as compared to erythrosin B which allows them to see slower molecular motions. Comparison of the lifetime plot as a function of temperature is shown between tryptophan and erythrosin B (Figure 1b), vanillin and erythrosin B (Figure 1c) and vanillin and tryptophan (Figure 1d). The log plot of average lifetime for the three probes is shown in Figure 1e.

Since tryptophan decays were also fitted with a two stretched exponential function a comparison was made with the beta values obtained by fitting erythrosin B decay to a single stretch exponential function (Figure 2). The beta values for tryptophan decays varied over a considerably wider range from -10°C ($\beta_1 = 0.77$) and ($\beta_2 = 0.30$) to 80°C ($\beta_1 = 0.24$) and ($\beta_2 = 0.22$). Whereas the β in case of erythrosin B didn't vary so much as a function of temperature from -10°C ($\beta_1 = 0.92$) to 80°C ($\beta_2 = 0.90$). Thus beta in case of tryptophan was significantly smaller than those for erythrosin B, suggesting larger heterogeneity in environments in the same glassy and melt region of sucrose as a function of temperature. These higher heterogeneities seen by tryptophan could be due to longer lifetime which allows it to see many other molecular motions as compared to the triplet state of erythrosin B (which is comparatively short lived).

The amplitudes of longer lifetime components decreased and that of shorter lifetime components increased as a function of temperature in case of both vanillin and tryptophan. Tryptophan showed three longer lifetime components (τ_1 , τ_2 and τ_3) that decreased in amplitudes (T_1 , T_2 and T_3) with increasing temperature and one shorter lifetime components (τ_4) that increased in amplitudes (T_4). Vanillin showed two longer lifetime components (τ_1 and τ_2) that decreased in amplitudes (V_1 and V_2) and two shorter lifetime components (τ_3 and τ_4) that increased in amplitudes (V_3 and V_4) with increasing temperature. Comparing the amplitudes of longer and shorter lifetime components of vanillin and tryptophan decays also revealed different details (Figure 3). There was no significant difference in the percentage of the longer (Figure 4a) and shorter (Figure 4b)

lifetime component between vanillin and tryptophan. In the glassy region for both tryptophan and vanillin, 70-80% of probes were distributed in rigid environments and 30-20% of them were present in mobile environments.

Temperature dependence of the rate constant for total decay of the triplet state for erythrosin B, vanillin and tryptophan is shown in Figure 5a. The decay rates were highest for erythrosin B followed by vanillin and tryptophan. Temperature dependence of the rate of non-radiative decay to S_0 (k_{NR}) is plotted in Figure 5b. The non-radiative decay rate which is an indicator of matrix mobility was highest is erythrosin B followed by vanillin and tryptophan. This indicates that erythrosin B probably senses faster motions compared to vanillin and tryptophan which also sense slower motions. The intrinsic rate of internal conversion affects k_{NR} : Ery B appears to have a much faster intrinsic rate. The Arrhenius plot of the total rate constant k_P and rate of non-radiative decay k_{NR} for the three probes is shown in Figure 6a and 6b, respectively.

The Arrhenius plot of $\ln(k_{NR})$ was biphasic in case of erythrosin B and triphasic in case of vanillin and tryptophan. The activation energies at low and high temperature for erythrosin B were $E_{aL} = 1.2 \text{ kJ mol}^{-1}$ and $E_{aH} = 10.2 \text{ kJ mol}^{-1}$, and it showed a transition temperature at $\sim 58^\circ\text{C}$ (close to T_g of sucrose $\sim 65^\circ\text{C}$). The activation energies for vanillin at low and high temperatures were $E_{aL} = 13.8 \text{ kJ mol}^{-1}$ and $E_{aH} = 72.3 \text{ kJ mol}^{-1}$, the two transition points were at $\sim 40^\circ\text{C}$. The activation energies for tryptophan at low and high temperatures were $E_{aL} = 23.9 \text{ kJ mol}^{-1}$ and $E_{aH} = 107.43 \text{ kJ mol}^{-1}$, the transition points

was at $\sim 30^{\circ}\text{C}$. The activation energies at low and high temperatures varied such that erythrosin B > vanillin > tryptophan (Table 1).

In glass to liquid transition, molecular mobility is present as α relaxation in the T_g zone; as temperature is lowered below T_g molecular mobility is present as β and γ (in some cases δ) relaxations also called secondary relaxations (Ediger et al., 1996; Hancock and Zografi 1997; Vyazovkin and Dranca, 2006). The α relaxation is thought to reflect changes in local segmental motions (Hill and Tant, 1998). The secondary relaxations are due to vibrations of atoms or bonds, or reorientation of small group of atoms (Debenedetti and Stillinger, 2001).

The sequence of non-radiative decay rate as a function of temperature (which is an indicator of matrix mobility) in amorphous sucrose film was erythrosin B > vanillin > tryptophan. Erythrosin B indicated a transition temperature $\sim 58^{\circ}\text{C}$ (close to T_g of sucrose). Thus erythrosin was more sensitive a probe to motions above T_g (with α relaxations) than below T_g . Whereas vanillin showed transitions much below T_g at 40°C , similarly tryptophan showed transition temperatures around 30°C .

In sucrose (using dielectric spectroscopy) three relaxation processes have been reported at temperatures 126°C to 74°C (α -relaxation), 72°C to 12°C (β -relaxation) and 6°C to -145°C (γ -relaxation) (Kaminski et al., 2008).

At high temperature translational mobility becomes activated and glass transition occurs (Champion et al., 2000; Zallen, 1998). In amorphous sucrose, glass to liquid transition, molecular mobility is presented as α relaxation in the T_g zone. The α relaxation corresponds to translational and rotational motion of molecules that support flow in the melt. As temperature is lowered below T_g molecular mobility is presented as β and γ relaxations also called secondary relaxations (Ediger et al., 1996; Hancock and Zografi, 1997; Vyazovkin and Dranca, 2006). In the glass the local vibrational and rotational motions help hydroxyl groups reorient around the probe molecules. The sub- T_g relaxations (β, γ) have been reported in amorphous sucrose due to localized motions (Le Meste et al., 2002; Wagner and Richert, 1998, 1999). A recent study by Kaminski et al in addition to commonly observed primary and secondary relaxation, have reported presence of slower secondary relaxation lying in between the two (Kaminski et al., 2008). The β relaxation in sucrose is considered to be the universal Johari-Goldstein. β relaxation observed in other sugars too (Ngai and Paluch, 2004; Johari and Goldstein, 1970; Ngai, 1998; 2003; Ngai et al., 2006; Capaccioli et al., 2006; Bohmer et al., 2006, Kaminski et al., 2006), which involves rotation of both monosaccharide (glucose and fructose) rings and is coupled with possible translational motion of the entire molecule (Poppe and Van Halbeek, 1992). The rotation of the two rings round each other is also considered to be one of possibility of β relaxation in sucrose. The γ relaxation is being found to be result of internal motion (backbone rotation) within the monosaccharide (glucose and fructose) presence in the sucrose.

At temperature below T_g molecular mobility is presented as β and γ , maybe vanillin and tryptophan were more sensitive to β and γ relaxations. Compared to α relaxation which have higher activation energy and is usually associated with the cooperative global translational motion of the matrix molecules, β relaxation is a secondary relaxation which requires less activation energy (Champion et al, 2003). Thus vanillin and tryptophan are sensitive to glassy state motions in way that erythrosin B is not.

Conclusion

The phosphorescence from each probe erythrosin B, vanillin and tryptophan was successfully utilized to measure molecular mobility on three different time scales corresponding to each probe.

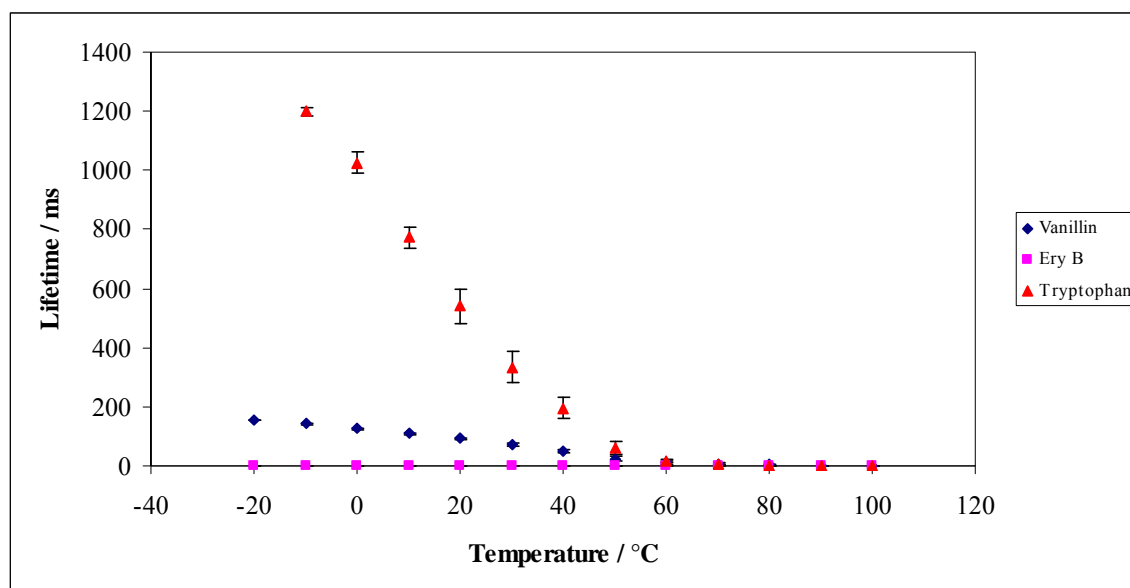
Figure VIc-1a

Figure VIc-1a: Comparison of average lifetime of erythrosin B (single stretch exponential fit), vanillin (multi exponential fit) and tryptophan (multi exponential fit) dispersed in amorphous films of sucrose equilibrated against nitrogen as a function of temperature. The data was calculated every 10°C from -20°C to 100°C.

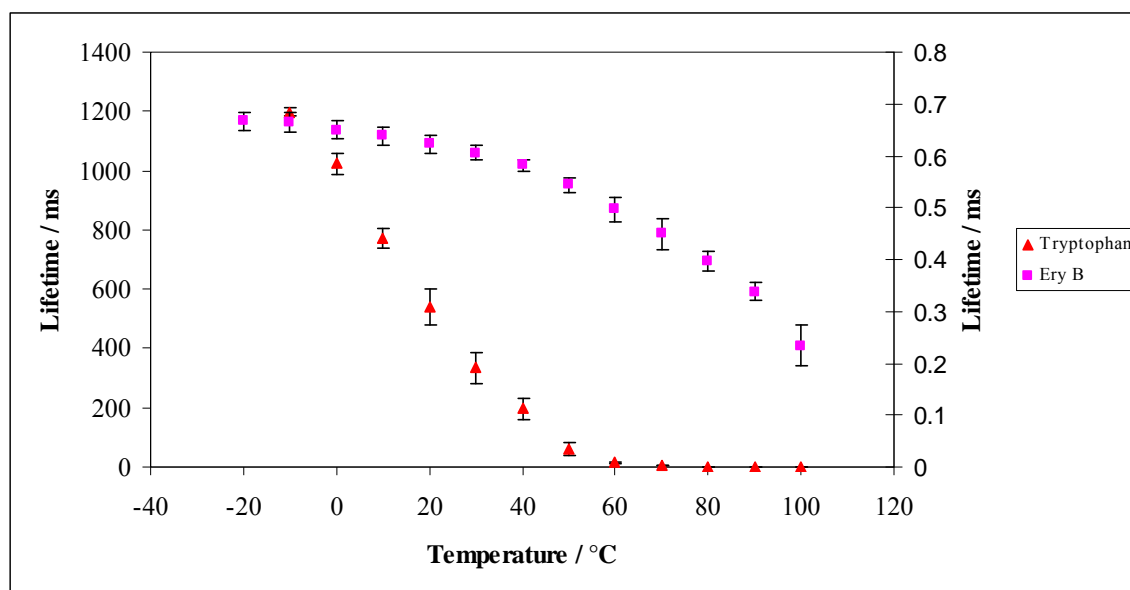
Figure VIc-1b

Figure VIc-1b: Comparison of average lifetime of erythrosin B (single stretch exponential fit) and tryptophan (multi exponential fit) dispersed in amorphous films of sucrose equilibrated against nitrogen as a function of temperature. The data was calculated every 10°C from -20°C to 100°C.

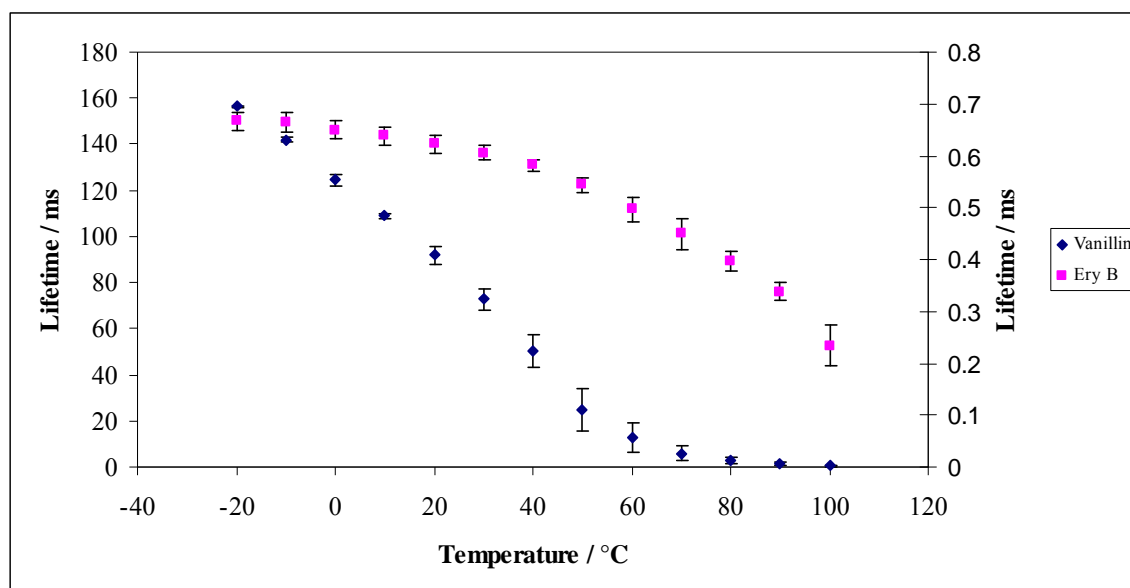
Figure VIc-1c

Figure VIc-1c: Comparison of average lifetime of erythrosin B (single stretch exponential fit) and vanillin (multi exponential fit) dispersed in amorphous films of sucrose equilibrated against nitrogen as a function of temperature. The data was calculated every 10°C from -20°C to 100°C.

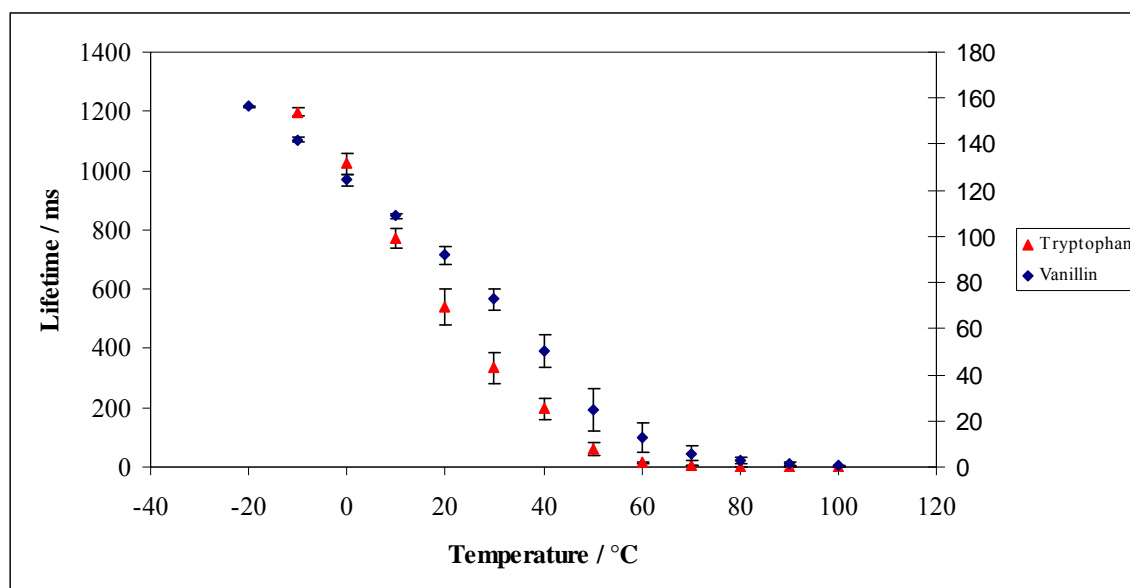
Figure VIc-1d

Figure VIc-1d: Comparison of average lifetime of vanillin (multi exponential fit) and tryptophan (multi exponential fit) dispersed in amorphous films of sucrose equilibrated against nitrogen as a function of temperature. The data was calculated every 10°C from -20°C to 100°C.

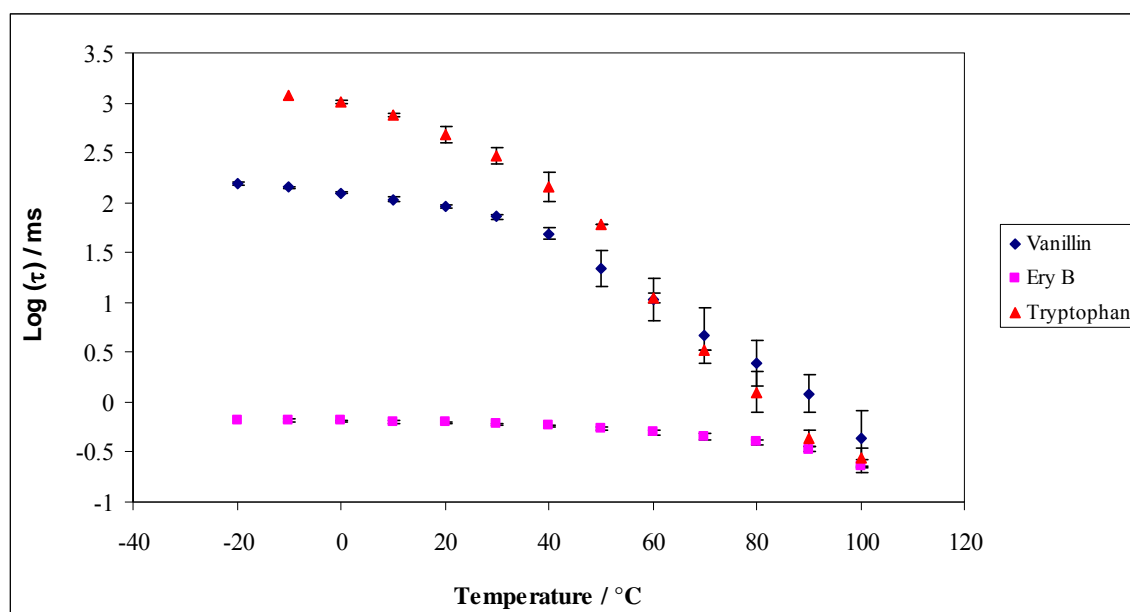
Figure VIc-1e

Figure VIc-1e: Comparison of log of average lifetime of vanillin (multi exponential fit), erythrosin B (stretch exponential fit) and tryptophan (multi exponential fit) dispersed in amorphous films of sucrose equilibrated against nitrogen as a function of temperature. The data was calculated every 10 $^{\circ}\text{C}$ from -20 $^{\circ}\text{C}$ to 100 $^{\circ}\text{C}$.

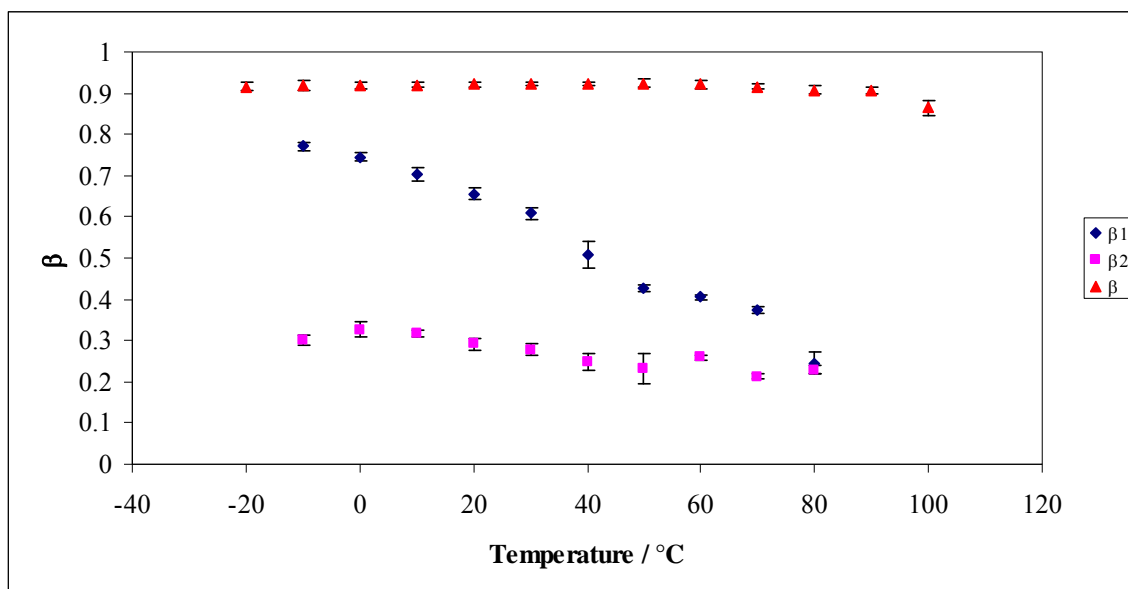
Figure VIc-2

Figure VIc-2: Comparison of temperature dependent of stretching exponent for tryptophan decay (β_1 (♦) and β_2 (■)) and erythrosin B decay (β (▲)) from fits to a stretched exponential model of the intensity decay in amorphous sucrose films.

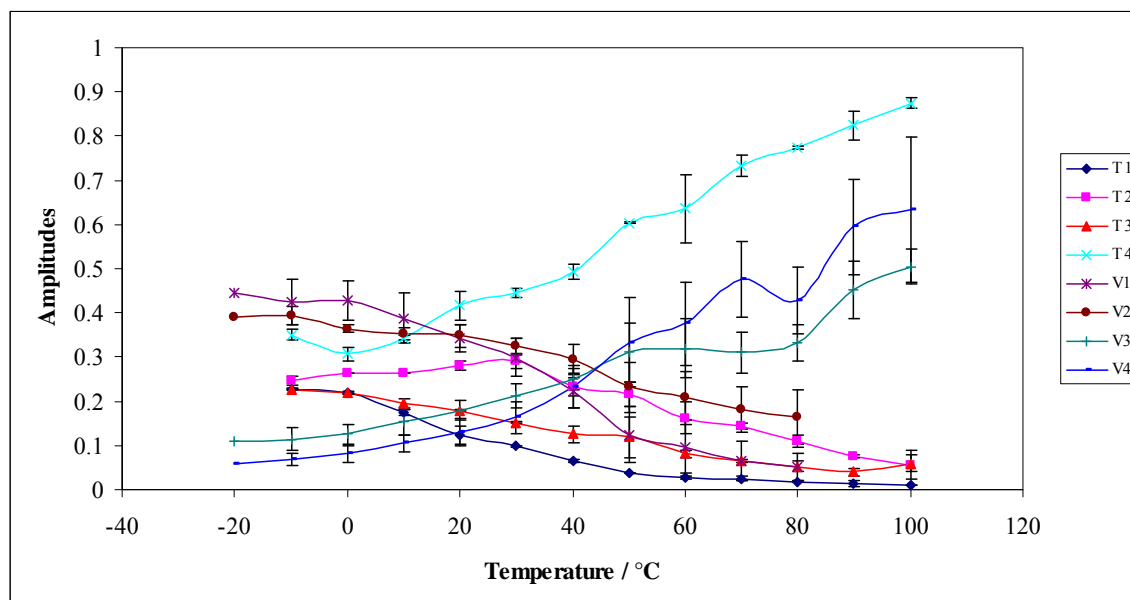
Figure VIc-3

Figure VIc-3: Comparison of intensity decay fit parameters amplitude for tryptophan and vanillin in amorphous films of sucrose in nitrogen as a function of temperature. The data was calculated every 10°C from -20°C to 100°C. In case of tryptophan the amplitudes T1 (♦), T2 (■) and T3 (▲) correspond to the longer life time components (τ_1 , τ_2 , τ_3) and T4 (*) correspond to the shorter lifetime components (τ_4). In case of vanillin the amplitudes V1 (*), V2 (●) correspond to the longer life time components (τ_1 , τ_2), V3 (+) and V4 (-) correspond to the shorter lifetime components (τ_3 , τ_4).

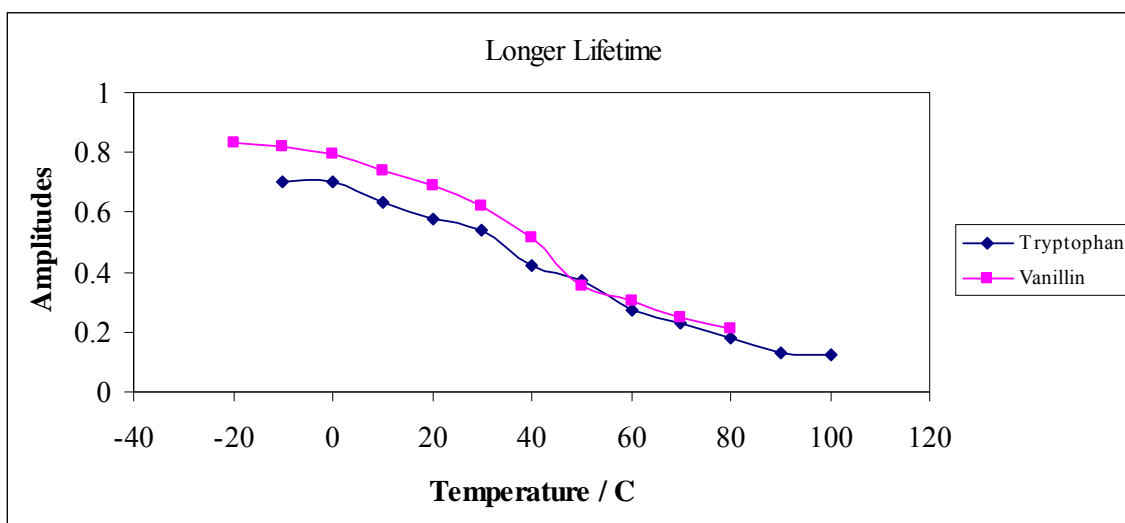
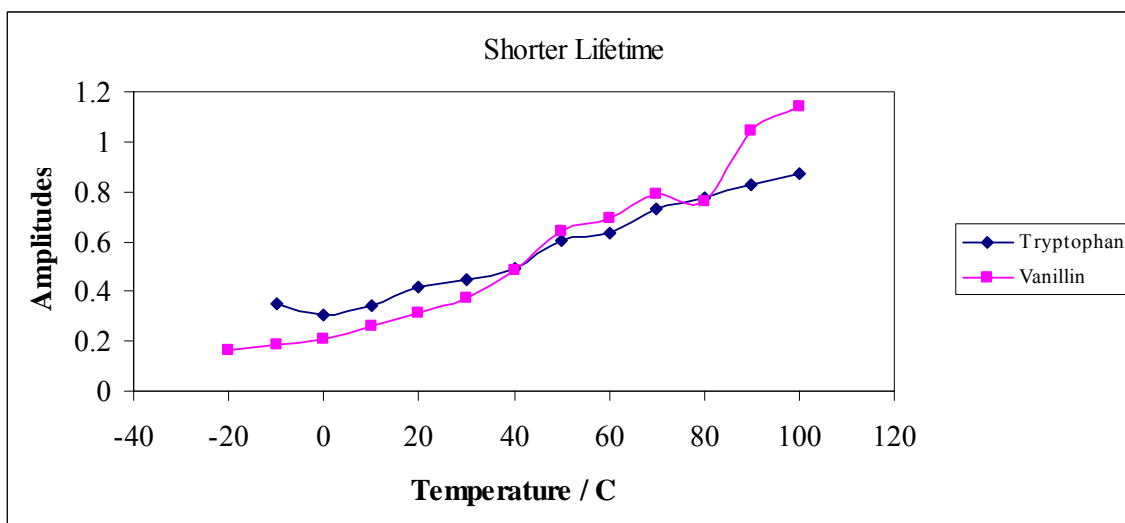
Figure VIc-4a*Figure VIc-4b*

Figure VIc-4a and 4b: Comparison of sum of amplitude for longer lifetime components (4a) and shorter lifetime components (4b) for tryptophan and vanillin in amorphous films of sucrose in nitrogen as a function of temperature. The data was calculated every 10°C from -20°C to 100°C.

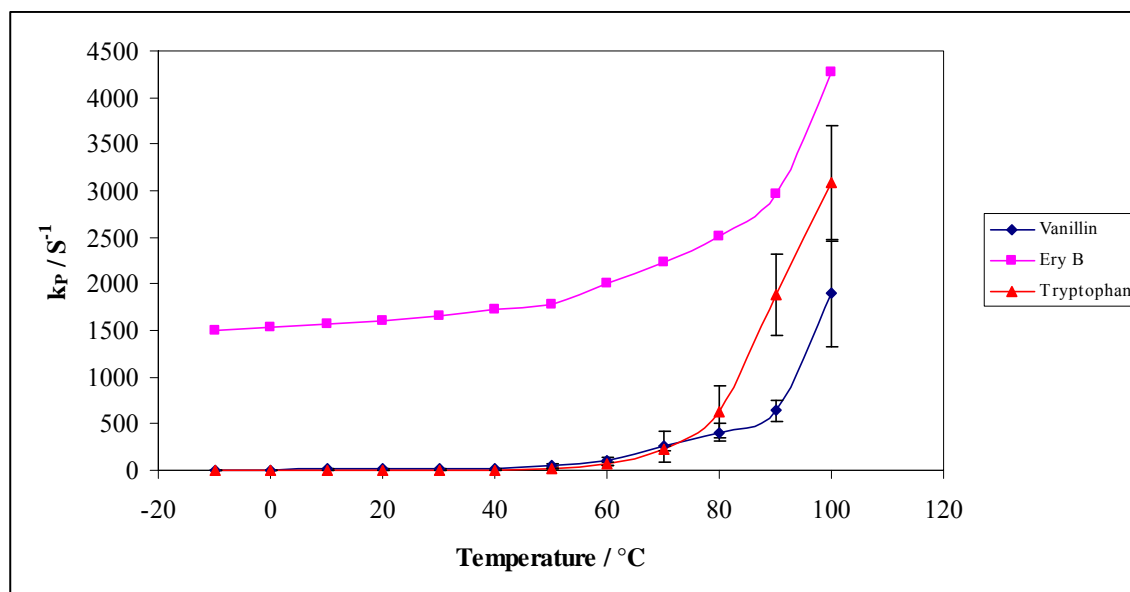
Figure VIc-5a

Figure VIc-5a: Temperature dependence of the total rate constant for decay of the triplet state ($k_P = k_{RP} + k_{TS0} + k_{TS1}$) for erythrosin B, vanillin and tryptophan in amorphous sucrose over the temperature range from -20°C to 100°C; values were calculated from the lifetime data.

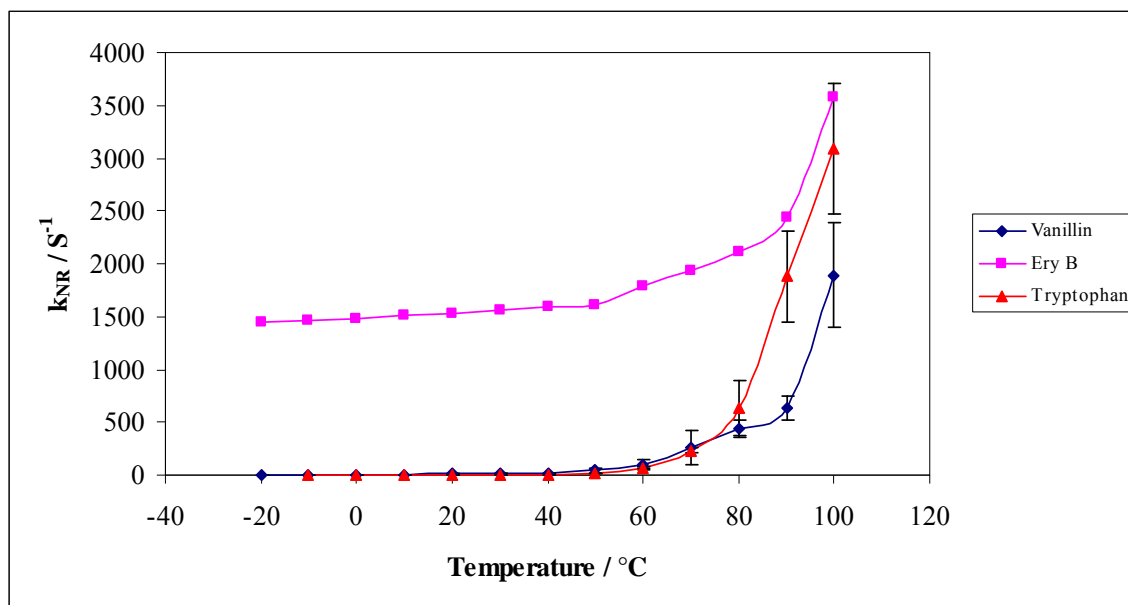
Figure VIc-5b

Figure VIc-5b: Temperature dependence of the rate of non-radiative decay to S_0 (k_{NR}) calculated for erythrosin B, vanillin and tryptophan in amorphous sucrose over the temperature range from -20°C to 100°C .

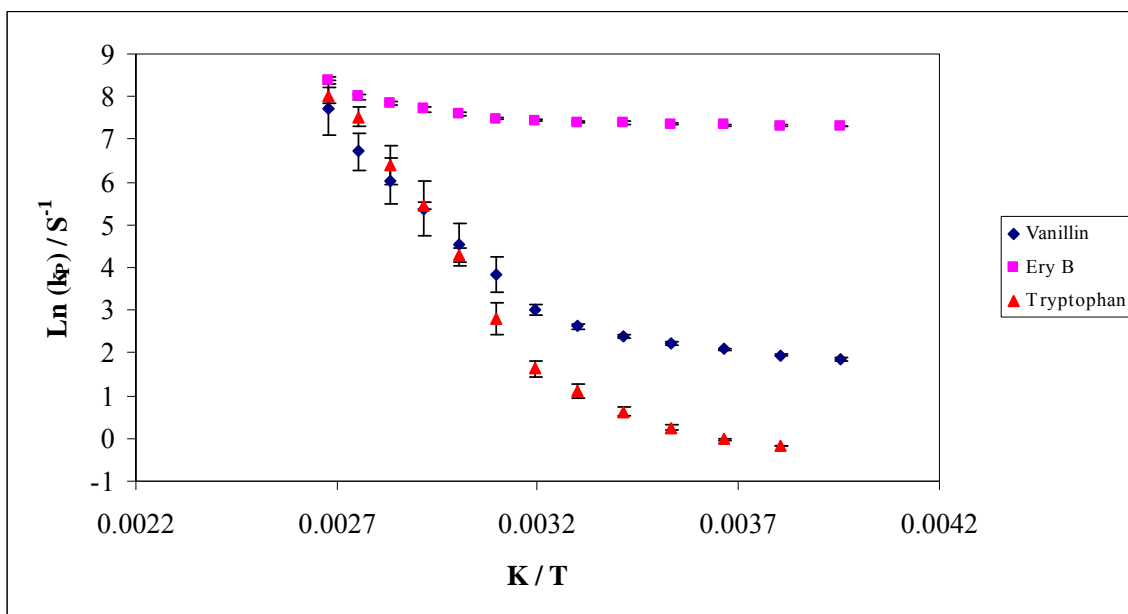
Figure VIc-6a

Figure VIc-6a: The Arrhenius plot of the rate of (k_p) calculated for erythrosin B, vanillin and tryptophan in amorphous sucrose over the temperature range from -20°C to 100°C .

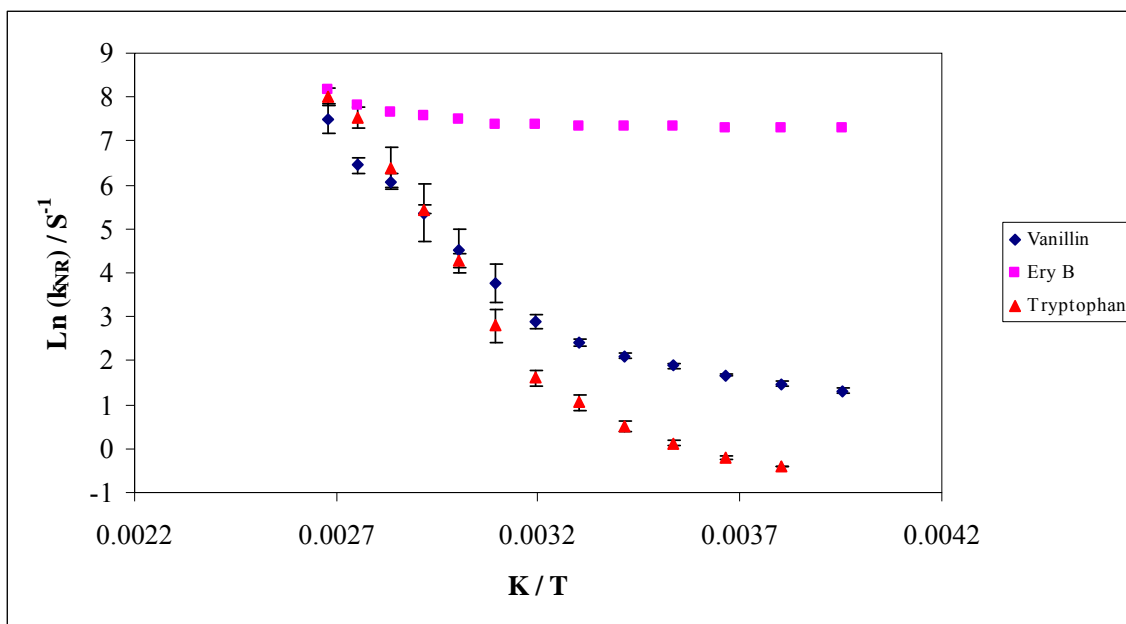
Figure VIc-6b

Figure VIc-6b: The Arrhenius plot of the rate of non-radiative decay to S_0 (k_{NR}) for erythrosin B, vanillin and tryptophan in amorphous sucrose over the temperature range from -20°C to 100°C .

Table VIc-1

Table VIc-1: The activation energies and transition temperatures of erythrosin B, vanillin and tryptophan in amorphous sucrose film.

Probe	E_{a_L} kJ / mol⁻¹	E_{a_H} kJ / mol⁻¹	T / C	τ_0 / ms
Ery B	1.2	10.2	58	26
Vanillin	13.84	72.32	40	372
Tryptophan	23.9	107.43	30	6000

References

- Bishai, F., Kuntz, E. and Augenstein, L. Intra and intermolecular factors affecting the excited states of aromatic amino acids. *Biochimica et Biophysica Acta*. 140 (1967). 381-394.
- Bohmer, R., Diezemann, G., Geil, B., Hinze, G., Nowaczyk, A and Winterlich, A. Correlation of primary and secondary relaxations in a super-cooled liquid. *Physical Review Letter*. 97 (2006). 135701-135702.
- Capaccioli, S., Kessairi, K., Prevosto, D., Lucchesi, M., Ngai, K. L. Genuine Johari-Goldstein beta-relaxations in glass-forming binary mixtures. *Journal of non crystalline solids*. 352 (2006). 4643.
- Champion, D., Le Meste, M. and Simatos, D. Towards an improved understanding of glass transition and relaxations in foods: molecular mobility in the glass transition range. *Trends in Food Science and Technology*. 11 (2000). 41-55.
- Debenedetti, P.G., and Stillinger, F. H. Supercooled liquids and the glass transition. *Nature*. 410 (2001). 259-267.
- Duchowicz, R., Ferrer, M.L. and Acuna, A.U. Kinetic spectroscopy of erythrosin phosphorescence and delayed fluorescence in aqueous solution at room temperature. *Photochemistry and Photobiology*. 68 (1998). 494-501.
- Ediger, M.D., Angell, C.A. and Nagel, S.R. Supercooled Liquids and Glasses. *Journal of Physical Chemistry*. 100 (1996). 13200-13212
- Hancock, B.C. and Zografi, G. Characteristics and significance of amorphous state in pharmaceutical systems. *Journal of Pharmaceutical Sciences* 86 (1997). 1-12.
- Kaminski, K., Kaminski, E., Hensel-Bielowka, S., Chelmecka, E., Pluch, M., Ziolo, J., Włodarczyk, P and Ngai, K. L. Identification of the molecular motions responsible for the slower secondary (β) relaxation in sucrose. *Journal of Physical Chemistry*. Xxx (2008).A-G.
- Kaminski, K., Kaminski, E., Paulch. M., Ziolo, J and Ngai, K. L. The true Johari-Goldstein β -relaxation of monosaccharides. *Journal of Physical Chemistry*. 110 (2006). 25045-25049.
- Le Meste, M., Champion, D., Roudau,t G., Blond, G. and Simatos, D. Glass transition and food technology: A critical appraisal. *Journal of Food Science*. 67 (2002). 2444-2458.
- Ngai, K. L and Paluch, M. J. Classification of secondary relaxation in glass-formers based on dynamic properties. *Journal of Chemical Physics*. 120 (2004). 857-873.

- Ngai, K. L. Relation between some secondary relaxations and the α -relaxations in glass-forming materials according to the coupling model. *Journal of Chemical Physics*. 109 (1998). 6982.
- Ngai, K. L. An extended coupling model description of the evolution of dynamics with time in supercooled liquids and ionic conductors. *Journal of Physics: Condensed Matters*. 15 (2003). S1107-1125.
- Ngai, K. L., Casalini, R., Capaccioli, S., Paluch, M and Roland, C. M. *Advanced Chemical Physics*. 133B (2006). 497.
- Poppe, L., Van Halbeek, H. J. The rigidity of sucrose: just an illusion? *American Chemical Society*. 114 (1992). 1092-1094.
- Vyazovkin, S. and Dranca, I. Probing beta relaxations in pharmaceutically relevant glasses by using DSC. *Pharmaceutical Research* 23 (2006). 422-28.
- Wagner, H. and Richert, R. Equilibrium and non-equilibrium type beta relaxations: D-Sorbitol versus o-Terphenyl. *Journal of Physical Chemistry* 103 (1999): 4071-77.
- Wagner, H. and Richert, R. Spatial uniformity of the beta relaxation in D-sorbitol. *Journal of Non-crystalline Solids*. 242 (1998). 19-24.
- Zallen, R. *The Physics of Amorphous Solids*. John Wiley and Sons, New York (1998).

Chapter VII : Protein (α -lactalbumin)

α -lactalbumin: α -lactalbumin is a small (14.3 kDa) globular calcium metalloprotein (Hendrix et al., 1996; Brew and Grobler, 1992; Wong et al., 1996). It is the second most common protein in bovine whey (20% of total whey protein). It has an ellipsoid shape with two distinct lobes divided by a cleft; one lobe is comprised of four helices and the other lobe is comprised of two β -strands with a loop-like chain. The bovine protein has 123 amino acids and contains four tryptophans (W26, W60, W104, and W118) and eight cysteine residues involved in four stable disulfide bonds with no free thiol groups (Vanaman et al., 1970). The three dimensional structure of the protein is known from crystallography (Acharya et al., 1989). The native calcium metalloprotein is referred to as holo α -lactalbumin and when calcium is removed from the structure it is referred to as apo α -lactalbumin. All α -lactalbumin species bind calcium at one strong affinity site, which dramatically affects its biophysical properties. α -lactalbumin on removal of calcium at low salt concentration and neutral pH is known to exist in a molten globule state (Ku wajima, 1996). In molten globule state α -lactalbumin includes native-like secondary structure (Hiroka and Sugai, 1984), a slightly expanded structure (10-20% larger radius) (Dolgikh et al., 1985), and an absence of tertiary structure packing (Ku wajima et al., 1976).

The apo form conformer has a much lower transition temperature ($T_d \sim 38^\circ \text{C}$) and renaturation ability than the holo form and has been referred to as more heat labile. We made films in absence of calcium to investigate the solid-state mobility of molten globule

state of amorphous α -lactalbumin. The current study focuses on using steady-state and time-resolved phosphorescence of the intrinsic tryptophan and extrinsic erythrosin B and vanillin to monitor molecular mobility as a function of temperature in amorphous solid dry films of α -lactalbumin (refers to apo form hence forth unless otherwise mentioned) in the molten globule state. The three probes selected differ in the triplet excited state lifetime where the lifetimes increase in the order of erythrosin B < vanillin < tryptophan. The idea is that longer lifetime probes may help to access other modes of motion that affects the proteins functionality in films, and will help determine whether slower molecular motions may be occurring in the amorphous α -lactalbumin matrix as a function of temperature. The structural and dynamic heterogeneity that has been observed on the millisecond time scale may be considerably different over seconds timescale.

Figure VII-1

Structure of Bovine α -lactalbumin



www.pdb.org

Amorphous Proteins: The physical properties of amorphous solid proteins are important for the texture of protein containing foods, the stability of pharmaceuticals, the viability of seeds and pores and the permeability of edible films (Slade, 1989; Hill et al., 2005; Buitink and Leprince, 2004; Krochta and DeMulder, 1997). Two main factors affecting the physical properties of amorphous solid protein include the 3D structure and molecular mobility. The physical change (in terms of molecular mobility) occurring in amorphous solid proteins are very important in defining their shelf-life and quality (Slade and Levine, 1991; Tolstoguzov, 2000; Walters, 2004). Molecular mobility in this context represents different types of motions, vibrations of atoms or bonds, reorientations of small groups of atoms, translational motion of molecules or segments of polymers (Le Meste et al., 2002), that are activated at specified conditions (Ludescher et al., 2001). The most common way of forming amorphous solid proteins are by rapid cooling of liquid melt, but there are many other routes to an amorphous state such as spray drying, freeze drying, extrusion, grinding, milling, etc (Liu et al., 2006). When solid proteins are dried they become amorphous. Different processes like dehydration restrict translational, rotational and vibrational motions in proteins that are important for biological functions (Rupley and Careri, 1991).

As compiled by Hill et al., 2005, proteins show many degrees of molecular motion like molecular vibrations, rotation of amino acids side chains, to more global larger scale motions of entire protein segments, depending on internal and external environmental conditions (Brooks et al., 1998). Stability of solid proteins (Lai and Topp, 1999) is strongly affected by temperature, water, pH, presence of any protectants, etc., and these

factors are known to affect dynamics of proteins (molecular mobility). Residual water has significant effect on solid state stability of proteins (Towns, 1995). The kinetics of various physical and chemical processes is strongly affected by the degrees of molecular mobility in amorphous solid proteins and hence is of concern to us. Changes in relaxation time can be an indicator of the tendency for physical or chemical instability in the amorphous state.

Protein Motions: Proteins show broad distribution of motions ranging from 10^{-15} to 10^4 s. Proteins motion include bond vibrations, side chain rotations, surface loops wiggling, domains flexing at connecting bonds, and the entire structure fluctuating to assemble the most stable structure (Ludescher, 1990). Thus, proteins have several degrees of motions; these motions are desirable to keep protein flexible enough to perform lots of functions, but in cases where motions lead to unfolding causing loss of its functionality it is highly undesirable. For example, proteins are thought to lose stability (Vanderheeren and Hanssens, 1994) due to preferential orientation of amino acids when exposed to air-water or liquid-water interfaces (Hill et al., 2005). Molecular mobility of proteins in solid state is not fully characterized.

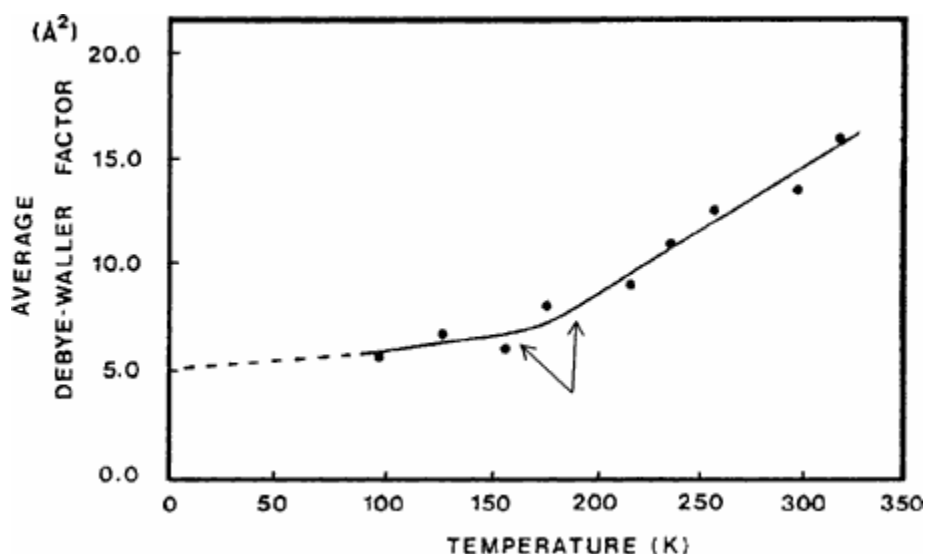
Fully hydrated proteins are known to show dynamic transition which is identified with polymer glass transition when cooled near the temperature called the dynamical transitions T_d , the so called glass transition in protein which is reminiscent of the α , β motions in glasses (Hill et al., 2005). The glass transition involves a change in the protein or polymer backbone (translational motions) and the lower temperature motions (β and γ)

involves side chain motions. Above T_d , dynamic behavior is dominated by highly temperature dependent, large-scale, anharmonic, collective motion of bonded and non-bonded atoms superimposed on small amplitude vibrational motions, whereas below T_d , nearly small-amplitude, harmonic vibrations exist with a temperature dependence similar to the harmonic atomic vibrations in small molecule crystals (Hill et al., 2005).

Amorphous protein solids are glassy when dry and rubbery when moist and exhibit broad thermal transitions between these states. Broad thermal softening transitions have been seen in calorimetric studies of lysozyme, hemoglobin, and myoglobin (Sartor and Johari, 1994) (Figure VII-2).

Figure VII-2

Dynamic transitions in Proteins



(Adapted from Hill et al., 2005)

Proteins demonstrate many degrees of molecular motions (Table 1). Motions in proteins cover time scales from femtoseconds (individual bond vibrations) to picoseconds (small group fluctuations) to nano and microseconds and longer (collective motions of groups of bonded and non-bonded atoms) and corresponding distance scales from fractions to an Angstrom.

Table VII-1

Characteristic motions of globular proteins

Local motions (0.01-5 Å, 10^{-15} - 10^{-1} s)

Atomic fluctuations

Side chain motions

Loop motions

Terminal arm motions

Rigid body motions (1-10 Å, 10^{-9} -1 s)

Helix motions

Domains (hinge bending) motions

Subunit motions

Larger-scale motions (>5 Å, 10^{-7} - 10^4 s)

Helix-coil transitions

Dissociation/association and coupled structural changes

Opening and distortional fluctuations

Folding and unfolding transitions

(Adopted from Brooks et al., 1998)

Studies have used dielectric relaxation (Gangasharan and Murthy, 1993; Chan et al., 1986; Faivre et al., 1999; Richert, 2001), mechanical spectroscopy (Faivre et al., 1999), FTIR (Wolkers et al., 1998), NMR (Moran and Jeffrey, 1999; Van Dusschoten et al., 1999), and ESR (Buitink et al., 2000) to study molecular mobility in food matrices. Also there are other methods to study protein dynamics; fluorescence and phosphorescence spectroscopy with the help of intrinsic (e.g., tryptophan) probe or extrinsic covalently attached organic dye (e.g., erythrosin B) has been widely used to study their dynamics in solution and in solid state (McGown and Nithipatikom, 2000). Due to the timescale of excited singlet state, fluorescence spectroscopy responds to molecular events in the range of 10^{-7} - 10^{-11} s and those of excited triplet state in case of phosphorescence spectroscopy respond to molecular event in the ms to s (Parker, 1968; Lakowicz, 1999). Molecular mobility can be detected within the local environment of a probe using phosphorescence spectroscopy as it is a sensitive site specific method (Shirke and Ludescher, 2005, 2006a, 2006b; Simon-Lukasik and Ludescher, 2006a, 2006b, 2004). It is very important that a probe should have high quantum yield of phosphorescence emission and the lifetime of emission should be within the timescale for monitoring motions (Lettinga et al., 2000).

Molecular Probes: Phosphorescence can be obtained from probes that can be divided into two categories: intrinsic or extrinsic probes. Extrinsic probes could be either covalently attached (e.g., erythrosin isothiocyanate attached to a protein surface; (Simon-Lukasik and Ludescher, 2004) or dispersed (e.g., erythrosin isothiocyanate dispersed in sucrose matrix: Pravinata et al., 2005). The intrinsic probe could be naturally occurring amino acid residue in proteins (e.g., tryptophan: Mazhul et al., 2002) and thus could provide site

specific dynamics information (Hurtubise et al., 1997). The different time scales of motions demand different probes; for example slower motions like the ones that occur in viscous glass demand using long-lifetime chromophores as compared to say if the medium was water (Lakowicz, 1999).

A probe observes molecular mobility during its excited state lifetime, and for slower motions (Craig et al., 1999) longer lifetime probes are more suitable and the opposite is true for faster motions. A probe should have high quantum yield of phosphorescence emission and the lifetime of emission should be within the timescale for monitoring motions (Lettinga et al., 2000). Organic dyes having easily populated stable triplet states, offer good choice as probes and are referred to as triplet probes (Parker, 1968).

Different probes will have different lifetime based on their molecular structure and environment in which they are present; the lifetime could also vary based on the sensitivity of the probe. Molecular probes report on the properties of the molecular environment around the probe. Different probes provide different information with respect to mobility.

As discussed above luminescence signal from spectroscopic probes erythrosin B, tryptophan, and vanillin are sensitive to mobility in amorphous solids. These three probes differ, where tryptophan is an intrinsic probe and erythrosin B and vanillin are extrinsic dispersed probes and have different lifetime and thus will monitor mobility in different time scales.

Probes emitted photons that can be characterized by their energy, their intensity and their polarization. Measurements of these luminescence characteristics can describe mobility and interaction within a specific size and time scales, depending on the chosen probe's size, lifetime and its specific location in a matrix.

References

- Acharya, K. R., Stuart, D. I., Walker, N. P., Lewis, M., and Phillips, D. C. Refined structure of baboon alpha-lactalbumin at 1.7 Å resolution. Comparison with C-type lysozyme *Journal of Molecular Biology* **208** (1989). 99-127.
- Brew, K. and Grobler, J. A. In advanced dairy chemistry: proteins. Edited by P. F. Fox. Elsevier Applied Science., New York. (1992). 191-229.
- Brooks, C.L. III, Gruebele, M., Onuchic, J.N. and Wolynes, P.G. Chemical physics of protein folding. *Proceedings of National Academy of Sciences of USA*. 95 (1998). 11037-11038.
- Buitink, L. and Leprince, O. Glass formation in plant anhydrobiotes: survival in the dry state. *Cryobiology* 48 (2004). 215-28.
- Chan, R. K., Pathmanathan, K. and Johari, G. P. Dielectric relaxations in the liquid and glassy states of glucose and its water mixture. *Journal of Physical Chemistry*. 90 (1986). 6358-6362.
- Craig, D.Q., Royall, P.G., Kett, V.L. and Hopton, M.L. The relevance of the amorphous state of pharmaceutical dosage forms: glassy drugs and freeze dried systems. *International Journal of Pharmaceutics*. 179 (1999). 179-207.
- Dolgikh, D. A., Abaturov, L. V., Bolotina, I. A. Compact state of a protein molecule with pronounced small-scale mobility: bovine α-lactalbumin. *European Biophysics Journal*. **13** (1985) 109-121.
- Faivre, A., Niquet, G., Maglione, M., Fornazero, J., Jal, J. F. and David, L. Dynamics of sorbitol and maltitol over a wide temperature range. *European Physical Journal B; Condensed Matter*. 10 (1999). 277-286.
- Gangasharan and Murthy, S. S. N. Study of α , β and γ relaxation processes in some supercooled liquids and supercooled plastic crystals. *Journal of Chemical Physics*. 99 (1993). 9865-9873.
- Hendrix, T.M., Griko, Y. and Privalov, P. Energetic of structural domains in alpha-lactalbumin. *Protein Science* 5 (1996). 923-931.
- Hill, J.J., Shalaev, E.Y. and Zografi, G. Thermodynamic and dynamic factors involved in the stability of native proteins structure in amorphous solids in relation to levels of hydration. *Journal of Pharmaceutical Sciences* 94 (2005). 1636-67.
- Hiroka, Y., Sugai, S. Thermodynamics of thermal unfolding of bovine apo- α -Lactalbumin. *International Journal of Peptide Protein Research*. 23 (1984). 535-542.

- Hurtubise, R.J. Phosphorimetry: Theory Instrumentation, and Applications. VCH Publishers, Inc, New York (1990).
- Hurtubise, R.J. Solid matrix luminescence analysis: photophysics, physicochemical interactions and applications. *Analytical Chimica Acta*. 351 (1997). 1-22.
- Krochta, J. M., DeMulder-Johnston, C. Edible and biodegradable polymer films: challenges and opportunities. *Food Technology*. 51 (1997). 61-74.
- Kuwajima, K. The molten globule state of alpha-lactalbumin. *The FASEB Journal*. 10 (1996). 102-109.
- Kuwajima, K., Nitta, K., Yoneyama, M and Sugai, S. Three-. state denaturation of c-lactalbumin by guanidine hydro-. Chloride. *Journal of Molecular Biology*. 106 (1976). 359-373.
- Lai, M.C. and Topp, E.M. Solid state chemical stability of protein and peptides. *Journal of Pharmaceutical Sciences*. 88 (1999). 489-500.
- Lakowicz, J.R. Principles of Fluorescence Spectroscopy. Second edition, Kluwer Academic/Plenum Press, New York (1999).
- Le Meste, M., Champion, D., Roudaut, G., Blond, G. and Simatos, D. Glass transition and food technology: A critical appraisal. *Journal of Food Science*. 67 (2002). 2444-2458.
- Lettinga, M.P., Zuilhof, H. and van Zandvoort, M.A. Phosphorescence and fluorescence characterization of fluorescein derivatives immobilized in various polymers matrices. *Physical Chemistry Chemical Physics*. 2 (2000). 3697-3707.
- Liu, Y., Bhandari, B. and Zhou, W. Glass transition and enthalpy relaxation of amorphous food saccharides: A review. *Journal of Agricultural and Food Chemsitry*. 54 (2006). 5701-5717.
- Ludescher, R.D., Shah, N.K., McCaul, C.P. and Simon, K.V. Beyond Tg: optical luminescence measurements of molecular mobility in amorphous solid foods. *Food Hydrocolloids* 15 (2001). 331-339.
- Ludescher, R.D. Molecular dynamics of food proteins: Experimental techniques and observations. *Trends in Food Science and Technology*. 1 (1990). 145-149.
- Mazhul, V.M, Zaitseva, E.M and Shcherbin, D.G. Phosphorescence of tryptophan residues of proteins at room temperature. *Journal of Applied Spectroscopy*. 69 (2002). 213-219.

- McGown, L.B. and Nithipatikom, K. Molecular fluorescence and phosphorescence. *Applied Spectroscopy Reviews*. 35 (2000). 353-393.
- Moran, G. R. and Jeffrey, K. R. A study of the molecular motion in glucose/water mixtures using deuterium nuclear magnetic resonances. *Journal of Chemical Physics*. 110 (1999). 3472-3483.
- Parker, C.A. *Photoluminescence of Solutions*. Elsevier Pub Co., Amsterdam (1968).
- Pravinata, L.V., You, Y. and Ludescher, R.D. Erythrosin B phosphorescence monitors molecular mobility and dynamic heterogeneity in amorphous sucrose. *Biophysical Journal*. 88 (2005). 3551-3561.
- Richert, R. Spectral selectivity in the slow beta relaxation of a molecular glass. *Europhysics Letters*. 54 (2001). 767-773.
- Rupley, J. A. and Careri, G. Protein hydration and function. *Advanced Protein Chemistry*. 41 (1991). 37-172.
- Sartor, G. and Johari, G. P. Calorimetric studies of the kinetic unfreezing of molecular motions in hydrated lysozyme, hemoglobin, and myoglobin. *Biophysical Journal*. 66 (1994). 249-258.
- Shirke, S. and Ludescher, R.D. Dynamic site heterogeneity in amorphous maltose and maltitol from spectral heterogeneity in erythrosin B phosphorescence. *Carbohydrate Research*. 340 (2005). 2661-2669.
- Shirke, S. and Ludescher, R.D. Dynamic site heterogeneity in amorphous lactose and lactitol from spectral heterogeneity in erythrosin B phosphorescence. *Biophysical Chemistry*. 123 (2006). 122-33.
- Shirke, S. and Ludescher, R.D. Molecular mobility and glass transition in amorphous glucose, maltose and maltotriose. *Carbohydrate Research*. 340 (2006). 2654-2660.
- Simon-Lukasik, K.V. and Ludescher, R.D. Effect of plasticizer on dynamic site heterogeneity in cold-cast gelatin films. *Food Hydrocolloids*. 20 (2006). 88-95.
- Simon-Lukasik, K.N. and Ludescher, R.D. Molecular mobility in water and glycerol plasticized cold and hot cast gelatin films. *Food Hydrocolloids*. 20 (2006). 96-105.
- Simon-Lukasik, K.V. and Ludescher, R.D. Erythrosin B phosphorescence as a probe of oxygen diffusion in amorphous gelatin films. *Food Hydrocolloids*. 18 (2004). 621-630.
- Slade, L. and Levine, H. A food polymer science approach to structure interactions. *Advances in experimental medicine and biology*. 302 (1991). 29-101.

- Slade, L., Levine, H., Finley, J. W. In protein quality and effects of processing; Phillips, R. D., Finley, J. W., eds., Marcel and Dekker Inc, New York. (1989).
- Tolstoguzov, V.B. The importance of glassy biopolymer components in food. *Nahrung*. 44 (2000). 76-84.
- Towns J.K. Moisture content in proteins: its effect and measurements. *Journal of Chromatography*. 705 (1995). 115-127.
- Van Dusschoten, D., Tracht, U., Heuer, A. and Spiess, H. W. Site specific rotational mobility of anhydrous glucose near the glass transition as studied by 2D echo decay ¹³C NMR. *Journal of Physical Chemistry*. 103 (1999). 8359-8364.
- Vanaman, T. C., Brew, K. and Hill, R. J. *Journal of Biological Chemistry*. 245 (1970). 4583-4585.
- Vanderheeren, G. and Hanssens, I. Thermal unfolding of bovine alpha lactalbumin. *The Journal of Biological Chemistry*. 269 (1994). 7090-94.
- Walters, C. Temperature dependency of molecular mobility in preserved seeds. *Biophysical Journal*. 86 (2004). 1253-58.
- Wolkers, W.F., Oldenholf, H., Alberda, M. and Hoekstra, F. A. A Fourier transform infrared microspectroscopy study of sugar glasses: application to anhydrobiotic higher plant cells. *Biochimica Biophysica Acta*. 1379 (1998). 83-96.
- Wong, D. W. S., Camirand, W. M. and Pavlath, A. E. structures and functionalities of milk proteins. *Critical Review in Food Science and Nutrition*. 36 (1996). 807-841.
- www.pdb.org

Chapter VII-a: Effect of temperature on molecular mobility, oxygen permeability, and dynamic site heterogeneity in amorphous α -lactalbumin films

Introduction

Erythrosin B is the most widely used phosphorescent probe of the molecular mobility of water soluble and membrane bound proteins because of its large extinction coefficient and high phosphorescence quantum yield even in aqueous solution. Erythrosin B (Ery B) has 98% of excited molecules converting to triplet state and has high phosphorescence quantum yield (Garland and Moore, 1979) and is thus considered as an ideal probe for phosphorescence studies. The phosphorescence of erythrosin B is due to the xanthene ring with four iodine atoms. Erythrosin B is one of the most sensitive and commonly used triplet probes in the study of μ s dynamics of large proteins in solution and in biomembranes. Erythrosin B has been used to monitor molecular mobility in many simple amorphous systems such as sucrose (Pravinata et al., 2005), gelatin (Simon-Lukasik and Ludescher, 2006a, 2006b), bovine serum albumin (Nack and Ludescher, 2006), β -lactoglobulin (Sundaresan and Ludescher, 2007) and glucose, maltose and maltotriose (Shirke and Ludescher, 2006a, 2006b). This study provides useful information about molecular events in amorphous α -lactalbumin using erythrosin B.

Oxygen is a contact quencher of the excited triplet state; phosphorescence can thus be used as a sensitive indicator of oxygen diffusion in amorphous solid proteins. Measurements of phosphorescence emission and lifetimes from Ery B labeled gelatin films (Simon-Lukasik and Ludescher, 2004) , amorphous BSA (Nack and Ludescher,

2006) and amorphous β -lactoglobulin (Sundaresan and Ludescher, 2007) have indicated its utility to monitor oxygen diffusion.

Amorphous solids due to dynamic heterogeneity (Ediger, 2000; Sillescu, 1999) may have distinct dynamic regions (high density or low density) and show different relaxation times (Liu et al., 2006; Shamblin et al., 1999. Sillescu, (1999) has extensively reviewed the existence of heterogeneity in glass forming liquids and polymers, by compiling different experimental techniques like NMR, dielectric and optical experiments which indicate the presence of dynamical heterogeneity (Sillescu, 1999; Richert1997, 2001). Dynamic site heterogeneity has being studied by Ludescher and colleagues using phosphorescence spectroscopy in various amorphous solids. Phosphorescence emission from Ery B has been shown to be distributed among dynamically distinct sites in different amorphous matrices like gelatin (Simon-Lukasik and Ludescher, 2006a, 2006b), maltose and maltitol (Shirke and Ludescher, 2005), lactose and lactitol (Shirke and Ludescher, 2006a, 2006b), amorphous sucrose (Pravinata et al., 2005) and in amorphous bovine serum albumin (Nack and Ludescher, 2006). It has been shown that in these amorphous solids different sites vary in overall molecular mobility indicating the presence of dynamic heterogeneity.

We report here a comparable phosphorescence study of molecular mobility, oxygen permeability and dynamic site heterogeneity in amorphous α -lactalbumin films using steady state and time-resolved intensity decays from dispersed Ery B. In this study we measure the local molecular mobility in amorphous α -lactalbumin films as a function of

temperature using phosphorescence spectroscopy based on emissions from Ery B dispersed in the matrix. We report here a comparable phosphorescence study of oxygen permeability in amorphous α -lactalbumin films using erythrosin B phosphorescence.

Materials and Methods

Sample preparation: Purified α -lactalbumin (calcium depleted) was obtained from Sigma Chemical Company (St Louis, MO) and used as received. In order to define and minimize the presence of counter ions, α -lactalbumin was dissolved in distilled deionized water at 10 mg/ml, placed in a cellulose dialysis tube having a 1 kDa molecular weight cutoff (Spectrum, Houston, TX), dialyzed against 0.1 M potassium chloride for at least 36 hours with frequent changes of buffer, and then dialyzed extensively against distilled deionized water. All dialysis was carried out at 4°C. The solution was then filtered through a 0.2 μ m Acrodisc membrane filter (Pall Gellman Laboratory, Ann Arbor, MI) to remove particulate matter. The concentration of the protein after dialysis was determined by absorbance at 280 nm using an extinction coefficient of 28,500 $\text{M}^{-1}\text{cm}^{-1}$ (Kronman and Andreotti, 1964).

A 10 mg/ml stock solution of Ery B free acid (Molecular Probes, Inc., Eugene, OR) was prepared in N,N-dimethylformamide (DMF) (Sigma-Aldrich, Milwaukee, WI); DMF has negligible effects on the spectroscopic properties of the probe in amorphous sucrose at a variety of concentrations (Pravinata et al., 2005). This concentration was selected to simplify the addition of the probe to the α -lactalbumin solution, and the solvent was selected for probe stability during long term storage. The probe was added to the α -lactalbumin solution at a molar ratio of 1:4 (dye: α -lactalbumin). At this concentration it was determined that the Ery B does not aggregate, existing only as individual molecules monitoring the molecular mobility of the protein.

Preparation of protein films: The amorphous films were made by pipetting 20 μL of the solution (Ery B + α -lactalbumin) onto quartz slides (13 mm x 30 mm x 0.6 mm) (NSG Precision Cells, Farmingdale, NY) and spreading the solution over an area approximately 15 mm x 10 mm. Before use, to improve the surface activity for spreading the solutions, the slides were soaked in Terg-A-Zyme (Alconox, Inc., NY) soap solution, washed with double distilled water, rinsed with ethanol and dried in acetone. After spreading (~ 0.05 mm thick), the slides were dried under constant flow of air for 30 minutes, allowing the films to set, and then transferred to a desiccators over phosphorus pentoxide for at least one week, where the water activity is not greater than 0.01. The slides were stored at $23.0 \pm 1^\circ\text{C}$, protected from light to prevent any photo bleaching of the Ery B and desiccant was refreshed as needed to maintain a relative humidity close to 0%.

Luminescence Measurements: Luminescence measurements were made using a Cary Eclipse fluorescence spectrophotometer (Varian Instruments, Walnut Creek, CA). Quartz slides were placed in a standard quartz fluorescence cuvette, which was capped with a lid having inlet and outlet ports for gas lines. The cuvette was flushed with a gentle stream of nitrogen for 15 minutes prior to data collection to eliminate oxygen. An oxygen-free nitrogen stream was generated by passage of high purity nitrogen through a Supelco (Bellefonte, PA) carrier gas purifier. The temperature of the cuvette holder was controlled by a thermoelectric cooler (Quantum Northwest, Spokane, WA); the temperature of the cuvette was monitored directly using a thermocouple in the cuvette. The films were equilibrated for 15 minutes at each temperature before collecting data.

The Cary Eclipse uses a pulsed lamp and collects emission intensity in analog mode; data were not collected within the first 0.1-0.2 ms to suppress fluorescence coincident with the lamp pulse. Delayed luminescence emission spectra were collected from 535 to 800 nm (10 nm bandwidth) using excitation at 500 nm (20 nm bandwidth) over the temperature range from -20°C to 100°C . Each data point was collected from a single flash with 0.2 ms delay, 5.0 ms gate time, and 0.02 s total decay time.

Phosphorescence emission spectra measured as a function of time delay following excitation at 500 nm (bandwidth 20 nm) were collected from 620-750 nm (bandwidth 10 nm) with gate time of 0.5 ms, number of flashes = 1 and varying delay times of 0.1, 0.6, 1.1, 1.6 and 2.1 ms. The phosphorescence spectra collected as a function of temperature in the presence of nitrogen were converted to intensity versus frequency (cm^{-1}) and analyzed to obtain the peak frequency and spectral bandwidth using eq. (1) and (2).

Lifetime measurements were made in the presence of nitrogen ($-\text{O}_2$) or in presence of air ($+\text{O}_2$) as a function of temperature. The samples were excited at 540 nm (20 nm bandwidth) and emission transients collected at 680 nm (20 nm bandwidth) at temperatures ranging from -20°C to 100°C . Each decay transient was the sum of 50 cycles, and for each cycle data were collected from a single lamp flash with a delay of 0.1 ms, 0.02 ms gate time and 4.0 ms total decay time. All measurements were made in quadruplicate.

The intensity decays of Ery B were also measured as a function of excitation wavelength using emission at 690 nm (bandwidth 20 nm); excitation wavelength was varied from 460 to 580 nm (bandwidth 10 nm). Measurements of intensity decays were also measured as a function of emission wavelength using excitation at 540 nm (bandwidth 20 nm); emission wavelength was varied from 660 to 760 nm (bandwidth 10 nm). The measurements were made at varying temperatures from -20°C to 120°C in the presence of nitrogen or air. The intensity was collected as a function of time following the lamp flash over a total window of 4 ms following a delay time of 0.1 ms and using a gate time of 0.02 ms; 50 cycles were summed to get a single decay. The intensity decay was analyzed using the stretch-exponential decay function (Eq. 3).

Data Analysis

Delayed luminescence spectra were fitted to a sum of two log normal functions using the program NFIT (Island Products, Galveston, TX). The emission peak energy (ν_p) and bandwidth (full-width-at-half-maximum, FWHM) of the emission bands were determined by fitting both delayed fluorescence and phosphorescence emission as a function of frequency (in cm^{-1}) to a log normal function Equation 1 (Maroncelli and Fleming, 1987).

$$I(\nu) = I_0 \exp \left\{ -\ln(2) \left[\ln(1 + 2b(\nu - \nu_p)/\Delta)/b \right]^2 \right\} \quad (1)$$

In this equation I_0 is the maximum emission intensity, ν_p is the peak energy (in cm^{-1}) of the emission maximum, Δ is a line width parameter, and b is an asymmetry parameter. The FWHM is related to b and Δ (Maroncelli and Fleming, 1987) Equation 2.

$$\Gamma = \Delta \sinh(b)/b \quad (2)$$

The time-resolved phosphorescence emission spectra collected as a function of delay time and temperature were also analyzed using eq. (1) and (2).

Intensity decay transits were analyzed using a non-linear least squares iterative fitting procedure using the program NFIT (Island Products, Galveston, TX). Fits were judged satisfactory if the r^2 values were in the range of 0.995-1.0, and the modified residual $[(\text{data-fit})/\text{data}^{1/2}]$ varied randomly about zero. Intensity decays were clearly non-exponential and were analyzed using the stretched exponential or Kohlrausch-Williams-Watts (KWW) model Equation 3. This model has being shown to be appropriate to describe the wide distribution of relaxation times (Champion et al., 2000) for the molecular processes that depopulate excited states in amorphous solids.

$$I(t) = I(0) \exp\{-(t/\tau)^\beta\} + C \quad (3)$$

Where $I(0)$ is the initial amplitude at time zero, τ is the Kohlrausch-Williams-Watt lifetime, and β is the stretching exponent, which varies from 0 to 1 and quantifies the non-exponential nature of the decay, and C is a constant; β provides a measure of the width of the distribution of lifetimes required to fit the intensity decay; the smaller the value of β , the wider the distribution of lifetimes (Lindsey and Patterson, 1980).

Photophysical Scheme: The phosphorescence lifetimes were interpreted in terms of the rate constants associated with the various processes that contribute to the de-excitation of the excited triplet state of the probe Equation 4 (Duchowicz et al., 1998).

$$\tau^{-1} = k_P = k_{RP} + k_{TS1} + k_{TS0} + k_Q[\text{O}_2] \quad (4)$$

In this expression, k_{RP} is the rate of radiative decay of the triplet state (phosphorescence) its value for erythrosin is 41s^{-1} (Lettinga et al., 2000; Duchowicz et al., 1998) . The term k_{TS1} is the rate for thermally activated reverse intersystem crossing from the triplet to the singlet excited state; it has an exponential dependence on the energy gap (ΔE_{TS}) between the singlet and the triplet state Equation 5:

$$k_{TS1}(T) = k_{TS1}^0 \exp(-\Delta E_{TS}/RT) \quad (5)$$

The value of ΔE_{TS} was calculated from the slope of the natural logarithm of the ratio of the emission intensity due to delayed fluorescence (I_{DF}) and phosphorescence (I_P) plotted versus $1/T$ Equation 6; I_{DF} and I_P were determined from log normal analysis of the emission spectra.

$$d [\ln (I_{DF}/I_P)]/d(1/T) = - \Delta E_{TS}/R \quad (6)$$

(Where $R = 8.314 \text{ J K}^{-1} \text{ mol}^{-1}$). The value of k_{TS1} was calculated from equation 5 using $k_{TS1}^0 = 6.5 \times 10^7 \text{ s}^{-1}$ and $\Delta E_{TS} = 31.9 \text{ kJ mol}^{-1}$. Intersystem crossing to the ground state S_0 , which reflects relaxation of the probe from the excited triplet state to the ground state without the emission of a photon, has rate k_{TS0} . The value of k_{TS0} was calculated from the lifetime in the presence of nitrogen ($-O_2$) (where $k_Q[O_2]$ is negligible) using Eq. 4. The rate of collisional quenching of the excited triplet state of the probe by oxygen is $k_Q[O_2]$. The values of $k_Q[O_2]$ was calculated from the difference in the inverse lifetime in the presence of air ($+O_2$) and nitrogen ($-O_2$) using Equation 7.

$$k_Q[O_2] = 1/\tau(\text{air}) - 1/\tau(N_2) \quad (7)$$

Results

Delayed emission spectra: The delayed luminescence spectra of Ery B dispersed in amorphous α -lactalbumin films (in the presence of nitrogen) as a function of temperature are plotted in Figure 1. These spectra exhibited maxima at ~ 565 nm and ~ 695 nm corresponding to delayed fluorescence and phosphorescence emission bands, respectively. Delayed, or E-type, fluorescence reflects emission to the ground state (S_0) from a singlet state (S_1) that has been repopulated by reverse intersystem crossing from the triplet state (T_1) (Parker, 1968). The phosphorescence band reflects emissions from the triplet state (T_1) to the ground state (S_0). The delayed emission spectra were collected over the temperature range -20°C to 100°C . Delayed emission showed a decrease in phosphorescence intensity as a function of temperature; the delayed fluorescence intensity increased continuously from -20°C to 100°C , as expected from a thermally stimulated processes.

The intensity ratio when plotted as a Van't Hoff plot of $\ln(I_{\text{DF}}/I_{\text{P}})$ vs. $1/T$ (using the maximum emission intensity determined from fitting spectra to a log-normal function) was linear over the entire range of measured temperature (with $R^2 > 0.995$ for all curves) with no systematic deviation (data not shown); the slope provides an estimate of the energy gap, ΔE_{TS} , between the lowest triplet (T_1) and singlet (S_1) states. The value of $\Delta E_{\text{TS}} = 31.9 \pm 0.9 \text{ kJ mol}^{-1}$ in presence of nitrogen was not significantly different than in presence of air ($\Delta E_{\text{TS}} = 31.55 \pm 0.8 \text{ kJ mol}^{-1}$). These values were significantly higher than that for Ery B in ethanol, $28.5 \text{ kJ mole}^{-1}$ (Duchowicz, 1998), but slightly smaller than the values for Ery B in amorphous films of bovine serum albumin ($32.9 \pm 0.5 \text{ kJ mol}^{-1}$)

(Nack and Ludescher, 2006) and β -lactoglobulin ($33.6 \pm 0.8 \text{ kJ mol}^{-1}$) (Sundaresan and Ludescher, 2007), suggesting that the specific structure of the matrix influences the triplet-singlet energy gap.

The peak energy (ν_p) and bandwidth (Γ) for both delayed fluorescence and phosphorescence were determined by fitting emission spectra to a sum of two log-normal functions. The values of ν_p and Γ for the phosphorescence band varied systematically as a function of temperature (Figure 2). There was a gradual decrease in the emission energy at low temperature, -20°C to 10°C , followed by steeper decrease above 10°C . The decrease in ν_p reflects an increase in the rate of dipolar relaxation around the triplet excited state (Lakowicz, 1999). The emission bandwidth (Γ) remained constant from -20°C to 10°C , increased gradually over the temperature interval from 20°C to 80°C , and increased sharply at higher temperature. The increase in Γ at elevated temperatures reflects an increase in the extent of inhomogeneous broadening of the spectra due to changes in the interaction of Ery B molecules with the surrounding matrix. The increase in dipolar relaxation rate was thus accompanied by an increase in the width of the distribution of energetically different environments. An Arrhenius plot of the inverse phosphorescence intensity ($1/I_p$), where I_p was determined by fitting the emission spectra to a log-normal function (data not shown) was biphasic; the transition temperature (determined from intersection of lines fit to points at low and high temperature) was estimated to be $\sim 50^\circ\text{C}$.

Phosphorescence lifetimes: Phosphorescence intensity decays of Ery B in amorphous α -lactalbumin films at 20°C in the presence of nitrogen (-O₂) and air (+O₂) are plotted in Figure 3 along with the modified residuals for fits to these decays using a stretched exponential model function (Eq. 3, Materials and Methods). The modified residuals for these fits varied randomly around zero, indicating that the stretched exponential function provided a statistically satisfactory fit to these data. All intensity decay data over the temperature interval from -20°C to 100°C were well fitted using a stretched exponential function. A stretched exponential function has also been shown to provide a statistically satisfactory fit to intensity decays of Ery B dispersed in amorphous gelatin (Simon-Lukasik and Ludescher, 2006a, 2006b), bovine serum albumin (Nack and Ludescher, 2006) and β -lactoglobulin (Sundaresan and Ludescher, 2007) under all conditions measured.

The phosphorescence intensity decreased with increasing temperature in absence and presence of oxygen, indicating an increase in triplet state quenching rates with increase in temperature; the results of these analyses are plotted in Figure 4a. The Ery B lifetime in the absence of oxygen was 0.56 ms at -20°C and decreased to 0.1 ms at 100°C; the decrease was gradual at low temperature and more dramatic at higher temperature. The decrease in lifetime with temperature in the absence of oxygen is the result of an increase in both k_{TS1} , the rate of reverse intersystem crossing to the excited singlet state (S_1), and k_{TS0} , the rate of intersystem crossing to a highly excited vibration of the singlet S_0 manifold followed by vibrational relaxation to the ground vibrational state (see Eq. 4 and analysis in Materials and Methods). The rate k_{TS0} reflects the extent to which molecular

motions within the matrix are able to facilitate dissipation of the vibrational energy of the highly excited probe into the matrix (Fischer et al., 2002; Vanderkooi and Berger, 1989) and is an indicator of matrix mobility.

The lifetime at -20°C in the presence of oxygen was 0.54 ms and identical within error to the value in the absence of oxygen, indicating that oxygen quenching was negligible at low temperature. The lifetime in the presence of oxygen, however, was significantly smaller than the lifetime in the absence of oxygen at all temperatures above 0°C , decreasing to as low as 0.06 ms at 100°C , indicating that oxygen quenching was thermally activated at about 0°C and above. Based on measurements in the presence and absence of oxygen on the same slide, comparison of the phosphorescence intensity I_p , determined from log-normal fits to the emission spectra, of films in the presence and absence of oxygen also indicated that oxygen effectively quenched the probe emission at all temperatures above 0°C (data not shown).

The stretching exponent β is a measure of the width of the distribution of lifetimes required to fit the intensity decay (Lindsey and Patterson, 1980; Richer, 2002); it provides a measure of the dynamic heterogeneity of the matrix and varies primarily due to variability in k_{TS0} (Pravinata et al., 2005). The value of β decreased linearly and equivalently with temperature in both the presence and absence of oxygen from a maximum of ~ 0.85 at -20°C to ~ 0.8 at 60°C . Above 60°C , however, β was lower in the presence of oxygen, decreasing to ~ 0.75 in the absence of oxygen and ~ 0.65 in the presence of oxygen at 100°C . There was significant difference in β in the presence and

absence of oxygen above 80°C, as shown in Figure 4b. The lower value, and thus a broader distribution of lifetimes, in the presence of oxygen (Lindsey and Patterson, 1980) may reflect additional heterogeneity due to variations in the magnitude of the oxygen quenching constant $k_Q [O_2]$.

Photophysical rate constants: The photophysical rate constants corresponding to various de-excitation processes provide insight into the effect of temperature on matrix mobility and oxygen permeability. The rates of collisional quenching k_{TS0} and oxygen quenching $k_Q [O_2]$ were calculated from lifetimes in the presence of nitrogen and air (using eq. 4 and 7; see Materials and Methods for details). The magnitude of k_{TS0} increased gradually at low temperatures and much more steeply at temperatures above ~50°C (Figure 5a). The oxygen quenching constant is the product of a rate constant k_Q , which is proportional to the diffusion coefficient of oxygen through the protein matrix, and the solubility of oxygen in the matrix $[O_2]$; it is thus proportional to the oxygen permeability. The oxygen quenching rate $k_Q [O_2]$ was calculated from the difference between k_P in the presence of nitrogen and air using Eq. 7. The magnitude of $k_Q [O_2]$ increased gradually at low temperatures and much more rapidly at temperatures above ~50°C as shown in Figure 5b.

Arrhenius plots of these rates are depicted in Figure 5b. The Arrhenius plot of k_{TS0} was essentially biphasic, exhibiting a change in slope at ~50°C indicated a dynamic transition in amorphous α -lactalbumin. The activation energies, determined from the slopes at low (–20°C to 50°C) and high (60°C to 100°C) temperature, were 1.89 kJ mol^{–1} and 8.46 kJ mol^{–1}, respectively; these values reflect the activation energy for the matrix motions that

effectively dissipate the excess probe vibrational energy into the matrix. The Arrhenius plot of $k_Q[\text{O}_2]$, on the other hand, was essentially linear over the entire temperature range; the single activation energy of $28.99 \text{ kJ mol}^{-1}$ reflects the activation energy for oxygen permeability through the α -lactalbumin matrix.

The rate $k_Q[\text{O}_2]$ varied with k_{TS0} over nearly three orders of magnitude change in the oxygen quenching constant (Figure 6), suggesting that matrix mobility directly modulated O_2 permeability in this protein matrix. The biphasic nature of the plot revealed a break point at 10°C . Similar, though subtly different, correlations between oxygen permeability and matrix mobility were also seen in amorphous thin films of BSA (Nack and Ludescher, 2006) and β -lactoglobulin (Sundaresan and Ludescher, 2007) using the same technique.

Phosphorescence lifetime as a function of excitation and emission wavelength:

Phosphorescence intensity decays were measured as a function of excitation (480 to 560 nm) and emission (660 to 760 nm) wavelength every 20 nm at temperatures ranging from -20°C to 120°C in the presence of nitrogen ($-\text{O}_2$) and air ($+\text{O}_2$). All decays were well analyzed using a stretched exponential decay function; the lifetimes and stretching exponents in nitrogen and in air are plotted versus wavelength in Figures 7 and 8, respectively. The lifetime varied systematically across both the excitation and emission band in nitrogen and in air.

In the presence of nitrogen the lifetime exhibited a systematic increase with increasing excitation wavelength at most temperatures (Figure 7a). However, the lifetimes decreased monotonically with increasing emission wavelength from -20°C to 20°C; for example, values of the lifetime at 20°C ranged from as high as 0.50 ms at 660 nm to as low as 0.38 ms at 760 nm. However, in the temperature range from 40°C to 100°C, lifetimes increased with increasing wavelength at the blue edge to a maximum at 660-680 nm and then decreased at higher wavelengths, while at 120°C the lifetime was approximately constant with emission wavelength. Comparable variations in lifetime with emission wavelength have been reported previously with this probe in amorphous sucrose (Pravinata et al., 2005), amorphous BSA (Nack and Ludescher, 2006), amorphous maltose and maltitol (Shirke and Ludescher, 2005), amorphous lactose and lactitol (Shirke and Ludescher, 2006a, 2006b) and amorphous gelatin (Simon-Lukasik and Ludescher, 2004). Such behavior provides strong evidence for dynamic site heterogeneity within the amorphous solid protein in which individual probes reside in distinct local environments with distinct molecular mobility. Systematic variations in the value of β across both the excitation and emission band indicate that the local environments also varied in the extent of dynamic heterogeneity (Figure 7b).

The lifetime variation across the excitation band in the presence of oxygen, however, was quite different from that seen in nitrogen; the lifetimes were significantly lower than those in nitrogen at the blue edge and increased sharply until they were nearly identical to those in nitrogen at the red edge of the excitation band at all temperatures (Figure 8a). The lifetime variation across the emission band in air was essentially identical to that in

nitrogen (Figure 8a), except that the lifetimes were displaced to lower values at temperatures above 0°C. Systematic variations in the value of β across both the excitation and emission band in the presence of oxygen indicated that the local environments also varied in the extent of dynamic heterogeneity (Figure 8b).

A comparison plot of lifetime and β in presence and absence of oxygen is shown in Figure 9a and 9b, respectively.

The oxygen quenching rate $k_Q[\text{O}_2]$ as a function of emission and excitation wavelength was calculated from the difference between k_P in the presence of nitrogen and air (Figure 10a). The magnitude of $k_Q[\text{O}_2]$ varied across the emission and excitation bands indicating that the local environments varied in the magnitude of oxygen quenching rates. The activation energies (E_A) for the motions that led to oxygen quenching were obtained from Arrhenius analysis of plots of $\ln k_Q[\text{O}_2]$ versus $1/T$. The values were essentially linear with wavelength at each temperature. E_A varied between 25.1 kJ mol⁻¹ to 39.5 kJ mol⁻¹ as a function of emission wavelength and between 27.1 kJ mol⁻¹ and 32.6 kJ mol⁻¹ as a function of excitation wavelength (Figure 10b).

The variation in lifetimes with emission wavelength could reflect variations in the underlying photophysical rate constant k_{TS0} with wavelength. Arrhenius analysis of the temperature dependence of the rate constants k_P at each wavelength provides an estimate of the apparent activation energy E_A for collisional quenching k_{TS0} . The activation energies for the motions that quenched the triplet state were obtained from Arrhenius

plots of $\ln k_{TS0}$ versus $1/T$ (Figure 10b). These values at low (-20°C to 20°C) and high temperatures (40°C to 120°C) are plotted in Figure 10b. The activation energy was five times larger at high temperature than at the low temperature, ranging from 11.1 kJ mol^{-1} to 16.4 kJ mol^{-1} at high temperature and almost constant around 2 kJ mol^{-1} at low temperature across the emission band. E_A was large at shorter wavelength at higher temperature. Similar variations in E_A with emission wavelength for Ery B have been reported in other amorphous biomaterial. The values varied from 18.1 kJ mol^{-1} to 13.7 kJ mol^{-1} at high temperature and remained around 2 kJ mol^{-1} at low temperature as a function of excitation wavelength without any systematic variations. Comparisons of the activation energies for $k_Q[\text{O}_2]$ and k_{TS0} as a function of emission and excitation wavelength are plotted in Figure 10b.

Time-resolved phosphorescence emission spectra: Phosphorescence emission spectra were collected as a function of delay time from 0.1 to 2.1 ms following excitation at temperatures ranging from -20°C to 80°C (data not shown); the peak emission energy and bandwidth determined from analysis of these spectra using a log-normal function are plotted in Figure 11 and Figure 12 respectively. The emission spectra increased in energy (blue-shifted) with increasing delay time at all temperatures. Such behavior is inconsistent with a model in which dipolar relaxation around the excited triplet state generates red-shifted emission for those probes that have longer lifetimes; it is, however, consistent with a site heterogeneity model in which individual probes are distributed among pre-existing environments whose physical properties are such that those molecules with long lifetimes have blue-shifted emission (Pravinata et al., 2005; Nack

and Ludescher, 2006; Shirke and Ludescher, 2005, 2006). These data provide direct evidence that probes in environments with shorter lifetime have red-shifted emission spectra and probes in environments with longer lifetime have blue-shifted emission spectra. A plot of bandwidth as function of delay time at different temperatures is shown in Figure 12.

Discussion

Two general modes of matrix molecular mobility, dipolar relaxation and collisional quenching, modulate the emission energy and lifetime of the excited triplet state of Ery B (Ref 31). Dipolar relaxation in the matrix generates new interactions that can stabilize the excited state (Demchenko, 1988) of erythrosin B and lower the emission energy of the phosphorescence emission while molecular collision with the excited triplet state dissipate excess vibrational energy of the probe into the matrix and lower the emission intensity and lifetime. In addition, since oxygen is a contact quencher of the excited triplet state of Ery B phosphorescence can be used as a sensitive indicator of oxygen diffusion in amorphous solid proteins (Sundaresan and Ludescher, 2007; Nack and Ludescher, 2006; Simon-Lukasik and Ludescher, 2004).

Matrix Molecular Mobility: The thermal response of peak emission reflects the affect of temperature on increasing the rate of dipolar relaxation around the excited triplet state of Ery B. Surface polar groups in α -lactalbumin are the origins of dipolar relaxation. The large increase in FWHM at higher temperatures indicated inhomogeneous broadening corresponding to increase in the width of the distribution of energetically distinct matrix environments in the amorphous α -lactalbumin films. Peak frequency indicated presence of softening transition at $\sim 10^{\circ}\text{C}$ respectively, and FWHM indicated presence of transition at $\sim 10^{\circ}\text{C}$ and $\sim 90^{\circ}\text{C}$. A softening transition has been observed using Ery B in amorphous films of bovine serum albumin (BSA) at $\sim 60^{\circ}\text{C}$ (Nack and Ludescher, 2006), and in amorphous films of β -lactoglobulin showed a distinct softening transition at $\sim 80^{\circ}\text{C}$ (Sundaresan and Ludescher, 2007). This difference might be attributed to the way Ery B

probes interacts with the different protein matrices BSA, β -lactoglobulin and α -lactalbumin.

The rate of collisional quenching k_{TS0} which is modulated by the physical state of the amorphous matrix (Fischer et al., 2002; Vanderkooi and Berger, 1989) reflects not only the way excited triplet state is vibrationally coupled to the singlet ground state but also the way ground state vibrational energy is dissipated from the excited probe into the surrounding matrix. The magnitude of k_{TS0} , was $\sim 1724 \text{ s}^{-1}$ was slightly larger for Ery B in amorphous α -lactalbumin than observed in amorphous BSA ($\sim 1600 \text{ s}^{-1}$) (Nack and Ludescher, 2006) and amorphous β -lactoglobulin films (1710 s^{-1}) (Sundaresan and Ludescher, 2007) at -20°C . This indicates that the sequence of matrix mobility is BSA (60 KDa) < β -lactoglobulin (18 KDa) < α -lactalbumin (14 KDa), which is also the sequence for decrease in molecular size. The Arrhenius plot of collisional quenching rate k_{TS0} showed a distinct break indicating presence of softening transition at $\sim 50^\circ\text{C}$ in amorphous α -lactalbumin films.

In amorphous α -lactalbumin the activation energy for collisional quenching, at low temperature was 1.89 kJ mol^{-1} and at high temperature was 8.46 kJ mol^{-1} . The 1.89 kJ mol^{-1} is the activation energy for motions within the glassy protein that activate vibrational relaxation of the highly excited probe while the activation energy 8.46 kJ mol^{-1} is the activation energy for motions within the protein that activate probe vibrational relaxation. The small values of E_A in the glass suggest that the motions that activate vibrational relaxation are small amplitude, local motions. Whereas the higher values in

the rubbery state indicate modes of protein motion involve significantly larger segments of the protein structure.

The comparison of E_A among amorphous BSA, β -lactoglobulin and α -lactalbumin at higher temperature indicated that BSA (Nack and Ludescher, 2006) had the lowest $E_A = 7.9 \text{ kJ mole}^{-1}$ followed by α -lactalbumin $E_A = 8.46 \text{ kJ mole}^{-1}$ and β -lactoglobulin (Sundaresan and Ludescher, 2007) $E_A = 21.4 \text{ kJ mole}^{-1}$. The E_A at low temperature also followed the same pattern where BSA had $E_A = 1.4 \text{ kJ mole}^{-1}$, α -lactalbumin $E_A = 1.89 \text{ kJ mole}^{-1}$ and β -lactoglobulin $E_A = 2.35 \text{ kJ mole}^{-1}$. Thus β -lactoglobulin showed higher activation energy as compared to BSA and α -lactalbumin both in the glass and in the rubbery state.

The values of β decreased approximately linearly with temperature. As lifetime is dependent on k_{TS0} this decrease in β reflects a broadening in the distribution of dynamically distinct environments with different values of k_{TS0} . Thus at higher temperature amorphous α -lactalbumin matrix had faster rate of collisional quenching and a broader distribution of environments. The lower values of β in presence of oxygen at high temperatures indicates addition heterogeneity associated with oxygen quenching constant $k_Q[\text{O}_2]$.

Oxygen Permeability: Oxygen quenching of phosphorescence has been used to probe the presence of oxygen in amorphous materials (Simon-Lukasik and Ludescher, 2004; Nack and Ludescher, 2006; Sundaresan and Ludescher, 2007). The measurements of

phosphorescence lifetime in the presence and absence of oxygen indicated that oxygen quenching was negligible at low temperatures but became more significant at higher temperatures. There appears to be an onset temperature, 0°C, and a threshold level of molecular mobility at which O₂ could gain entry into the matrix. The α -lactalbumin film is thus more rigid to oxygen in the glassy state at low temperature and less rigid and more permeable to oxygen in the rubbery state. A similar onset temperature for oxygen permeability was observed in amorphous BSA (0°C) and amorphous β -lactoglobulin (10°C) films.

The rate constants k_P and k_{TS0} of the excited triplet state of Ery B in amorphous α -lactalbumin films were affected by both temperature and oxygen. The product of k_Q (rate of oxygen diffusion) and oxygen solubility (O₂), $k_Q[O_2]$ has been shown to be directly correlated to the rigidity of protein matrix (Simon-Lukasik and Ludescher, 2004; Strambini and Cioni, 1999). As seen in (Figure 6) there was an approximately linear relationship between the oxygen quenching constant $k_Q[O_2]$ and the collisionally activated non-radiative decay rate k_{TS0} which suggests that matrix mobility directly modulates O₂ permeability. The $k_Q[O_2]$ increases dramatically above ~50°C Figure 5a. The Arrhenius plot of oxygen quenching did not show any distinct break point.

A similar correlation between mobility and oxygen permeability was also observed using erythrosin B in BSA and β -lactoglobulin (Nack and Ludescher, 2006; Sundaresan and Ludescher, 2007). The activation energy for the molecular motions that control oxygen permeability in amorphous α -lactalbumin, 29.9 kJ mol⁻¹, was significantly larger than

that observed for collisional quenching, 1.89 kJ mol^{-1} and 8.46 kJ mol^{-1} at low and high temperatures, respectively. The single activation energy for oxygen permeability was very comparable to those observed for amorphous BSA films ($E_A = 29.9 \text{ kJ mol}^{-1}$) but significantly different than those observed for amorphous β -lactoglobulin films which had two activation energies 20.8 kJ mol^{-1} and 54.8 kJ mol^{-1} corresponding to low and high temperatures. Thus the activation energy was much higher in β -lactoglobulin as compared to BSA and α -lactalbumin which have similar values.

Dynamic Transitions in amorphous α -lactalbumin: Proteins are shown to exhibit a dynamic transition T_d at temperatures near 200K. This transition, due to its similarity to the high temperature dynamical transition seen in amorphous dry proteins, is often referred as a glass transition (Ringe and Petsko, 2003). Above proteins dynamic transition T_d (similar to T_g), the dynamic behavior is thought to be highly temperature dependent and shows an-harmonic vibrations and below T_d harmonic vibrations are more prevalent (e.g., localized atomic fluctuations).

Analysis of the temperature dependence of the k_{TS0} and $k_Q[\text{O}_2]$ suggest that the protein undergoes a softening transition at around $\sim 40\text{-}50^\circ\text{C}$. The Arrhenius plot of I_p also showed a break point at $\sim 50^\circ\text{C}$. For the holo form of α -lactalbumin (calcium containing) various denaturation temperatures (T_m) have being reported in the literature ranging from ($\sim 61^\circ\text{C}$ - 70°C) (Hendrix et al., 2000; Boye et al., 1997). However there is a 20°C decrease in T_m when calcium is removed (Bernal and Jelen, 1984). The apo α -lactalbumin (calcium depleted) form has a much lower transition temperature ($T_d \sim 38^\circ\text{C}$) (Hendrix et

al., 2000; Relkin et al., 1993) and has been referred to as more heat labile than the holo form. The transitions observed around $\sim 50^{\circ}\text{C}$ in amorphous α -lactalbumin matrix could reflect denaturation which occurs near $\sim 38^{\circ}\text{C}$. But the lifetime versus temperature curves are superimposable during heating and cooling (data not shown) and thus denaturation was possibly not the reason for these transitions. The other possibility is that it reflects a glass like transition (Hill et al., 2000). The softening transition seen in apo α -lactalbumin at $\sim 50^{\circ}\text{C}$ may thus correspond to a glass transitions within the amorphous α -lactalbumin matrix. A study of molecular mobility and oxygen permeability in amorphous films using erythrosin B phosphorescence in bovine serum albumin (BSA) showed a softening transition at $\sim 60^{\circ}\text{C}$, possibly corresponding to the glass transition within the native BSA molecules in the films (Nack and Ludescher, 2006). A similar such transition was observed in β -lactoglobulin at 80°C (Sundaresan and Ludescher, 2007). In case of α -lactalbumin emission energy and bandwidth also showed much steeper changes above 10°C . And also the plot of $k_Q[\text{O}_2]$ versus k_{TS0} showed a distinct point at $\sim 10^{\circ}\text{C}$ which may be correlated with the points of dynamic transition in amorphous α -lactalbumin. It is possible that there is another softening transition in α -lactalbumin at 10°C which is close to 0°C the onset temperature for oxygen permeability.

Thus, these spectroscopic measures were clear indicators of molecular mobility in amorphous α -lactalbumin indicating that protein undergoes softening transitions at $\sim 50^{\circ}\text{C}$ and at $\sim 10^{\circ}\text{C}$.

Dynamic Site Heterogeneity: The spectral heterogeneities reported here for Ery B phosphorescence in amorphous α -lactalbumin matrix are similar to those reported previously for the same probe in amorphous BSA (Nack and Ludescher, 2006), sucrose (Pravinata et al., 2005), maltose and maltitol (Shirke and Ludescher, 2005), lactose and lactitol (Shirke and Ludescher, 2006a, 2006b) and gelatin (Simon-Lukasik and Ludescher, 2006a, 2006b). The various photophysical events in these matrices indicate that Ery B molecules are distributed among different environments in the amorphous matrices that differ in overall molecular mobility. Ery B emission energy, bandwidth, variations in lifetime and stretching exponent across the emission band indicated that probes are distributed among dynamically distinct matrix sites, indicating the presence of matrix heterogeneity.

The lifetimes in presence of nitrogen were higher than in presence of oxygen as a function of emission and excitation wavelength at all the temperatures above 0°C and showed similar wavelength variation. The variation in lifetime (and thus k_{TS0}) across the emission band provides an indicator of dynamic heterogeneity. The probes with blue-shifted emission having higher energy triplet state are in matrix sites with slower dipolar relaxation rates. Whereas the probes with red-shifted emission having lower energy triplet state are in sites with faster dipolar relaxations rates. The probes in sites with blue-shifted emission have longer lifetime and thus smaller values of k_{TS0} and those in sites with red-shifted emission have shorter lifetime and thus larger values of k_{TS0} . Rigid sites with slower dipolar relaxation rates and slower collisional quenching rates have lower overall molecular mobility. Mobile sites have faster dipolar relaxation and faster

collisional quenching rates. In the α -lactalbumin matrix, decrease in emission energy across the emission band is not consistent with the standard relaxation model (Pravinata et al., 2005). However, this decrease is consistent with the dynamic site heterogeneity model in which probes are distributed in sites with different mobility both in presence and absence of oxygen. Similar spectral heterogeneities of Ery B were observed in other amorphous biomaterials like amorphous BSA (Nack and Ludescher, 2006) and gelatin (Simon-Lukasik and Ludescher, 2005). These heterogeneities thus support the physical model for dynamic heterogeneities generated in super-cooled liquids and amorphous polymers (Sillescu, 1999; Ediger, 2000; Richer, 2002), where several techniques have indicated that pure super-cooled liquids and solids composed of either small molecules or polymers exhibit dynamic heterogeneity through space and time.

The values of the stretching exponent β varied in the range from ~ 0.8 - 0.6 in amorphous α -lactalbumin matrix as a function of emission and excitation wavelengths both in presence and absence of oxygen. The Ery B probes thus appears to be distributed among environmentally different sites in the matrix differing in matrix mobility, providing an indication of a continuous distribution rather than discrete classes of sites in the amorphous solids. Temperature had a greater effect in varying the distribution of these local mobilities. The stretching exponent β was high and didn't change significantly at low temperature indicating lower matrix heterogeneity. A broader lifetime distribution at higher temperature is due to higher range of mobility. As a function of excitation wavelength the β values were significantly different in presence of oxygen as compared to in absence except at peak 520 nm. Similarly as a function of emission wavelength the

β values were not significantly different in presence and absence of oxygen except at peak ~ 700 nm.

The activation energy obtained from the Arrhenius plot of $\ln k_{TS0}$ was distinctly higher at high temperature as compared to low temperature. At low temperature there was no significant change in activation energy as a function of emission and excitation wavelength but at high temperature the values varied as a function of emission and excitation wavelength. The blue shifted probes had higher apparent activation energies $E_A = 16.5 \text{ kJ mole}^{-1}$ for collisional quenching than red shifted probes $E_A = 11.1 \text{ kJ mole}^{-1}$. The E_A value of k_{TS0} at various wavelength provides insight on the variation of matrix mobility in the α -lactalbumin matrix. The higher values of E_A provide evidence that the slower molecular mobility in rigid sites reflects the collective motions of larger regions of the protein matrix. A similar observation was also made for Ery B in amorphous BSA, amorphous sucrose, amorphous maltose and maltitol and amorphous lactose and lactitol.

The local environments in amorphous α -lactalbumin also varied in the extent of oxygen quenching rates with different activation energies. The magnitude of $k_Q[O_2]$ varied across the emission and excitation bands indicating that the local environments varied in the magnitude of oxygen quenching rates. The activation energies for $k_Q[O_2]$ were significantly higher than those for k_{TS0} . The activation energies for $k_Q[O_2]$ varied as a function of emission and excitation wavelength indicating presence of heterogeneity in different sites.

Measurements of emission energy as a function of delay time showed that as the delay time increased the peak frequency increased. The short delay time reflects the average emission energy from all the chromophores distributed and the long delay time is indicative of the emission energies due to high energy sites that have long lived chromophores. Except at high temperature, the bandwidth did not change with increasing delay time, indicating that the dynamic heterogeneity was approximately equal across these different matrix environments.

These findings thus suggest the existence of a coupling between the rates of dipolar relaxations and molecular collisions within the amorphous α -lactalbumin matrix, which gives rise to dynamic site heterogeneity.

Conclusion

Phosphorescence of Ery B in amorphous α -lactalbumin matrix clearly provided insight into the molecular mechanisms controlling oxygen transport through the protein matrix. The thermal behavior of emission energy, bandwidth, $k_Q[\text{O}_2]$ and k_{TS0} indicated that the α -lactalbumin matrix undergoes a softening transition at $\sim 10^\circ\text{C}$ and $\sim 40\text{-}50^\circ\text{C}$. The linear dependence of $k_Q[\text{O}_2]$ over k_{TS0} provides evidence that oxygen transport is controlled by local molecular mobility of the matrix. Spectral heterogeneities in Ery B provide direct evidence to support the dynamic site heterogeneity model. The heterogeneity is shown to increase in presence of quenching molecule oxygen. Temperature shows profound effect in modulating the matrix heterogeneity.

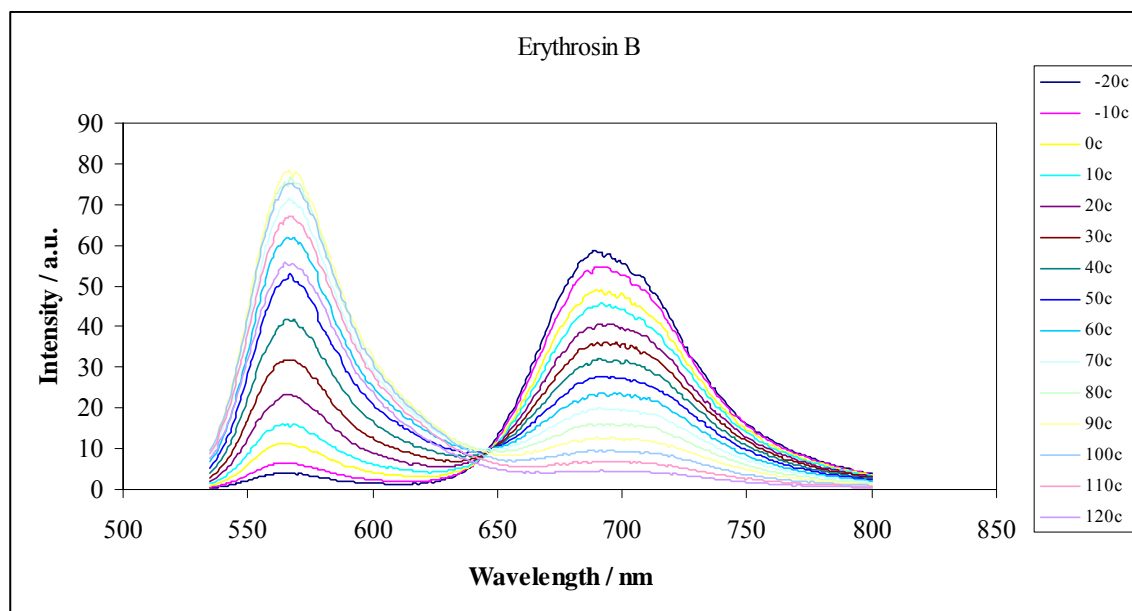
Figure VIIa-1

Figure VIIa-1: Delayed emission spectra of erythrosin B in amorphous α -lactalbumin films as a function of temperature (excitation at 500 nm). The spectra were collected at 10°C intervals from -20 to 120°C (the curves follow this order from high to low intensity at ~690nm).

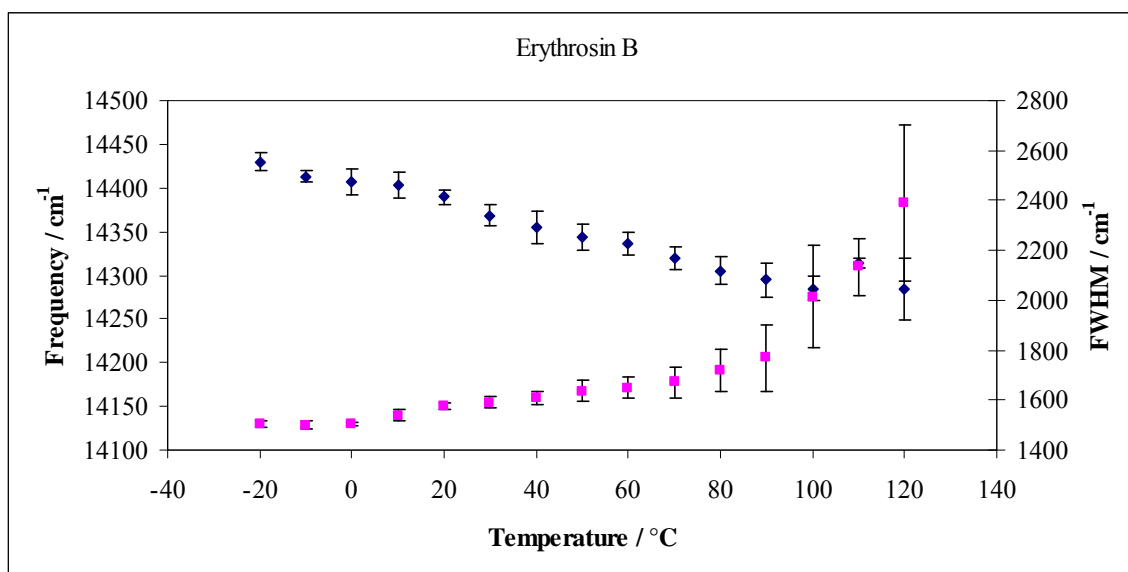
Figure VIIa-2

Figure VIIa-2: Peak energy ν_p (\diamond , left hand scale) and bandwidth (\blacksquare , right hand scale) for phosphorescence emission from erythrosin B in α -lactalbumin films as a function of temperature. The delayed emission spectra collected as a function of temperature (Figure 1) were analyzed using a log-normal function as described in Materials and Methods.

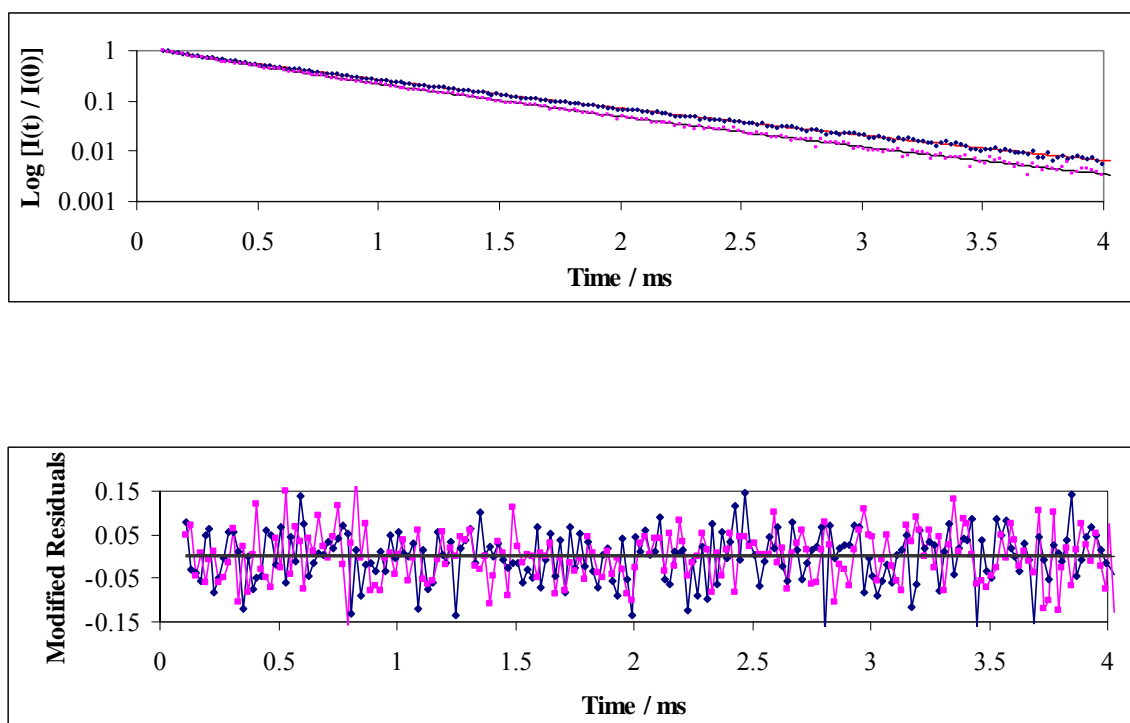
Figure VIIa-3

Figure VIIa-3: (a) Normalized phosphorescence intensity decay $[I(t)/I(0)]$ of erythrosin B dispersed in amorphous α -lactalbumin film at 20°C in the presence of nitrogen (♦) and air (■). The solid lines through the data are fits using a stretched exponential function with following parameters $\tau = 0.475$ ms and $\beta = 0.806$ for data in nitrogen and $\tau = 0.356$ ms and $\beta = 0.806$ for data in air. (b) The modified residuals $[(\text{Data}-\text{Fit})/\text{Data}^{1/2}]$ for these fits to data in the presence of nitrogen (dotted line) and air (solid line).

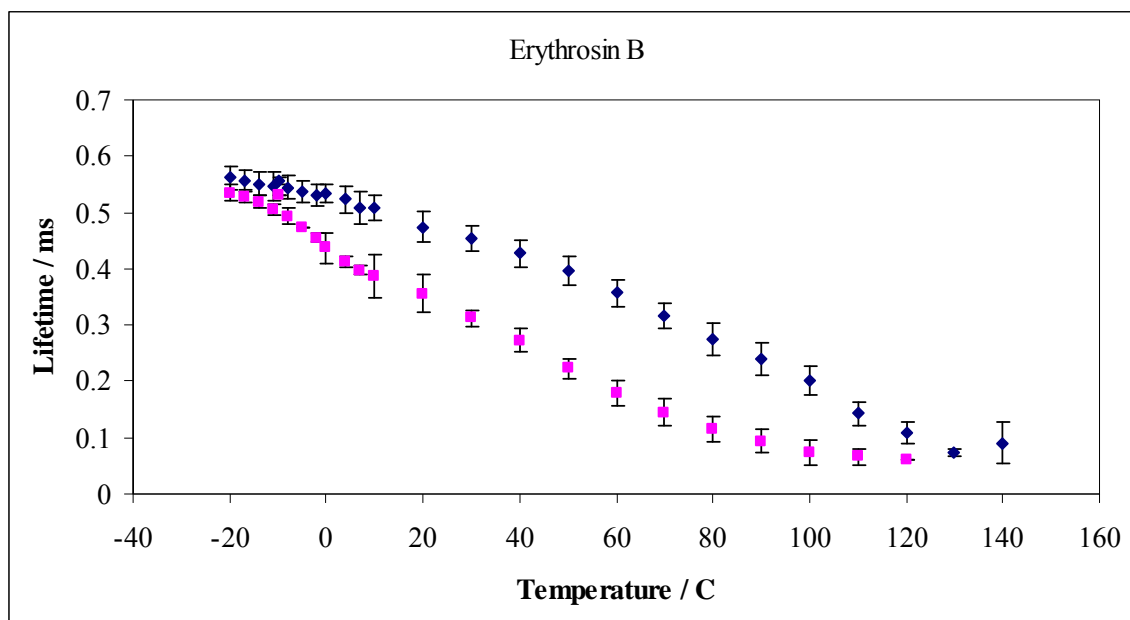
Figure VIIa-4a

Figure VIIa-4a: Lifetime τ (a) from a stretched exponential model fit to phosphorescence intensity decay data from erythrosin B in α -lactalbumin films equilibrated against nitrogen (♦) and air (■).

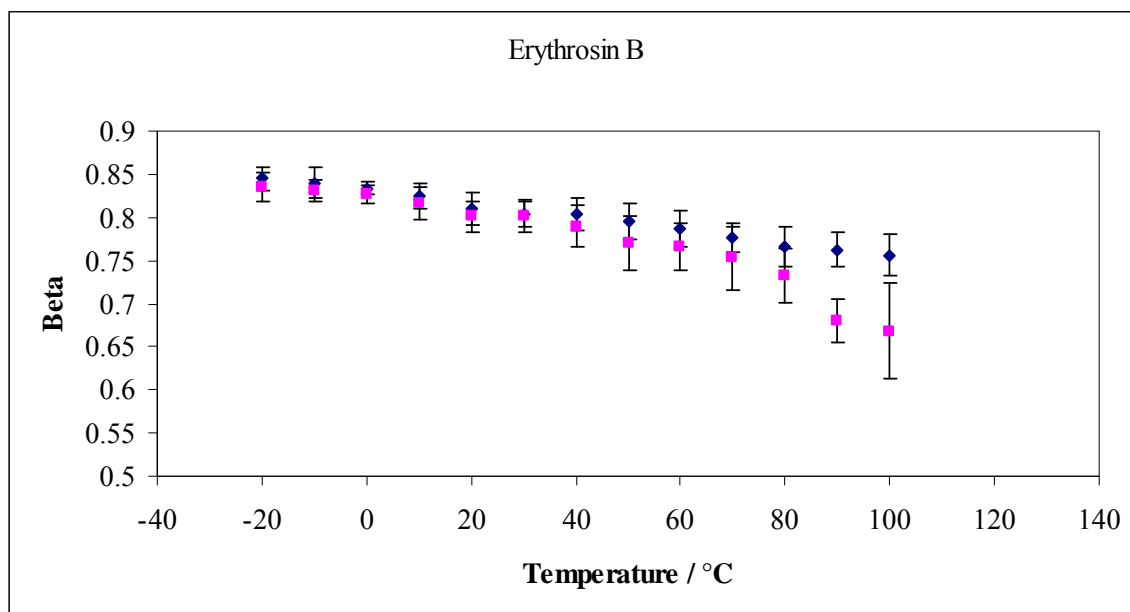
Figure VIIa-4b

Figure VII-4b: Stretched exponential model fit to phosphorescence intensity decay data from erythrosin B in α -lactalbumin films equilibrated against nitrogen (♦) and air (■).

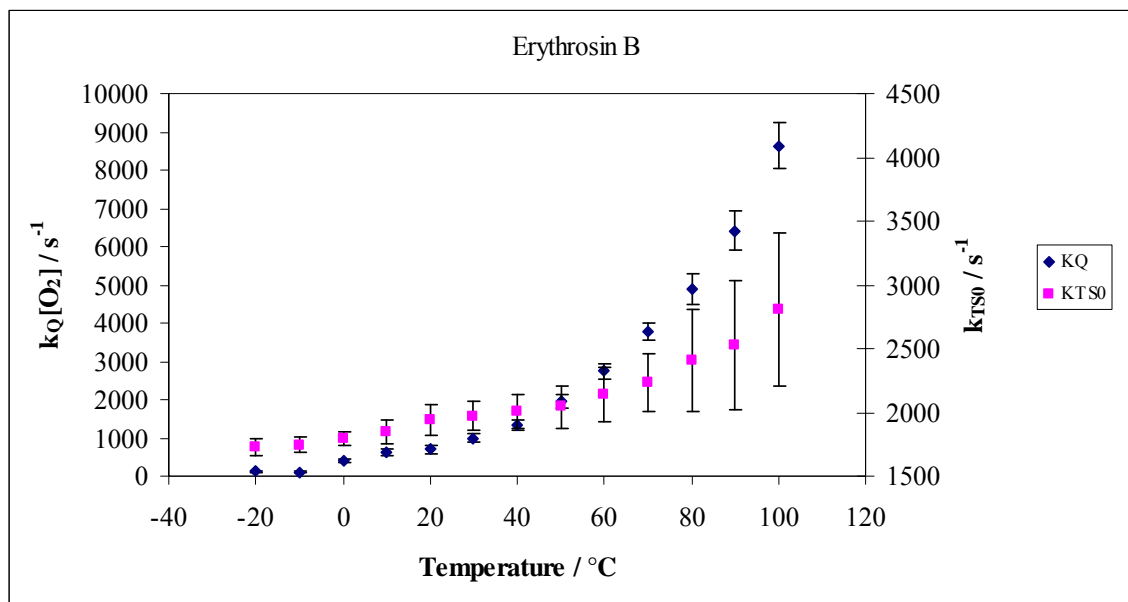
Figure VIIa-5a

Figure VIIa-5a. The effect of temperature on the triplet state de-excitation rates for collisional quenching k_{TS0} (■) and oxygen quenching $k_Q [O_2]$ (◆).

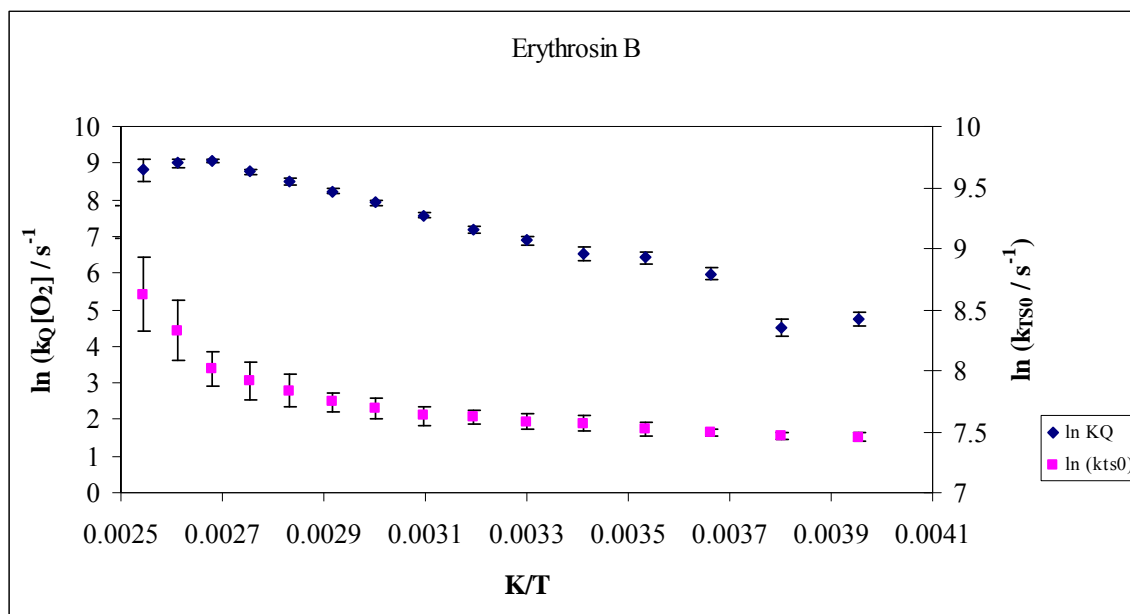
Figure VIIa-5b

Figure VIIa-5b. Arrhenius plot for the rates of collisional quenching k_{TS0} (■) and oxygen quenching k_Q [O₂] (◆). Rates calculated from the lifetime data in Figure 4a.

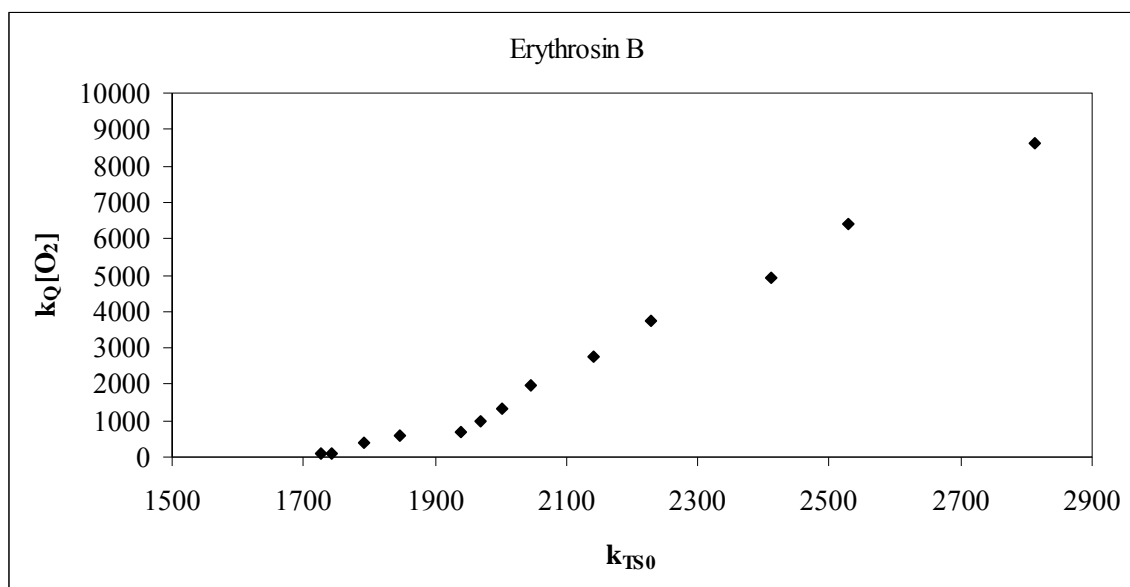
Figure VIIa-6**Figure VIIa-6:** Dependence of $k_Q [\text{O}_2]$ on $k_{\text{TS}0}$.

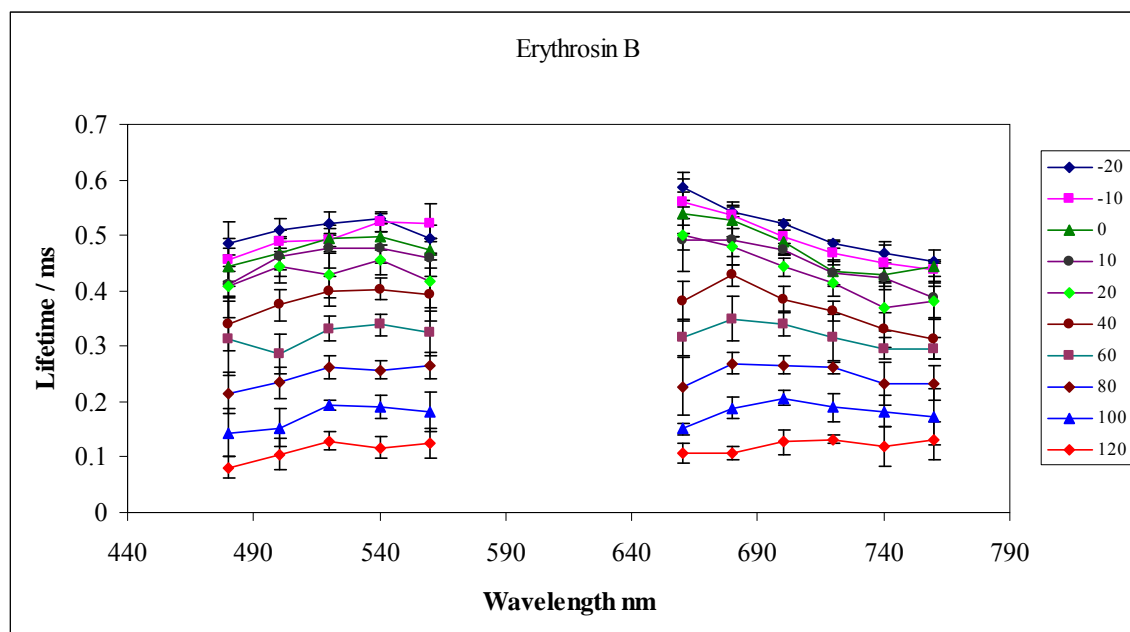
Figure VIIa-7a

Figure VIIa-7a: Lifetime from a stretched exponential model fit to phosphorescence intensity decay data from erythrosin B in amorphous α -lactalbumin films collected as a function of emission wavelength (with excitation at 540 nm) and excitation wavelength (with emission at 690 nm). Data collected at 20°C intervals from -20°C to 120°C in presence of nitrogen.

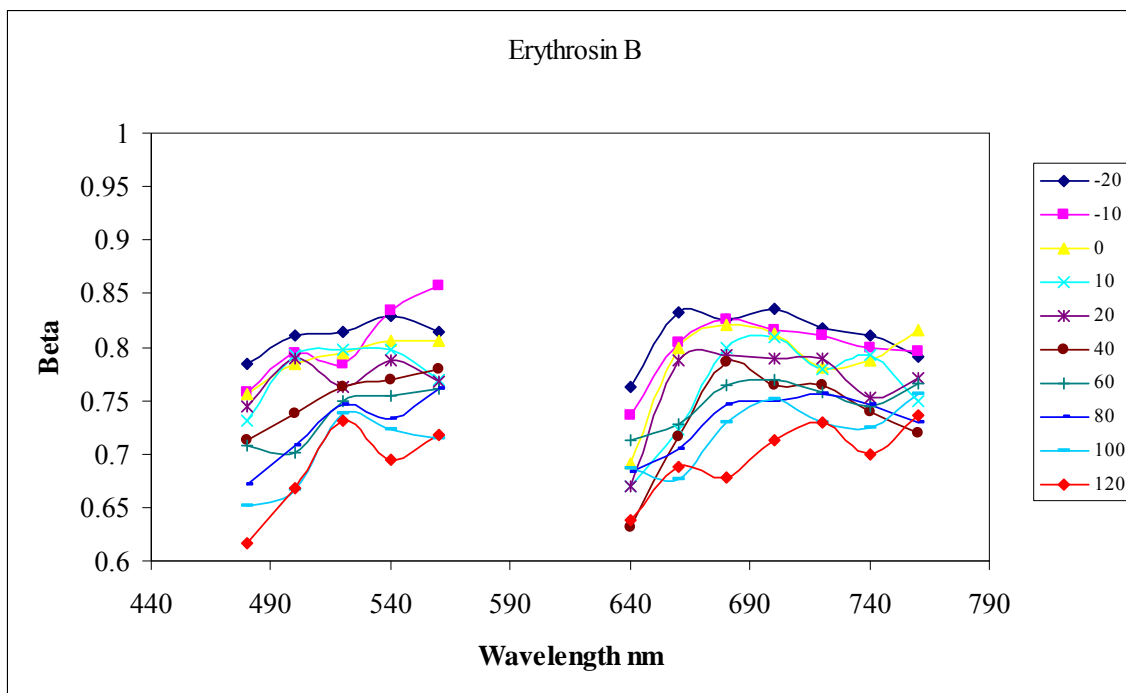
Figure VIIa-7b

Figure VIIa-7b: Stretching exponents from a stretched exponential model fit to phosphorescence intensity decay data from erythrosin B in amorphous α -lactalbumin films collected as a function of emission wavelength (with excitation at 540 nm) and excitation wavelength (with emission at 690 nm). Data collected at 20°C intervals from -20°C to 120°C in presence of nitrogen.

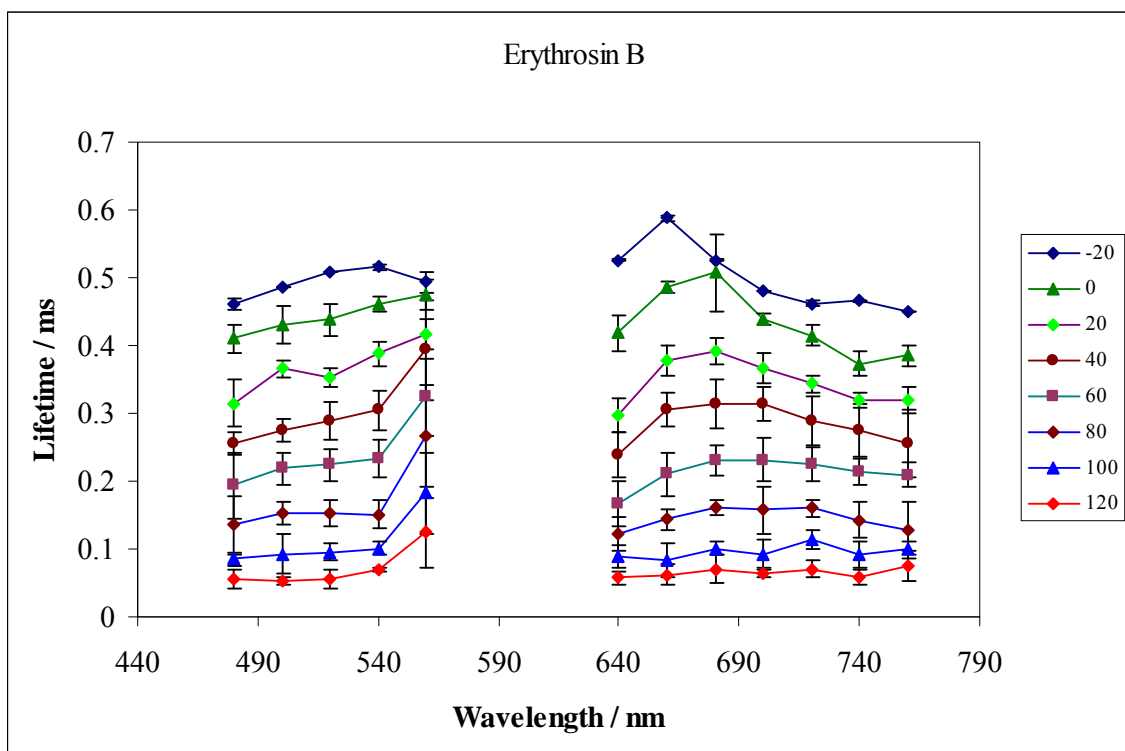
Figure VIIa-8a

Figure VIIa-8a: Lifetime from a stretched exponential model fit to phosphorescence intensity decay data from erythrosin B in amorphous α -lactalbumin films collected as a function of emission wavelength (with excitation at 540 nm) and excitation wavelength (with emission at 690 nm). Data collected at 20°C intervals from -20°C to 120°C in presence of oxygen.

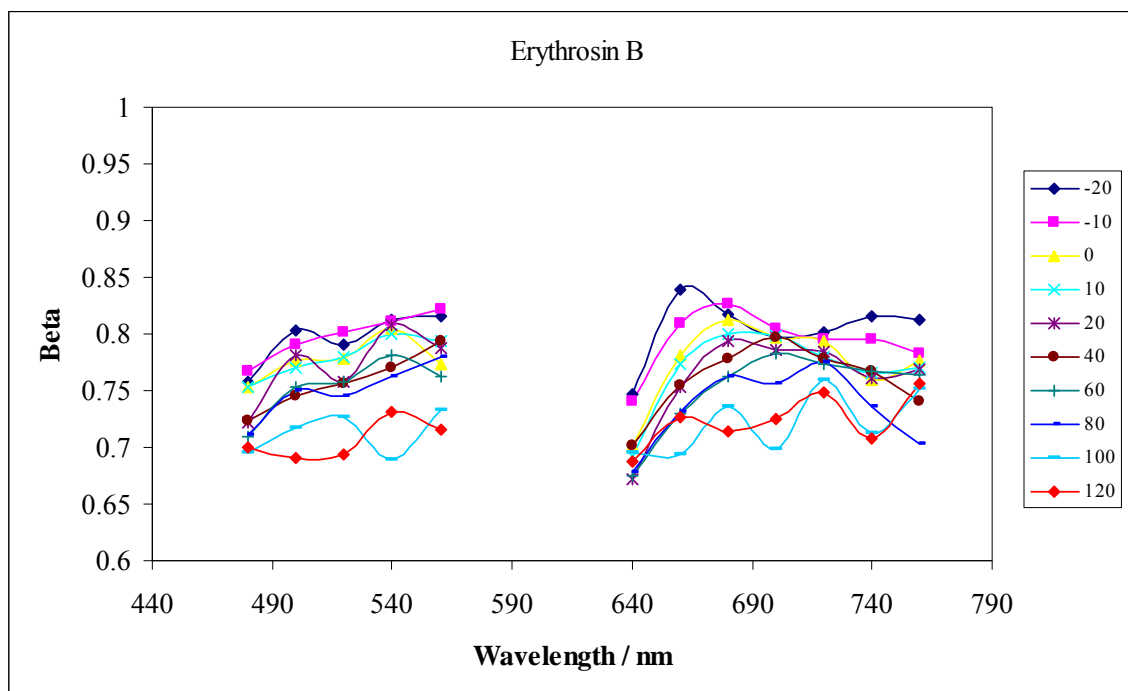
Figure VIIa-8b

Figure VIIa-8b: Stretching exponents from a stretched exponential model fit to phosphorescence intensity decay data from erythrosin B in amorphous α -lactalbumin films collected as a function of emission wavelength (with excitation at 540 nm) and excitation wavelength (with emission at 690 nm). Data collected at 20°C intervals from -20°C to 120°C in presence of oxygen.

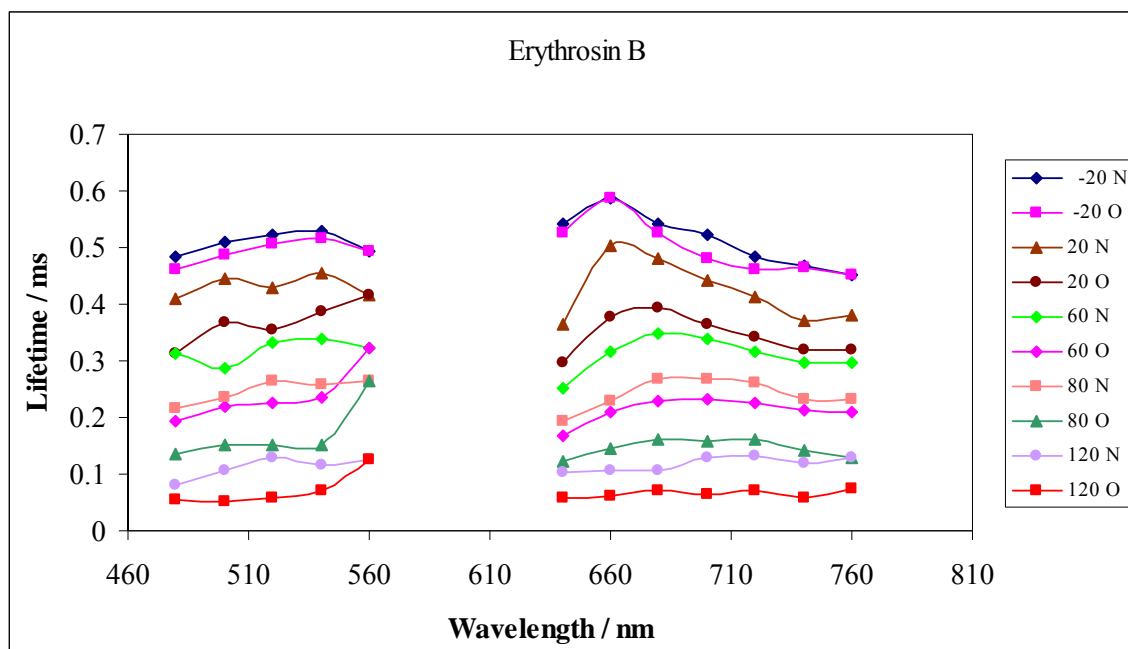
Figure VIIa-9a

Figure VIIa-9a: Comparison of lifetime in presence and absence of oxygen from a stretched exponential model fit to phosphorescence intensity decay data from erythrosin B in amorphous α -lactalbumin films collected as a function of emission wavelength (with excitation at 540 nm) and excitation wavelength (with emission at 690 nm). Data collected at 20°C intervals from -20°C to 120°C.

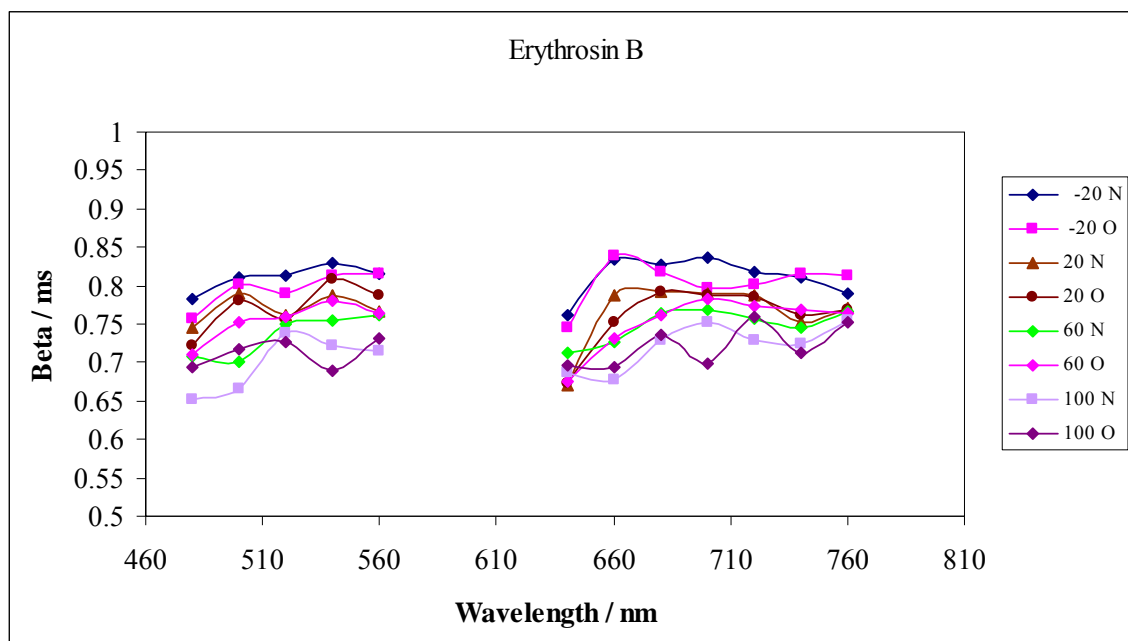
Figure VIIa-9b

Figure VIIa-9b: Comparison of stretching exponents in presence and absence of oxygen from a stretched exponential model fit to phosphorescence intensity decay data from erythrosin B in amorphous α -lactalbumin films collected as a function of emission wavelength (with excitation at 540 nm) and excitation wavelength (with emission at 690 nm). Data collected at 20°C intervals from -20°C to 100°C.

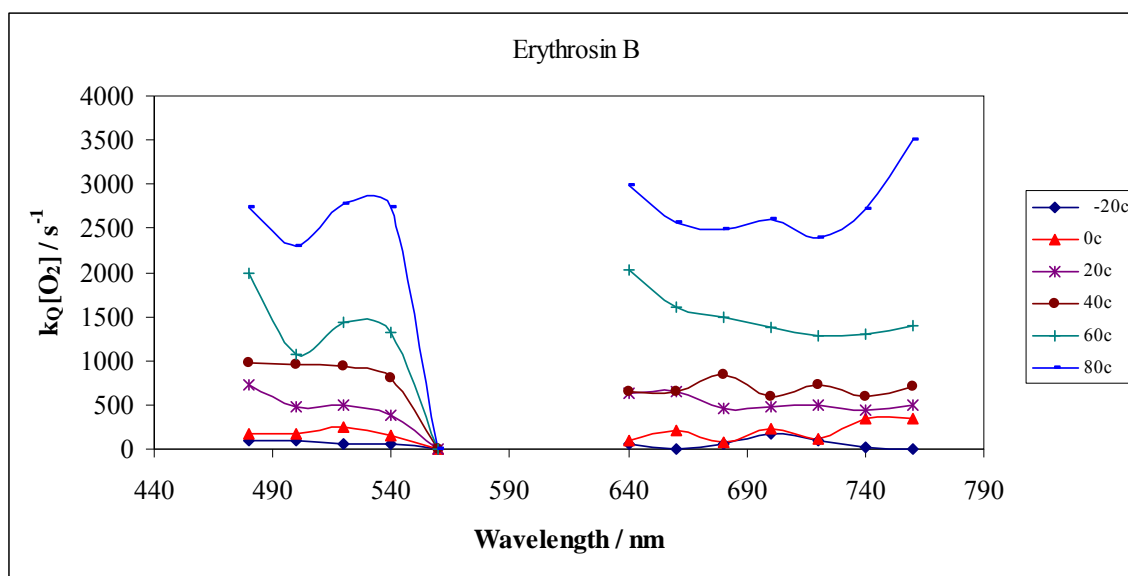
Figure VIIa-10a

Figure VIIa-10a: The temperature dependence for the rate for oxygen quenching $k_Q[O_2]$ in amorphous α -lactalbumin films collected as a function of emission wavelength (with excitation at 540 nm) and excitation wavelength (with emission at 690 nm). Data was calculated from the lifetime data in Figures 7 and 8, data at -20°C (♦), 0°C (▲), 20°C (*), 40°C (■), 60°C (||) and 80°C (-).

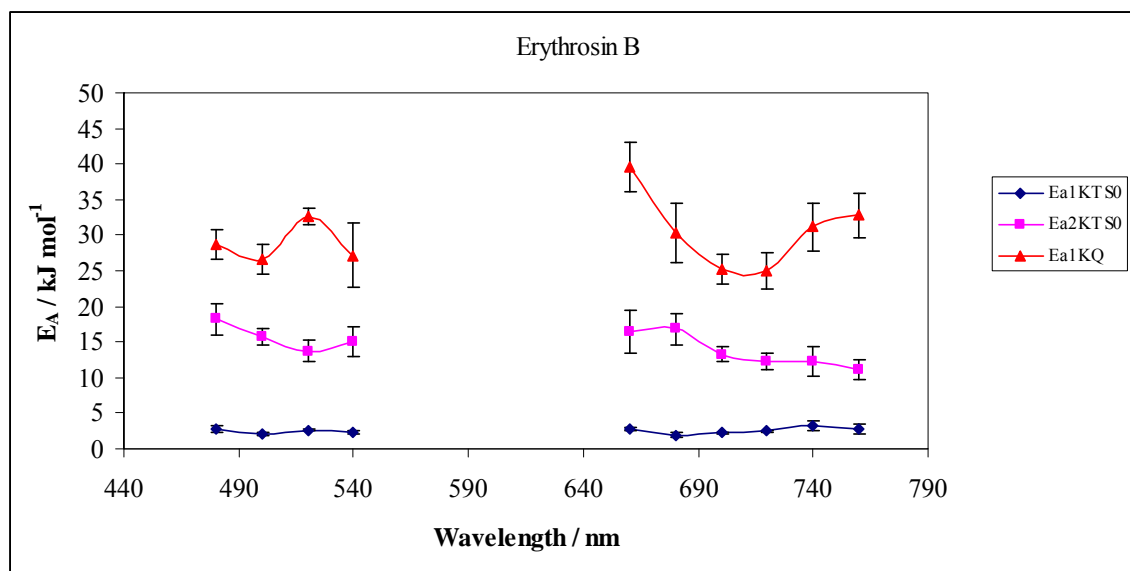
Figure VIIa-10b

Figure VIIa-10b: Activation energies for collisional quenching k_{TS0} at low temperature (\blacklozenge from -20°C to 20°C) and high temperature (\blacksquare from 40°C to 120°C) and the oxygen quenching $k_Q[\text{O}_2]$ (\blacktriangle) calculated from the lifetime data in Figure 7 and 8, as a function of emission wavelength (with excitation at 540 nm) and excitation wavelength (with emission at 690 nm). The activation energies were obtained from slopes Arrhenius plots of k_{TS0} and $k_Q[\text{O}_2]$.

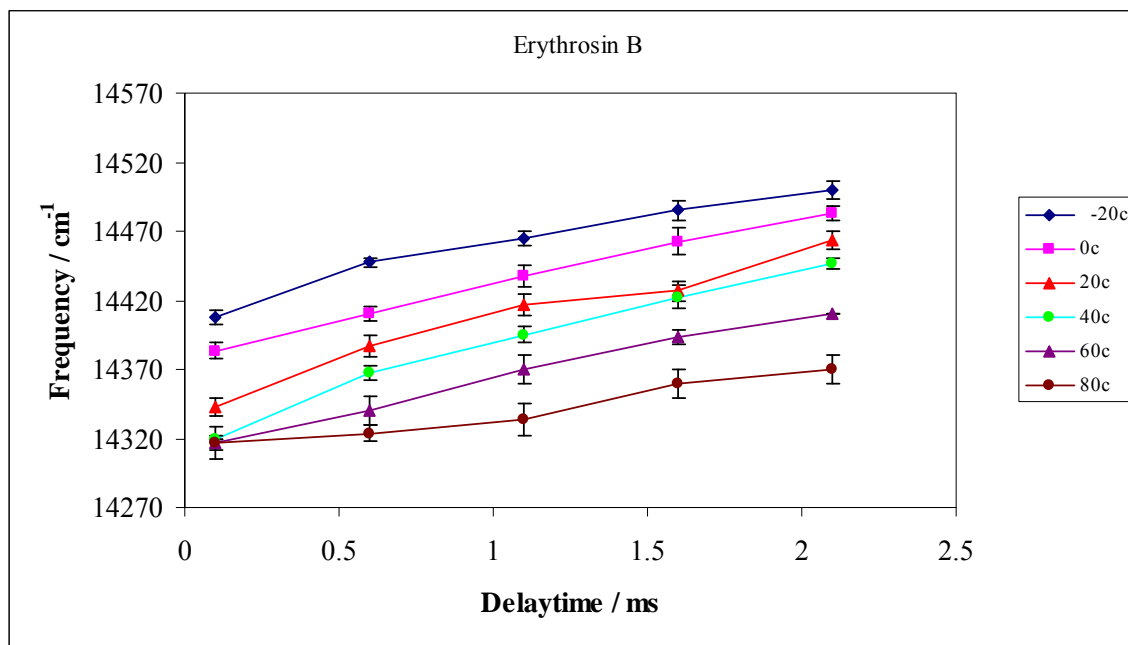
Figure VIIa-11

Figure VIIa-11. Effect of delay time on the peak frequency of the phosphorescence emission spectra of erythrosin B dispersed in amorphous α -lactalbumin film at -20°C (\blacklozenge), 0°C (\blacksquare), 20°C (\blacktriangle), 40°C (\bullet), 60°C (\blacktriangle) and 80°C (\bullet) determined from time resolved emission spectra; peak frequency was calculated from analysis of emission spectra using a log-normal function.

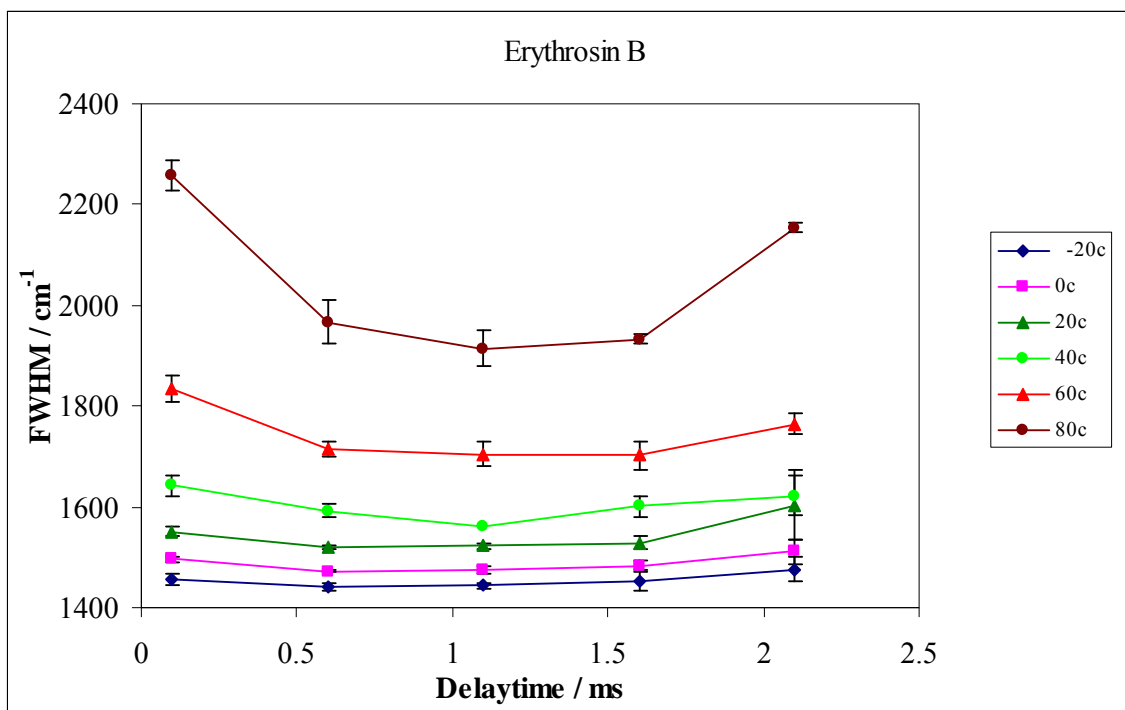
Figure VIIa-12

Figure VIIa-12. Effect of delay time on the bandwidth of the phosphorescence emission spectra of erythrosin B dispersed in amorphous α -lactalbumin film at -20°C (\blacklozenge), 0°C (\blacksquare), 20°C (\blacktriangle), 40°C (\bullet), 60°C (\blacktriangle) and 80°C (\bullet) determined from time resolved emission spectra; peak frequency was calculated from analysis of emission spectra using a log-normal function.

References

- Champion, D., Le Meste, M. and Simatos, D. Towards an improved understanding of glass transition and relaxations in foods: molecular mobility in the glass transition range. *Trends in Food Science and Technology*. 11 (200). 41-55.
- Demchenko, A. P. Site selective excitation: a new dimension in protein membrane spectroscopy. *Trends in Biochemical Sciences*. 13 (1988). 374-377.
- Duchowicz, R., Ferrer, M. L. and Acuna, A. U. Kinetic spectroscopy of erythrosin phosphorescence and delayed fluorescence in aqueous solution at room temperature. *Photochemistry and Photobiology*. 68 (1998). 494-501.
- Ediger, M. D., Angell, C. A. and Nagel, S. R. Supercooled Liquids and Glasses. *Journal of Physical Chemistry*. 100 (1996). 13200-13212.
- Fischer, C. J., Gafni, A., Steel, D. G. and Schauerte, J. A. The triplet-state lifetime of indole in aqueous and viscous environments: significance to the interpretation of room temperature phosphorescence in proteins. *Journal of the American Chemical Society*. 124 (2004). 10359-10266.
- Garland, P. B. and Moore, C. H. Phosphorescence of protein-bound eosin and erythrosin: A possible probe for measurements of slow rotational mobility. *Biochemistry Journal*. 183 (1979). 561-572.
- Hill, J. J., Shalaev, E. Y. and Zograf, G. Thermodynamic and dynamic factors involved in the stability of native proteins structure in amorphous solids in relation to levels of hydration. *Journal of Pharmaceutical Sciences*. 94 (2005). 1636-1667.
- J. I. Boye, I. Alli and A. A. Ismail. Use of differential scanning calorimetry and infrared spectroscopy in the study of thermal and structural stability of (α -lactalbumin *Journal of Agriculture and Food Chemistry* **45**, 1116-1125 (1997).
- Kronman, M. J. and Andreotti, R. E. Inter and intramolecular interactions of alpha lactalbumin. *Protein Science*. 3 (1964). 1145-1151.
- Lakowicz, J. R. *Principles of Fluorescence Spectroscopy*. Second ed. New York: Kluwer Academic/Plenum Press. (1999).
- Lettinga, M. P., Zuilhof, H. and van Zandvoort, M. A. M. J. Phosphorescence and fluorescence characterization of fluorescein derivatives immobilized in various polymers matrices. *Physical Chemistry Chemical Physics*. 2 (2000): 3697-3707.
- Lindsey, C. P. and Patterson, G. D. Detailed comparison of the Williams-Watts and Cole-Davidson functions. *Journal of Chemical Physics*. 2 (1980). 3348-3357.

- Liu, Y., Bhandari, B. and Zhou, W. Glass transition and enthalpy relaxation of amorphous food saccharides: A review. *Journal of Agricultural and Food Chemistry*. 54 (2006). 5701-5717.
- Ediger, M. D. Spatially heterogeneous dynamics in supercooled liquids. *Annual Review In Physical Chemistry*. 51 (2000). 99-128.
- Maroncelli, M. and Fleming, G. R. Picosecond salvation dynamics of coumarin 153: The importance of molecular aspects of salvation. *Journal of Chemical Physics*. 86 (1987). 6221-6239.
- Nack, T. J. and Ludescher, R. D. Molecular mobility and oxygen permeability in amorphous bovine serum albumin films. *Food Biophysics*. 1 (2006). 151-162.
- Relkin, P., Launay, B. and Eynard, L. Effect of sodium and calcium addition on thermal denaturation of apo- α -lactalbumin: a Differential Scanning Calorimetric Study. *Journal of Dairy Science*. 76 (1993). 36-47.
- Parker, C.A. *Photoluminescence of Solutions*. Amsterdam: Elsevier Pub Co. (1968).
- Pravinata, L. C. *Molecular Mobility of Amorphous Sucrose Detected by Phosphorescence of Erythrosin B and Eosin Y*. Diss. Rutgers University, NJ. (2003).
- Pravinata, L.V., You, Y. and Ludescher, R. D. Erythrosin B phosphorescence monitors molecular mobility and dynamic heterogeneity in amorphous sucrose. *Biophysical Journal*. 88 (2005). 3551-3561.
- Richert, R. *Journal of Physical Condens Matter*. 14 (2002). R738-R803.
- Richert, R. Evidence of dynamic heterogeneity near T_g from the time resolved inhomogeneous broadening of optical line shapes. *Journal of Physical Chemistry* 101 (1997). 6323-6326.
- Richert, R. Spectral selectivity in the slow beta relaxation of a molecular glass. *Europhysics Letters*. 54 (2001). 767-773.
- Richert, R. Triplet state salvation dynamics: Basics and applications. *Journal of Chemical Physics*. 113 (2000). 8404-8429.
- Ringe, D. and Petsko, G. A. The glass transition in protein dynamics: what it is? Why it occurs and how to exploit it. *Biophysical Chemistry*. 105 (2003). 667-680.
- Shamblin, S.L., Tang, X. L., Chang, L. Q., Hancock, B.C. and Pikal, M. J. Characterization of the time scales of molecular motion in pharmaceutically important glasses. *Journal of Physical Chemistry*. 103 (1999). 4113-4121.

- Shirke, S. and Ludescher, R. D. Dynamic site heterogeneity in amorphous maltose and maltitol from spectral heterogeneity in erythrosin B phosphorescence. *Carbohydrate Research*. 340 (2005). 2661-2669.
- Shirke, S. and Ludescher, R. D. Dynamic site heterogeneity in amorphous lactose and lactitol from spectral heterogeneity in erythrosin B phosphorescence. *Biophysical Chemistry*. 123 (2006a). 122-133.
- Shirke, S. and Ludescher, R. D. Molecular mobility and glass transition in amorphous glucose, maltose and maltotriose. *Carbohydrate Research*. 340 (2006b). 2654-2660.
- Sillescu, H. J. Heterogeneity at the glass transition: a review. *Journal of Non-Crystalline Solids*. 243 (1999). 81-108.
- Simon-Lukasik K. V. and Ludescher, R. D. Effect of plasticizer on dynamic site heterogeneity in cold-cast gelatin films. *Food Hydrocolloids*. 20 (2006a). 88-95.
- Simon-Lukasik, K. V. and Ludescher, R. D. Molecular mobility in water and glycerol plasticized cold and hot cast gelatin films. *Food Hydrocolloids*. 20 (2006b). 96-105.
- Simon-Lukasik, K. V., and Ludescher, R. D. Erythrosin B phosphorescence as a probe of oxygen diffusion in amorphous gelatin films. *Food Hydrocolloids*. 18 (2004). 621-630.
- Strambini, G. B. and Cioni, P. Pressure temperature effects on oxygen quenching in protein phosphorescence. *Journal of American Chemical Society*. 121 (1999). 8337-8344.
- Sundaresan, K. V. and Ludescher, R. D. Molecular mobility and oxygen permeability in amorphous beta-lactoglobulin films. *Food Hydrocolloids*. 22 (2007). 403-413.
- Hendrix, T., Griko, Y. V. and Privalov, P. L. A calorimetric study of the influence of calcium on the stability of bovine alpha-lactalbumin. *Biophysical Chemistry*. 84 (2000). 27-34.
- Bernal, V. and Jelen, P. Effect of Calcium Binding on Thermal Denaturation of Bovine {alpha} -Lactalbumin. *Journal of Dairy Science*. 67 (1984). 2452-2454.
- Vanderkooi, J. M. and Berger, J. W. Excited triplet state used to study biological macromolecules at room temperature. *Biochimica et Biophysica Acta: Bioenergetics*. 976 (1989). 1-27.

Chapter VIIb: Investigating the molecular mobility of the amorphous α -lactalbumin matrix using the phosphorescence of intrinsic probe (tryptophan).

Introduction

Tryptophan is a naturally occurring amino acid whose fluorescence and phosphorescence are sensitive to the physical properties of the local environment. Tryptophan has been shown to exhibit strong room temperature phosphorescence emission after excluding oxygen in many proteins (Vanderkooi et al., 1987). Tryptophan absorbs in the UV region, centered at 280 nm, due to the aromatic indole chromophore. Tryptophan shows strong phosphorescence at room temperature in viscous media. Its phosphorescence lifetime at 77K is 5-6s (Strambini and Gonnelli, 1985). Tryptophan is the most commonly used intrinsic probe in study of protein dynamics (Lakowicz, 1999). Tryptophan phosphorescence can be as long as 1-2 s in proteins and thus could measure slower motions that are un-measurable with most other triplet probes (Thomas, 1986). The phosphorescence lifetime of tryptophan is sensitive to mobility of the local environment and the probe is useful to measure motions on the millisecond time scale in rigid environments (Ludescher et al., 2001; Strambini and Gonnelli, 1985). Tryptophan phosphorescence, for example, has been used to study the internal mobility of proteins in solution (Papp and Vanderkooi, 1989) and in the solid state (Shah and Ludescher, 1995) on the milliseconds to seconds timescale; the long lifetime of this probe provides support for the presence of rigid, glassy regions within even fully hydrated proteins. Also the triplet state of indole has been shown to have a strong dependence of the radiation-less deactivation rate on medium viscosity, the lifetime of tryptophan decreases from 6.5s in a

glassy matrix to 1.2 ms in aqueous solutions at ambient temperature (Strambini and Gonnelli, 1995).

Trp phosphorescence in protein is many orders of magnitude longer than Trp fluorescence (Vanderkooi et al., 1987) and is sensitive to hydration-related dynamics (Strambini and Gabellieri, 1984; Shah and Ludescher, 1993). Gabellieri and Strambini (2001) have measure Trp phosphorescence in amorphous protein films as a method to probe the subtle protein structural changes that occur within protein, which may have eventual application in sensor technology (Strambini and Strambini 2000). Phosphorescence emission from intrinsic tryptophan has been used to monitor the effect of hydration on the internal molecular mobility of the protein lysozyme (Shah and Ludescher, 1992, 1993; Subramaniam et al., 2006). Tryptophan has also been used as a dispersed probe in studying molecular mobility in amorphous sucrose (McCaul and Ludescher, 1999; Shah and Ludescher, 1995). However, tryptophan as a probe for protein dynamic study has several disadvantages: a) Most proteins have several tryptophans making it difficult to study site selectively. b) Tryptophan may not be present in a protein. c) Tryptophan has to be buried in a rigid environment for phosphorescence in solution. d) The tryptophan signal could be quenched by several quenchers (e.g., disulfide), and energy transfer among chromophores can complicate the interpretations (Vanderkooi et al., 1990).

In spite of all the issues associated with use of tryptophan as a triplet state probe it still is a great choice when present intrinsically. The intrinsic nature makes the tryptophan

phosphorescence measurable in solid-state proteins (almost exclusively from Trp) as a useful tool in probing slower motions and molecular dynamic environments on the very local level. The empirical relationship between phosphorescence lifetime at RT and micro-viscosity established by Strambini and Gonnelli (1985) has allowed estimates of the local flexibility associated with Trp in proteins (Strambini et al., 1987; Strambini and Gabellieri, 1989).

The bovine α -lactalbumin protein contains four intrinsic tryptophans (W26, W60, W104, and W118). The current study focuses on using steady state and time-resolved phosphorescence of the tryptophan probe to monitor molecular mobility in thin films of amorphous α -lactalbumin (apo: calcium depleted) as a function of temperature. The results from this study will also be compared to measurements of mobility made in α -lactalbumin matrix using erythrosin B and vanillin.

Materials and Methods

Sample preparation: Purified α -lactalbumin (calcium depleted) was obtained from Sigma Chemical Company (St Louis, MO) and used as received. In order to define and minimize the presence of counter ions, α -lactalbumin was dissolved in distilled deionized water at 10 mg/ml, placed in a cellulose dialysis tube having a 1 kDa molecular weight cutoff (Spectrum, Houston, TX), dialyzed against 0.1 M potassium chloride for at least 36 hours with frequent changes of buffer, and then dialyzed extensively against distilled deionized water. All dialysis was carried out at 4°C. The solution was then filtered through a 0.2 μ m Acrodisc membrane filter (Pall Gellman Laboratory, Ann Arbor, MI) to remove particulate matter. The concentration of the protein after dialysis was determined by absorbance at 280 nm using an extinction coefficient of 28,500 $\text{M}^{-1}\text{cm}^{-1}$ (Kronman and Andreotti, 1964).

Preparation of protein films: The amorphous films were made by pipetting 20 μ L of the α -lactalbumin solution onto quartz slides (13 mm x 30 mm x 0.6 mm) (NSG Precision Cells, Farmingdale, NY) and spreading the solution over an area approximately 15 mm x 10 mm. Before use, to improve the surface activity for spreading the solutions, the slides were soaked in Terg-A-Zyme (Alconox, Inc., NY) soap solution, washed with double distilled water, rinsed with ethanol and dried in acetone. After spreading (~0.05 mm thick), the slides were dried under constant flow of air for 30 minutes, allowing the films to set, and then transferred to a desiccators over phosphorus pentoxide for at least one week, where the water activity is not greater than 0.01. The slides were stored at $23.0 \pm$

1°C, protected from light to prevent any photo bleaching of the tryptophan and desiccant was refreshed as needed to maintain a relative humidity close to 0%.

Luminescence Measurements: Luminescence measurements were made using a Cary Eclipse fluorescence spectrophotometer (Varian Instruments, Walnut Creek, CA). Quartz slides were placed in a standard quartz fluorescence cuvette, which was capped with a lid having inlet and outlet ports for gas lines. The cuvette was flushed with a gentle stream of nitrogen for 15 minutes prior to data collection to eliminate oxygen. An oxygen-free nitrogen stream was generated by passage of high purity nitrogen through a Supelco (Bellefonte, PA) carrier gas purifier. The temperature of the cuvette holder was controlled by a thermoelectric cooler (Quantum Northwest, Spokane, WA); the temperature of the cuvette was monitored directly using a thermocouple in the cuvette. The films were equilibrated for 15 minutes at each temperature before collecting data.

The Cary Eclipse uses a pulsed lamp and collects emission intensity in analog mode; data were not collected within the first 0.1-0.2 ms to suppress fluorescence coincident with the lamp pulse. Delayed luminescence emission spectra were collected from 400 to 600 nm (10 nm bandwidth) using excitation at 280 nm (20 nm bandwidth) over the temperature range from -20°C to 60°C. Each data point was collected from a single flash with 0.2 ms delay, 950 ms gate time, and 1 s total decay time.

Lifetime measurements were made in the presence of nitrogen (-O₂) as a function of temperature. The samples were excited at 280 nm (20 nm bandwidth) and emission

transients collected at 455 nm (20 nm bandwidth) at temperatures ranging from -20°C to 100°C . Each decay transient was the sum of 50 cycles, and for each cycle data were collected from a single lamp flash with a delay of 0.2 ms. Windows for gate time and total decay time were varied at each temperature. All measurements were made in quadruplicate.

Data Analysis

Emission Energy as a function of temperature: Delayed luminescence spectra were fitted to a sum of two log normal functions using the program Igor (Wavemetrics, Inc., Lake Oswego, OR). The emission peak energy (ν_p) and bandwidth (full-width-at-half-maximum, FWHM) of the emission bands were determined by fitting phosphorescence emission as a function of frequency (in cm^{-1}) to a log normal function Equation 1 (Maroncelli and Fleming, 1987).

$$I(\nu) = I_0 \exp \left\{ -\ln(2) \left[\ln \left(1 + 2b(\nu - \nu_p)/\Delta \right) / b \right]^2 \right\} \quad (1)$$

In this equation I_0 is the maximum emission intensity, ν_p is the peak energy (in cm^{-1}) of the emission maximum, Δ is a line width parameter, and b is an asymmetry parameter.

The FWHM is related to b and Δ Equation 2 (Maroncelli and Fleming, 1987).

$$\Gamma = \Delta \sinh(b)/b \quad (2)$$

Phosphorescence Intensity: Phosphorescence lifetimes were determined with the statistical program Igor (Wavemetrics, Inc., Lake Oswego, OR). The phosphorescence intensity decay were collected as described above and were fitted using a multi-exponential functions (Shamblin et al., 2000). Fits were judged satisfactory if the r^2

values were in the range of 0.995-1.0 and the modified residuals $((\text{data} - \text{fit})/\text{data}^{1/2})$ varied randomly about zero. The phosphorescence intensity decay were collected as described above and were also fitted using a multi-exponential functions (Shamblin et al., 2000). The multi-exponential model is as show in Equation 3. τ_i are decay times, α_i represent the amplitudes of the components at $t = 0$ and n is the number of decay times. The average lifetime was calculated using Equation 4.

$$I(t) = \sum_{i=1}^n \alpha_i \exp(-t/\tau_i) \quad (3)$$

$$\tau_{\text{Avg}} = \sum_{i=1}^n \alpha_i \tau_i / \sum_{i=1}^n \alpha_i \quad (4)$$

Photo-physical Scheme: The lifetime is the average amount of time a molecule spends in the excited state. There are several different deactivation processes via phosphorescence emission (with rate constant k_{RP}), non-radiative relaxation (K_{TS0}) and collisional quenching ($k_Q [Q]$). The phosphorescence lifetimes were used to calculate the rate constants associated with the various processes that depopulate the excited triplet state. The lifetime τ is related to the rate constants for de-excitation of the triplet excited state of the probe according to the following Equation 5 (Papp and Vanderkooi, 1989).

$$1/\tau = k_{RP} + k_{NR} + k_Q [Q] = k_P \quad (5)$$

Here $k_P (=1/\tau)$ is the total decay rate. The rate of radiative decay k_{RP} of the ground state is fixed and not influenced by the matrix. k_{NR} is the rate of non-radiative decay to the singlet state followed by vibrational relaxation to S_0 due to collisional quenching. The magnitude of k_{NR} reflects factors associated with the mechanism by which the excited T_1 state is coupled to highly excited vibrations of the S_0 ground state as well as external factors associated with the mechanism by which the ground state vibrational energy can dissipate from the excited state into the surrounding matrix (Fischer et al., 2002; Vanderkooi and Berger, 1989). As the efficiency of external vibrational dissipation is related to overall mobility of the matrix, the magnitude of k_{NR} provides a measure of matrix mobility. One common method for restricting the collisional deactivation is to super cool analyte solutions with liquid nitrogen to a rigid glass. The term $k_Q [Q]$ refers to the collisional quenching due to interaction between the excited chromophore and quencher. Oxygen is an efficient quencher of tryptophan phosphorescence i.e. it reduces the intensity and lifetime. Therefore the measurements were conducted under N_2

atmosphere. The collisional quenching rate constant can thus be excluded in the absence of a quencher molecule, and Equation 5 simplified to Equation 6.

$$1/\tau = k_{RP} + k_{NR} = k_P \quad (6)$$

The phosphorescence emission rate constant k_{RP} for tryptophan is known ($1/6 \text{ s}^{-1}$) (Bishai et al., 1967). It is obtained from the lifetime of tryptophan at temperature where non-radiative rates are negligible (77K).

Results

Delayed emission spectra: The delayed luminescence spectra of intrinsic tryptophan in amorphous α -lactalbumin films (in the presence of nitrogen) as function of temperature are plotted in Figure 1. Phosphorescence spectra possess a 0-0 band at ~ 415 nm and a second emission maximum around 440 nm. The phosphorescence band reflects emission from the triplet state (T_1) to the ground state (S_0). The delayed emission spectra were collected over the temperature range -20°C to 60°C . Delayed emission showed a decrease in phosphorescence intensity as a function of temperature as expected from thermally stimulated processes. The normalized plots of phosphorescence intensity versus temperature are shown in Figure 2. The plot shows, as the temperature increases, the peak intensity of the emission spectra decreases.

The emission spectra were fitted using a two log-normal function (Equation 1 Materials and Methods). Phosphorescence spectra appear in the form of a series of vibronic transitions reflecting transitions from the lowest vibration level of the triplet state to various vibrational levels of the ground singlet state. The shoulder band at high frequency side of the phosphorescence emission arises from an electronic transition in which the vibrations in the molecule resides in the $\nu = 0$ level both before and after the transitions (0-0 band) and the main band that appears as the peak of the phosphorescence emission arises from an electronic transition in which the vibrations in the molecule reside in the $\nu = 0$ level before and the 1 level after the transition (0-1 band). The peak frequencies PF1 and PF2 (Figure 3a and 3b) decrease linearly at low temperature. Above 25°C the emission spectra are broadened and only fitted to a one log-normal function (PF). The PF

shows dramatic decrease and the slope becomes more negative at high temperatures. This decrease is due to increase in the average extent of matrix dipolar relaxation around the excited triplet state. There was a gradual decrease in the emission energy at low temperature, -20°C to 40°C , followed by steeper decrease above 40°C .

The bandwidths FWHM1 and FWHM2 (Figure 3a and 3b) increased gradually with temperature and much more dramatically at high temperature, reflecting a large increase in the range of energetically distinct environments. The emission bandwidth (Γ) remained constant from -20°C to 15°C , increased gradually over the temperature interval from 20°C to 40°C , and increased sharply at higher temperature. The decrease in emission energy and the broadening of emission spectra with an increase in temperature can be explained with a solvent relaxation mechanism (Pravinata et al., 2005). With increase in temperature the reorientation of dipoles of protein molecules around tryptophan's excited state becomes faster. Peak frequency indicated presence of transition at $\sim 40^{\circ}\text{C}$ and FWHM indicated presence of transition at $\sim 30^{\circ}\text{C}$.

Phosphorescence lifetimes: The phosphorescence intensity decays collected as a function of temperature were fitted using a multi-exponential function. These lifetimes reflect the sample of all possible dynamic sites average because the peak excitation and peak emission wavelength were used. The intensity decay at 20°C is plotted in Figure 4 along with a fit using a multi-exponential function (Eq. 3, Materials and Methods). The modified residuals for this fit varied randomly around zero, indicating that this functions

provided a statistically satisfactory fit to these data (Figure 4). Lifetime is the average time a molecule spends in the excited state and is an indicator of the rigidity of the matrix.

All intensity decay data over the temperature interval from -20°C to 100°C were well fitted using a multi-exponential function and two physically important parameters lifetime τ and amplitude α were obtained. The lifetimes of tryptophan as a function of temperature are shown in Figure 5a. The log plots for lifetime is shown in Figure 5b. In case of multi-exponential function the four lifetime components at 20°C were $\tau_1 = 126.7$ ms, $\tau_2 = 20.0$ ms, $\tau_3 = 3.3$ ms and $\tau_4 = 0.46$ ms indicating the presence of local environment with ~ 300 fold difference in mobility. The plot of amplitudes of each lifetime component for as a function of temperature is shown in Figure 6. The amplitudes of longer lifetime and shorter lifetime components did not change as a function of temperature. The long lifetime component contributed 13% and the short component contributed 87% to the emission as a function of temperature.

The average lifetime was calculated using Eq. 4 and is plotted in Figure 7. The Arrhenius plot of average decay rate (Figure 8b) shows a transition point at $\sim 38^{\circ}\text{C}$. The Arrhenius plots of the inverse of individual lifetime components τ_1 , τ_2 , τ_3 and τ_4 are shown in Figure 8a. The transition temperatures and activation energies from Arrhenius plots of individual lifetime components are as compiled in Table 1. The Arrhenius plots of $\ln k_p$ for lifetime component τ_1 and τ_2 (longer lifetimes) showed a transition temperature at 35°C and 38°C respectively. The Arrhenius plot of $\ln k_p$ for lifetime component τ_3 and τ_4 (shorter lifetimes) did not show any transition temperature. The Arrhenius plot of $\ln k_p$ (average

lifetime) showed transition temperature of 38°C with activation energies at low and high temperature of 14.4 kJ mol⁻¹ and 27.9 kJ mol⁻¹ respectively (Table 1).

Temperature dependence of the total rate constant for non-radiative decay of the triplet state ($k_P = k_{RP} + k_{TS0} + k_{TS1}$) calculated from the average lifetime from a multi exponential fit over the temperature range from -20°C to 100°C is shown in Figure 9. The k_{NR} term is a rate constant for non-radiative decay; it is the actual measure of the effect of the motion that quenches probes excited triplet state and was obtained from eq. 6. The k_{NR} values were calculated by subtracting the phosphorescence emission rate constant ($1/\tau = 1/6$ s at 77K) from the inverse of the lifetime. A plot of k_{NR} as a function of temperature are represented in Figure 9. The Arrhenius plot of k_{NR} is as shown in Figure 10. The activation energy obtained from the slope of the fit line in this plot is the activation energy of the motions which quench probes excited triplet state (Table 1).

Discussion

Matrix Molecular Mobility: α -lactalbumin contains four tryptophan residues at positions W (26), W (60), W (104) and W (118). Proteins show a single peak without evidence of spectrum heterogeneity in presence of more than two tryptophan residues. This could be due to small differences in emission wavelength among the tryptophan residues. As these tryptophans are present in distinct environments, the emission spectra from amorphous α -lactalbumin films do not show clearly resolved bands, but occur as single 0-1 bands containing a 0-0 shoulder. The emission peak appeared at ~ 450 nm with a shoulder at ~ 415 nm. As the temperature increased, the peak at 415 nm shifted to the red due to solvent relaxation and was eventually un-resolvable at least above 25°C , but the peak at 450 nm remained all the way up to 60°C . The shoulder disappearance could be due to just broadening of the spectra which makes resolution impossible. Phosphorescence spectra of protein in solid solution at 77K possess a 0-0 band between 406-415 nm (Longworth, 1971) and a second emission maximum around 440 nm.

The thermal response of peak emission reflects the affect of temperature on increasing the rate of dipolar relaxation around the excited triplet state of tryptophan (Stratt and Maroncelli, 1996; Richert, 2000). Surface polar groups like side-chain hydroxyl, amino, and carboxyl groups in α -lactalbumin are the origins of dipolar relaxation. The large increase in FWHM at higher temperatures indicated inhomogeneous broadening corresponding to increase in the width of the distribution of energetically distinct matrix environments in the amorphous α -lactalbumin films. Peak frequency indicated presence of a softening transition at $\sim 40^{\circ}\text{C}$ and FWHM indicated presence of softening transition

at $\sim 15^{\circ}\text{C}$ and $\sim 41^{\circ}\text{C}$. The increase in matrix mobility seen at $\sim 30^{\circ}\text{C}$ thus appears to reflect an increase in the ability of these groups to reorient around the tryptophan triplet state.

All the lifetime components decreased drastically with increase in temperature from -20°C to 100°C (Figure 5). The decrease in lifetime occurs because of an increase in the rate of collisional quenching from interaction of the probe with the protein matrix and/or increase of vibrational relaxation. The average lifetime varied from ~ 17.5 ms at -20°C to 1 ms at 100°C , indicating ~ 17.5 -fold decrease in mobility. The measured lifetime reflects tryptophan's sensitivity to the internal dynamics of the protein structure. The phosphorescence decay times are sensitive to minor perturbations to the internal conformational flexibility of globular proteins. In environments with more mobility, tryptophan has a shorter lifetime (Strambini and Gonnelli, 1985) as a result of quenching. In the environments with higher lifetimes, probe senses lower mobility and is less easily quenched.

In solid state proteins have shown lifetimes shorter only by a factor of 2 to 5 compared to those obtained at 77K (Strambini and Gabellieri, 1984). In absence of solvent at room temperature lifetimes of about 1 second were found for several proteins (Saviotti, 1975). The observed lifetimes of tryptophan in dry films of amorphous α -lactalbumin at room temperature are 126 ms, 20 ms, 3.3 ms and 0.5 ms with an average lifetime of 7.2 ms, thus indicating presence of very mobile environments.

The triplet state lifetime decreases due to many reasons such as tryptophan is buried or exposed to surface, presence of a quencher; these two have been discussed in detail in the next section. Phosphorescence decay measurements in the absence of Trp quencher interactions provide information pertaining to protein conformational dynamics. The triplet state lifetime is also reduced due to increase in non-radiative decay constants (Birks, 1970). The non-radiative decay constant k_{NR} because of its sensitivity to collision between matrix groups and probe, provides an estimate of the overall matrix mobility. The non radiative quenching rate showed a constant increase from 56.9 s^{-1} (-20°C) to 1058.1 s^{-1} (100°C), with a transition temperature at 40°C . The Arrhenius plot of $\ln k_{NR}$ showed transition temperature of 40°C with activation energies at low and high temperature of 14.4 kJ mol^{-1} and 27.8 kJ mol^{-1} , respectively. Collisional quenching in α -lactalbumin at low temperature involved local motions with small activation energy and more delocalized, collective motions with higher, activation energy at high temperatures.

Dynamic Transitions in amorphous α -lactalbumin: Proteins are shown to exhibit a dynamic transition at temperatures near 200K. This transition due to its similarity to the high temperature dynamical transition seen in amorphous dry proteins is often referred as glass transition (Ringe and Petsko, 2003). Above proteins dynamic transition temperature T_d (similar to T_g), the dynamic behavior is thought to be highly temperature dependent and shows an-harmonic vibrations and below T_d harmonic vibrations are more prevalent (e.g., localized atomic fluctuations).

Analysis of the temperature dependence of the peak frequency, bandwidth and lifetime suggest that the protein undergoes a softening transition at around $\sim 40^{\circ}\text{C}$. There are two possible physical origins from this softening: protein denaturation or protein glass transition.

For the holo form of α -lactalbumin (calcium containing) various denaturation temperatures (T_m) have been reported in the literature ranging from ($\sim 61^{\circ}\text{C}$ to 70°C) (Hendrix et al., 2000; Boye et al., 1997). However, there is a 20°C decrease in T_m when calcium is removed (Bernal and Jelen., 1984). The apo α -lactalbumin (calcium depleted) form has a much lower transition temperature ($T_d \sim 38^{\circ}\text{C}$) (Hendrix et al., 2000; Relkin et al., 1993) and has been referred to as more heat labile than the holo form. The transitions observed around $\sim 40^{\circ}\text{C}$ in amorphous α -lactalbumin matrix could reflect denaturation which occurs near $\sim 38^{\circ}\text{C}$. A similar study in amorphous α -lactalbumin films using Ery B as a phosphorescence probe showed a softening transition at $\sim 50^{\circ}\text{C}$ (Chapter VIIa).

The other possibility is that it reflects a glass -like transition (Hill et al., 2000). The softening transition seen in apo α -lactalbumin at $\sim 40^{\circ}\text{C}$ may thus correspond to a glass transition within the amorphous α -lactalbumin matrix. A study of molecular mobility and oxygen permeability in amorphous films using erythrosin B phosphorescence in bovine serum albumin (BSA) showed a softening transition at $\sim 60^{\circ}\text{C}$, possibly corresponding to the glass transition within the native BSA molecules in the films (Nack and Ludescher, 2006). A similar such transition was observed in β -lactoglobulin at 80°C (Sundaresan and

Ludescher, 2007). In a study by Shah and Ludescher by applying a continuous flow of oxygen free nitrogen of known relative humidity to hydrated hen egg white (HEW) lysozyme dry powder, it was observed that both RTP intensity and lifetime decreased in a non linear pattern (Shah and Ludescher, 1993). This was interpreted in terms of induction of softening transition in HEW on hydration.

Thus these spectroscopic measures were clear indicators of molecular mobility in amorphous α -lactalbumin indicating that protein undergoes a softening transition at $\sim 40^\circ\text{C}$.

Correlating lifetime components to tryptophans: The phosphorescence lifetimes of tryptophan in α -lactalbumin fitted to a four exponential function. As α -lactalbumin has four tryptophan residues, each lifetime component can, in principle be, associated with one of the four tryptophan residues W26, W60, W104 and W118. The four tryptophan residues of concern in α -lactalbumin and their locations in the 3D structure are shown in Figure 11. The lifetimes were very diverse showing almost 300 fold variation at 20°C ($\tau_1 = 126.7$ ms, $\tau_2 = 20.0$ ms, $\tau_3 = 3.3$ ms and $\tau_4 = 0.46$ ms). Triplet lifetime as long as 1-2 s is observed when tryptophan residues are buried within seemingly inflexible domains in globular proteins (Saviotti and Galley, 1974; Vanderkooi et al., 1987; Strambini et al., 1990). On the other hand, tryptophans in more mobile environments possess lifetimes of 1-2 ms (Strambini and Gonnelli, 1995; Gonnelli and Strambini, 1995).

Associating observed lifetimes with a particular tryptophan residue in a protein with multiple tryptophans residues is very difficult. However, surface accessibility of tryptophan residues could help us in making this assignment, as Trp residues hidden in the relatively rigid core of the protein are quenched with much lower probability than solvent-exposed Trp residues. The water accessible surface area for each tryptophan residue was calculated as 0 (W26), 6.1 (W60), 12.4 (W104) and 28.1 Å (W118) (with help from Dr Peter Kahn using Pymol). The surface accessible area for the four tryptophan residues in α -lactalbumin is shown in Figure 12. The surface accessible area indicates that all tryptophan residues are in a fairly buried environment and are capable of emitting phosphorescence. As phosphorescence derives only from those tryptophan residues that are buried within the protein structure, the absence of this type of residue does not show any phosphorescence in proteins (Vanderkooi et al., 1987; Saviotti, 1975; Wright et al., 1992).). Comparing the surface accessible area among the four residues indicates that W26 is the most buried tryptophan followed by W60 and W104, and W118 is the most exposed residue. In proteins Trp residues are buried in the interior of the molecules as a result of polypeptide folding which provides a viscous or rigid environment for the buried tryptophan residues. It is tempting to associate the diversity in lifetimes with variations in the flexibility of the local regions in which the four tryptophan residues are buried, with long lifetime components associated with tryptophans buried in rigid protein regions and shorter lifetimes associated with residues in peripheral regions. W26, totally inaccessible and buried in the protein core, is thus associated with the longest lifetime component. W118, which has the highest accessible surface area, is thus associated with the shortest lifetime component.

The phosphorescence lifetime associated with a particular tryptophan residue provides information on a specific protein domain within the structure. Thus these tryptophan residues could provide information about particular domains (where they reside) within the protein. RTP lifetimes of Trp residues in different protein or different domains within the same protein have been shown to vary considerably in the absence of dissolved oxygen (Vanderkooi et al., 1987). This diversity in lifetimes is clearly associated with the variations in flexibility of the domains in which the Trp residues are buried (Saviotti and Galley, 1974).

The local environments of different protein domains have no influence on Trp phosphorescence lifetimes at 77K and are essentially constant (5-6 seconds). RTP is more sensitive to quenching than phosphorescence at 77K where diffusional motions are absent. However presence of internal or external quenching could greatly influence the phosphorescence lifetime. Internal factors are those existing within the protein structure, while external factors are considered to be those added to the protein solution.

A number of molecules are identified with the ability to quench the phosphorescence of buried tryptophan efficiently (Callhoun et al., 1988; Vanderkooi, 1990). Some of the most notable ones are solvent dissolved oxygen molecule, species such as NO, CO, H₂S, and CS₂ (Geacintov et al., 1972; Strambini, 1987a; Calhoun et al., 1988), and acrylamide (Ghiron et al., 1988). A group of larger and polar quenchers, including ethanethiol, methyl vinyl ketone, nicotinamide, cinnamide and quinaldic acid, were also shown to

affect the phosphorescence of buried tryptophan through a long range radiationless process (Calhoun et al., 1988).

In the absence of external quenching the main contributor to quenching includes internal factors such as disulfide linkage (Li et al., 1992; Schutz et al., 1974; Bent and Hayon, 1975). The disulfide quenching mechanism has been proposed to be a one electron transfer from the excited state of tryptophan to disulfide (Li et al., 1992; Schutz et al., 1974) at the triplet level, and disulfides have been shown to quench triplet tryptophan at RT (Bent and Hayon, 1975). The disulfide linkage in close proximity to tryptophan residues has been demonstrated to shorten phosphorescence lifetime of tryptophan at 77K (Churchich, 1964; Cowgill, 1967; Longworth, 1971; vandevan, 1987). There is no quantitative report on the distances dependence of the rate constants for disulfide quenching at RT; however recent data suggests that it is only effective over a few angstroms (Gonnelli and Strambini, 1995). Presence of a disulfide bond as close as $\sim 4\text{\AA}$ at 77K has been shown to cause quenching in a protein decreasing the lifetime to 0.5-2 seconds (Li et al., 1989). In α -lactalbumin the four disulfide bonds include Cys6-Cys120, Cys61-Cys77, Cys73-Cys91 and Cys28-Cys111. The four tryptophan residues and the disulfide linkages and their locations in the 3D structure are shown in Figure 13. Only tryptophan W118, which has the highest accessible surface area, is also in close proximity ($\sim 3.4\text{\AA}$) to a disulfide bond Cys28-Cys111.

The relative motion of tryptophan with its neighboring groups also contributes to the widely varied lifetimes observed in different proteins. The RTP lifetime of Trp in protein

has recently been observed to be shortened in the presence of several amino acids in the solvent, with Cys and ionized Tyr being the most effective and protonated Tyr and protonated His less effective. At this time the mechanism is not known (Gonnelli and Strambini, 1995).

Two tryptophan residues at a distance of 6\AA to 16\AA (Galley, 1976) could interact at singlet and singlet state through electronic energy transfer, whereas triplet-triplet energy transfer could occur at much shorter distance (Terenin and Ermolaev, 1956). This energy transfer thus could complicate the assignments of phosphorescence spectra and lifetimes.

Thus the above analysis needs a more detailed investigation in terms of the various local environments of each tryptophan residues before the exact assignments of lifetimes could be made.

Conclusion

Measurement of tryptophan phosphorescence in α -lactalbumin films provides useful information in terms of molecular events in the proteins and also provides evidence for dynamic transition within amorphous solid α -lactalbumin films. The decrease in emission energy with temperature reflects increase in rate of dipolar relaxation around the excited triplet state. The increase in FWHM at elevated temperatures reflects an increase in the extent of inhomogeneous broadening of the spectra due to interactions of tryptophan with the surrounding matrix. The phosphorescence lifetime was fitted using a four exponential function over the whole temperature range. These spectroscopic measures of thermally-activated molecular mobility in amorphous α -lactalbumin suggest that the amorphous solid protein undergoes a softening transition at $\sim 40^{\circ}\text{C}$, W26, totally solvent inaccessible and buried in the protein core, is associated with the longest lifetime component. W118, which has the highest accessible surface area and is also in close proximity ($\sim 3.4 \text{ \AA}$) to a disulfide bond, a known quencher of tryptophan phosphorescence, is associated with the shortest lifetime component. The phosphorescence lifetime and emission wavelength associated with a particular tryptophan residue thus could provide information on the mobility of specific domains within the protein structure.

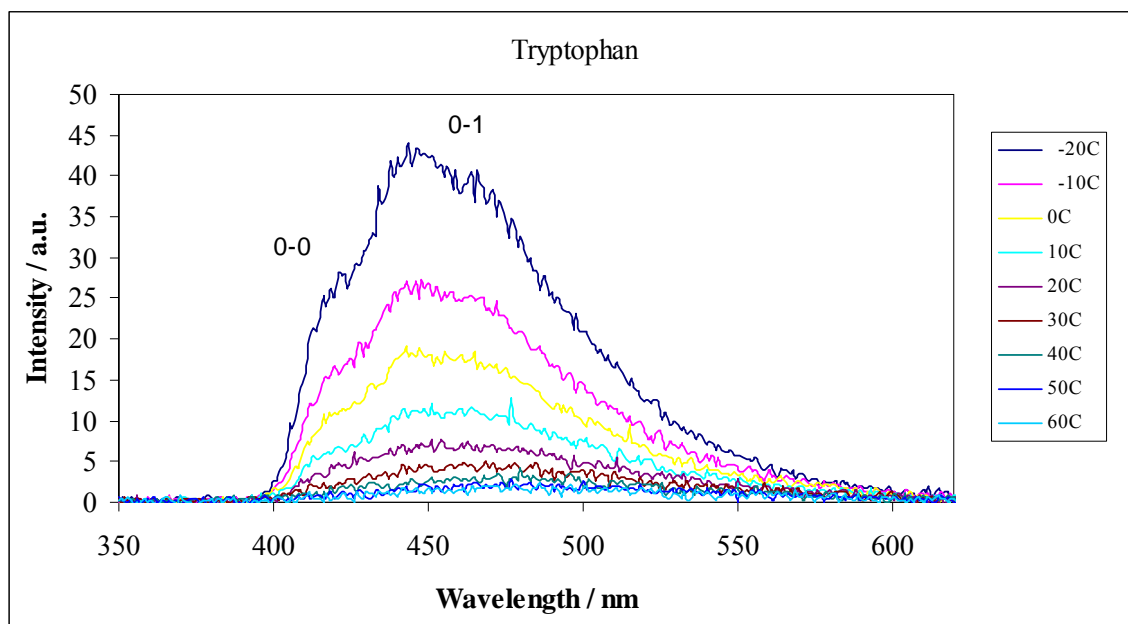
Figure VIIb-1

Figure VIIb-1: Delayed emission spectra of tryptophan in amorphous α -lactalbumin films as a function of temperature (excitation at 280 nm). The spectra were collected at 10°C intervals from -20°C to 60°C (the curves follow this order from high to low intensity at ~450 nm).

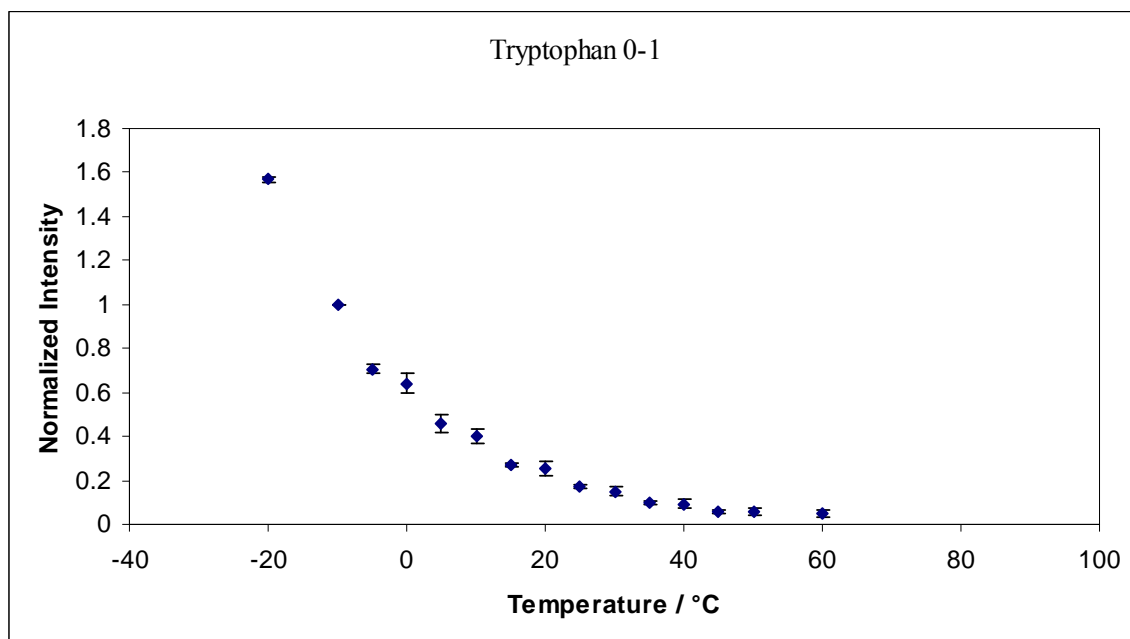
Figure VIIb-2a

Figure VIIb-2a: The effect of temperature on the phosphorescence emission intensity of tryptophan in amorphous α -lactalbumin films as a function of temperature equilibrated against nitrogen. Intensity (I_P) was determined from analysis of the phosphorescence emission band (Figure 2) using a log-normal function (eq. (1), Materials and Methods). The intensity was normalized to -10°C.

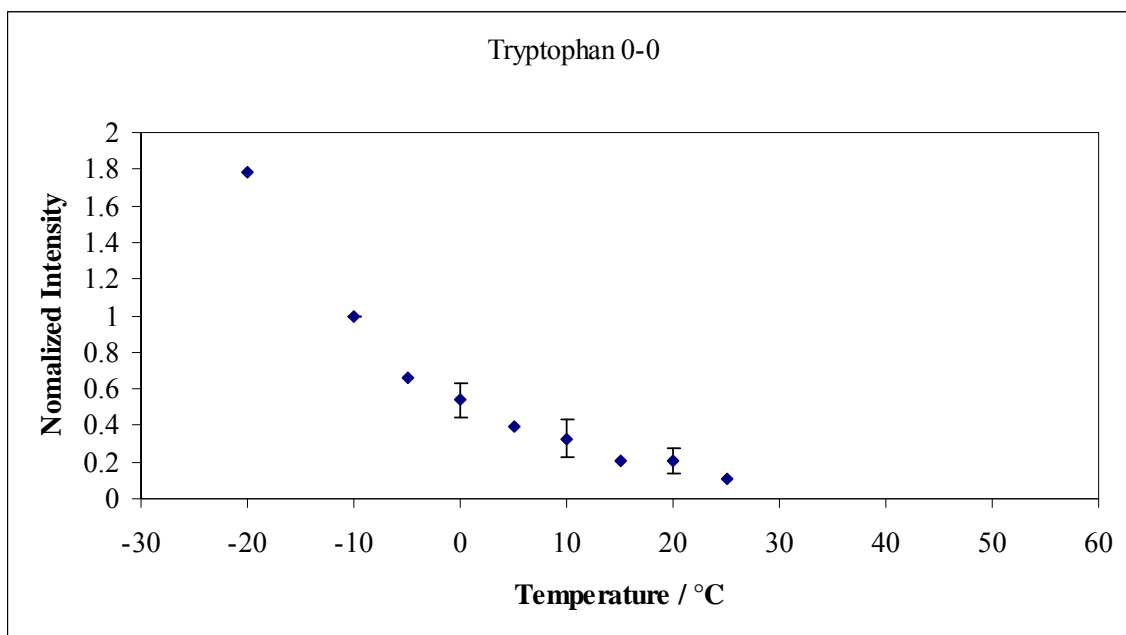
Figure VIIb-2b

Figure VIIb-2b: The effect of temperature on the phosphorescence emission intensity of tryptophan in amorphous α -lactalbumin films as a function of temperature equilibrated against nitrogen. Intensity (I_P) was determined from analysis of the phosphorescence emission band (Figure 2) using a log-normal function (eq. (1), Materials and Methods).

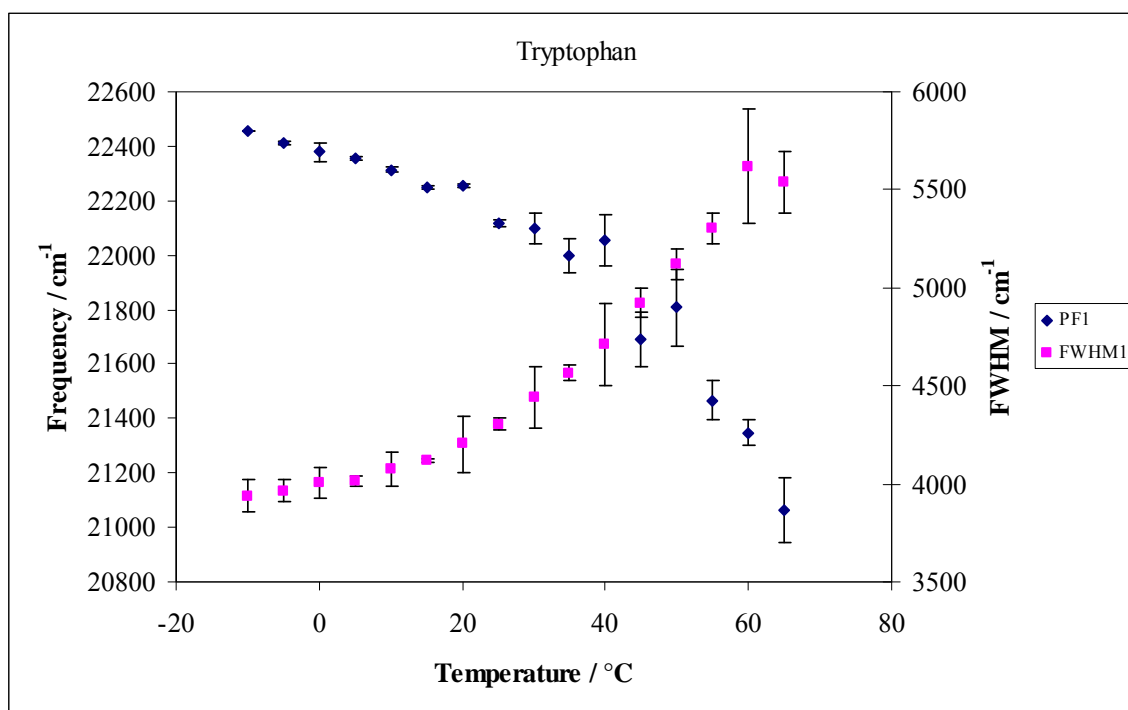
Figure VIIb-3a

Figure VIIb-3a: Peak energy ν_p (♦, left hand scale) and bandwidth (■, right hand scale) for phosphorescence emission from tryptophan in α -lactalbumin films as a function of temperature.

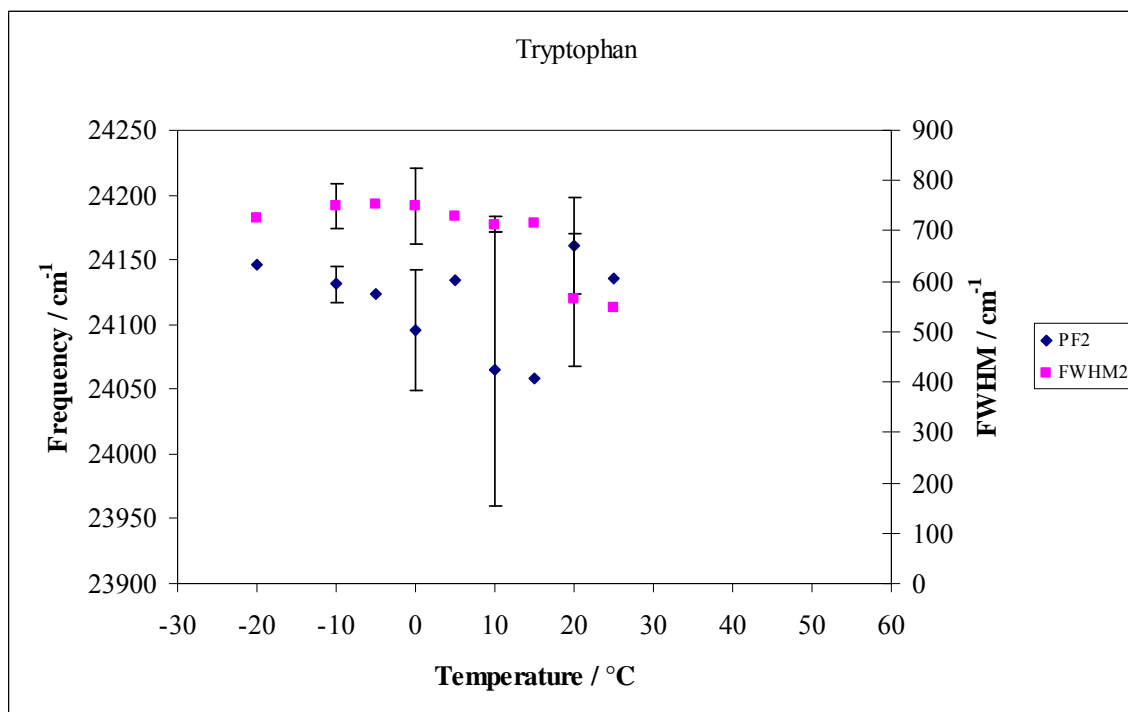
Figure VIIb-3b

Figure VIIb-3b: Peak energy ν_p (♦, left hand scale) and bandwidth (■, right hand scale) for phosphorescence emission from tryptophan in α -lactalbumin films as a function of temperature.

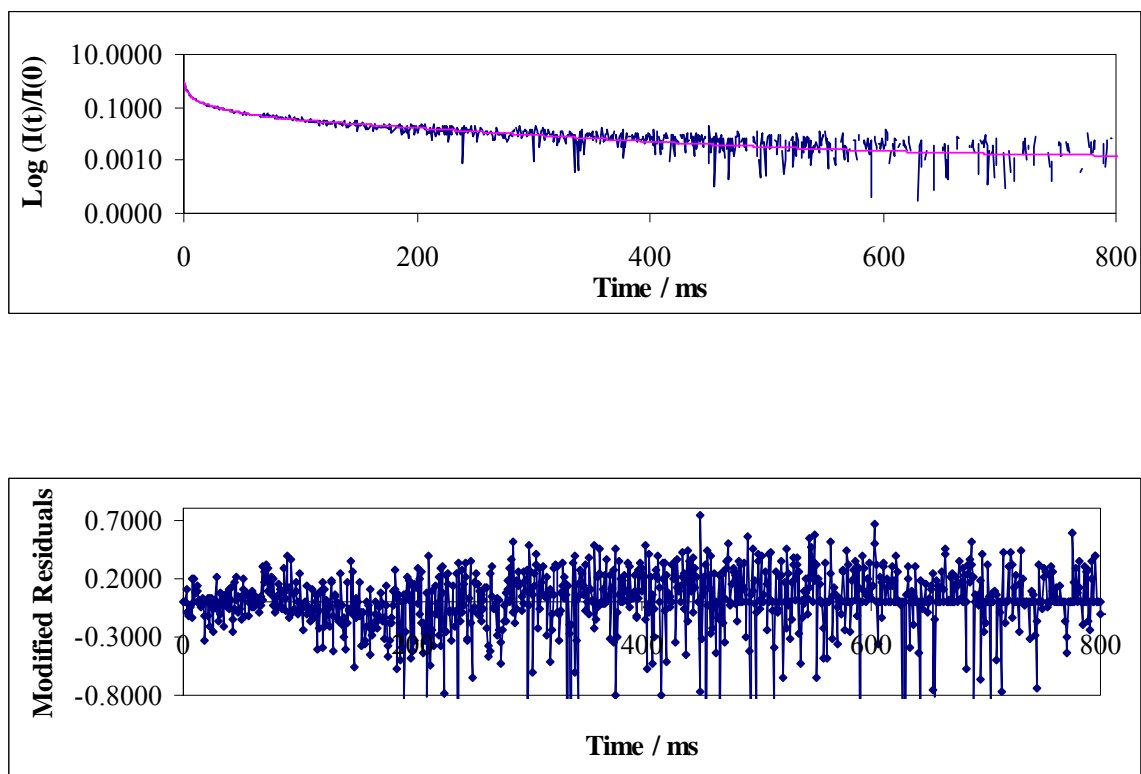
Figure VIIb-4

Figure VIIb-4: (a) Normalized phosphorescence intensity decay $[I(t)/I(0)]$ of tryptophan in amorphous α -lactalbumin film at 20°C in the presence of nitrogen (\blacklozenge). The solid lines through the data are fits using a multi-exponential function. (b) The modified residuals $[(\text{Data-Fit})/\text{Data}^{1/2}]$ for these fits to data in the presence of nitrogen (dotted line).

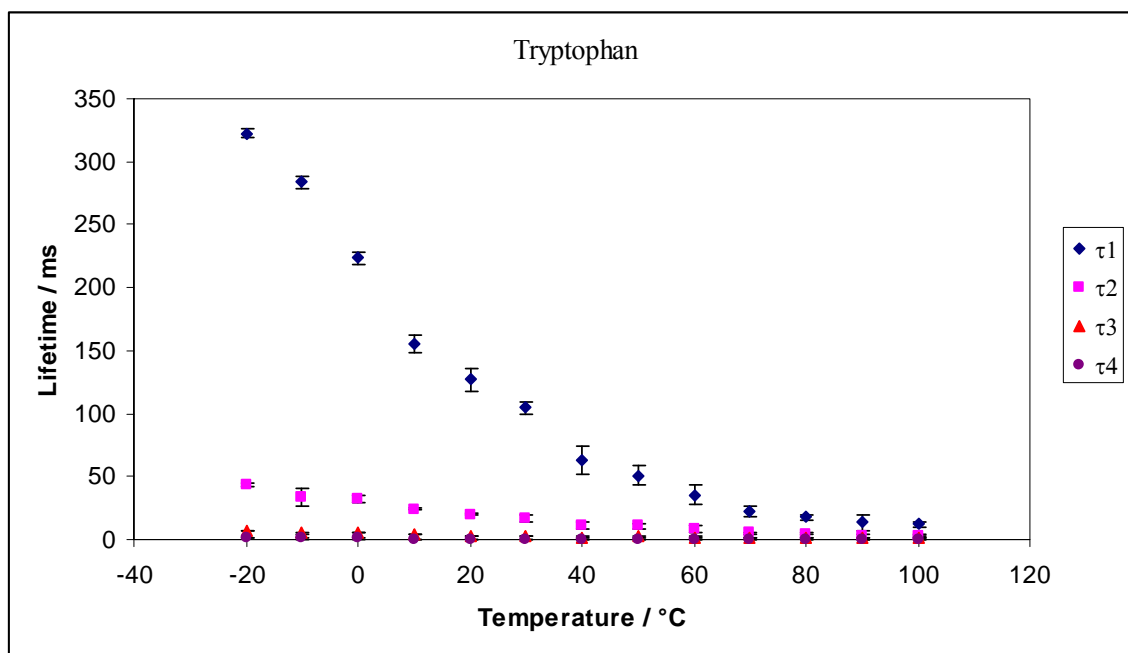
Figure VIIb-5a

Figure VIIb-5a: Lifetime components τ_1 (\blacklozenge), τ_2 (\blacksquare), τ_3 (\blacktriangle), τ_4 (\bullet) obtained from a multi-exponential model fit (Eq. (3), Materials and Methods) to phosphorescence intensity decay data from tryptophan in amorphous α -lactalbumin films equilibrated against nitrogen as a function of temperature. The data was calculated every 10°C from -20°C to 100°C.

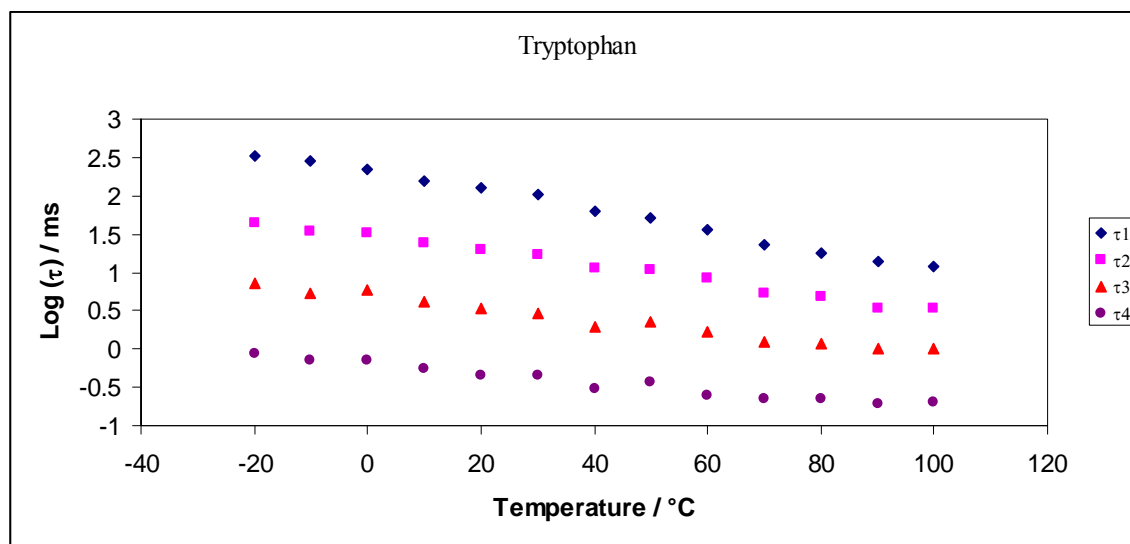
Figure VIIb-5b

Figure VIIb-5b: Log plot of lifetime components τ_1 (\blacklozenge), τ_2 (\blacksquare), τ_3 (\blacktriangle), τ_4 (\bullet) obtained from a multi-exponential model fit (Eq. (3), Materials and Methods) to phosphorescence intensity decay data from tryptophan in amorphous α -lactalbumin films equilibrated against nitrogen as a function of temperature. The data was calculated every 10°C from -20°C to 100°C.

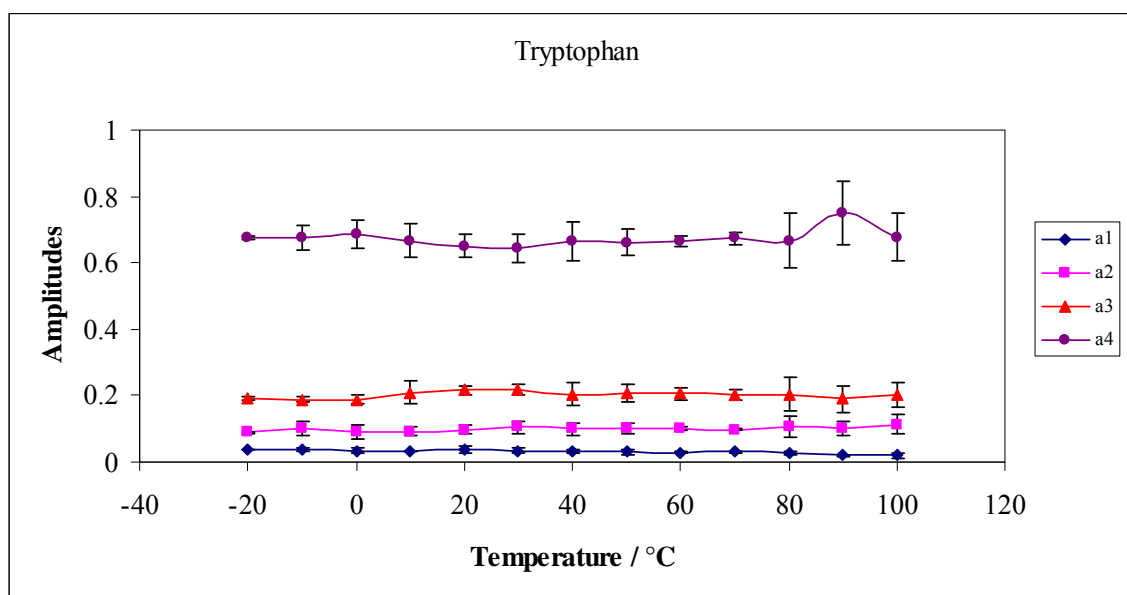
Figure VIIb-6

Figure VIIb-6: Intensity decay fit parameters amplitude for tryptophan in amorphous α -lactalbumin films in nitrogen as a function of temperature. The data was calculated every 10°C from -20°C to 100°C. The amplitudes a_1 (♦) and a_2 (■) correspond to the longer life time components (τ_1 , τ_2) and a_3 (▲) and a_4 (●) correspond to the shorter lifetime components (τ_3 , τ_4). The amplitudes were obtained from a multi exponential model fit (Eq. (3), Materials and Methods) to phosphorescence intensity decay data from tryptophan in amorphous α -lactalbumin films equilibrated against nitrogen as a function of temperature

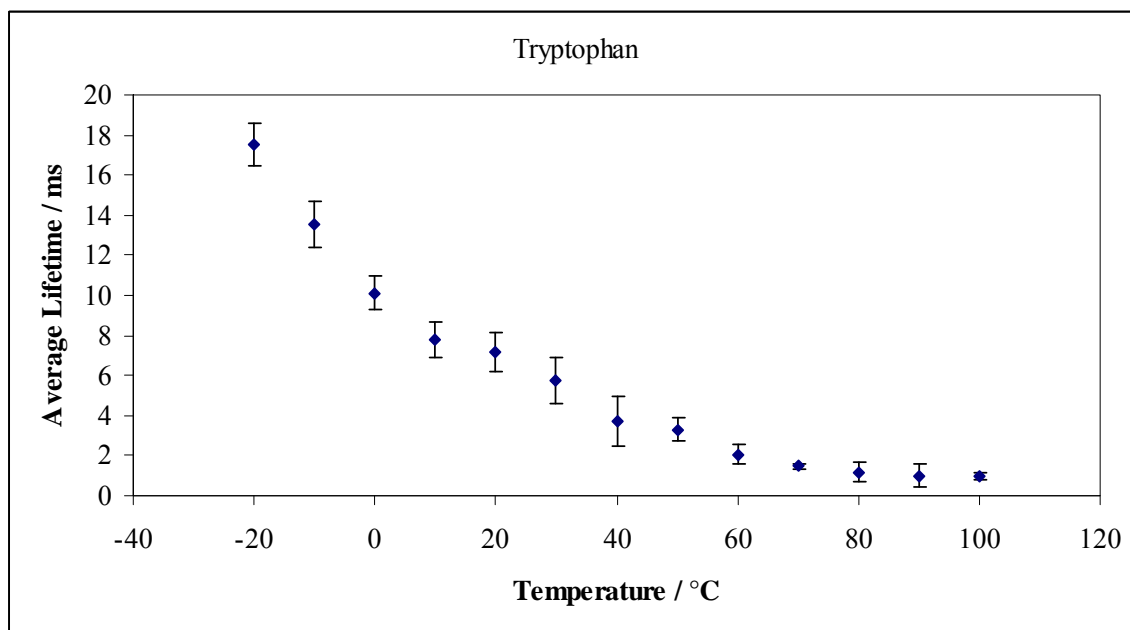
Figure VIIb-7

Figure VIIb-7: Average lifetime from a multi-exponential model fit (Eq. (4), Materials and Methods) to phosphorescence intensity decay data from tryptophan in amorphous α -lactalbumin films equilibrated against nitrogen as a function of temperature. The data was calculated every 10°C from -20°C to 100°C.

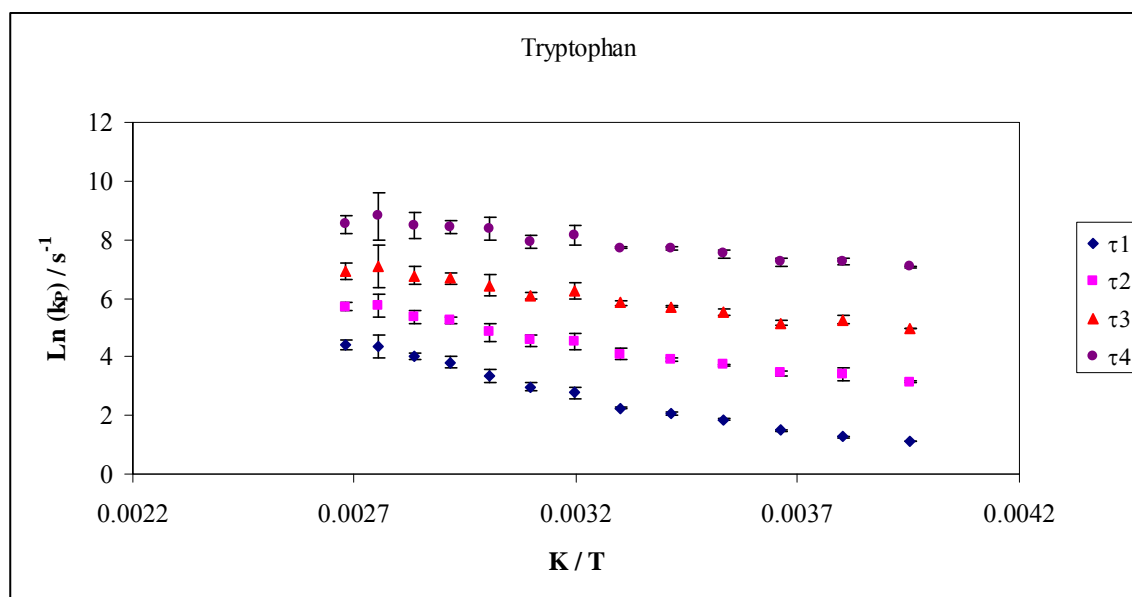
Figure VIIb-8a

Figure VIIb-8a: The Arrhenius plot of the individual lifetime component τ_1 (\blacklozenge), τ_2 (\blacksquare), τ_3 (\blacktriangle) and τ_4 (\bullet) of tryptophan in amorphous α -lactalbumin as a function of inverse of temperature.

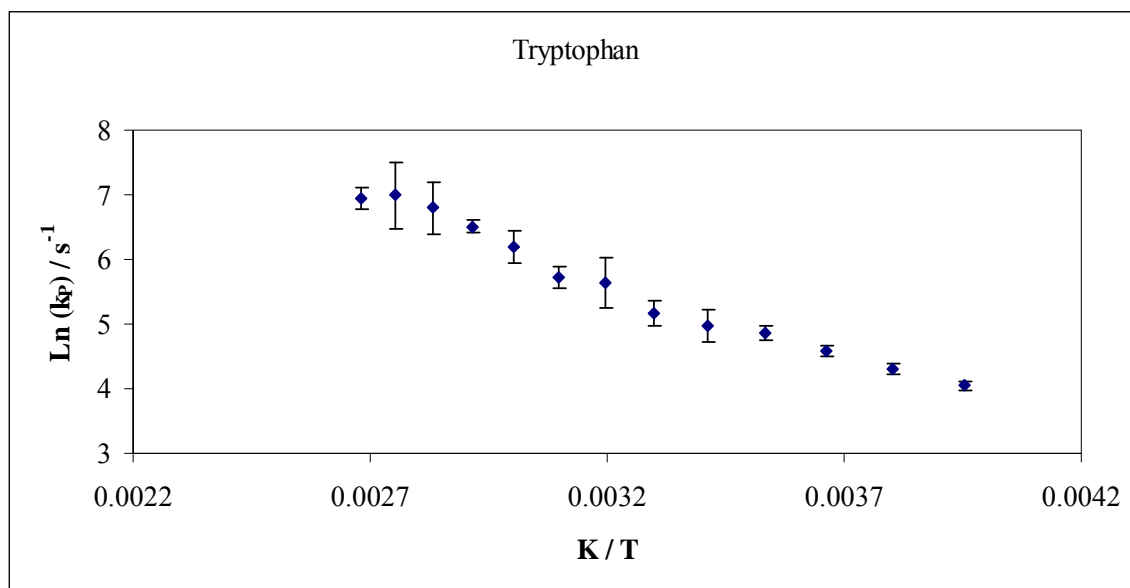
Figure VIIb-8b

Figure VIIb-8b: The Arrhenius plot of the average lifetime of tryptophan in amorphous α -lactalbumin as a function of inverse of temperature.

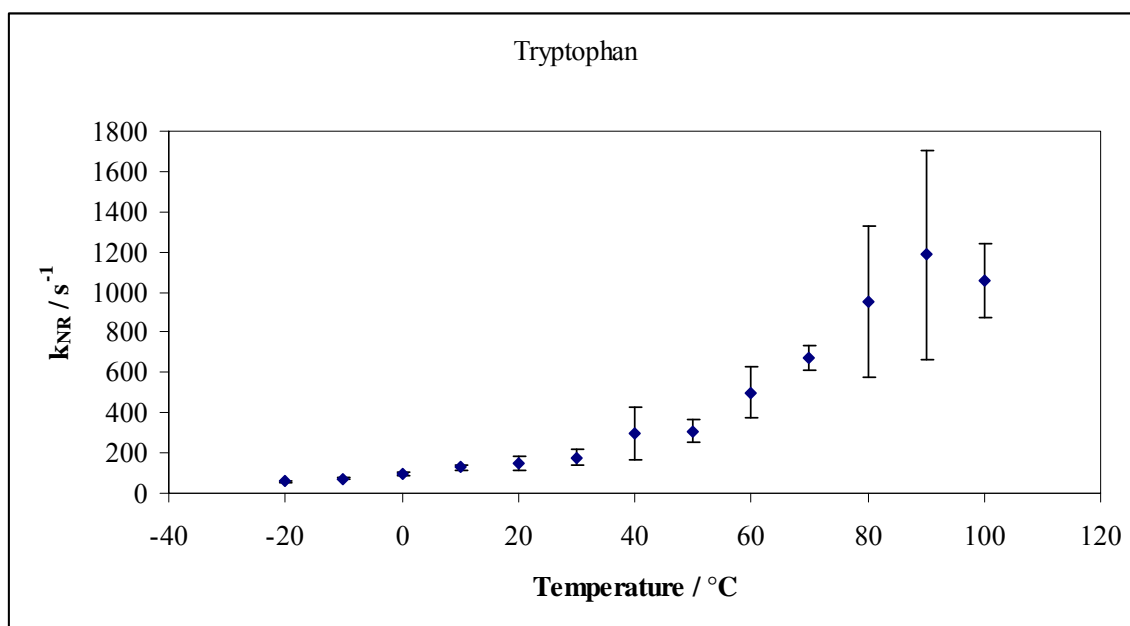
Figure VIIb-9

Figure VIIb-9: Temperature dependence of the total non-radiative decay rate of the triplet state k_{NR} ($k_p = k_{RP} + k_{NR}$) to So of tryptophan in amorphous α -lactalbumin film over the temperature range from -20°C to 100°C, values were calculated from the lifetime data.

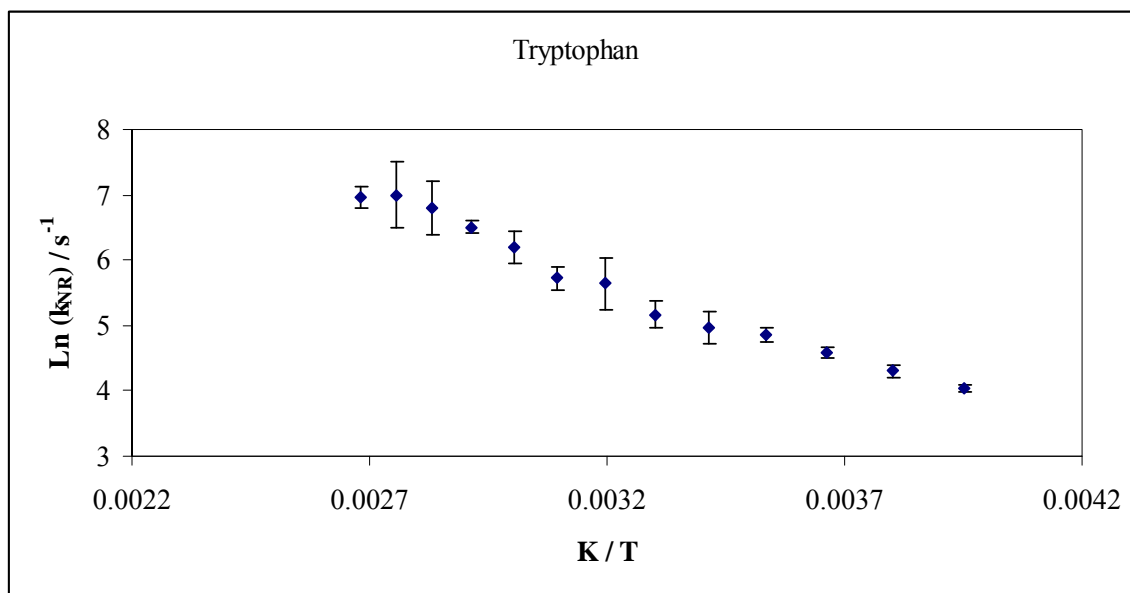
Figure VIIb-10

Figure VIIb-10: The Arrhenius plot of the total non-radiative decay rate of the triplet state k_{NR} ($k_{\text{p}} = k_{\text{RP}} + k_{\text{NR}}$) to So of tryptophan in amorphous α -lactalbumin film as function of inverse of temperature.

Figure VIIb-11

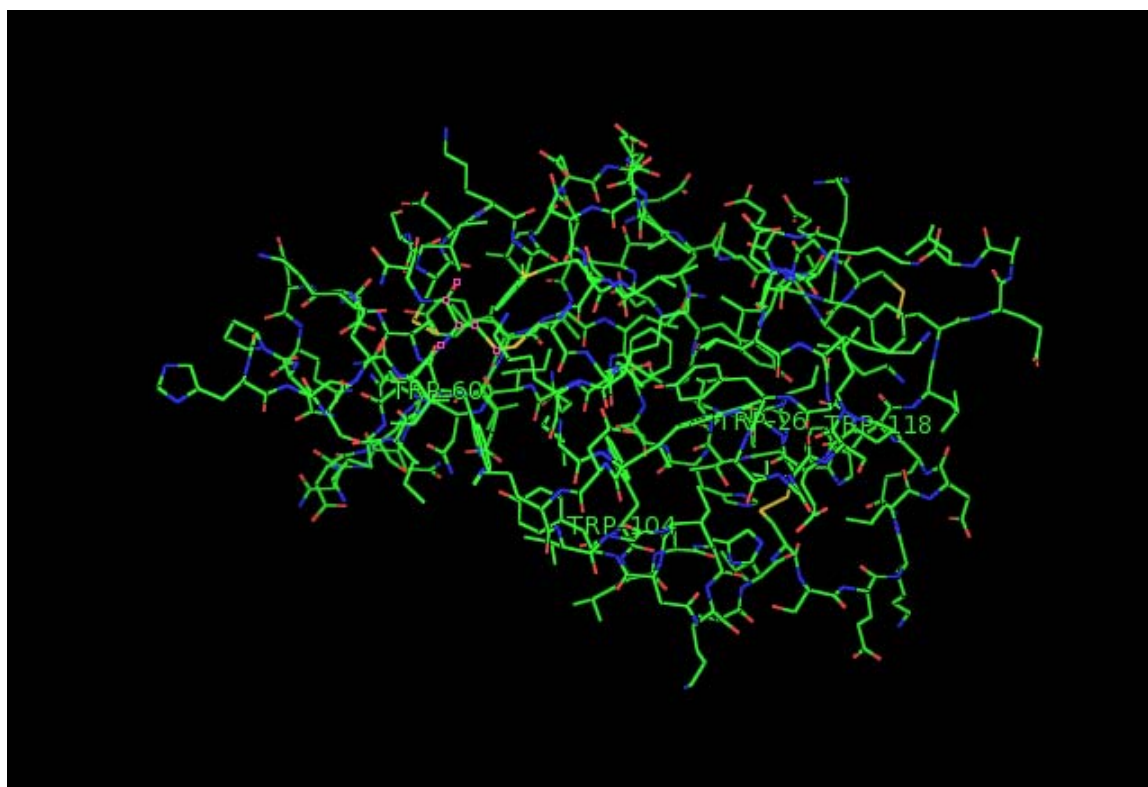


Figure VIIb-11: The structure of α -lactalbumin showing positions of tryptophan residues (Pymol).

Figure VIIb-12

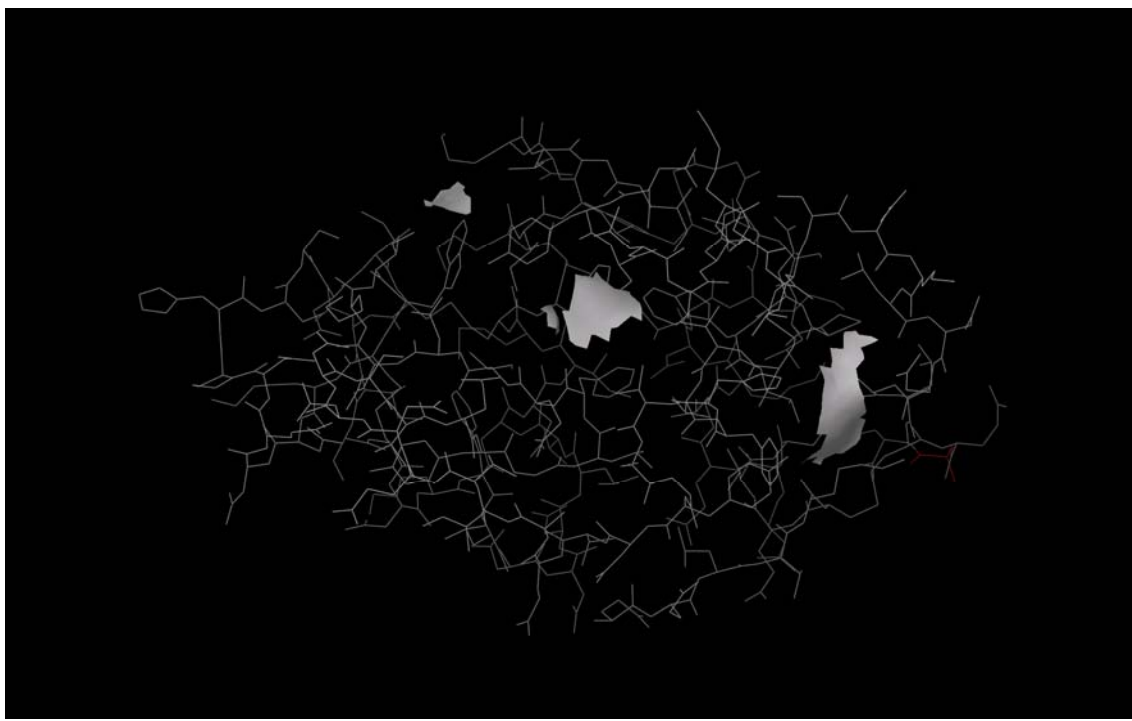


Figure VIIb-12: The surface accessible area of tryptophan residues (Pymol).

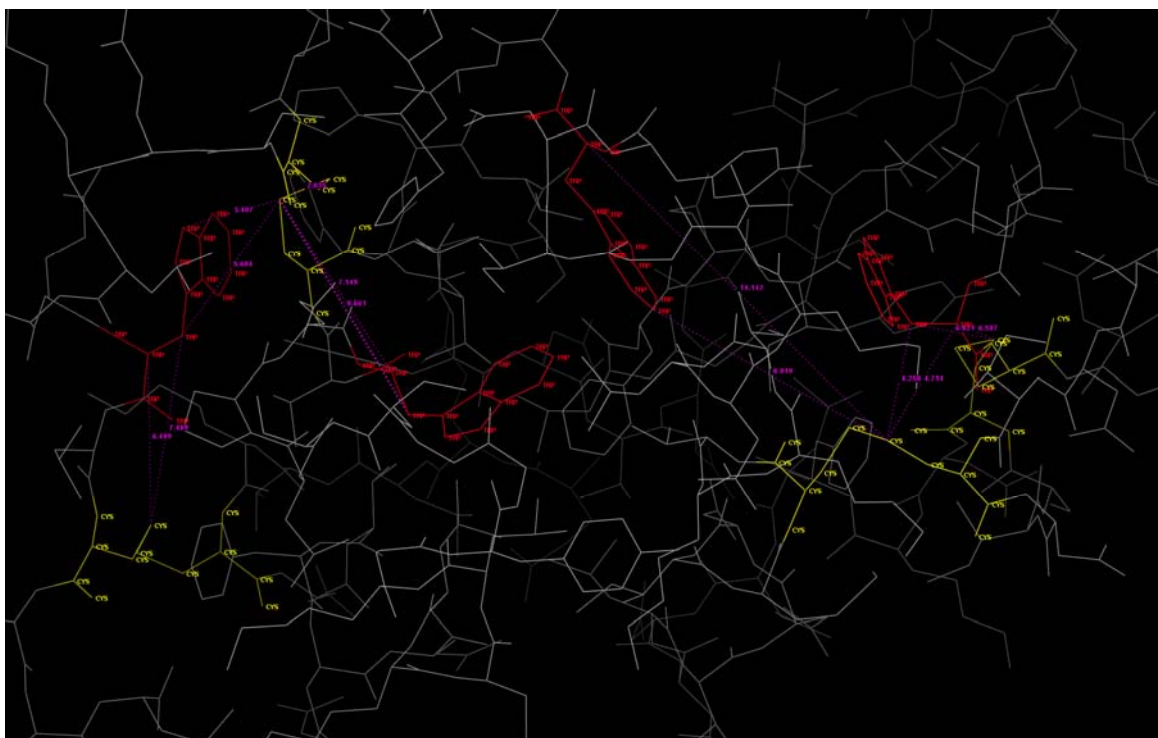
Figure VIIb-13

Figure VIIb-13: The distance calculation between tryptophan residues and disulphide bond (Pymol).

Table VIIb-1

Table VIIb-1: Calculated activation energy E_a for each individual lifetime components τ_1 , τ_2 , τ_3 and τ_4 and average lifetime at low, intermediate and high temperature.

Lifetime	Temperature	Equation	R^2	E_a KJ / mol	Transition Temperatures °C
τ_1	LT	$y = -1841.1x + 8.3284$	0.98	15.31	35
	HT	$y = -3484.4x + 13.868$	0.98	28.97	
τ_2	LT	$y = -1441.7x + 8.8242$	0.97	11.99	38
	HT	$y = -2888.7x + 13.615$	0.97	24.02	
τ_3	HT	$y = -1731.2x + 11.67$	0.96	14.39	-
τ_4	HT	$y = -1341.4x + 12.284$	0.95	11.15	-
τ_{Avg}	LT	$y = -1733.4x + 10.915$	0.99	14.40	38
	HT	$y = -3350.3x + 16.249$	0.98	27.90	
$\ln(k_{NR})$	LT	$y = -1736.4x + 10.924$	0.99	14.44	40
	HT	$y = -3351.4x + 16.252$	0.98	27.86	

References

- Bent, D. V. and Hayon, E. Excited state chemistry of aromatic amino acids and related peptides. III. Tryptophan *Journal of American Chemical Society*. 97 (1975). 2612-2619.
- Birks, J. B. *Photophysics of Aromatic Molecules*. New York: John Wiley and Sons. (1970).
- Bishai, F., Kuntz, E. and Augenstein, L. Intra and intermolecular factors affecting the excited states of aromatic amino acids. *Biochimica et Biophysica Acta*. 140 (1967). 381-394.
- Callhoun, D. B., Englander, S. W., Wright, W. W. and Vanderkooi, J. M. Quenching of room temperature protein phosphorescence by added small molecules. *Biochemistry*. 27 (1988). 8466-8474.
- Chen, R. Apparent stretched exponential luminescence decay in crystalline solids. *Journal of Luminescence*. 102-103 (2003). 510-518.
- Churchich, J. E. Effect of dioxane on the dissociation and activity in bovine-liver catalase. *Biochimica Biophysica Acta*. 92 (1964). 194-197.
- Cowgill, R. W. Fluorescence quenching by disulfide and sulfhydryl groups *Biochimica Biophysica Acta*. 140 (1967). 37-44.
- Fischer, C. J., Gafni, A., Steel, D. G. and Schauerte, J. A. The triplet-state lifetime of indole in aqueous and viscous environments: significance to the interpretation of room temperature phosphorescence in proteins. *Journal of the American Chemical Society*. 124 (2004). 10359-10266.
- Gabellieri, E. and Strambini, G. B. Structural perturbations of azurin deposited on solid matrices as revealed by tryptophan phosphorescence. *Biophysical Journal*. 80 (2001). 2431-2438.
- Galley, W. C. In *Biochemical Fluorescence: Concepts* (Edited by Chen R.F. and Edelhoch, H) Marcel and Dekker, Vol II (1976). 409-439.
- Geacintov, N. E., Benson, R., and Pomeranz, S. B. *Chemistry Physics Letter*. 17 (1972). 280-282.
- Ghiron, C., Bazin, M and Santu, R. Determination of the acrylamide quenching constant for protein and model indole triplets. *Photochemistry and Photobiology*. 48 (1988). 539-543.

- Gonnelli, M and Strambini, G. B. Phosphorescence lifetime of tryptophan in proteins Biochemistry. 34 (1995). 13874-13857.
- Hendrix, T. M., Griko, Y. and Privalov, P. Energetics of structural domains in alpha lactalbumin. Protein Science. 5 (1996). 923-931.
- Boye, J. I., Alli, I. and Ismail, A. A. Use of differential scanning calorimetry and infrared spectroscopy in the study of thermal and structural stability of (α -lactalbumin Journal of Agriculture and Food Chemistry. 45 (1997). 1116-1125.
- Kronman, M. J. and Andreotti, R. E. Inter and intramolecular interactions of alpha lactalbumin. Protein Science. 3 (1964). 1145-1151.
- Lakowicz, J. R. Principles of Fluorescence Spectroscopy. Second ed. New York: Kluwer Academic/Plenum Press. (1999).
- Li, Z., Bruce, A., and Galley, W. C. Temperature dependence of the disulfide perturbation to the triplet state of tryptophan. Biophysical Journal. 61 (1992). 1364-1371.
- Li, Z., Lee, W. E., and Galley, W. C. Distance dependence of the tryptophan-disulfide interaction at the triplet level from pulsed phosphorescence studies on a model system. Biophysical Journal. 56 (1989). 361-367.
- Longworth, J. W. Luminescence of polypeptides and proteins. In excited states of protein and nucleic acids (Edited by R. F. Steiner and L. Weinryb). Plenum Press, NY. (1971). 3190384.
- Ludescher, R.D., Shah, N. K., McCaul, C. P. and Simon-Lukasik, K. V. Beyond Tg: optical luminescence measurements of molecular mobility in amorphous solid foods. Food Hydrocolloids. 15 (2001). 331-339.
- Maroncelli, M. and Fleming, G. R. Picosecond salvation dynamics of coumarin 153: The importance of molecular aspects of salvation. Journal of Chemical Physics. 86 (1987). 6221-6239.
- McCaul, C. P. and Ludescher, R. D. Room temperature phosphorescence from tryptophan and halogenated tryptophan analogs in amorphous sucrose. Photochemistry and Photobiology. 70 (1999). 166-1671.
- Nack, T. J. and Ludescher, R. D. Molecular mobility and oxygen permeability in amorphous bovine serum albumin films. Food Biophysics. 1 (2006). 151-162.
- Relkin, P., Launay, B. and Eynard, L. Effect of sodium and calcium addition on thermal denaturation of apo- α -lactalbumin: a Differential Scanning Calorimetric Study. Journal of Dairy Science. 76 (1993). 36-47.

- Papp, S. and Vanderkooi, J. M. Tryptophan phosphorescence at room temperature as a tool to study protein structure and dynamics. *Photochemistry and Photobiology*. 49 (1989). 775-784.
- Pravinata, L.V., You, Y. and Ludescher, R. D. Erythrosin B phosphorescence monitors molecular mobility and dynamic heterogeneity in amorphous sucrose. *Biophysical Journal*. 88 (2005). 3551-3561.
- Richert, R. Triplet state salvation dynamics: Basics and applications. *Journal of Chemical Physics*. 113 (2000). 8404-8429.
- Saviotti, M. L. Room temperature phosphorescence and the dynamic aspects of protein structure Ph. D Thesis. McGill University, Montreal, Canada. (1975).
- Shah, N. K. and Ludescher, R. D. Hydration and the internal dynamics of hen egg white lysozyme. *Proceedings of SPIE*. 1640 (1992). 174-179.
- Shah, N. K. and Ludescher, R. D. Influence of hydration on the internal dynamics of hen egg white lysozyme in the dry state. *Photochemistry and Photobiology*. 58 (1993). 169-174.
- Shah, N. K. and Ludescher, R. D. Phosphorescence of probes of the glassy state in amorphous sucrose. *Biotechnology Progress*. 11 (1995). 540-544.
- Shamblin, S., Hancock, B. C., Dupuis, Y. and Pikal M. J. Interpretation of relaxation time constants for amorphous pharmaceutical systems. *Journal of Pharmaceutical Sciences*. 89 (2000). 417-427.
- Strambini, G. B. and Gonnelli, M. Tryptophan phosphorescence in fluid solution. *Journal of American Chemical Society*. 117 (1995). 7646-7651.
- Strambini, G. B. and Gabellieri, E. Intrinsic phosphorescence from proteins in the solid state. *Photochemistry Photobiology*. 39 (1984). 725-729.
- Strambini, G. B. and Gonnelli, M. The indole nucleus triplet-state lifetime and its dependence on solvent microviscosity. *Chemical Physics Letters*. 115 (1985). 196-200.
- Strambini, G. B. Quenching of alkaline phosphatase phosphorescence by O₂ and NO. Evidence for inflexible regions of protein structure. *Biophysical Journal*. 52 (1987). 23-28.
- Strambini, G. B. and Gabeillieri, E. *Photochemical Photobiology*. 51 (1990). 643-648.

- Stratt, R. M. and Maroncelli, M. Nonreactive dynamics in solution: the emerging molecular view of solvation dynamics and vibrational relaxations. *Journal of Physical Chemistry*. 100 (1996). 12981-12996.
- Subramaniam, V., Gafni, A. and Steel, D. G. Time-resolved tryptophan phosphorescence spectroscopy: A sensitive probe of protein folding and structure. *IEEE Journal of Selected Topics in Quantum Electronics*. 2 (2006). 1107-1114.
- Sundaresan, K. V. and Ludescher, R. D. Molecular mobility and oxygen permeability in amorphous beta-lactoglobulin films. 22 (2007). 403-413.
- Sviotti, M. L. and Galley, W. C. *Proceeding of National Academics of Sciences, USA*. 71 (1974). 4154-4158.
- Terenin, A. N. and Ermoleav, V. A. *Trans Faraday Society*. 52 (1956). 1042-1046.
- Thomas D. *Rotational Diffusion of Membranes*. Ed. Ragan C.I and Cherry R.J. *Analysis of membrane proteins*. London: Chapman and Hall. (1986). 377-394.
- Bernal, V. and Jelen, P. Effect of Calcium Binding on Thermal Denaturation of Bovine α -Lactalbumin. *Journal of Dairy Science*. 67 (1984). 2452-2454
- vande Van, M., Han, M., Walbridge, D., Knutson, J., Shin, D., Ainfinsen, C. B. and Brand, L. *Biophysical Journal*. 51 (1987). 275a.
- Vanderkooi, J.M., Englander, S.W., Papp, S., Wright, W.W. and Owen, C.S. Long range electron exchange measured in proteins by quenching of tryptophan phosphorescence. *Proceedings of National Academy of Sciences of USA*. 87 (1990). 5099-5103.
- Vanderkooi, J. M. and Berger, J. W. Excited triplet state used to study biological macromolecules at room temperature. *Biochimica et Biophysica Acta: Bioenergetics*. 976 (1989). 1-27.
- Vanderkooi, J. M., Maniara, Green, T. J. and Wilson, D. F. An optical method for measurement of dioxygen concentration based upon quenching of phosphorescence. *Journal of Biological Chemistry*. 262 (1987). 5476-5482.
- Wright, W. W., Owen, C. S. and Vanderkooi. Wright, W. W., Owen, C. S. and Vanderkooi, *Journal of Molecular Biochemistry*. 31 (1992). 6538-6544. *Journal of Molecular Biochemistry*. 31 (1992). 6538-6544.

Chapter VIIc: Investigating the molecular mobility of the amorphous α -lactalbumin matrix using the phosphorescence of extrinsic probe (vanillin).

Introduction

We have recently shown that vanillin can be used as a triplet state probe to monitor molecular mobility in amorphous solids (Chapter II). Vanillin phosphorescence lifetime and emission energy were found to be extremely sensitive to the local environment in amorphous solids (sucrose, protein) in the glassy state and at the glass-to-rubber transition into the melt. Vanillin was also shown to be promising in reporting molecular mobility in amorphous sucrose film in the dual probe combination study using erythrosin B and tryptophan (Chapter X). There are many different techniques used to study protein motions such as H-exchange, NMR and electron microscopy, each providing information of protein motions on different time scales (Linderstrom-Lang, 1958; Schellman, 1964; Kuwajima et al., 1983). Room temperature phosphorescence has been used to investigate protein motions (Vanderkooi et al., 1987; Cioni and Strambini, 1989; Strambini et al., 1990). The current study focuses on using steady state and time-resolved phosphorescence of the vanillin probe to monitor molecular mobility in thin films of amorphous α -lactalbumin (apo: calcium depleted) as a function of temperature. The results from this study will also be compared to measurements of mobility made in α -lactalbumin matrix using erythrosin B and tryptophan.

Materials and Methods

Sample preparation: Purified α -lactalbumin (calcium depleted) was obtained from Sigma Chemical Company (St Louis, MO) and used as received. In order to define and minimize the presence of counter ions, α -lactalbumin was dissolved in distilled deionized water at 10 mg/ml, placed in a cellulose dialysis tube having a 1 kDa molecular weight cutoff (Spectrum, Houston, TX), dialyzed against 0.1 M potassium chloride for at least 36 hours with frequent changes of buffer, and then dialyzed extensively against distilled deionized water. All dialysis was carried out at 4°C. The solution was then filtered through a 0.2 μ m Acrodisc membrane filter (Pall Gellman Laboratory, Ann Arbor, MI) to remove particulate matter. The concentration of the protein after dialysis was determined by absorbance at 280 nm using an extinction coefficient of 28,500 $\text{M}^{-1}\text{cm}^{-1}$ (Kronman and Andreotti, 1964).

Vanillin: A 66mM stock solution of vanillin (Sigma-Aldrich, Milwaukee, WI) was prepared in distilled deionized water. This concentration was selected to simplify the addition of the probe to the protein solution. For measuring phosphorescence in amorphous solid, vanillin was added to the protein solution at a molar ratio of 1:1 (dye: protein). Other ratios 1:3, 1:5 and 1:10 were also tested to study the effect of probe concentration.

Preparation of protein films: The amorphous films were made by pipetting 20 μ L of the solution (α -lactalbumin + vanillin) onto quartz slides (13 mm x 30 mm x 0.6 mm) (NSG Precision Cells, Farmingdale, NY) and spreading the solution over an area approximately

15 mm x 10 mm. Before use, to improve the surface activity for spreading the solutions, the slides were soaked in Terg-A-Zyme (Alconox, Inc., NY) soap solution, washed with double distilled water, rinsed with ethanol and dried in acetone. After spreading (~0.05 mm thick), the slides were dried under constant flow of air for 30 minutes, allowing the films to set, and then transferred to a desiccators over phosphorus pentoxide for at least one week, where the water activity is not greater than 0.01. The slides were stored at $23.0 \pm 1^{\circ}\text{C}$, protected from light to prevent any photo bleaching of the vanillin and desiccant was refreshed as needed to maintain a relative humidity close to 0%.

Instrumentation: Measurements were made on a Cary Eclipse fluorescence spectrophotometer (Varian Instruments, Walnut Creek, CA). This instrument, which collects in analog mode, uses a high intensity pulsed lamp and a time delay was employed to avoid any fluorescence during the lamp pulse. The temperature was controlled by using a TLC 50 thermoelectric heating/cooling system (Quantum Northwest, Spokane, WA). The TLC-50 sample compartment was fitted with a jacketed cover. The measurements were made in absence of oxygen (Nitrogen was purged for 15 minutes). Nitrogen stream was generated by passage of high purity nitrogen through a Supelco (Bellefonte, PA) carrier gas purifier. Quartz slides were placed in the standard 1cm x 1cm x 1cm quartz fluorescence cuvette, which was capped with a lid having inlet and outlet ports of gas lines.

Luminescence Measurements: The Cary Eclipse uses a pulsed lamp and collects emission intensity in analog mode; data were not collected within the first 0.1-0.2 ms to suppress fluorescence coincident with the lamp pulse.

Delayed luminescence emission spectra of vanillin in amorphous protein were collected from 400 to 800 nm (10 nm bandwidth) using excitation at 320 nm (20 nm bandwidth) over the temperature range from -20°C to 100°C . Each data point was collected from a single flash with 0.2 ms delay, 100 ms gate time, and 0.12 s total decay time. The phosphorescence spectra collected as a function of temperature in the presence of nitrogen, were converted to intensity versus frequency (cm^{-1}) and analyzed to obtain the peak frequency and spectral bandwidth using eq. (1) and (2) (Maroncelli and Fleming 1987).

Lifetime measurements were made as a function of temperature. The samples were excited at 320 nm (20 nm bandwidth) and emission transients collected at 490 nm (20 nm bandwidth) at temperature ranging from -20°C to 100°C . Each decay was the average of 50 cycles, and for each cycle data was collected from a single flash with a delay of 0.2 ms, windows for gate time and total decay time were varied at each temperature. All measurements were made in quadruplicate.

Data Analysis

Emission Energy as a function of temperature: Emission spectra were fit using the program Igor (Wavemetrics, Inc., Lake Oswego, OR) to a log-normal function over the temperature range Equation 1.

$$I(\nu) = I_0 \exp \left\{ -\ln(2) \left(\frac{\ln[1 + 2b(\nu - \nu_p) / \Delta]}{b} \right)^2 \right\} \quad (1)$$

In this equation I_0 is the maximum intensity of the emission spectra, ν_p is the frequency (in cm^{-1}) of the emission maximum, Δ is a line width parameter, and b is an asymmetry parameter. The bandwidth of the emission, the full width at half maximum (Γ), is related to b and Δ Equation 2.

$$\Gamma = \Delta \left(\frac{\sinh(b)}{b} \right) \quad (2)$$

Phosphorescence Intensity: Phosphorescence lifetimes were determined with the statistical program Igor (Wavemetrics, Inc., Lake Oswego, OR). The phosphorescence intensity decays were collected as described above and were fitted using a multi-exponential function for vanillin (Shamblin et al., 2000). Fits were judged satisfactory if the r^2 values were in the range of 0.995-1.0 and the modified residuals $((\text{data} - \text{fit})/\text{data}^{1/2})$ varied randomly about zero.

Multi-exponential function: The multi-exponential model is as show in Equation 3. τ_i are decay times, α_i represent the amplitudes of the components at $t = 0$ and n is the number of decay times. The average lifetime was calculated using Equation 4.

$$I(t) = \sum_{i=1}^n \alpha_i \exp(-t/\tau_i) \quad (3)$$

$$\tau_{\text{Avg}} = \sum_{i=1}^n \alpha_i \tau_i / \sum_{i=1}^n \alpha_i \quad (4)$$

Photophysical Scheme: The phosphorescence lifetimes were interpreted in terms of the rate constants associated with the various processes that contribute to the de-excitation of the excited triplet state of the probe (Duchowicz., 1998). The phosphorescence lifetimes were used to calculate the rate constants associated with the various processes that depopulate the excited triplet state. The term $k_P (=1/\tau)$ is the total decay rate, k_{RP} is the rate of radiative decay of the triplet state. The magnitude of k_{NR} reflects factors associated with the mechanism by which the excited T_1 state is coupled to highly excited vibrations of the S_0 ground state as well as external factors associated with the mechanism by which the ground state vibrational energy can dissipate from the excited state into the surrounding matrix (Fischer et al., 2002; Vanderkooi and Berger, 1989). As the efficiency of external vibrational dissipation is related to overall mobility of the matrix, the magnitude of k_{NR} provides a measure of matrix mobility. The term $k_Q [Q]$ refers to the

collisional quenching due to interaction between the excited chromophore and a quencher molecule for example triplet state oxygen.

The lifetime τ is related to the rate constants for de-excitation of the triplet excited state of the probe according to the following Equation 5 (Papp and Vanderkooi, 1989).

$$1/\tau = k_{RP} + k_{NR} (T) + k_Q [Q] = k_P \quad (5)$$

Here $k_P (=1/\tau)$ is the total decay rate, k_{RP} is the rate of radiative decay of the ground state ($1/6 \text{ s}^{-1}$), k_{NR} is the rate of non-radiative decay to the singlet state followed by vibrational relaxation to S_0 due to collisional quenching. The term $k_Q [Q]$ refers to the collisional quenching due to interaction between the excited chromophore and a quencher molecule for example triplet state oxygen.

Results

Delayed emission spectra: The delayed luminescence spectra of extrinsic vanillin in amorphous α -lactalbumin films (in the presence of nitrogen) as a function of temperature are plotted in Figure 1. The emission spectra showed maxima at ~ 490 nm. The phosphorescence band reflects emissions from the triplet state (T_1) to the ground state (S_0). The delayed emission spectra were collected over the temperature range -20°C to 100°C . Delayed emission showed a decrease in phosphorescence intensity as a function of temperature as expected from thermally stimulated processes. The normalized plots of phosphorescence intensity versus temperature are shown in Figure 2. The plot shows, as the temperature increases, the peak intensity of the emission spectra decreases.

The peak energy (ν_p) and bandwidth (Γ) were determined by fitting emission spectra to a log-normal function. The values of ν_p and Γ for the phosphorescence band varied systematically as a function of temperature (Figure 3). There was a steeper decrease in the emission energy as a function of temperature from -20°C to 30°C than from 40°C to 80°C , followed by steeper decrease above 90°C . The decrease in ν_p reflects an increase in the rate of dipolar relaxation around the triplet excited state (Lakowicz, 1999). The emission bandwidth (Γ) remained constant from -20°C to 50°C , and increased gradually over the temperature interval from 60°C to 100°C . The increase in Γ at elevated temperatures reflects an increase in the extent of inhomogeneous broadening of the spectra due to changes in the interaction of vanillin molecules with the surrounding matrix.

Phosphorescence lifetimes: The phosphorescence intensity decays collected as a function of temperature were fitted using a multi-exponential function. These lifetimes reflect the ensemble average of all dynamic environments because the peak excitation and peak emission wavelength were used. The intensity decays are plotted in Figure 4 along with fits using a multi-exponential function. The modified residuals for these fits varied randomly around zero, indicating that these functions provided a statistically satisfactory fit to these data (Figure 4). Lifetime is the average time a molecule spends in the excited state and is the indicator of the rigidity of the matrix.

All intensity decay data over the temperature interval from -20°C to 100°C were well fitted using multi-exponential function and two physically important parameters lifetime τ and amplitude α were obtained. The lifetimes of vanillin as a function of temperature are shown in Figure 5a. The log plots for lifetime is shown in Figure 5b. In case of multi-exponential function the four lifetime components at 20°C were $\tau_1 = 94.6$ ms, $\tau_2 = 24.2$ ms, $\tau_3 = 4.8$ ms and $\tau_4 = 0.74$ ms indicating the presence of local environments with ~ 130 fold difference in mobility. The plot of the amplitudes of each life time component for as a function of temperature is shown in Figure 6. The amplitudes a_1 and a_2 of the longer lifetimes, decreased and amplitude a_4 of shorter lifetime component increased as a function of temperature. The amplitude a_3 for τ_3 did not change as a function of temperature. The long lifetime components ($a_1 + a_2$) contributed 10-40% and the short component contributed 60-88% to the emission as a function of temperature.

The average lifetime was calculated using Eq. 4 and is plotted in Figure 7. Arrhenius plots of the inverse of individual lifetime components τ_1 , τ_2 , τ_3 and τ_4 are shown in Figure 8a. The transition temperatures and activation energies for individual lifetime components are compiled in Table 1. The Arrhenius plot of $\ln k_p$ for lifetime component τ_1 and τ_2 (longer lifetimes) showed transition temperatures at 50°C and 50°C, respectively. The Arrhenius plot of $\ln k_p$ for lifetime component τ_3 and τ_4 (shorter lifetimes) show transition temperature at 60°C and 68°C. The Arrhenius plot of $\ln k_p$ (average lifetime) showed transition temperature of 50°C with activation energies at low and high temperature as 10.0 kJ mol⁻¹ and 46.4 kJ mol⁻¹, respectively (Table 1).

Temperature dependence of non-radiative decay of the triplet state is shown in Figure 9. The k_{NR} term is a rate constant for non-radiative decay; it is the actual measure of the effect of the motion that quenches probes excited triplet state. The k_{NR} values were calculated by subtracting the phosphorescence emission rate constant ($1/\tau$ at 77K) from the inverse of the lifetime. Plot of k_{NR} as a function of temperature is in Figure 9. The Arrhenius plot of k_{NR} is shown in Figure 10. The activation energy obtained from the slope of fit line in this plot is the activation energy of the motions which quench probes excited triplet state are shown in Table 1.

Discussion

We have recently shown that the phosphorescence from vanillin provides information about matrix molecular mobility in amorphous solid sugars (Chapter II). Vanillin phosphorescence was found to be sensitive to both dipolar relaxation around the excited triplet state that lowers the emission energy and molecular collision with the triplet state that lowers the emission intensity and lifetime. Similar phosphorescence behavior for vanillin dispersed in thin dry films of α -lactalbumin indicates that amorphous protein exhibits a similar pattern of molecular mobility.

Matrix Molecular Mobility: The thermal response of peak emission reflects the effect of temperature on increasing the rate of dipolar relaxation around the excited triplet state of vanillin. Surface polar groups like side-chain hydroxyl, amino, and carboxyl groups in α -lactalbumin are the origins of dipolar relaxation. The large increase in FWHM at higher temperatures indicated inhomogeneous broadening corresponding to increase in the width of the distribution of energetically distinct matrix environments in the amorphous α -lactalbumin films. Peak frequency did not indicate presence of any softening transition. FWHM indicated presence of softening transition above $\sim 50^{\circ}\text{C}$. The increase in matrix mobility seen at $\sim 50^{\circ}\text{C}$ thus appears to reflect an increase in the ability of these groups to reorient around the tryptophan triplet state. The effect of temperature is diminishing at high temperature on emission energy, suggesting that something is going on but that is not softening phase.

The photophysical analysis of vanillin indicates that the triplet state lifetime decreases with temperature because of thermal activation of the rates of collisionally activated non-radiative decay to the ground state (k_{NR}). The non-radiative decay rate provides an estimate of matrix mobility. The magnitude of k_{NR} increased moderately at low and more dramatically at high temperature with a transition temperature of $\sim 50^\circ\text{C}$. The activation energy for motions associated with k_{NR} was 10.6 kJ mol^{-1} at low temperature and 46.9 kJ mol^{-1} at high temperature. The activation energy at low temperature were similar to those seen for vanillin in amorphous sucrose (Chapter II) in the glass (12.3 kJ mol^{-1}) suggesting that comparable molecular motions caused quenching in both amorphous sucrose and amorphous α -lactalbumin. But the activation energies at high temperature were significantly different in amorphous α -lactalbumin as compared to amorphous sucrose (29 kJ mol^{-1} and 72 kJ mol^{-1}), suggesting that different molecular motions caused quenching in both amorphous sucrose and amorphous α -lactalbumin.

Collisional quenching in α -lactalbumin involves local motions with small activation energy at temperatures below the softening transition temperature (50°C) and more delocalized collective motions with larger activation energy at temperatures above the softening transition.

Dynamic Transition: Two spectroscopic measures, bandwidth and lifetime, indicate that the protein undergoes a softening transition at $\sim 50^\circ\text{C}$. The softening transition could be due to protein denaturation or protein glass transition. The apo α -lactalbumin (calcium depleted) form has a much lower transition temperature ($T_d \sim 38^\circ\text{C}$) and has been

referred to as more heat labile than the holo form. Thus, softening transition could be attributed to denaturation process seen in α -lactalbumin. However, a study conducted in our lab using Ery B in amorphous α -lactalbumin in the same temperature -20°C to 100°C , showed the variation in emission lifetime to be reversible upon heating and cooling, such behavior is not expected for denaturation in the solid phase. Thus one could rule out the possibility of denaturation.

Proteins are shown to exhibit a dynamic transition T_d (Hill et al., 2005) at temperatures near 200K. This transition due to its similarity to the high temperature dynamical transition seen in amorphous dry proteins is often referred as glass transition (Ringe and Petsko, 2003). Above proteins dynamic transition T_d (similar to T_g), the dynamic behavior is thought to be highly temperature dependent and shows an-harmonic vibrations and below T_d harmonic vibrations are more prevalent (e.g., localized atomic fluctuations). The softening transition seen in α -lactalbumin at $\sim 50^{\circ}\text{C}$ may thus correspond to a glass transition within the α -lactalbumin molecule in the film.

Conclusion

We have used phosphorescence from the vanillin to characterize the molecular mobility as a function of temperature in amorphous solid α -lactalbumin films. Emission spectra provided information of how temperature modulates the emission energy and bandwidth. The emission energy decreased as a function of temperature without any transition point. The bandwidth increased gradually at low temperature and more steeply at high temperature indicating a softening transition of the protein matrix at $\sim 50^{\circ}\text{C}$ - 60°C . Lifetime decreased as a function of temperature. Arrhenius analysis of the rate constant for nonradiative collisional quenching indicated an increase in quenching indicative of matrix softening at $\sim 50^{\circ}\text{C}$ - 60°C . These results enrich our molecular understanding of the intrinsic mobility of proteins within the amorphous solid phase, provide evidence for dynamic transition within solid α -lactalbumin.

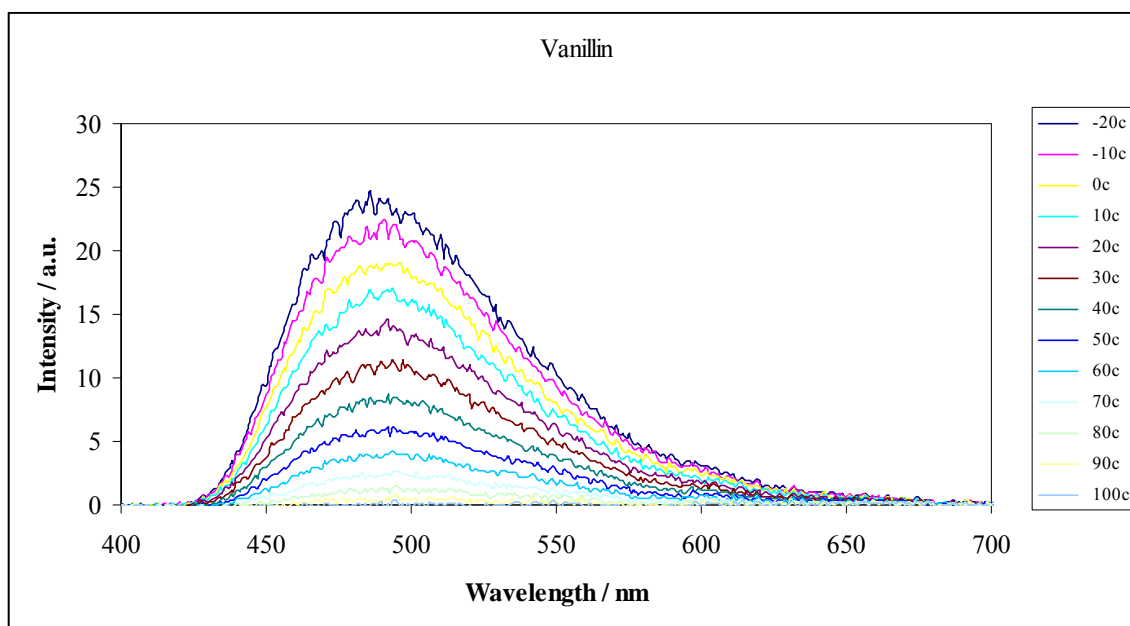
Figure VIIc-1

Figure VIIc-1: Delayed emission spectra of vanillin in amorphous α -lactalbumin films as a function of temperature (excitation at 320 nm). The spectra were collected at 10°C intervals from -20°C to 100°C (the curves follow this order from high to low intensity at ~490 nm).

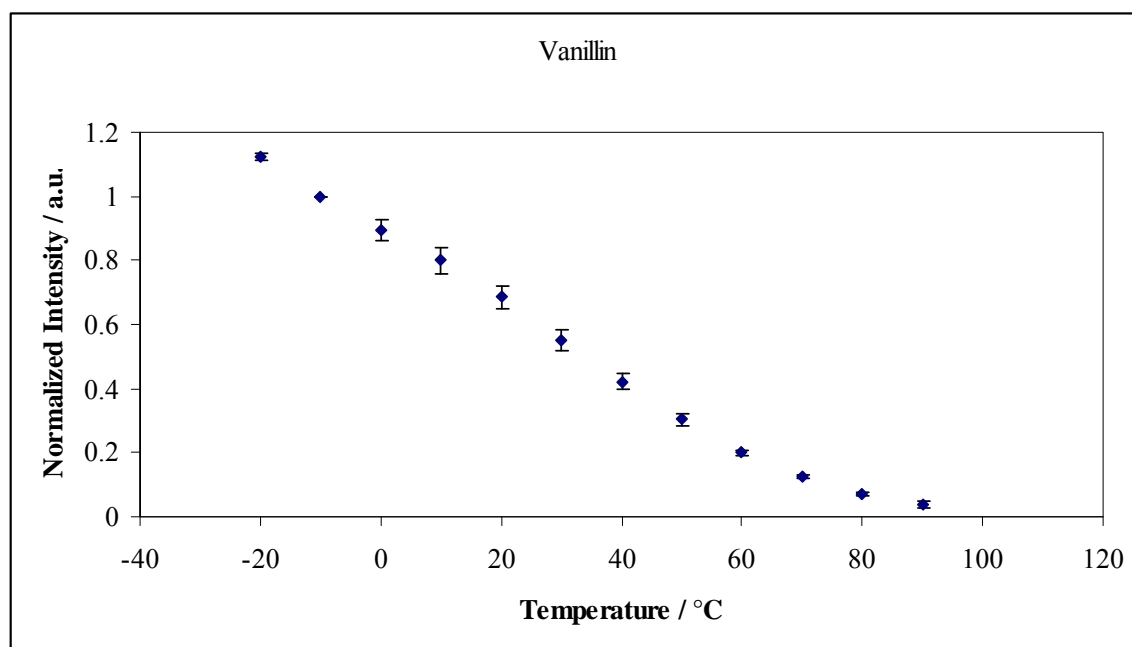
Figure VIIc-2

Figure VIIc-2: The effect of temperature on the phosphorescence emission intensity of vanillin in amorphous α -lactalbumin films as a function of temperature equilibrated against nitrogen. Intensity (I_P) was determined from analysis of the phosphorescence emission band (Figure 2) using a log-normal function (eq. (1), Materials and Methods). The data was normalized to -20°C.

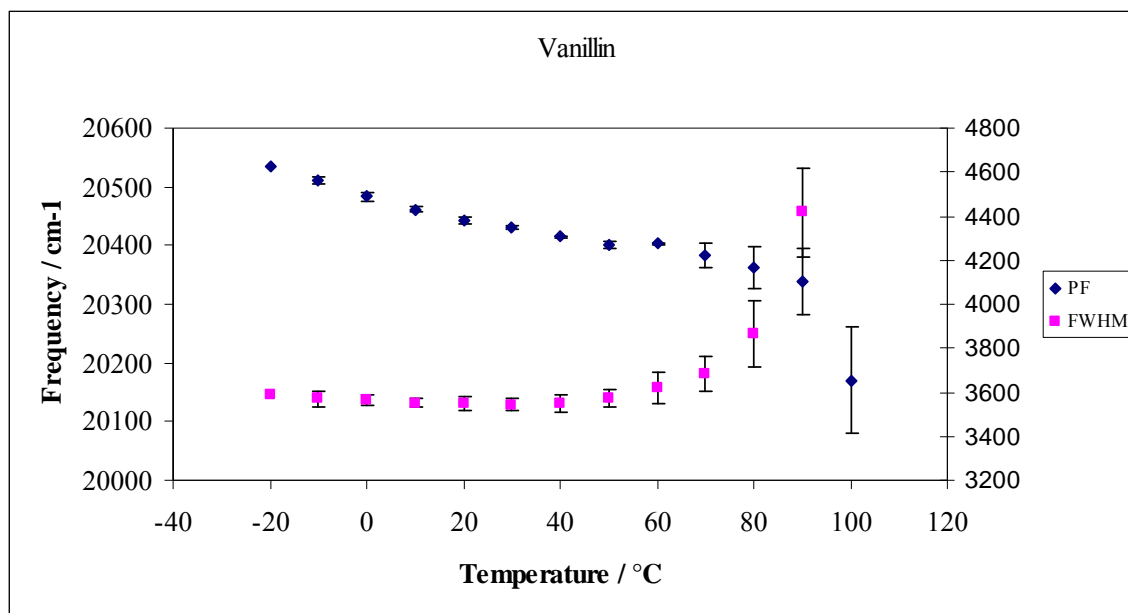
Figure VIIc-3

Figure VIIc-3: Peak energy ν_p (♦, left hand scale) and bandwidth (■, right hand scale) for phosphorescence emission from vanillin in α -lactalbumin films as a function of temperature.

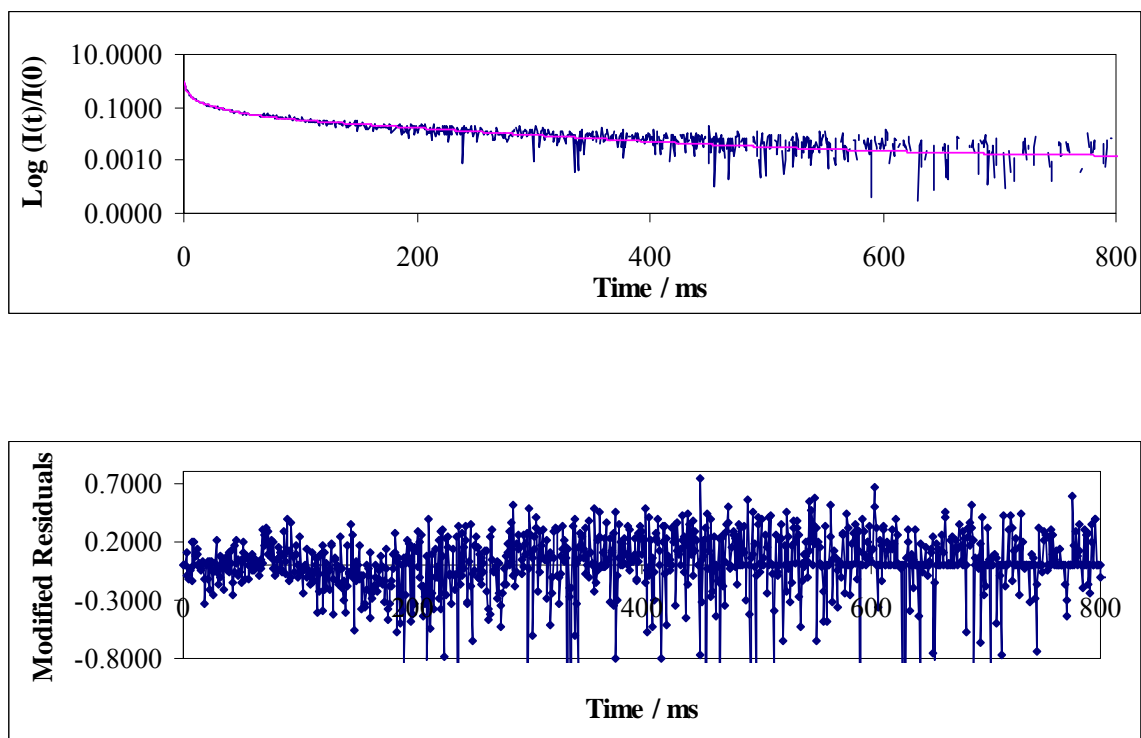
Figure VIIc-4

Figure VIIc-4: (a) Normalized phosphorescence intensity decay $[I(t)/I(0)]$ of vanillin dispersed in amorphous α -lactalbumin film at 20°C in the presence of nitrogen (\blacklozenge). The solid lines through the data are fits using a multi-exponential function. (b) The modified residuals $[(\text{Data}-\text{Fit})/\text{Data}^{1/2}]$ for these fits to data in the presence of nitrogen (dotted line).

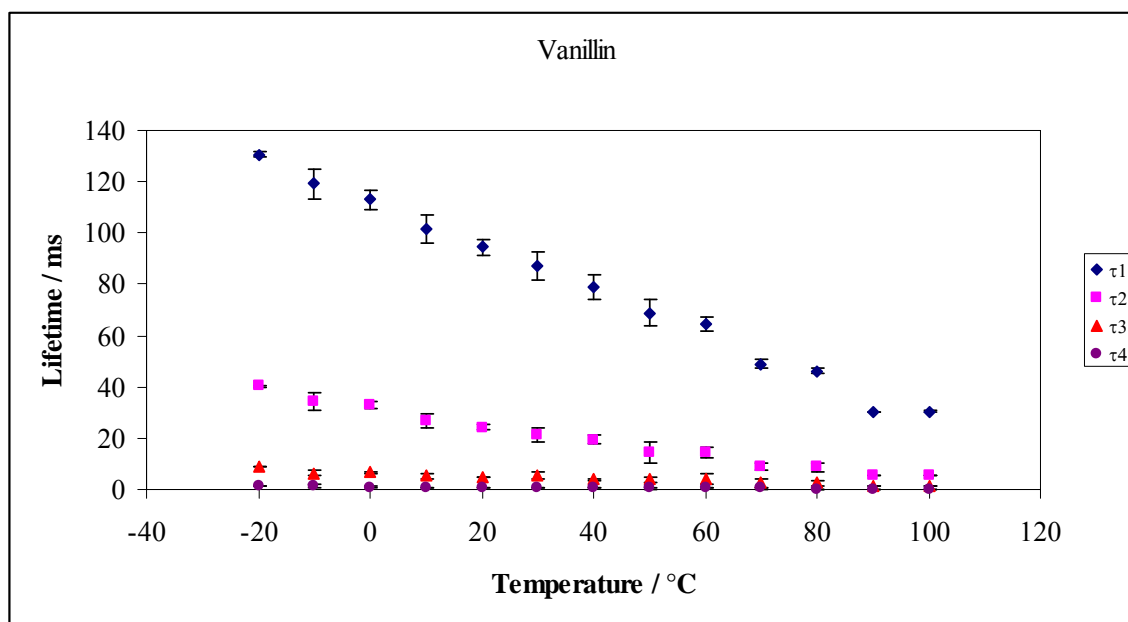
Figure VIIc-5a

Figure VIIc-5a: Lifetime components τ_1 (\blacklozenge), τ_2 (\blacksquare), τ_3 (\blacktriangle), τ_4 (\bullet) obtained from a multi-exponential model fit (Eq. (3), Materials and Methods) to phosphorescence intensity decay data from vanillin dispersed in amorphous α -lactalbumin films equilibrated against nitrogen as a function of temperature. The data was calculated every 10°C from -20°C to 100°C.

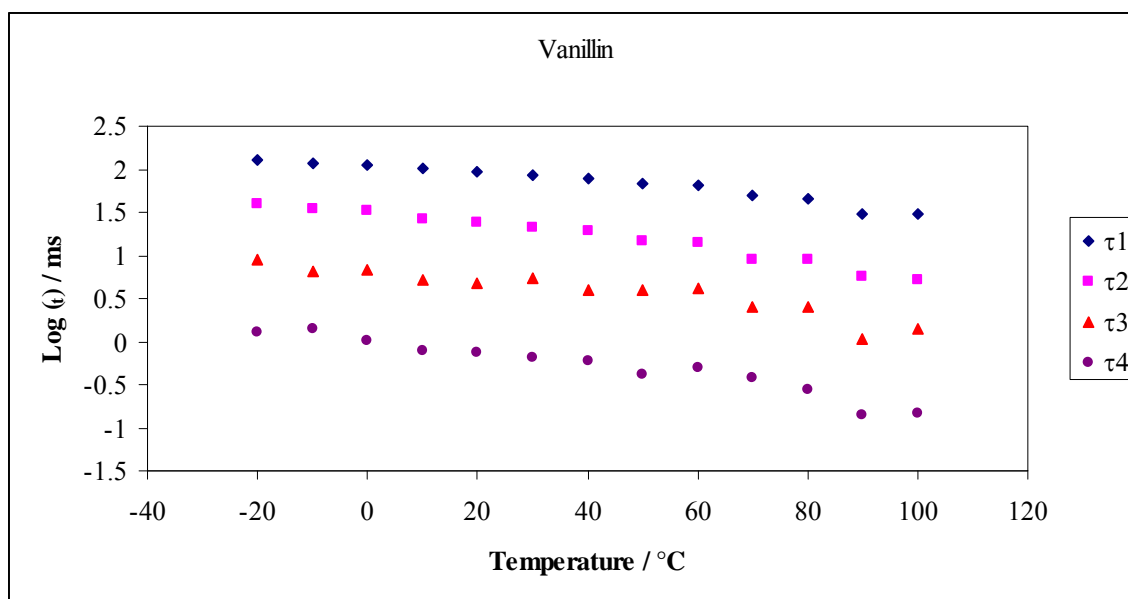
Figure VIIc-5b

Figure VIIc-5b: The log plot of lifetime components τ_1 (\blacklozenge), τ_2 (\blacksquare), τ_3 (\blacktriangle), τ_4 (\bullet) obtained from a multi-exponential model fit (Eq. (3), Materials and Methods) to phosphorescence intensity decay data from vanillin dispersed in amorphous α -lactalbumin films equilibrated against nitrogen as a function of temperature. The data was calculated every 10°C from -20°C to 100°C.

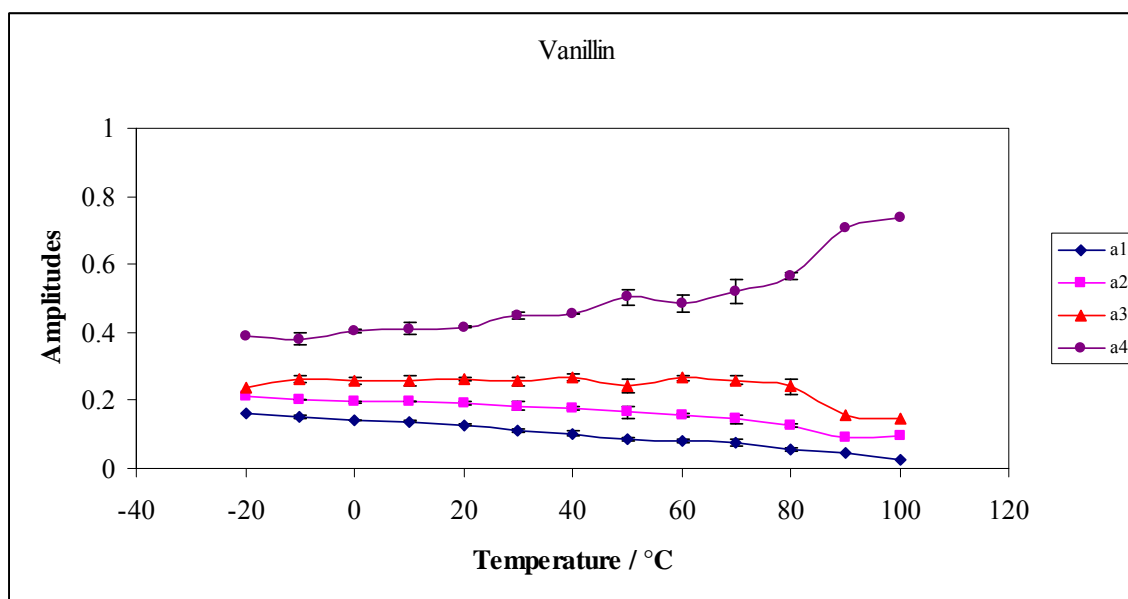
Figure VIIc-6

Figure VIIc-6: Intensity decay fit parameters amplitude for vanillin in amorphous α -lactalbumin films in nitrogen as a function of temperature. The data was calculated every 10 °C from -20 °C to 100 °C. The amplitudes a_1 (♦) and a_2 (■) correspond to the longer life time components (τ_1 , τ_2) and a_3 (▲) and a_{14} (●) correspond to the shorter lifetime components (τ_3 , τ_4). The amplitudes were obtained from a multi exponential model fit (Eq. (3), Materials and Methods) to phosphorescence intensity decay data from vanillin dispersed in amorphous α -lactalbumin films equilibrated against nitrogen as a function of temperature

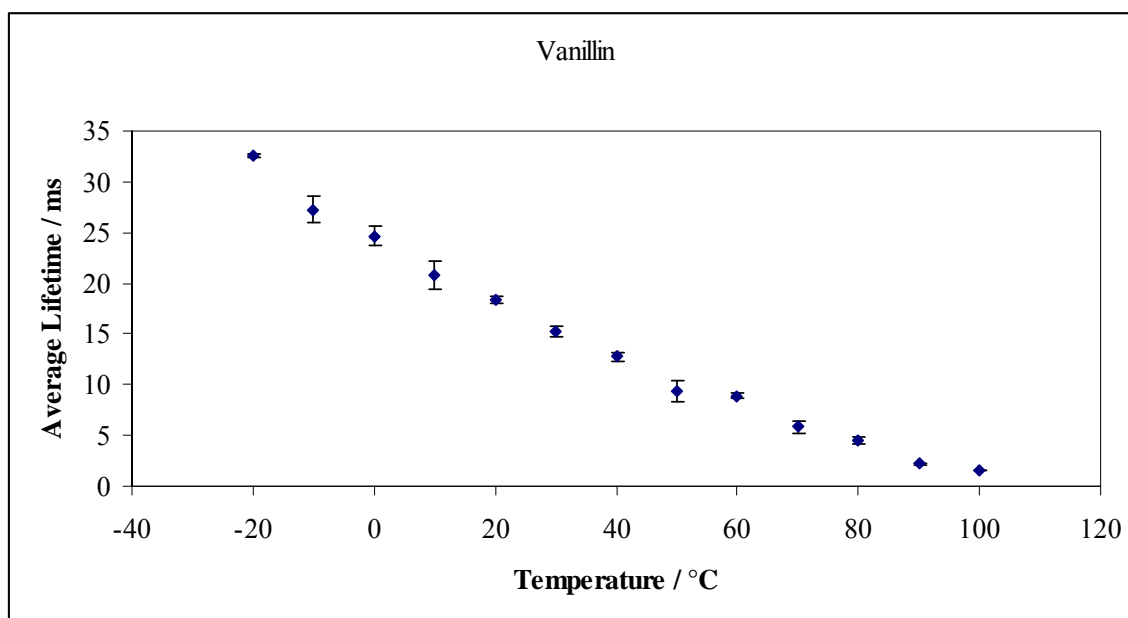
Figure VIIc-7

Figure VIIc-7: Average lifetime from a multi-exponential model fit (Eq. (4), Materials and Methods) to phosphorescence intensity decay data from vanillin dispersed in amorphous α -lactalbumin films equilibrated against nitrogen as a function of temperature. The data was calculated every 10°C from -20°C to 100°C.

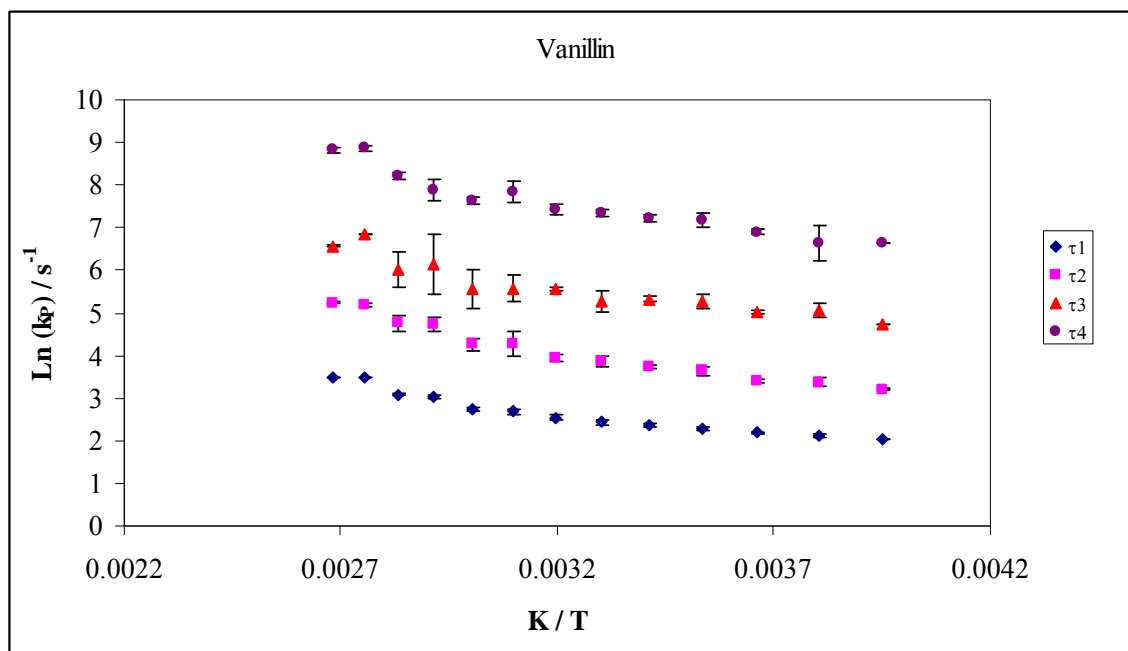
Figure VIIc-8a

Figure VIIc-8a: The Arrhenius plot of the individual lifetime component τ_1 (\blacklozenge), τ_2 (\blacksquare), τ_3 (\blacktriangle) and τ_4 (\bullet) of vanillin in amorphous α -lactalbumin as a function of temperature.

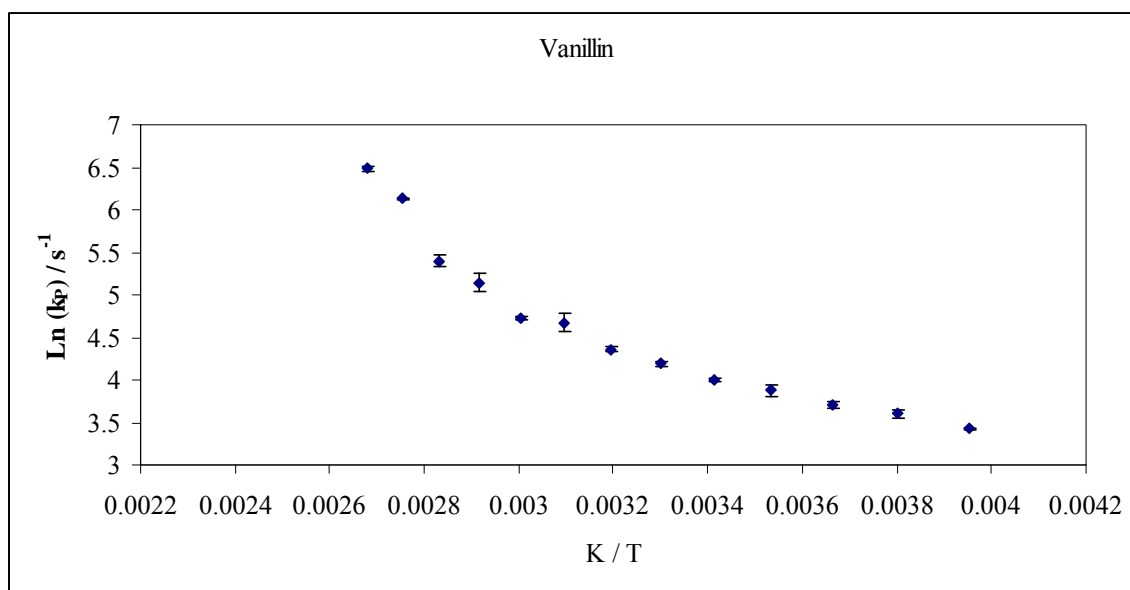
Figure VIIc-8b

Figure VIIc-8b: The Arrhenius plot of the average lifetime of vanillin in amorphous α -lactalbumin as a function of inverse of temperature.

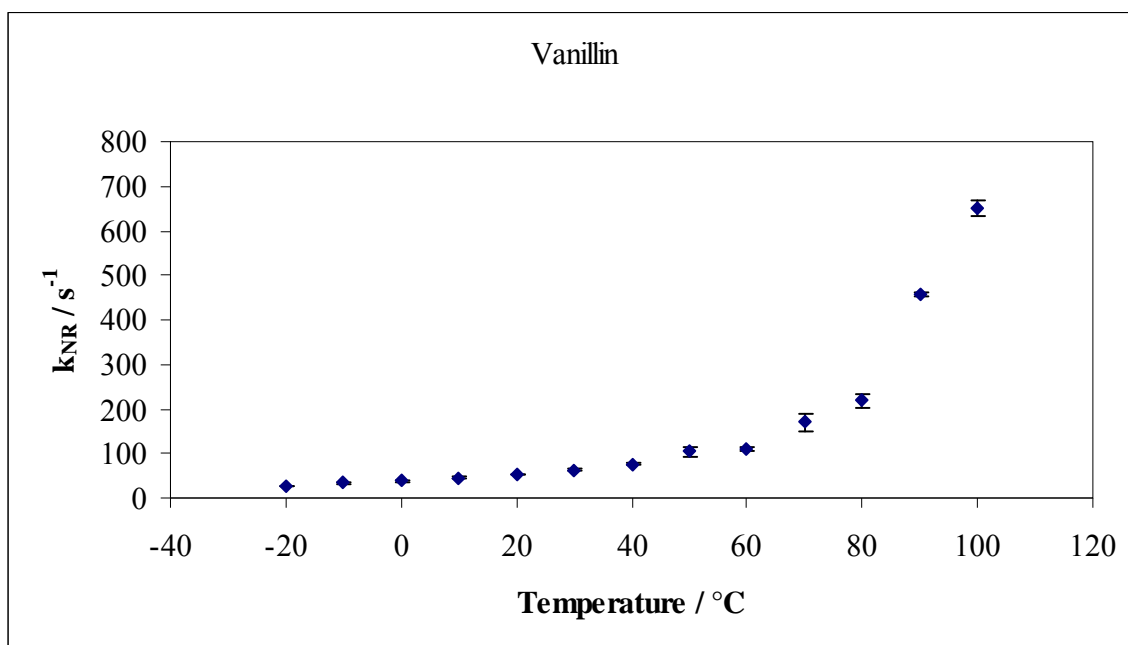
Figure VIIc-9

Figure VIIc-9: Temperature dependence of the total non-radiative decay rate of the triplet state k_{NR} ($k_p = k_{RP} + k_{NR}$) to S_0 of vanillin in amorphous α -lactalbumin film over the temperature range from -20°C to 100°C , values were calculated from the lifetime data.

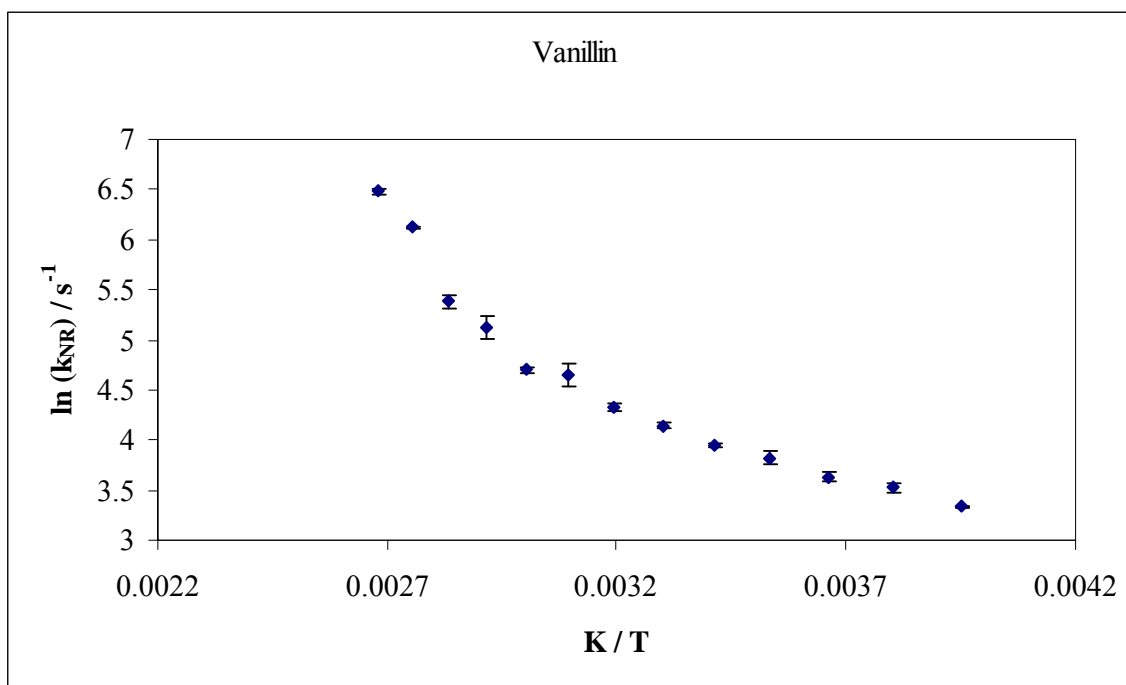
Figure VIIc-10

Figure VIIc-10: The Arrhenius plot of the total non-radiative decay rate of the triplet state k_{NR} ($k_p = k_{RP} + k_{NR}$) to So of vanillin in amorphous α -lactalbumin film as function of inverse of temperature.

Table VIIc-1

Table VIIb-1: Calculated activation energy E_a for each individual lifetime components τ_1 , τ_2 , τ_3 and τ_4 and average lifetime at low, intermediate and high temperature.

Lifetime	Temperature	Equation	R^2	E_a KJ / mol	Transition Temperatures °C
τ_1	LT	$y = -655.49x + 4.6098$	0.99	5.45348516	50
	HT	$y = -2464.9x + 10.158$	0.92	20.4931786	
τ_2	LT	$y = -986.76x + 7.0996$	0.98	8.20392264	50
	HT	$y = -2642.3x + 12.353$	0.92	21.9680822	
τ_3	LT	$y = -841.65x + 8.1543$	0.9	6.9974781	60
	HT	$y = -10427x + 35.559$	1	86.690078	
τ_4	LT	$y = -1165.1x + 11.186$	0.95	9.6866414	68
	HT	$y = -4857.3x + 22.122$	0.94	40.3835922	
τ_{Avg}	LT	$y = -1203.4x + 8.1522$	0.99	10.0050676	50
	HT	$y = -5581.1x + 21.412$	0.97	46.4012654	
$\ln(k_{NR})$	LT	$y = -1276.4x + 8.3513$	0.99	10.6119896	50
	HT	$y = -5643.6x + 21.577$	0.97	46.9208904	

References

- Duchowicz, R., Ferrer, M. L. and Acuna, A. U. Kinetic spectroscopy of erythrosin phosphorescence and delayed fluorescence in aqueous solution at room temperature. *Photochemistry and Photobiology*. 68 (1998). 494-501.
- Fischer, C. J., Gafni, A., Steel, D. G. and Schauerte, J. A. The triplet-state lifetime of indole in aqueous and viscous environments: significance to the interpretation of room temperature phosphorescence in proteins. *Journal of the American Chemical Society*. 124 (2004). 10359-10266.
- Hill, J. J., Shalaev, E. Y. and Zografi, G. Thermodynamic and dynamic factors involved in the stability of native proteins structure in amorphous solids in relation to levels of hydration. *Journal of Pharmaceutical Sciences*. 94 (2005). 1636-167.
- Kronman, M. J. and Andreotti, R. E. Inter and intramolecular interactions of alpha lactalbumin. *Protein Science*. 3 (1964). 1145-1151.
- Lakowicz, J. R. *Principles of Fluorescence Spectroscopy*. Second ed. New York: Kluwer Academic/Plenum Press. (1999).
- Maroncelli, M. and Fleming, G. R. Picosecond salvation dynamics of coumarin 153: The importance of molecular aspects of salvation. *Journal of Chemical Physics*. 86 (1987). 6221-6239.
- Papp, S. and Vanderkooi, J. M. Tryptophan phosphorescence at room temperature as a tool to study protein structure and dynamics. *Photochemistry and Photobiology*. 49 (1989). 775-784.
- Ringe, D. and Petsko, G. A. The glass transition in protein dynamics: what it is? Why it occurs and how to exploit it, *Biophysical Chemistry*. 105 (2003). 667-680.
- Shamblin, S., Hancock, B.C., Dupuis, Y. and Pikal, M. J. Interpretation of relaxation time constants for amorphous pharmaceutical systems. *Journal of Pharmaceutical Sciences*. 89 (2000). 417-427.
- Strambini, G. B. and Gabeillieri, E. *Photochemical Photobiology*. 51 (1990). 643-648.
- Vanderkooi, J. M. and Berger, J. W. Excited triplet state used to study biological macromolecules at room temperature. *Biochimica et Biophysica Acta: Bioenergetics*. 976 (1989). 1-27.
- Vanderkooi, J. M., Maniara., Green, T. J. and Wilson, D. F. An optical method for measurement of dioxygen concentration based upon quenching of phosphorescence. *Journal of Biological Chemistry*. 262 (1987). 5476-5482.

Chapter VII d: Comparing the molecular mobility of the amorphous α -lactalbumin matrix using the phosphorescence of extrinsic probe (vanillin and erythrosin B) and intrinsic tryptophan.

Results and Discussion

Vanillin (Chapter VII c), tryptophan (Chapter VII b) and erythrosin B (Chapter VII a) have been used in amorphous α -lactalbumin to study molecular mobility as a function of temperature. This chapter aims at making a comparison among the three probes for molecular mobility measurements.

In case of Ery B peak frequency indicated presence of softening transition at $\sim 10^{\circ}\text{C}$ and FWHM indicated presence of transition at $\sim 10^{\circ}\text{C}$. In case of vanillin peak frequency did not indicate presence of any softening transition, but FWHM indicated presence of transition above $\sim 50^{\circ}\text{C}$. In case of tryptophan peak frequency indicated presence of a softening transition at $\sim 40^{\circ}\text{C}$ and FWHM indicated presence of transition at $\sim 30^{\circ}\text{C}$.

Among the three, tryptophan is the intrinsic probe and erythrosin B and vanillin are extrinsic probes. The phosphorescence lifetimes of vanillin ($\tau_{77\text{K}} = 372 \text{ ms}$) and tryptophan ($\tau_{77\text{K}} = 6 \text{ s}$) are considerable longer than that of erythrosin B ($\tau_{77\text{K}} = 25 \text{ ms}$). Longer lived triplet probes (lifetimes of milliseconds to seconds) may help to access other modes of motion that affect the physical changes in the protein films. These probes could help detect slower molecular motions. The structural and dynamic heterogeneity that has been observed on the sub-millisecond time scale may be considerably different over whole millisecond to seconds.

Vanillin and tryptophan lifetime behavior are quite distinct and more dramatic than that seen with erythrosin B (Figure 1). As seen from Figure 1, in the glassy region, vanillin and tryptophan show dramatic decrease in lifetime as compared to erythrosin B whose lifetime shows a gradual decrease. This difference may be attributed to longer lifetimes of vanillin and tryptophan as compared to erythrosin B which allows them to sense slower molecular motions.

Temperature dependence of the total rate constant for radiative decay of the triplet state ($k_P = k_{RP} + k_{TS0} + k_{TS1}$) for erythrosin B, vanillin and tryptophan is shown in Figure 2a. Temperature dependence of the total rate constant for non-radiative decay of the triplet state (k_{NR}) for erythrosin B, vanillin and tryptophan is shown in Figure 3a. The non-radiative decay rate which is an indicator of matrix mobility was highest is erythrosin B followed by tryptophan and vanillin. Thus indicating that erythrosin B probably senses faster motions compared to vanillin and tryptophan which also sense slower motions. The Arrhenius plot of the total rate constant k_P and rate of non-radiative decay k_{NR} for the three probes are shown in Figures 2b and 3b, respectively. The activation energy and transition temperature obtained from the Arrhenius plots are compiled in Table 1.

The Arrhenius plot of $\ln(k_{NR})$ was biphasic in case of erythrosin B, vanillin and tryptophan. The activation energies at low and high temperature for erythrosin B were $E_{aL} = 1.89 \text{ kJ mol}^{-1}$ and $E_{aH} = 8.46 \text{ kJ mol}^{-1}$, and it showed a transition temperature at $\sim 50^\circ\text{C}$. The activation energies for vanillin at low and high temperatures were $E_{aL} = 10.6$

kJ mol^{-1} and $E_{\text{aH}} = 46.9 \text{ kJ mol}^{-1}$, the transition point was at 50°C . The activation energies for tryptophan at low and high temperatures were $E_{\text{aL}} = 14.4 \text{ kJ mol}^{-1}$ and $E_{\text{aH}} = 27.9 \text{ kJ mol}^{-1}$, the transition point was at 40°C . The activation energies at low temperatures varied such that erythrosin B > vanillin > tryptophan and at high temperature such as erythrosin B > tryptophan > vanillin.

The sequence of non-radiative decay rate (which is an indicator of matrix mobility) in amorphous sucrose film was erythrosin B > tryptophan > vanillin. Erythrosin B and vanillin indicated a transition temperature $\sim 50^{\circ}$. Whereas tryptophan showed transition temperature around 40°C . Lower transition temperature seen in tryptophan could be attributed to longer lifetime of tryptophan (6s) as compared to vanillin (372ms) and erythrosin B (25ms).

Conclusion

The phosphorescence from each probe erythrosin B, vanillin and tryptophan was successfully utilized to measure molecular mobility on three different time scales corresponding to each probe. Intrinsic tryptophan indicated presence of softening transition at $\sim 40^{\circ}\text{C}$ (close to $T_d = 38^{\circ}\text{C}$ for α -lactalbumin). The two extrinsic probes Ery B and vanillin indicated softening transition at around $\sim 50^{\circ}\text{C}$.

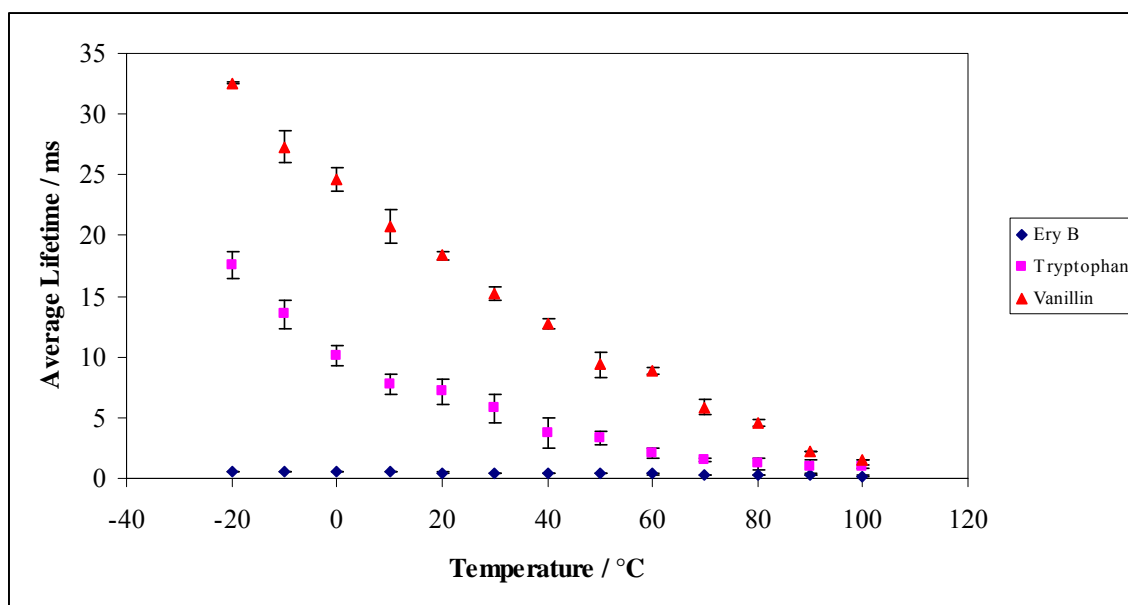
Figure VIIId-1a

Figure VIIId-1a: Comparison of average lifetime of erythrosin B (single stretch exponential fit), vanillin (multi exponential fit) and tryptophan (multi exponential fit) dispersed in amorphous films of α -lactalbumin equilibrated against nitrogen as a function of temperature. The data was calculated every 10°C from -20°C to 100°C.

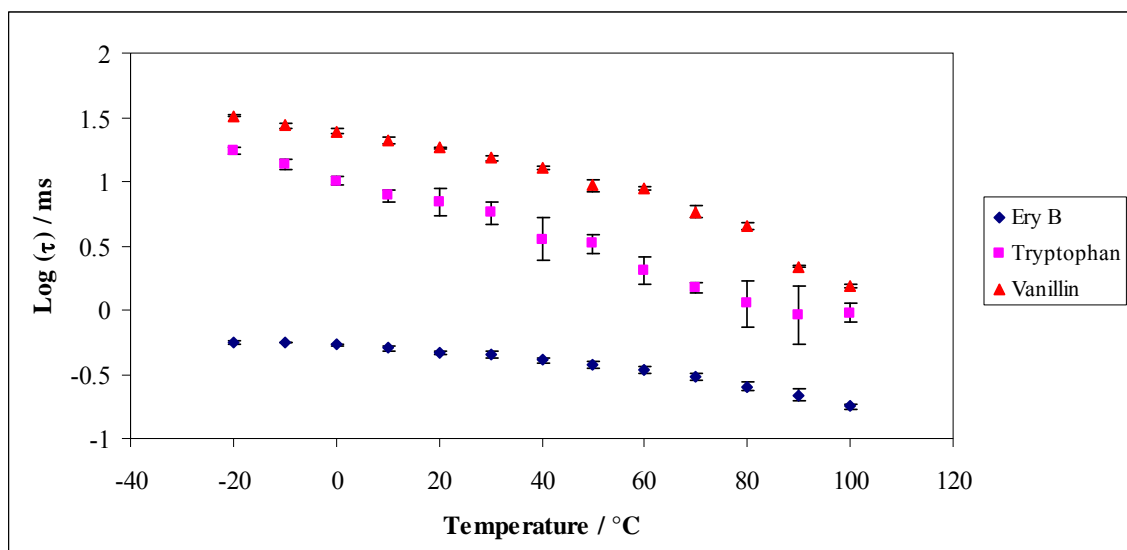
Figure VIIId-1b

Figure VIIId-1b: Comparison of log plot of average lifetime of erythrosin B (single stretch exponential fit), vanillin (multi exponential fit) and tryptophan (multi exponential fit) dispersed in amorphous films of α -lactalbumin equilibrated against nitrogen as a function of temperature. The data was calculated every 10 $^{\circ}\text{C}$ from -20 $^{\circ}\text{C}$ to 100 $^{\circ}\text{C}$.

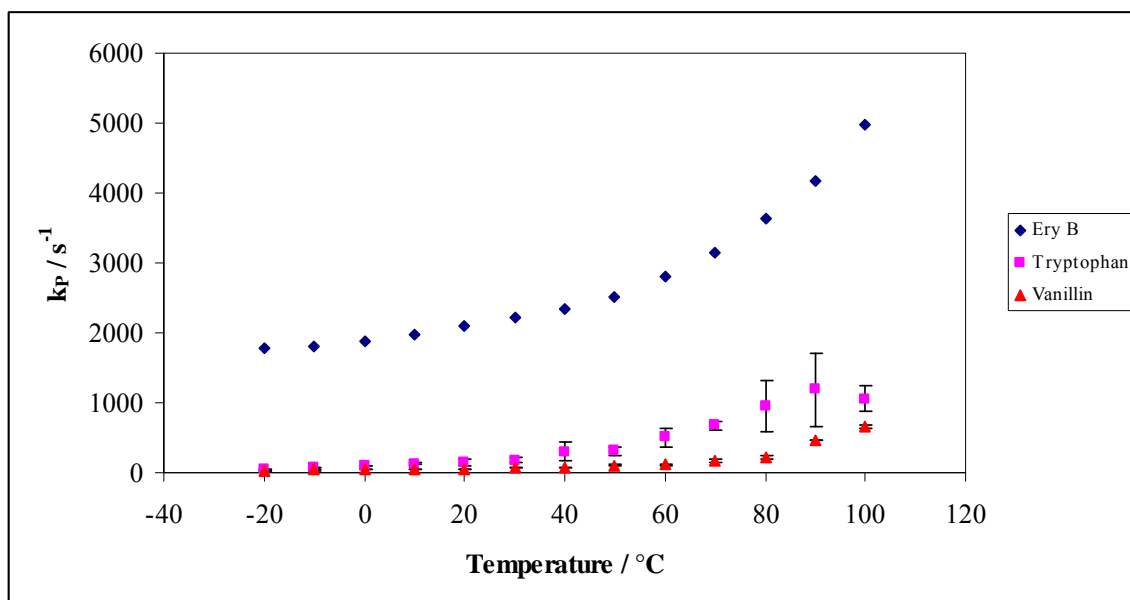
Figure VIId-2a

Figure VIId-2a: Comparison of k_P of erythrosin B, vanillin and tryptophan in amorphous films of α -lactalbumin equilibrated against nitrogen as a function of temperature.

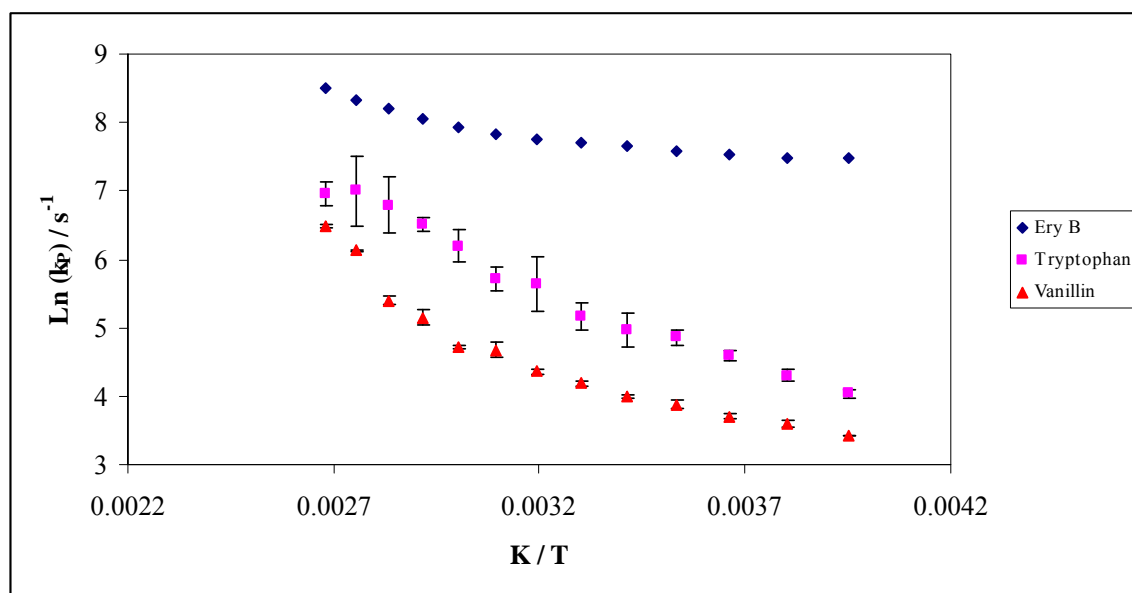
Figure VIIId-2b

Figure VIIId-2b: Comparison of $\text{Ln}(k_p)$ of erythrosin B, vanillin and tryptophan in amorphous films of α -lactalbumin equilibrated against nitrogen as a function of temperature.

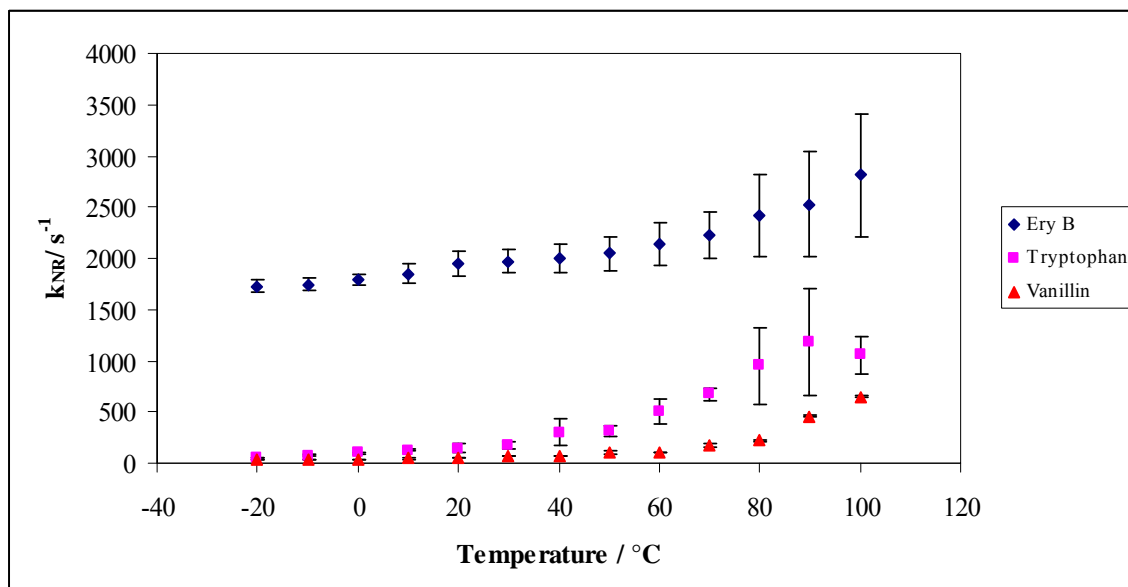
Figure VIIId-3a

Figure VIIId-3a: Comparison of k_{NR} average lifetime of erythrosin B (single stretch exponential fit), vanillin (multi exponential fit) and tryptophan (multi exponential fit) in amorphous films of α -lactalbumin equilibrated against nitrogen as a function of temperature. The data was calculated every 10°C from -20°C to 100°C.

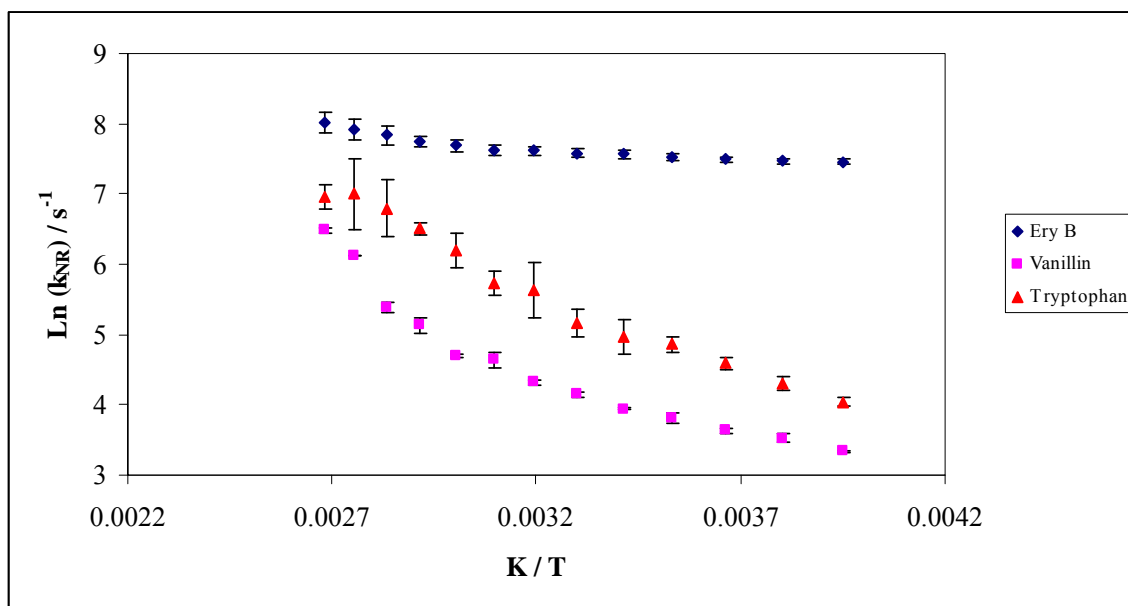
Figure VIId-3b

Figure VIId-3b: Comparison of Arrhenius plot of $\ln k_{NR}$ for erythrosin B, vanillin and tryptophan in amorphous films of α -lactalbumin equilibrated against nitrogen as a function of temperature.

Table VIId-1

Table VIId-1: Comparison of activation energy and transition temperature for erythrosin B, vanillin and tryptophan in amorphous α -lactalbumin.

Probe	Ea_L kJ / mol	Ea_H kJ / mol	T_N / °C	τ_0 / ms
Ery B	1.86	8.46	50	26
Vanillin	10.61	46.92	50	372
Tryptophan	14.44	27.86	40	6000

Chapter VIII: Investigating the potential of using multiple luminescent probes to understand the local dynamics in amorphous mixtures

Introduction

Amorphous solids are not just simple systems containing pure sugar or protein, but often are complex systems composed of sugar/protein, protein/lipid, sugar/polysaccharide or protein/polysaccharide combinations. Maltodextrin has been used in combination with other excipients including sugars, proteins and polysaccharides to protect enzymes (Rossi et al., 1997; Mazzobre et al., 1997; Corveleyn and Remon, 1996), microorganisms, (Oldenhof et al., 2005) and encapsulated lipids (Grattard et al., 2002). Lipids are incorporated in protein films either as an emulsion or coating to improve their barrier properties (Khwaldia et al., 2004). In food systems, the presence of sugars can influence protein functionality and the two are very commonly found in many dehydrated food products and amorphous ingredients (Bell et al., 1996). Excipients (such as sucrose or trehalose) are often used to protect proteins and peptides from various chemical and physical degradation processes (Lai and Topp, 1999). Sugar/protein mixtures are commonly used in food and pharmaceutical formulations (Lopez-Diez and Bone, 2000) where sugars serve as stabilizers and/or protectants for proteins (Kaushik and Bhat, 2003). Trehalose has being shown to stabilize proteins in the amorphous and dry state (Leslie et al., 1995) and sucrose glasses are cryoprotectant during anhydrobiosis (Crowe et al., 1998).

Amorphous proteins and sugars are dynamically complex system and could have compositional heterogeneity (e.g. mixtures of proteins and sugars) or structural

heterogeneity (e.g. different states glass/rubber) making it dynamically heterogeneous contributing different relaxation processes. Amorphous solids at temperatures below T_g are said to be glassy and above this temperature are said to be melt or rubbery (Champion et al., 2000). However the exact nature of interactions of protein and sugars is not well understood. Some of the theories propose that sugars acts as hydrant and substitute for water to protein through hydrogen bonding (Carpenter and Crowe, 1988, 1989; Mazzobre et al., 1997). The other theory proposes that sugar provides a glassy environment for protein restricting and preventing any conformational flexibility to unfold (Green and Angel 1988). The extent of hydrogen bonding along with amorphous glassy matrix could play a great role in preservation (Crowe et al., 1998). Hence more research is needed to understand which interactions control the stabilizing effect of sugars on proteins. Molecular mobility (in amorphous sucrose phase, amorphous protein phase and in the amorphous mixture) is known to contribute to physical changes in these amorphous mixtures thereby affecting their quality and performance.

In glass to liquid transition, molecular mobility is presented as α relaxation in the T_g zone; as temperature is lowered below T_g molecular mobility is presented as β and γ (in some cases δ) relaxations also called secondary relaxations (Ediger et al., 1996; Hancock and Zografi, 1995; Vyazovkin and Dranca, 2006). The α relaxation is thought to reflect changes in local segmental motions (Hill and Tant, 1998). The secondary relaxations are due to vibrations of atoms or bonds, or reorientation of small group of atoms (Debenedetti and Stillinger, 2001).

Proteins show thousands of potential modes of motion (Ludescher et al., 2001), and the dynamic events range from vibration of and rotation around bonds to local backbone motion, chain segmental motion, global structural perturbation of three dimensional structure, and to large-scale movement of interior regions during denaturation. Together these motions govern the stability of amorphous proteins. As compiled in Hill et al., (2005) the thermal stability of proteins is governed by connectivity and co-operativity between β -like motions that control α -like motions. Sucrose has been shown to have onset of molecular mobility below T_g in the glass using phosphorescence spectroscopy (Shah and Ludescher, 1995; Ludescher et al., 2001, Pravinata et al., 2005). In the glass there are some motions including vibrational modes of the 3D sugar lattice, and internal rotational modes of side chains.

A glass is composed of dense regions with restricted molecular mobility and less dense regions with excess free volume permitting the localized motions. The local motions (in protein or sucrose) could cause changes in physical properties of amorphous mixtures such as toughening, slower diffusion, increased density or decreased oxygen permeability (Fabienna et al., 2006) and hence are of concern to us. However we do not have a clear understanding of the local dynamics in amorphous mixtures thereby limiting our knowledge. It is important hence not only to consider the glass transition related changes but also understand the local dynamics of various participating components in these amorphous mixtures as stability of amorphous solid mixtures depends on the physical state of their individual constituent's components. For example, to understand the mechanism leading to stability by sugars to protein, it's important to study the molecular

interaction of sugar and protein mixtures. And to get a deeper appreciation of these interactions one needs to investigate the simultaneous measurement of molecular mobility in different components of amorphous mixtures like sugars and proteins.

Phosphorescence spectroscopy has been used to measure molecular mobility in protein and sugars and even their mixtures (Simon-Lukasik and Ludescher, 2006a, 2006b, 2004; Nack and Ludescher, 2006; Sundaresan and Ludescher, 2007; Pravinata et al., 2005) using a wide variety of single probes like Ery B, tryptophan and its analogs, vanillin, etc. and can be further extended to study the local dynamics in amorphous mixtures using multiple probes. For example erythrosin B in protein and vanillin in sucrose in sucrose/protein amorphous mixture could provide useful insight into the molecular dynamics and physical changes occurring in sugars and proteins. The two probes could be dispersed or covalently attached in amorphous systems.

The potential of using multiple probes for reporting molecular mobility in amorphous solids has never been studied so far; this would be the first of its kind. There are several questions that arise with this objective as mentioned below which have being addressed in this research. a) Can multiple probes be used to report molecular mobility in an amorphous matrix? b) Do probes interfere with each other either spectroscopically or physically (aggregate)/ and c) Is there any energy transfer between the probes and, if so, can it be exploited?

In this study molecular mobility was studied in amorphous sucrose films by monitoring phosphorescence from the dual probe combination of erythrosin B and vanillin. A comparison of the data was made with data obtained from individually dispersed probes in amorphous sucrose films. We found that there was no effect on phosphorescence measurement of erythrosin B and vanillin in presence of each other. This research thus opens a new world where one can investigate simultaneous measurements of mobility using multiple probes in amorphous sucrose which could be further extended for measurements in amorphous protein and sucrose mixtures.

Materials and Methods

Sucrose Solution: Sucrose solution was made as described in Pravinata et al 2005. Approximately 20 g of sucrose (99.5% pure; Sigma Chemical, St. Louis, MO) were dissolved in 100 mL of deionized water containing 0.5 g of activated charcoal to remove luminescent impurities. After stirring overnight, the charcoal was removed by vacuum filtration using ashless filter paper (Whatman No. 40, Whatman International, Maidstone, UK), additional charcoal was added, and the process repeated. Sucrose solution was made to a final concentration of 65–67 wt % sucrose; concentration was confirmed using a refractometer (NSG Precision Cells, Farmingdale, NY). This sucrose solution was filtered through a 0.2 μm membrane to remove particulates.

Erythrosin B: A 50mM stock solution of erythrosin B sodium salt (Molecular Probes, Inc., Eugene, OR) was prepared in distilled deionized water. This concentration was selected to simplify the addition of the probe to the sucrose solution. For measuring phosphorescence in amorphous sucrose films, erythrosin B was added to the sucrose solution at a molar ratio of 1:10⁴ (dye: sucrose). The ratio 1:10⁴ (dye: sucrose) was chosen as at this concentration it was determined that the probe does not aggregate, existing only as individual molecules monitoring the molecular mobility of the sucrose.

Vanillin: A 66mM stock solution of vanillin (Sigma-Aldrich, Milwaukee, WI) was prepared in distilled deionized water. This concentration was selected to simplify the addition of the probe to the sucrose solution. For absorbance, fluorescence and phosphorescence measurements the 66mM stock was diluted to 50 μM in distilled

deionized water. For measuring absorbance and phosphorescence in amorphous solid, vanillin was added to the sucrose solution at a molar ratio of $1:10^3$ (dye: sucrose). Other ratios $3:10^4$, $5:10^4$ and $2:10^3$ were also tested to study the effect of probe concentration. The ratio $1:10^3$ (dye: sucrose) was chosen as at this concentration it was determined that the probe does not aggregate, existing only as individual molecules monitoring the molecular mobility of the sucrose.

Sucrose films: To produce glassy sucrose films containing both erythrosin B at $(1:10^4)$ and vanillin at $(1:10^3)$, 20 μL of a sucrose solution containing erythrosin B and vanillin were spread on a quartz slide ($30 \times 13.5 \times 0.6$ mm; custom made by NSG Precision Cells, Farmingdale, NY). After spreading the solutions on the slides were then dried under a heat gun (Vidal Sassoon) for 5 min to a maximum temperature of $\sim 88^\circ\text{C}$ (measured using a thermocouple probe) and the final thickness was ~ 0.05 mm. The slides were stored at room temperature against P_2O_5 and Drierite, protected from the light to prevent any photobleaching, for at least 7 days before any phosphorescence measurements were made. The desiccant was refreshed as needed to maintain a relative humidity close to 0%.

Instrumentation: Measurements were made on a Cary Eclipse fluorescence spectrophotometer (Varian Instruments, Walnut Creek, CA). This instrument, which collects in analog mode, uses a high intensity pulsed lamp and a time delay was employed to avoid any fluorescence during the lamp pulse. The temperature was controlled by using a TLC 50 thermoelectric heating/cooling system (Quantum

Northwest, Spokane, WA). The TLC-50 sample compartment was fitted with a jacketed cover. The measurements were made in absence of oxygen (Nitrogen was purged for 15 minutes). Nitrogen stream was generated by passage of high purity nitrogen through a Supelco (Bellefonte, PA) carrier gas purifier. Quartz slides were placed in the standard 1cm x 1cm x 1cm quartz fluorescence cuvette, which was capped with a lid having inlet and outlet ports of gas lines.

Luminescence Measurements

Erythrosin B Protocol: The Cary Eclipse uses a pulsed lamp and collects emission intensity in analog mode; data were not collected within the first 0.1-0.2 ms to suppress fluorescence coincident with the lamp pulse. Delayed luminescence emission spectra were collected from 535 to 800 nm (10 nm bandwidth) using excitation at 500 nm (20nm bandwidth) over the temperature range from -20°C to 100°C . Each data point was collected from a single flash with 0.2 ms delay, 5.0 ms gate time, and 0.02 s total decay time. The phosphorescence spectra collected as a function of temperature in the presence of nitrogen, were converted to intensity versus frequency (cm^{-1}) and analyzed to obtain the peak frequency and spectral bandwidth using eq. (5) and (6) (Maroncelli and Fleming 1987). Lifetime measurements (for phosphorescence and delayed fluorescence) were made in the presence of nitrogen ($-\text{O}_2$) as a function of temperature. The samples were excited at 540 nm (20 nm bandwidth) and emission transients for phosphorescence and delayed fluorescence collected at 690 nm and 550 nm respectively (20 nm bandwidth) at temperatures ranging from -20°C to 100°C . Each decay transient was the sum of 50 cycles, and for each cycle data was collected from a single lamp flash with a delay of 0.1

ms, 0.06 ms gate time and 6.0 ms total decay time. All measurements were made in quadruplicate.

A similar measurement was also made for amorphous sucrose film containing just erythrosin B for comparison. To check for spectroscopic interference from vanillin, erythrosin B was also excited using vanillin protocol.

Vanillin Protocol: Delayed luminescence emission spectra of vanillin in amorphous sucrose were collected from 400 to 800 nm (10 nm bandwidth) using excitation at 320 nm (20 nm bandwidth) over the temperature range from -20°C to 100°C . Each data point was collected from a single flash with 0.2 ms delay, 100 ms gate time, and 0.12 s total decay time. The phosphorescence spectra collected as a function of temperature in the presence of nitrogen, were converted to intensity versus frequency (cm^{-1}) and analyzed to obtain the peak frequency and spectral bandwidth using eq. (5) and (6) (Maroncelli and Fleming, 1987). Lifetime measurements were made as a function of temperature. The samples were excited at 320 nm (20 nm bandwidth) and emission transients collected at 490 nm (20 nm bandwidth) at temperature ranging from -20°C to 100°C . Each decay was the average of 50 cycles, and for each cycle data was collected from a single flash with a delay of 0.2 ms, windows for gate time and total decay time were varied at each temperature. All measurements were made in quadruplicate.

A similar measurement was also made for amorphous sucrose film containing just vanillin for comparison. To check spectroscopic interference from erythrosin B, vanillin was also excited using erythrosin B protocol.

Photophysical Scheme: The phosphorescence lifetimes were interpreted in terms of the rate constants associated with the various processes that contribute to the de-excitation of the excited triplet state of the probe (Duchowicz et al., 1998). The phosphorescence lifetimes were used to calculate the rate constants associated with the various processes that depopulate the excited triplet state.

The term $k_P (=1/\tau)$ is the total decay rate, k_{RP} is the rate of radiative decay of the triplet state. The magnitude of k_{NR} reflects factors associated with the mechanism by which the excited T_1 state is coupled to highly excited vibrations of the S_0 ground state as well as external factors associated with the mechanism by which the ground state vibrational energy can dissipate from the excited state into the surrounding matrix (Fischer et al., 2002; Vanderkooi and Berger, 1989). As the efficiency of external vibrational dissipation is related to overall mobility of the matrix, the magnitude of k_{NR} provides a measure of matrix mobility. The term $k_Q [Q]$ refers to the collisional quenching due to interaction between the excited chromophore and a quencher molecule for example triplet state oxygen.

Erythrosin B: In case of erythrosin B, k_{RP} the rate of radiative decay of the triplet state (phosphorescence) is $41s^{-1}$ (Lettinga et al., 2000; Duchowicz et al., 1998). The term k_{TS1}

is the rate for thermally activated reverse intersystem crossing from the triplet to the singlet excited state; it has an exponential dependence on the energy gap (ΔE_{TS}) between singlet and the triplet state:

$$\tau^{-1} = k_P = k_{RP} + k_{TS1} + k_{NR} + k_Q [Q] \quad (1)$$

$$k_{TS1}(T) = k_{TS1}^0 \exp(-\Delta E_{TS}/RT) \quad (2)$$

The value of ΔE_{TS} was calculated from the slope of the natural logarithm of the ratio of the emission intensity due to delayed fluorescence (I_{DF}) and phosphorescence (I_P) plotted versus $1/T$; I_{DF} and I_P were determined from log normal analysis of the emission spectra.

$$d [\ln (I_{DF}/I_P)]/d(1/T) = \Delta E_{TS}/R \quad (3)$$

(Where $R = 8.314 \text{ J K}^{-1} \text{ mol}^{-1}$). The value of k_{TS1} was calculated from equation 5 using $k_{TS1}^0 = 3.0 \times 10^7 \text{ s}^{-1}$ and $\Delta E_{TS} = 31.9 \text{ kJ mol}^{-1}$. Intersystem crossing to the ground state S_0 , which reflects relaxation of the probe from the excited triplet state to the ground state without the emission of a photon, has rate k_{NR} . The value of k_{NR} was calculated from the lifetime in the presence of nitrogen ($-O_2$) (where $k_Q [O_2]$ is negligible) using Eq. 1.

Vanillin: In case of vanillin the term k_{TS1} is not relevant as there is no reverse intersystem crossing. The lifetime τ is related to the rate constants for de-excitation of the triplet excited state of the probe according to the following Equation 4 (Papp and Vanderkooi, 1989).

$$1/\tau = k_{RP} + k_{NR} (T) + k_Q [Q] = k_P \quad (4)$$

Here $k_p (=1/\tau)$ is the total decay rate, k_{RP} is the rate of radiative decay of the ground state (2.69 s^{-1}), k_{NR} is the rate of non-radiative decay to the singlet state followed by vibrational relaxation to S_0 due to collisional quenching. The term $k_Q [Q]$ refers to the collisional quenching due to interaction between the excited chromophore and a quencher molecule for example triplet state oxygen.

Data Analysis

Emission energy as a function of temperature: Delayed luminescence spectra collected were fitted to a log-normal function equation 5 for erythrosin B and vanillin using the program Igor (Wavemetrics, Inc., Lake Oswego, OR). In case of erythrosin B emission spectra was fitted using a log-normal two function in EVS and ES matrix. But in case of vanillin emission spectra was fitted to a log-normal three function in EVS matrix and to a log-normal one function in VS matrix. The emission peak energy (ν_p) and bandwidth (full-width-at-half-maximum, FWHM) of the emission bands were determined (Maroncelli and Fleming, 1987).

$$I(\nu) = I_0 \exp \left\{ -\ln(2) \left[\ln(1 + 2b(\nu - \nu_p)/\Delta)/b \right]^2 \right\} \quad (5)$$

In this equation I_0 is the maximum emission intensity, ν_p is the peak energy (in cm^{-1}) of the emission maximum, Δ is a line width parameter, and b is an asymmetry parameter. The FWHM is related to b and Δ as shown in equation 6.

$$\Gamma = \Delta \sinh(b)/b \quad (6)$$

Phosphorescence Intensity: Intensity decay transits were analyzed using a non-linear least squares iterative fitting procedure using the program Igor (Wavemetrics, Inc., Lake

Oswego, OR). Fits were judged satisfactory if the r^2 values were in the range of 0.995-1.0, and the modified residual $[(\text{data-fit})/\text{data}]^{1/2}$ varied randomly about zero.

Erythrosin B: Intensity decays in case of erythrosin B were clearly non-exponential and were analyzed using a stretched exponential function or Kohlrausch-Williams-Watts (KWW) model equation 7. This model has being shown to be appropriate to describe the wide distribution of relaxation times (Champion et al., 2000) for the molecular processes that depopulate excited states in amorphous solids (Pravinata et al., 2006; Nack and Ludescher, 2006; Sundaresan and Ludescher, 2007).

$$I(t) = I(0) \exp\{-(t/\tau)^\beta\} + C \quad (7)$$

Where $I(0)$ is the initial amplitude at time zero, τ is the Kohlrausch-Williams-Watt lifetime (Lindsey and Patterson, 1980), and β is the stretching exponent, which varies from 0 to 1 and quantifies the non-exponential nature of the decay, and C is a constant; β provides a measure of the width of the distribution of lifetimes required to fit the intensity decay; the smaller the value of β , the wider the distribution of lifetimes.

Vanillin: Intensity decays in case of vanillin were clearly non-exponential and were analyzed using a multi-exponential function. The multi-exponential model is as show in Equation 8. τ_i are decay times, α_i represent the amplitudes of the components at $t = 0$ and n is the number of decay times. The average lifetime was calculated using Equation 9.

$$I(t) = \sum_{i=1}^n \alpha_i \exp(-t/\tau_i) \quad (8)$$

$$\tau_{\text{Avg}} = \frac{\sum_{i=1}^n \alpha_i \tau_i}{\sum_{i=1}^n \alpha_i} \quad (9)$$

Spectroscopic interaction: As vanillin emits at ~500 nm which is the excitation wavelength for erythrosin B, there is a possibility of energy transfer between the two. In the EVS matrix when vanillin was excited at 320 nm we found some emission from erythrosin B too and this emission was higher than the emission for erythrosin B excited at 320 nm in the absence of vanillin. The peak emission (delayed fluorescence and phosphorescence) for erythrosin B at 320 nm excitation was normalized against emission at 500 nm and compared between EVS (erythrosin B: vanillin: sucrose matrix) and ES (erythrosin B: sucrose matrix) matrix using Equation 10a (phosphorescence) and 10b (delayed fluorescence).

EVS-E-320nm-P

EVS-E-500nm-P = Ratio A (10a)

ES-E-320nm-P

ES-E-500nm-P

EVS-E-320nm-DF

$$\frac{\text{EVS-E-500nm-DF}}{\text{ES-E-320nm-DF}} = \text{Ratio B} \quad (10b)$$

ES-E-320nm-DF

ES-E-500nm-DF

- Ratio = 1: means emission intensities match between ES and EVS
- Ratio > 1: means emission intensities are higher in EVS as compared to in ES
- Ratio < 1: means emission intensities are lower in EVS as compared to in ES

Table VIII-1

Emission Ratios

Peak emission intensity Ery B Phosphorescence in EVS-320nm (EVS-E-320nm-P)
 Peak emission intensity Ery B Phosphorescence in EVS-500nm (EVS-E-500nm-P)
 Peak emission intensity Ery B Phosphorescence in ES-320nm (ES-E-320nm-P)
 Peak emission intensity Ery B Phosphorescence in ES-500nm (ES-E-500nm-P)
 Peak emission intensity Ery B Delayed Fluorescence in EVS-320nm (EVS-E-320nm-DF)
 Peak emission intensity Ery B Delayed Fluorescence in EVS-500nm (EVS-E-500nm-DF)
 Peak emission intensity Ery B Delayed Fluorescence in ES-320nm (ES-E-320nm-DF)
 Peak emission intensity Ery B Delayed Fluorescence in ES-500nm (ES-E-500nm-DF)

Results

Delayed luminescence emission spectra were collected as a function of temperature in presence of nitrogen from erythrosin B and vanillin dispersed together in amorphous sucrose films (erythrosin + vanillin + sucrose, referred as EVS) and compared to spectra from individual probes dispersed singly in sucrose (erythrosin + sucrose, referred as ES) and (vanillin + sucrose, referred as VS). Three spectroscopic measures of molecular mobility were made: emission energy, emission bandwidth and emission lifetime.

Erythrosin B:

There was no shift observed in the emission spectra in EVS matrix as compared to the ES matrix.

Delayed Luminescence Spectra: The delayed luminescence spectra as a function of temperature of Ery B dispersed in amorphous ES or amorphous EVS films are plotted in Figure 1a and 1b, respectively. These spectra exhibited maxima at ~552 nm and ~670 nm corresponding to delayed fluorescence and phosphorescence emission bands, respectively. Delayed, or E-type, fluorescence reflects emission from a singlet state (S_1) that has been repopulated by reverse intersystem crossing from the triplet state (T_1) (Parker, 1968). Phosphorescence band reflects emission directly from the triplet state. The delayed emission spectra were collected over the temperature range -20°C to 100°C. Delayed emission spectra showed a decrease in phosphorescence intensity as a function of temperature; the delayed fluorescence intensity increased continuously from -20°C to

100°C as expected from thermally stimulated processes and the changes were comparable in the EVS and ES matrices.

The intensity ratio when plotted as a Van't Hoff plot of $\ln(I_{DF}/I_P)$ vs. $1/T$ (using the maximum emission intensity determined from fitting spectra to a log-normal function) was linear over the entire range of measured temperature (with $R^2 > 0.995$ for all curves) with no systematic deviation (Data not shown), the slope provides an estimate of the energy gap, ΔE_{TS} , between the lowest triplet (T_1) and singlet state (S_1). In ES matrix $\Delta E_{TS} = 35.3 \pm 0.4 \text{ kJ mol}^{-1}$ and in EVS it was $\Delta E_{TS} = 35.2 \pm 1.1 \text{ kJ mol}^{-1}$.

The peak energy (ν_p) and bandwidth (Γ) for both delayed fluorescence and phosphorescence were determined by fitting emission spectra to a sum of two log-normal functions (Eq. 5 and 6 Materials and Methods). The values of ν_p and Γ for the phosphorescence band varied systematically as a function of temperature in both ES and EVS as shown in Figure 2.

There was a gradual decrease in the peak emission energy at low temperature followed by a steeper decrease at higher temperature. The decrease in ν_p reflects an increase in the rate and extent of dipolar relaxation around the triplet excited state (Lackowicz, 1999). The emission bandwidth (Γ) increased gradually with temperature in the glass and much more dramatically in the melt. The increase in Γ at elevated temperatures reflects an increase in the extent of inhomogeneous broadening of the spectra due to energetic interactions of Ery B molecules with the surrounding matrix. This increase was gradual at

low temperature and much more dramatic at higher temperatures indicating increase in dipolar relaxation rate was accompanied by an increase in the distribution of energetically different environments.

The comparison between ES and EVS matrix indicated that erythrosin B peak frequency and FWHM were super-imposable within error as shown in Figure 2. This indicated that there is no interference from presence of vanillin to erythrosin B measurements. Erythrosin B was thus able to report about local dipolar relaxation in amorphous sucrose film in the presence of vanillin.

Phosphorescence Intensity Decay: A phosphorescence intensity decay of Ery B in EVS films at 20°C in the presence of nitrogen is plotted in Figure 3 along with the modified residuals for a fit to this decay using a stretched exponential model function (Eq. 7, Materials and Methods). The modified residuals for these fits varied randomly around zero, indicating that the stretched exponential function provided a statistically satisfactory fit to these data. All intensity decay data over the temperature interval from –20°C to 100°C were well fitted using a stretched exponential function. A stretched exponential function has also been shown to provide a statistically satisfactory fit to intensity decays of Ery B dispersed in amorphous sucrose (Pravinata et al., 2005), maltose and maltitol (Shirke and Ludescher, 2006a, 2006b), gelatin (Simon-Lukasik and Ludescher, 2006a, 2006b, 2004), bovine serum albumin (Nack and Ludescher, 2006) and β -lactoglobulin (Sundaresan and Ludescher, 2007) under all conditions measured.

The phosphorescence lifetime decreased with increasing temperature in both EVS and ES films, indicating an increase in triplet state quenching rates with increase in temperature (Figure 4a). The Ery B lifetime in the absence of oxygen was 0.66 ms at -20°C and decreased to 0.2 ms at 100°C ; the decrease was gradual at low temperature and more dramatic at higher temperature. The decrease in lifetime with temperature in the absence of oxygen is the result of an increase in both k_{TS1} , the rate of reverse intersystem crossing to the excited singlet state (S_1), and k_{TS0} , the rate of intersystem crossing to a highly excited vibration of the singlet S_0 manifold, followed by vibrational relaxation to the ground vibrational state (Eq. 1 Materials and Methods). The rate k_{TS0} reflects the extent to which molecular motions within the matrix are able to facilitate dissipation of the vibrational energy of the highly excited probe into the matrix (Fischer et al., 2002; Vanderkooi and Berger, 1989) and is an indicator of matrix mobility.

The stretching exponent β is a measure of the width of the distribution of lifetimes required to fit the intensity decay (Lindsey and Patterson, 1980; Richert, 2000); it provides a measure of the dynamic heterogeneity of the matrix and varies primarily due to variability in k_{TS0} (Pravinata et al., 2005). The value of β decreased linearly with temperature in the absence of oxygen from a maximum of ~ 0.92 at -20°C to ~ 0.86 at 100°C in both EVS and ES films (Figure 4b).

Comparing ES and EVS matrix, erythrosin B lifetime and beta values were found to be super imposable as shown in Figure 4a and 4b. This indicated that there is no interference from vanillin phosphorescence to erythrosin B measurements.

Vanillin:

Delayed Luminescence Spectra: The delayed emission spectra from vanillin (excited at 320 nm) in amorphous VS matrix (Figure 5a) showed one band and three bands in EVS matrix (Figure 5b). Vanillin phosphorescence emission in EVS and VS amorphous films appeared at ~500nm. The bands at ~550 nm and ~670 nm in EVS belong to erythrosin B excited at 320 nm. Vanillin phosphorescence was temperature dependent over the temperature range from -20°C to 100°C in both amorphous EVS and VS films, as expected. The decrease in phosphorescence intensity with increasing temperature results from thermally-stimulated deactivation processes (Parker, 1968).

The emission energy (ν_p) and bandwidth (Γ) were determined by fitting the phosphorescence emission spectra to a log-normal function (Eq. 5 and 6) Materials and Methods). The log-normal one function was used to fit the emission spectra for VS and log-normal three functions was used to fit the emission spectra for EVS matrix. The values of emission energy and bandwidth as a function of temperature are shown in Figure 6. There was a gradual decrease in the emission energy at low temperature followed by steeper decrease at higher temperatures, indicating an increase in the average rate and thus extent of matrix dipolar relaxation around the excited triplet state with a transition temperature above ~50°C. The peak frequency values as a function of temperature were found to be super-imposable for vanillin in EVS and VS matrix. The phosphorescence bandwidth increased gradually in the glass and then very sharply in the melt, reflecting a large increase in the range of energetically distinct matrix environments

in amorphous sucrose below and above T_g (Figure 6). The bandwidth increased linearly and gradually with temperature up to $\sim 60^\circ\text{C}$ and quiet dramatically at higher temperatures.

The peak frequency of vanillin phosphorescence was not affected by presence of erythrosin B in the EVS matrix and was comparable to the values in VS matrix. However the bandwidth values were found to be much higher in the EVS matrix as compared to in the VS matrix suggesting a broader distribution of energetically different environments arising from vanillin and erythrosin B emissions. The higher bandwidth could also be due to problems with data analysis as we are comparing three component fit to a one component fit. As the emission of erythrosin B in presence of vanillin with excitation at 320 nm, may be due to energy transfer, the absolute subtraction between the EVS-vanillin+erythrosin B spectra and ES-vanillin spectra was not possible to obtain just EVS-vanillin spectrum.

Phosphorescence Intensity Decays: Vanillin phosphorescence decay kinetics were also studied in the amorphous EVS films and compared with intensity decays from VS films. Time-resolved phosphorescence intensity decays of vanillin in amorphous films were measured over the temperature range from -20°C to 100°C . The intensity decays were fit using both stretched and multi-exponential function, but the best fit was generally obtained with a four-exponential function. The phosphorescence intensity decay of vanillin in amorphous EVS film at 20°C in the presence of nitrogen is plotted in Figure 7

along with the modified residuals for a fit using a four-exponential function (Eq. 8, Materials and Methods).

All intensity decays over the temperature interval from -20°C to 80°C were well fit using a four-exponential function and those for 90°C and 100°C was fit using a two-exponential function. This analysis indicated that the vanillin probe had multiple lifetimes in the amorphous EVS matrix at all temperatures. The phosphorescence intensity decreased with increasing temperature indicating an increase in triplet state quenching rates with increase in temperature, the results of these lifetime analyses for vanillin in EVS are plotted in Figure 8a. The decrease in lifetime as a function of temperature was dramatic both below and above T_g , indicating the presence of a range of molecular motions both below and above T_g . A comparison of individual lifetime components τ_1 , τ_2 , τ_3 and τ_4 for vanillin in EVS and VS is shown in Figure 8b (longer lifetimes) and 8c (shorter lifetimes). There was no significant difference in the individual lifetime component of vanillin in EVS and VS films.

The average lifetime calculated using Eq. 9 (Material and Methods) is plotted for EV and VS films in Figure 9 as a function of temperature. The average lifetime varied from ~150 ms at -20°C to ~0.5 ms at 100°C. The decrease in vanillin lifetime as a function of temperature corresponds to an increase in k_{NR} (Eq. 4, Materials and Methods), the rate of vibrational relaxation due to collisional quenching which is an indicator of the increase in matrix mobility. The decrease in lifetime was multi-phased as a function of temperature. A comparison plot of average lifetimes of Ery B and vanillin in the EVS amorphous

matrix is shown in Figure 9. The amplitudes of each lifetime component are plotted as a function of temperature in Figure 10. A comparison plot for amplitudes a_1 , a_2 , a_3 and a_4 between EVS and VS is shown in Figure 10a, 10b, 10c and 10d, respectively. The amplitudes of the longer lifetime components decreased and that of the shorter lifetime components increased as a function of temperature. The non-radiative decay rate reflects the sum of all collisional interaction between the matrixes and the probe and is sensitive to molecular environments, and changes in this decay rate with change in physical state of the probe environments strongly modulate the phosphorescence lifetime giving rise to multiple lifetimes.

The comparison between VS and EVS matrix, vanillin lifetime and amplitudes values were found to be super imposable. This indicated that there is no interference from erythrosin B phosphorescence to vanillin lifetime measurements.

The Arrhenius plot of natural log of k_p for average lifetime as function of inverse of temperature for vanillin and erythrosin B dispersed in EVS films is shown in Figure 11.

Spectroscopic interactions between Ery B and Vanillin: Erythrosin B was also excited at 320 nm (the excitation wavelength for vanillin) although vanillin did not show any excitation at 500 nm (the excitation wavelength for Ery B). The delayed fluorescence and phosphorescence peak intensity of erythrosin B were compared between EVS (obtained by fitting the EVS 320 nm spectra to a log-normal three function) and ES matrix (obtained by fitting the EVS 320 nm spectra to a log-normal two function) excited at

320nm using (Equation 10a Materials and Methods) for phosphorescence and Equation 10b for delayed fluorescence.

The delayed fluorescence emission of erythrosin B was found to be higher in the presence of vanillin as compared to in the absence (Figure 12a). However, there was no change in the emission of phosphorescence of erythrosin B in presence or absence of vanillin (Figure 12b). Thus may be a small amount of energy transfer occurred between vanillin and erythrosin B, as erythrosin B (acceptor) absorbs at 500 nm which is the emission wavelength for vanillin (donor). There probably was some amount of energy transfer between erythrosin B and vanillin that translated into higher emissions for delayed fluorescence. It is very surprising to believe this, as no higher emissions were observed in case of phosphorescence. Also the lifetime measurements of delayed fluorescence in presence or absence of vanillin showed no difference between EVS and ES films as shown in Figure 13. This observation could just be contribution from the data analysis, as the emission spectra of vanillin in EVS matrix was analyzed using log-normal three functions. As these measurements of intensity are based on log-normal three function analysis, it is probable that the delayed fluorescence intensity (which overlaps with vanillin phosphorescence) is artificially high due to problem with the analysis.

Discussion

This research investigated simultaneous measurements of mobility by using both erythrosin B and vanillin in amorphous matrix and demonstrates that multiple probes can be used to report molecular mobility in an amorphous matrix. Vanillin and erythrosin B in amorphous sucrose (where they co-existed) reported independently about molecular mobility. Emission energy and lifetimes were found to be super-imposable to data obtained from individual probes indicating no physical (aggregation) or spectroscopic interactions between Ery B and vanillin. Although Ery B showed no difference in the FWHM between ES and EVS matrix, vanillin did have higher FWHM values in EVS matrix as compared to in VS matrix. This increase in spectral broadening was due to emission from Ery B as it showed small amount when excitation was at 320nm (vanillin's excitation wavelength). This research thus opens a new world where one can investigate simultaneous measurements of mobility using multiple probes in amorphous solid mixtures.

Phase separations in protein/sugar matrix may remove the protecting effect of sugars on proteins. Phase separation is important in such sugar/protein mixtures to understand changes in the amorphous mixtures. These probes (Ery B and vanillin) could provide information by partitioning in different phases. Dispersible extrinsic probes have chemical properties that allow them to partition into and report on molecular properties of a specific phase of the system (such as protein surface or a lipid phase).

Storage stability in seeds is thought to be related to molecular mobility and packing density of the intracellular glass (Buitnik and Leprince, 2004). The glass dynamics mechanism (Frank et al., 1991; Slade and Levin, 1991) focuses on rigid, inert matrix formed by vitrification (glass formation) of stabilizers such as sugars. Glass formation is a purely kinetic mechanism, and the stability is expected to correlate to molecular mobility in the rigid matrix. On the other hand it was thought that below T_g , the free volume of an amorphous solid is reduced, which limits the diffusion of molecules (Miller et al., 1997), thus showing that the stability of protein/carbohydrate glasses depends largely on molecular mobility (Yoshioka et al 1997). The current research will be able to provide meaningful insight into these issues. Using multiple probes dispersed or covalently attached in a amorphous mixtures one will be able to generate a detailed understanding of different molecular processes associated with transitions below and above T_g . One can generate mobility maps which will provide useful insight as to how molecular mobility of protein and sugar molecules change in the amorphous mixtures.

The higher emission of delayed fluorescence for Ery B in presence of vanillin was thought to be due to energy transfer between the two probes. This energy transfer occurred probably between excited triplet state of vanillin and excited singlet state of erythrosin B as it contributed to more delayed fluorescence emissions without affecting the phosphorescence. This is hard to believe as energy transfer gives rise to excess delayed fluorescence but no excess phosphorescence. No change in lifetime of delayed fluorescence decay in presence or absence of vanillin was observed. Energy transfer is a process that occurs when emission energy of a donor appears as electronic excitation

energy of the acceptor molecule. For this process to take place the absorption spectrum of the acceptor must overlap with the emission of the donor (Lakowicz, 1999). Excitation energy could be transferred between molecules as far apart as 50Å , i.e., over distances considerably greater than collisional diameter (Parker, 1968). Energy exchange is not a diffusional process. As vanillin emits at 500 nm and erythrosin B is excited at $\sim 500\text{nm}$, higher emission may be due to energy transfer. This did not affect the phosphorescence measurements. It had no effect on measurements of emission energy and lifetime for both Ery B and vanillin in the EVS matrix. This energy transfer could provide some information about the regions in which these probes are dispersed, because for energy transfer to occur the acceptor/donor pair should not be over up to a distance of 50Å (Parker, 1968).

Consider an amorphous matrix which contains regions that are in the different phases. If the donor and the acceptor both partition into the same region, one expects the extent of energy transfer to be increased, relatively to that expected from a random distribution of donors and acceptors between the phases. Conversely if donor and acceptor partition into different phases, the extent of energy transfer will decrease relative to a random distribution. If an acceptor labeled lipid clusters around the protein, then the extent of energy transfer will be greater than expected for acceptor randomly dispersed. These all are just speculations where the knowledge of using multiple probes could be used but these need to be tested out before drawing conclusions.

This paper focuses on exploring the potential of using multiple probe combination of vanillin and erythrosin B dispersed in the simple system (amorphous sucrose) to report about local dynamics and the results are promising. This research can be further developed for studying the physical behaviors of each component in more complex systems.

Conclusions

This research investigated simultaneous measurements of mobility by using both erythrosin B and vanillin in amorphous matrix. This would be first of its kind where multiple probes are used in the same amorphous system. It has addressed answers to the following two important questions: a) Do chromophores interfere with each other or act individually and report on molecular mobility based on the environment they are present; and b) Is there any spectroscopic or physical interaction between the two probes.

The answers to both questions can be exploited in different ways. If two probes present in a matrix do not interfere they could be used to report on molecular mobility by partitioning them into two different phases, e.g., erythrosin B in protein and vanillin in sugar phase. If there is energy transfer between the two probes one can measure interaction between two sites in which these probes are present. For example, say erythrosin B is covalently attached to a protein and vanillin is dispersed in the sucrose matrix.

In case of erythrosin B and vanillin there was no spectroscopic interference observed and they both reported about matrix mobility independently. The only exception to this was higher emission of delayed fluorescence seen in erythrosin B in presence of vanillin, but this did not affect the phosphorescence measurement. This erythrosin B and vanillin combination can be used in the same amorphous matrix to report about molecular mobility independently.

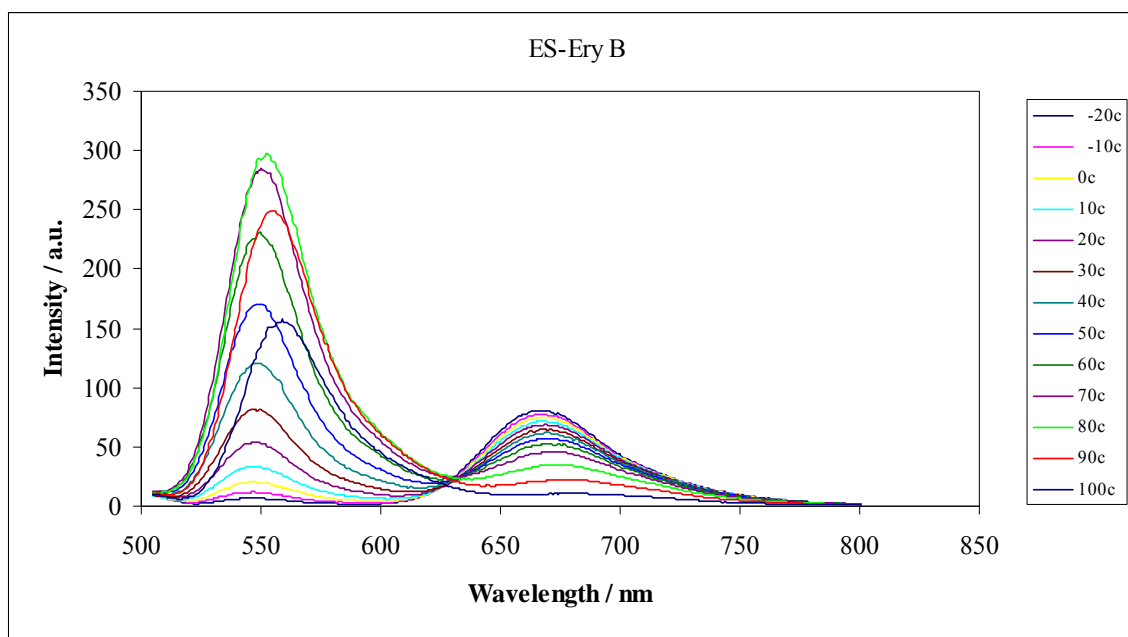
Erythrosin B***Figure VIII-1a***

Figure VIII-1a: Delayed emission spectra of erythrosin B dispersed in amorphous films of sucrose (referred as ES matrix) as a function of temperature (excitation at 500 nm). The spectra were collected at 10°C intervals from -20°C to 100°C (the curves follow this order from high to low intensity at ~690 nm).

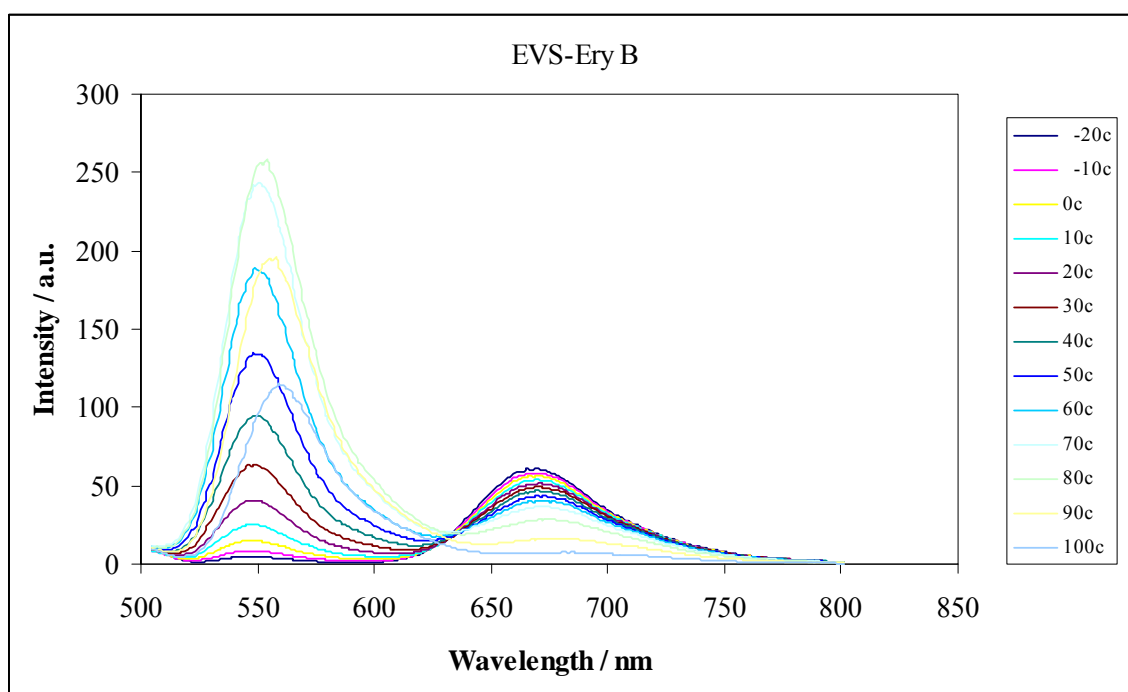
Figure VIII-1b

Figure VIII-1b: Delayed emission spectra of erythrosin B dispersed in amorphous films of sucrose also containing vanillin (referred as EVS matrix) as a function of temperature (excitation at 500 nm). The spectra were collected at 10°C intervals from -20°C to 100°C (the curves follow this order from high to low intensity at ~690 nm).

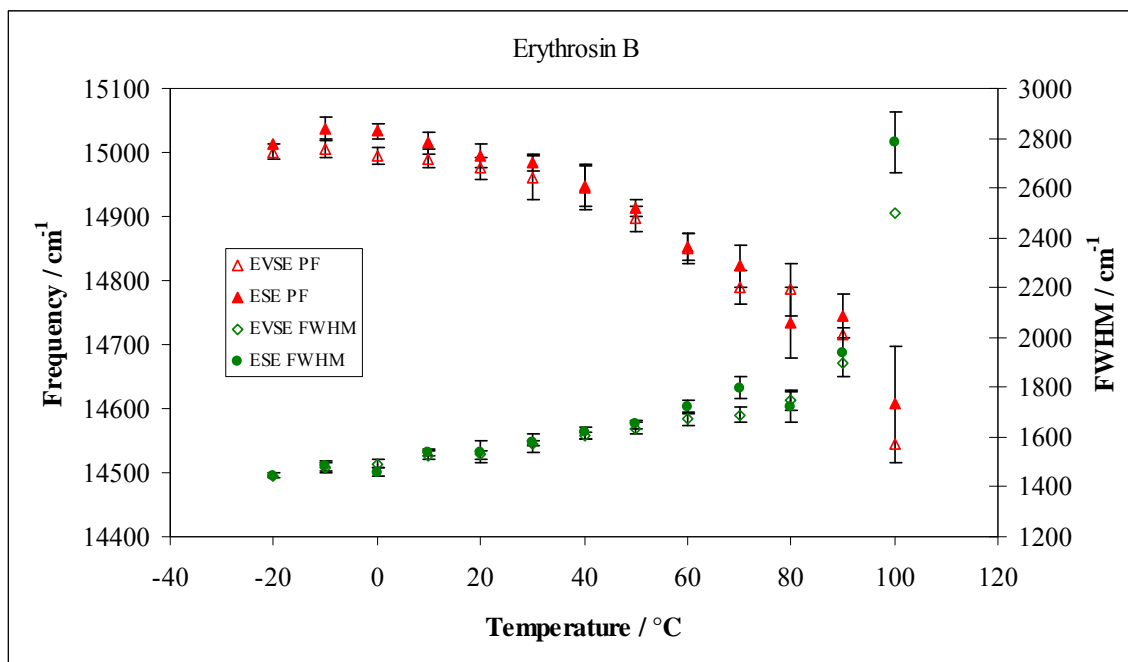
Figure VIII-2

Figure VIII-2: Peak energy ν_p (left hand scale) and bandwidth FWHM (right hand scale) for phosphorescence emission from erythrosin B in amorphous EVS and ES films as a function of temperature. The spectra were collected every 10°C from -20 to 100°C. The frequency is given by in (Δ) EVS matrix and by (\blacktriangle) in ES matrix. The FWHM is given by (\diamond) in EVS matrix and by (\blacklozenge) in ES matrix.

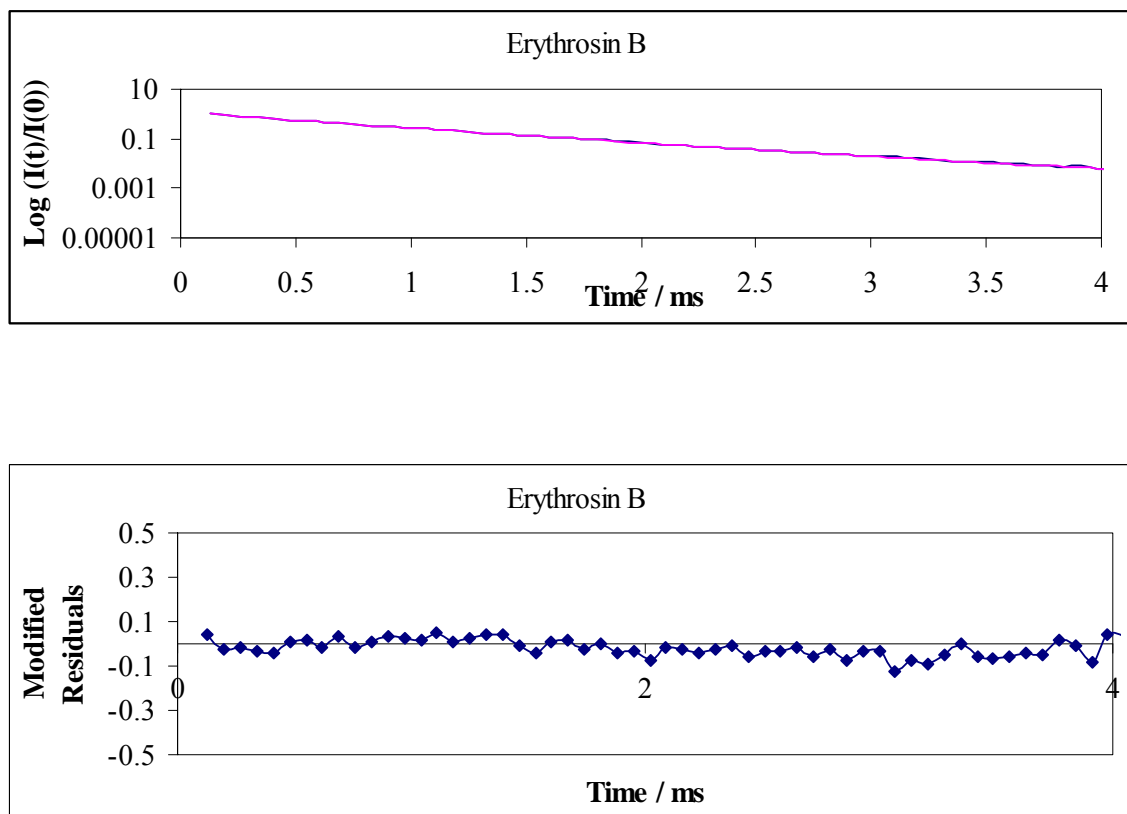
Figure VIII-3

Figure VIII-3: Normalized phosphorescence intensity decay $[I(t)/I(0)]$ of erythrosin B dispersed in amorphous EVS films at 20°C in the presence of nitrogen. The solid lines through the data are fits using a stretched-exponential function. Below is the plot of modified residuals $[(\text{Data-Fit})/\text{Data}^{1/2}]$ for these fits to data plotted in the presence of nitrogen.

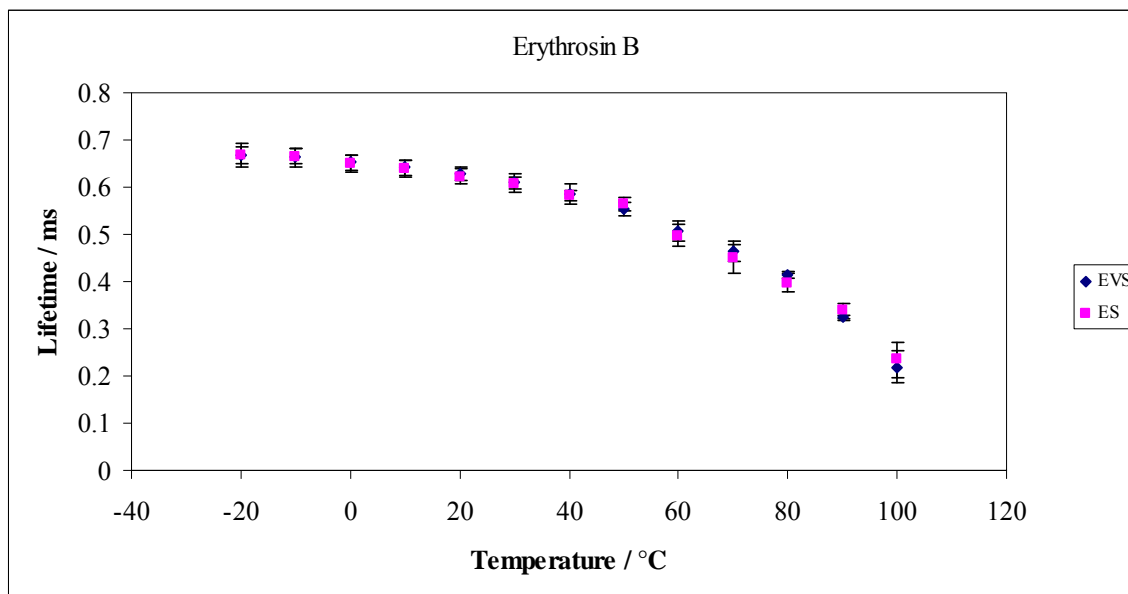
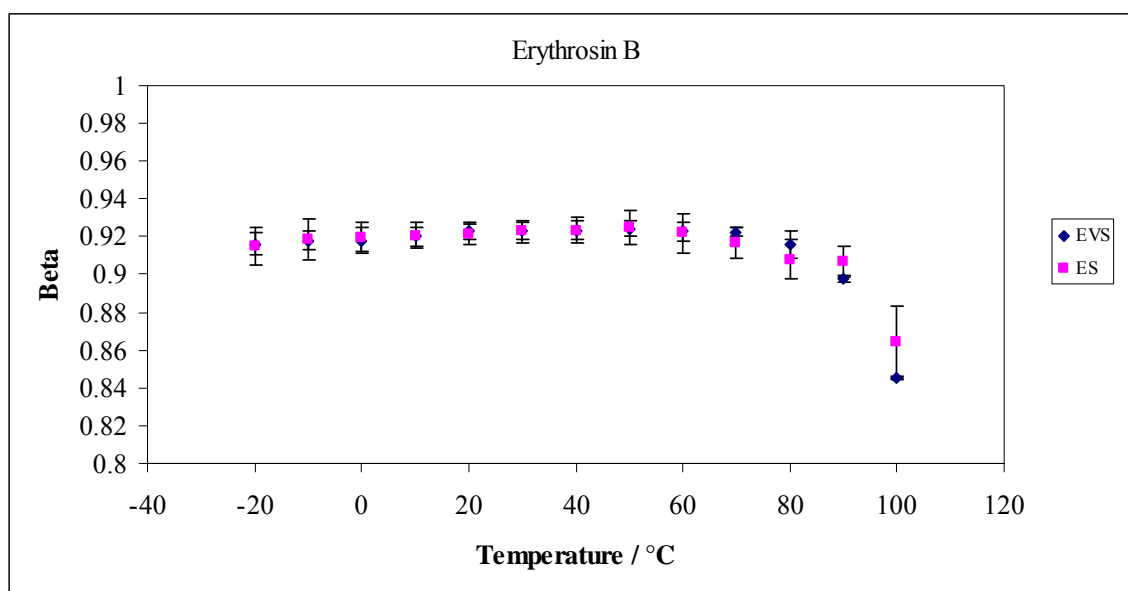
Figure VIII-4a**Figure VIII-4b**

Figure VIII 4a and 4b: Intensity decay fit parameters for erythrosin B in amorphous sucrose film ES (■) and EVS (◆). The values were measured every 10°C from -20°C to 100°C. The measurements were made in the absence of oxygen. (a) Stretched exponential lifetimes in nitrogen as a function of temperature. (b) Stretched exponential fitting parameter β as a function of temperature.

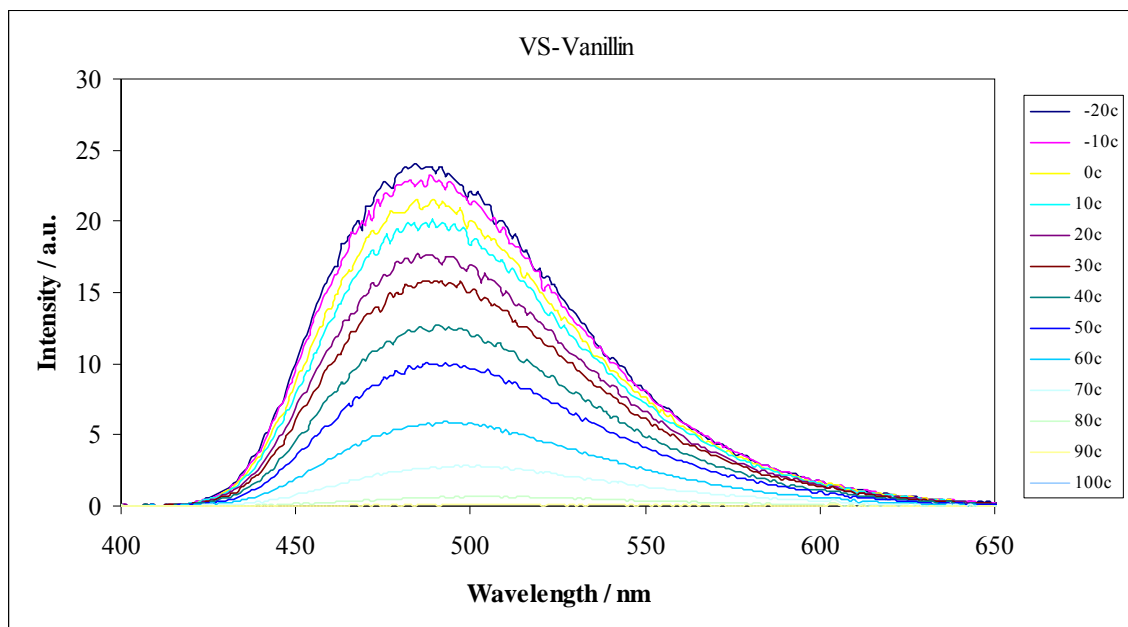
Vanillin**Figure VIII-5a**

Figure VIII-5a: Delayed emission spectra of vanillin in amorphous sucrose films (referred as VS) as a function of temperature (excitation at 320 nm). The spectra were collected at 10°C intervals from -20°C to 100°C (the curves follow this order from high to low intensity at ~490 nm).

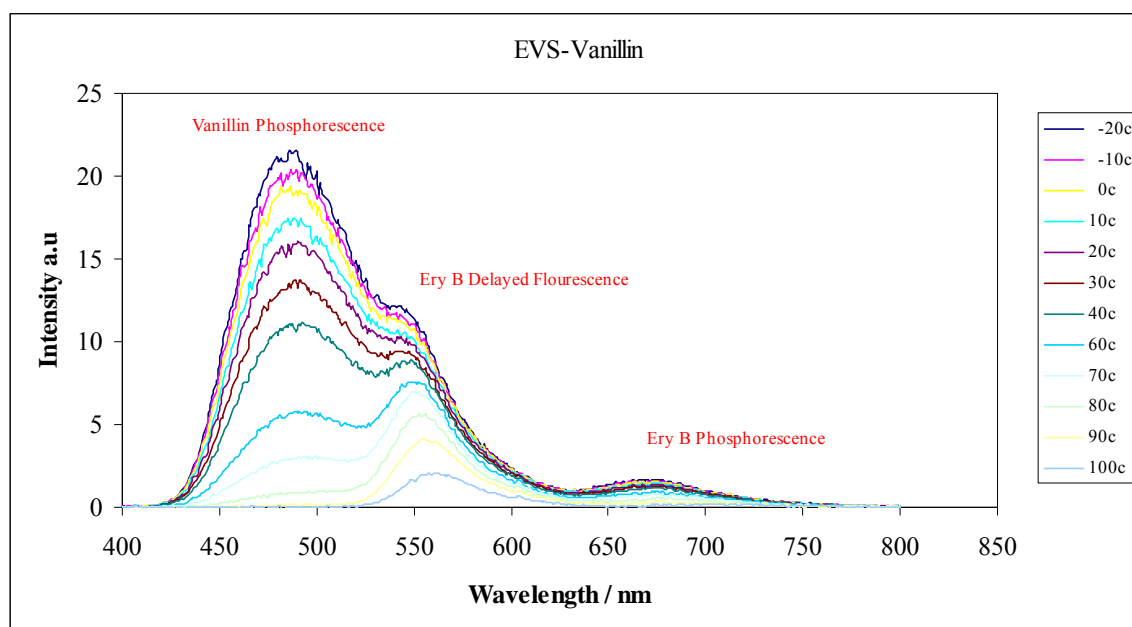
Figure VIII-5b

Figure VIII-5b: Delayed emission spectra of vanillin in amorphous sucrose films also containing erythrosin B (referred as EVS) as a function of temperature (excitation at 320 nm). The spectra were collected at 10°C intervals from -20°C to 100°C (the curves follow this order from high to low intensity at ~490 nm).

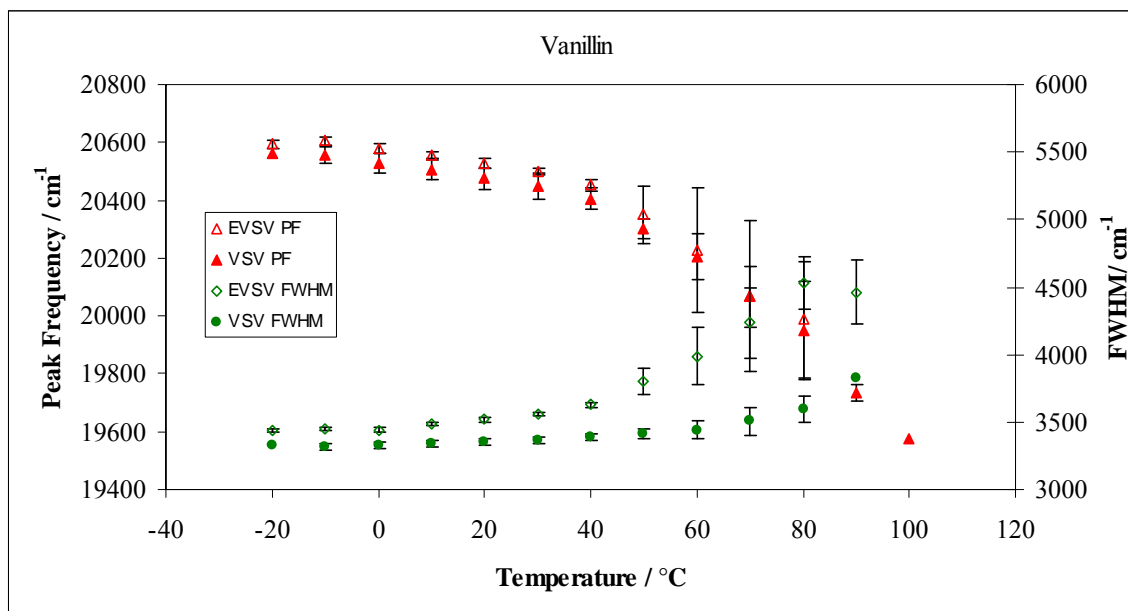
Figure VIII-6

Figure VIII-6: Peak energy ν_p (left hand scale) and bandwidth FWHM (right hand scale) for phosphorescence emission from vanillin in amorphous EVS and VS films as a function of temperature. The spectra were collected every 10°C from -20 to 100°C. The frequency is given by in (Δ) EVS matrix and by (\blacktriangle) in VS matrix. The FWHM is given by (\diamond) in EVS matrix and by (\blacklozenge) in VS matrix.

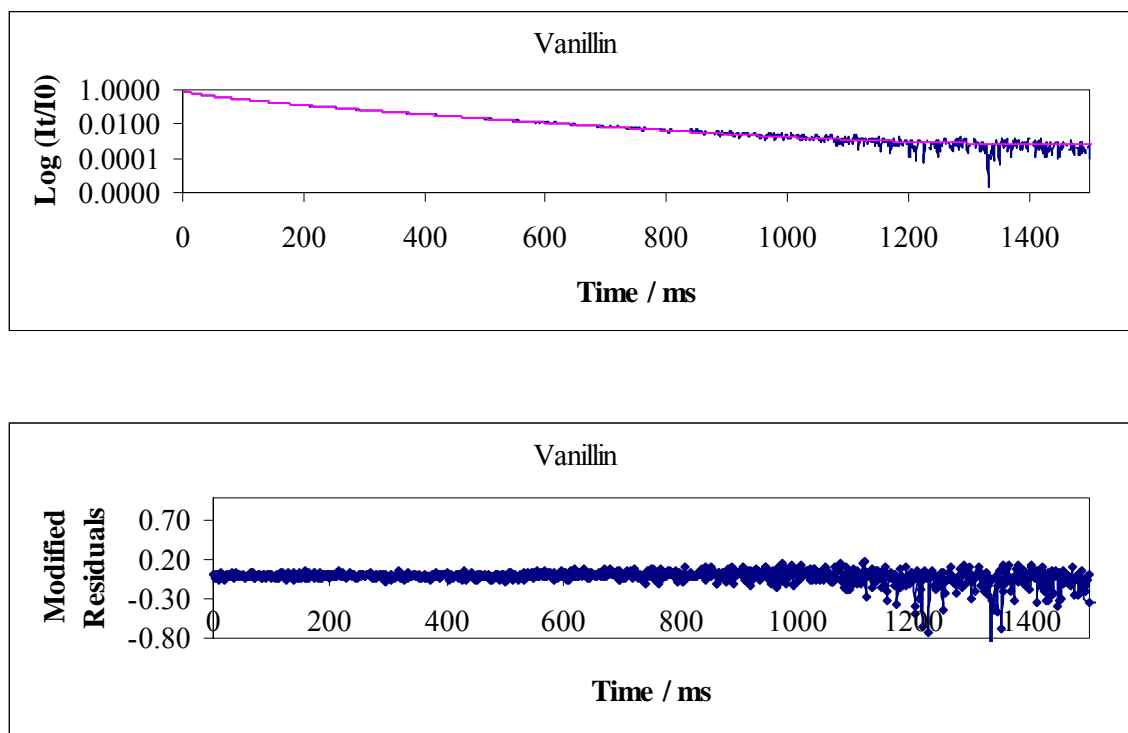
Figure VIII-7

Figure VIII-7: Normalized phosphorescence intensity decay $[I(t)/I(0)]$ of vanillin dispersed in amorphous EVS films at 20°C in the presence of nitrogen. The solid lines through the data are fits using a multi-exponential function. Below is the plot of modified residuals $[(\text{Data}-\text{Fit})/\text{Data}^{1/2}]$ for these fits to data plotted in the presence of nitrogen.

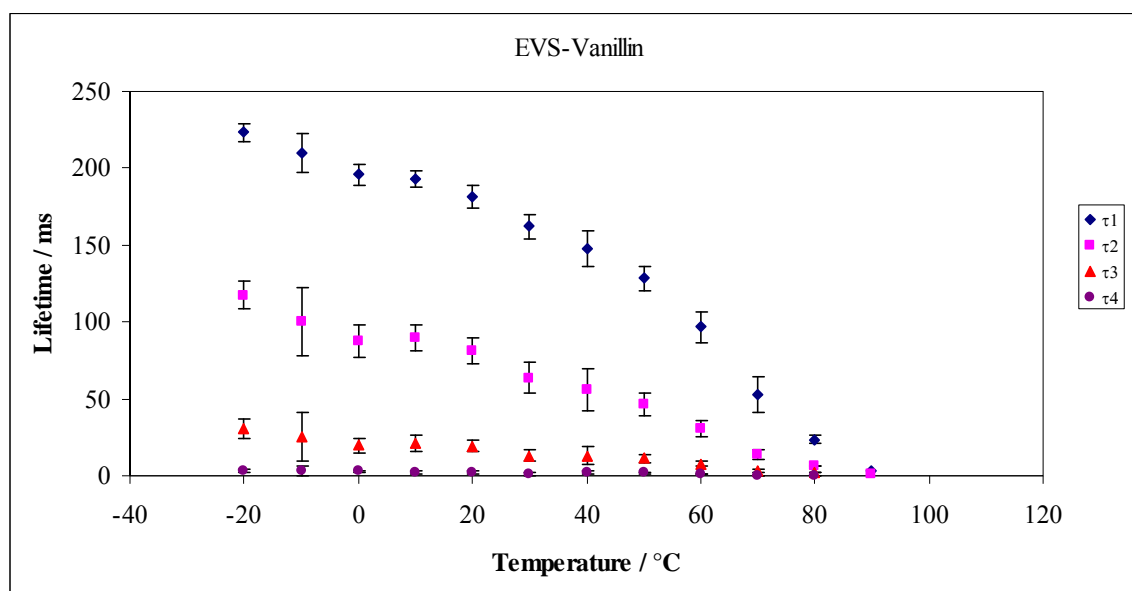
Figure VIII-8a

Figure VIII-8a: Lifetime components τ_1 (\blacklozenge), τ_2 (\blacksquare), τ_3 (\blacktriangle) and τ_4 (\bullet) obtained from a multi-exponential model fit (Eq. (8), Materials and Methods) to phosphorescence intensity decay data from vanillin dispersed in amorphous EVS films equilibrated against nitrogen as a function of temperature. The data was calculated every 10 $^{\circ}\text{C}$ from -20 $^{\circ}\text{C}$ to 100 $^{\circ}\text{C}$.

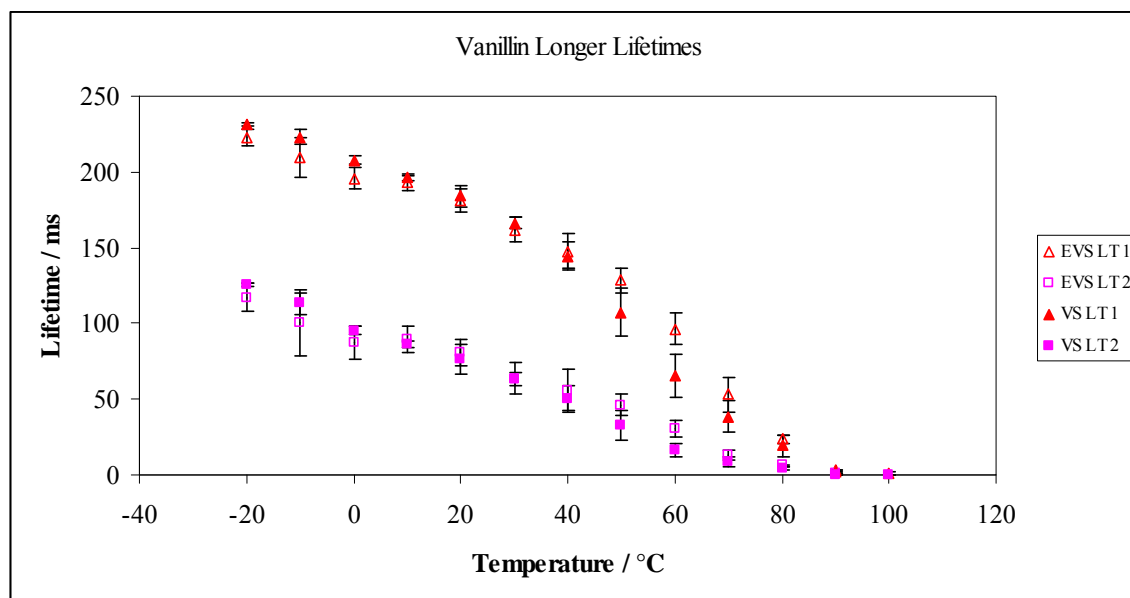
Figure VIII-8b

Figure VIII-8b: Comparison of longer lifetime components τ_1 (◆) and τ_2 (■) obtained from a multi-exponential model fit (Eq. (8), Materials and Methods) to phosphorescence intensity decay data from vanillin dispersed in amorphous EVS or VS films equilibrated against nitrogen as a function of temperature. The data was calculated every 10°C from -20°C to 100°C.

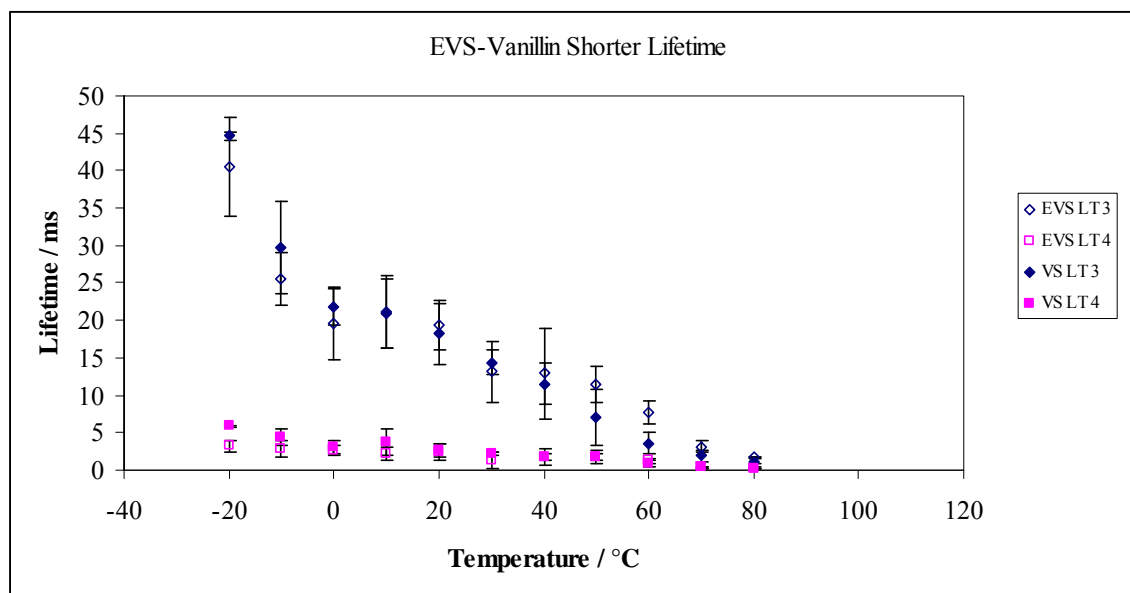
Figure VIII-8c

Figure VIII-8c: Comparison of shorter lifetime components τ_1 (◆) and τ_2 (■) obtained from a multi-exponential model fit (Eq. (8), Materials and Methods) to phosphorescence intensity decay data from vanillin dispersed in amorphous EVS or VS films equilibrated against nitrogen as a function of temperature. The data was calculated every 10°C from -20°C to 100°C.

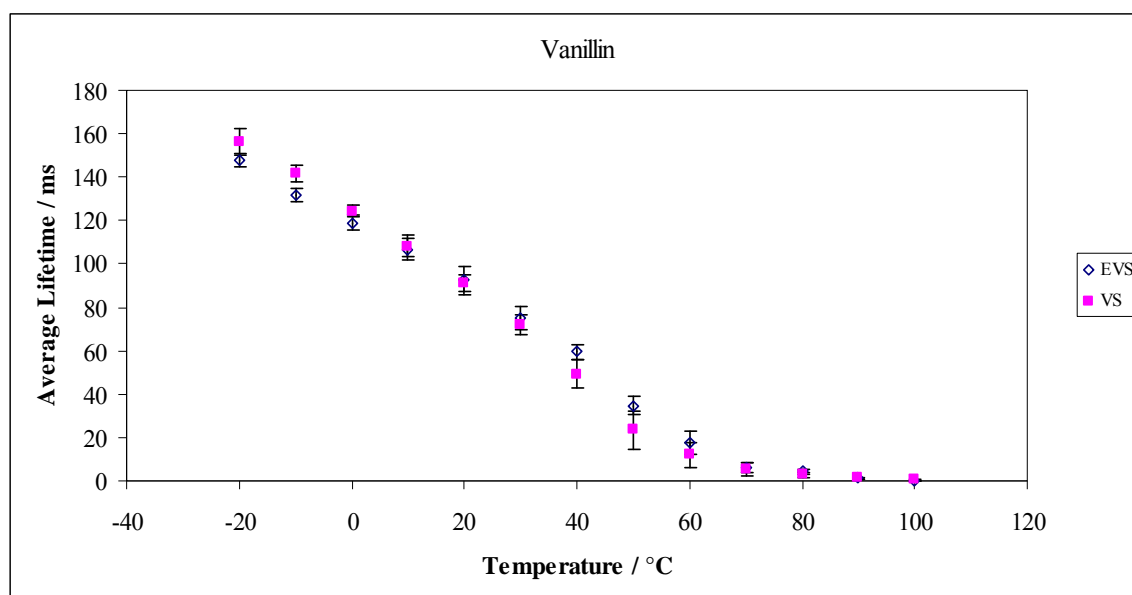
Figure VIII-9

Figure VIII-9: The average lifetime of vanillin in EVS (◆) and VS (■) films obtained from a multi-exponential model fit equilibrated against nitrogen as a function of temperature. The data were collected every 10°C from -20°C to 100°C.

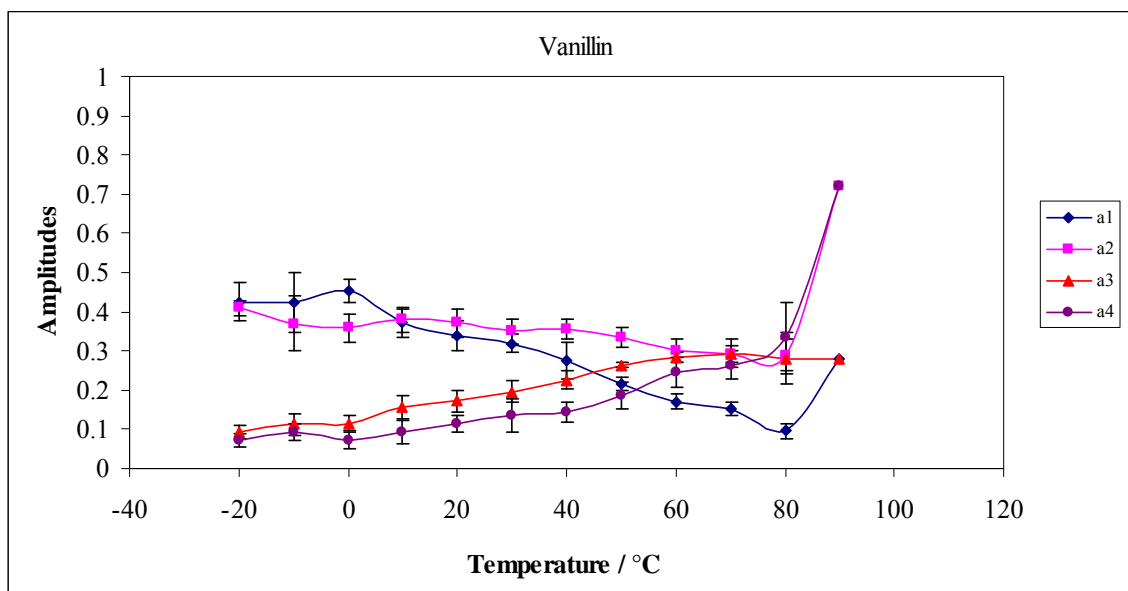
Figure VIII-10

Figure VIII-10: Intensity decay fit parameters amplitude for vanillin in amorphous EVS film in nitrogen as a function of temperature. The data was calculated every 10°C from -20°C to 90°C. The amplitudes a1 (♦) and a2 (■) correspond to the longer life time components (τ_1 , τ_2) and a3 (▲) and a4 (●) correspond to the shorter lifetime components (τ_3 , τ_4). The amplitudes were obtained from a multi exponential model fit (Eq. (8), Materials and Methods) to phosphorescence intensity decay data from vanillin dispersed in amorphous sucrose films equilibrated against nitrogen as a function of temperature.

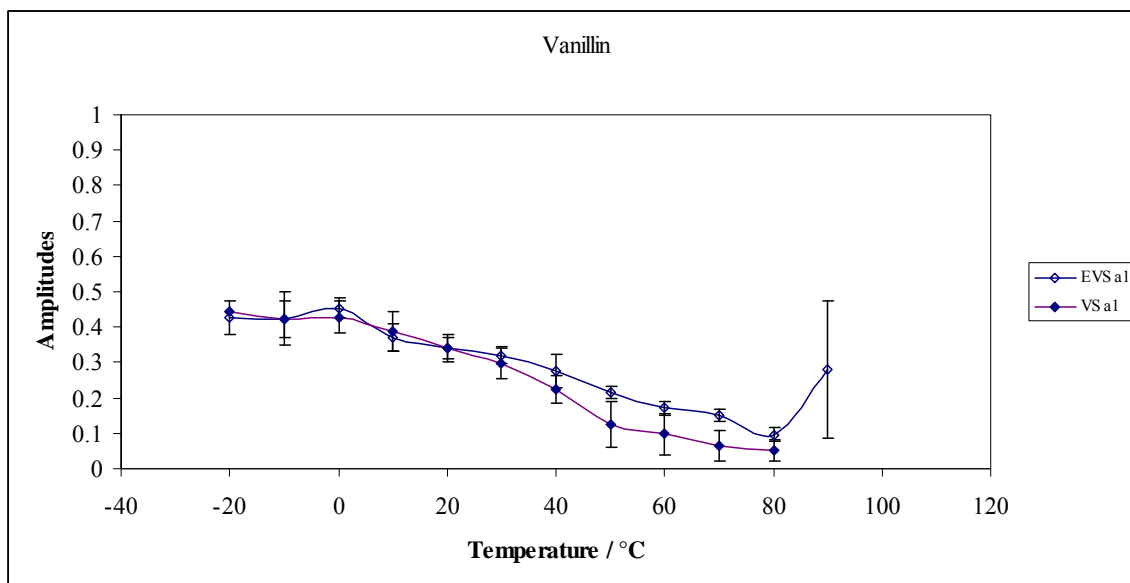
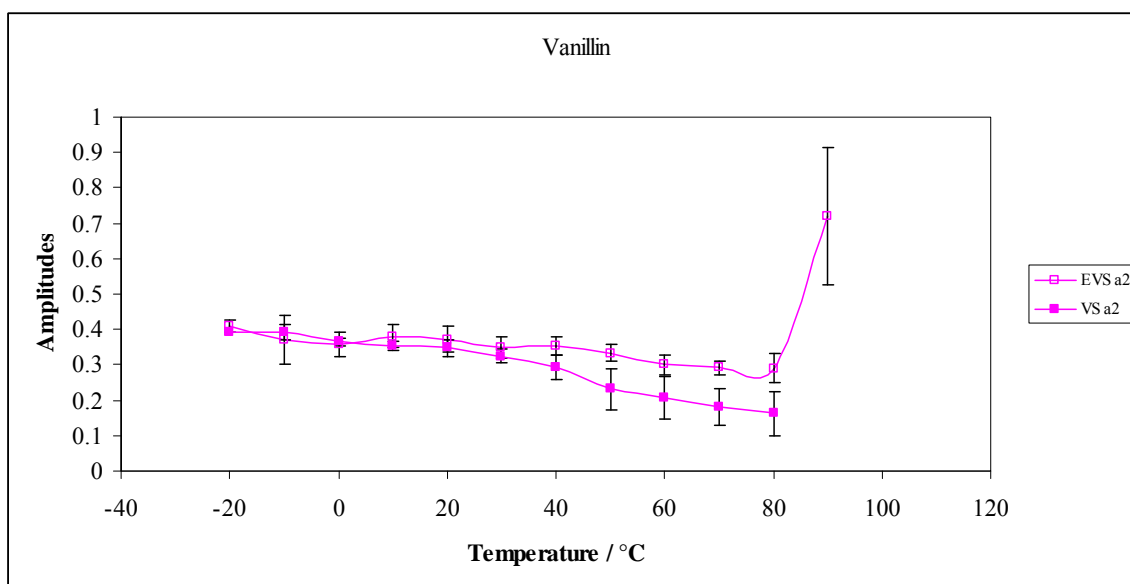
Figure VIII-10a*Figure VIII-10b*

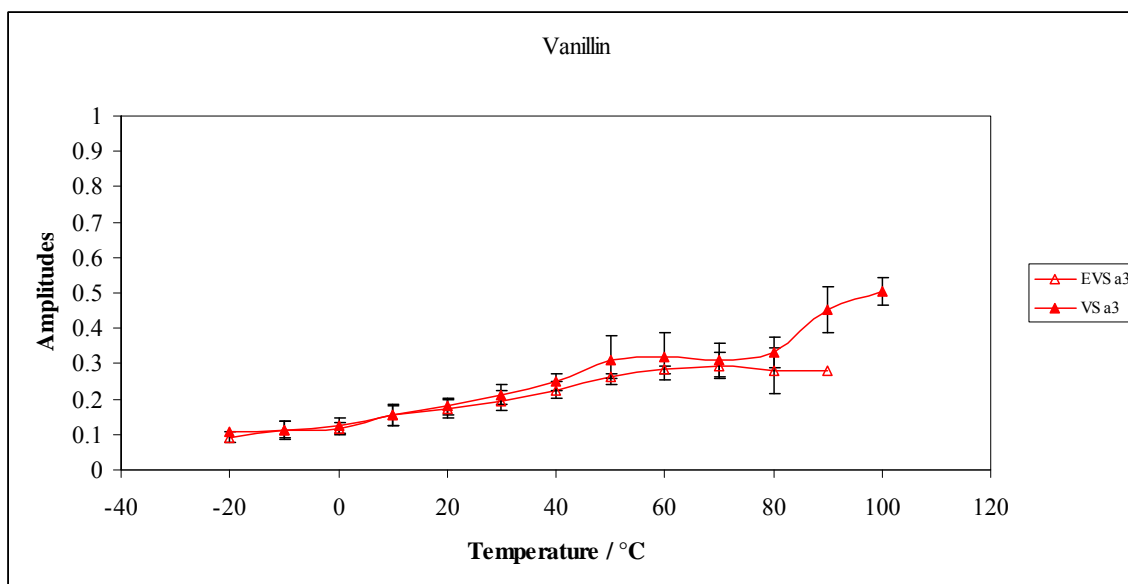
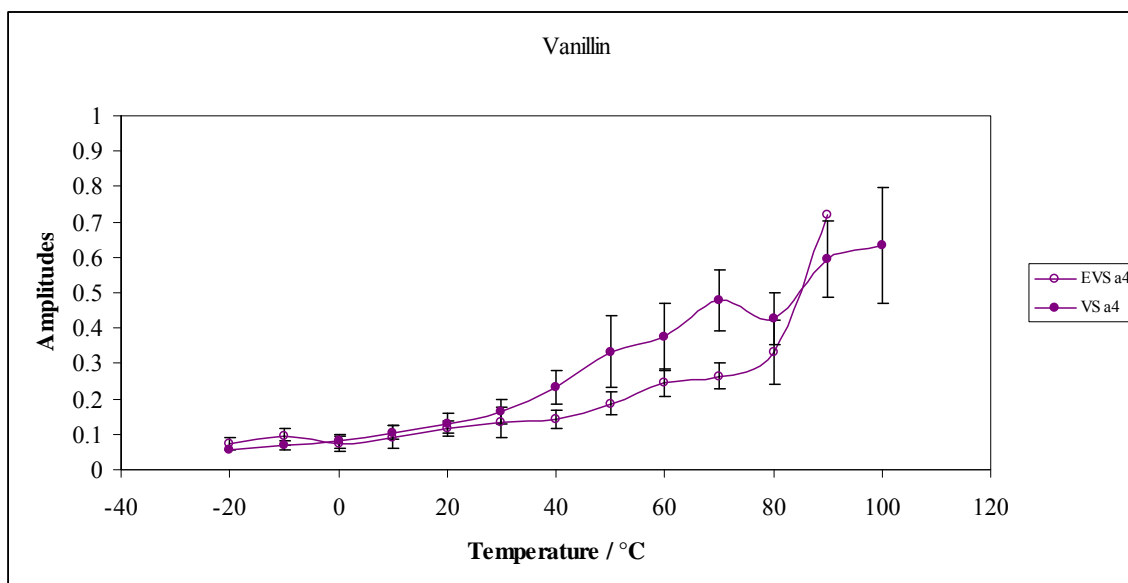
Figure VIII-10c*Figure VIII-10d*

Figure VIII-10a-10d: Comparison of intensity decay fit amplitudes for vanillin in amorphous EVS and VS film in nitrogen as a function of temperature.

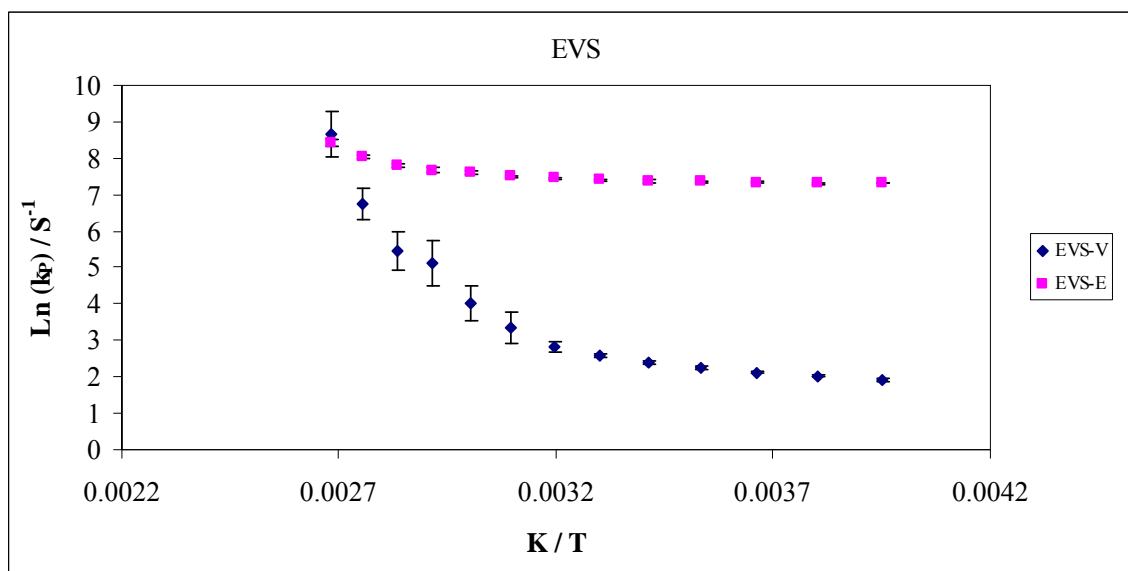
Figure VIII-11

Figure VIII-11: The Arrhenius plot of natural log of k_p for average lifetime as function of inverse of temperature for vanillin and erythrosin B dispersed in EVS films.

Energy Transfer between vanillin and erythrosin B:

Figure VIII-12a

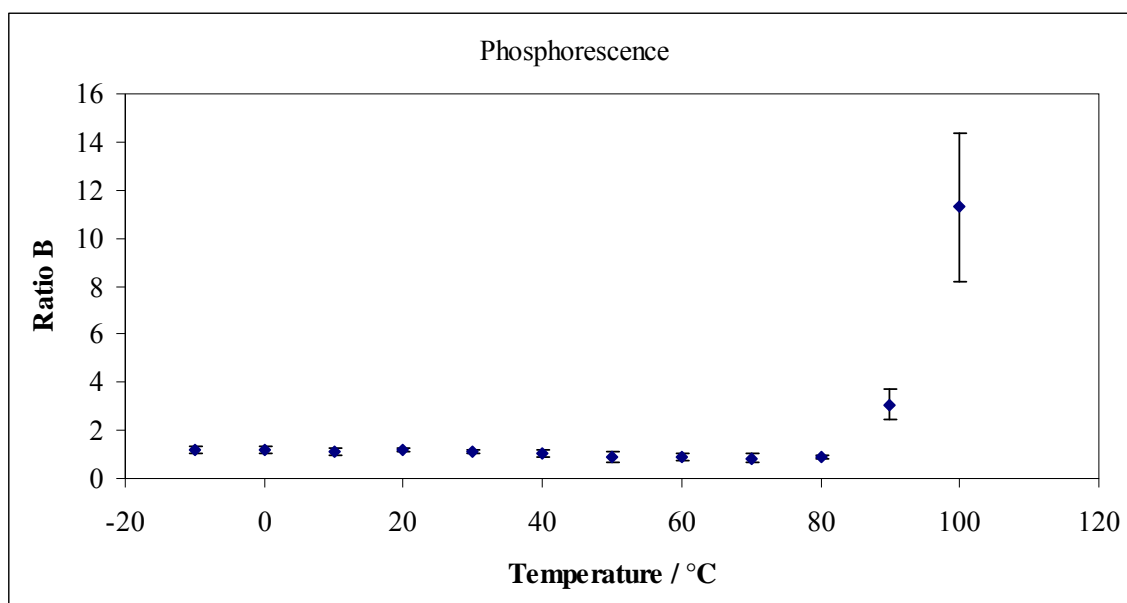


Figure VIII-12b

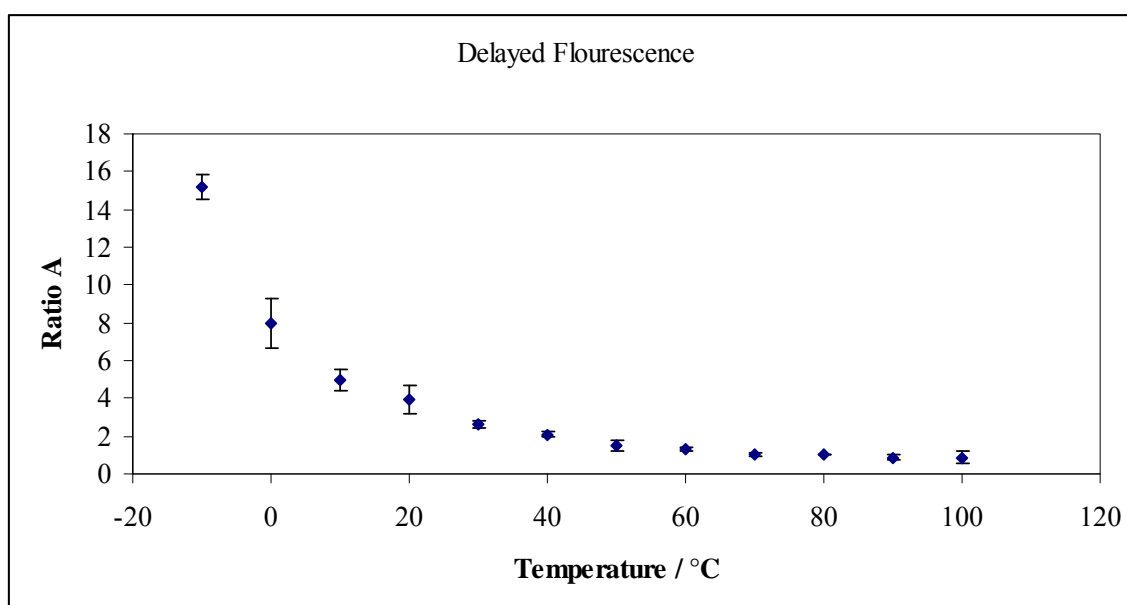


Figure 12a and 12b: Comparing the Ratio A and Ratio B corresponding to phosphorescence and delayed fluorescence of erythrosin B, respectively, as a function of temperature in absence of oxygen.

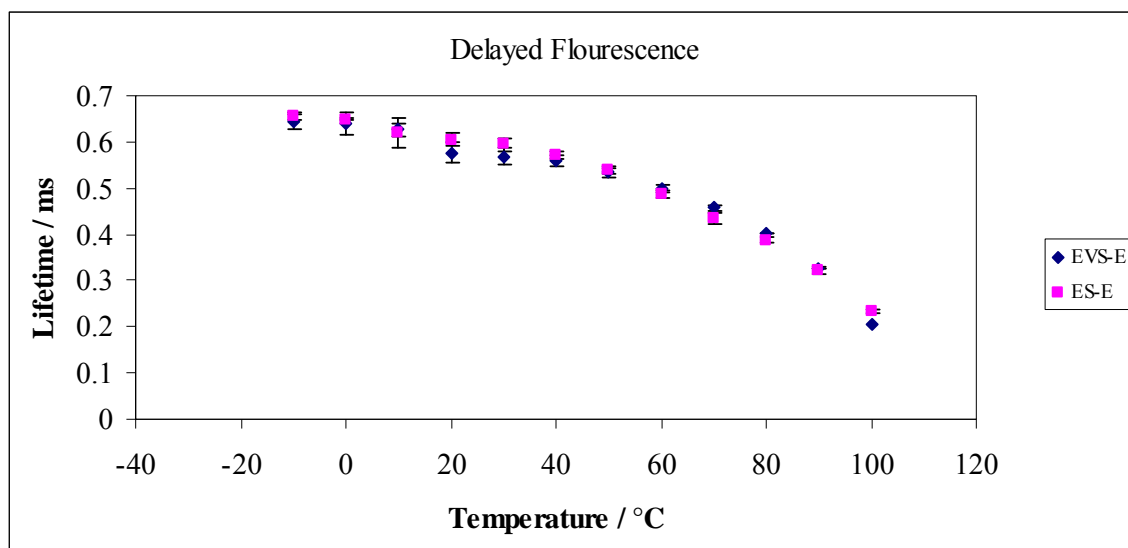
Figure VIII-13

Figure VIII-13: Comparing the delayed fluorescence lifetime of erythrosin B in EVS (♦) and ES (■) films. The values were measured every 10°C from -20°C to 100°C. The measurements were made in the absence of oxygen.

References

- Bell, L. N. and Hageman, M. J. Glass transition explanation for effect of polyhydroxy compounds on protein denaturation in dehydrated solids. *Journal of Food Science*. 61 (1996). 372-375.
- Buitink, L. and Leprince, O. Glass formation in plant anhydrobiotes: survival in the dry state. *Cryobiology*. 48 (2004). 215-228.
- Carpenter, J. F. and Crowe, J. H. An infrared spectroscopic study of the interactions of carbohydrates with dried proteins. *Biochemistry*. 28 (1989). 3916-3922.
- Carpenter, J. F. and Crowe, J. H. The mechanism of cryoprotection of proteins by solutes. *Cryobiology*. 25 (1988). 244-255.
- Champion, D., Le Meste, M. and Simatos, D. Towards an improved understanding of glass transition and relaxations in foods: molecular mobility in the glass transition range. *Trends in Food Science and Technology*. 11 (2000). 41-55.
- Corveleyn, S. and Remon, J. Maltodextrin as lyoprotectants in the lyophilization of a model protein, LDH. *Pharmaceutical Research*. 13 (1996). 146-150.
- Crowe, J. H., Carpenter, J. F. and Crowe, L. M. The role of vitrification in anhydrobiosis. *Annual Review Physiology*. 60 (1998). 73-103.
- Debenedetti, P. G. and Stillinger, F. H. Supercooled liquids and the glass transition. *Nature*. 410 (2001). 259-267.
- Duchowicz, R., Ferrer, M. L. and Acuna, A. U. Kinetic spectroscopy of erythrosin phosphorescence and delayed fluorescence in aqueous solution at room temperature. *Photochemistry and Photobiology*. 68 (1998). 494-501.
- Ediger, M. D., Angell, C. A. and Nagel, S. R. Supercooled Liquids and Glasses. *Journal of Physical Chemistry*. 100 (1996). 13200-13212.
- Fischer, C. J., Gafni, A., Steel, D. G. and Schauerte, J. A. The triplet-state lifetime of indole in aqueous and viscous environments: significance to the interpretation of room temperature phosphorescence in proteins. *Journal of the American Chemical Society*. 124 (2002). 10359-10266.
- Grattard, N., Salaun, E., Champion, D., Roudaut, G. and Le Meste, M. Influence of physical state and molecular mobility of freeze dried maltodextrin matrices on the oxidation rate of encapsulated lipids. *Journal of Food Science*. 67 (2002). 3002-3010.
- Green, J. L. and Angell, C. A. Phase relation and vitrification in saccharide-water solutions and trehalose anomaly. *Journal of Physical Chemistry* 93 (1989): 2880-82.

- Hancock, B. C. and Zografi, G. Characteristics and significance of amorphous state in pharmaceutical systems. *Journal of Pharmaceutical Sciences* 86 (1997): 1-12.
- Hill, J. J., Shalae, E. Y. and Zografi, G. Thermodynamic and dynamic factors involved in the stability of native proteins structure in amorphous solids in relation to levels of hydration. *Journal of Pharmaceutical Sciences*. 94 (2004). 1636-1667.
- Kaushik, J. K. and Bhat, R. Why is Trehalose an exceptional protein stabilizer? An analysis of thermal stability of proteins in the presence of the compatible osmolyte trehalose. *Journal of Biological Chemistry*. 278 (2003). 26458-26465.
- Khwaldia, K., Banon, S., Desobry, S. and Hardy, J. Mechanical and barrier properties of sodium caseinate-anhydrous milk fat edible films. *International Journal of Food Science and Technology*. 39 (2004). 403-411.
- Khwaldia, K., Perez, C., Banon, S., Desobry, S. and Hardy, J. Milk proteins for edible films and coatings. *Critical Review in Food Science and Nutrition*. 44 (2004). 239-251.
- Lai, M. C. and Topp, E. M. Solid state chemical stability of protein and peptides. *Journal of Pharmaceutical Sciences*. 88 (1999). 489-500.
- Lakowicz, J. R. *Principles of Fluorescence Spectroscopy*. Second ed. New York: Kluwer Academic/Plenum Press. (1999).
- Leslie, S. B., Israeli, E., Lighthart, B., Crowe, J. H. and Crowe, L. M. Trehalose and sucrose protect both membranes and proteins in intact bacteria during drying. *Applied and Environmental Microbiology*. 61 (1995). 3592-3597.
- Lettinga, M. P., Zuillhof, H. and Van Zandvoort, M. A. M. J. Phosphorescence and fluorescence characterization of fluorescein derivatives immobilized in various polymers matrices. *Physical Chemistry Chemical Physics*. 2 (2000). 3697-707.
- Lindsey, C. P. and Patterson, G. D. Detailed comparison of the Williams-Watts and Cole-Davidson functions. *Journal of Chemical Physics*. 2 (1980). 3348-3357.
- Lopez-Diez, E. C. and Bone, S. An investigation of water binding properties of protein and sugar systems. *Physics in Medicine and Biology*. 2 (2000). 3577-3588.
- Ludescher, R. D., Shah, N. K., McCaul, C. P. and Simon-Lukasik, K. V. Beyond Tg: optical luminescence measurements of molecular mobility in amorphous solid foods. *Food Hydrocolloids*. 15 (2001). 331-339.
- Maroncelli, M. and Fleming, G. R. Picosecond salvation dynamics of coumarin 153: The importance of molecular aspects of salvation. *Journal of Chemical Physics*. 86 (1987). 6221-6239.

- Mazzobre, M. F., del Pilar Buera, M. and Chirife, J. Protective role of trehalose on thermal stability of lactase in relation to its glass and crystal forming properties and effect of delaying crystallization. *Lebensm-Wiss. U.-Technol.* 30 (1997). 324-329.
- Miller, D.P., de Pablo, J.J. and Corti, H.R. Thermophysical properties of trehalose and its concentrated aqueous solutions. *Pharmaceutical Research*. 14 (1997). 578-589.
- Nack, T. J. and Ludescher, R. D. Molecular mobility and oxygen permeability in amorphous bovine serum albumin films. *Food Biophysics*. 1 (2006). 151-162.
- Oldenhof, H., Wolkers, W. F., Foneseca, F., Passot, S. and Marin, M. Effect of sucrose and maltodextrin on the physical properties and survival of air-dried *Lactobacillus bulgaris*: an in situ Fourier transform infrared spectroscopy study. *Biotechnology Progress*. 21 (2005). 885-892.
- Papp, S. and Vanderkooi, J. M. Tryptophan phosphorescence at room temperature as a tool to study protein structure and dynamics. *Photochemistry and Photobiology*. 49 (1989). 775-784.
- Parker, C. A. *Photoluminescence of Solutions*. Amsterdam: Elsevier Pub Co., (1968).
- Pravinata, L.V., You, Y. and Ludescher, R. D. Erythrosin B phosphorescence monitors molecular mobility and dynamic heterogeneity in amorphous sucrose. *Biophysical Journal*. 88 (2005). 3551-3561.
- Richert, R. Triplet state salvation dynamics: Basics and applications. *Journal of Chemical Physics*. 113 (2000). 8404-8429.
- Roosi, S., Buera, M. P., Moreno, S. and Chirife, J. Stabilization of the restriction enzyme EcoRI dried with trehalose and other selected glass forming solutes. *Biotechnology Progress*. 13 (1997). 609-616.
- Shah, N. K and Ludescher, R. D. Phosphorescence of probes of the glassy state in amorphous sucrose. *Biotechnology Progress*. 11 (1995). 540-544.
- Shirke, S. and Ludescher, R. D. Dynamic site heterogeneity in amorphous maltose and maltitol from spectral heterogeneity in erythrosin B phosphorescence. *Carbohydrate Research*. 340 (2005). 2661-2669.
- Shirke, S. and Ludescher, R. D. Dynamic site heterogeneity in amorphous lactose and lactitol from spectral heterogeneity in erythrosin B phosphorescence. *Biophysical Chemistry*. 123 (2006a). 122-133.
- Shirke, S. and Ludescher, R. D. Molecular mobility and glass transition in amorphous glucose, maltose and maltotriose. *Carbohydrate Research*. 340 (2006b), 2654-2660.

- Simon-Lukasik, K. V. and Ludescher, R. D. Effect of plasticizer on dynamic site heterogeneity in cold-cast gelatin films. *Food Hydrocolloids*. 20 (2006a). 88-95.
- Simon-Lukasik, K. V. and Ludescher, R. D. Molecular mobility in water and glycerol plasticized cold and hot cast gelatin films. *Food Hydrocolloids*. 20 (2006b). 96-105.
- Simon-Lukasik, K. V. and Ludescher, R. D. Erythrosin B phosphorescence as a probe of oxygen diffusion in amorphous gelatin films. *Food Hydrocolloids*. 18 (2004). 621-630.
- Slade, L. and Levine, H. A food polymer science approach to structure interactions. *Advances in experimental medicine and biology*. 302 (1991) 29-101.
- Sundaresan, K. V. and Ludescher, R. D. Molecular mobility and oxygen permeability in amorphous beta-lactoglobulin films. 22 (2007). 403-413.
- Vanderkooi, J. M. and Berger, J. W. Excited triplet state used to study biological macromolecules at room temperature. *Biochimica et Biophysica Acta: Bioenergetics*. 976 (1989). 1-27.
- Vyazovkin, S. and Dranca, I. Probing beta relaxations in pharmaceutically relevant glasses by using DSC. *Pharmaceutical Research*. 23 (2006). 422-28.
- Yoshioka, S., Aso, Y. and Kojima, S. Dependence of the molecular mobility and protein stability of freeze dried gamma globulin formulations on the molecular weight of dextran. *Pharmaceutical Research*. 14 (1997). 736-741.

CHAPTER IX: Investigating the potential of using multiple probes erythrosin B and tryptophan in amorphous sucrose films to report molecular mobility.

Introduction

This study is an extension of our previous work on using multi- probes combinations of erythrosin B and vanillin dispersed in amorphous sucrose film (Chapter VIII) used to report molecular mobility. Current research also recognizes the importance of understanding the local dynamics in amorphous mixtures (e.g., containing protein and sugars) using tryptophan and erythrosin B combination.

Tryptophan is a naturally occurring amino acid and has been shown to exhibit strong room temperature phosphorescence emission after excluding oxygen (Vanderkooi et al., 1987). Tryptophan phosphorescence has being found to be sensitive to the physical properties of the local environment (Strambini and Gonnelli, 1985). The long lifetime of this probe helps detect molecular motions present in the rigid, glassy regions within even fully hydrated proteins (Shah and Ludescher, 1992, 1993). Also, the triplet state of indole has being shown to have a strong dependence of the radiation-less deactivation rate on medium viscosity; the lifetime of tryptophan decreases from 6.5s in a glassy matrix to 1.2 ms in aqueous solutions at ambient temperature (Strambini and Gonnelli, 1995). Typtophan phosphorescence, for example, has been used to study the internal mobility of proteins in solution (Papp and Vanderkooi, 1989) and in the solid state (Shah and Ludescher, 1995) on the milliseconds to second timescale. Phosphorescence of tryptophan has been used to monitor molecular mobility of lysozyme (Shah and Ludescher, 1992, 1993). Previous studies have been conducted where phosphorescence

from the luminescent chromophores tryptophan (McCaul and Ludescher, 1999) and N-acetyltryptophanamide (NATA) (Shah and Ludescher, 1995) was used to probe the molecular dynamics of the glassy state and the glass-to-rubber transition in amorphous sucrose. Tryptophan has also been used to study molecular mobility in amorphous films of sucrose, maltose and trehalose where sucrose was found to be the most mobile matrix among the three (Zunic, 2004).

Erythrosin B (acid form) has been used to monitor molecular mobility in many simple amorphous systems such as sucrose (Pravinata et al., 2005 and Shah and Ludescher, 1995), gelatin (Simon-Lukasik and Ludescher, 2006a, 2006b), bovine serum albumin (Nack and Ludescher, 2006), and glucose, maltose and maltotriose (Shirke and Ludescher, 2006). Measurements of phosphorescence emission and lifetimes from erythrosin-labeled gelatin in amorphous solid films have indicated its utility to monitor oxygen diffusion (Simon-Lukasik and Ludescher, 2006a, 2006b). Erythrosin B has also been used to study plasticizer effects on molecular mobility (Simon-Lukasik and Ludescher, 2006a) and dynamic site heterogeneity (Simon-Lukasik and Ludescher 2006b) in amorphous gelatin films. Erythrosin B has also been used to detect dipolar relaxation and dynamic site heterogeneity in sugars and sugar alcohols (Shirke and Ludescher, 2005).

In this study molecular mobility was studied in the amorphous sucrose films by monitoring phosphorescence from dual probes combinations of erythrosin B and tryptophan. A comparison of the data was made with data obtained from individually dispersed probes in amorphous sucrose films. We found that there was no effect on

phosphorescence measurement of erythrosin B and tryptophan in presence of each other.

This research thus opens a new world where one can investigate simultaneous measurements of mobility using multiple probes in amorphous sucrose which could be further extended for measurements in amorphous mixtures.

Materials and Methods

Sucrose Solution: Sucrose solution was made as described in Pravinata et al 2005. Approximately 20 g of sucrose (99.5% pure; Sigma Chemical, St. Louis, MO) were dissolved in 100 mL of deionized water containing 0.5 g of activated charcoal to remove luminescent impurities. After stirring overnight, the charcoal was removed by vacuum filtration using ashless filter paper (Whatman No. 40, Whatman International, Maidstone, UK), additional charcoal was added, and the process repeated. Sucrose solution was made to a final concentration of 65–67 wt % sucrose; concentration was confirmed using a refractometer (NSG Precision Cells, Farmingdale, NY). This sucrose solution was filtered through a 0.2 μm membrane to remove particulates.

Erythrosin B: A 50mM stock solution of erythrosin B sodium salt (Molecular Probes, Inc., Eugene, OR) was prepared in distilled deionized water. This concentration was selected to simplify the addition of the probe to the sucrose solution. For measuring phosphorescence in amorphous sucrose films, erythrosin B was added to the sucrose solution at a molar ratio of 1:10⁴ (dye: sucrose). The ratio 1:10⁴ (dye: sucrose) was chosen as at this concentration it was determined that the probe does not aggregate, existing only as individual molecules monitoring the molecular mobility of the sucrose.

Tryptophan: A 50mM stock solution of tryptophan (Sigma Chemical, St. Louis, MO) was prepared in distilled deionized water. This concentration was selected to simplify the addition of the probe to the sucrose solution. For measuring phosphorescence in amorphous sucrose films, tryptophan was added to the sucrose solution at a molar ratio of

1:500 (dye: sucrose). The ratio 1:500 (dye: sucrose) was chosen as at this concentration it was determined that the probe does not aggregate, existing only as individual molecules monitoring the molecular mobility of the sucrose.

Sucrose films: To produce glassy sucrose films containing both erythrosin B at $(1:10^4)$ and vanillin at $(1:10^3)$, 20 μL of a sucrose solution containing erythrosin B and vanillin were spread on a quartz slide ($30 \times 13.5 \times 0.6$ mm; custom made by NSG Precision Cells, Farmingdale, NY). After spreading the solutions on the slides were then dried under a heat gun (Vidal Sassoon) for 5 min to a maximum temperature of $\sim 88^\circ\text{C}$ (measured using a thermocouple probe) and the final thickness was ~ 0.05 mm. The slides were stored at room temperature against P_2O_5 and Drierite, protected from the light to prevent any photobleaching, for at least 7 days before any phosphorescence measurements were made. The desiccant was refreshed as needed to maintain a relative humidity close to 0%.

Instrumentation: Measurements were made on a Cary Eclipse fluorescence spectrophotometer (Varian Instruments, Walnut Creek, CA). This instrument, which collects in analog mode, uses a high intensity pulsed lamp and a time delay was employed to avoid any fluorescence during the lamp pulse. The temperature was controlled by using a TLC 50 thermoelectric heating/cooling system (Quantum Northwest, Spokane, WA). The TLC-50 sample compartment was fitted with a jacketed cover. The measurements were made in absence of oxygen (Nitrogen was purged for 15 minutes). Nitrogen stream was generated by passage of high purity nitrogen through a

Supelco (Bellefonte, PA) carrier gas purifier. Quartz slides were placed in the standard 1cm x 1cm x 1cm quartz fluorescence cuvette, which was capped with a lid having inlet and outlet ports of gas lines.

Luminescence Measurements

The Cary Eclipse uses a pulsed lamp and collects emission intensity in analog mode; data were not collected within the first 0.1-0.2 ms to suppress fluorescence coincident with the lamp pulse.

Erythrosin B Protocol: Delayed luminescence emission spectra were collected from 535 to 800 nm (10 nm bandwidth) using excitation at 500 nm (20nm bandwidth) over the temperature range from -10°C to 100°C . Each data point was collected from a single flash with 0.2 ms delay, 5.0 ms gate time, and 0.02 s total decay time. The phosphorescence spectra collected as a function of temperature in the presence of nitrogen, were converted to intensity versus frequency (cm^{-1}) and analyzed to obtain the peak frequency and spectral bandwidth using eq. (1) and (2) (Maroncelli and Fleming, 1987). Lifetime measurements (for phosphorescence and delayed fluorescence) were made in the presence of nitrogen ($-\text{O}_2$) as a function of temperature. The samples were excited at 540 nm (20 nm bandwidth) and emission transients collected at 680 nm (20 nm bandwidth) at temperatures ranging from -10°C to 100°C . Each decay transient was the sum of 50 cycles, and for each cycle data was collected from a single lamp flash with a delay of 0.1 ms, 0.06 ms gate time and 6.0 ms total decay time. All measurements were made in quadruplicate. A similar measurement was also made for amorphous sucrose

film containing just erythrosin B for comparison. To check for spectroscopic interference from tryptophan, erythrosin B was also excited using tryptophan protocol.

Tryptophan Protocol: Delayed luminescence emission spectra were collected from 350 to 600 nm (10 nm bandwidth) using excitation at 280 nm (20nm bandwidth) over the temperature range from -10°C to 100°C . Each data point was collected from a single flash with 0.2 ms delay, 10.0 ms gate time, and 1.0 s total decay time. The phosphorescence spectra collected as a function of temperature in the presence of nitrogen, were converted to intensity versus frequency (cm^{-1}) and analyzed to obtain the peak frequency and spectral bandwidth using eq. (1) and (2) (Maroncelli and Fleming, 1987). Lifetime measurements were made in the presence of nitrogen ($-\text{O}_2$) as a function of temperature. The samples were excited at 280 nm (20 nm bandwidth) and emission transients collected at 455 nm (20 nm bandwidth) at temperatures ranging from -10°C to 100°C . Each decay transient was the sum of 50 cycles, and for each cycle data was collected from a single lamp flash with a delay of 0.2 ms. Windows for gate time and total decay time were varied at each temperature. All measurements were made in quadruplicate. A similar measurement was also made for amorphous sucrose film containing just tryptophan for comparison. To check for spectroscopic interference from erythrosin B, tryptophan was also excited using erythrosin B protocol.

Data Analysis

Emission Energy as a function of temperature: Emission spectra were fit using the program Igor (Wavemetrics, Inc., Lake Oswego, OR) to a log-normal function over the temperature range Equation 1.

$$I(\nu) = I_0 \exp \left\{ -\ln(2) \left(\frac{\ln[1 + 2b(\nu - \nu_p) / \Delta]}{b} \right)^2 \right\} \quad (1)$$

In this equation I_0 is the maximum intensity of the emission spectra, ν_p is the frequency (in cm^{-1}) of the emission maximum, Δ is a line width parameter, and b is an asymmetry parameter. The bandwidth of the emission, the full width at half maximum (Γ), is related to b and Δ Equation 2.

$$\Gamma = \Delta \left(\frac{\sinh(b)}{b} \right) \quad (2)$$

Phosphorescence Intensity: Phosphorescence lifetimes were determined with the statistical program Igor (Wavemetrics, Inc., Lake Oswego, OR). The phosphorescence intensity decays were collected as described above and were fitted using a stretch exponential function for erythrosin B and multi-exponential function for tryptophan (Chen, 2003; Shamblin et al., 2000). Fits were judged satisfactory if the r^2 values were in the range of 0.995-1.0 and the modified residuals $((\text{data} - \text{fit})/\text{data}^{1/2})$ varied randomly about zero.

Multi-exponential function: The multi-exponential model is as show in Equation 3. τ_i are decay times, α_i represent the amplitudes of the components at $t = 0$ and n is the number of decay times. The average lifetime was calculated using Equation 4.

$$I(t) = \sum_{i=1}^n \alpha_i \exp(-t/\tau_i) \quad (3)$$

$$\tau_{\text{Avg}} = \sum_{i=1}^n \alpha_i \tau_i / \sum_{i=1}^n \alpha_i \quad (4)$$

Stretched exponential function: Intensity decays were analyzed using a stretched exponential function or Kohlrausch-Williams-Watts (KWW) model equation 5. This model has being shown to be appropriate to describe the wide distribution of relaxation times (Champion et al., 2000) for the molecular processes that depopulate excited states in amorphous solids (Pravinata et al., 2005; Nack and Ludescher, 2006). The average lifetime was calculated using Equation 6.

$$I(t) = I(0) \exp\{-(t/\tau_i)^\beta\} + C \quad (5)$$

$$\tau_{\text{Avg}} = \tau \cdot \Gamma(1/\beta)/\beta \quad (6)$$

Where $I(0)$ is the initial amplitude at time zero, τ is the Kohlrausch-Williams-Watt lifetime (Lindsey and Patterson, 1980), and β is the stretching exponent, which varies from 0 to 1 and quantifies the non-exponential nature of the decay, and C is a constant; β provides a measure of the width of the distribution of lifetimes required to fit the intensity decay; the smaller the value of β , the wider the distribution of lifetimes.

Photophysical Scheme: The phosphorescence lifetimes were interpreted in terms of the rate constants associated with the various processes that contribute to the de-excitation of the excited triplet state of the probe (Duchowicz et al., 1998). The phosphorescence lifetimes were used to calculate the rate constants associated with the various processes that depopulate the excited triplet state.

The term $k_P (=1/\tau)$ is the total decay rate, k_{RP} is the rate of radiative decay of the triplet state. The magnitude of k_{NR} reflects factors associated with the mechanism by which the excited T_1 state is coupled to highly excited vibrations of the S_0 ground state as well as external factors associated with the mechanism by which the ground state vibrational energy can dissipate from the excited state into the surrounding matrix (Fischer et al., 2002; Vanderkooi and Berger, 1989). As the efficiency of external vibrational dissipation is related to overall mobility of the matrix, the magnitude of k_{NR} provides a measure of matrix mobility. The term $k_Q [Q]$ refers to the collisional quenching due to interaction

between the excited chromophore and a quencher molecule for example triplet state oxygen.

Erythrosin B: In case of erythrosin B, k_{RP} the rate of radiative decay of the triplet state (phosphorescence) is 41s^{-1} (Leetinga, 2000; Duchowicz et al., 1998). The term k_{TS1} is the rate for thermally activated reverse intersystem crossing from the triplet to the singlet excited state; it has an exponential dependence on the energy gap (ΔE_{TS}) between singlet and the triplet state:

$$\tau^{-1} = k_P = k_{RP} + k_{TS1} + k_{NR} + k_Q [Q] \quad (7)$$

$$k_{TS1}(T) = k_{TS1}^0 \exp(-\Delta E_{TS}/RT) \quad (8)$$

The value of ΔE_{TS} was calculated from the slope of the natural logarithm of the ratio of the emission intensity due to delayed fluorescence (I_{DF}) and phosphorescence (I_P) plotted versus $1/T$; I_{DF} and I_P were determined from log normal analysis of the emission spectra.

$$d [\ln (I_{DF}/I_P)]/d(1/T) = \Delta E_{TS}/R \quad (9)$$

(Where $R = 8.314 \text{ J K}^{-1} \text{ mol}^{-1}$). The value of k_{TS1} was calculated from equation 8 using $k_{TS1}^0 = 3.0 \times 10^7 \text{ s}^{-1}$ and $\Delta E_{TS} = 31.9 \text{ kJ mol}^{-1}$ (calculated using equation 9). Intersystem crossing to the ground state S_0 , which reflects relaxation of the probe from the excited triplet state to the ground state without the emission of a photon, has rate k_{NR} . The value

of k_{NR} was calculated from the lifetime in the presence of nitrogen ($-O_2$) (where $k_Q [O_2]$ is negligible) using Eq. 7.

Tryptophan: In case of tryptophan the term k_{TS1} is not relevant as there is no reverse intersystem crossing. The lifetime τ is related to the rate constants for de-excitation of the triplet excited state of the probe according to the following Equation 10 (Papp and Vanderkooi, 1989).

$$1/\tau = k_{RP} + k_{NR} (T) + k_Q [Q] = k_P \quad (10)$$

Here $k_P (=1/\tau)$ is the total decay rate, k_{RP} is the rate of radiative decay of the ground state ($1/6 \text{ s}^{-1}$), k_{NR} is the rate of non-radiative decay to the singlet state followed by vibrational relaxation to S_0 due to collisional quenching. The term $k_Q [Q]$ refers to the collisional quenching due to interaction between the excited chromophore and a quencher molecule for example triplet state oxygen.

Results and Discussion

Delayed luminescence emission spectra were collected as a function of temperature in the presence of nitrogen from erythrosin B and tryptophan dispersed together in amorphous sucrose films (erythrosin B + tryptophan + sucrose referred as TES) and compared to spectra from individual probes dispersed singly in sucrose (erythrosin B + sucrose referred as ES) and (tryptophan + sucrose referred as TS). Three spectroscopic measures of molecular mobility were made: emission energy, emission bandwidth and emission lifetime.

Erythrosin B:

There was no shift observed in the emission spectra in TES matrix as compared to the ES matrix.

Delayed Luminescence Spectra: The delayed luminescence spectra as a function of temperature of erythrosin B dispersed in amorphous ES or amorphous TES films are plotted in Figure 1a and 1b, respectively. These spectra exhibited maxima at ~552 nm and ~670 nm corresponding to delayed fluorescence and phosphorescence emission bands, respectively. Delayed, or E-type, fluorescence reflects emission from a singlet state (S_1) that has been repopulated by reverse intersystem crossing from the triplet state (T_1). Phosphorescence band reflects emissions directly from the triplet state. The delayed emission spectra were collected over the temperature range from -10°C to 100°C. Delayed emission spectra showed a decrease in phosphorescence intensity as a function of temperature; the delayed fluorescence intensity increased continuously from -10°C to

100°C as expected from a thermally stimulated processes and the changes were comparable in the TES and ES matrices.

The intensity ratio when plotted as a Van't Hoff plot of $\ln(I_{DF}/I_P)$ vs. $1/T$ (using the maximum emission intensity determined from fitting spectra to a log-normal function) was linear over the entire range of measured temperature (with $R^2 > 0.995$ for all curves) with no systematic deviation (Data not shown), the slope provides an estimate of the energy gap, ΔE_{TS} , between the lowest triplet (T_1) and singlet state (S_1). In ES matrix the values of $\Delta E_{TS} = 35.3 \pm 0.4 \text{ kJ mol}^{-1}$ and in EVS it was $\Delta E_{TS} = 34.5 \pm 1.1 \text{ kJ mol}^{-1}$.

The peak energy (ν_p) and bandwidth (Γ) for both delayed fluorescence and phosphorescence were determined by fitting emission spectra to a log-normal function (Eq. 1 and 2 Materials and Methods). The values of ν_p and Γ for the phosphorescence band varied systematically as a function of temperature as shown in Figure 2.

There was a gradual decrease in the peak emission energy at low temperature followed by a steeper decrease at higher temperature. The decrease in ν_p reflects increase in the rate and extent of dipolar relaxation around the triplet excited state. The emission bandwidth (Γ) increased gradually with temperature in the glass and much more dramatically in the melt. The increase in Γ at elevated temperatures reflects an increase in the extent of inhomogeneous broadening of the spectra due to energetic interactions of Ery B molecules with the surrounding matrix. This increase was gradual at low temperature and much more dramatic at higher temperatures indicating that the increase in dipolar

relaxation rate was accompanied by an increase in the distribution of energetically different environments.

The comparison between ES and TES matrix indicated that erythrosin B peak frequency and FWHM were generally super-imposable within error as shown in Figure 2. This indicated that there is no interference from presence of tryptophan to erythrosin B measurements. Erythrosin B was thus able to report about local dipolar relaxation in amorphous sucrose film in the presence of tryptophan.

Phosphorescence Intensity Decay: A phosphorescence intensity decay of erythrosin B in TES films at 20°C in the presence of nitrogen is plotted in Figure 3 along with the modified residuals for a fit to this decay using a stretched exponential model function (Eq. 5 and 6, Materials and Methods). The modified residuals for these fits varied randomly around zero, indicating that the stretched exponential function provided a statistically satisfactory fit to these data. All intensity decay data over the temperature interval from -10°C to 100°C were well fitted using a stretched exponential function. A stretched exponential function has also been shown to provide a statistically satisfactory fit to intensity decays of erythrosin B dispersed in amorphous sucrose (Pravinata et al., 2005), maltose and maltitol (Shirke and Ludescher, 2006, 2005), gelatin (Simon-Lukasik and Ludescher, 2006a, 2006b, 2004), bovine serum albumin (Nack and Ludescher, 2006) and β -lactoglobulin (Sundaresan and Ludescher, 2007) under all conditions measured.

The phosphorescence lifetime decreased with increasing temperature in both TES and ES films, indicating an increase in triplet state quenching rates with increase in temperature (Figure 4a). The erythrosin B lifetime in the absence of oxygen was 0.65 ms at -10°C and decreased to 0.32 ms at 100°C ; the decrease was gradual at low temperature and more dramatic at higher temperature. The decrease in lifetime with temperature in the absence of oxygen is the result of an increase in both k_{TS1} , the rate of reverse intersystem crossing to the excited singlet state (S_1), and k_{TS0} , the rate of intersystem crossing to a highly excited vibration of the singlet S_0 manifold, followed by vibrational relaxation to the ground vibrational state (Eq. 7 Materials and Methods). The rate k_{TS0} reflects the extent to which molecular motions within the matrix are able to facilitate dissipation of the vibrational energy of the highly excited probe into the matrix (Fischer et al., 2002; Vanderkooi and Berger, 1989) and is an indicator of matrix mobility.

The stretching exponent β is a measure of the width of the distribution of lifetimes required to fit the intensity decay (Lindsey and Patterson, 1980; Richert, 2000); it provides a measure of the dynamic heterogeneity of the matrix and varies primarily due to variability in k_{TS0} . The value of β decreased linearly with temperature in the absence of oxygen from a maximum of ~ 0.92 at -20°C to ~ 0.90 at 100°C in both TES and ES films (Figure 4b).

The comparison between ES and TES matrix, erythrosin B lifetime and beta values were found to be super imposable as shown in Figure 4a and 4b. This indicated that there is no interference from tryptophan phosphorescence to erythrosin B measurements.

Tryptophan:

Delayed Luminescence Spectra: The delayed emission spectra from tryptophan (excited at 280 nm) in amorphous TS and TES matrix are shown in Figure 5a and 5b, respectively. Tryptophan phosphorescence emission in TS and TES amorphous films appeared at ~450 nm. Tryptophan phosphorescence was temperature dependent over the temperature range from -10°C to 100°C in both amorphous TS and TES films. The decrease in phosphorescence intensity with increasing temperature results from thermally-stimulated deactivation processes (Parker, 1968).

The emission energy (ν_p) and bandwidth (Γ) were determined by fitting the phosphorescence emission spectra to a log-normal function (Eq. 1 and 2), Materials and Methods). The values of emission energy and bandwidth as a function of temperature are shown in Figure 6a and Figure 6b, respectively. There was a sharp decrease in the emission energy at low temperature followed by a steeper decrease at higher temperatures, indicating an increase in the average rate and thus extent of matrix dipolar relaxation around the excited triplet state with a transition temperature above ~50°C. The peak frequencies PF1, PF2 and PF3 (Figure 6a) decreased linearly in the glass at low temperature. Above 50°C the emission spectrum broadened and was fitted to a log-normal one function (PF2). The PF2 shows dramatic decrease and the slope became more negative above T_g of sucrose. The peak frequency values as a function of temperature were found to be super-imposable for tryptophan in TS and TES matrix.

The phosphorescence bandwidth increased gradually in the glass and then very sharply in the melt, reflecting a large increase in the range of energetically distinct matrix environments in amorphous sucrose below and above T_g (Figure 6b). The bandwidths FWHM1, FWHM2 and FWHM3 increased gradually with temperature in the glass and FWHM2 much more dramatically in the melt, reflecting a large increase in the range of energetically distinct environment above T_g . The bandwidth values as a function of temperature were found to be super-imposable for tryptophan in TS and TES matrix.

The peak frequency and bandwidth of tryptophan phosphorescence was not affected by presence of erythrosin B in the TES matrix and was comparable to the values in TS matrix.

Phosphorescence Intensity Decays: Tryptophan phosphorescence decay kinetics were also studied in the amorphous TES films and compared with intensity decays from TS films. Time-resolved phosphorescence intensity decays of tryptophan in amorphous films were measured over the temperature range from -10°C to 100°C . The intensity decays were fitted using multi-exponential function, but the best fit was generally obtained with a four-exponential function. The phosphorescence intensity decays of tryptophan in amorphous TES film at 20°C in the presence of nitrogen is plotted in Figure 7 along with the modified residuals for a fit using a four-exponential function (Eq. 3, Materials and Methods).

All intensity decays over the temperature interval from -10°C to 100°C were well fit using a four-exponential function. This analysis indicated that the tryptophan probe had multiple lifetimes in the amorphous TES matrix at all temperatures. The phosphorescence intensity decreased with increasing temperature indicating an increase in triplet state quenching rates with increase in temperature, the results of these lifetime analyses for tryptophan in TES are plotted in Figure 8a. The decrease in lifetime as a function of temperature was dramatic both below and above T_g , indicating the presence of a range of molecular motions both below and above T_g . A comparison of individual lifetime components τ_1 , τ_2 , τ_3 and τ_4 for tryptophan in TES and TS is shown in Figure 8b (longer lifetimes) and 8c (shorter lifetimes). There was no significant difference in the individual lifetime component of tryptophan in TES and TS films.

The average lifetime calculated using Eq. 4 (Material and Methods) is plotted in Figure 9 as a function of temperature. The average lifetime varied from ~ 1100 ms at -10°C to ~ 0.1 ms at 100°C . The decrease in tryptophan lifetime as a function of temperature corresponds to an increase in k_{NR} (Eq. 10, Materials and Methods), the rate of vibrational relaxation due to collisional quenching which is an indicator of the increase in matrix mobility. The decrease in lifetime was multi-phasic as a function of temperature. A comparison plot of average lifetimes of tryptophan in the TES and TS amorphous matrix is as shown in Figure 9. The average lifetimes of tryptophan were super-imposable and followed the same trend in TES and TS matrix. The amplitudes of each lifetime component in TES are plotted as a function of temperature in Figure 10. The amplitudes of the longer lifetime components decreased and that of the shorter lifetime components

increased as a function of temperature. A comparison of amplitudes a_1 , a_2 , a_3 and a_4 for tryptophan in TS and TES matrix is shown in Figure 10a, 10b, 10c and 10d, respectively. The non-radiative decay rate reflects the sum of all collisional interaction between the matrixes and the probe and is sensitive to molecular environments, and changes in this decay rate with change in physical state of the probe environments strongly modulate the phosphorescence lifetime giving rise to multiple lifetimes.

The comparison between TS and TES matrix, tryptophan lifetime and amplitudes values were found to be super imposable. This indicated that there is no interference from erythrosin B phosphorescence to tryptophan lifetime measurements.

The Arrhenius plot of natural log of k_p for average lifetime as function of inverse of temperature for tryptophan and erythrosin B dispersed in TES films is shown in Figure 11.

Conclusion

This research has investigated simultaneous measurements of mobility by using both erythrosin B and tryptophan in amorphous matrix. This would be a unique combination of probes, as they reported about molecular mobility independently without interfering with each other. Also there was no spectroscopic or physical interaction seen between erythrosin B and tryptophan. This research can be further developed for studying the physical behaviors of amorphous mixtures containing protein (tryptophan) and sugar (erythrosin B).

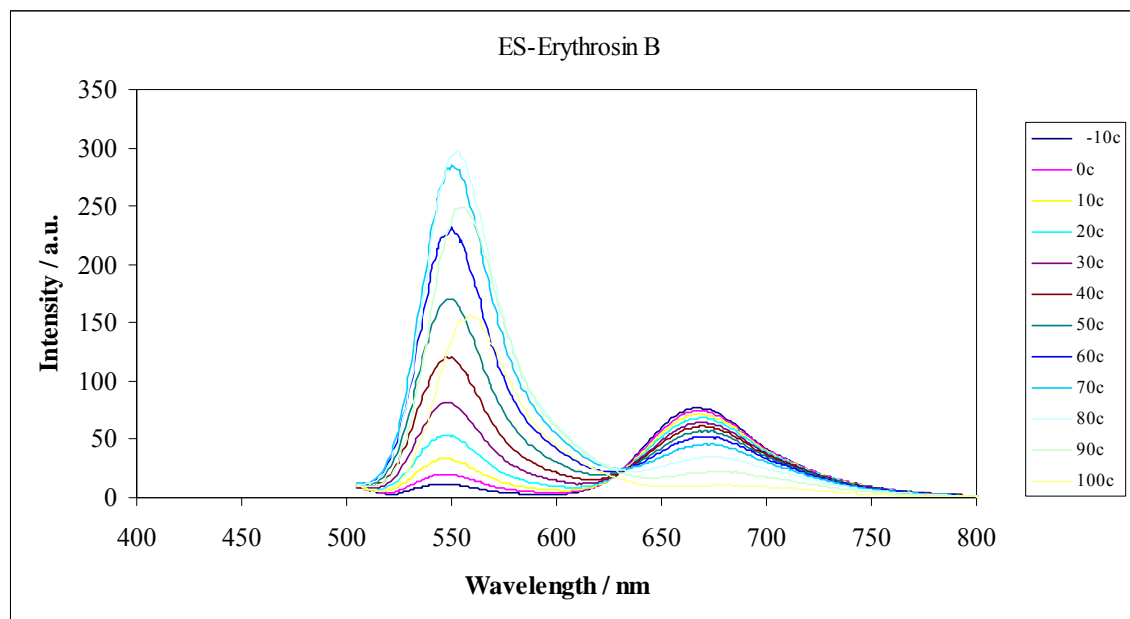
Erythrosin B**Figure IX-1a**

Figure IX-1a: Delayed emission spectra of erythrosin B dispersed in amorphous films of sucrose (referred as ES matrix) as a function of temperature (excitation at 500 nm). The spectra were collected at 10°C intervals from -10°C to 100°C (the curves follow this order from high to low intensity at ~690 nm).

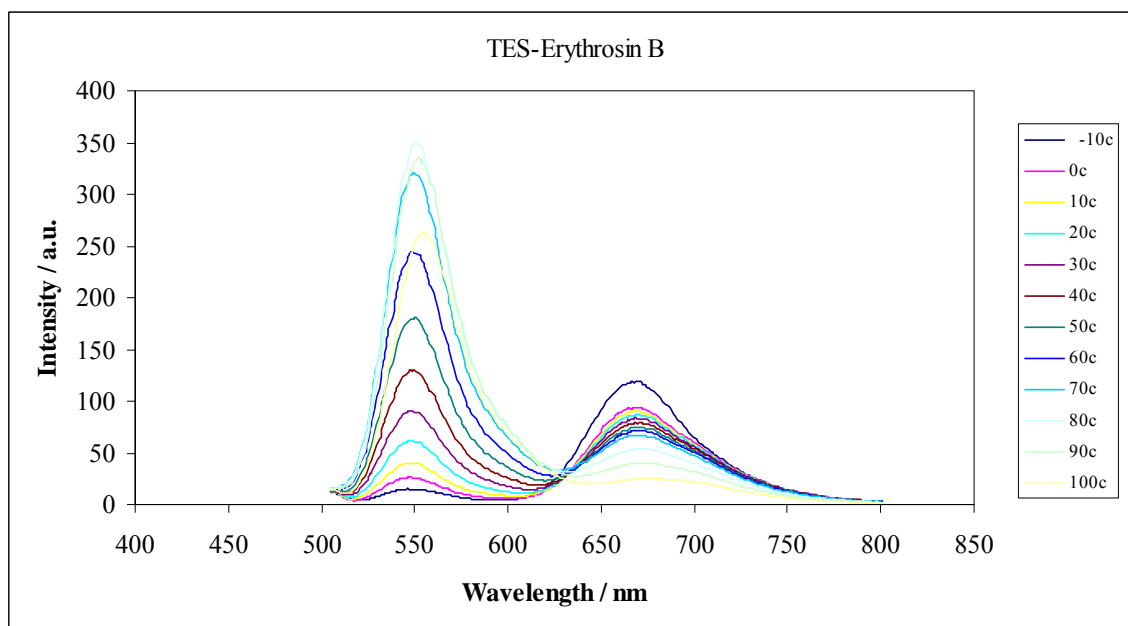
Figure IX-1b

Figure IX-1b: Delayed emission spectra of erythrosin B dispersed in amorphous films of sucrose also containing tryptophan (referred as TES matrix) as a function of temperature (excitation at 500 nm). The spectra were collected at 10°C intervals from -10°C to 100°C (the curves follow this order from high to low intensity at ~690 nm).

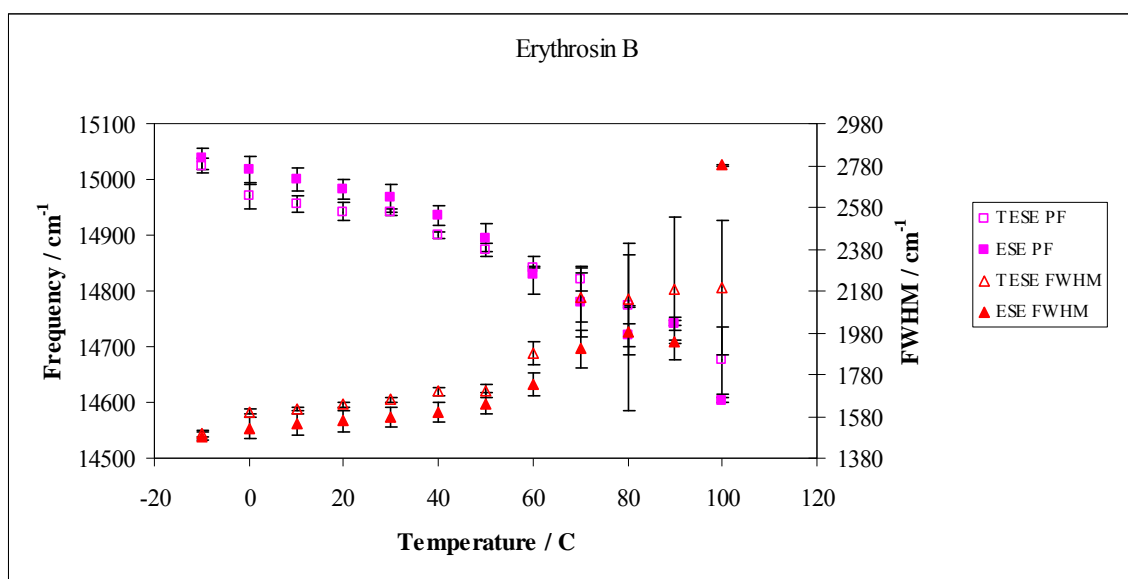
Figure IX-2

Figure IX-2: Peak energy ν_p (left hand scale) and bandwidth FWHM (right hand scale) for phosphorescence emission from erythrosin B in amorphous TES and ES films as a function of temperature. The spectra were collected every 10°C from -10°C to 100°C. The frequency is given by in (Δ) TES matrix and by (\blacktriangle) in ES matrix. The FWHM is given by (\diamond) in TES matrix and by (\blacklozenge) in ES matrix.

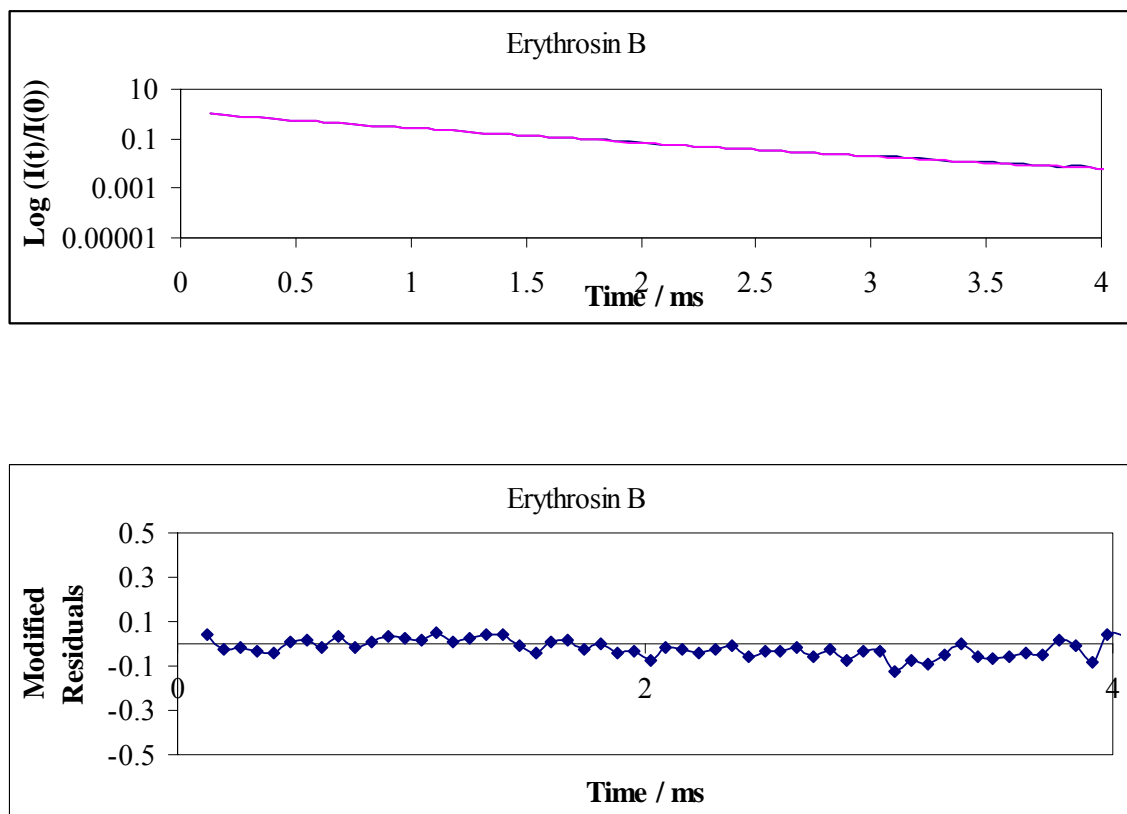
Figure IX-3

Figure IX-3: Normalized phosphorescence intensity decay $[I(t)/I(0)]$ of erythrosin B dispersed in amorphous TES films at 20°C in the presence of nitrogen. The solid lines through the data are fits using a stretched-exponential function. Below is the plot of modified residuals $[(\text{Data}-\text{Fit})/\text{Data}^{1/2}]$ for these fits to data plotted in the presence of nitrogen.

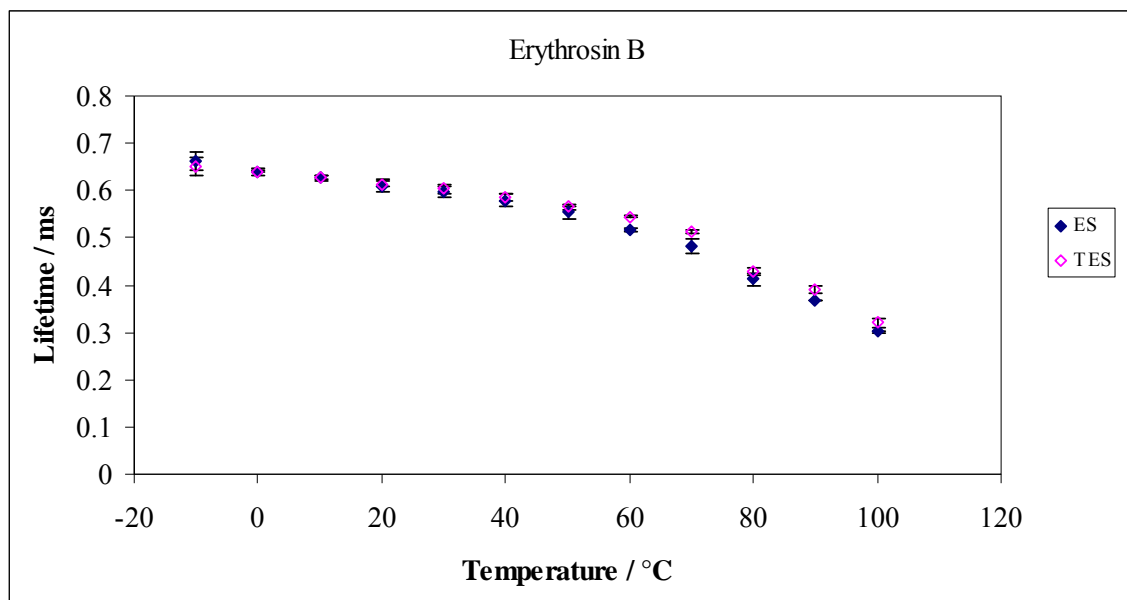
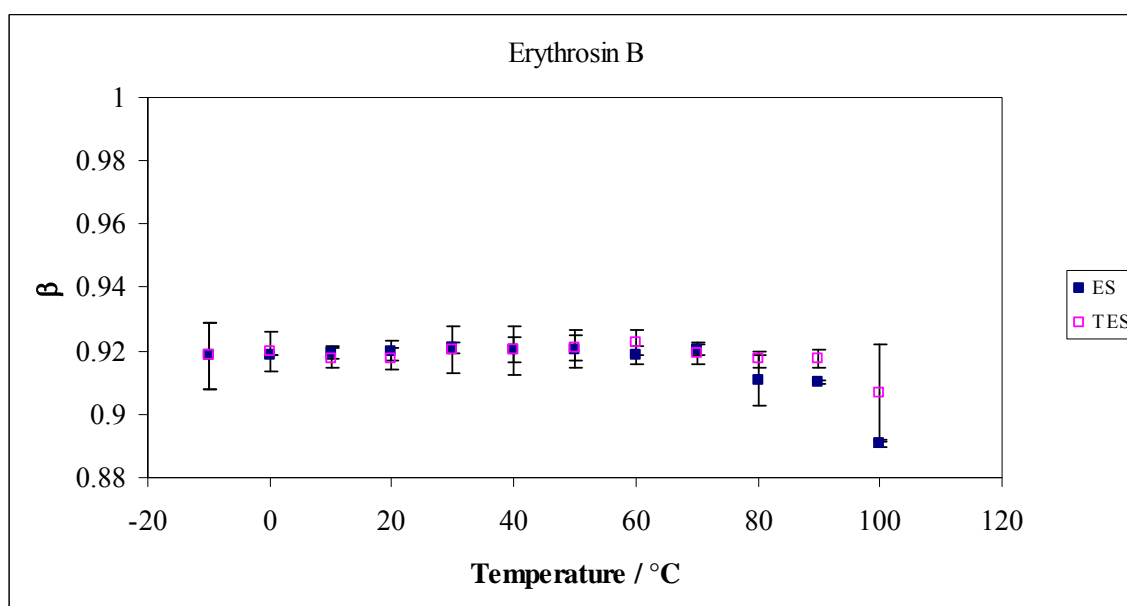
Figure IX-4a**Figure VIII-4b**

Figure IX 4a and 4b: Intensity decay fit parameters for erythrosin B in amorphous sucrose film ES and TES. The values were measured every 10°C from -10°C to 100°C. The measurements were made in the absence of oxygen. (a) Stretched exponential lifetimes in nitrogen as a function of temperature. (b) Stretched exponential fitting parameter β as a function of temperature.

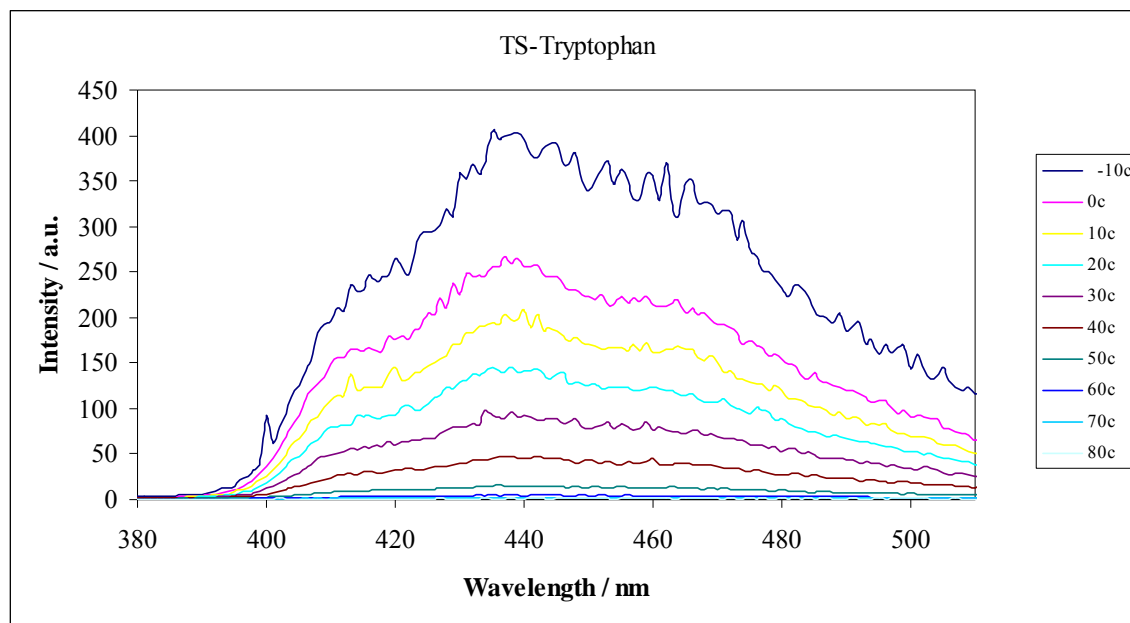
Tryptophan**Figure IX-5a**

Figure IX-5a: Delayed emission spectra of tryptophan dispersed in amorphous films of sucrose (referred as TS) as a function of temperature (excitation at 280 nm). The spectra were collected at 10°C intervals from -10°C to 80°C (the curves follow this order from high to low intensity at ~455 nm).

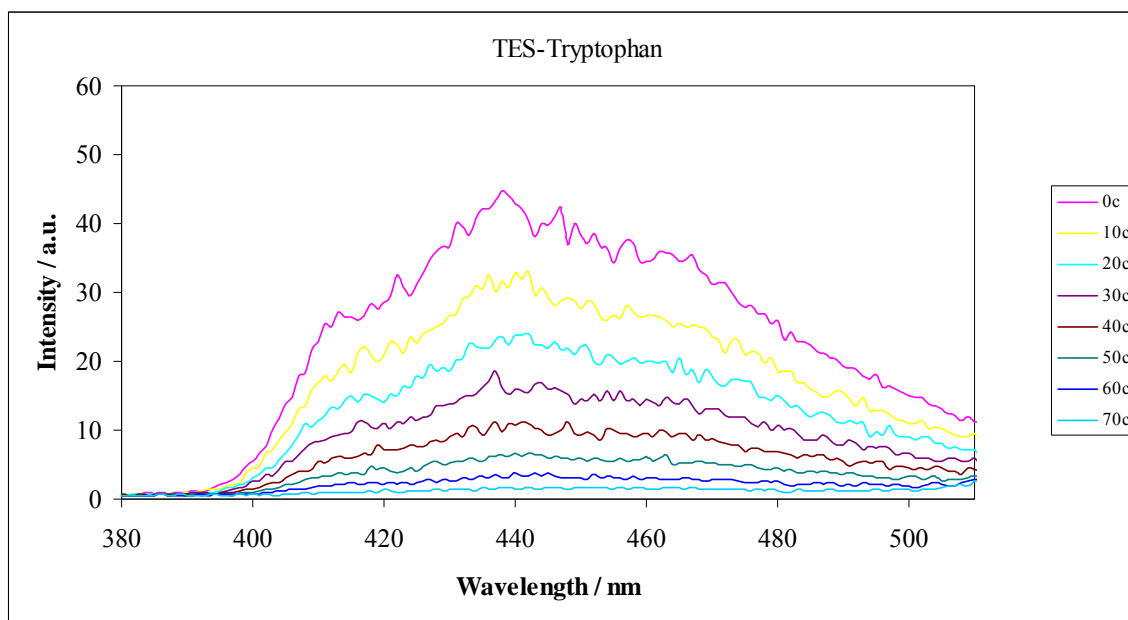
Figure IX-5b

Figure IX-5b: Delayed emission spectra of tryptophan dispersed in amorphous films of sucrose also containing erythrosin B (referred as TES matrix) as a function of temperature (excitation at 280 nm). The spectra were collected at 10°C intervals from - 0°C to 70°C (the curves follow this order from high to low intensity at ~455 nm).

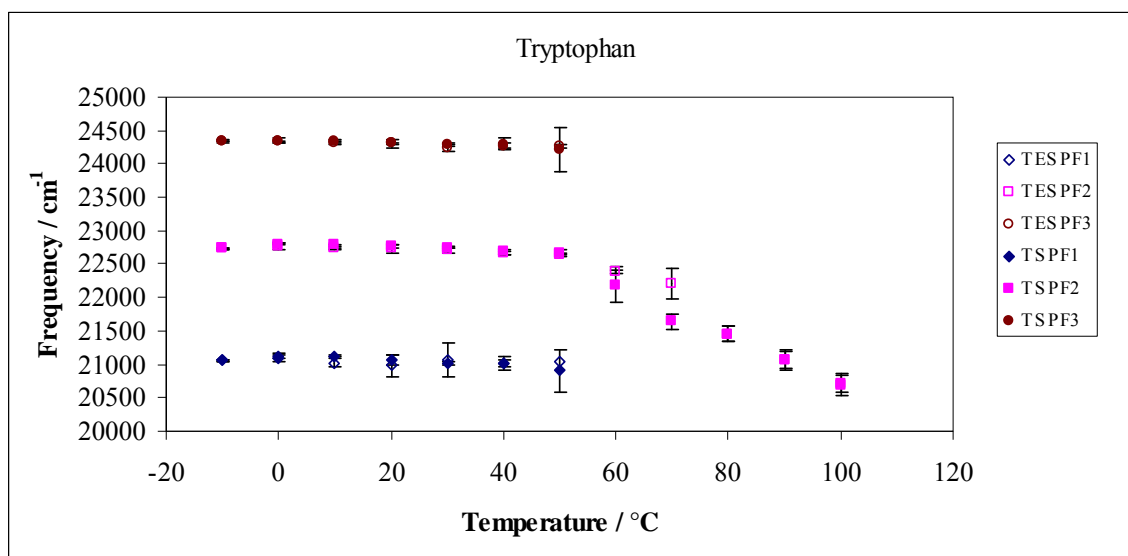
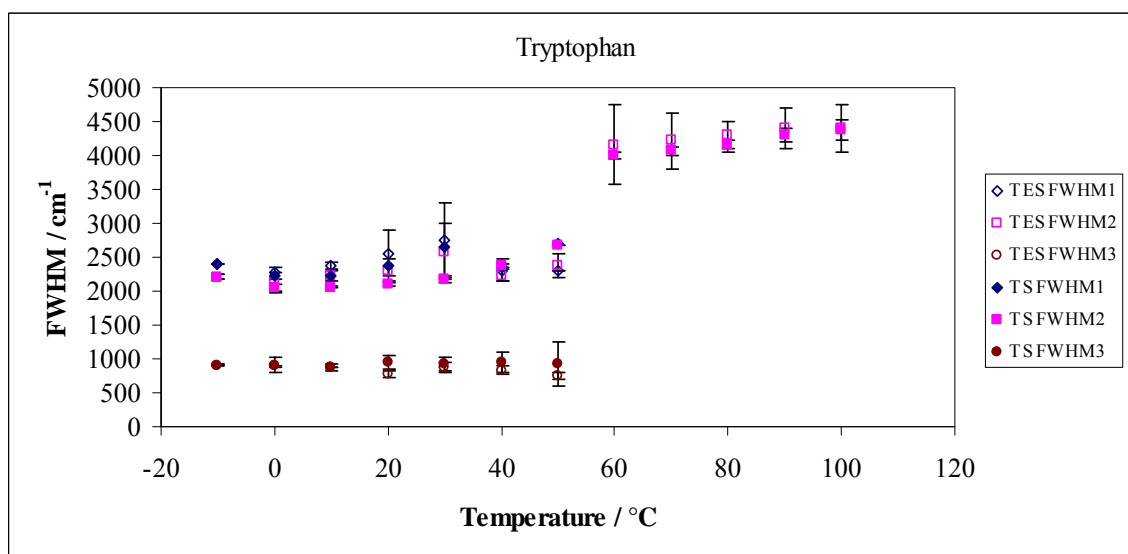
Figure IX-6a**Figure IX-6b**

Figure IX-6a and 6b: Peak energy ν_p (6a) and bandwidth (6b) for phosphorescence emission from tryptophan in amorphous films of TS and TES as a function of temperature. The delayed emission spectra collected as a function of temperature (Figure 5a and 5b) were analyzed using log-normal functions as described in Materials and Methods using eq. (1) and (2).

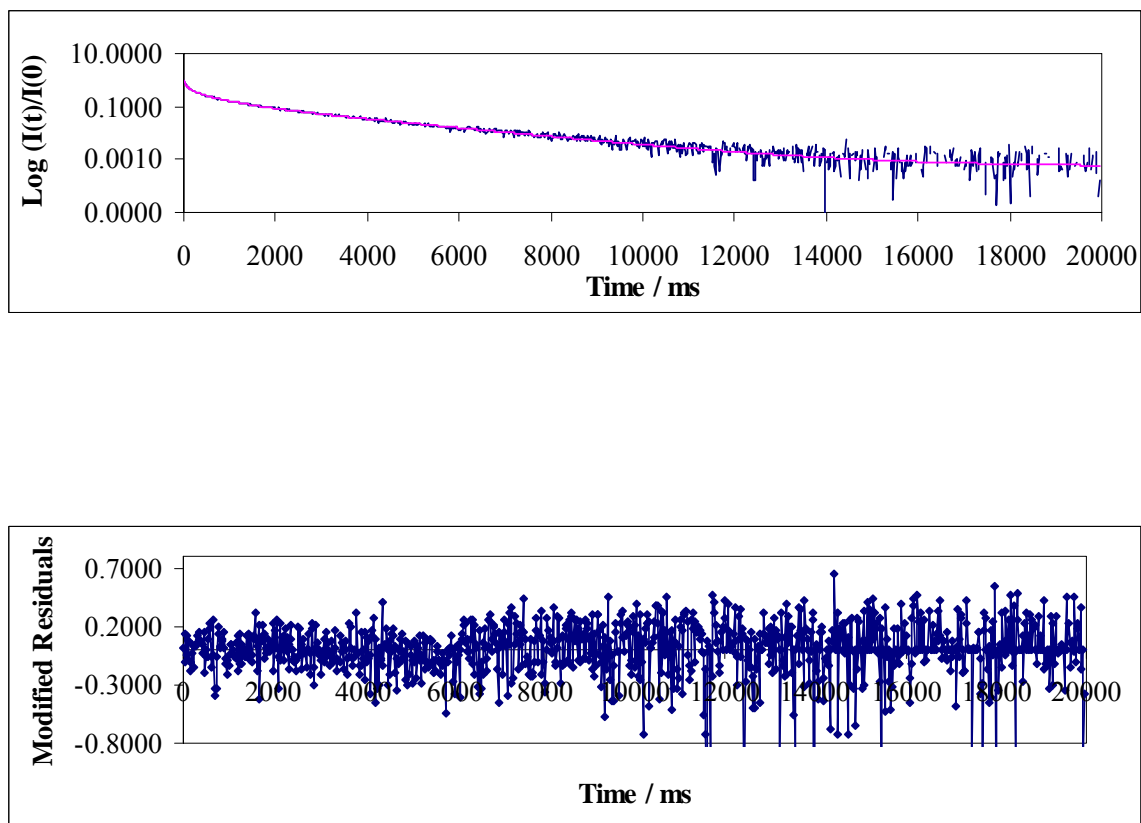
Figure IX-7

Figure IX-7: Normalized phosphorescence intensity decay $[I(t)/I(0)]$ of tryptophan dispersed in amorphous TES films at 20°C in the presence of nitrogen. The solid lines through the data are fits using a multi-exponential function. Below is the plot of modified residuals $[(\text{Data}-\text{Fit})/\text{Data}^{1/2}]$ for these fits to data plotted in the presence of nitrogen.

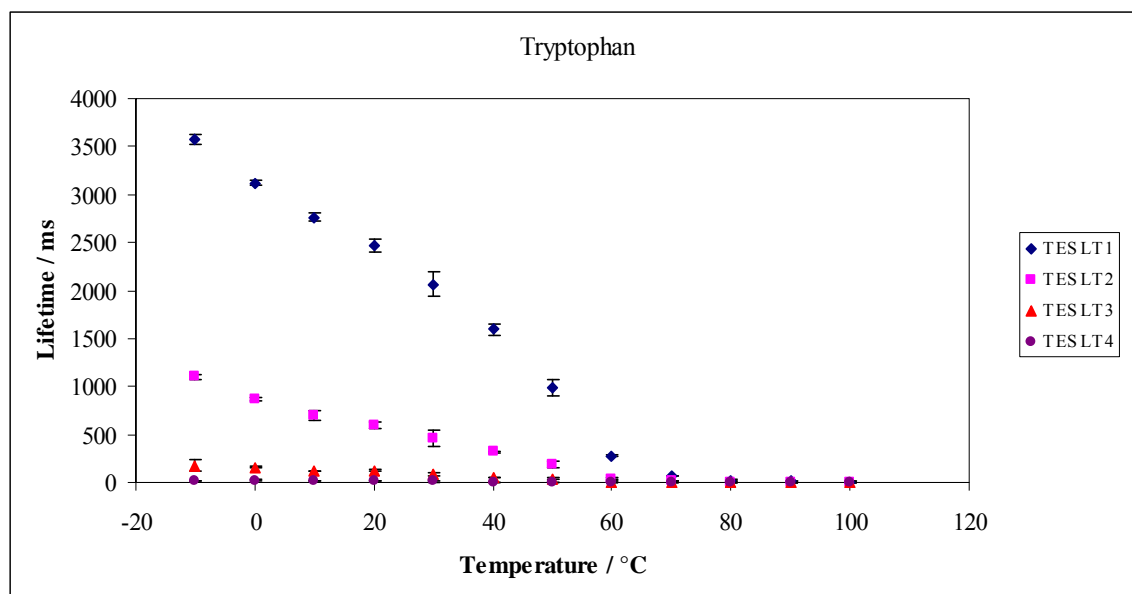
Figure IX-8a

Figure IX-8a: Lifetime components τ_1 (\blacklozenge), τ_2 (\blacksquare), τ_3 (\blacktriangle) and τ_4 (\bullet) obtained from a multi-exponential model fit to phosphorescence intensity decay data from tryptophan dispersed in amorphous films of TES equilibrated against nitrogen as a function of temperature. The data was calculated every 10°C from -10°C to 100°C.

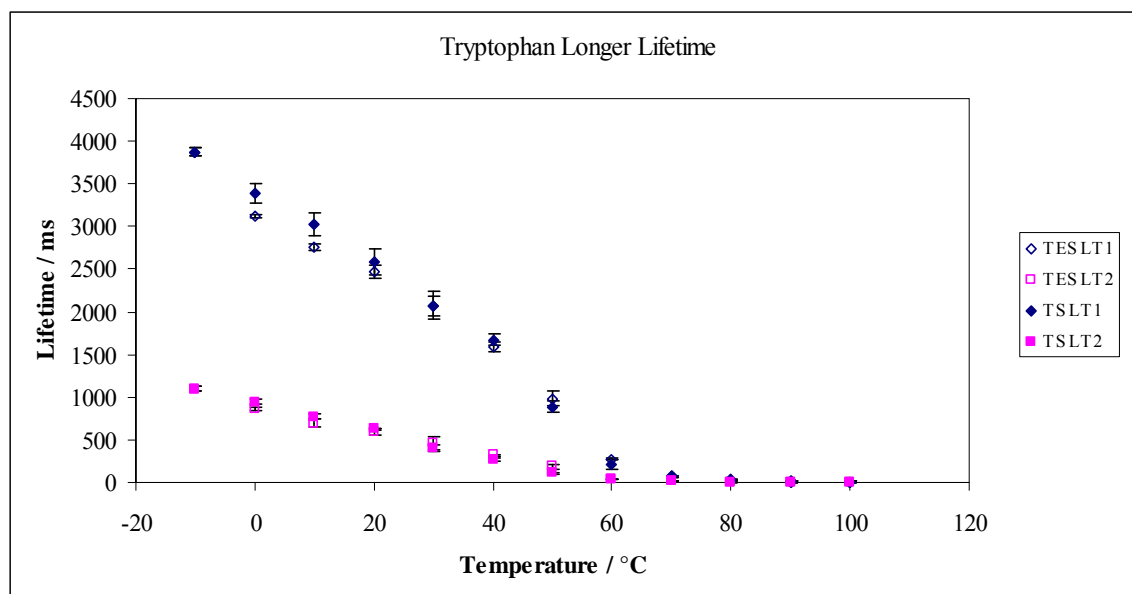
Figure IX-8b

Figure IX-8b: Comparison of longer lifetime components τ_1 (◆) and τ_2 (■) obtained from a multi-exponential model fit (Eq. (3), Materials and Methods) to phosphorescence intensity decay data from tryptophan dispersed in amorphous TES or TS films equilibrated against nitrogen as a function of temperature. The data was calculated every 10°C from -10°C to 100°C.

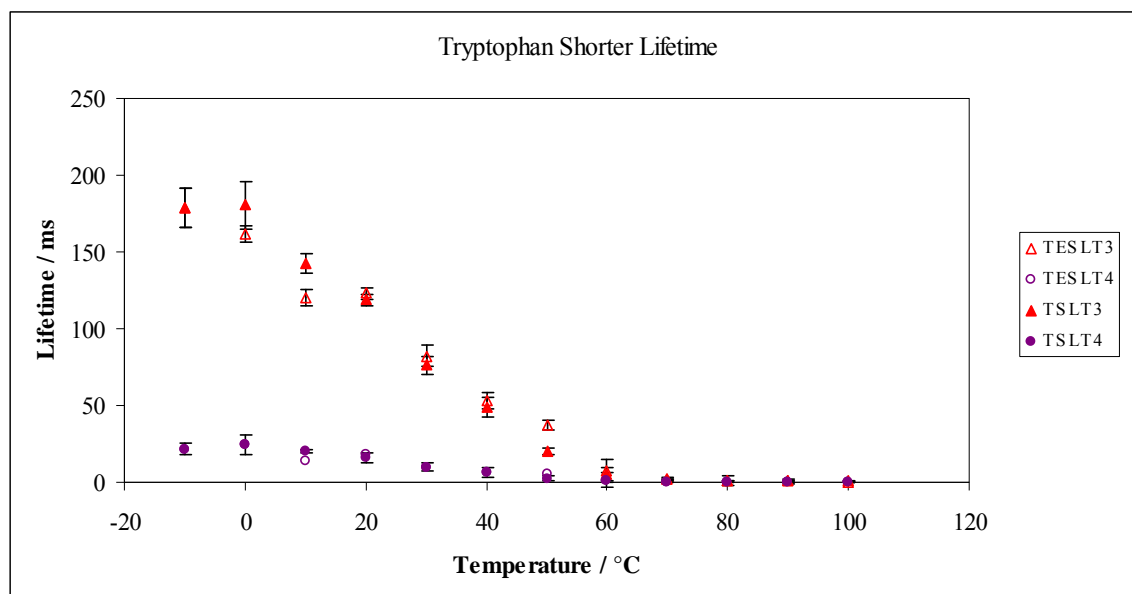
Figure IX-8c

Figure IX-8c: Comparison of shorter lifetime components τ_1 (\blacklozenge) and τ_2 (\blacksquare) obtained from a multi-exponential model fit (Eq. (3), Materials and Methods) to phosphorescence intensity decay data from tryptophan dispersed in amorphous TES or TS films equilibrated against nitrogen as a function of temperature. The data was calculated every 10°C from -10°C to 100°C.

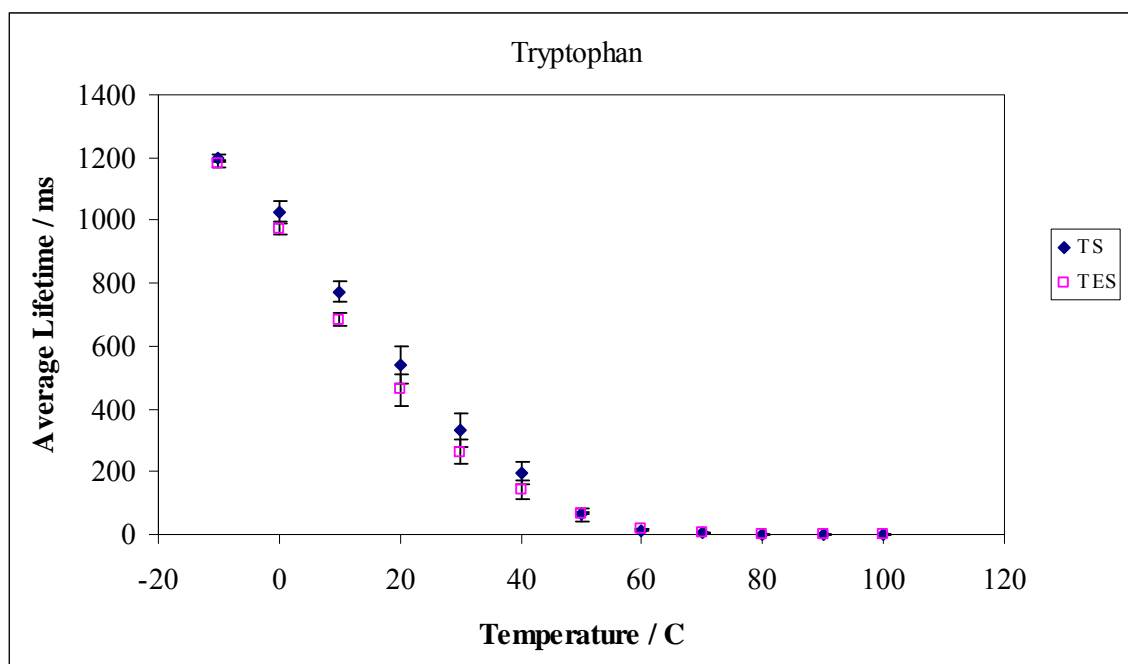
Figure IX-9

Figure IX-9: The average lifetime of tryptophan in TES and TS films obtained from a multi-exponential model fit equilibrated against nitrogen as a function of temperature. The data were collected every 10°C from -10°C to 100°C.

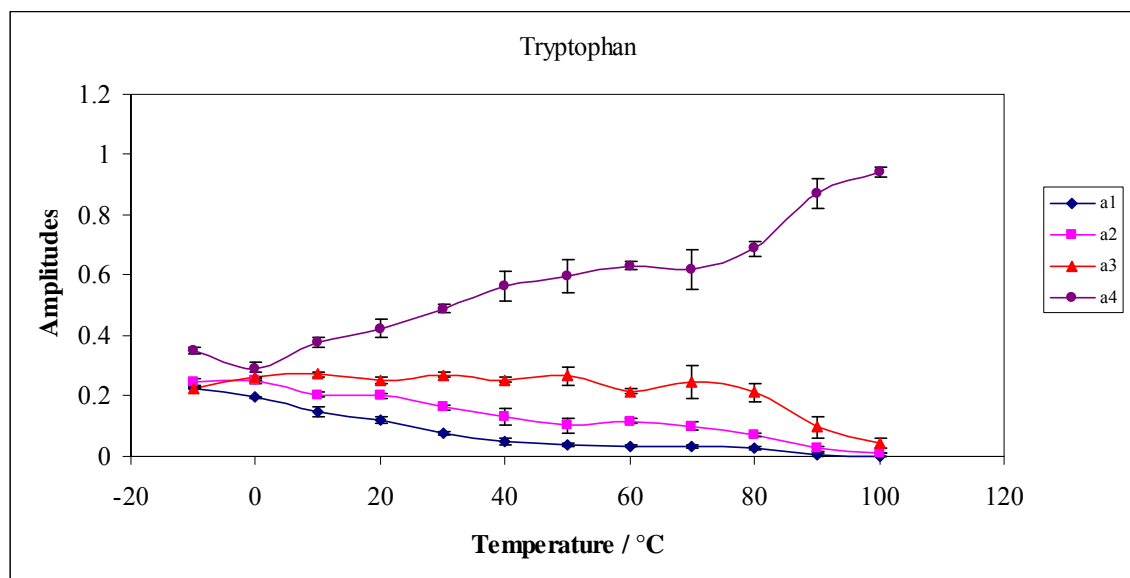
Figure IX-10

Figure IX-10: Intensity decay fit parameters amplitude for tryptophan in amorphous TES film in nitrogen as a function of temperature. The data was calculated every 10°C from -10°C to 100°C. The amplitudes a1 (♦) and a2 (■) correspond to the longer life time components (τ_1 , τ_2) and a3 (▲) and a4 (●) correspond to the shorter lifetime components (τ_3 , τ_4). The amplitudes were obtained from a multi exponential model fit (Eq. (3), Materials and Methods) to phosphorescence intensity decay data from tryptophan dispersed in TES films equilibrated against nitrogen as a function of temperature.

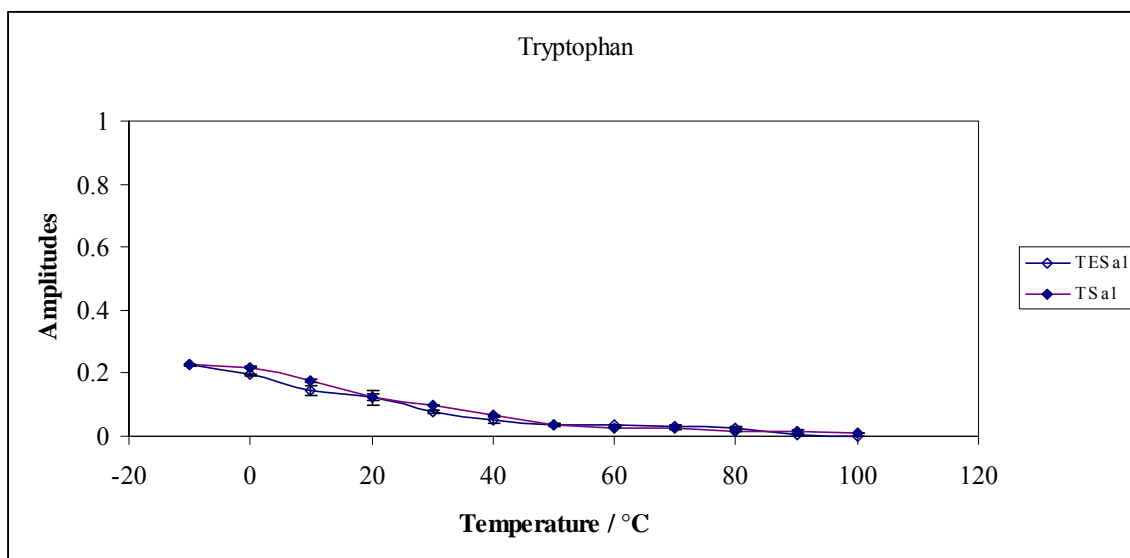
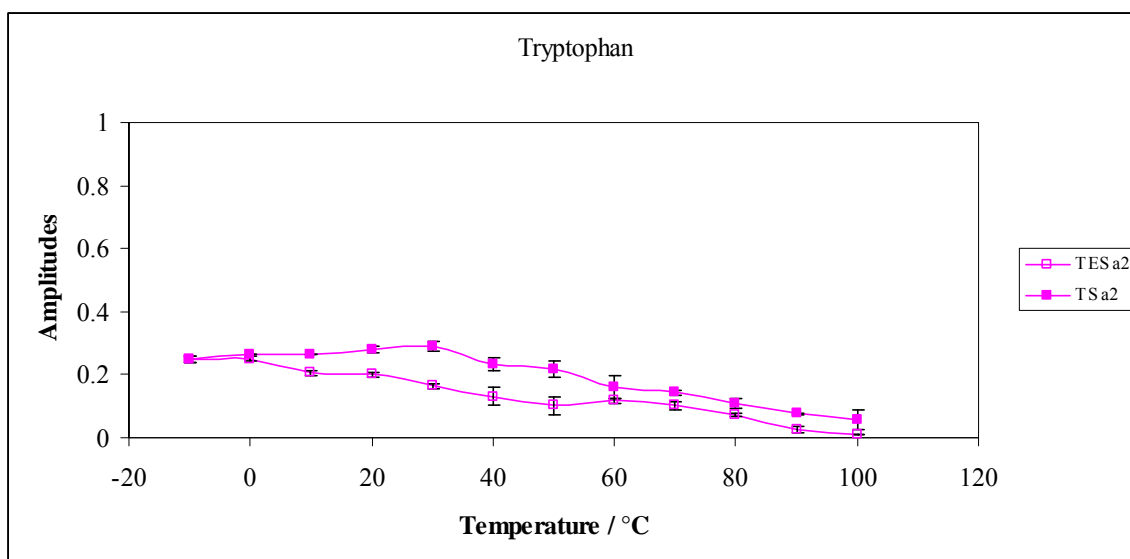
Figure IX-10a*Figure IX-10b*

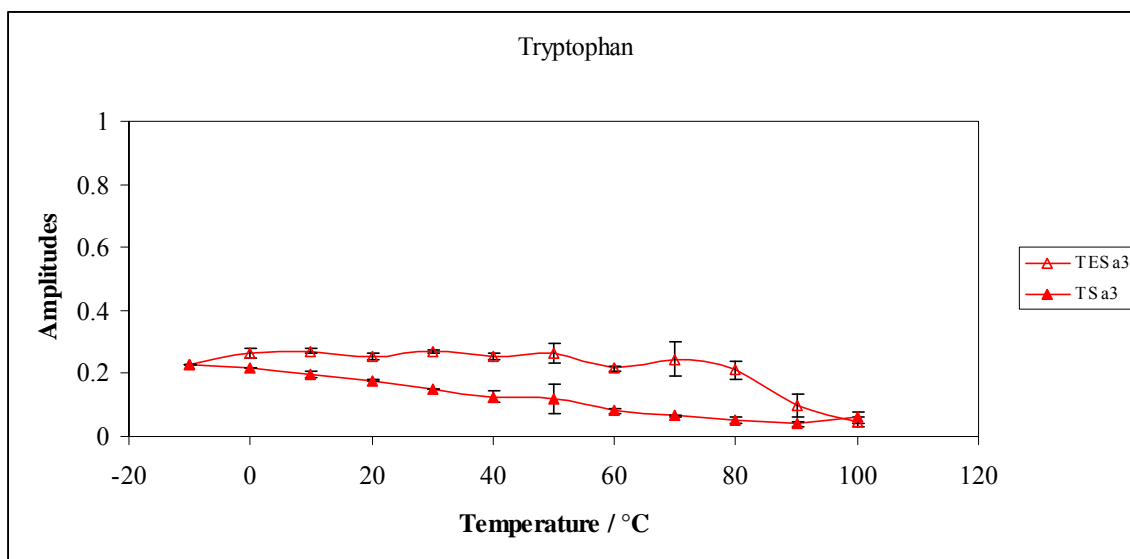
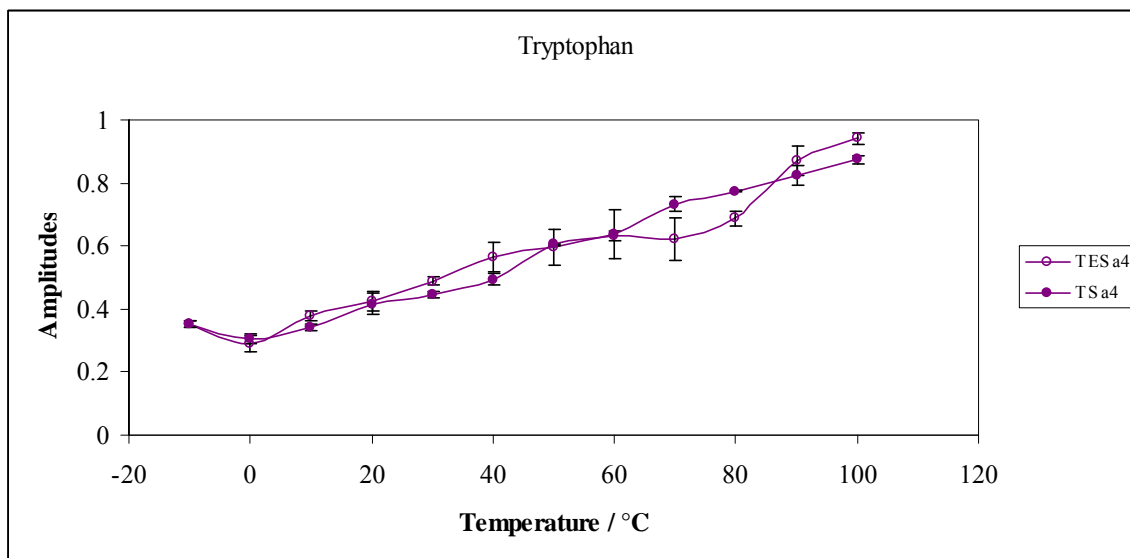
Figure IX-10c**Figure IX-10d**

Figure IX-10a-10d: Comparing the intensity decay fit amplitudes for tryptophan in amorphous TES and TS film in nitrogen as a function of temperature.

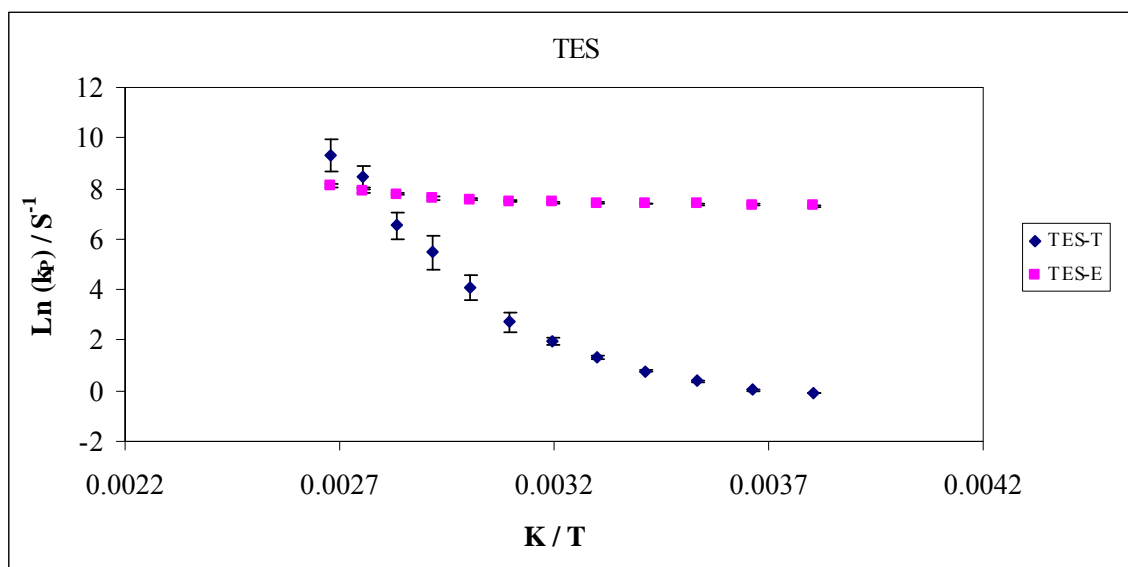
Figure IX-11

Figure IX-11: The Arrhenius plot of natural log of k_p for average lifetime as function of inverse of temperature for tryptophan and erythrosin B dispersed in TES films.

References

- Champion, D., Le Meste, M. and Simatos, D. Towards an improved understanding of glass transition and relaxations in foods: molecular mobility in the glass transition range. *Trends in Food Science and Technology*. 11 (2000). 41-55.
- Chen, R. Apparent stretched exponential luminescence decay in crystalline solids. *Journal of Luminescence*. 102-103 (2003). 510-518.
- Duchowicz, R., Ferrer, M. L. and Acuna, A. U. Kinetic spectroscopy of erythrosin phosphorescence and delayed fluorescence in aqueous solution at room temperature. *Photochemistry and Photobiology*. 68 (1998). 494-501.
- Fischer, C. J., Gafni, A., Steel, D. G. and Schauerte, J. A. The triplet-state lifetime of indole in aqueous and viscous environments: significance to the interpretation of room temperature phosphorescence in proteins. *Journal of the American Chemical Society*. 124 (2004). 10359-10266.
- Lettinga, M. P., Zuilof, H. and Van Zandvoort, M. A. M. J. Phosphorescence and fluorescence characterization of fluorescein derivatives immobilized in various polymers matrices. *Physical Chemistry Chemical Physics*. 2 (2000). 3697-3707.
- Lindsey, C. P. and Patterson, G. D. Detailed comparison of the Williams-Watts and Cole-Davidson functions. *Journal of Chemical Physics*. 2 (1980). 3348-3357.
- Maroncelli, M. and Fleming, G. R. Picosecond salvation dynamics of coumarin 153: The importance of molecular aspects of salvation. *Journal of Chemical Physics*. 86 (1987). 6221-6239.
- McCaul, C. P. and Ludescher, R. D. Room temperature phosphorescence from tryptophan and halogenated tryptophan analogs in amorphous sucrose. *Photochemistry and Photobiology*. 70 (1999). 166-171.
- Nack, T. J. and Ludescher, R. D. Molecular mobility and oxygen permeability in amorphous bovine serum albumin films. *Food Biophysics*. 1 (2006). 151-162.
- Papp, S. and Vanderkooi, J. M. Tryptophan phosphorescence at room temperature as a tool to study protein structure and dynamics. *Photochemistry and Photobiology*. 49 (1989). 775-784.
- Pravinata, L.V., You, Y. and Ludescher, R. D. Erythrosin B phosphorescence monitors molecular mobility and dynamic heterogeneity in amorphous sucrose. *Biophysical Journal*. 88 (2005). 3551-3561.
- Richert, R. Triplet state salvation dynamics: Basics and applications. *Journal of Chemical Physics*. 113 (2000). 8404-8429.

- Shah, N. K. and Ludescher, R. D. Hydration and the internal dynamics of hen egg white lysozyme. *Proceedings of SPIE*. 1640 (1992). 174-179.
- Shah, N. K. and Ludescher, R. D. Influence of hydration on the internal dynamics of hen egg white lysozyme in the dry state. *Photochemistry and Photobiology*. 58 (1993). 169-174.
- Shah, N. K. and Ludescher, R. D. Phosphorescence of probes of the glassy state in amorphous sucrose. *Biotechnology Progress*. 11 (1995). 540-544.
- Shamblin, S., Hancock, B. C., Dupuis, Y. and Pikal, M. J. Interpretation of relaxation time constants for amorphous pharmaceutical systems. *Journal of Pharmaceutical Sciences*. 89 (2000). 417-427.
- Shirke, S. and Ludescher, R. D. Dynamic site heterogeneity in amorphous lactose and lactitol from spectral heterogeneity in erythrosin B phosphorescence. *Biophysical Chemistry*. 123 (2006). 122-133.
- Shirke, S. and Ludescher, R. D. Dynamic site heterogeneity in amorphous maltose and maltitol from spectral heterogeneity in erythrosin B phosphorescence. *Carbohydrate Research*. 340 (2005). 2661-2669.
- Simon-Lukasik, K. V. and Ludescher, R. D. Effect of plasticizer on dynamic site heterogeneity in cold-cast gelatin films. *Food Hydrocolloids*. 20 (2006a). 88-95.
- Simon-Lukasik, K. V. and Ludescher, R. D. Molecular mobility in water and glycerol plasticized cold and hot cast gelatin films. *Food Hydrocolloids*. 20 (2006b). 96-105.
- Strambini, G. B. and Gonnelli, M. The indole nucleus triplet-state lifetime and its dependence on solvent microviscosity. *Chemical Physics Letters*. 115 (1985). 196-200.
- Sundaresan, K. V. and Ludescher, R. D. Molecular mobility and oxygen permeability in amorphous beta-lactoglobulin films. 22 (2007). 403-413.
- Vanderkooi, J. M. and Berger, J. W. Excited triplet state used to study biological macromolecules at room temperature. *Biochimica et Biophysica Acta: Bioenergetics*. 976 (1989). 1-27.
- Vanderkooi, J. M., Maniara, Green, T. J. and Wilson, D. F. An optical method for measurement of dioxygen concentration based upon quenching of phosphorescence. *Journal of Biological Chemistry*. 262 (1987). 5476-5482.

- Zunic, A. Molecular mobility of amorphous disaccharide studied by tryptophan luminescence. Master Thesis. Rutgers University. New Brunswick, NJ. (2004).

CHAPTER X: Investigating the potential of using multiple probes vanillin and tryptophan in amorphous sucrose films to report molecular mobility.

Introduction

This study is an extension of our previous work on the probe combinations erythrosin B: vanillin and erythrosin B: tryptophan dispersed in amorphous sucrose film (Chapter VIII and IX) used to report molecular mobility. Current research also recognizes the importance of understanding the local dynamics in amorphous mixtures using the tryptophan and vanillin combination.

We have recently shown that vanillin can be used as a triplet state probe to monitor molecular mobility in amorphous solids (Chapter II). Vanillin phosphorescence lifetime and quantum yield were found to be extremely sensitive to the local environment in amorphous solid sucrose or protein in the glassy state and at the glass-to-rubber transition into the melt. Vanillin was also shown to be promising in reporting molecular mobility in amorphous sucrose films in the dual probe combination with erythrosin B (Chapter VIII).

Tryptophan is a naturally occurring amino acid and has been shown to exhibit strong room temperature phosphorescence emission after excluding oxygen in proteins (Vanderkooi et al., 1987; Simon-Lukasik and Ludescher, 2006a, 2006b) and sugars (McCaul and Ludescher, 1999, Shah and Ludescher, 1995, Zunic, 2004). Tryptophan phosphorescence has been found to be sensitive to the physical properties of the local environment (Ludescher, 2001, Strambini and Gonnelli, 1985). Also the triplet state of indole has been shown to have a strong dependence of the radiation-less deactivation

rate on medium viscosity; the lifetime of tryptophan decreases from 6.5s in a glassy matrix to 1.2 ns in aqueous solutions at ambient temperature (Strambini and Gonnelli, 1995).

In this study molecular mobility was studied in the amorphous sucrose films by monitoring phosphorescence from dual probe combinations of vanillin: tryptophan. A comparison of the data was made with data obtained from individually dispersed probes in amorphous sucrose films.

Materials and Methods

Sucrose Solution: Sucrose solution was made as described in Pravinata et al 2005. Approximately 20 g of sucrose (99.5% pure; Sigma Chemical, St. Louis, MO) were dissolved in 100 mL of deionized water containing 0.5 g of activated charcoal to remove luminescent impurities. After stirring overnight, the charcoal was removed by vacuum filtration using ashless filter paper (Whatman No. 40, Whatman International, Maidstone, UK), additional charcoal was added, and the process repeated. Sucrose solution was made to a final concentration of 65–67 wt % sucrose; concentration was confirmed using a refractometer (NSG Precision Cells, Farmingdale, NY). This sucrose solution was filtered through a 0.2 μm membrane to remove particulates.

Tryptophan: A 50mM stock solution of tryptophan (Sigma Chemical, St. Louis, MO) was prepared in distilled deionized water. This concentration was selected to simplify the addition of the probe to the sucrose solution. For measuring phosphorescence in amorphous sucrose films, tryptophan was added to the sucrose solution at a molar ratio of 1:500 (dye: sucrose). The ratio 1:500 (dye: sucrose) was chosen as at this concentration it was determined that the probe does not aggregate, existing only as individual molecules monitoring the molecular mobility of the sucrose.

Vanillin: A 66mM stock solution of vanillin (Sigma-Aldrich, Milwaukee, WI) was prepared in distilled deionized water. This concentration was selected to simplify the addition of the probe to the sucrose solution. For absorbance, fluorescence and phosphorescence measurements the 66mM stock was diluted to 50 μM in distilled

deionized water. For measuring absorbance and phosphorescence in amorphous solid, methyl vanillin was added to the sucrose solution at a molar ratio of $1:10^3$ (dye: sucrose). Other ratios $3:10^4$, $5:10^4$ and $2:10^3$ were also tested to study the effect of probe concentration. The ratio $1:10^3$ (dye: sucrose) was chosen as at this concentration it was determined that the probe does not aggregate, existing only as individual molecules monitoring the molecular mobility of the sucrose.

Sucrose films: To produce glassy sucrose films containing both erythrosin B at $(1:10^4)$ and vanillin at $(1:10^3)$, 20 μL of a sucrose solution containing erythrosin B and vanillin were spread on a quartz slide ($30 \times 13.5 \times 0.6$ mm; custom made by NSG Precision Cells, Farmingdale, NY). After spreading the solutions on the slides were then dried under a heat gun (Vidal Sassoon) for 5 min to a maximum temperature of $\sim 88^\circ\text{C}$ (measured using a thermocouple probe) and the final thickness was ~ 0.05 mm. The slides were stored at room temperature against P_2O_5 and Drierite, protected from the light to prevent any photobleaching, for at least 7 days before any phosphorescence measurements were made. The desiccant was refreshed as needed to maintain a relative humidity close to 0%.

Instrumentation: Measurements were made on a Cary Eclipse fluorescence spectrophotometer (Varian Instruments, Walnut Creek, CA). This instrument, which collects in analog mode, uses a high intensity pulsed lamp and a time delay was employed to avoid any fluorescence during the lamp pulse. The temperature was controlled by using a TLC 50 thermoelectric heating/cooling system (Quantum

Northwest, Spokane, WA). The TLC-50 sample compartment was fitted with a jacketed cover. The measurements were made in absence of oxygen (Nitrogen was purged for 15 minutes). Nitrogen stream was generated by passage of high purity nitrogen through a Supelco (Bellefonte, PA) carrier gas purifier. Quartz slides were placed in the standard 1cm x 1cm x 1cm quartz fluorescence cuvette, which was capped with a lid having inlet and outlet ports of gas lines.

Luminescence Measurements

The Cary Eclipse uses a pulsed lamp and collects emission intensity in analog mode; data were not collected within the first 0.1-0.2 ms to suppress fluorescence coincident with the lamp pulse.

Tryptophan Protocol: Delayed luminescence emission spectra were collected from 350 to 600 nm (10 nm bandwidth) using excitation at 280 nm (20nm bandwidth) over the temperature range from -10°C to 100°C . Each data point was collected from a single flash with 0.2 ms delay, 10 ms gate time, and 1.0 s total decay time. The phosphorescence spectra collected as a function of temperature in the presence of nitrogen, were converted to intensity versus frequency (cm^{-1}) and analyzed to obtain the peak frequency and spectral bandwidth using eq. (1) and (2) (Maroncelli and Fleming, 1987). Lifetime measurements were made in the presence of nitrogen ($-\text{O}_2$) as a function of temperature. The samples were excited at 280 nm (20 nm bandwidth) and emission transients collected in TVS at 405 nm, TS (a) 455 nm and TS (b) 405 nm (20 nm bandwidth) at temperatures ranging from -10°C to 100°C . Each decay transient was the

sum of 50 cycles, and for each cycle data was collected from a single lamp flash with a delay of 0.2 ms. Windows for gate time and total decay time were varied at each temperature. All measurements were made in quadruplicate. A similar measurement was also made for amorphous sucrose film containing just tryptophan for comparison. To check for spectroscopic interference from vanillin, tryptophan was also excited using vanillin protocol.

Vanillin Protocol: Delayed luminescence emission spectra of vanillin in amorphous sucrose were collected from 400 to 800 nm (10 nm bandwidth) using excitation at 320 nm (20 nm bandwidth) over the temperature range from -10°C to 100°C . Each data point was collected from a single flash with 0.2 ms delay, 100 ms gate time, and 0.12 s total decay time. The phosphorescence spectra collected as a function of temperature in the presence of nitrogen, were converted to intensity versus frequency (cm^{-1}) and analyzed to obtain the peak frequency and spectral bandwidth using eq. (1) and (2) (Maroncelli and Fleming, 1987). Lifetime measurements were made as a function of temperature. The samples were excited at 320 nm (20 nm bandwidth) and emission transients collected at 490 nm (20 nm bandwidth) at temperature ranging from -10°C to 100°C . Each decay was the average of 50 cycles, and for each cycle data was collected from a single flash with a delay of 0.2 ms, windows for gate time and total decay time were varied at each temperature. All measurements were made in quadruplicate. A similar measurement was also made for amorphous sucrose film containing just vanillin for comparison. To check spectroscopic interference from tryptophan, vanillin was also excited using tryptophan protocol.

Data Analysis

Emission Energy as a function of temperature: Emission spectra were fit using the program Igor (Wavemetrics, Inc., Lake Oswego, OR) to a log-normal function over the temperature range Equation 1.

$$I(\nu) = I_0 \exp \left\{ -\ln(2) \left(\frac{\ln[1 + 2b(\nu - \nu_p) / \Delta]}{b} \right)^2 \right\} \quad (1)$$

In this equation I_0 is the maximum intensity of the emission spectra, ν_p is the frequency (in cm^{-1}) of the emission maximum, Δ is a line width parameter, and b is an asymmetry parameter. The bandwidth of the emission, the full width at half maximum (Γ), is related to b and Δ Equation 2.

$$\Gamma = \Delta \left(\frac{\sinh(b)}{b} \right) \quad (2)$$

Phosphorescence Intensity: Phosphorescence lifetimes were determined with the statistical program Igor (Wavemetrics, Inc., Lake Oswego, OR). The phosphorescence intensity decays were collected as described above and were fitted using a multi-exponential function for tryptophan and vanillin (Shamblin et al., 2000). Fits were judged satisfactory if the r^2 values were in the range of 0.995-1.0 and the modified residuals $((\text{data} - \text{fit})/\text{data}^{1/2})$ varied randomly about zero.

Multi-exponential function: The multi-exponential model is as show in Equation 3. τ_i are decay times, α_i represent the amplitudes of the components at $t = 0$ and n is the number of decay times. The average lifetime was calculated using Equation 4.

$$I(t) = \sum_{i=1}^n \alpha_i \exp(-t/\tau_i) \quad (3)$$

$$\tau_{\text{Avg}} = \sum_{i=1}^n \alpha_i \tau_i / \sum_{i=1}^n \alpha_i \quad (4)$$

Photophysical Scheme: The phosphorescence lifetimes were interpreted in terms of the rate constants associated with the various processes that contribute to the de-excitation of the excited triplet state of the probe (Duchowicz et al., 1998). The phosphorescence lifetimes were used to calculate the rate constants associated with the various processes that depopulate the excited triplet state. The term k_p ($=1/\tau$) is the total decay rate, k_{RP} is the rate of radiative decay of the triplet state. The magnitude of k_{NR} reflects factors associated with the mechanism by which the excited T_1 state is coupled to highly excited vibrations of the S_0 ground state as well as external factors associated with the mechanism by which the ground state vibrational energy can dissipate from the excited state into the surrounding matrix (Fischer et al., 20002; Vanderkooi and Berger, 1989). As the efficiency of external vibrational dissipation is related to overall mobility of the matrix, the magnitude of k_{NR} provides a measure of matrix mobility. The term k_Q [Q]

refers to the collisional quenching due to interaction between the excited chromophore and a quencher molecule for example triplet state oxygen.

Tryptophan and Vanillin: The lifetime τ is related to the rate constants for de-excitation of the triplet excited state of the probe according to the following Equation 5 (Papp and Vanderkooi, 1989).

$$1/\tau = k_{RP} + k_{NR} (T) + k_Q [Q] = k_P \quad (5)$$

Here $k_P (=1/\tau)$ is the total decay rate, k_{RP} is the rate of radiative decay of the ground state, k_{NR} is the rate of non-radiative decay to the singlet state followed by vibrational relaxation to S_0 due to collisional quenching. The term $k_Q [Q]$ refers to the collisional quenching due to interaction between the excited chromophore and a quencher molecule for example triplet state oxygen.

Results and Discussion

Delayed luminescence emission spectra were collected as a function of temperature in presence of nitrogen from vanillin and tryptophan dispersed together in amorphous sucrose films (vanillin + tryptophan + sucrose referred as TVS) and compared to spectra from individual probes dispersed singly in sucrose (vanillin + sucrose referred as VS) and (tryptophan + sucrose referred as TS). Three spectroscopic measures of molecular mobility were made: emission energy, emission bandwidth and emission lifetime.

Vanillin:

Delayed Luminescence Spectra: The delayed emission spectra from vanillin (excited at 320 nm) in amorphous VS and TVS matrix are shown in Figure 1a and 1b, respectively. Vanillin phosphorescence emission in VS and TVS amorphous films appeared at ~490nm. Vanillin phosphorescence was temperature dependent over the range from -10°C to 100°C in both amorphous VS and TVS films. The decrease in phosphorescence intensity with increasing temperature results from thermally-stimulated deactivation processes (Parker, 1968).

The emission energy (γ_p) and bandwidth (Γ) were determined by fitting the phosphorescence emission spectra to a log-normal function Eq. 1 and 2 (Materials and Methods). The values of emission energy and bandwidth as a function of temperature are shown in Figure 2. There was a gradual decrease in the emission energy at low temperature followed by a steeper decrease at higher temperatures, indicating an increase in the average rate and thus extent of matrix dipolar relaxation around the excited triplet

state. The peak frequency values as a function of temperature were found to be super-imposable for vanillin in VS and TVS matrix (Figure 2). The phosphorescence bandwidth increased gradually in the glass and then very sharply in the melt, reflecting a large increase in the range of energetically distinct matrix environments in TVS matrix below and above T_g (Figure 2). A comparison of bandwidth between VS and TVS matrix is shown in Figure 2; the values were super-imposable.

Phosphorescence Intensity Decays: Vanillin phosphorescence decay kinetics were studied in the amorphous TVS films and compared with intensity decays from VS films. Time-resolved phosphorescence intensity decays of vanillin in amorphous films were measured over the temperature range from -10°C to 100°C . The intensity decay were fitted using a multi-exponential function. The phosphorescence intensity decays of vanillin in amorphous TVS film at 20°C in the presence of nitrogen is plotted in Figure 3 along with the modified residuals for a fit using a four-exponential function (Eq. 3, Materials and Methods).

All intensity decays over the temperature interval from -10°C to 100°C were well fit using a four-exponential function. This analysis indicated that the vanillin probe had multiple lifetimes in the amorphous TVS matrix at all temperatures. The phosphorescence intensity decreased with increasing temperature indicating an increase in triplet state quenching rates with increase in temperature; the results of these lifetime analyses for vanillin in TVS are plotted in Figure 4a. The decrease in lifetime as a function of temperature was dramatic both below and above T_g , indicating the presence

of a range of molecular motions both below and above T_g . A comparison of individual lifetime components τ_1 , τ_2 , τ_3 and τ_4 for vanillin in TVS and VS is shown in Figure 4b (longer lifetimes) and 4c (shorter lifetimes). In general there was no significant difference in the individual lifetime component of vanillin in TVS and VS films.

The average lifetime calculated using Eq. 4 (Material and Methods) is plotted in Figure 5 as a function of temperature. The average lifetime varied from ~ 150 ms at -10°C to ~ 0.8 ms at 100°C . The decrease in vanillin lifetime as a function of temperature corresponds to an increase in k_{NR} (Eq. 4, Materials and Methods), the rate of vibrational relaxation due to collisional quenching which is an indicator of the increase in matrix mobility. The decrease in lifetime was multi-phasic as a function of temperature. A comparison plot of average lifetimes of vanillin in the TVS and VS amorphous matrix is shown in Figure 5. The amplitudes of each lifetime component in TVS are plotted as a function of temperature in Figure 6. The amplitudes of the longer lifetime components decreased and that of the shorter lifetime components increased as a function of temperature. The non-radiative decay rate reflects the sum of all collisional interactions between the matrix and the probe and is sensitive to molecular environments, and changes in this decay rate with change in physical state of the probe environments strongly modulate the phosphorescence lifetime giving rise to multiple lifetimes.

In comparison between VS and TVS matrix, vanillin lifetime and amplitudes values were found to be super-imposable. This indicated that there is no interference from tryptophan phosphorescence to vanillin lifetime measurements.

Tryptophan:

The delayed emission spectra from tryptophan (excited at 280 nm) in amorphous TS and TVS matrix is shown in Figure 7a and 7b, respectively. As seen from Figure 7b, the tryptophan emission spectra in TVS matrix appear different than that seen in Figure 7a. This is due to simultaneous emission from vanillin as it also gets excited at 280 nm (excitation wavelength for tryptophan). Thus vanillin emission interferes with tryptophan emission. The spectra's of tryptophan in presence of vanillin looked like vanillin spectra (in absence of tryptophan), and the intensities of this spectra was much higher even when vanillin is excited in the same matrix at 320 nm (Figure 7b vs. Figure 1b), it is likely that there is energy transfer from tryptophan to vanillin since tryptophan emission overlaps with vanillin absorption.

Tryptophan emits phosphorescence from 380 nm to 530 nm with a peak at 455 nm, and vanillin emits phosphorescence from 420 nm to 600 nm with a peak at ~490 nm. It was difficult to resolve the emission spectra of tryptophan in presence of vanillin. In the region between 380 nm to 420 nm only tryptophan emits and there is no emission observed from vanillin, so tryptophan lifetimes were measured by collecting emission at 405 nm and compared to tryptophan emission (in TS matrix) at 455 nm and 405 nm. The intensity decays were fitted using multi-exponential function. The phosphorescence intensity decay of tryptophan in amorphous TVS film at 20°C in the presence of nitrogen is plotted in Figure 8 along with the modified residuals for a fit using a four-exponential function (Eq. 8, Materials and Methods).

Time-resolved phosphorescence intensity decay of tryptophan in amorphous films were measured over the temperature range from -10°C to 100°C. All intensity decays over the temperature interval from -10°C to 100°C were well fit using a four-exponential function. This analysis indicated that the tryptophan probe had multiple lifetimes in the amorphous TVS matrix at all temperatures. The phosphorescence intensity decreased with increasing temperature indicating an increase in triplet state quenching rates with increase in temperature, the results of these lifetime analyses for tryptophan in TVS are plotted in Figure 9a.

A comparison of individual lifetime components τ_1 , τ_2 , τ_3 and τ_4 for tryptophan in TVS (emission at 405 nm), TS (a) (emission at 455 nm) and TS (b) (emission at 405 nm) is shown in Figure 10a, 10b, 10c, and 10d, respectively. There was no significant difference in the individual lifetime components of tryptophan in TVS and TS films.

A comparison of average lifetimes is shown in Figure 11. There was no significant difference in the average lifetimes in TS matrix for emissions at 455 nm or 405 nm. However the average lifetime was lower in TVS as compared to TS up to 40°C, and above 50°C there was no significant difference in the lifetime. This difference was due to differences in the amplitudes among the emission from TVS (at 405 nm), TS (a) (at 455 nm) and TS (b) (at 405 nm).

The amplitudes of the longer lifetime components in TVS decreased and that of the shorter lifetime component increased as a function of temperature (Figure 12). A comparison of amplitudes a_1 , a_2 , a_3 and a_4 in TVS and TS (a) (emission at 455 nm) and TS (b) (emissions at 405 nm) is shown in Figure 13a, 13b, 13c and 13d. The amplitudes differed among TVS, TS (a) and TS (b) decays. The amplitude a_1 followed the trend where it was not different for emission at 455 nm and 405 nm in TS matrix, but these values were significantly higher in TVS at 405 nm. The amplitudes a_2 and a_3 were higher in TS (a) > TS (b) > TVS. There was no significant difference in the amplitude a_4 among the three.

Thus number of probes emitting at 455 nm were highest as compared to probes emitting at 405 nm, however this affected the average lifetime of tryptophan at 405 nm in TVS matrix. The Arrhenius plot for $\ln(k_p)$ of TS (a), TS (b) and TVS is shown in Figure 14a. There was no significant difference among the three.

The Arrhenius plot of natural log of k_p for average lifetime as function of inverse of temperature for tryptophan and vanillin dispersed in TVS films is shown in Figure 14b.

Conclusion

This research investigated simultaneous measurements of mobility by using vanillin and tryptophan in amorphous matrix. There was no spectroscopic or physical interaction seen from tryptophan for measurements of vanillin in the TVS matrix. However vanillin shows excitation at 280 nm (excitation wavelength for tryptophan) and emission from 420 nm to 600 nm which interfered with tryptophan measurements. There is a possibility that there was energy transfer from tryptophan to vanillin. Tryptophan emits from 380 nm to 520 nm, to avoid interference from vanillin emissions, the decays were collected at 405 nm. Although the individual lifetimes did not differ at 405 nm and 455 nm, but the average lifetimes were seen to be different. This difference was due to higher number of emitting probes in case of emissions at 455 nm as compared to at 405 nm.

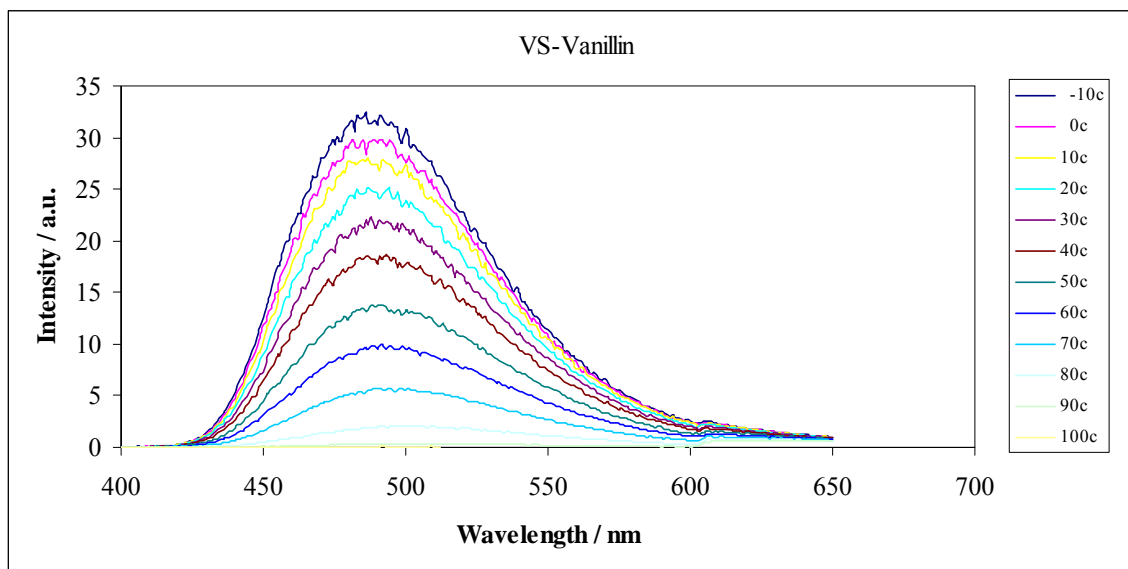
Vanillin**Figure X-1a**

Figure X-1a: Delayed emission spectra of vanillin dispersed in amorphous films of sucrose (referred as VS matrix) as a function of temperature (excitation at 320 nm). The spectra were collected at 10°C intervals from -10°C to 100°C (the curves follow this order from high to low intensity at ~490 nm).

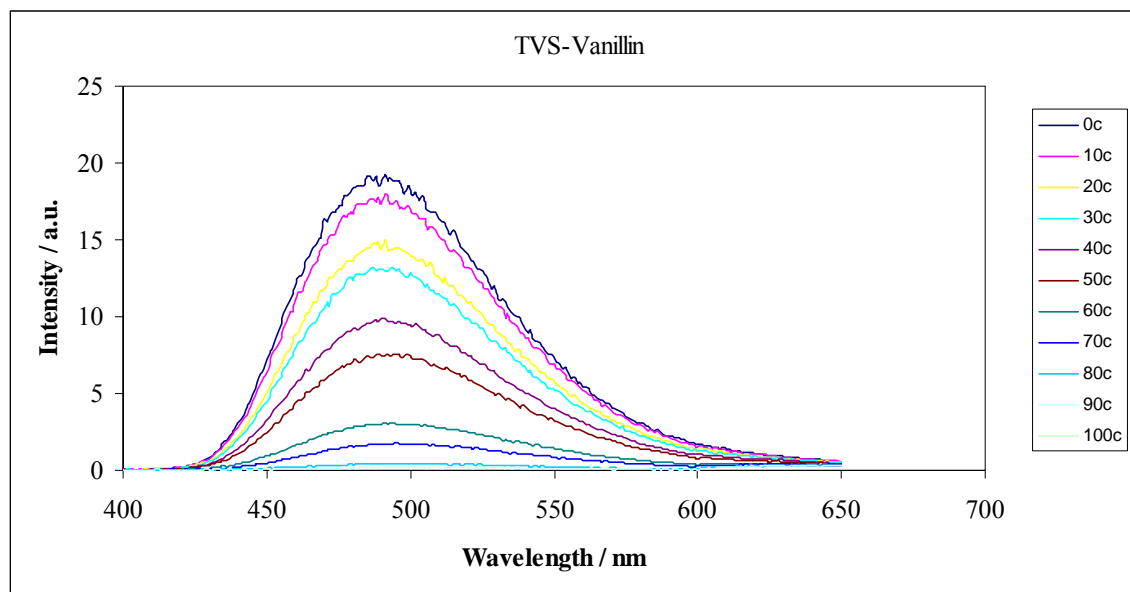
Figure X-1b

Figure X-1b: Delayed emission spectra of vanillin dispersed in amorphous films of sucrose containing tryptophan (referred as TVS matrix) as a function of temperature (excitation at 320 nm). The spectra were collected at 10°C intervals from 0°C to 100°C (the curves follow this order from high to low intensity at ~490 nm).

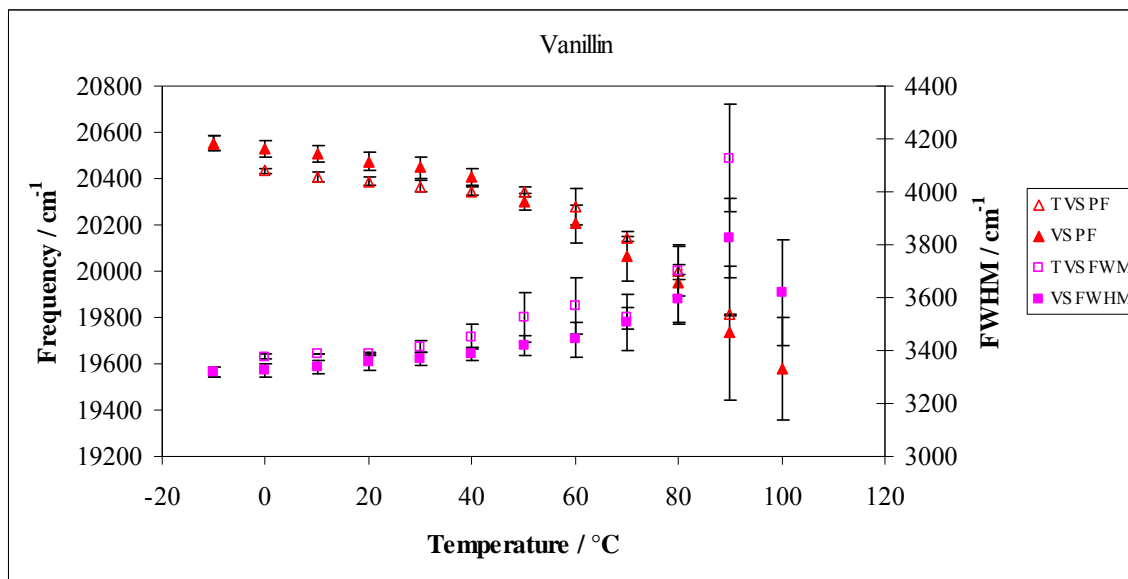
Figure X-2

Figure X-2: Peak energy ν_p (left hand scale) and bandwidth FWHM (right hand scale) for phosphorescence emission from vanillin in amorphous TVS and VS films as a function of temperature. The spectra were collected every 10°C from -10°C to 100°C. The frequency is given by in (Δ) TVES matrix and by (\blacktriangle) in VS matrix. The FWHM is given by (\diamond) in TVS matrix and by (\blacklozenge) in VS matrix.

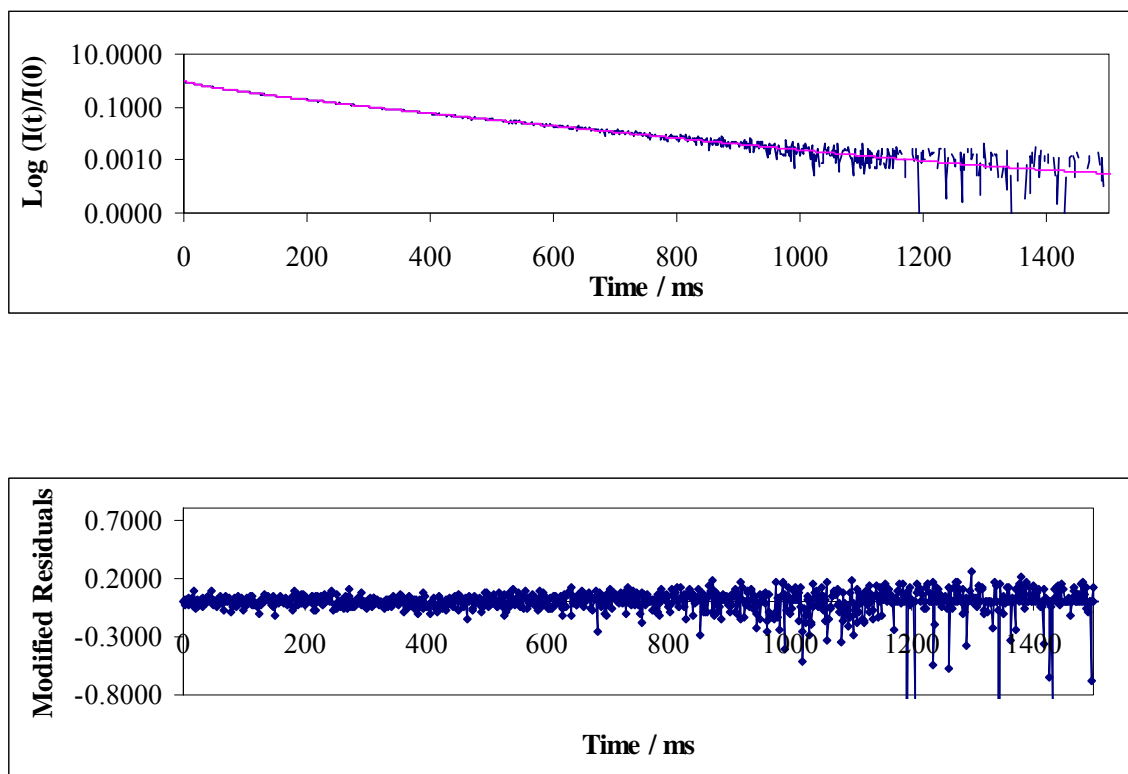
Figure X-3

Figure X-3: Normalized phosphorescence intensity decay $[I(t)/I(0)]$ of vanillin dispersed in amorphous TVS films at 20°C in the presence of nitrogen. The solid lines through the data are fits using a stretched-exponential function. Below is the plot of modified residuals $[(\text{Data}-\text{Fit})/\text{Data}^{1/2}]$ for these fits to data plotted in the presence of nitrogen.

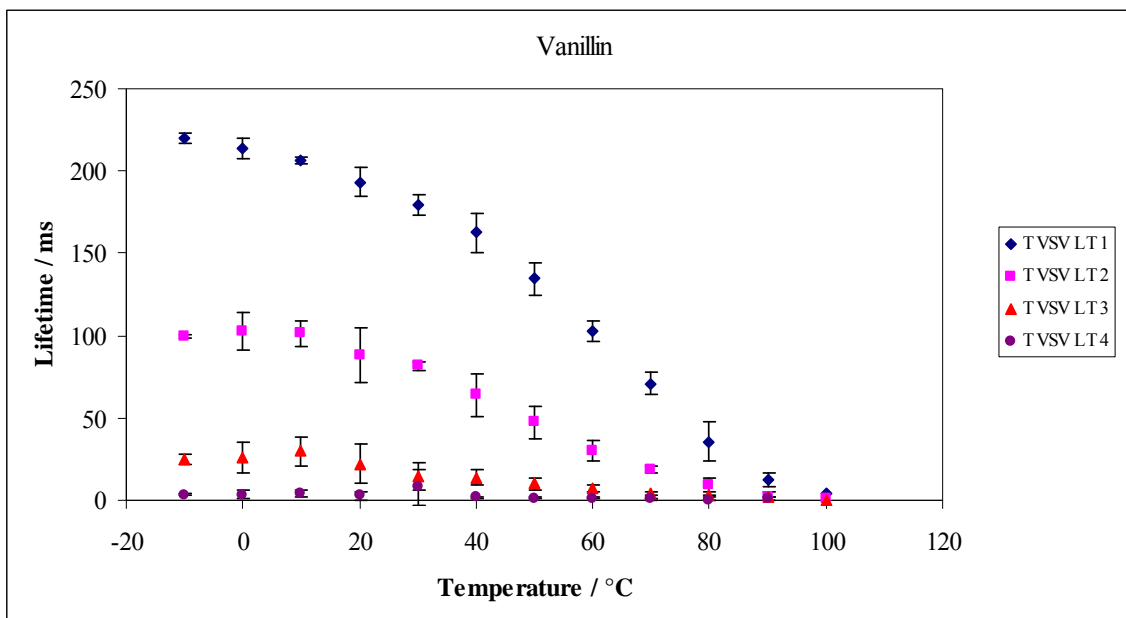
Figure X-4a

Figure X-4a: Lifetime components τ_1 (\blacklozenge), τ_2 (\blacksquare), τ_3 (\blacktriangle) and τ_4 (\bullet) obtained from a multi-exponential model fit to phosphorescence intensity decay data from vanillin dispersed in amorphous films of TVS equilibrated against nitrogen as a function of temperature. The data was calculated every 10°C from -10°C to 100°C.

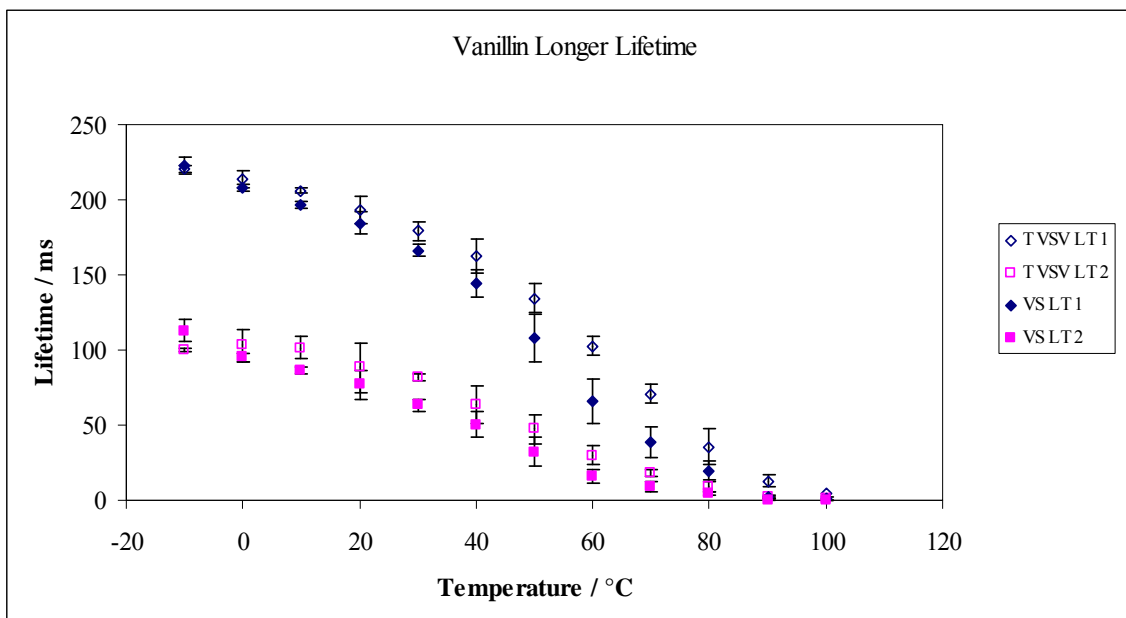
Figure X-4b

Figure X-4b: Comparison of longer lifetime components τ_1 (◆) and τ_2 (■) obtained from a multi-exponential model fit (Eq. (3), Materials and Methods) to phosphorescence intensity decay data from vanillin dispersed in amorphous TVS or VS films equilibrated against nitrogen as a function of temperature. The data was calculated every 10°C from -10°C to 100°C.

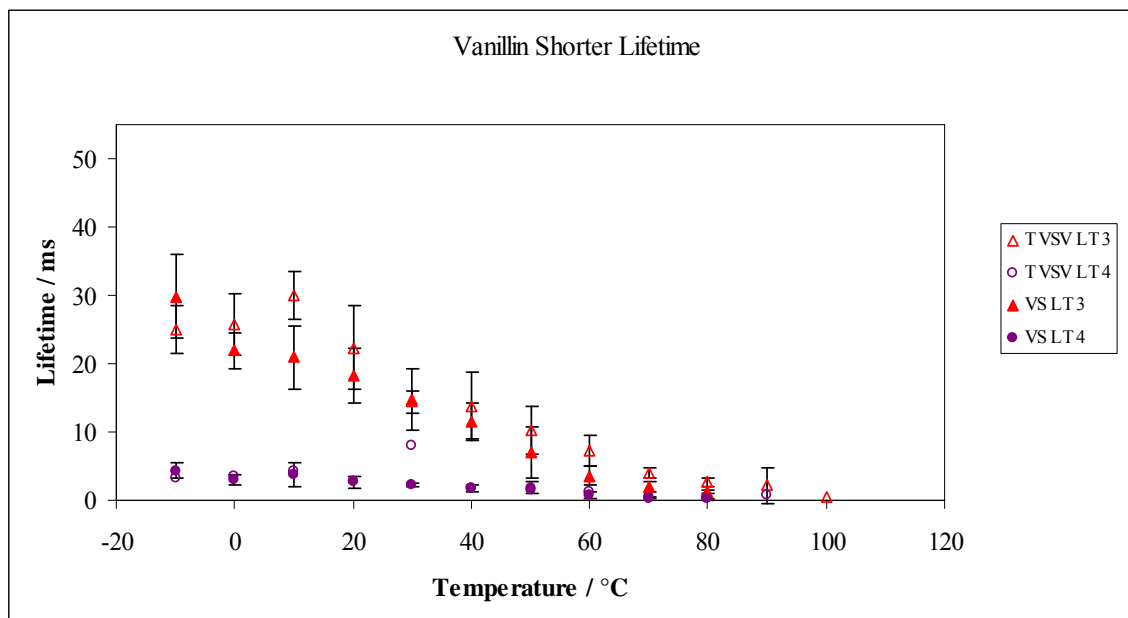
Figure X-4c

Figure X-4c: Comparison of shorter lifetime components τ_1 (\blacklozenge) and τ_2 (\blacksquare) obtained from a multi-exponential model fit (Eq. (3), Materials and Methods) to phosphorescence intensity decay data from vanillin dispersed in amorphous TVS or VS films equilibrated against nitrogen as a function of temperature. The data was calculated every 10°C from -10°C to 100°C.

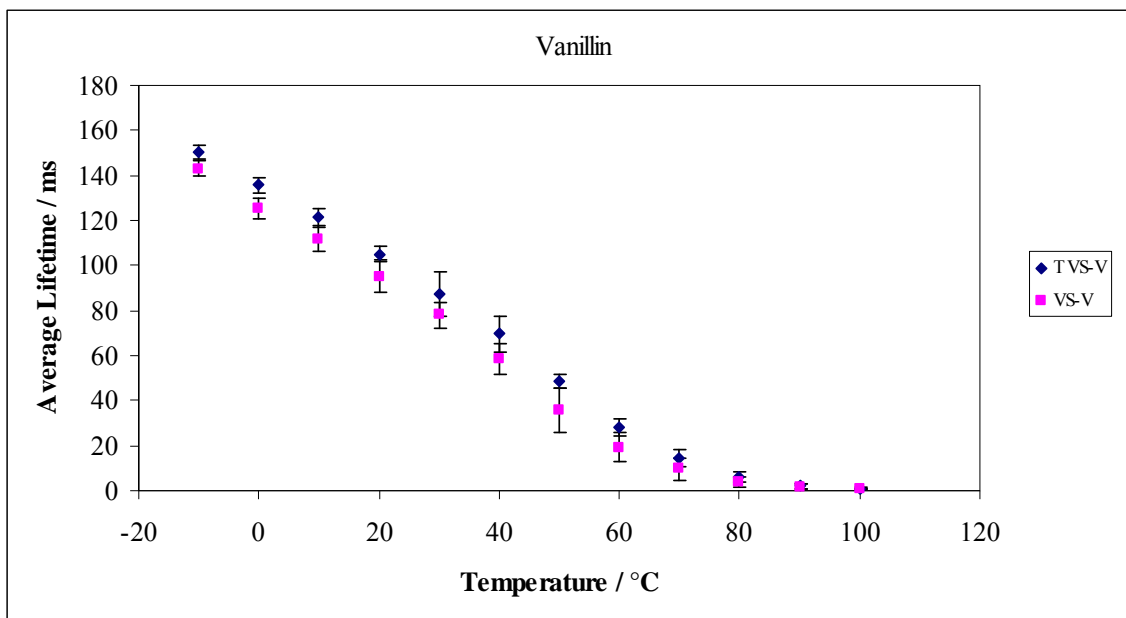
Figure X-5

Figure X-5: The average lifetime of vanillin in TVS (■) and VS (◆) films obtained from a multi-exponential model fit equilibrated against nitrogen as a function of temperature. The data were collected every 10°C from -10°C to 100°C.

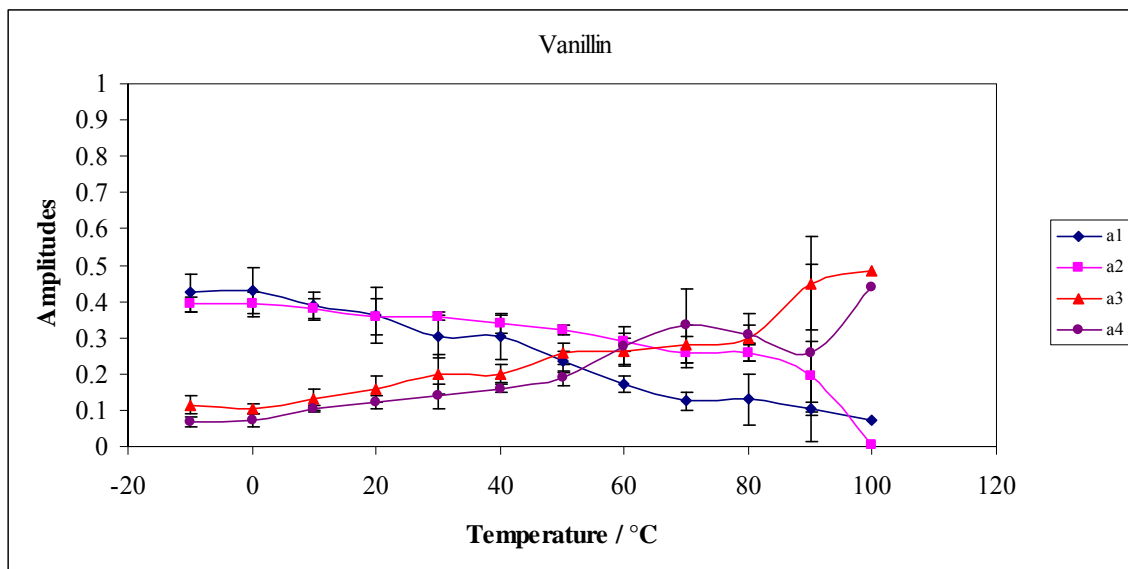
Figure X-6

Figure X-6: Intensity decay fit parameters amplitude for vanillin in amorphous TVS film in nitrogen as a function of temperature. The data was calculated every 10°C from -10°C to 100°C. The amplitudes a1 (♦) and a2 (■) correspond to the longer life time components (τ_1 , τ_2) and a3 (▲) and a4 (●) correspond to the shorter lifetime components (τ_3 , τ_4). The amplitudes were obtained from a multi exponential model fit (Eq. (3), Materials and Methods) to phosphorescence intensity decay data from vanillin dispersed in TVS films equilibrated against nitrogen as a function of temperature.

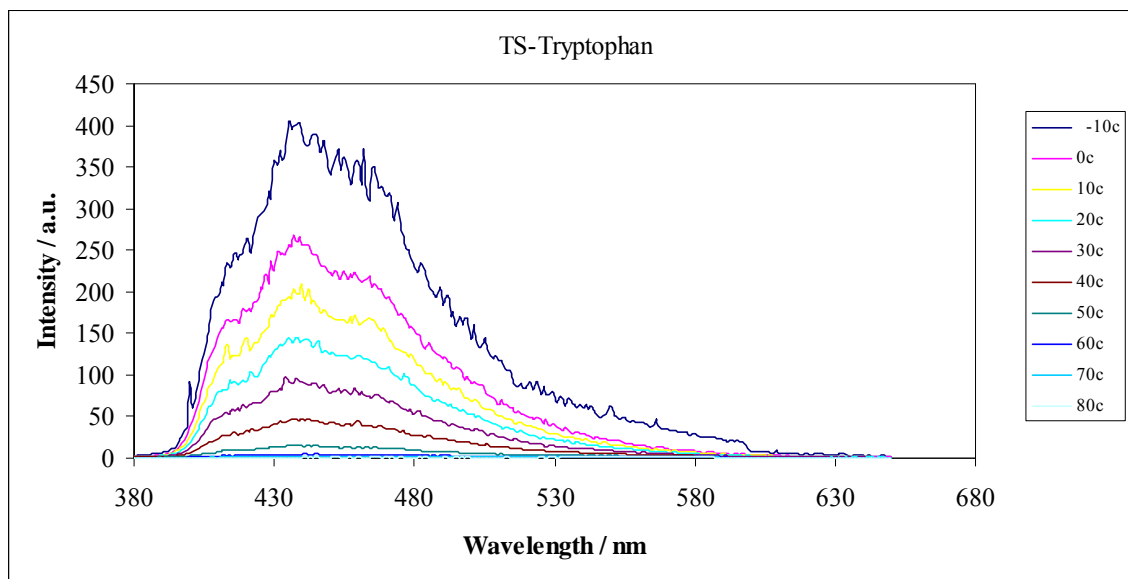
Tryptophan**Figure X-7a**

Figure X-7a: Delayed emission spectra of tryptophan dispersed in amorphous films of sucrose (referred as TS) as a function of temperature (excitation at 280 nm). The spectra were collected at 10°C intervals from -10°C to 80°C (the curves follow this order from high to low intensity at ~455 nm).

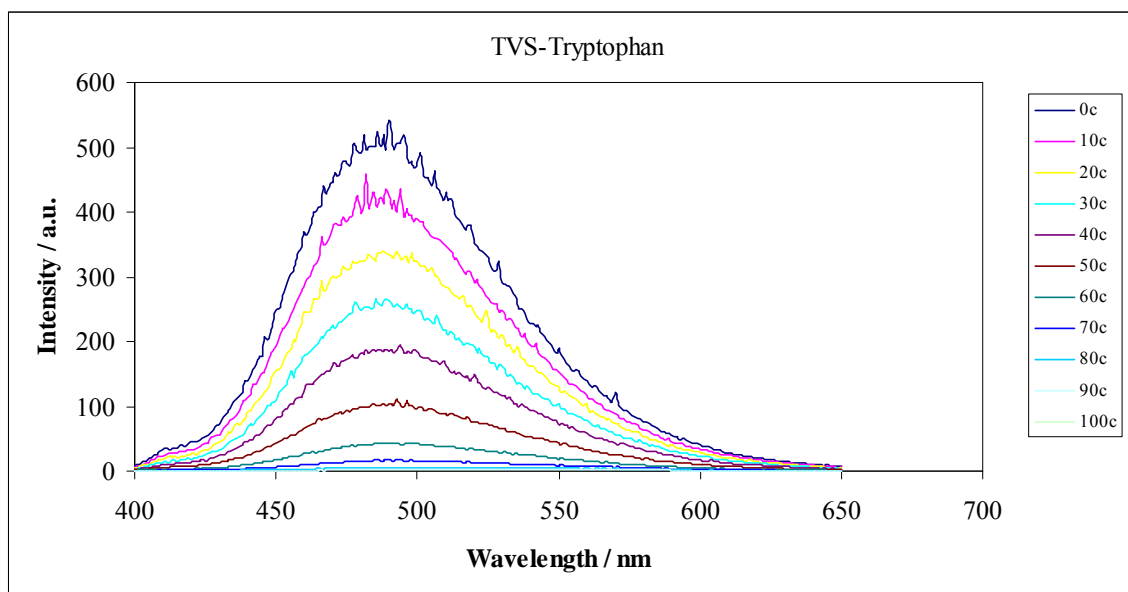
Figure X-7b

Figure X-7b: Delayed emission spectra of tryptophan dispersed in amorphous films of sucrose also containing vanillin (referred as TVS) as a function of temperature (excitation at 280 nm). The spectra were collected at 10°C intervals from 0°C to 100°C (the curves follow this order from high to low intensity at ~455 nm).

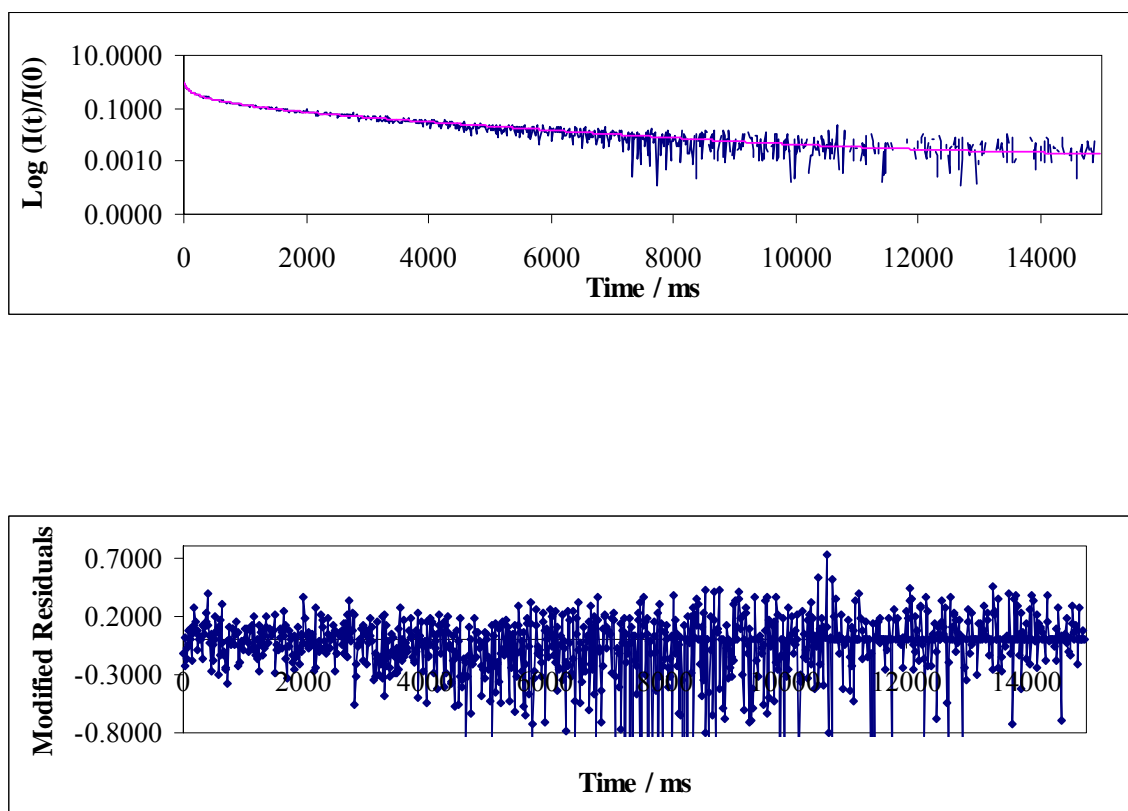
Figure X-8

Figure X-8: Normalized phosphorescence intensity decay $[I(t)/I(0)]$ of tryptophan dispersed in amorphous TVS films at 20°C in the presence of nitrogen. The solid lines through the data are fits using a multi-exponential function. Below is the plot of modified residuals $[(\text{Data}-\text{Fit})/\text{Data}^{1/2}]$ for these fits to data plotted in the presence of nitrogen. The data was collected at 405 nm.

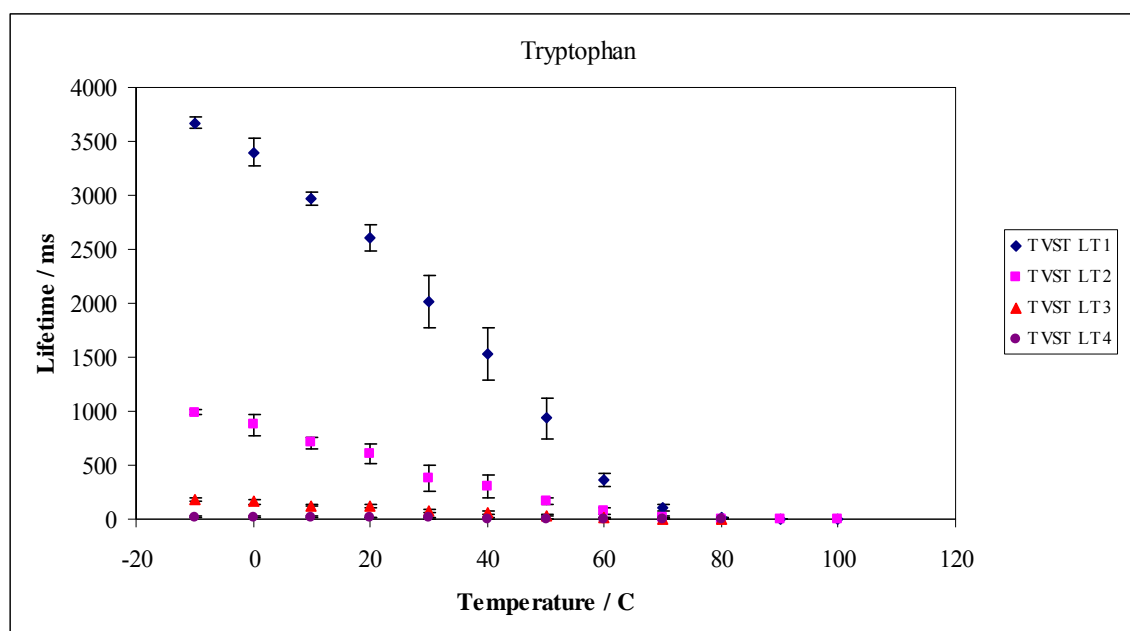
Figure X-9a

Figure X-9a: Lifetime components τ_1 (\blacklozenge), τ_2 (\blacksquare), τ_3 (\blacktriangle) and τ_4 (\bullet) obtained from a multi-exponential model fit to phosphorescence intensity decay data from tryptophan dispersed in amorphous films of TVS equilibrated against nitrogen as a function of temperature. The data was calculated every 10°C from -10°C to 100°C.

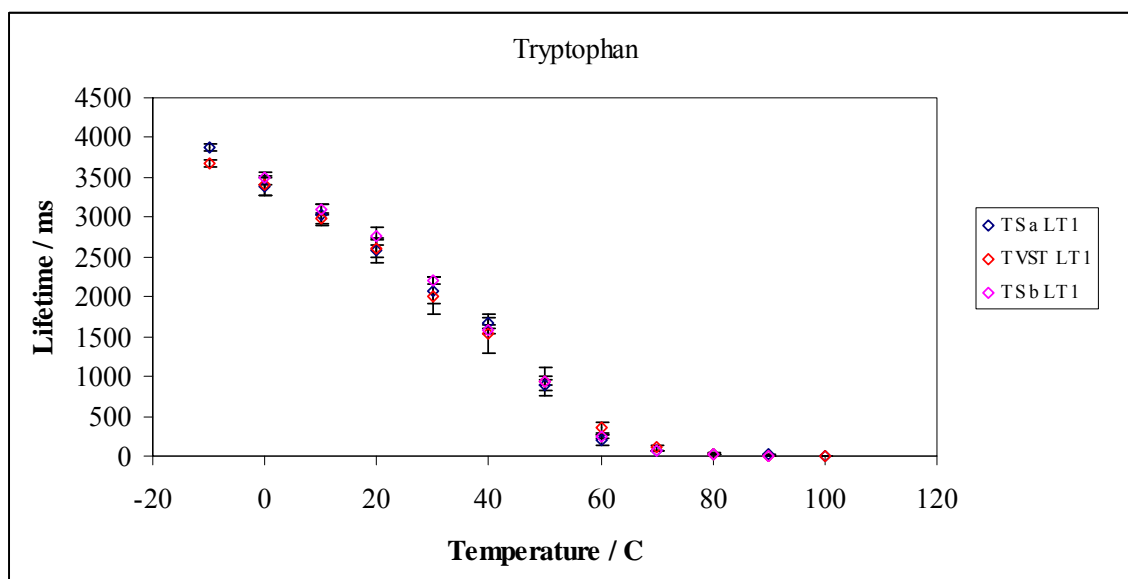
Figure X-10a

Figure X-10a: Comparison of longer lifetime component τ_1 obtained from a multi-exponential model fit (Eq. (3), Materials and Methods) to phosphorescence intensity decay data from tryptophan dispersed in amorphous TVS (\diamond) (emissions at ~ 405 nm) or TS a (\diamond) (emissions at ~ 455 nm) or TS b (\diamond) (emissions at ~ 405 nm) films equilibrated against nitrogen as a function of temperature. The data was calculated every 10°C from -10°C to 100°C.

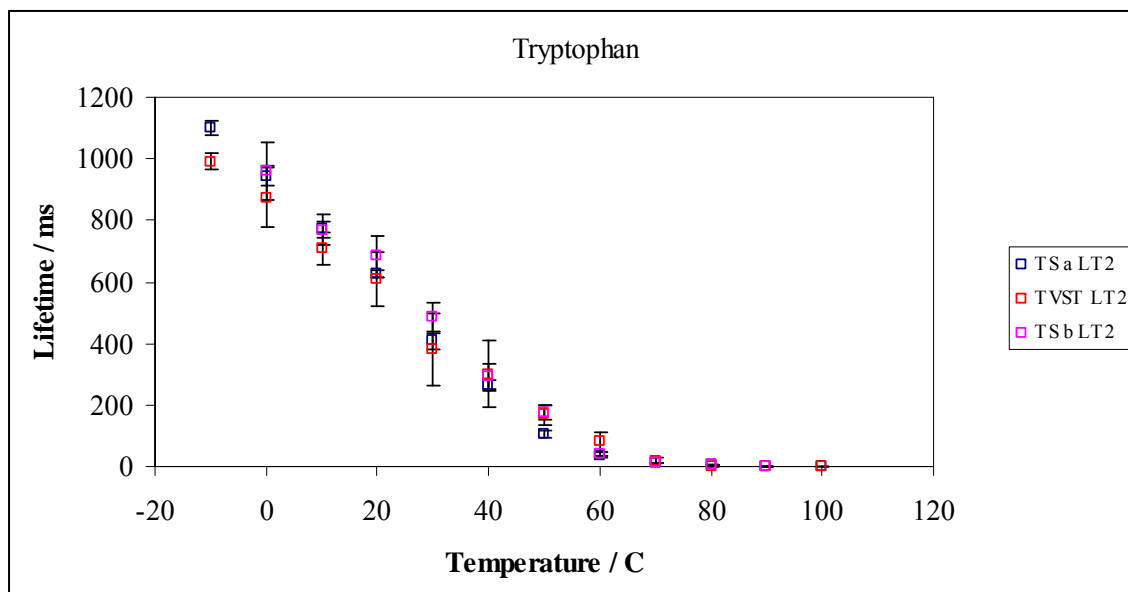
Figure X-10b

Figure X-10b: Comparison of longer lifetime component τ_2 obtained from a multi-exponential model fit (Eq. (3), Materials and Methods) to phosphorescence intensity decay data from tryptophan dispersed in amorphous TVS (\square) (emissions at ~ 405 nm) or TS a (\square) (emissions at ~ 455 nm) or TS b (\square) (emissions at ~ 405 nm) films equilibrated against nitrogen as a function of temperature. The data was calculated every 10°C from -10°C to 100°C .

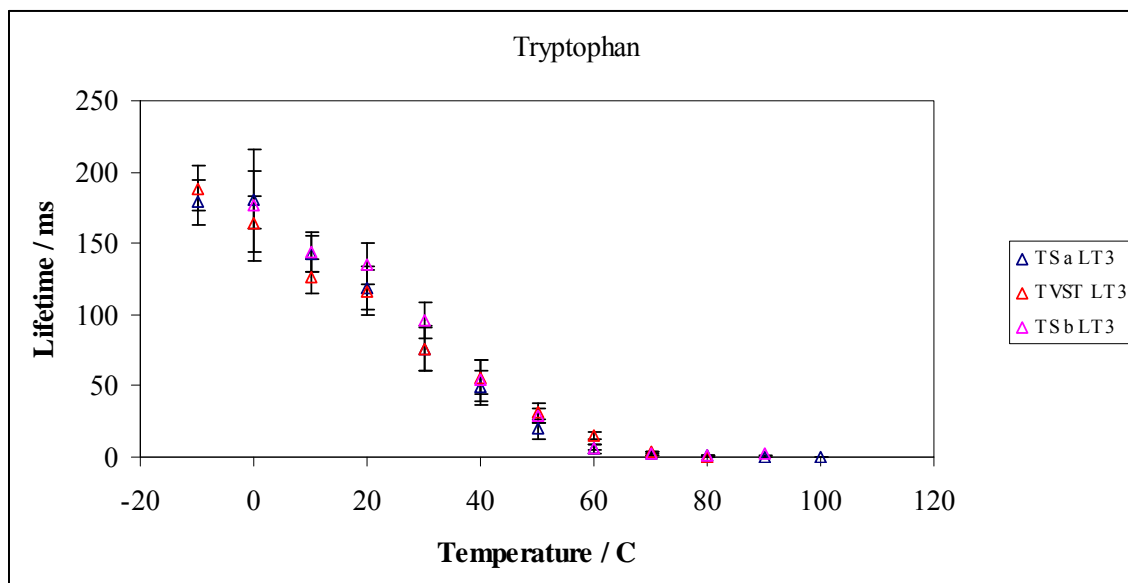
Figure X-10c

Figure X-10c: Comparison of shorter lifetime component τ_3 obtained from a multi-exponential model fit (Eq. (3), Materials and Methods) to phosphorescence intensity decay data from tryptophan dispersed in amorphous TVS (Δ) (emissions at ~ 405 nm) or TS a (Δ) (emissions at ~ 455 nm) or TS b (Δ) (emissions at ~ 405 nm) films equilibrated against nitrogen as a function of temperature. The data was calculated every 10°C from -10°C to 100°C .

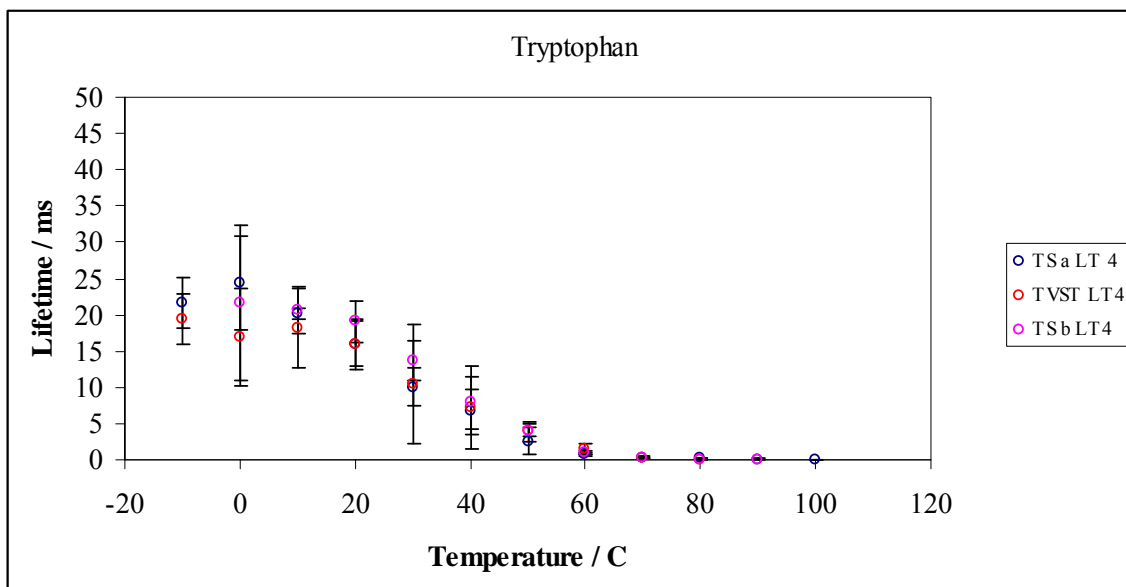
Figure X-10d

Figure X-10d: Comparison of shorter lifetime component τ_4 obtained from a multi-exponential model fit (Eq. (3), Materials and Methods) to phosphorescence intensity decay data from tryptophan dispersed in amorphous TVS (○) (emissions at ~ 405 nm) or TS a (○) (emissions at ~ 455 nm) or TS b (○) (emissions at ~ 405 nm) films equilibrated against nitrogen as a function of temperature. The data was calculated every 10°C from -10°C to 100°C .

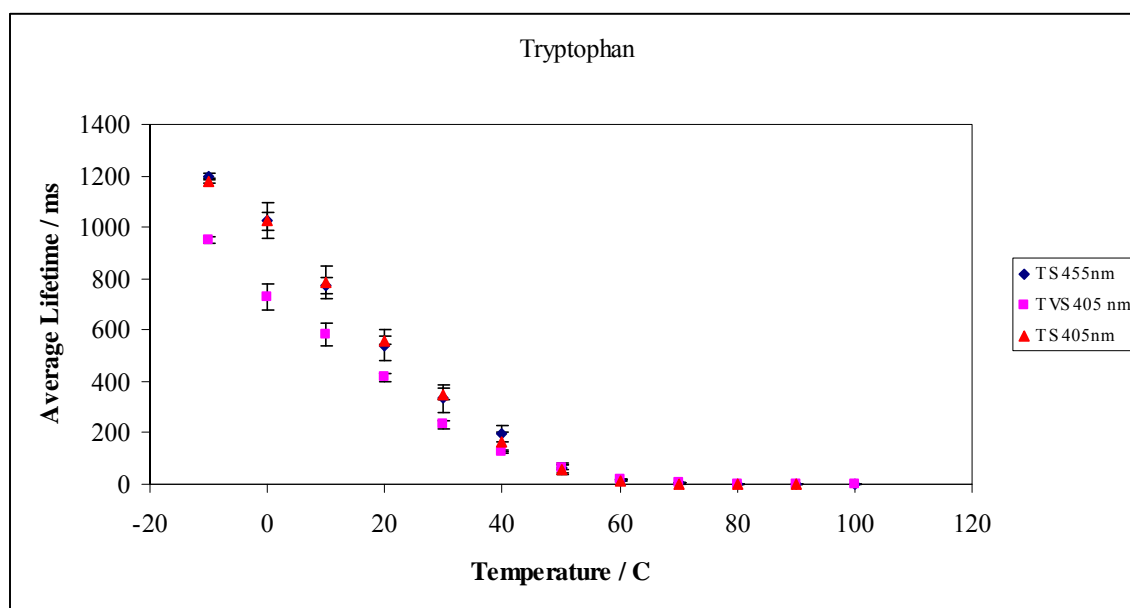
Figure X-11

Figure X-11: The average lifetime of tryptophan in TVS 405 nm (■), TS 455 nm (◆) and TS 405 nm (▲) films obtained from a multi-exponential model fit equilibrated against nitrogen as a function of temperature. The data were collected every 10°C from -10°C to 100°C.

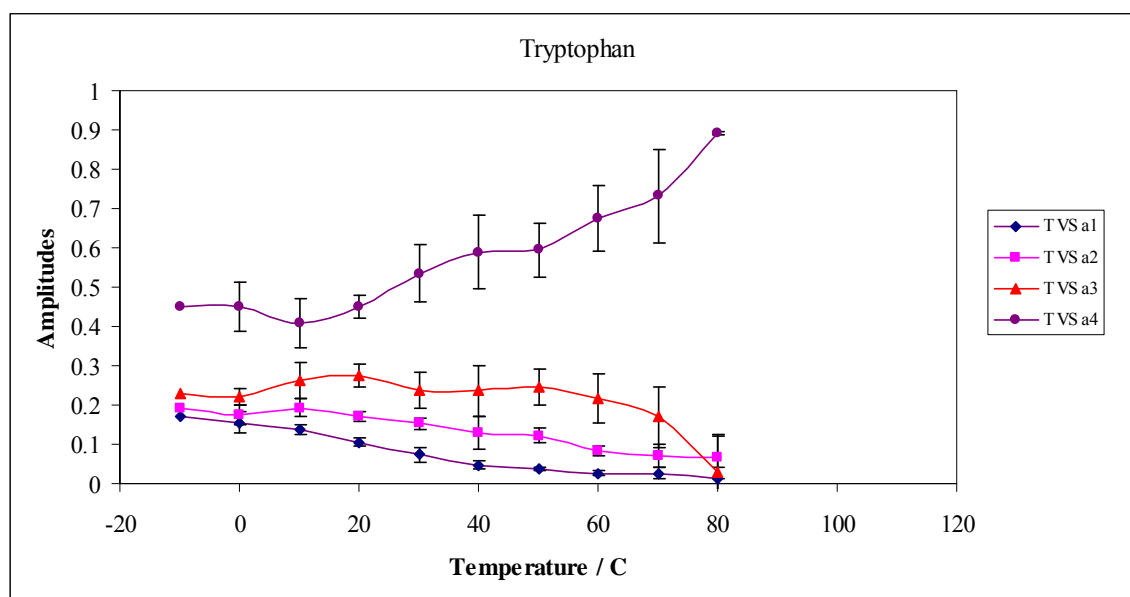
Figure X-12

Figure X-12: Intensity decay fit parameters amplitude for tryptophan in amorphous TVS film in nitrogen as a function of temperature. The data was calculated every 10°C from -10°C to 80°C. The amplitudes a1 (♦) and a2 (■) correspond to the longer life time components (τ_1 , τ_2) and a3 (▲) and a4 (●) correspond to the shorter lifetime components (τ_3 , τ_4). The amplitudes were obtained from a multi exponential model fit (Eq. (3), Materials and Methods) to phosphorescence intensity decay data from tryptophan dispersed in TVS films equilibrated against nitrogen as a function of temperature.

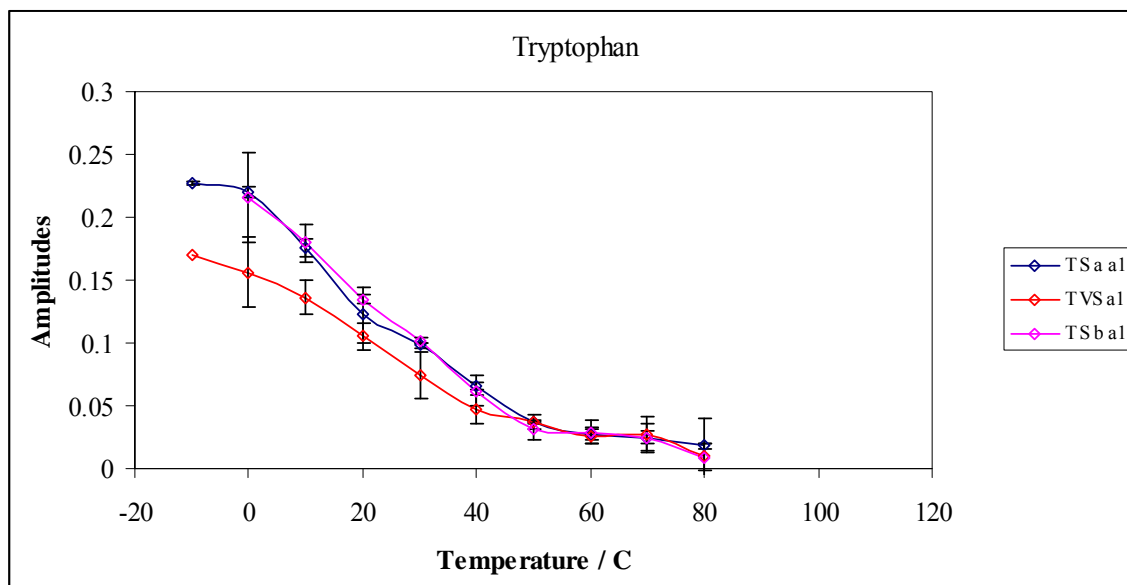
Figure X-13a

Figure X-13a: Comparison of longer lifetime amplitude a_1 obtained from a multi-exponential model fit (Eq. (3), Materials and Methods) to phosphorescence intensity decay data from tryptophan dispersed in amorphous TVS (\diamond) (emissions at ~ 405 nm) or TS a (\diamond) (emissions at ~ 455 nm) or TS b (\diamond) (emissions at ~ 405 nm) films equilibrated against nitrogen as a function of temperature. The data was calculated every 10°C from -10°C to 80°C .

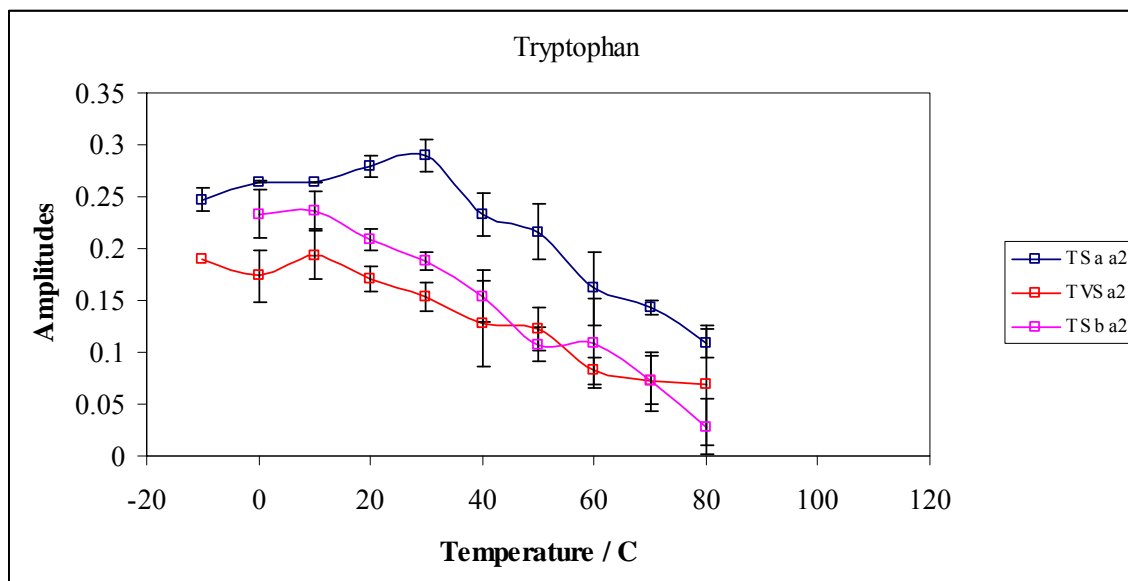
Figure X-13b

Figure X-13b: Comparison of longer lifetime amplitude a2 obtained from a multi-exponential model fit (Eq. (3), Materials and Methods) to phosphorescence intensity decay data from tryptophan dispersed in amorphous TVS (\square) (emissions at ~ 405 nm) or TS a (\square) (emissions at ~ 455 nm) or TS b (\square) (emissions at ~ 405 nm) films equilibrated against nitrogen as a function of temperature. The data was calculated every 10°C from -10°C to 80°C .

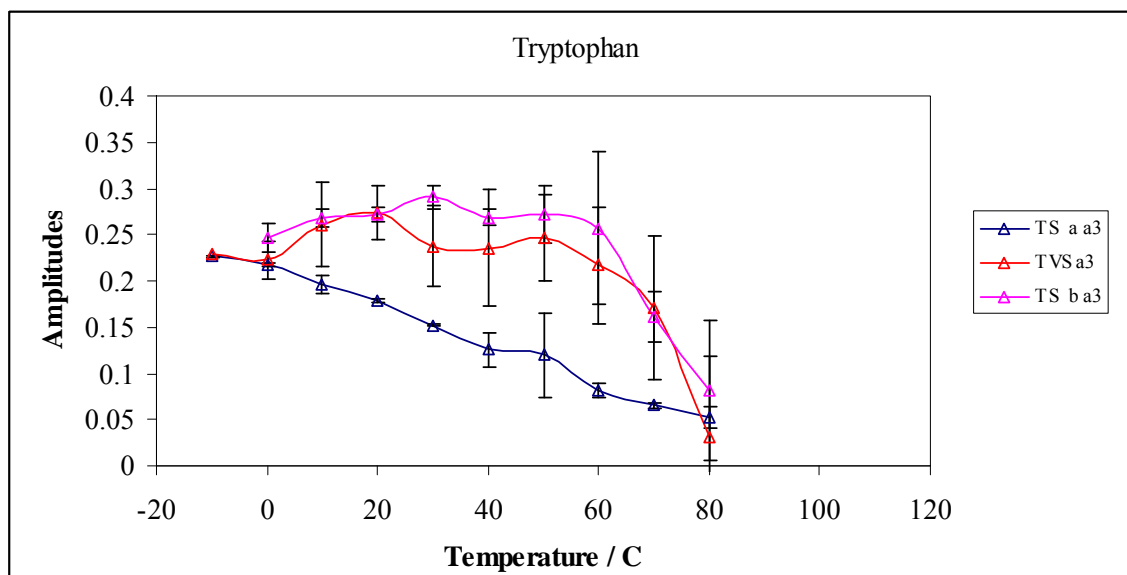
Figure X-13c

Figure X-13c: Comparison of shorter lifetime amplitude a_3 obtained from a multi-exponential model fit (Eq. (3), Materials and Methods) to phosphorescence intensity decay data from tryptophan dispersed in amorphous TVS (Δ) (emissions at ~ 405 nm) or TS a (Δ) (emissions at ~ 455 nm) or TS b (Δ) (emissions at ~ 405 nm) films equilibrated against nitrogen as a function of temperature. The data was calculated every 10°C from -10°C to 80°C .

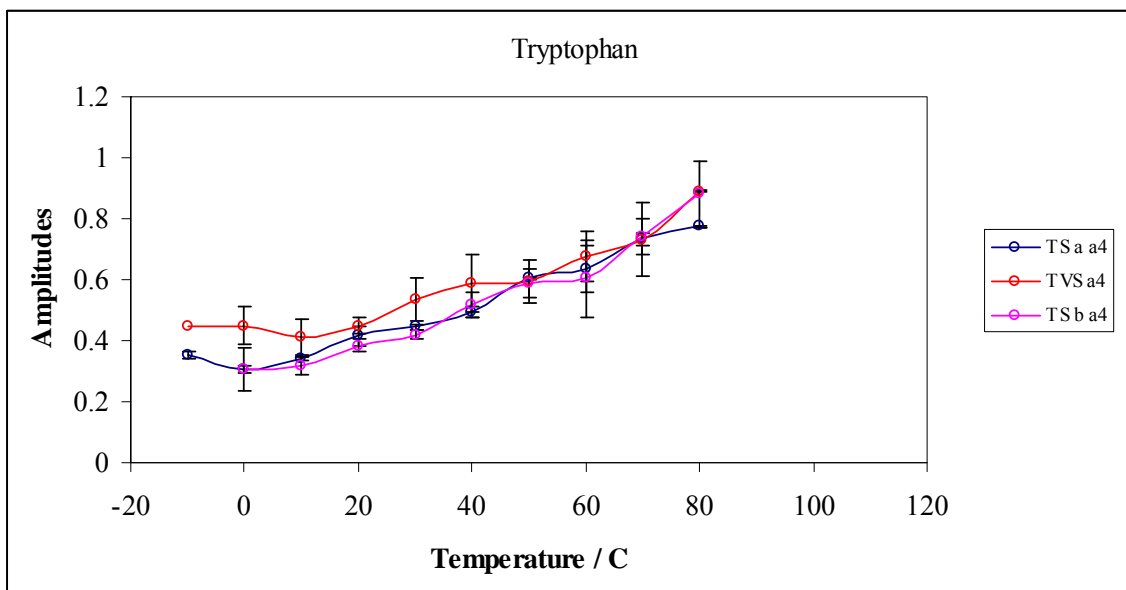
Figure X-13d

Figure X-13d: Comparison of shorter lifetime component a4 obtained from a multi-exponential model fit (Eq. (3), Materials and Methods) to phosphorescence intensity decay data from tryptophan dispersed in amorphous TVS (○) (emissions at ~ 405 nm) or TS a (○) (emissions at ~ 455 nm) or TS b (○) (emissions at ~ 405 nm) films equilibrated against nitrogen as a function of temperature. The data was calculated every 10°C from -10°C to 80°C.

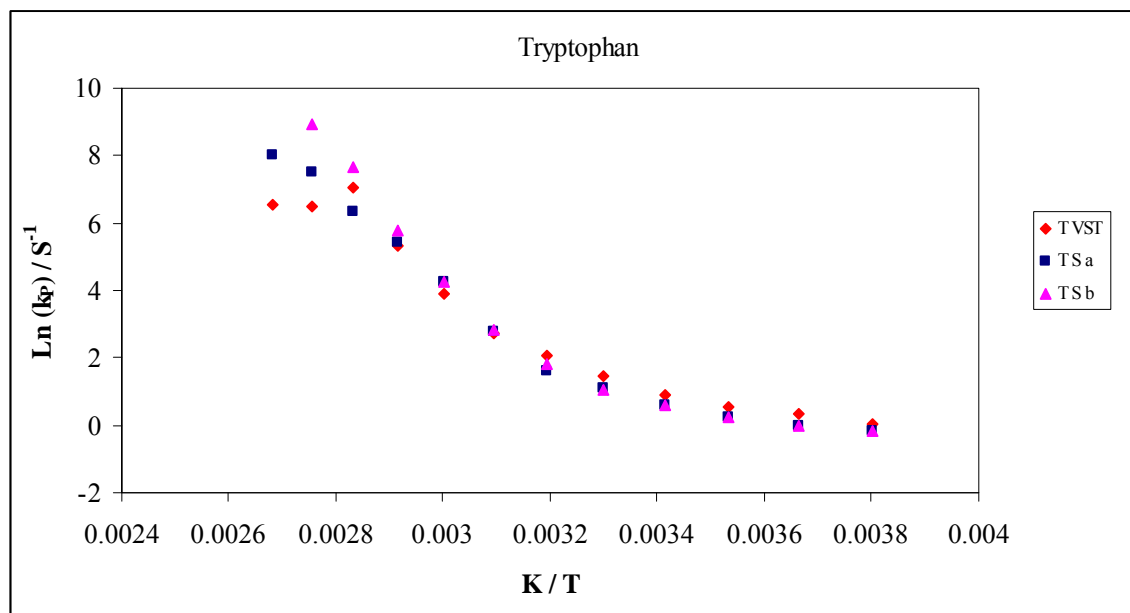
Figure X-14a

Figure X-14a: The Arrhenius plot of natural log of k_p for average lifetime as function of inverse of temperature for tryptophan dispersed in TVS (emissions at 405 nm), TS a (emissions at 455nm) and b (emissions at 405 nm) films.

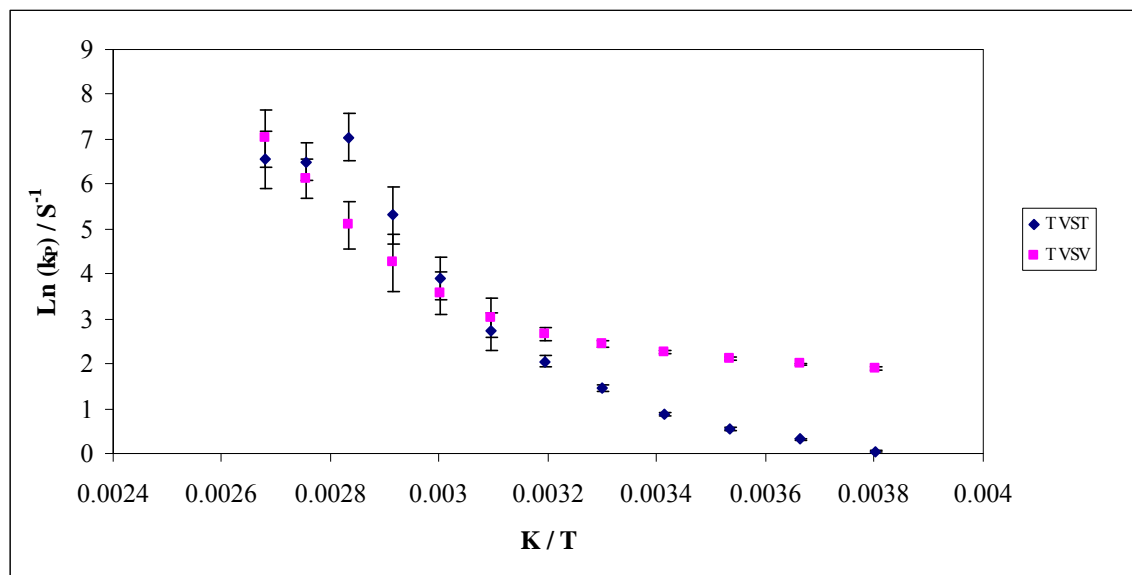
Figure X-14b

Figure X-14b: The Arrhenius plot of natural log of k_p for average lifetime as function of inverse of temperature for tryptophan and vanillin dispersed in TVS films.

References

- Champion, D., Le Meste, M. and Simatos, D. Towards an improved understanding of glass transition and relaxations in foods: molecular mobility in the glass transition range. *Trends in Food Science and Technology*. 11 (2000). 41-55.
- Chen, R. Apparent stretched exponential luminescence decay in crystalline solids. *Journal of Luminescence*. 102-103 (2003). 510-518.
- Duchowicz, R., Ferrer, M. L. and Acuna, A.U. Kinetic spectroscopy of erythrosin phosphorescence and delayed fluorescence in aqueous solution at room temperature. *Photochemistry and Photobiology*. 68 (1998). 494-501.
- Fischer, C. J., Gafni, A., Steel, D. G. and Schauerte, J. A. The triplet-state lifetime of indole in aqueous and viscous environments: significance to the interpretation of room temperature phosphorescence in proteins. *Journal of the American Chemical Society*. 124 (2004). 10359-10266.
- Lettinga M.P et al. Phosphorescence and fluorescence characterization of fluorescein derivatives immobilized in various polymers matrices. *Physical Chemistry Chemical Physics* 2 (2000): 3697-707.
- Lindsey, C. P. and Patterson, G. D. Detailed comparison of the Williams-Watts and Cole-Davidson functions. *Journal of Chemical Physics*. 2 (1980). 3348-3357.
- Maroncelli, M. and Fleming, G. R. Picosecond salvation dynamics of coumarin 153: The importance of molecular aspects of salvation. *Journal of Chemical Physics*. 86 (1987). 6221-6239.
- McCaul, C. P. and Ludescher, R. D. Room temperature phosphorescence from tryptophan and halogenated tryptophan analogs in amorphous sucrose. *Photochemistry and Photobiology*. 70 (1999). 166-171.
- Nack, T. J. and Ludescher, R. D. Molecular mobility and oxygen permeability in amorphous bovine serum albumin films. *Food Biophysics*. 1 (2006). 151-162.
- Papp, S. and Vanderkooi, J. M. Tryptophan phosphorescence at room temperature as a tool to study protein structure and dynamics. *Photochemistry and Photobiology*. 49 (1989). 775-784.
- Pravinata, L. V., You, Y. and Ludescher, R. D. Erythrosin B phosphorescence monitors molecular mobility and dynamic heterogeneity in amorphous sucrose. *Biophysical Journal*. 88 (2005). 3551-3561.
- Richert, R. Triplet state salvation dynamics: Basics and applications. *Journal of Chemical Physics*. 113 (2000). 8404-8429.

- Shah, N. K. and Ludescher, R. D. Hydration and the internal dynamics of hen egg white lysozyme. *Proceedings of SPIE*. 1640 (1992). 174-179.
- Shah, N. K. and Ludescher, R. D. Influence of hydration on the internal dynamics of hen egg white lysozyme in the dry state. *Photochemistry and Photobiology*. 58 (1993). 169-174.
- Shah, N. K. and Ludescher, R. D. Phosphorescence of probes of the glassy state in amorphous sucrose. *Biotechnology Progress*. 11 (1995). 540-544.
- Shamblin, S., Hancock, B. C., Dupuis, Y. and Pikal, M. J. Interpretation of relaxation time constants for amorphous pharmaceutical systems. *Journal of Pharmaceutical Sciences*. 89 (2000). 417-427.
- Shirke, S. and Ludescher, R. D. Dynamic site heterogeneity in amorphous lactose and lactitol from spectral heterogeneity in erythrosin B phosphorescence. *Biophysical Chemistry*. 123 (2006). 122-133.
- Shirke, S. and Ludescher, R. D. Dynamic site heterogeneity in amorphous maltose and maltitol from spectral heterogeneity in erythrosin B phosphorescence. *Carbohydrate Research*. 340 (2005). 2661-2669.
- Simon-Lukasik, K. V. and Ludescher, R. D. Effect of plasticizer on dynamic site heterogeneity in cold-cast gelatin films. *Food Hydrocolloids*. 20 (2006a). 88-95.
- Simon-Lukasik, K. V. and Ludescher, R. D. Molecular mobility in water and glycerol plasticized cold and hot cast gelatin films. *Food Hydrocolloids*. 20 (2006b). 96-105.
- Strambini, G. B. and Gonnelli, M. The indole nucleus triplet-state lifetime and its dependence on solvent microviscosity. *Chemical Physics Letters*. 115 (1985). 196-200.
- Sundaresan, K. V. and Ludescher, R. D. Molecular mobility and oxygen permeability in amorphous beta-lactoglobulin films. 22 (2007). 403-413.
- Vanderkooi, J. M. and Berger, J. W. Excited triplet state used to study biological macromolecules at room temperature. *Biochimica et Biophysica Acta: Bioenergetics*. 976 (1989). 1-27.
- Vanderkooi, J. M., Maniara, Green, T. J. and Wilson, D. F. An optical method for measurement of dioxygen concentration based upon quenching of phosphorescence. *Journal of Biological Chemistry*. 262 (1987). 5476-5482.
- Zunic, A. Molecular mobility of amorphous disaccharide studied by tryptophan luminescence. Master Thesis. Rutgers University. New Brunswick, NJ. (2004).

CURRICULUM VITA

Rashmi S. Tiwari

Education

Mumbai University

Major: Chemistry, Physics and Mathematics

August 1993 – May 1996

Degree: Bachelor of Science in Chemistry, May 1996

Mumbai University

Major: Food Science and Technology

August 1996 – May 1999

Degree: Bachelor of Science in Food Technology, May 1999

Florida State University

Major: Food Science and Nutrition

August 2001- May 2004

Degree: Master of Science, May 2004

Rutgers, The State University of New Jersey

Major: Food Science with an emphasis in Food Chemistry

August 2004- May 2008

Degree: Ph. D. Food Science, October 2008